

# Concentration and Recovery of Positively Buoyant Cenospheres using an Inverted REFLUX Classifier

A thesis submitted for the degree of

Doctor of Philosophy

By

Ali Kiani

July 2016



*The thesis contains no material which has been accepted for the award of any other degree or diploma in any university or other tertiary institution and, to the best of my knowledge and belief, contains no material previously published or written by another person, except where due reference has been made in the text. I give consent to the final version of my thesis being made available worldwide when deposited in the University's Digital Repository\*\*, subject to the provisions of the Copyright Act 1968.*

*\*\*Unless an Embargo has been approved for a determined period.*

*I hereby certify that the work embodied in this thesis contains a published paper/s/scholarly work of which I am a joint author. I have included as part of the thesis a written statement, endorsed by my supervisor, attesting to my contribution to the joint publication/s/scholarly work.*

.....  
Ali Kiani

.....  
Kevin Galvin

## **Acknowledgements**

I would like to acknowledge the people who have contributed to the production of my dissertation.

Most importantly, I would like to deeply thank my principal supervisor, Professor Kevin Galvin, for his valuable guidance, useful advice, understanding and great supports. Studying under his supervision, I had the chance to gain valuable experience and learn many useful skills for my future career and life.

I would also like to thank my co-supervisor, Doctor James Zhou, who provided me with very useful hints and comments, encouragement and supervision. His understanding at my difficult time made him like a close friend for me.

Doctor Simon Iveson had a great contribution to my thesis, as he always kindly listened and gave me encouragement and advice. I deeply appreciate his very useful comments in different stages of my study as well as his patience and time in reading my thesis.

I am also greatly thankful to Mark Mason for his kindness, patience and help during my PhD. His support in the laboratory during my PhD was exceptional for me. Many thanks also to my colleagues, especially Jamie, Anthony and Kim for their friendship, communication and help.

I am also very grateful to Professor Behdad Moghtaderi for helping me to keep my spirit up during my life in Australia.

At last, but not least, I would like to thank my immediate family for their kind supports and love during my life and study. Special thanks go to my wife for her love, understanding, patience, help and kindness. This thesis was impossible to be accomplished without their supports.

Finally, I would like to appreciate the financial supports including the scholarships from the University of Newcastle, and the grants provided by the Australian Research Council and Vecor Australia.

## **Table of Contents**

<b>List of Figures</b>	<b>x</b>
<b>List of Tables</b>	<b>xix</b>
<b>Abstract</b>	<b>xxi</b>
<b>Publications</b>	<b>xxiv</b>
<b>Awards</b>	<b>xxv</b>
<b>Nomenclature</b>	<b>xxvi</b>
<b>CHAPTER 1 INTRODUCTION</b>	<b>1</b>
<b>1.1 Aim of Thesis</b>	<b>2</b>
<b>1.2 Background</b>	<b>4</b>
<b>1.3 Thesis Objectives</b>	<b>7</b>
<b>1.4 Outlines of Thesis</b>	<b>8</b>
<b>CHAPTER 2 GRAVITY SEPARATION FUNDAMENTAL CONCEPTS</b>	<b>10</b>
<b>2.1 Introduction</b>	<b>11</b>
<b>2.2 Isolated particle settling in a fluid</b>	<b>11</b>
2.2.1 Drag force	11
2.2.2 Particle terminal settling velocity	14
2.2.3 Other factors affecting the settling velocity	16
2.2.3.1 Particle shape and size	16
2.2.3.2 Particle surface roughness	19
2.2.3.3 Container walls	21
<b>2.3 Hindered settling</b>	<b>21</b>
2.3.1 Modified Stokes' law	22
2.3.2 Richardson and Zaki equation	23
2.3.3 Other studies on hindered settling	24
<b>2.4 Fluidization</b>	<b>27</b>

2.4.1 Packed bed	27
2.4.2 Fluidized beds	28
2.4.3 Density definitions in fluidization	32
2.4.4 Particle entrainment (elutriation)	33
<b>2.5 Particle segregation and dispersion</b>	<b>34</b>
<b>2.6 Fine particle beneficiation technologies</b>	<b>38</b>
2.6.1 Gravity separation methods	39
2.6.2 Particle size classification	40
2.6.3 Enhanced gravity separation methods	41
<b>2.7 Summary</b>	<b>42</b>
<b>CHAPTER 3 BULK STREAMING MOTION AND INCLINED SETTLING</b>	<b>43</b>
<b>3.1 Introduction</b>	<b>44</b>
<b>3.2 Bulk streaming motion</b>	<b>44</b>
3.2.1 Evidence for bulk streaming motion	44
3.2.2 Conditions for the development of bulk streaming motion	49
3.2.3 Similar phenomena to bulk streaming	54
3.2.3.1 Clustering and streaming in a gas-solid fluidized bed	54
3.2.3.2 Shear thinning behaviour of concentrated suspensions	55
<b>3.3 Inclined settling</b>	<b>56</b>
<b>3.4 REFLUX™ Classifier</b>	<b>62</b>
3.4.1 The Laskovski et al. correlation	65
3.4.2 Elutriation models for laminar high-shear flow in narrow channels	68
<b>3.5 Combined effects of Inclined Settling and Bulk Streaming Motion</b>	<b>72</b>
<b>3.6 The Potential for separating cenospheres from fly ash in an Inverted REFLUX™ Classifier</b>	<b>75</b>
<b>3.7 Summary</b>	<b>77</b>
<b>CHAPTER 4 FLY ASH AND CENOSPHERE CHARACTERIZATION</b>	<b>78</b>
<b>4.1 Introduction</b>	<b>80</b>

<b>4.2 Experimental</b>	<b>80</b>
4.2.1 Experimental procedure	80
4.2.1.1 Cenosphere grade	80
4.2.1.2 Particle size	81
4.2.1.3 Particle density	82
4.2.1.4 Feed semi-batch fractionation	82
<b>4.3 Results and Discussion</b>	<b>84</b>
4.3.1 Morphology and compositions	84
4.3.2 Feed fractionation using the semi-batch REFLUX™ Classifier	86
4.3.3 Particle size and density	90
<b>4.4 Conclusions</b>	<b>92</b>
<b>CHAPTER 5 PRELIMINARY EXPERIMENTS ON UPGRADING POSITIVELY BUOYANT PARTICLES USING AN INVERTED REFLUX™ CLASSIFIER</b>	<b>93</b>
<b>5.1 Introduction</b>	<b>95</b>
<b>5.2 Background</b>	<b>95</b>
<b>5.3 Experimental</b>	<b>96</b>
5.3.1 Experimental equipment	96
5.3.2 Feed preparation	99
5.3.3 Experimental procedure	100
5.3.4 Samples analysis for grade and recovery	101
5.3.4.1 Gas pycnometry method	101
5.3.4.2 Sink-float separation method	102
5.3.5 Mass balance reconciliation technique	103
5.3.6 Particle size measurement	103
<b>5.4 Results and Discussion</b>	<b>104</b>
5.4.1 Model feed	104
5.4.1.1 Separation at different product fluxes	106
5.4.2 Fly ash feed	111
5.4.2.1 Separation at a high solids concentration	112
5.4.2.2 Zero-fluidization water effects	112
5.4.2.3 Effects of different operating conditions	114
5.4.2.3.1 Influence of fluidization rate	115
5.4.2.3.2 Influence of the feed rate	118

5.4.2.3.3 Influence of the split ratio	125
5.4.2.4 Variation in recovery with particle size	126
5.4.2.5 Combined effects of product rate and fluidization rate	128
5.4.2.6 Density-based classification of cenospheres and fly ash in the IRC™	129
<b>5.5 Conclusions</b>	<b>130</b>
<b>CHAPTER 6 ENHANCED RECOVERY AND CONCENTRATION OF CENOSPHERES FROM FLY ASH PARTICLES IN THE INVERTED REFLUX™ CLASSIFIER</b>	<b>132</b>
<b>6.1 Introduction</b>	<b>134</b>
<b>6.2 Background</b>	<b>134</b>
<b>6.3 Experimental</b>	<b>138</b>
6.3.1 Equipment	138
6.3.2 Methodology	138
6.3.3 Measurements	139
6.3.3.1 Sink-float experiments	139
6.3.3.2 The particle size distribution	140
6.3.3.3 Fly ash properties	141
<b>6.4 Results and Discussion</b>	<b>142</b>
6.4.1 The effects of the dense medium on the separation of positively buoyant cenospheres from fly ash in the IRC™	143
6.4.2 Dense medium effects on the particles size classification in the IRC™	146
6.4.3 Varying product split at the optimum feed pulp density	151
6.4.4 Effect of the feed throughput at the optimum feed pulp density	153
6.4.5 Grade-Recovery curve	155
<b>6.5 Conclusions</b>	<b>156</b>
<b>CHAPTER 7 A PILOT SCALE STUDY OF CENOSPHERE RECOVERY AND CONCENTRATION IN THE INVERTED REFLUX™ CLASSIFIER</b>	<b>158</b>
<b>7.1 Introduction</b>	<b>160</b>
<b>7.2 Materials and Methods</b>	<b>160</b>
7.2.1 Pilot scale Inverted REFLUX™ Classifier	160
7.2.2 Experimental procedure	162

7.2.3 Data analysis	163
7.2.3.1 Grade and recovery	164
7.2.3.2 Particle size and density	164
<b>7.3 Results and Discussion</b>	<b>165</b>
7.3.1 Variation of the feed split ratio	166
7.3.2 Density and size classification of cenospheres and fly ash	172
7.3.3 Separation of cenospheres from fly ash at different feed throughputs	177
<b>7.4 Conclusions</b>	<b>182</b>
<b>CHAPTER 8 MULTI-STAGE CONCENTRATION OF CENOSPHERES IN FLY ASH</b>	<b>184</b>
<b>8.1 Introduction</b>	<b>186</b>
<b>8.2 Experimental</b>	<b>186</b>
8.2.1 Materials	186
8.2.2 Methods	186
8.2.3 Data analysis	187
<b>8.3 Results and Discussion</b>	<b>189</b>
8.3.1 Upgrading cenospheres from a low-grade fly ash feed	190
8.3.2 Upgrading cenospheres from a high-grade fly ash feed	191
8.3.2.1 Product grades and cenosphere recovery	192
8.3.2.2 Size and density of cenospheres in the multi-stage IRC™ process	198
<b>8.4 Conclusions</b>	<b>202</b>
<b>CHAPTER 9 THE PERFORMANCE OF THE ONE-STAGE INVERTED REFLUX™ CLASSIFIER PROCESS IN SEPARATION OF CENOSPHERES FROM DIFFERENT FLY ASH FEEDS</b>	<b>203</b>
<b>9.1 Introduction</b>	<b>205</b>
<b>9.2 Experimental</b>	<b>205</b>
<b>9.3 Results and Discussion</b>	<b>206</b>
<b>9.4 Conclusions</b>	<b>212</b>

<b>CHAPTER 10 CONCLUSIONS AND RECOMMENDATIONS</b>	<b>213</b>
<b>10.1 Conclusions</b>	<b>214</b>
<b>10.2 Recommendations</b>	<b>218</b>
<b>Reference</b>	<b>220</b>
<b>Appendix A: IRC™ raw experimental and reconciled data and results (grade and recovery by the sink-float method)</b>	<b>234</b>
<b>Appendix B: IRC™ raw experimental data and results (grade and recovery by pycnometry)</b>	<b>269</b>
<b>Appendix C: Size distribution data and partition numbers</b>	<b>275</b>
<b>Appendix D: Double fractionation data obtained from the RC™</b>	<b>316</b>
<b>Appendix E: The concentration induced enhancement obtained in Chapter 6, Runs 1-5 at different pulp densities</b>	<b>320</b>
<b>Appendix F: Three different models in predicting cenosphere hindered rise velocity in suspensions at different solids concentrations</b>	<b>321</b>
<b>Appendix G: Cumulative size distribution of cenospheres and fly ash in the preliminary and main feeds used in multi-stage study in Chapter 8.</b>	<b>322</b>
<b>Appendix H: Sample calculations</b>	<b>323</b>
<b>Appendix I: Photos of the experiments and laboratory and pilot scale Inverted REFLUX™ Classifier</b>	<b>332</b>

## List of Figures

- Figure 1.1: SEM images on feed fly ash, (A) Floated cenospheres and (B) sinks coal fly ash using a sink-float funnel. The background material was ink used to hold the particles in their place and hence is not related to the fly ash particles. The length scales are 100  $\mu\text{m}$  in both images. 2
- Figure 1.2: A schematic diagram of the Inverted REFLUX<sup>TM</sup> Classifier. 3
- Figure 2.1: Forces acting on a negatively buoyant spherical particle of diameter  $d_p$  settling in a fluid at its terminal settling velocity  $u_t$ . 12
- Figure 2.2: Standard drag curve for spherical particles in a fluid (Clift & Gauvin, 1970). 13
- Figure 2.3: Drag curves for non-spherical particles falling in a fluid as a function of particle sphericity,  $\psi$ . The volume equivalent spherical diameter  $d_v$  is used to calculate  $C_D$  and  $Re_p$  (Rhodes, 1998). 19
- Figure 2.4: Drag coefficient versus Reynolds number for particles with different surface roughness (Hoerner, 1958), where  $\Delta$  = Ditto, Behind the turbulent screen,  $\diamond$  = NACA, through resting air,  $\star$  = NACA, Variable-density tunnel,  $\times$  = Ditto, Surface roughness 0.03,  $\bullet$  = Hoerner, In open water, and  $+$  = In wind tunnel with surface roughness of 0.003. 20
- Figure 2.5: A packed bed (left hand side) and a fluidized bed (right hand side). 27
- Figure 2.6: Pressure drop vs. fluid velocity illustrating common behaviours and the location of the minimum fluidization velocity (Yang, 2003). 30
- Figure 2.7: (a) Packed bed, (b) Minimum fluidization, (c) Particulate fluidization, (d) Bubbling fluidization, (e) Axial slugging, (f) Flat slugging, (g) Turbulent fluidization, and (h) Pneumatic transport (Kunii & Levenspiel, 1991). 32
- Figure 2.8: Particle segregation in a fluidized bed at six different fluidization velocities in increasing order from a to f. The open and closed symbols show the volume fractions of low density and high density particles, respectively. Lines show model predictions (Galvin et al., 2006). 36
- Figure 2.9: Photos of the phase inversion which occurred in a binary mixture of small dense and large light particles as the fluid velocity increased from 0.012 m/s to 0.042 m/s (Galvin et al., 2002). 37
- Figure 2.10: A simple plot of a partition curve. 41
- Figure 3.1: The variation in the settling rate of the falling-spheres as a function of the concentration of the suspended-spheres. Mixture made up of methyl-methacrylate polymer

(falling-spheres) and polystyrene (suspended-spheres) in aqueous solutions of lead nitrate (Whitmore, 1954). 45

Figure 3.2: Settling patterns of a suspension containing positively and negatively buoyant particles (Weiland & McPherson, 1979). 46

Figure 3.3: The dependence of (a) negatively-buoyant particle relative settling rate on the concentration of positively-buoyant particles  $\phi_L$ , and (b) light particle settling rate on the concentration of heavy particles  $\phi_H$  (Fessas and Weiland, 1981 & 1982). 47

Figure 3.4: Streaming structures observed in a suspension containing negatively-buoyant particles with different densities. It is noted that properties of these systems are indicated in Table 3.1 (Weiland et al., 1984). 49

Figure 3.5: Photographs of the four different types of internal structures or streams observed by Batchelor & Van Rensburg (1986) which they classified as: a) blobs with tail and a good photographic contrast; b) blobs and a good contrast; c) columns with head and a fair contrast; and d) streaming columns with poor contrast. 51

Figure 3.6: The regime map proposed by Batchelor and Van Rensburg (1986) to show instabilities for a suspension containing positively and negatively buoyant particles when  $\lambda = 1$ , and  $\gamma = -1$ . System types:  $\times$  indicates unstable systems,  $\blacktriangledown$  indicates the systems studied by Fessas and Weiland (1981 & 1984) classified as being marginally unstable and  $\circ$  indicates the stable region. 52

Figure 3.7: Regime map showing the ( $\times$ ) unstable, ( $\blacksquare$ ) marginally unstable and ( $\circ$ ) stable systems when  $\phi_1 = \phi_2 = 0.15$  (Batchelor & Van Rensburg, 1986). 53

Figure 3.8: Formation of particles clusters in a gas-solid fluidized bed (Li et al., 1991). 55

Figure 3.9: Shear thinning behaviour developed in a concentrated suspension at high shear rates (Rhodes, 2007). 56

Figure 3.10: (a) Inclined settler related to the PNK theory (Hill et al., 1977), and (b) Inclined settling considering a more complex clear water-suspension interface (Zahavi & Rubin, 1975). 58

Figure 3.11: A simplified model for predicting the particles settling velocity in an inclined container (Davis et al., 1982). 60

Figure 3.12: A continuous inclined settling of a suspension with four different species.  $Q_o$  was adjusted such that only the two smallest species could be carried to the overflow (Davis & Gecol, 1996). 62

Figure 3.13: A fluidized bed with a system of inclined channels installed at its different vertical positions (Galvin & Nguyentranlam, 2002). 63

Figure 3.14: (a) A schematic of a simplified system containing an inclined channel and a fluidized bed (Galvin & Nguyentranlam, 2002), and (b) a more complex analysis of the system (Doroodchi et al., 2004). 64

Figure 3.15: (a) A representation of the REFLUX™ Classifier as set up for semi-batch fractionation tests. In semi-batch tests, there is no underflow removal and no feed addition other than the initial batch of feed solids (Laskovski et al., 2006) & (b) A schematic diagram of the REFLUX™ Classifier showing its main dimensions (Li et al., 2014). 65

Figure 3.16: (a) The parabolic velocity profile for laminar flow in a narrow channel gives (b) a near linear velocity field close to the wall, such that the local conveying velocity  $u$  experienced by particles is approximately proportional to their size (Galvin et al., 2009). 70

Figure 3.17: The dependency of elutriation velocity on the particles size for (a) a conventional elutriator and (b) a REFLUX™ Classifier with 1.77 mm spacing (Galvin et al., 2009). 70

Figure 3.18: The equilibrium condition for a particle in a channel subjected to a laminar flow (Galvin & Liu, 2011). 71

Figure 3.19: A system of light (white) and heavy particles (pink) in an inclined vessel at volume fractions of (a) 0.08 for each one, and (b) 0.20 and 0.15 for light and heavy ones, respectively (Law et al., 1988). 73

Figure 3.20: Dependency of the light particles' velocity relative to their terminal velocity ( $u_{lb}^\theta/u_{lm}^0$ ) on the angle of inclination  $\theta$  of the channel for different initial concentrations of heavy particles  $\phi_{hb}$  (MacTaggart et al., 1988). 75

Figure 3.21: (a) A schematic diagram of an Inverted REFLUX™ Classifier and (b) bulk streaming motion phenomenon hypothesised to occur for ● negatively buoyant fly ash and ○ positively buoyant cenospheres. 76

Figure 4.1: (a) A sink-float funnel, (b) a top view photo of the sink-float funnel showing the entrained fly ash and unburnt carbon particles with the cenospheres, (c) the released fly ash and unburnt carbon particles, and (d) obtained clean cenospheres at the end of the sink-float test. 81

Figure 4.2: A simple representation of a semi-batch REFLUX™ Classifier process. 83

Figure 4.3: (a) A spherical cenosphere (Length Scale = 10  $\mu\text{m}$ ), (b) a broken cenosphere (Length Scale = 20  $\mu\text{m}$ ), (c) an unburnt carbon particle and (d) heavy particles in fly ash (silica, alumina, calcium and unburnt carbon). In (c) & (d), the length scales shown are 200  $\mu\text{m}$ . 84

Figure 4.4: X-ray spectroscopy component analyses of (a) unburnt carbon particles, (b) dense fly ash particles, (c) silicate fly ash particles and (d) cenosphere particles. 86

Figure 4.5: Cumulative yield at different density cut points (preliminary experiment).	88
Figure 4.6: Cumulative yield at different density cut points (main experiment).	90
Figure 4.7: The mass-based and volume-based fractions of cenospheres and fly ash less than a given particle size.	91
Figure 4.8: The volume-based size distributions of cenospheres particles at different density intervals in $\text{kg/m}^3$ .	92
Figure 5.1: A schematic representation of the Inverted REFLUX™ Classifier used in this study.	98
Figure 5.2: The fluidization water distributor with 4 water inlets to the chamber and 14 holes in each face of the distributor.	98
Figure 5.3: Separating funnels used for sink-float measurements of the grade of cenospheres in product, tailings and feed samples.	103
Figure 5.4: The volume frequency size distributions of the cenospheres and silica fractions in the model feed of Run 1 (raw data).	105
Figure 5.5: Product grade and cenosphere recoveries obtained at different overflow product fluxes for the model feed at constant feed and wash water fluxes of $7.0 \text{ m}^3/(\text{m}^2 \text{ h})$ and $0.87 \text{ m}^3/(\text{m}^2 \text{ h})$ , respectively (based on balanced data). The error bars show the span of calculated recoveries based on the raw measurements of feed, product and tailings masses.	107
Figure 5.6: Floats volume frequency size distributions in the product, tailings and feed streams from Run 2 on the model feed at a product flux of $0.17 \text{ m}^3/(\text{m}^2 \text{ h})$ . Raw data measured using Malvern 2000.	108
Figure 5.7: Partition of cenospheres to the product stream for experiments with the model feed at a volumetric flux of $6.7 \text{ m}^3/(\text{m}^2 \text{ h})$ and slurry with 8.3% solids by mass. Curves based on material-balanced data.	110
Figure 5.8: Product grade obtained at different product fluxes in the IRC™ at feed solids concentration of about 50 wt.% (Runs 5-8).	113
Figure 5.9: Cenosphere recovery for entire size range obtained at different product fluxes (Runs 5-8) in the IRC™ at feed solids concentration of about 50 wt.% based on reconciled data.	113
Figure 5.10: The volume frequency size distributions of the floats and sinks fractions in the fly ash feed slurry of Runs 9-20 as measured by a Malvern Mastersizer Model 2000 (raw data).	114

Figure 5.11: The influence of fluidization water on (A) product solid flux (B) product solid density (C) grade of cenospheres in product (D) recovery of cenospheres in product. Note that at the fluidization water flux of about $0.35 \text{ m}^3/(\text{m}^2 \text{ h})$ , the measured average solids density was about $1630 \text{ kg/m}^3$ (Graph B), so it makes no sense to calculate grades or recoveries based on an assumed fly ash density of $1600 \text{ kg/m}^3$ .	118
Figure 5.12: The investigation of feed flux variation (with ratio of product volumetric flux to feed volumetric flux set equal to 0.2) on (A) product solid flux (B) product solid density (C) grade of cenospheres in product (D) recovery of cenospheres in product.	121
Figure 5.13: The investigation of feed flux variation (with ratio of product volumetric flux to feed volumetric flux set equal to 0.4) on (A) product solid flux (B) product solid density (C) grade of cenospheres in product (D) recovery of cenospheres in product.	124
Figure 5.14: Grade and recovery of cenospheres at different split ratios (Runs 9-11).	125
Figure 5.15: Volume-based recovery of cenospheres obtained at different split ratios for the full particles size range compared with recoveries based only on particles larger than $50 \mu\text{m}$ (Runs 9-11).	126
Figure 5.16: Partition curves at different split ratios (based on volume-balance reconciled data) (Runs 9-11).	127
Figure 5.17: Product grade versus ( $P - W$ ) parameter for the experiments at different operating conditions.	128
Figure 5.18: Recovery versus ( $P - W$ ) parameter for the experiments at different operating conditions.	129
Figure 6.1: The rise velocity of cenospheres in fly ash slurry at different feed pulp densities predicted by three different models.	136
Figure 6.2: The visual sign of the streams forming against the downward facing surface of the Inclined channel.	137
Figure 6.3: (a) Sink and float analysis using a separating funnel, (b) entrained cenospheres recovered from the sinks fraction.	140
Figure 6.4: Volume frequency size distributions of floats cenospheres and sinks fly ash fractions in feed on a log scale (based on the unreconciled raw data).	141
Figure 6.5: Feed cenosphere volume frequency size distributions in Runs 1-5 as measured by the Malvern Mastersizer 2000. It is noted that the small peaks at particle sizes smaller than $30 \mu\text{m}$ are mainly due to the fine cenospheres and fly ash misplacement in the sink-float separation method.	144

- Figure 6.6: Dependence of product grade from Runs 1-5 (different feed pulp densities (PD)) on the difference between the product and fluidization volumetric fluxes, ( $P - W$ ). 145
- Figure 6.7: Recovery of cenospheres at different feed pulp densities from Runs 1-5 (based on reconciled data). 146
- Figure 6.8: Cenosphere volume frequency size distributions in the feed, product and tailing for Run 4, conducted at 38.1 wt.% feed pulp density (unreconciled raw data). 147
- Figure 6.9: Partitioning to the product for different feed pulp densities (PD) (based on the mass-balance reconciled results). 150
- Figure 6.10: Concentration induced throughput advantage (Eq. 6.1) of the Inverted REFLUX™ Classifier. The curve is based on the  $d_{50}$  values while the error bars denote values ranging from the  $d_{25}$  to the  $d_{75}$  (see Appendix E & H). The dashed horizontal line denotes the base-line for the Inverted REFLUX™ Classifier. 151
- Figure 6.11: Grade and recovery of cenospheres as a function of product flux for Runs 6-8 at the optimum feed pulp density of 40 wt. % and a feed solids flux of 4.7 t/(m<sup>2</sup> h) (based on the reconciled data). 152
- Figure 6.12: The effect of the feed flux on the product grade, at the optimum feed pulp density (PD) of about 40 wt.% (based on the mass balance reconciled results). 154
- Figure 6.13: The effect of the feed flux on the cenosphere recovery, at the optimum feed pulp density of about 40 wt.% (based on the reconciled results). 154
- Figure 6.14: The grade-recovery curves for experiments conducted at different feed volumetric fluxes. The Chapter 5 results were based on pulp density of 30-32 wt.%, and feed grade 0.51 wt.%. All other data are based on Run 4 and Runs 6-10 involving a pulp density of 38.1 to 41.5 wt.% solids, and feed grade of 0.81 to 1.08 wt.%. 156
- Figure 7.1: (a) A schematic representation and (b) A photo of the experimental set up. 161
- Figure 7.2: Cenospheres and fly ash volume frequency size distributions in the feed (based on the raw data). 164
- Figure 7.3: The suspension density formed in the vertical section of the IRC™ above the feed point versus time at different feed split ratios with the feed solids throughput and fluidization water flux kept constant at 4.1 t/(m<sup>2</sup> h) and 0.83 m<sup>3</sup>/(m<sup>2</sup> h), respectively. 167
- Figure 7.4: Variation of the average density of cenospheres in product at different feed split ratios (raw data) with the feed solids throughput and fluidization water fluxes kept constant at 4.1 t/(m<sup>2</sup> h) and 0.83 m<sup>3</sup>/(m<sup>2</sup> h), respectively. 168

Figure 7.5: Variation of the average size of cenospheres in product at different feed split ratios (raw data) with the feed solids throughput and fluidization water flux kept constant at 4.1 t/(m<sup>2</sup> h) and 0.83 m<sup>3</sup>/(m<sup>2</sup> h), respectively. 169

Figure 7.6: Recovery of cenospheres obtained at different yields from the pilot scale IRC<sup>TM</sup> (based on the reconciled data) with the feed solids throughput and fluidization water flux kept constant at 4.1 t/(m<sup>2</sup> h) and 0.83 m<sup>3</sup>/(m<sup>2</sup> h), respectively. 170

Figure 7.7: Product grades obtained at different yields from the pilot scale IRC<sup>TM</sup> (based on the reconciled data) with the feed solids throughput and fluidization water flux kept constant at 4.1 t/(m<sup>2</sup> h) and 0.83 m<sup>3</sup>/(m<sup>2</sup> h), respectively. 171

Figure 7.8: The bed density and product grade at different feed split ratios at the steady state condition. 171

Figure 7.9: The grade-recovery curve achieved for the pilot scale IRC<sup>TM</sup> at a solid throughput of 4.1 t/(m<sup>2</sup> h) (based on the mass balanced data) with the fluidization water fluxes kept constant at 0.83 m<sup>3</sup>/(m<sup>2</sup> h). The feed solids throughput and fluidization water flux were about 4.7 t/(m<sup>2</sup> h) and 1.0 m<sup>3</sup>/(m<sup>2</sup> h) in the laboratory scale runs. The feed pulp density was around 40 wt.% at both scales. 172

Figure 7.10: The volume frequency size distributions of sink fly ash particles in the product, tailings and feed for Run 3 (based on the raw data). 173

Figure 7.11: The volume frequency size distributions of float cenosphere particles in product, tailings and feed for Run 3 (based on the raw data). 174

Figure 7.12: The partition curves for Run 1, 2, 3 and 6 (based on the reconciled data). 175

Figure 7.13: The bed density variation with time at different feed fluxes in the pilot scale IRC<sup>TM</sup>. Fluidization water flux, feed volumetric split ratio and feed pulp density were maintained approximately constant at 0.83 m<sup>3</sup>/(m<sup>2</sup> h), 16 vol.% and 40 wt.% respectively. 178

Figure 7.14: The bed density and product grade at different feed fluxes, at steady state. 178

Figure 7.15: The variation of product grades at different feed slurry mass fluxes (based on the mass balanced data), comparing this chapter's pilot-scale results with the laboratory-scale results from Chapter 6. Fluidization water flux, feed volumetric split ratio and feed pulp density were maintained approximately constant at 0.83 m<sup>3</sup>/(m<sup>2</sup> h), 16 vol.% and 40 wt.% respectively in the pilot scales runs, while the feed volumetric split ratio was slightly higher at 20 vol.% in the lab scale runs. 179

Figure 7.16: The recovery of cenospheres at different feed slurry mass fluxes (based on the reconciled data) comparing the present pilot-scale results with the laboratory-scale results from Chapter 6. Fluidization water flux, feed volumetric split ratio and feed pulp density were maintained approximately constant at 0.83 m<sup>3</sup>/(m<sup>2</sup> h), 16 vol.% and 40 wt.%

respectively in the pilot scales runs, while the feed volumetric split ratio was slightly higher at 20 vol.% in the lab scale runs.	180
Figure 7.17: Product grade and cenospheres recovery obtained from different runs in the pilot scale IRC™ (Runs 1-6).	181
Figure 8.1: A schematic diagram of the three-stage IRC™ process.	187
Figure 8.2: The cenosphere floats and fly ash sinks particle size distributions in the feed used for the preliminary two-stage trials.	188
Figure 8.3: SEM images showing (A) the floats fraction and (B) the sinks fraction obtained from a sink-float separation of the preliminary fly ash feed containing 0.33 wt.% cenospheres, and (C) the floats fraction and (D) the sinks fraction obtained from a sink-float separation of the main fly ash feed containing about 0.9 wt.% cenospheres. The 100 μm length scale is shown in the bottom left hand corner of each image. Note the background material, on which the samples rest, is unrelated to the fly ash.	189
Figure 8.4: Product grade of cenospheres at different stages of the process.	193
Figure 8.5: Cenospheres incremental recovery obtained at different stages of the process.	194
Figure 8.6: Cumulative upgrade after each stage of the process.	195
Figure 8.7: Cumulative cenosphere recovery after each stage of the process.	195
Figure 8.8: Product grade and cenospheres recovery obtained from the third stage of the process at different product fluxes.	197
Figure 8.9: Grade-recovery curve for each stage of the process.	198
Figure 8.10: Size distributions of cenospheres in the product at different stages of the process.	199
Figure 8.11: Partitioning to product obtained at different stages of the process.	200
Figure 8.12: Average density of all product solids and only the cenospheres in the product at different stages of the process.	201
Figure 9.1: Volume size distributions of cenospheres in the different fly ash feeds.	207
Figure 9.2: Product grades obtained from IRC™ in separating cenospheres from different fly ash feeds (Runs 1, 2 and 3).	209
Figure 9.3: Cenosphere recovery obtained for different fly ash feeds processed in the IRC™.	210

Figure 9.4: Volume-based frequency size distribution of cenospheres in product, tailings and feed for Run 3. 211

Figure 9.5: The size partition curves obtained for Feeds 2 and 3 (Runs 2 and 3). 211

## List of Tables

Table 2.1: Drag coefficient and terminal velocity for spherical particles in different flow regimes (Heiskanen, 1993; Rhodes, 1998).	15
Table 2.2: $n$ values for the Richardson-Zaki equation (Richardson & Zaki, 1954a; Richardson & Zaki, 1954b).	24
Table 3.1: Properties of the systems in which an enhancement in the settling or rise velocity of species was reported (Batchelor & Van Rensburg, 1986).	48
Table 3.2: The dependency of the superficial velocity in fluidized beds and the REFLUX™ Classifier on particles size at different regimes (Laskovski et al., 2006).	68
Table 3.3: Properties of the system and geometrical dimensions of the vessels used to examine the combined effects of Boycott and bulk streaming motion phenomenon (MacTaggart et al., 1988).	74
Table 4.1: Double fractionation data of a typical fly ash feed sample (Preliminary experiment).	87
Table 4.2: Interpolation of data in Table 4.1 to obtain the density distribution (Preliminary experiment).	87
Table 4.3: Double fractionation data of a typical fly ash feed sample (main experiment).	89
Table 4.4: Interpolation of data in Table 4.3 to obtain the density distribution (main experiment).	89
Table 5.1: Experimental parameters and results obtained from the four runs using the model feed. Note that the mass of cenospheres in the tailings samples, all samples of Run 4 and the feed sample of Run 3 were too small for the gas pycnometry method to measure their density.	106
Table 5.2: Experimental parameters in different runs on real fly ash feed (based on raw data).	111
Table 5.3: $d_{25}$ , $d_{50}$ , $d_{75}$ and $I$ for the runs at different product fluxes (Runs 9-11).	127
Table 5.4: Density of cenospheres and fly ash in feed, tailings and product of Runs 5, 6 & 7.	129
Table 5.5: Mass and density of cenospheres in feed, product and tailings for different size ranges (Run 5 based on reconciled data).	130

Table 6.1: Details of the 10 experiments carried out using a raw fly ash feed. All data shown is mass-balance reconciled except for the total volumetric flow rate values which are based on the raw data.	143
Table 6.2: $I$ , $d_{50}$ values, theoretical and actual throughput advantage for Runs 1-5 (based on the reconciled results).	150
Table 7.1: Summary of experimental results, operating conditions, and parameters based on the reconciled data (note that the section labelled “Experimental conditions” is based on the raw data).	166
Table 7.2: $d_{50}$ and $I$ obtained at different split ratios (Runs 1, 2, 3 and 6).	175
Table 7.3: Arithmetic average size and density of cenospheres and fly ash in product, tailings and feed for Run 3 (based on the raw Malvern & pycnometry data).	176
Table 8.1: Product grade and cenosphere recovery achieved at different stages of the process.	191
Table 8.2: The operating parameters (based on raw data) and the obtained results (based on mass-balanced data) for the three-stage separation in the IRC™.	192
Table 8.3: $d_{50}$ and imperfection ( $I$ ) (Wills, 1996) showing the quality of separation in each stage.	200
Table 9.1: Average size and density of the fly ash and the cenospheres at different feeds.	206
Table 9.2: The experimental parameters and the results obtained from the separation of cenospheres from different fly ash feeds in the IRC™.	208

## Abstract

This thesis is concerned with investigating the application of the Inverted REFLUX™ Classifier (IRC™) for separating positively buoyant particles from other negatively buoyant particles. This innovative technology was investigated here for the first time to recover valuable cenospheres, less dense than water, from the fly ash waste of a coal fired power station. Annually, millions of tonnes of fly ash generated from burning coal are discarded to the land surrounding power stations, causing long-lasting environmental and health issues. Fly ash contains valuable components such as cenospheres, unburnt carbon, metals and trace elements. The cenospheres are hollow micro-shells consisting of oxides of silicon and aluminium. These particles represent one of the most valuable components found in fly ash, but at low levels of order 1 wt.%. The particles offer superior properties such as high insulation, high strength, and low density, and hence are valued sometimes up to \$ 2000 per tonne. They are positively buoyant in water, and hence wet gravity separation offers the potential for their separation from the negatively buoyant fly ash particles. In this study, wet gravity separation in an Inverted REFLUX™ Classifier was investigated to recover and concentrate cenospheres.

The Inverted REFLUX™ Classifier (IRC™) consisted of 1-metre long parallel inclined channels located underneath a 1-metre long vertical liquid fluidized bed. Downwards fluidization was supplied through a distributor at the top for the purpose of washing high density slimes from the low density cenospheres. The inclined channels enhanced the segregation rate of the cenosphere particles leading to a throughput advantage over a conventional fluidized bed. Following preliminary experiments it was shown, using the correlation derived by Laskovski et al. (2006), the throughput advantage of the IRC™ was 32. In other words, for a given separation performance, the feed rate per unit of vessel area to the IRC™ can be increased to a level 32 times higher than for a conventional fluidized bed. These preliminary studies were based on using a model feed, a mixture of commercial cenospheres and silica flour. Then, a real fly ash feed containing around 0.51 wt.% cenospheres was used. At a solids throughput of about 2.3 t/(m<sup>2</sup> h), a product grade of 76 wt.% and a recovery of about 42 wt.% were obtained, corresponding to an upgrade of about 151. By increasing the product rate, the recovery of cenospheres increased to about 64 wt.%, while the upgrade was reduced to 33.

A more systematic study was then conducted using a new feed consisting of about 1 wt.% cenospheres, focussed on the role of the solids concentration in effecting enhanced segregation. Based on the study by Batchelor and Van Rensburg (1986), it was hypothesised that a bulk streaming phenomenon should develop in the inclined channels at sufficiently high cenosphere and fly ash concentrations. Different feed solids concentrations from 10 wt.% to 46 wt.% were used, for a fixed feed flow rate, fluidization rate, and volumetric split between the overflow and underflow. As the feed solids concentration increased from 10.1 wt.% to about 38.1 wt.%, the recovery of the cenospheres increased from 61.7 wt.% to an optimum recovery of 89.9 wt.%, before declining rapidly to a recovery of 60.2 wt.% at a feed solids concentration of about 46.4 wt.%. At the optimum feed solids concentration of 38.1 wt.%, the solids throughput was a remarkable  $3.1 \text{ t}/(\text{m}^2 \text{ h})$ , and the upgrade in the cenospheres concentration was 58.6.

The overall throughput advantage at the optimum condition was found to be 54, based on a partition curve analysis of the separation size of the cenospheres. More detailed analysis indicated that the inclined channels delivered a throughput advantage of 18, hence it was concluded that a further throughput advantage of 3 was most likely due to the bulk streaming phenomenon. The sharpest size classification was also evident at the optimum feed solids concentration, providing the  $d_{25} = 31.5 \text{ }\mu\text{m}$ ,  $d_{50} = 36.5 \text{ }\mu\text{m}$ , and  $d_{75} = 50.0 \text{ }\mu\text{m}$ . The separation performance at the optimum feed solids concentration was further investigated at different feed flow rates and product split ratios, in order to provide the optimum operating conditions to be used in the pilot scale investigation.

The potential to scale-up the process by a factor of 10 was investigated using a pilot scale device with cross-section  $0.3 \text{ m} \times 0.3 \text{ m}$ . The separation performance in the pilot scale IRC™ was compared with that obtained from the laboratory scale performance. The results were found to be consistent. At a solids throughput of about  $4.1 \text{ t}/(\text{m}^2 \text{ h})$ , a cenosphere recovery of about 80 wt.% and a high upgrade of 19 were achieved while at a lower product split ratio, a slightly lower recovery of 75 wt.% and a higher upgrade of 38 were achieved. This part of the study provides the necessary basis for justifying a full scale investigation of this technology.

The potential benefits of a multi-stage arrangement were also investigated. A fly ash feed with the cenosphere grade of about 0.9 wt.% was subjected to a three-stage IRC™ separation.

At the end of the process, a very high grade product of about 97 wt.% (almost pure on a volume basis) was achieved. However, the overall three stage recovery fell to around 50 wt.%, mainly due to the low separation efficiency in Stage 2 of the process. In fact, the second stage involved a very dilute feed, and hence a likely explanation is the lack of the bulk streaming phenomenon under these conditions. It is therefore concluded that the single stage separation offers the best option.

A further fly ash feed containing larger cenospheres at an even higher cenosphere concentration was examined in the IRC™. At a high solids throughput of 4.9 t/(m<sup>2</sup> h), the cenosphere recovery was found to be 93 wt.%, and product grade 80 wt.%. This final study demonstrated the remarkable separation performance that can be achieved, and the fact that in the presence of larger cenospheres high recoveries and upgrades are possible at even higher solids throughputs. The work was also consistent with the earlier findings which show the benefit of a higher cenosphere feed concentration in promoting the bulk streaming phenomenon.

This study has investigated for the first time an entirely new technology for separating very low grade buoyant particles from a very high concentration of ultrafine high density particles. The approach is effectively an inverted application of the REFLUX™ Classifier. This thesis has therefore incorporated the analysis developed for the REFLUX™ Classifier, providing a clear basis for assessing this new, inverted, system. Through this approach it has been possible to infer the existence of hydrodynamic benefits that arise from operating at higher concentrations, and in turn elevated solids processing rates. Further investigation of the bulk streaming phenomenon within inclined systems is recommended in order to identify the precise onset of the phenomenon. This benefit has not previously been identified in the separation of cenospheres from fly ash. The overall findings from this study demonstrate a separation performance significantly better than achieved previously by any other technology to date.

## Publications

### *Journals*

- **Kiani, A.,** Zhou, J. & Galvin, K.P. (2015). Upgrading of Positively Buoyant Particles Using an Inverted Reflux Classifier. *Advance Powder Technology*, 26, 119-125.
- **Kiani, A.,** Zhou, J. & Galvin, K.P. (2015). Enhanced Recovery and Concentration of Positively Buoyant Cenospheres from Negatively Buoyant Fly ash Particles using the Inverted Reflux Classifier. *Minerals Engineering*, 79, 1-9.
- **Kiani, A.,** Zhou, J. & Galvin, K.P. (2015). A Pilot Scale Study of Cenosphere Recovery and Concentration using the Inverted Reflux Classifier, *Minerals Engineering*, 79, 17-23.
- **Kiani, A.,** Zhou, J. & Galvin, K.P. (2015). Multi-stage concentration of cenospheres in fly ash using the Inverted Reflux Classifier. *Coal Combustion and Gasification Products*, 7, 40-46.
- **Kiani, A.,** Zhou, J. & Galvin, K.P. (2016). Detailed Characterization and Separation of Fly Ash Fed to the Inverted Reflux Classifier. *Fuel Processing Technology*, DOI: 10.1016/j.fuproc.2016.04.028.
- Li, J., Agarwal, A., Iveson, S.M., **Kiani, A.,** Dickinson, J., Zhou, J. & Galvin, K.P. (2014). Recovery and Concentration of Buoyant Cenospheres using an Inverted Reflux Classifier. *Fuel Processing Technology*, 123, 127–139.

### *Conferences*

- **Kiani, A.,** Zhou, J. & Galvin, K.P., Upgrading of Cenosphere in Fly ash using a Series of Inverted Reflux Classifier, WOCA conference, USA, 4-7 May, 2015.
- **Kiani, A.,** Zhou, J. & Galvin, K.P., Gravity Separation of Positively Buoyant Cenospheres from Different Fly ash Waste Streams using the Inverted Reflux Classifier, ICCS&T, Melbourne, Australia, 27 Sep - 1 Oct, 2015.
- **Kiani, A.,** Zhou, J. & Galvin, K.P., Upgrading of Positively Buoyant Particles Using an Inverted Reflux Classifier, Chemeca Conference, Brisbane, Australia, 2013.
- **Kiani, A.,** Zhou, J. & Galvin, K.P., Gravity separation of cenospheres using a laboratory inverted Reflux Classifier, Australasian Particle Technology Society (APTS) Inaugural Student Conference - Sunshine Coast, 27 – 29 Sep 2013.

## **Awards**

- Most Outstanding Student Oral Presentation at WOCA International Conference 2015.

## Nomenclature

Symbol	Definition	Units
$F_W$	Gravitational force	N
$F_B$	Buoyancy force	N
$F_D$	Drag force	N
$u_t$	Terminal velocity	m/s
$d_p$	Particle diameter	m
$u_r$	Relative velocity	m/s
$Re_p$	Reynolds Number	-
$C_D$	Drag coefficient	-
$R'$	Force per projected area	N
$m$	Particle mass	kg
$a$	Particle acceleration	m/s <sup>2</sup>
$F_I$	Inertial force	N
$F_F$	Net weight force	N
$V$	Particle volume	m <sup>3</sup>
$g$	Gravitational acceleration	m/s <sup>2</sup>
$A$	Particle cross-sectional area	m <sup>2</sup>
$Ar$	Archimedes Number	-
$d_v$	Volume-equivalent spherical diameter	m
$d_s$	Surface-area equivalent spherical diameter	m
$S$	Particle surface area	m <sup>2</sup>
$d_{sv}$	Particle sauter diameter	m
$d_{St}$	Particle Stokes' diameter	m
$N$	Total number of particles	-
$n_i$	Total number of ith particles	-
$d_g$	Particles size geometric mean	m
$f_w$	Wall factor	-
$u_{tD}$	Particle settling velocity in the tube or pipe	m/s
$u_{t\infty}$	Particle settling velocity in an infinite fluid	m/s
$D$	Tube or pipe diameter	m
$u_p$	Hindered settling velocity	m/s
$u_f$	local fluid interstitial velocity	m/s

$n$	Richardson-Zaki constant	-
$P'$	Pressure	Pa
$H_0$	Bed initial height	m
$K_3$	Particle shape and surface factor	-
$u_s$	Superficial fluid velocity	m/s
$S_v$	Surface area per unit volume of particles	1/m
$H$	Bed height	m
$U_{mf}$	Minimum fluidization velocity	m/s
$Re_{mf}$	Reynolds number in minimum fluidization	-
$L_m$	Bed length when the bed is fixed	m
$L_{mf}$	Bed length in minimum fluidization	m
$L_f$	Bed length in fluidization	m
$z'$	Distance from base of the vessel	m
$U_i$	Local segregation velocity	m/s
$U_{mi}$	Maximum possible segregation velocity	m/s
$D$	Dispersion coefficient	m <sup>2</sup> /s
$r$	Particle radius	m
$F''$	Hindering factor	-
$d_{25}$	Particle diameter with 25% possibility to be in product	m
$d_{50}$	Particle diameter with 50% possibility to be in product	m
$d_{75}$	Particle diameter with 75% possibility to be in product	m
$I$	Imperfection	-
$E_p$	Ecart probable	Kg/m <sup>3</sup>
$t$	Time	s
$U_H$	Heavy particles velocity in the presence of light particles	m/s
$U_H^0$	Heavy particles velocity in the absence of the light particles	m/s
$U_L$	Light particles velocity in the presence of heavy particles	m/s
$U_L^0$	Light particles velocity in the absence of heavy particles	m/s
$I'$	Indication of stability in the suspensions	-
$h$	Water layer thickness	m
$h(t)$	Clear water layer thickness at time $t$	m
$u$	Settling velocity in a vertical tube	m/s
$h'$	Clear water layer underneath the downward facing wall	m

$U'$	Settling velocity in an inclined container	m/s
$Gr$	Grashof number	-
$l$	Characteristic length of macroscale motions	m
$Q_o$	Overflow rate	m <sup>3</sup> /s
$Q_u$	Underflow rate	m <sup>3</sup> /s
$Q_f$	Feed rate	m <sup>3</sup> /s
$B$	Vertical section width	m
$H$	Vertical section height	m
$L$	Plates length	m
$z$	Channels spacing	m
$t'$	Plates thickness	m
$F'$	Theoretical throughput advantage	-
$U$	Superficial velocity in the RC <sup>TM</sup>	m/s
$x$	Particle distance from the upward facing plate	m
$L_f$	Critical lift force	N
$F_n$	Net weight force acting perpendicular to the plate	N
$u_{lb}^\theta$	Light particles velocity at different inclination angle	m/s
$u_{lm}^0$	Light particles terminal velocity in a vertical channel	m/s
$X_c$	Product grade	-
$R$	Cenosphere recovery	-
$M_{solid}$	Total mass of solids	kg
$R_{Vc}$	Volume-based recovery	-
$R_{Mc}$	Mass-based recovery	-
$P$	Product flux	m <sup>3</sup> /(m <sup>2</sup> h)
$F$	Feed flux	m <sup>3</sup> /(m <sup>2</sup> h)
$W$	Fluidization water flux	m <sup>3</sup> /(m <sup>2</sup> h)
<b>Greek Letters</b>		
$\mu$	Fluid viscosity	Pa.s
$\rho_f$	Fluid density	kg/m <sup>3</sup>
$\rho_p$	Particle density	kg/m <sup>3</sup>
$\psi$	Sphericity	-
$\chi$	Shape factor	-
$\mu_e$	Effective suspension viscosity	Pa.s

$f(\varepsilon)$	Viscosity function	-
$\rho_{susp}$	Effective suspension density	kg/m <sup>3</sup>
$\varepsilon$	Voidage or volume fraction of the fluid	-
$\phi$	Solids volume fraction	-
$f(\phi_f)$	Particles concentration factor	-
$\phi_{pi}$	$i_{th}$ species volumetric concentration	-
$\phi_f$	Fluid volume concentration	-
$\Delta$	Difference	-
$\varepsilon_{mf}$	Bed voidage in minimum fluidization	-
$\phi_i$	Local volume concentration of $i_{th}$ species	-
$\phi_{ni}$	$i_{th}$ species local concentration relative to the mono-component zone	-
$\phi_{mi}$	$i_{th}$ species concentration in the mono-component zone	-
$\alpha'$	Adjustable parameter	-
$\alpha$	Adjustable parameter	-
$\phi_L$	Light particles concentration	-
$\phi_H$	Heavy particles concentration	-
$\lambda$	The ratio of species radii	-
$\gamma$	The ratio of species reduced densities	-
$\phi_0$	Suspensions initial solids volume fraction	-
$\Lambda$	ratio of Grashof number to Reynolds number	-
$\theta$	Inclination angle relative to the horizontal	°
$\eta$	Segregation efficiency	-
$\gamma$	Shear rate	s <sup>-1</sup>
$\rho_s$	Dense fly ash density	kg/m <sup>3</sup>
$\rho_c$	Cenosphere density	kg/m <sup>3</sup>
$\rho_{solids}$	Solids density	kg/m <sup>3</sup>
$\rho_{cF}$	Density of cenosphere in feed	kg/m <sup>3</sup>
$\rho_{cP}$	Density of cenosphere in product	kg/m <sup>3</sup>

# **Chapter 1**

## **Introduction**

## 1.1 Aim of Thesis

Figure 1.1 shows SEM images of cenospheres and fly ash generated as by-products from a coal fired power station in Australia. A large proportion of fly ash waste has been discarded to lands around the power stations. The fly ash waste has the potential to cause long-lasting environmental problems as land availability for further disposal around some power stations has become scarce. If the useful particles present in the fly ash can be recovered and concentrated, this waste may be considered a resource, not a problem.

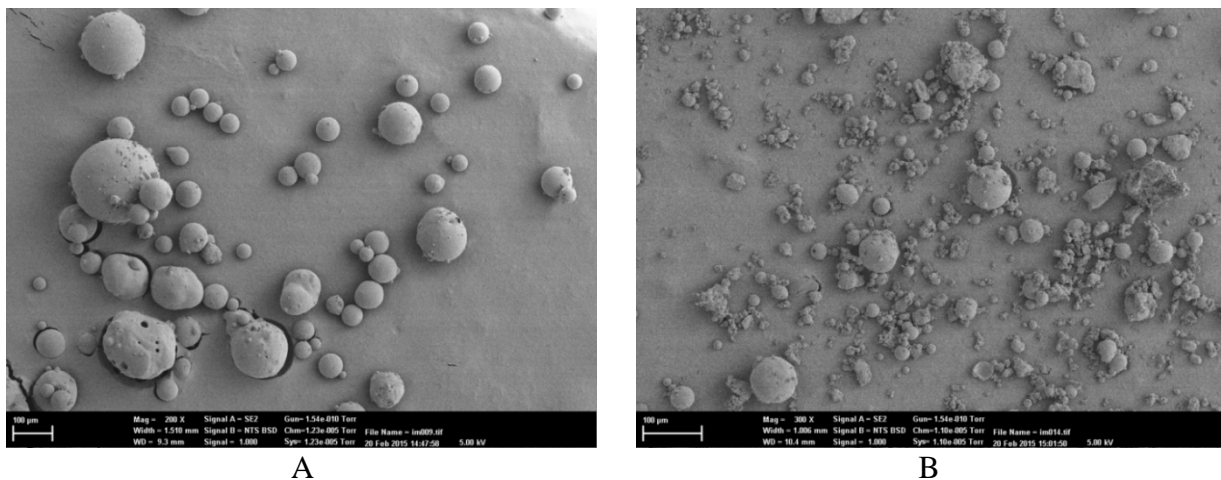


Figure 1.1: SEM images on feed fly ash, (A) Floated cenospheres and (B) sinks coal fly ash using a sink-float funnel. The background material was ink used to hold the particles in their place and hence is not related to the fly ash particles. The length scales are 100 µm in both images.

Cenospheres, hollow spherical particles, are one of the most useful components found in fly ash waste. The grade of cenospheres in fly ash has decreased recently due to the modifications made to burners of the power stations. Therefore the current method of cenospheres separation, scooping the particles from the surface of the ash ponds, is even less efficient. Moreover, in the conventional method, the cenospheres product is contaminated by the low density fine fly ash particles. Therefore there is a need for an efficient method for separation of cenospheres from fly ash.

This thesis is mostly focused on an innovative method of recovery and concentration of the valuable cenospheres from fly ash waste referred to as the Inverted REFLUX™ Classifier (IRC™). As shown in Figure 1.2, this approach consists of a liquid fluidized bed located

vertically above a system of inclined channels. The high segregation rate through the inclined channels causes that the fine and low density cenospheres to return to the vertical section of the IRC™ for recovery via the product overflow. A fluidization water chamber is also installed at the top of the IRC™, distributing water in order to wash the fine and dense fly ash particles away from the cenosphere product. Therefore this innovative system can be potentially considered as an efficient method for concentration and recovery of cenospheres from fly ash.

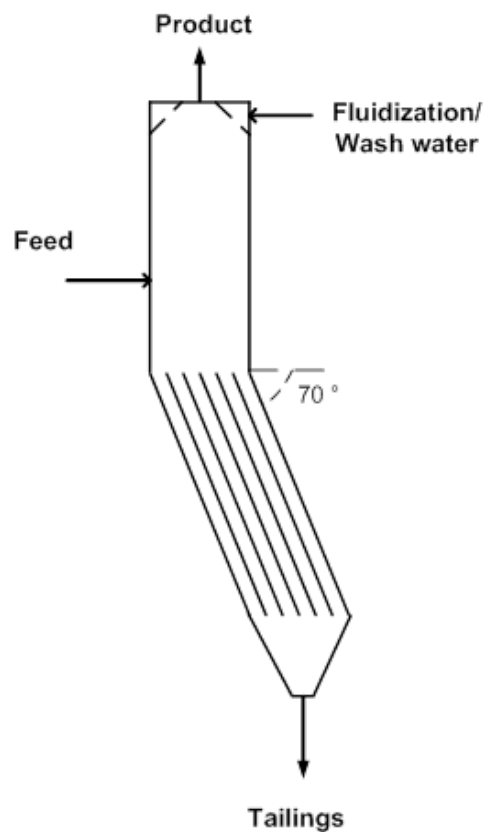


Figure 1.2: A schematic diagram of the Inverted REFLUX™ Classifier.

It is noted that this study is focussed on the separation of cenospheres which are lower in density than water. In fact the term cenospheres, as applied in this study, is reserved for particles less dense than water. It is recognised, however, that there are hollow spheres of density higher than water, but these are not addressed in this study.

## 1.2 Background

Fly ash is a waste produced as a by-product from burning coal in coal-fired power station units worldwide. It is reported that the production of coal ash worldwide is about 600 million tonnes per year with fly ash constituting approximately 80% of this (Joshi and Lothia, 1997). The production of fly ash in Australia is reported to be about 18 million tonnes per year (ADAA, 2005), and the production of fly ash in the USA was estimated to be around 52 million tonnes in 2012 (ACAA, 2014). Even though many applications have been recently found for fly ash, about 60% of it continues to be discarded to lands surrounding the power stations (ADAA, 2005) and as a worldwide average only 16% of fly ash is reused (Joshi and Lothia, 1997). Owing to the presence of toxic trace elements and fine particles in fly ash waste, this waste can cause environmental and respiratory problems (Jankowski et al., 2006; Aziz et al., 2010; Tsiridis et al., 2012).

Therefore a driving motivation behind studies that have focused on fly ash treatment involve firstly, minimizing the disposal cost and the area of land affected by this disposal, secondly, achieving a financial return from reusing this material, and finally, replacing scarce or expensive resources (Ahmaruzzaman, 2010). A significant portion of the fly ash waste is used in the cement industry. However, the power stations have been recently forced to retrofit low NO<sub>x</sub> burners. This modification has led to the production of fly ash with higher unburnt carbon content, reducing the use of the fly ash in cement, and other potential applications (Huang et al., 2003). Therefore the separation of unburnt carbons, magnetic particles and cenosphere particles is crucial.

Cenospheres are one of the most valuable materials found in fly ash. While the density of ash materials in cenospheres is larger than 2000 kg/m<sup>3</sup>, the density of the cenospheres particles can be as low as 400 kg/m<sup>3</sup> due to their hollow structures (Raask, 1985). Conversely, there are some hollow cenospheres which are denser than water, however, in practice, the ash particles which are lower in density than water have been collected as “cenospheres” (Raask, 1968; Vassilev & Vassileva, 1996; Kruger, 1997). These hollow silica-alumina microspheres provide a range of superior properties, being low weight, chemically inert, good in packing, good insulators, offering excellent mechanical strength. Owing to these properties, cenospheres have a wide variety of potential applications including lightweight concrete, cement, light composite materials, filtering media and insulators (Lilkov et al., 1999; Blanco

et al., 2000; McBride et al., 2002; Chalivendra et al., 2003). As a result, cenospheres are typically valued in excess of \$2000 per tonne. On the other hand, being very fine between 45 and 150 microns (Raask, 1968) and light, cenospheres can cause respiratory diseases (Fenelonov, 2010) if left in ash ponds and allowed to dry.

Cenospheres are typically very fine with a low density between  $400 \text{ kg/m}^3$  and  $900 \text{ kg/m}^3$ . In mineral processing, flotation is normally applied to the separation of fine particles. Here, cenospheres and fly ash have similar surface properties making flotation inefficient. Dry separation is also ineffective due to the significant difference between the density of cenospheres and fly ash and the density of air. Given a significant difference between the densities of cenospheres, fly ash and water, wet gravity separation is the most appropriate option for separation of these particles.

In the conventional method of cenospheres separation, the coarse cenospheres particles are scooped from the top of the ash ponds. However, the settling velocity of fine fly ash particles is very low, causing contamination to the product. Furthermore, fine cenospheres are very difficult to recover as their rise velocities are significantly lower. The modifications on power stations burners have also resulted in a significant drop in the grade of cenospheres in fly ash to the order of 1% by mass. Therefore, the current method of cenospheres separation is uneconomic. An efficient method applied to separate cenospheres from fly ash needs to address the above mentioned problems.

Settling and rise velocities of particles mostly depend on their size and density. These velocities are very small for fine particles and those having a slight density difference with respect to water. The velocity of a particle in a suspension can also be affected by the presence of other particles, defined as the suspension hindrance effect. The Richardson and Zaki equation (Richardson and Zaki, 1954a) can be accurately applied to estimate the hindered settling velocity of particles in one-component suspensions.

There is an ambiguity in the hydrodynamic behaviour of multi-component suspensions. Asif (1997) and Masliyah (1979) studied such suspensions by considering the effective density of the suspensions. This led to a modified form of the Richardson and Zaki equation for the multi-component suspensions in Asif's study, and a new equation dependent on the suspension density in Masliyah's study. Owing to the slow segregation of particles

specifically in concentrated suspensions, methods for increasing the settling or rise velocity of particles need to be used. The most common method used to increase the velocity of particles is flocculation. Other approaches include centrifugal forces, and inclined settlers.

Boycott (1920) reported that blood corpuscles settled quicker in a tilted tube compared to a vertical one. Based on this observation, many investigations have been carried out on inclined settlers (Zahavi and Rubin, 1975; Acrivos and Herbolzheimer, 1979; Herbolzheimer and Acrivos, 1981). These investigations led to the development of the lamellae thickener which has been used in solid-liquid separation. In order to increase the capacity of this method of separation, the use of multi-channel inclined separators was crucial. However the uniform and even distributions of feed through the inclined channels, required for obtaining the same quality of product from all channels, was very difficult. Use of a fluidized bed combined with the inclined settlers, referred to as the REFLUX™ Classifier addressed this difficulty. This new method of separation, the REFLUX™ Classifier, has been recently investigated in detail (Laskovski et al., 2006; Galvin and Liu, 2011; Galvin, 2012).

The inclined channels used in the REFLUX™ Classifier increases the segregation rate of particles, resulting in a throughput advantage that is defined as the fluid velocity required to just retain a particle (with the size of  $d$  and the density of  $\rho$ ) within the inclined channels compared to the terminal settling velocity of the same particle (Laskovski et al., 2006). This parameter can be maximized to 1 for conventional fluidized beds given the fluid velocity cannot overtake the terminal settling velocity of the finest target particle.

Another phenomenon adding more complexity to the multi-component suspensions is the bulk streaming phenomenon (Whitmore, 1955; Weiland and McPherson, 1979; Fessas and Weiland, 1981; Fessas and Weiland, 1984) which can be used to increase the segregation rates of particles in the suspensions. This phenomenon results from the instabilities in the suspensions. The particles tend to gather together and form particle clusters, and hence significantly move quicker in the suspension (Batchelor and Van Rensburg, 1986) *en-masse*. This phenomenon was reported to be largely dependent on the particles size and density and also the volume fractions of the species in the suspensions.

### 1.3 Thesis Objectives

In this study, an efficient novel method, an Inverted REFLUX™ Classifier (IRC™), has been used to recover and concentrate positively buoyant cenospheres in fly ash. Using the specific operating conditions, the streaming phenomenon is hypothesized to develop and lead to an increase in the particle segregation rates. In fact the separation of cenospheres from fly ash can be promoted using the combined effects of the fluidization, the bulk streaming motion and the inclined settling.

Therefore, the objectives of this thesis are:

- 1) To thoroughly characterize a typical fly ash and cenospheres in terms of chemical composition and surface morphology, and size and density distributions.
- 2) To examine the potential of a laboratory scale IRC™ in recovering and concentrating positively buoyant particles.
- 3) To apply this innovative method (i.e. the IRC™) to the separation of positively buoyant cenospheres from negatively buoyant waste fly ash.
- 4) To examine the effects of different operating parameters on the separation of cenospheres from fly ash in the laboratory scale IRC™.
- 5) To achieve an enhanced separation of cenospheres from fly ash using the combined effects of the Boycott and bulk streaming motion phenomena.
- 6) To study scale up of this method of cenospheres separation in a pilot scale IRC™.
- 7) To maximize the concentration of cenospheres in fly ash using multi-stage IRC™ processes.
- 8) To examine the separation of cenospheres from different fly ash streams in the IRC™.

## 1.4 Outlines of Thesis

This thesis aims to investigate a novel method, referred to the Inverted REFLUX™ Classifier to achieve the separation of cenospheres from fly ash. Chapter 2 provides a comprehensive literature review concerning the fundamentals of this study, including particle properties, particle settling, suspension hydrodynamics, gravity separation and fluidization. The chapter also introduces the recent developments in this area, specifically the methods for the enhancement of particle settling rate. Chapter 3 provides a detailed background of the bulk streaming motion phenomenon in multi-component suspensions. In this chapter, the inclined settling is then comprehensively discussed, introducing the innovative method of particle separation referred to as the REFLUX™ Classifier. The background and details of this novel method are outlined in this chapter.

In Chapter 4, a typical fly ash and cenospheres feed are characterized, providing information about the surface properties and size and density distributions of the particles. Chapter 5 presents the preliminary experiments carried out to investigate the potential of the Inverted REFLUX™ Classifier in separating cenospheres from fly ash. Firstly, the potential of the IRC™ in separating positively buoyant particles are reported using a model feed, a mixture of commercial cenospheres and silica flour. Then the separation of cenospheres from real fly ash feed is investigated. This chapter concludes by examining the effects of different operating parameters on the separation performance, providing a clear basis for conducting a more rigorous study of the system.

Chapter 6 is concerned with the effect of feed solids concentration on the recovery of cenospheres in the IRC™, the objective being to assess the potential for bulk streaming and hence concentration induced enhancement of the separation. The cenospheres size classification and the theoretical and actual throughput advantage of the IRC™ are also analysed in this chapter, to reveal the best performance of the IRC™ over a range of feed solids concentrations. The second aim of this chapter is to further explore the cenospheres separation process at different operating conditions while applying the optimum feed solids concentration.

Chapter 7 investigates the cenospheres separation from fly ash using a pilot scale IRC™, about 10 fold larger in area than the laboratory scale. The results are compared with those

presented in the previous chapter to verify the scale up performance of the pilot scale IRC™. In Chapter 8, multi-stage separation of cenospheres from two different types of fly ash is examined, the goal being to achieve the highest possible product grade. Finally in Chapter 9, a fly ash feed containing larger cenospheres at a higher concentration is examined, and the separation performance is compared with the results of previous chapters.

Chapter 10 provides a summary of all chapters, and is followed by the conclusions of this thesis. Some recommendations are made concerning future theoretical and experimental directions.

## **Chapter 2**

# **Gravity Separation Fundamental Concepts**

## 2.1 Introduction

Regardless of variations in other properties such as size, shape, hydrophobicity, magnetic susceptibility or electrical conductivity, the most appropriate method to use for separating positively and negatively buoyant particles is a wet density-based separation (wet gravity separation) where the density of the liquid medium is between that of the two solid species being separated. Therefore in this chapter the fundamentals of wet gravity separation, fluidization and particle settling are introduced and discussed.

The first step in describing particle-liquid systems is to study single particle settling in a Newtonian fluid and then extend this to more complicated cases involving large numbers of particles, such as occurs in sedimentation and fluidization (Rhodes, 1998).

## 2.2 Isolated particle settling in a fluid

### 2.2.1 Drag force

When a particle is placed in a fluid it starts to accelerate due to the net weight force of the particle in the fluid, governed by the gravitational  $F_W$  and buoyancy  $F_B$  forces. As the velocity increases, the drag force  $F_D$  also increases, resulting in the net force acting on the particle decreasing until it approaches zero. When there is no net force acting on the particle, there is no longer any acceleration, and hence the particle has reached its terminal settling velocity,  $u_t$  (Gregory, 2005). A schematic diagram of these forces is shown in Figure 2.1.

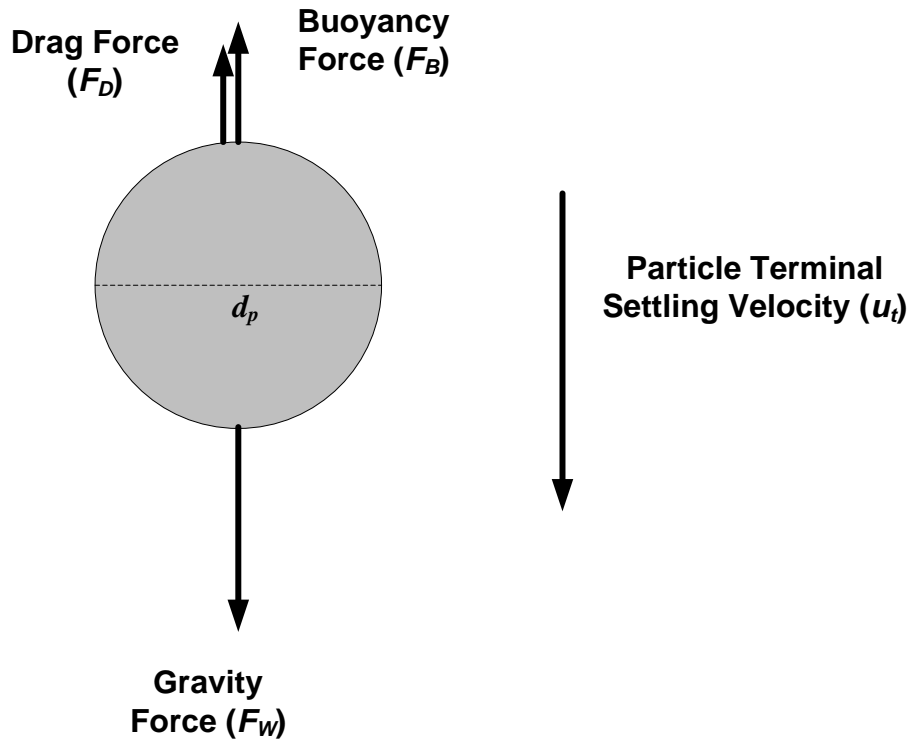


Figure 2.1: Forces acting on a negatively buoyant spherical particle of diameter  $d_p$  settling in a fluid at its terminal settling velocity  $u_t$ .

The drag force resisting the motion of a particle in a fluid consists of two parts, pressure (or form) drag and shear stress (or skin friction or viscous) drag. For a smooth sphere in a very slow steady flow or creeping motion, these are given by Stokes' law (Stokes, 1851):

$$\text{Pressure drag force} = \pi d_p \mu u_r \quad (2-1)$$

$$\text{Shear stress drag force} = 2\pi d_p \mu u_r \quad (2-2)$$

Hence the total drag force is:

$$\text{Total drag force} = 3\pi d_p \mu u_r \quad (2-3)$$

where  $d_p$  is the particle diameter,  $\mu$  is the fluid viscosity and  $u_r$  is the particle velocity relative to the fluid. This theoretical equation predicts the total drag force with less than 9 % error, for particles with a Reynolds number smaller than 1 (Rhodes, 1998). The Reynolds number of a particle depends on its size and velocity, and the fluid properties, defined as:

$$Re_p = \rho_f \mu_r d_p / \mu \quad (2-4)$$

The drag coefficient is defined as:

$$C_D = R' / (1/2 \rho_f \mu_r^2) \quad (2-5)$$

where  $R'$  is the force per unit projected area of the particle, and for a spherical particle is equal to  $F_D / (\pi d_p^2 / 4)$ . For a single sphere settling in a fluid under creeping motion conditions where viscous forces dominate over inertial forces, Stokes law can be applied to explicitly calculate the drag coefficient. At higher velocities, however, inertia becomes significant and no theoretical solution exists to relate the drag coefficient to the Reynolds number, hence the data from empirical correlations or standard drag curves should be used (Rhodes, 1998). Figure 2.2 shows the drag curve for spherical particles (Clift & Gauvin, 1970; Turton & Levenspiel, 1986; Rhodes, 1998).

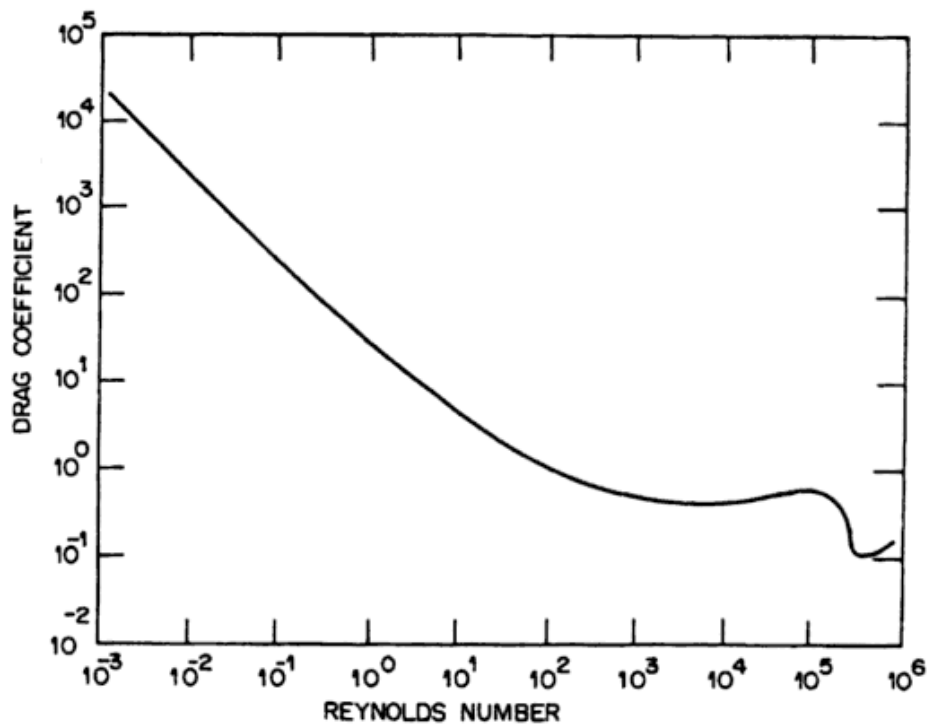


Figure 2.2: Standard drag curve for spherical particles in a fluid (Clift & Gauvin, 1970).

### 2.2.2 Particle terminal settling velocity

For a particle falling through a fluid, based on Newton's Second Law of Motion, the force balance becomes,

$$F_I + F_D + F_F = ma \quad (2-6)$$

where  $F_I$  is the inertial force,  $F_D$  is the fluid drag force,  $F_F$  is the net weight force of the particle in the fluid,  $m$  and  $a$  are the particle's mass and acceleration, respectively. At its terminal velocity, the particle is no longer accelerating ( $a = 0$ ), and the inertial force is equal to zero (Rushton et al., 1996). Hence the Equation 2-6 can be written as:

$$F_D + F_F = 0 \quad (2-7)$$

where  $F_F = F_W + F_B = (\rho_p - \rho_f)Vg$ ,  $V$  is the particle volume,  $\rho_p$  is the particle density and  $g$  is the gravitational acceleration.  $F_W$  and  $F_B$  are the gravity and buoyancy forces acting on a particle as shown in Figure 2.1. It is noted that in Equations 2-6 and 2-7 the downward direction is considered to be positive.

There is no explicit equation to be used for calculating  $F_D$  outside the creeping flow regime, and hence dimensional analysis is applied using empirical results. For an incompressible Newtonian fluid, the drag force depends on the particle diameter ( $d_p$ ), fluid density and viscosity ( $\rho_f$  and  $\mu$ ) and fluid velocity relative to the particle ( $u_r$ ). The drag force can be expressed using two dimensionless numbers, drag coefficient and Reynolds number.

$$F_D = 1/2 C_D A \rho_f u_r^2 \quad (2-8)$$

$C_D$  is the drag coefficient, a dimensionless number which is a function of the Reynolds number and particle shape and orientation.  $A$  is the cross-sectional area of the particle perpendicular to the direction of motion. Note that in a free fall or rise, the fluid velocity around the particles is equal to the free terminal settling velocity of the particle (Seville et al., 1997). At low Reynolds numbers, combining Equations 2-7 and 2-8, gives the drag coefficient as being inversely related to the Reynolds number as shown below:

$$C_D = 24/Re_p \quad (2-9)$$

As shown in Figure 2.2, the drag coefficient was also found to be constant at around 0.44 at high Reynolds numbers (Newton's regime). Therefore, using Equations 2-7, 2-8 and 2-9, for spherical particles falling in the Stokes regime:

$$u_t = d_p^2(\rho_p - \rho_f)g/18\mu \quad (2-10)$$

and in the Newtonian regime where  $C_D = 0.44$ ,

$$u_t = 1.74[d_p(\rho_p - \rho_f)g/\rho_f]^{0.5} \quad (2-11)$$

where  $u_t$  is the particle terminal settling velocity. No theoretical equation exists for calculating  $C_D$  and  $u_t$  in the intermediate regime. For this regime, using the proposed relationship between  $u_t$  and different parameters such as  $d_p$ ,  $\rho_p$ ,  $\rho_f$  and  $\mu$ , many correlations have been suggested for calculating the drag force and then the terminal settling velocity (Heiskanen, 1993). Table 2.1 shows the drag coefficient and terminal settling velocity for different regimes for a spherical particle.

Table 2.1: Drag coefficient and terminal velocity for spherical particles in different flow regimes (Heiskanen, 1993; Rhodes, 1998).

Regime	Reynolds number	Drag Coefficient, $C_D$	Terminal velocity
Stokes	$Re_p < 0.3$	$C_D = 24/Re_p = 24\mu/(\rho_f d_p u_t)$	$u_t = (\rho_p - \rho_f)d_p^2 g/(18\mu)$
Intermediate	$0.3 < Re_p < 500$	$C_D = 24/Re_p + 0.44$ (Dallavale, 1948)	$u_t = 0.153(\rho_p - \rho_f)^{5/7} d_p^{8/7} g^{5/7}/\mu^{3/7} \rho_f^{2/7}$
Newton	$500 < Re_p < 2 \times 10^5$	$C_D = 0.44$	$u_t = 1.74[(\rho_p - \rho_f)gd_p/\rho_f]^{1/2}$

There are also several correlations in the literature for calculating the drag coefficient and the terminal velocity, which are valid for a wide range of Reynolds numbers, such as Equation 2-12 proposed by Turton and Levenspiel (1986):

$$C_D = 24(1 + 0.173Re_p^{0.657})/Re_p + 0.413/(1 + 16300Re_p^{-1.09}) \quad (2-12)$$

and the correlation of Zigrang and Sylvester (1981) which can be used to explicitly calculate the terminal velocity of particles written as:

$$Re_p = [(14.51 + 1.83(g(\rho_p - \rho_f) \rho_f)^{0.5} d_p^{1.5}/\mu)^{0.5} - 3.81]^2 \quad (2-13)$$

Equation 2-13 is valid for  $Re_p \leq 2 \times 10^5$ .

### 2.2.3 Other factors affecting the settling velocity

In addition to the size and density of particles, there are several other factors which can also affect the settling behaviour of particles in a given fluid. These include particle shape, roughness, and wall effects.

#### 2.2.3.1 Particle shape and size

The shapes of particles affects the drag force and hence the particle settling velocity. For non-spherical particles, the drag force also depends on the orientation of particles. The sphericity is a parameter indicating how close the shape of a particle is to a sphere. Based on Wadell (1933), the sphericity can be defined as:

$$\psi = \frac{\text{surface area of a spherical particles with the same volume as the particle}}{\text{surface area of the particle}} \quad (2-14)$$

The effect of the shape on the drag force is significantly more in the Newton's and intermediate regimes than that in the Stokes' regime. In the Stokes' regime, non-spherical particles fall through the fluid in an orientation in which their longest surface is parallel to the oncoming fluid, while in the Newton's regime they fall with their longest surface perpendicular to the oncoming fluid (Rhodes, 1998).

A variety of particle shape exists, most of which are irregular. Different definitions can be used to characterize the size of such particles. Which definition should be used depends on the intended purpose. One of the most common ones is the volume-equivalent spherical diameter,  $d_v$ , defined as the diameter of a sphere with the same volume as the particle:

$$d_v = (6V/\pi)^{1/3} \quad (2-15)$$

where  $V$  is the particle volume and  $d_v$  is independent of the particle orientation. This definition can be useful when the particle volume is an important factor in controlling its behaviour. In the case of particle settling, the volume of the particle determines the net gravity-buoyancy force on the particle, an important consideration.

Another commonly used size definition is the surface-area equivalent spherical diameter,  $d_s$ , defined as the diameter of a sphere with the same surface area  $S$  as the particle:

$$d_s = (S/\pi)^{1/2} \quad (2-16)$$

where  $d_s$  is independent of the particle's orientation. For a non-porous particle, the surface area controls the skin friction drag, so it affects the settling velocity of particles, especially in the Stokes regime. Therefore  $d_s$  is an important definition in studying the hydrodynamic behaviours of particles. For porous particles, it becomes important to distinguish between internal and external surface area, as only the external surface area directly controls fluid drag. The internal porosity will, however, be significant in determining the weight of the particle, depending on whether it is filled with gas or liquid.

The Sauter diameter ( $d_{sv}$ ) is defined as the diameter of a sphere with the same ratio of particle volume to surface area, given by:

$$d_{sv} = (6V/S) = (d_v^3/d_s^2) \quad (2-17)$$

This diameter conserves the ratio of body forces (proportional to volume) and drag forces (proportional to surface area) and so is often important in applications involving a balance of these two forces, such as in fluidization.

The other important definition of size is the Stokes' diameter defined as the diameter of a sphere with the same density and settling velocity as the particle. It is defined as:

$$d_{St} = [18\mu u_t/(\rho_p - \rho_f)g]^{1/2} \quad (2-18)$$

where  $u_t$  is the particle terminal velocity. This definition is an important factor in the applications involving the hydrodynamic behaviour of the particle such as in fluidized beds (Seville et al., 1997).

Systems often contain a wide size range of particles, so it is very important to accurately measure the size distributions as particles with different sizes may behave differently. The size distributions can be reported based on number, mass or volume. The distributions are also presented in two different forms, frequency distributions and cumulative distributions (Seville et al., 1997; Rhodes, 1998). The sieve and laser scattering machine are two common methods for measuring particles size distributions, providing the mass-based and volume-based size distributions, respectively. These two size distributions should be the same if all particles have a constant density.

Particles of different size can show quite different hydrodynamic behaviours, so it can be problematic trying to characterize a broad size distribution by a single average size. Nevertheless, this is often done in order to reduce complexity. Different definitions of average particle size can be used. The simplest one, the arithmetic mean, is defined as the summation of particles' diameters divided by the total number of particles. Another important one is the geometric mean defined as  $d_g = [d_{p1}^{n1} d_{p2}^{n2} d_{p3}^{n3} \dots d_{pi}^{ni}]^{1/N}$ .

To take the effect of particle shape into account when studying particle motion in a fluid, a shape factor ( $\chi$ ) is defined. It is defined as the ratio of the resistance forces on the particle and on a sphere with the same volume and velocity settling in the Stokes' regime (Seville et al., 1997). Hence:

$$\chi = F_D / (3\pi\mu u_t d_v) \quad (2-19)$$

There are also some figures and correlations which can be used for directly calculating the drag force that applies to non-spherical particles (Miltzer et al., 1989; Haider & Levenspiel, 1989; Clift et al., 1978). For instance, Figure 2.3 shows how particle sphericity affects the drag coefficient for isometric particles.

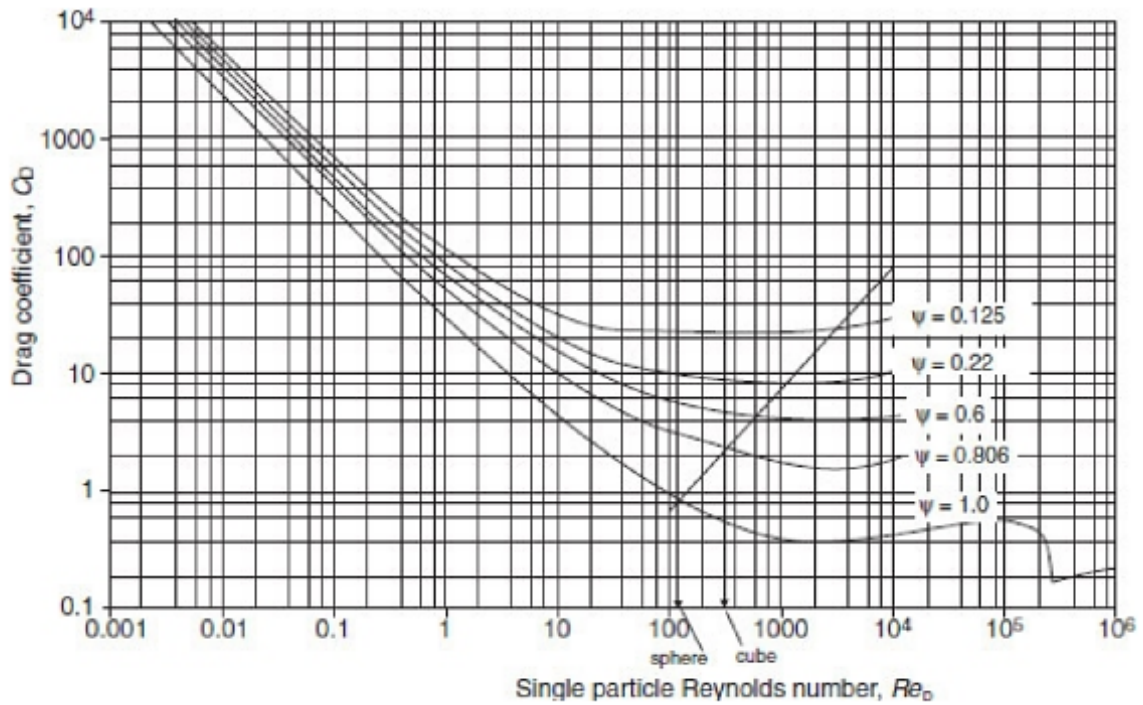


Figure 2.3: Drag curves for non-spherical particles falling in a fluid as a function of particle sphericity,  $\psi$ . The volume equivalent spherical diameter  $d_v$  is used to calculate  $C_D$  and  $Re_p$  (Rhodes, 1998).

One correlation to calculate the drag coefficient of non-spherical particles is that suggested by Haider and Levenspiel (1989):

$$C_D = \frac{24}{Re_p} [1 + (8.1716e^{-4.0655\psi}) Re_p^{0.0964+0.5565\psi}] + \frac{73.69e^{-5.0748\psi} Re_p}{(Re_p + 5.378 e^{6.2122\psi})} \quad (2-20)$$

where  $Re_p$  is the particles Reynolds number and  $\psi$  is the sphericity.

### 2.2.3.2 Particle surface roughness

Another factor which should be considered in studying particle sedimentation is particle surface roughness. The effect of roughness is most significant in controlling the transition of the boundary layer from laminar to turbulent. This delays the detachment of the boundary layer from the rear of the particle, thus allowing more pressure recovery in the flow which can result in a form drag reduction of over 80 %. For a smooth sphere, the transition occurs at the Reynolds numbers between about  $2.5 \times 10^5$  and  $5 \times 10^5$  (Graf, 1984). As the particle

surface roughness increases, the transition occurs earlier and so the reduction in the drag coefficient occurs earlier (Hoerner, 1958). Figure 2.4 shows the effect of particle surface roughness on the early occurrence of the transition to the turbulent boundary layer regime and the drag coefficient reduction. Prior to this transition, the surface roughness has a less dramatic effect on the drag coefficient. In the creeping flow regime, the literature is unclear as to whether particle surface roughness has a significant effect. Some workers report a decrease in drag coefficient with increasing roughness (Selberg & Nicholls, 1968; Sivier & Nicholls, 1969), whereas others report no effect (Lanchester, 1907; Arnold, 1911). The effects, if any, of surface roughness on the drag force are hard to quantify due to the difficulties in measuring the surface roughness (Graf, 1984).

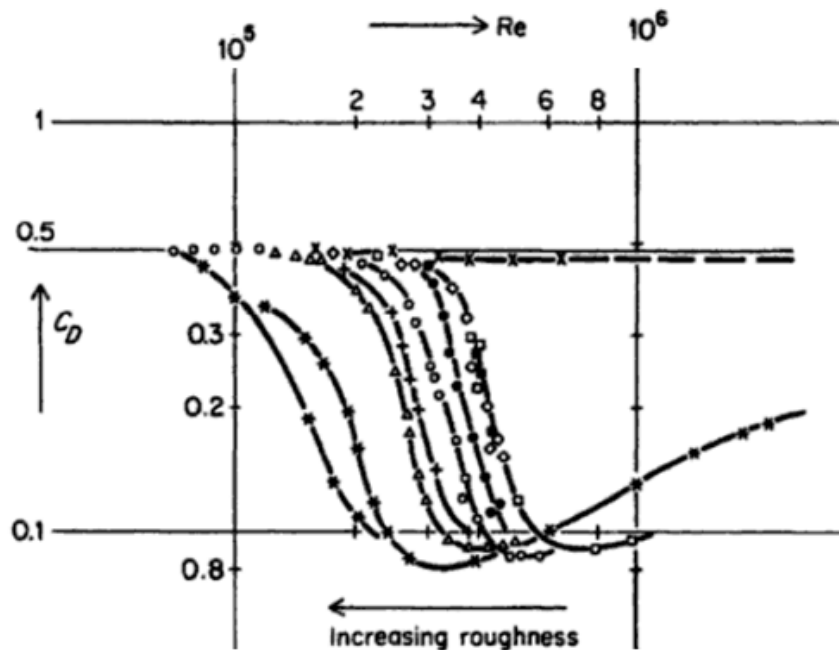


Figure 2.4: Drag coefficient versus Reynolds number for particles with different surface roughness (Hoerner, 1958), where  $\Delta$  = Ditto, Behind the turbulent screen,  $\diamond$  = NACA, through resting air,  $\star$  = NACA, Variable-density tunnel,  $\times$  = Ditto, Surface roughness 0.03,  $\bullet$  = Hoerner, In open water, and  $+$  = In wind tunnel with surface roughness of 0.003.

### 2.2.3.3 Container walls

Container walls act to reduce the rate of particle settling. When particles are settling in a container, the displaced fluid moves in the opposite direction to the particles. Hence there is a higher particle-fluid relative velocity. The presence of the container walls also increases the shear gradient and hence increases the shear force acting on the particles.

When a particle is falling along the axis of a tube or pipe, a factor is defined to correct the settling velocity considering the effects of the wall. This wall factor ( $f_w$ ) is the ratio of the particle settling velocity in the tube or pipe ( $u_{tD}$ ) to that in an infinite fluid ( $u_{t\infty}$ ). Several correlations for calculation of the wall factor in a wide range of Reynolds numbers proposed by Faxen (1923), Munroe (1888-89) and Francis (1933) are respectively indicated below:

$$f_w = 1 - 2.1(d_p / D), Re_p \leq 0.3, d_p/D \leq 0.1 \quad (2-21)$$

$$f_w = 1 - (d_p/D)^{1.5}, 10^3 \leq Re_p \leq 10^4, 0.1 \leq d_p/D \leq 0.8 \quad (2-22)$$

$$f_w = (1 - (d_p/D))^{2.25}, Re_p \leq 0.3, d_p/D \leq 0.97 \quad (2-23)$$

where  $d_p$  and  $D$  are the particle and tube diameter, respectively.

## 2.3 Hindered settling

The settling velocity of particles in a suspension is different to that of an isolated particle in an infinite fluid. In this situation, whilst the particles may not be touching, the small distance between the particles affects their behaviour in the suspension. The reduced settling velocity of particles in a suspension is called the hindered settling velocity. The hydrodynamics of particles in settling suspensions has been studied closely (Zimmels, 1988, 1985; Happel & Brenner, 1965). Some of the mechanisms include:

1. The decreased cross-sectional area available for the displaced fluid to move upward forces it to flow more quickly, leading to an increase in the shear force acting on the particles.

2. The narrower inter-particle gaps for the fluid flow also increases the shear gradients, which increases the drag force acting on the particles.

3. Changing the hydrodynamic diffusion defined as the motion caused by the particles interactions (Davis, 1996; Zimmels, 1988, 1985). In a pulp with a high solids concentration, collisions occur which dissipate energy and cause divergence in the settling paths. This causes the particles to settle more slowly (Heiskanen, 1993; Seville et al., 1997).

These hindered settling effects are sometimes discussed in terms of the suspension acting as a fluid with a higher effective density and viscosity than the pure liquid. This analogy works well when considering a large individual particle settling in a suspension of fine particles. However, there is considerable debate in the literature as to whether this is a valid perspective when considering the settling of a particle in a suspension of other particles of similar size (Di Felice & Gibilaro, 1988; Clift et al., 1987; Gibilaro et al., 1987; Jean & Fan, 1986; Gibilaro et al., 1986; Epstein & Leclair, 1985; Reed & Anderson, 1980).

### 2.3.1 Modified Stokes' law

Stokes' law can be still applied to slow settling particles in a concentrated suspension by applying the concepts of an effective suspension density and viscosity:

$$\mu_e = \mu/f(\varepsilon) \quad (2-24)$$

$$\rho_{susp} = \varepsilon\rho_f + (1 - \varepsilon)\rho_p \quad (2-25)$$

where  $\varepsilon$  is the voidage or volume fraction of the fluid,  $\rho_f$  and  $\rho_p$  are the densities of fluid and solid, respectively, and  $f(\varepsilon)$  is a function modifying the viscosity. Applying the suspension effective viscosity and density to Equation 2-9, the drag coefficient is calculated as:

$$C_D = 24\mu_e/(u_r \rho_{susp} d_p) \quad (2-26)$$

For a particle falling through a concentrated suspension, using the force balance Equation 2-6 together with Equations 2-24, 2-25 and 2-26:

$$u_r = u_t \varepsilon f(\varepsilon) \quad (2-27)$$

where  $u_r$  is the settling velocity of a particle relative to the fluid, influenced by the presence of the other particles in the suspension, or the relative hindered settling velocity, defined as  $u_p - u_f$ . Therefore, in the Stokes regime the following equation has been proposed (Rhodes, 1998; Haider & Levenspiel, 1989):

$$u_r = g d_p^2 (\rho_s - \rho_f) (\varepsilon) f(\varepsilon) / (18\mu) \quad (2-28)$$

### 2.3.2 Richardson and Zaki equation

Considering batch settling in a cylinder or tube, the total flux should be equal to zero, and hence:

$$u_p(1 - \varepsilon) + u_f(\varepsilon) = 0 \quad (2-29)$$

Considering  $u_r = u_p - u_f$ , and applying Equation 2-28:

$$u_p = u_t \varepsilon^2 f(\varepsilon) \quad (2-30)$$

Theoretically, the viscosity function was calculated by Einstein (1906) to be  $\varepsilon^{2.5}$  for a suspension of neutrally buoyant particles with less than 10 vol.% solids (Rhodes, 1998). Alternatively, the semi-empirical correlations derived by Thomas (1965) (Eqn. 2-31) and Gibilaro et al., (2007) (Eqn. 2-32) can be used to calculate the effective viscosity of suspensions.

$$\mu_e/\mu = 1 + 2.5 \phi + 10.05 \phi^2 + 0.00273 \exp(16.6 \phi) \quad (2-31)$$

$$\mu_e/\mu = (1 - \phi)^{-2.8} \quad (2-32)$$

where  $\mu_e$  is the suspension effective density, and  $\phi$  is the solids volume fraction of suspensions. For a non-fluctuating system with negligible particle-particle interactions, Richardson and Zaki (1954a) experimentally found that the hindered settling velocity is

related to the voidage or solids volume fraction and unhindered terminal settling velocity with a power  $n$  related to the Reynolds number and the container diameter ( $D$ ):

$$u_p = u_t \varepsilon^n = u_t (1 - \phi)^n \quad (2-33)$$

where  $\varepsilon$  is the voidage,  $\phi$  is the solids volume fraction of the suspension and  $u_t$  is the unhindered terminal settling velocity. As shown in Table 2.2, for particles with diameter of  $d_p$  the index  $n$  depends on the particle's Reynolds number and the container diameter.

Table 2.2:  $n$  values for the Richardson-Zaki equation (Richardson & Zaki, 1954a; Richardson & Zaki, 1954b).

$Re_p$ at terminal velocity	Value of $n$
$Re_p \leq 0.2$	4.6
$0.2 < Re_p < 1$	$(4.35 + 17.5 d_p / D) Re_p^{-0.03}$
$1 \leq Re_p < 200$	$(4.45 + 18 d_p / D) Re_p^{-0.1}$
$200 \leq Re_p < 500$	$4.45 Re_p^{-0.1}$
$500 \leq Re_p$	2.4

More recently, Khan and Richardson (1989) proposed a general correlation for the calculation of  $n$  at any Reynolds numbers as below:

$$(4.8 - n) / (n - 2.4) = 0.043 Ar^{0.57} [1 - 2.4(d_p/D)^{0.27}] \quad (2-34)$$

$$Ar = [\rho_f (\rho_p - \rho_f) g d_p^3 / \mu^2] \quad (2-35)$$

where  $Ar$  is the Archimedes number, and  $d_p$  and  $D$  are the particle and vessel diameters.

### 2.3.3 Other studies on hindered settling

For a suspension containing identical particles, a modified form of Equation 2-33 can be used to describe the slip velocity of a species. However, it is more complex for a suspension of particles with different densities. Some models have been proposed for such suspensions (Asif, 1997; Masliyah, 1979). In both these studies, the effective density of suspension based on the total solids concentration was defined and considered in calculating the velocity of particles in the suspensions. This led to a new form of the Richardson and Zaki equation introduced in Asif's study as:

$$u_r = u_t[(\rho_p - \rho_{susp})/(\rho_p - \rho_f)]^{n-1} \quad (2-36)$$

where  $u_t$  is the particle free-settling terminal velocity,  $u_r$  is the velocity of the particle relative to the fluid in the suspension with a local bulk density of  $\rho_{susp}$ , and  $\rho_p$  is the particle density.

Masliyah (1979) also developed a general equation to calculate the slip velocity of a species in a multi-component suspension by considering the suspension effective density and viscosity as two important factors,

$$u_r = u_{pi} - u_f = g d_i^2 f(\phi_f) (\rho_{pi} - \rho_{susp}) / 18 \mu \quad (2-37)$$

where  $u_{pi}$  and  $u_f$  are the  $i_{th}$  particle species velocity and the local fluid interstitial velocity relative to a stationary point, respectively.  $\rho_{susp}$  is the suspension density calculated as  $\sum (\phi_{pi} \rho_{pi}) + \phi_f \rho_f$  where  $\phi_f$  and  $\phi_{pi}$  are the fluid and  $i_{th}$  species volumetric concentrations.  $f(\phi_f)$  is a factor related to the particle concentration, defined by (Richardson & Zaki, 1954b).

$$f(\phi_f) = (\phi_f)^{2.7} \quad (2-38)$$

It is noted that  $\phi_f$  is the volume fraction of the fluid, which is the same parameter as  $\varepsilon$  used in Equation 2-33.

The velocity of the  $i_{th}$  component in the concentrated suspension is calculated as (Masliyah, 1979),

$$u_{pi} = g \phi_f^{2.7} / 18 \mu [d_i^2 (1 - \phi_{pi}) (\rho_{pi} - \rho_{susp}) - d_j^2 \phi_{pj} (\rho_{pj} - \rho_{susp})] \quad (2-39)$$

There is still quite an ambiguity in the literature in predicting the hindered settling velocity of particles in a multi-component suspension. In particular, the equations mentioned predict completely different species velocity in a suspension containing both positively and negatively buoyant particles. In such suspensions, as the heavy particles settle, the displaced water moves upward and this enhances the rise velocity of the light particles, which is

obviously in contradiction with the model of Richardson and Zaki (1954a, 1954b). Moreover, for a suspension containing solids denser than water, increasing the suspension pulp density leads to a rise in the effective density of the suspension and hence increases the buoyancy driving force of the light particles (Asif, 1997; Masliyah, 1979). On the other hand, the increased effective viscosity of the suspension hinders the rise velocity of the light particles.

To illustrate the issues, consider a mixture of 100  $\mu\text{m}$  particles of two species with density 800  $\text{kg/m}^3$  and 2000  $\text{kg/m}^3$  respectively, suspended in water. Assume that the volume fraction of the light and heavy particles in the suspension are 2 %, and 25 %, respectively. From Equation 2-13, the terminal rise velocity of the light species is 1.04 m/s. Based on Equation 2-33, assuming  $n = 4.6$ , the hindered rise velocity of the light particles is calculated to be 0.24 m/s. Now, using Equation 2-36 proposed by Asif (1997), the rise velocity of the light species is 41.6 m/s, whereas Equation 2-39 proposed by Masliyah (1979) predicts this velocity to be only 1.46 m/s. So both Masliyah's and Asif's models predict the rise velocity of light particles in the suspension would be larger than the particles' terminal velocity (although they differ in how large the increase is), whilst the Richardson-Zaki equation predicts this velocity to be lower than the terminal velocity.

There is little information in the literature to provide a comparison between the experimental data and the models predictions for systems containing particles with different densities, particularly, for mixtures of negatively and positively buoyant species. For suspensions containing negatively buoyant species with similar densities, Equation 2-33 was found to be valid in predicting the experimental data (Lockett & Al-Habbouby, 1973), while for a system of different densities species (both heavier than the fluid), the experimental data could only be predicted by considering the difference between the particles and suspension densities (Eqn. 2-39) (Richardson & Meikle, 1961). More detailed consideration of these issues is presented and discussed in Chapter 6 alongside experimental data for the fly ash-cenosphere system.

Another complication that can emerge in such systems is when the particles of a particular species congregate together, forming plumes with an enhanced rise or settling velocity. This effect, referred to as "Bulk Streaming Motion", is thoroughly reviewed in Chapter 3.

## 2.4 Fluidization

When a fluid flows upwards through a bed of negatively-buoyant particles, initially the bed remains in a packed state with the particles remaining in permanent contact with one another. However, as the fluid velocity increases, eventually the drag forces exceed the attractive forces between the particles, and the particles become fluidized. These two hydrodynamic phenomena, the packed bed and fluidized bed, are shown in Figure 2.5.

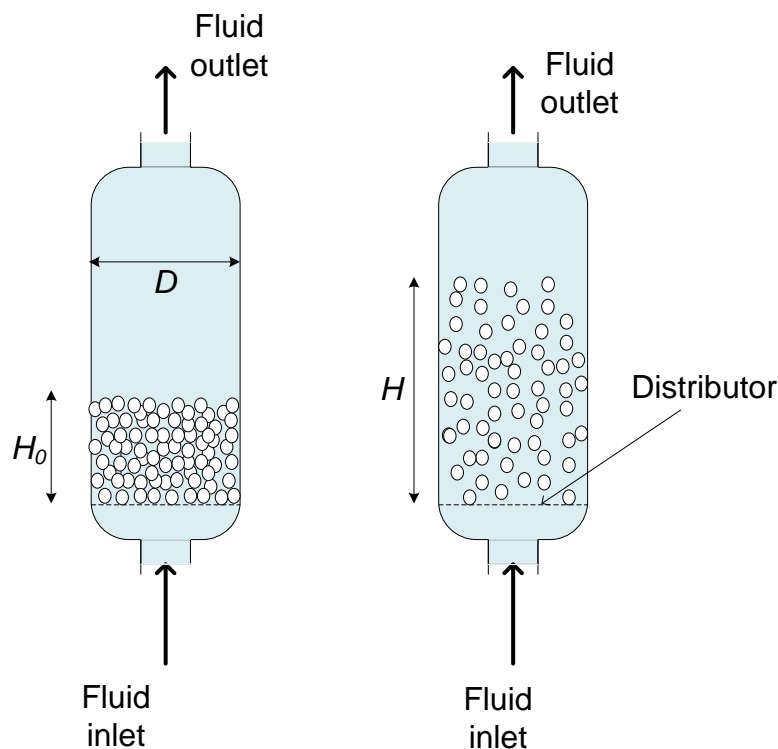


Figure 2.5: A packed bed (left hand side) and a fluidized bed (right hand side).

### 2.4.1 Packed bed

When the fluid velocity is not sufficient to lift the particles, the bed remains in a packed bed state. There are many applications which involve packed bed behaviour. A fluid passing through a filter cake is one of the most common applications. In such a process, knowing the relationship between the flow rate and pressure drop  $\Delta P$  is often important. Different correlations have been proposed, usually based on the Darcy study (Darcy, 1856). For laminar flow through a randomly packed bed of particles, the Carman-Kozeny equation can be used (Kozeny, 1927, 1933; Carman, 1937):

$$(-\Delta P)/H_0 = K_3 [(1 - \varepsilon)^2/\varepsilon^3] \mu u_s S_v^2 \quad (2-40)$$

where  $H_0$  is the height of the packed bed,  $u_s$  is the superficial fluid velocity,  $\varepsilon$  is the bed voidage,  $\mu$  is the fluid viscosity,  $S_v$  is the surface area per unit volume of particles, calculated to be  $6/d_p$  for monosized spherical particles, and  $K_3$  depends on the particle shape and surface properties, and is found to be about 5. Hence for a bed of monosized spheres with a diameter of  $d_p$ , the above equation becomes:

$$(-\Delta P)/H_0 = 180[(1 - \varepsilon)^2/\varepsilon^3] \mu u_s^2/d_p^2 \quad (2-41)$$

An equation for predicting the pressure drop of a turbulent flow through a randomly packed bed of monosized spheres is (Rhodes, 1998):

$$(-\Delta P)/H_0 = 1.75[(1 - \varepsilon)/\varepsilon^3] \rho \mu_s^2/d_p \quad (2-42)$$

Replacing  $d_p$  with  $d_{sv}$ , Equations 2-41 and 2-42 can also be applied to systems with non-spherical particles of varying size. The Ergun Equation combines the two and can be used to calculate the pressure drop across a wide range of Reynolds numbers, from laminar through to turbulent flow (Ergun, 1952):

$$(-\Delta P)/H_0 = 150[(1 - \varepsilon)^2/\varepsilon^3] \mu u_s^2/d_{sv}^2 + 1.75[(1 - \varepsilon)/\varepsilon^3] \rho \mu_s^2/d_{sv} \quad (2-43)$$

As expected, the effect of fluid viscosity is not significant in the turbulent regime (i.e. the second term), while it is important in the first term which is related to the laminar regime. By using this equation, the total frictional pressure loss is calculated. To obtain the total pressure drop, the hydrostatic pressure drop should be added. The hydrostatic pressure loss depends on the height of the bed and fluid density. This can become significant in liquid systems.

## 2.4.2 Fluidized beds

As the fluid velocity through a bed of particles is increased, eventually the drag force matches the net weight of the particles, after which the particles lift and become supported by the fluid flow and the bed is said to be fluidized. With further increases in fluid velocity, other phenomena such as channelling, spouting or slugging can occur (Yang, 2003). However,

these are rare in liquid-fluidized systems (Rhodes, 1998; Kunii & Levenspiel, 1991), so are not discussed further here.

Based on the force balance written for the bed, the pressure drop through the fluidized bed is equal to:

$$\Delta P'/H = (1 - \varepsilon)(\rho_p - \rho_f)g \quad (2-44)$$

The fluid velocity needed to achieve incipient fluidization of a bed of particles is called the minimum fluidization velocity  $U_{mf}$ . One method for determining this velocity experimentally is to measure the pressure drop over the column at different superficial fluid velocities. The velocity, at which the pressure drop in the chamber stops increasing and becomes constant, is the minimum fluidization velocity. Figure 2.6 shows such a plot of pressure drop through a bed versus the superficial velocity. Line FG shows the fluidization region while the points B and B' reflect the extra force initially needed to overcome the inter-particle forces in compacted powders. The curve ACDEFG indicates a normal fluidization curve which first levels off at the minimum fluidization velocity. It is noted that partial segregation occurs when a wide range of particles size is involved, leading to the partial fluidization shown as the curves AC'EFG and AC''EFG.

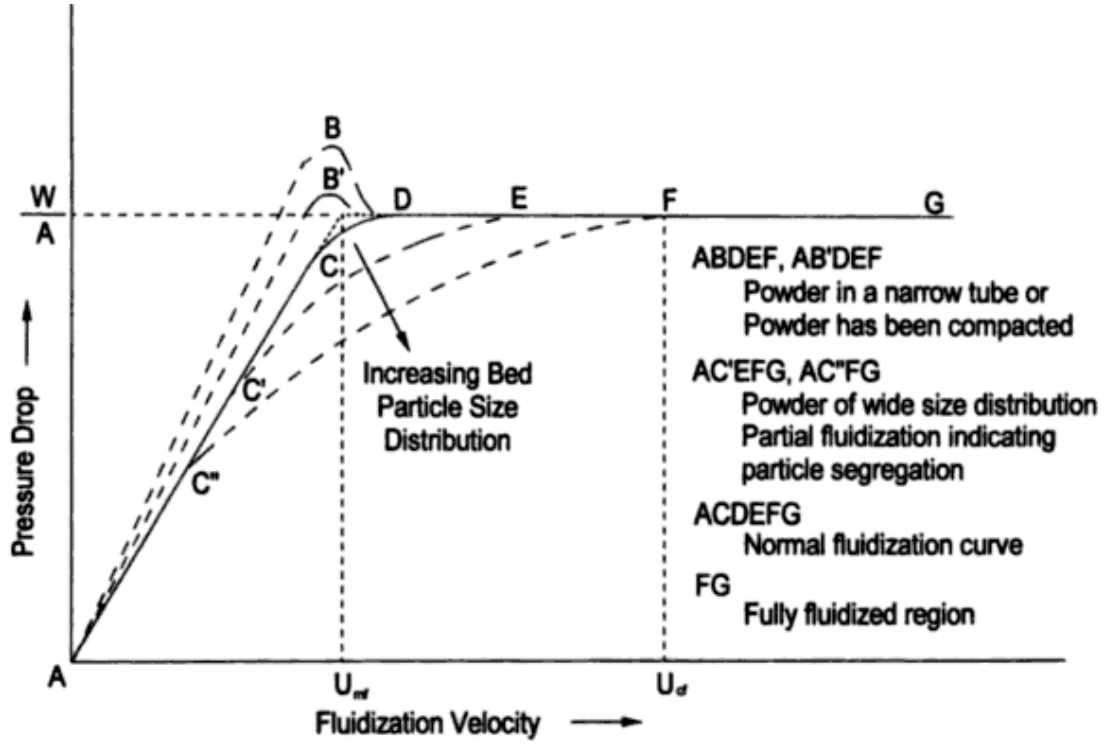


Figure 2.6: Pressure drop vs. fluid velocity illustrating common behaviours and the location of the minimum fluidization velocity (Yang, 2003).

According to Figure 2.6, when increasing the fluid velocity through a packed bed of particles, the pressure drop increases to a maximum point, and then levels off when the bed starts to fluidize. At the minimum fluidization velocity, the pressure drop calculated using Equations 2-43 and 2-44 should be equal. Therefore using these equations, a formula for the minimum fluidization velocity can be derived (Rhodes, 1998):

$$Ar = 150(1 - \epsilon_{mf})^2 Re_{mf}/\epsilon_{mf}^3 + 1.75(Re_{mf}^2)/\epsilon_{mf}^3 \quad (2-45)$$

Assuming  $\epsilon_{mf} = 0.4$ ,

$$Ar = 1652 Re_{mf} + 24.51 Re_{mf}^2 \quad (2-46)$$

where

$$Ar = [\rho_f (\rho_p - \rho_f) g d_{sv}^3 / \mu^2] \quad (2-47)$$

$$Re_{mf} = (U_{mf} d_{sv} \rho_f) / \mu \quad (2-48)$$

It is noted that these equations can be used to calculate the minimum fluidization velocity only if the voidage at minimum fluidization is known. There are numerous correlations in the literatures for predicting the minimum fluidization velocity. The following correlation can be used for the calculation of the minimum fluidization velocity for Reynolds number between 0.01 and 1000 (Wen & Yu, 1966):

$$Re_{mf} = 33.7[(1 + 3.59 \times 10^{-5} Ar_v)^{0.5} - 1] \quad (2-49)$$

where  $Ar_v$  is calculated based on  $d_v$ , the volume equivalent spherical diameter. In gas fluidization, the above equation is more suitable for particles larger than 100  $\mu\text{m}$ , and the correlation proposed by Baeyens and Geldart (1974) can be used to calculate the minimum fluidization velocity for the particles smaller than 100  $\mu\text{m}$ .

$$U_{mf} = (\rho_p - \rho_f)^{0.934} g^{0.934} d_{sv}^{1.8} / (\mu^{0.87} \rho_f^{0.066}) \quad (2-50)$$

Figure 2.7 shows what happens after minimum fluidization in both solid-gas and solid-liquid fluidized beds (Kunii & Levenspiel, 1991). As the fluid velocity increases, the bed initially may expand uniformly (smooth or “particulate” fluidization). However, in gas fluidized systems, the regime of fluidization usually changes to bubbling behaviour, then turbulent fluidization and eventually pneumatic transport (Yang, 2003). In narrow vessels, slugging behaviour can also occur. It is noted that there is usually no bubbling fluidization for liquid-solid systems except in rare cases involving very dense particles and/or low density liquids (Rhodes, 1998; Kunii & Levenspiel, 1991).

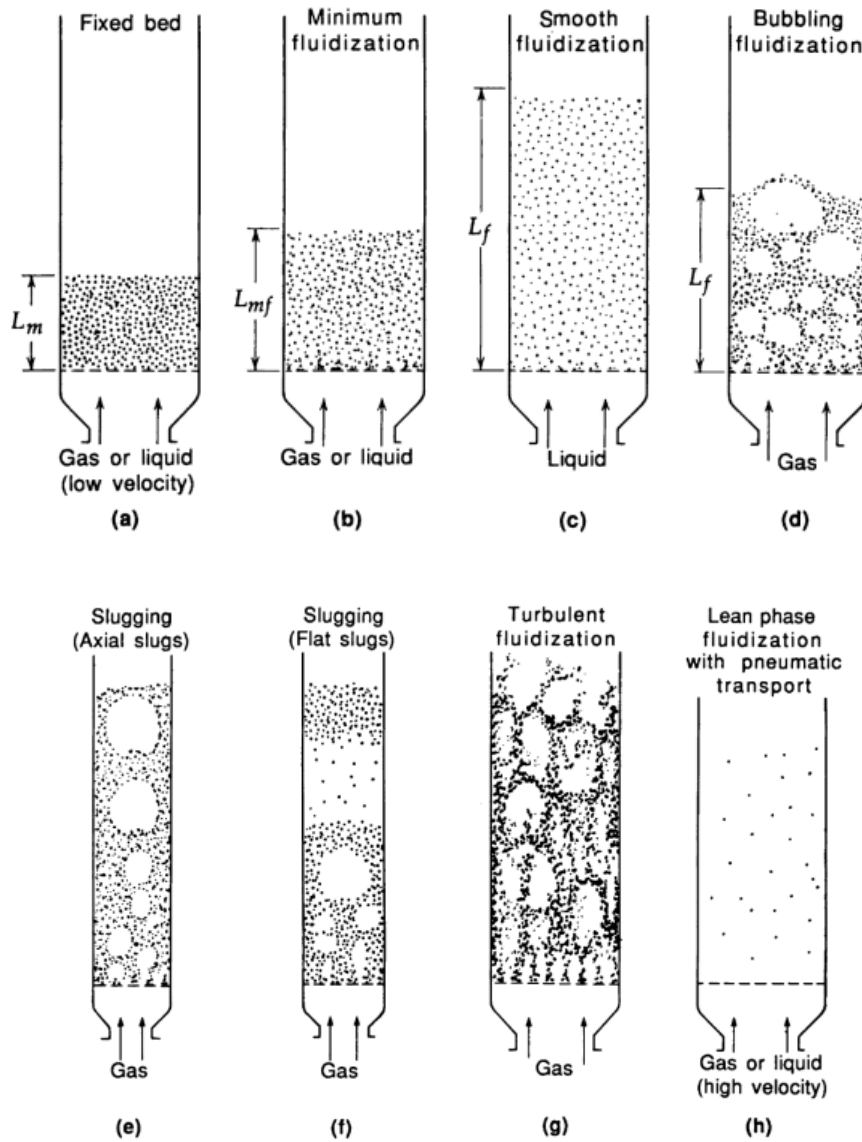


Figure 2.7: (a) Packed bed, (b) Minimum fluidization, (c) Particulate fluidization, (d) Bubbling fluidization, (e) Axial slugging, (f) Flat slugging, (g) Turbulent fluidization, and (h) Pneumatic transport (Kunii & Levenspiel, 1991).

### 2.4.3 Density definitions in fluidization

The particle density used in fluidization correlations should be the apparent density, defined as the ratio of the particle mass to the volume that is “seen” by the surrounding fluid. So the total volume used in calculating the density should include the internal pore volume. Therefore a method such as gas pycnometry which does not measure pore volume will measure the so-called skeletal or true density of the particle, which is greater than the apparent density of porous particles. It is noted that the density measured by the water pycnometry method depends on how well the water wets the particles and whether water is

given enough time to penetrate into the pores of the particles. If it does completely penetrate, then it gives the same result as the gas pycnometry method. Different definitions can be seen as below (Rhodes, 1998):

$$\text{Apparent density} = \frac{\text{mass of the particle and liquid inside the particle's pores}}{\text{hydrodynamic volume of the particle}}$$

(2-51)

$$\text{Absolute (true or skeletal) density} = \frac{\text{mass of particle}}{\text{volume of the solid phase excluding the pores}}$$

(2-52)

Another density is the bed density defined as:

$$\text{Bed density} = \frac{\text{mass of the particles in a bed}}{\text{volume of the bed}}$$

(2-53)

which includes the inter-particle voidage, as well as the intra-particle voidage. Thus bed density is always lower than the apparent and true densities.

#### **2.4.4 Particle entrainment (elutriation)**

Entrainment and elutriation are two terms used to describe the removal of particles from a bed by the fluid. As previously mentioned, a particle falling in a fluid accelerates until it reaches its terminal settling velocity at which point the forces on the particle are balanced. Now if the fluid velocity in the upward direction is higher than the settling velocity of the particle then the fluid entrains the particles and carries them in the upwards direction. The bursting of bubbles at the bed surface can be another cause of particle elutriation (Yang, 2003). Some correlations for the calculation of the entrainment rates in gas-solid fluidized beds have been proposed by Geldart et al. (1979) for particles larger than 100  $\mu\text{m}$ , and by Zenz and Weil (1958) for particles smaller than 100  $\mu\text{m}$ . However, bubbling fluidization is not a feature of most liquid-fluidized systems and so is not considered further in this thesis.

## 2.5 Particle segregation and dispersion

Particles with different properties such as density and size tend to separate from each other. This phenomenon referred to as particle segregation is very important in both mixers and separators. In separators, segregation is used in an attempt to separate particles based on differences in their properties (usually density is the property of most interest). This process is opposed by dispersion or mixing phenomena.

Williams (1990 & 1976) proposed four different general mechanisms for segregation in non-fluidized systems. Trajectory segregation occurs when particles are projected horizontally. Percolation is the tendency of fine particles to fall down through the gaps between larger particles. Large particles can also rise to the surface of a bed due to vibration. Elutriation segregation occurs when fine particles are entrained and carried to the surface of a bed by a fluid moving upwards through the interstitial gaps between larger particles.

As the interstitial fluid velocity is increased, the bed of particles eventually becomes fully fluidized, and dispersion and segregation phenomena must be considered. As previously discussed, in a liquid fluidized bed increasing fluid velocity generally gives uniform or smooth expansion of the bed. In these cases the empirical Richardson and Zaki equation (Eqn. 2-33) can be used to predict the height and porosity of the bed. However, the behaviour of liquid fluidized beds containing particles with different sizes or densities can be quite complex with the possibility of segregation occurring.

Dispersion is a phenomenon that promotes mixing and thus opposes segregation. It is analogous to the diffusion process, where species naturally move from high to low concentration regions, as a result of the random small-scale movements caused by inter-particle collisions and interaction with the fluid. In a gas-solid fluidized bed, dispersion is dominant due to the agitation caused by bubbles. However, in liquid-solid fluidized beds it is possible for segregation to become significant enough that useful separations can be performed on the basis of differences in particle size and/or density.

In a mixture of species with different sizes and densities, each species tends to segregate and form a mono-component zone. In a general binary system, two mono-component zones of each species and one transient zone containing both species may be formed. The distribution

of the species in the mixed zone is controlled by the balance between dispersion and segregation of each species, and this is what controls the equilibrium concentration profile (Galvin et al., 2006). The balance between dispersion and segregation at steady state was proposed as (Kennedy & Bretton, 1966):

$$D_i d\phi_i/dz' = U_i\phi_i \quad (2-54)$$

where  $U_i$  is the local segregation velocity,  $\phi_i$  is the local volume fraction of species  $i$ ,  $d\phi_i/dz'$  is the local concentration gradient and  $D_i$  is the dispersion coefficient and  $z'$  is the distance from the base of the vessel. The local segregation velocity of species  $i$  was proposed by Asif and Petersen (1993) as:

$$U_i = U_{mi} (1 - \phi_{ni}) \quad (2-55)$$

where  $U_{mi}$  is the maximum possible segregation velocity occurring when species  $i$  is immersed in a mono-component zone of the other species.  $\phi_{ni}$  is calculated as  $\phi_i / \phi_{mi}$  when  $\phi_i$  and  $\phi_{mi}$  are the species  $i$  local concentration and its concentration in the mono-component zone, respectively. When  $\phi_{ni}$  is approaching zero, one particle of species  $i$  is present in a mono-component zone of other species and hence has the maximum segregation velocity. On the other hand, when  $\phi_{ni}$  is approaching 1, one particle of species  $i$  is in a mono-component zone of the same species and hence no segregation occurs (Galvin et al., 2006).

Batchelor (1988) proposed that the dispersion coefficient could be calculated as:

$$D = \alpha' r u_s \quad (2-56)$$

where  $r$  is the particle radius,  $u_s$  is the fluid superficial velocity and  $\alpha'$  is an adjustable parameter varying between 8 and 12 depending on the species volume fractions (Davis & Hassen, 1988). Galvin et al. (2006) used a simple analysis based on the mean free path between particles to predict the dispersion coefficient. They suggested that the dispersion coefficient should be proportional to  $d_p u_f / \phi$ , where  $u_f$  is interstitial fluid velocity,  $\phi$  is the volume fraction of solids, and  $d_p$  is the particles diameter. So they proposed the dispersion coefficient as:

$$D = \alpha d_p u_f / \phi \quad (2-57)$$

where  $\alpha$  is an adjustable parameter. Based on this equation, the dispersion coefficient varies through the fluidized bed as the interstitial fluid velocity varies, whereas Equation 2-56 predicts a constant dispersion coefficient in a given system.

By applying Equations 2-55 and 2-57 to Equation 2-54, the volume fractions of each species through the fluidized bed can be calculated. Figure 2.8 shows the experimental data and the model prediction of Patel et al. (2008) and Galvin et al. (2006) for the segregation in a two-component suspension at different fluid superficial velocities.

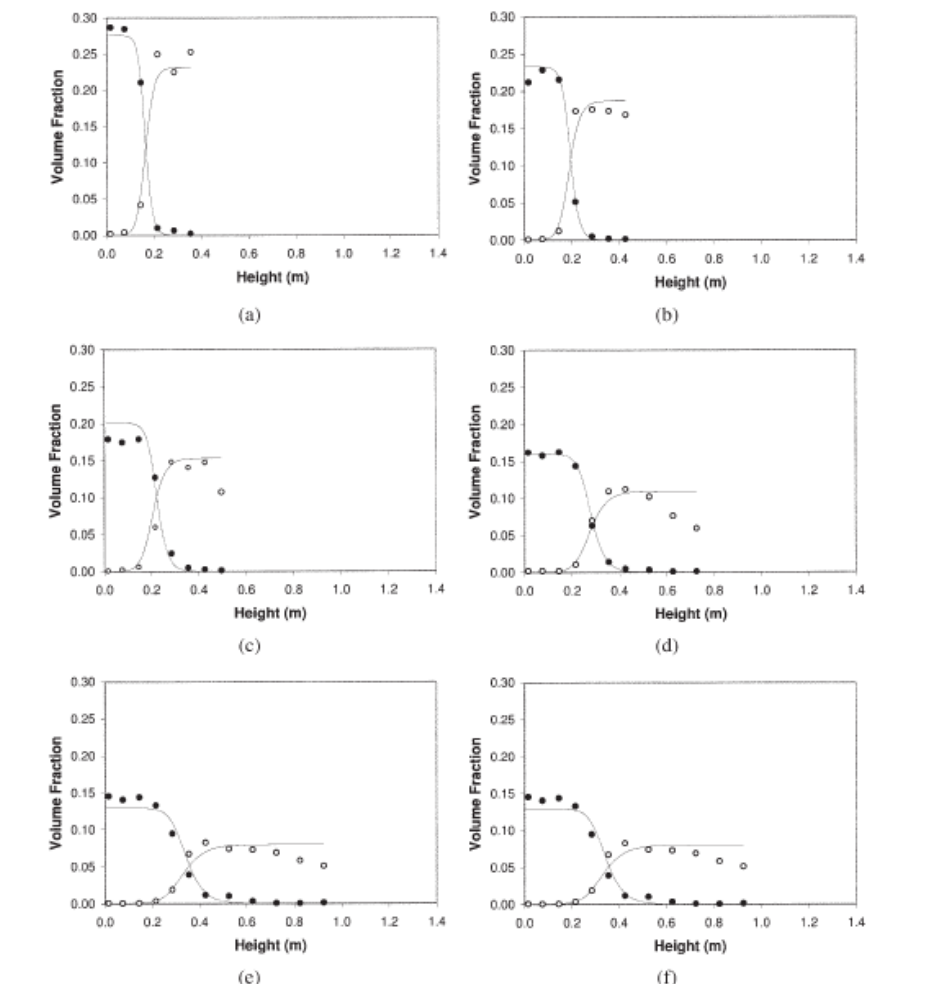


Figure 2.8: Particle segregation in a fluidized bed at six different fluidization velocities in increasing order from a to f. The open and closed symbols show the volume fractions of low density and high density particles, respectively. Lines show model predictions (Galvin et al., 2006).

One of the very interesting phenomena in fluidization is phase inversion (Moritomi et al., 1982). When a mixture of small dense particles and large low-density particles are fluidized, initially the small dense ones form a layer at the base of the bed while the large light particles tend to be in the upper section of the bed. By increasing the fluid velocity, dispersion occurs and a well-mixed zone containing both species emerges. Further increasing the fluid velocity leads to the reformation of the segregated zones, but this time with a (much more dilute) layer of large light particles at the base and the layer of small dense particles in the upper zone (Galvin et al., 2002). Figure 2.9 illustrates this phenomenon.

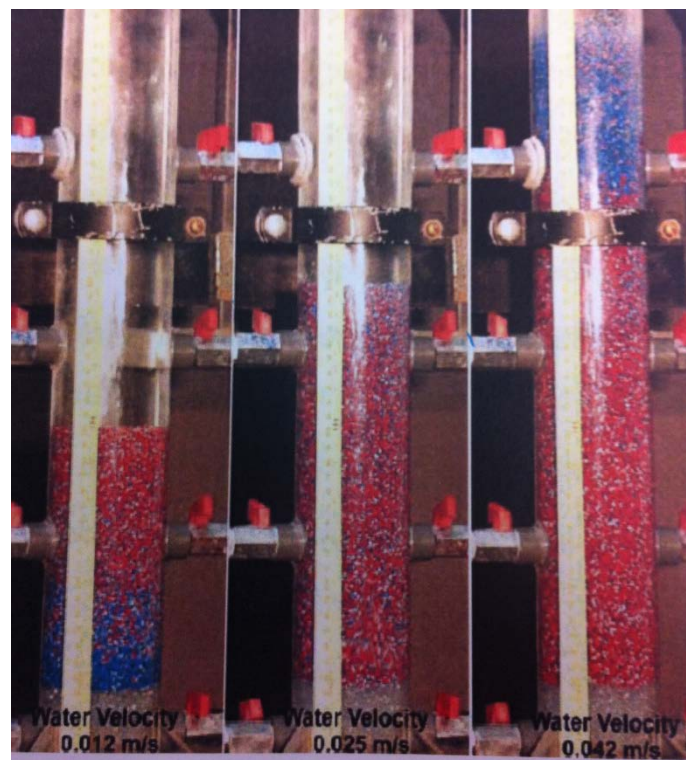


Figure 2.9: Photos of the phase inversion which occurred in a binary mixture of small dense and large light particles as the fluid velocity increased from 0.012 m/s to 0.042 m/s (Galvin et al., 2002).

In fact in a mixture of fine and coarse particles forming a suspension with total solids fraction of  $\phi$ , the slip velocities of both species are the same. Initially if the mixing was to cease, then the fine particles would move downward and the coarse particles move upward compared to the vessel i.e. in this case, the slip velocity of fine particles is greater than that of the coarse ones. However once inversion has occurred, if mixing were to cease, then the slip velocity of

the coarse particles would be greater. Therefore the slip velocity models such as those proposed by Richardson and Zaki (1954b) and Di Felice (1995) which are dependent only on the volume fractions of solids encountered limitations in predicting the phase inversion phenomenon in the fluidized beds (Asif, 1998). Some more generalized models have been proposed by considering the effective density of the suspension and its influence on each species' settling behaviour (Masliyah, 1979). Later Asif (1997) and then Galvin et al. (1999) further empirically investigated the effect of the suspension density, and proposed the following equation:

$$F'' = (u_p - u_f)/u_t = [(\rho_p - \rho_{susp})/(\rho_p - \rho_f)]^{n-1} \quad (2-58)$$

where  $F''$  is the hindering factor defined as the ratio of the slip velocity and the terminal velocity. For systems containing different density particles, this model was found to provide some explanation of the phase inversion phenomenon.

## 2.6 Fine particle beneficiation technologies

Sedimentation processes, which depend on the settling velocity of the particles, are relatively low throughput, decreasing as the separation sizes decreases. Generally, froth flotation has been applied to the treatment of particles smaller than 150  $\mu\text{m}$ . However, gravity separators have been developed to target these fine particles. Working with gravity separators has several advantages over froth flotation. Firstly, particle density is a more reliable indicator of average particle composition than the surface composition. Values locked inside gangue material will not be “seen” by flotation, but still influence the particle density. Secondly the density of a particle remains almost constant whereas a particle's surface properties can vary with the chemical environment and vary due to oxidation, etc. Further, gravity separation can be applied at much higher throughput when the target particle size exceeds about 100  $\mu\text{m}$ . However, below this size the throughput declines markedly (Honaker & Forrest, 2003).

The settling velocity of particles in a given fluid depends only on particle size and density. For two particles with the same density, the larger one settles faster, whereas for particles with the same size, the denser one settles faster. So for a suspension of particles with different sizes and densities, fine particles with high densities can have the same settling velocity as

some of the coarser low-density particles. The size ratio of particles with different densities, which have the same free settling velocities, is known as the free settling ratio:

$$d_{p2}/d_{p1} = [(\rho_{p1} - \rho_f) / (\rho_{p2} - \rho_f)]^n \quad (2-59)$$

where  $n = 0.5$  for the Stokes regime (small particles),  $n = 1$  for Newtonian regime (large particles) and  $0.5 < n < 1$  for the intermediate regime (intermediate sized particles) (Heiskanen, 1993). When this factor is larger than 2.5, positive or negative, gravity separation is relatively easy (Wills, 1997). In a system containing both positively and negatively buoyant particles, the free settling ratio becomes negative, reflecting the movements of the species in opposite directions. In theory, a perfect separation of species can be achieved in such a system with a fluid density between the species' densities. However the misplacement of fine particles is inevitable, especially when the absolute value of the free settling ratio is less than 2.5.

### **2.6.1 Gravity separation methods**

Many different gravity separation techniques have been developed to process particles and separate them. An overview of these separation techniques can be found in Burt (1985) and Wills (1997). Jigs, pinched sluices and Reichert cones are gravity separators which can be used efficiently for coarse particle separation (Wills, 1997). Spirals are another gravity concentrator and have been used for many years in different fields such as separating heavy mineral sands. However, Sanders (2007) reports that this separator is essentially ineffective for particles smaller than 125  $\mu\text{m}$ .

Float-sink processes, which are generally run as batch systems, are the simplest of the gravity separation methods, offering a high efficiency and sharp separation at any given density. Here, the particles with a density higher than the fluid sink and particles less dense than the fluid float. In theory, this method of separation only depends on the density of the particles, not their size. However, in practice, the small particles have low settling or rising velocities, hence this approach can be very slow. Further, the ultra-fine particles increase the viscosity and hence decrease the particle settling velocity. Therefore this method of separation is inefficient for separation of fine particles if they have only a short residence time.

Dense medium cyclones are used widely in the coal and mineral industries. The high centrifugal force provided by these cyclones make them a powerful method for separating fine particles compared to other methods of gravity separation. However applying this method to the separation of very fine particles becomes problematic as it becomes difficult to effectively separate the medium particles for re-use. They can be also used for classifying particles based on their density and/or size, and also for dewatering (Sander, 2007).

A fluidized bed classifier (also called teeter bed or hindered bed classifier) is a vessel which separates particles based on their hindered settling velocity. Two distinct zones are formed in the vessel: there is a lower fluidized zone with a high concentration of particles and also an upper zone with low concentration. Particles with high settling velocity move downward and exit in the underflow and particles with lower settling velocity are entrained into the overflow. These devices are typically used for size classification. However they can be used for density separation if the feed particle size range is narrow. Specifically, if the diameter ratio of the largest low density particle to the smallest high density particle is less than the free settling ratio, then theoretically a density separation can be achieved. Otherwise, misplacement of particles is inevitable. In reality, there is always some extent of misplacement of coarse low density particles into the high density underflow and vice versa (Heiskanen, 1993).

### **2.6.2 Particle size classification**

To show particle size classification, one approach is to plot the recovery of the particles as a function of the particle size, forming the so-called partition curve. A sample partition curve is shown in Figure 2.10 presenting the important parameters such as  $d_{25}$ ,  $d_{50}$  and  $d_{75}$  defined as the particle sizes with 25 %, 50 % and 75 % probability of entering the product respectively. From these, the imperfection  $I = (d_{75} - d_{25})/(2d_{50})$ , an indication of the separation sharpness, can be also calculated (Wills, 1997).

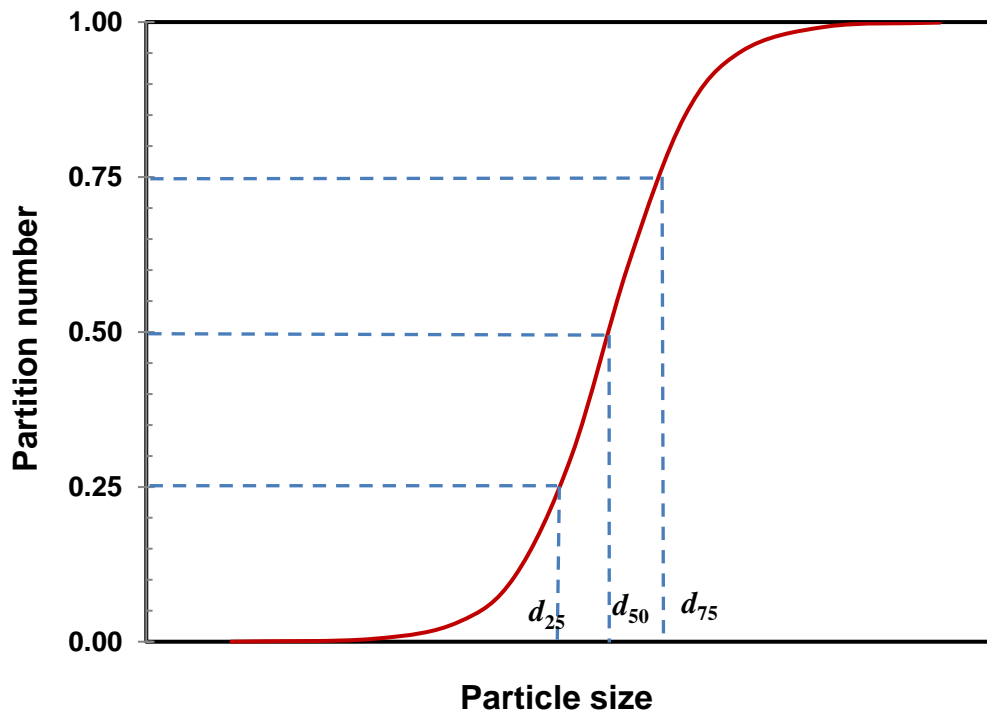


Figure 2.10: A simple plot of a partition curve.

### 2.6.3 Enhanced gravity separation methods

The velocity of fine particles is much lower in more concentrated suspensions. Therefore to increase the separation efficiency in terms of throughput and separation sharpness, methods to increase the settling rates are commonly used. One of the most effective methods for increasing the sedimentation rate is to operate gravitational separators using a centrifugal force. This approach can increase the body force by more than 100 times normal gravity. Three examples include centrifugal jigs, centrifugal films and centrifugal teetered beds (Cole & Dunne, 2012). Recently, a centrifugal REFLUX™ Classifier has been studied and applied to the separation of particles (Galvin & Dickinson, 2013).

Flocculation is another common method used to increase the settling rate of fine particles. However the flocculants need to selectively flocculate only one of the species to be effective in particle-particle separations, and hence their usage in beneficiation is limited. Other important phenomena include the bulk streaming effect comprehensively discussed by Batchelor and Van Rensburg (1986), and inclined settling based on the observation made by Boycott (1920). These play a significant role inside the inverted REFLUX™ Classifier, so are covered in Chapter 3.

## 2.7 Summary

In this chapter, the concepts of particle settling and gravity separation were reviewed. The effects of different parameters such as particle size, surface roughness and sphericity on the terminal settling velocity of particles have been described. Then the behaviour of particles in a concentrated suspension was reviewed, introducing the concept of hindered settling velocity. The mechanisms involved in hindered settling were discussed and different models proposed for its calculation including the commonly-used Richardson and Zaki equation. It was found that there is still confusion in the literature surrounding how to predict the hindered settling velocity of multi-component suspensions, particularly those containing mixtures of both positively and negatively buoyant particles. This chapter also briefly reviewed packed bed and fluidization behaviour. The segregation, dispersion and phase inversion phenomena that occur in fluidized beds were discussed, including the predictive models. This chapter concluded with a brief mention of some of the different methods of fine particle separation currently used commercially. The methods for increasing the sedimentation rate were noted, including the subject of the next chapter, inclined settling and the bulk streaming formation.

## **Chapter 3**

# **Bulk Streaming Motion and Inclined Settling**

### 3.1 Introduction

This chapter studies two important hydrodynamic phenomena that can be used to increase particle segregation rates. The first is the bulk streaming motion phenomenon, the tendency of particles to gather together and move *en masse*. These particles can form a streaming motion leading to an increase in their settling rates. The conditions under which this streaming phenomenon develops are discussed, with regime maps presented for two specific cases.

Inclined settling is the second phenomenon reviewed in this chapter, applicable for increasing particle segregation rates. Using inclined surfaces, the effective area for sedimentation increases. The particles settle a short distance onto settle the surface, before sliding down *en masse* with other settled particles. In the case of positively-buoyant particles the motion proceeds in the upwards direction.

New developments in these areas are reviewed, including discussion of how these phenomena potentially combine and contribute to the separation performance inside a REFLUX™ Classifier.

### 3.2 Bulk streaming motion

#### 3.2.1 Evidence for bulk streaming motion

As previously discussed in Chapter 2, there is confusion concerning the hydrodynamic behaviour of suspensions containing different density particles. More specifically, three different models were shown to provide completely different predictions of the particle velocity in a mixture of negatively and positively buoyant particles. Thus many researchers have focused on the influence of suspension concentration on the settling or rise velocity of mixtures of particles with different densities. One of the earliest studies was that of Whitmore (1954), which investigated a system containing a suspending fluid with a density of 1.0558 g/cm<sup>3</sup>, falling-spheres with a density of 1.1881 g/cm<sup>3</sup> and a particle size of 96 µm, and suspended-spheres of the same size as the falling-spheres and the same density of suspending fluid. They found that for total solids concentrations below about 10 vol.%, increasing the concentration of the suspended-spheres causes a decrease in the segregation rate of the falling-spheres. However, above 10 vol.%, the settling rate increases significantly. This

behaviour was attributed to hydrodynamic forces between the particles creating instabilities in the suspension. These instabilities led to the formation of vertical streams, and hence increased the settling velocities due to pluming effects. There is, however, a limit to this effect. Relative settling rates defined as a ratio of the falling-sphere velocity in the presence of the suspended-spheres to that in the absence of the suspended-spheres peaked at a total solids concentration of about 37 vol.%. Beyond this, the dense packing of the system starts to become significant. Figure 3.1 shows the variation of the falling-sphere velocity as a result of increasing the concentration of the suspended-spheres.

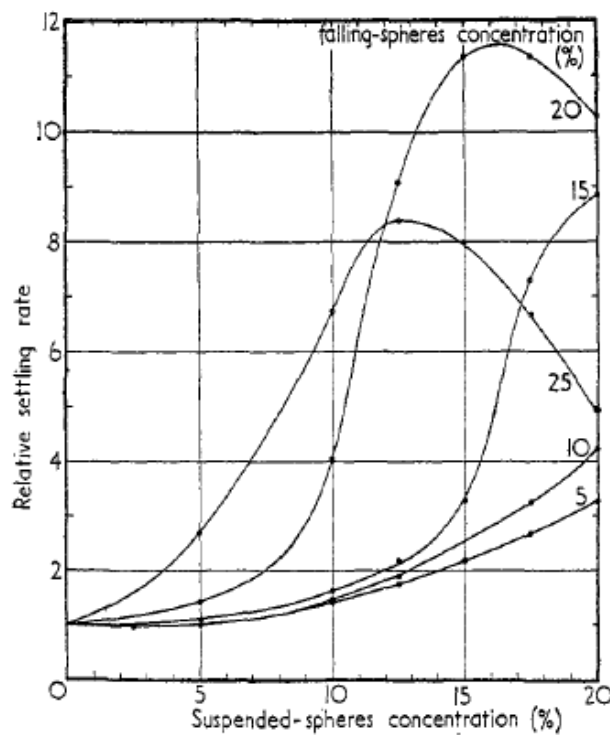


Figure 3.1: The variation in the settling rate of the falling-spheres as a function of the concentration of the suspended-spheres. Mixture made up of methyl-methacrylate polymer (falling-spheres) and polystyrene (suspended-spheres) in aqueous solutions of lead nitrate (Whitmore, 1954).

Weiland and McPherson (1979) extended Whitmore's study, examining the presence of a positively-buoyant phase and its effects on settling suspensions. They suggested that the presence of a large number of positively-buoyant particles can induce significant density convection in the suspensions. A schematic diagram of the settling pattern in their system is shown in Figure 3.2. The effect of positively buoyant particles on the sedimentation rate of heavy particles was also reported to be more significant than the effect of neutrally-buoyant

particles reported in Whitmore's study. Both these studies used a measurement technique which was capable of causing convection in the suspensions, and hence potentially led to inaccuracy in their conclusions (Fessas & Weiland, 1981).

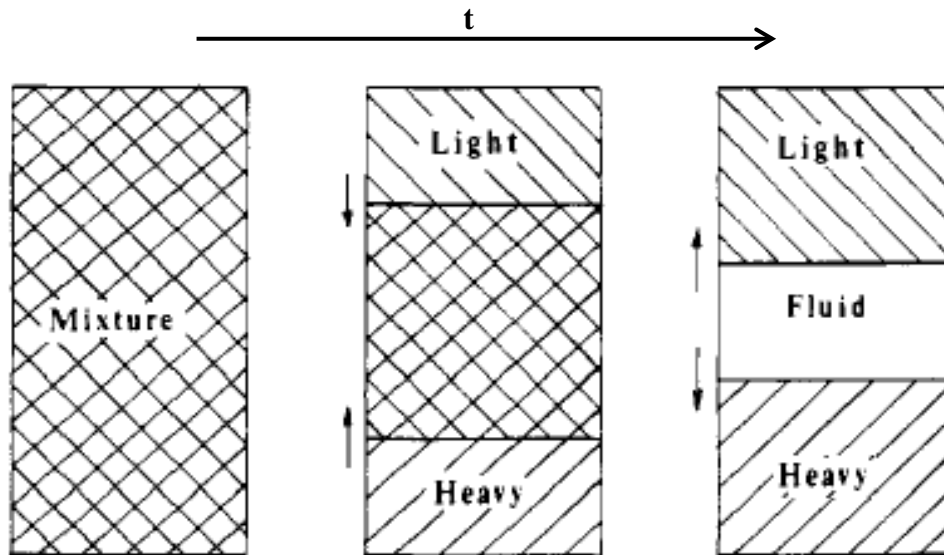


Figure 3.2: Settling patterns of a suspension containing positively and negatively buoyant particles (Weiland & McPherson, 1979).

Fessas and Weiland (1981) investigated the effects of buoyant particles on the sedimentation of heavy particles using a method that caused no disturbance to the suspension behaviour. They coated particles with a fluorescent dye and measured the behaviours by illuminating with ultraviolet light. Fessas and Weiland qualitatively observed the formation of clusters in the suspensions, moving up and down, forming a pathway for other clusters to move and hence forming a chain of clusters in the suspensions. This interesting behaviour can induce a bulk convective effect and hence increases the rate of settling. Figure 3.3(a) shows the velocity of heavy particles in the presence of positively-buoyant particles relative to that in the absence of the positively-buoyant particles ( $U_H/U_H^0$ ). The system used in their study contained an aqueous solution of thallium formate with a density of  $2.24 \text{ g/cm}^3$  as the suspending fluid, negatively-buoyant and positively-buoyant particles with densities of  $2.96 \text{ g/cm}^3$  and  $1.4 \text{ g/cm}^3$  and Sauter mean size of  $100 \text{ }\mu\text{m}$ , and  $107 \text{ }\mu\text{m}$ , respectively.

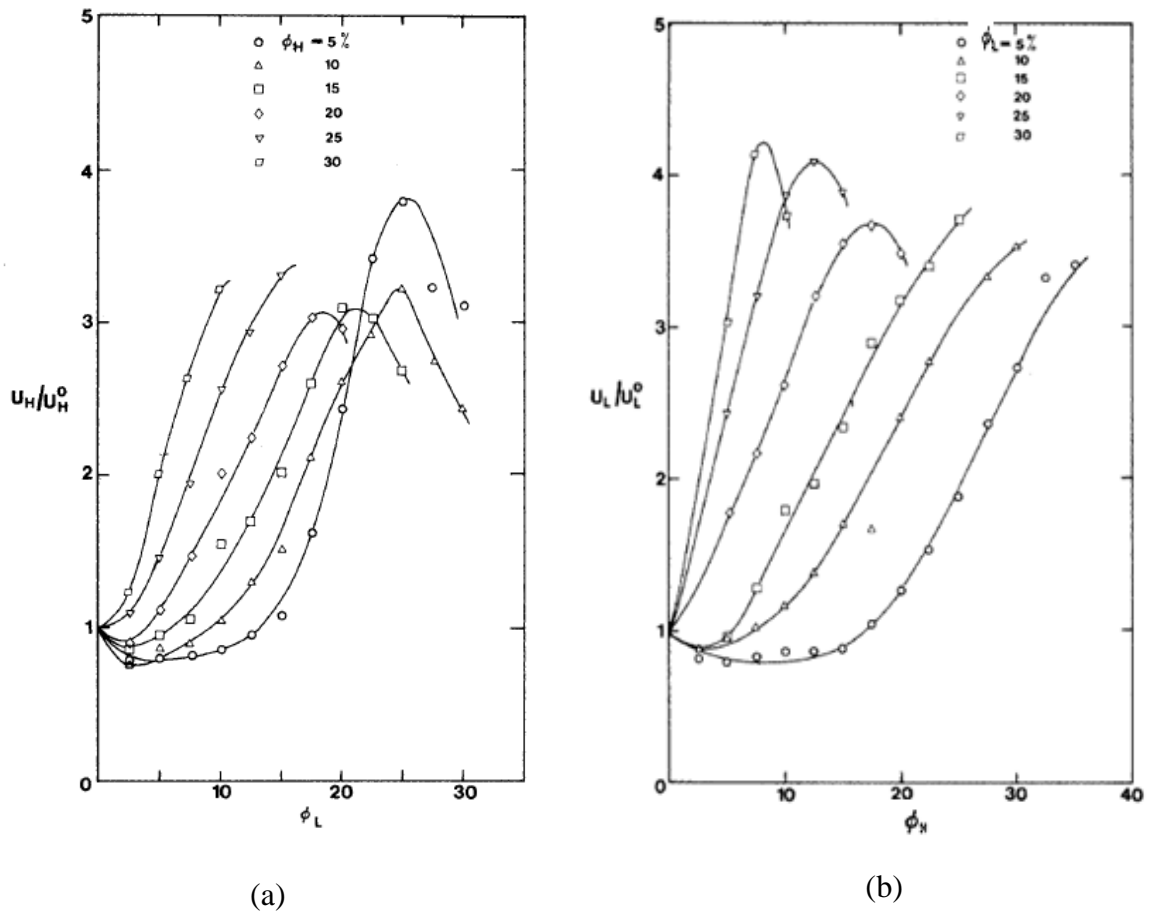


Figure 3.3: The dependence of (a) negatively-buoyant particle relative settling rate on the concentration of positively-buoyant particles  $\phi_L$ , and (b) light particle settling rate on the concentration of heavy particles  $\phi_H$  (Fessas and Weiland, 1981 & 1982).

In 1982, they extended this work further and suggested that the effects of the buoyant particles are much more significant when the density of the heavy particles is closer to the density of the fluid (Fessas & Weiland, 1982). Also, larger buoyant particles are much more effective than small ones in increasing the settling rate of the heavy particles. As shown in Figure 3.3(b), the rise velocity of positively-buoyant particles could also be increased by the presence of a heavy species (Fessas & Weiland, 1982).

Table 3.1 summarises the studies in which enhanced settling velocities in bi-dispersed systems has been observed. According to these studies, at low total solids concentrations, the effect of the second species is to decrease the settling velocity of the other species, presumably due to standard hindered settling mechanisms. Only at higher total solids

concentrations are the particles in close enough proximity for the clustering and streaming phenomena to occur.

Table 3.1: Properties of the systems in which an enhancement in the settling or rise velocity of species was reported (Batchelor & Van Rensburg, 1986).

	Whitmore (1955)	Weiland & McPherson (1979)	Fessas & Weiland (1981)	Weiland et al., (1984)			Fessas & Weiland (1984)	
				A	B	C		
<b>Suspending Fluid</b>								
$\rho_f$ (g/cm <sup>3</sup> )	1.06	1.10	2.24	1.12	1.06	1.12	1.59	2.24
$\mu$ (g/(cm.s))	0.011	0.019	0.021	0.049	0.018	0.049	0.015	0.021
<b>Particles 1</b>								
$(\rho_1 - \rho_f)$ (g/cm <sup>3</sup> )	0.13	0.28	0.72	0.28	1.40	0.28	0.92	0.72
$r_1$ ( $\mu$ m)	48	100	50	69	45	109	24	58
$Re_1$	0.032	0.800	0.101	0.009	0.091	0.037	0.019	0.152
$\phi_1$	Various	Various	Various	0.175	0.175	0.143	Various	Various
<b>Particles 2</b>								
$(\rho_2 - \rho_f)/(\rho_1 - \rho_f)$	0	-0.21	-1.17	-1.88	0.25	1.0	-0.20	-1.17
$r_2/r_1$	1.02	1.00	1.08	1.00	1.00	0.63	2.02	1.00
$\phi_2$	various	Various	Various	0.165	0.175	0.095	Various	Various

However, although streaming is often suggested as the cause of the enhanced settling rate, most of these studies do not actually provide any details about such structures or the mechanisms behind their formation (Batchelor & Van Rensburg, 1986). Fessas and Weiland's study (1984) was the only one reporting the appearance of vertical fingers or streams, referred to as "lateral separation". They described these fingers as vertical streaming columns 3.5 mm in diameter containing mostly the less populous species. These were reported to move through the high concentration of the more populous species, and thus result in a significant buoyancy driving force and a bulk movement in the suspensions. They were also the first ones reporting such hydrodynamics behaviour for bi-dispersed suspensions of negatively-buoyant particles with different densities. Figure 3.4 shows a photo of this phenomenon which occurs in such suspensions (Weiland et al., 1984). Thus prior to Batchelor and Van Rensburg's study in 1986 there was a lack of information about the mechanisms behind this phenomenon and the critical conditions under which it may develop.

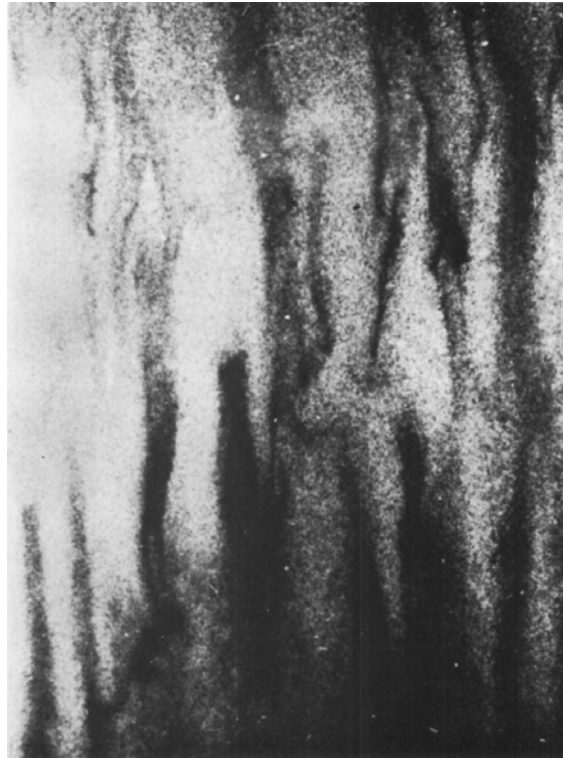


Figure 3.4: Streaming structures observed in a suspension containing negatively-buoyant particles with different densities. It is noted that properties of these systems are indicated in Table 3.1 (Weiland et al., 1984).

### 3.2.2 Conditions for the development of bulk streaming motion

Batchelor and Van Rensburg (1986) investigated the mechanisms behind settling velocity enhancement in concentrated bi-disperse suspensions. Their preliminary results showed and confirmed that for a suspension containing two types of particles between 10 and 100  $\mu\text{m}$  in size at specific concentrations, uniformly dispersed, and settling under gravity, the particles of each species tend to gather together and move as streams. They referred to this phenomenon as bulk streaming motion and presented photographs to show its origin and details.

They examined different case studies in detail to investigate the conditions under which bulk streaming motion develops. Four dimensionless numbers were defined to specify different suspensions. The ratio of species radii ( $\lambda = d_1/d_2$ ), the ratio of their reduced densities  $\gamma = (\rho_2 - \rho_f)/(\rho_1 - \rho_f)$ , and the volume fractions of each species ( $\phi_1$  and  $\phi_2$ ). They studied two cases, firstly the systems with constant  $\lambda$  and  $\gamma$  and various  $\phi_1$  and  $\phi_2$ , and secondly for constant  $\phi_1$  and  $\phi_2$  they examined different  $\lambda$  and  $\gamma$  values. The instability caused by small disturbances to

the statistically homogenous bi-dispersed suspension was found to be the reason for the bulk streaming motion. Regime maps were suggested for each case showing the instability in the suspension which led to an enhancement in the rate of particles settling or rising. It should be noted that owing to the random nature of the streaming structures that emerge, this phenomenon was very difficult to quantify. Therefore all the conclusions were taken using from a sequence of photographs and visual observations for two specific cases (Batchelor and Van Rensburg, 1986).

**Case 1:** In the first case,  $\lambda = 1$ , and  $\gamma = -1$ , hence the system contained two species of the same size, but with positively buoyant and negatively buoyant species relative to the suspending fluid. In this case, at the end of a settling test in a vessel, two layers formed, a layer of light particles at the top and a layer of high density particles at the bottom of the vessel. As shown in Figure 3.5, they qualitatively defined four different classes of streaming/clustering behaviour. Blobs with a tail and a good photographic contrast (Figure 3.5a) were shown to occur when the volume fractions of both species were large and nearly equal. Blobs with good contrast and columns with good contrast are shown in Figures 3.5b and 3.5c. Streaming columns with poor contrast are shown in Figure 3.5d. Good contrast indicates that the streams formed primarily from one species. Poor contrast indicates that the stream or cluster is difficult to recognise as it still contains significant concentrations of both species (Batchelor & Van Rensburg, 1986).

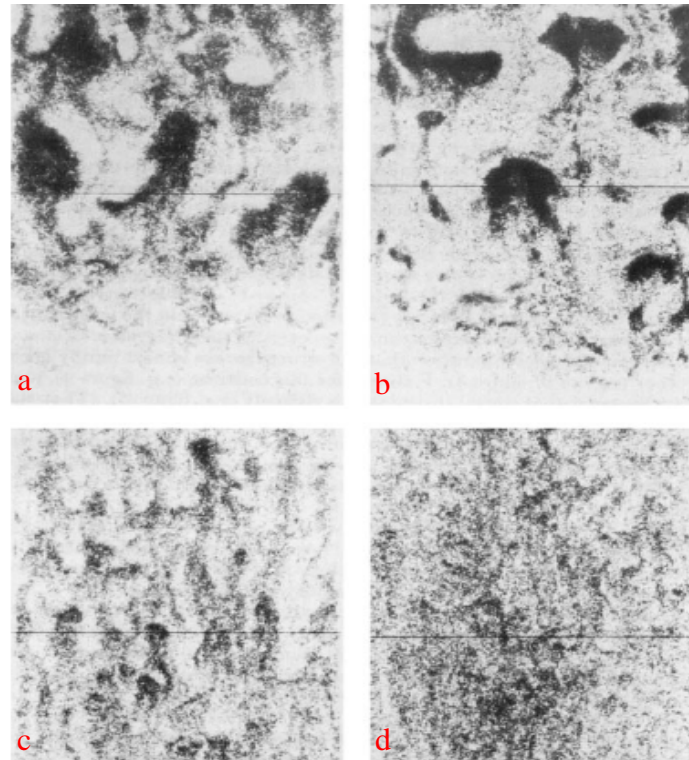


Figure 3.5: Photographs of the four different types of internal structures or streams observed by Batchelor & Van Rensburg (1986) which they classified as: a) blobs with tail and a good photographic contrast; b) blobs and a good contrast; c) columns with head and a fair contrast; and d) streaming columns with poor contrast.

The regime map reported for Case 1, which is a system containing both positively and negatively buoyant particles, is shown in Figure 3.6. When the initial volume fractions of species are larger in a suspension, it is more likely to form blobs consisting mostly of one species, which shows a good separation. This behaviour leads to a significant buoyancy driving force. If the volume fractions of solids are small and the system is still unstable, the structures or streams formed in the suspension are classified as columns showing a poor separation. For stable systems, no coherent streaming structure is formed, although the small cluster formation may still exist in some cases. The classification called “marginally unstable” means that the formation of structures or streams is unclear and contrast is poor. In such systems, a slight increase in the mean velocity of the suspension may happen.

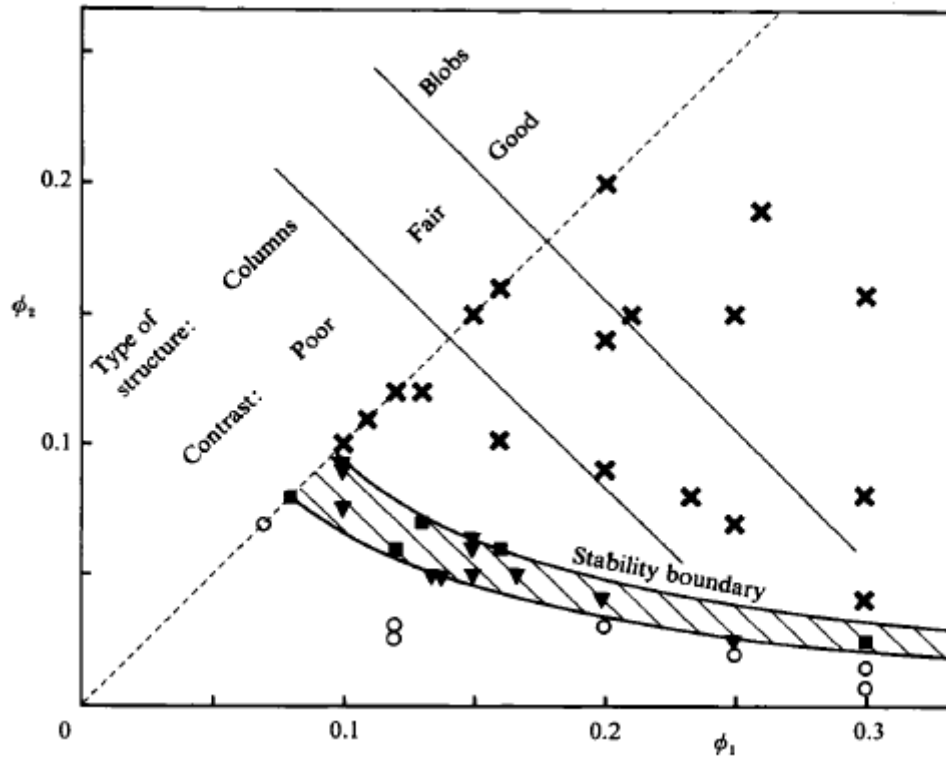


Figure 3.6: The regime map proposed by Batchelor and Van Rensburg (1986) to show instabilities for a suspension containing positively and negatively buoyant particles when  $\lambda = 1$ , and  $\gamma = -1$ . System types:  $\times$  indicates unstable systems,  $\blacktriangledown$  indicates the systems studied by Fessas and Weiland (1981 & 1984) classified as being marginally unstable and  $\circ$  indicates the stable region.

**Case 2:** The second case studied by Batchelor and Van Rensburg (1986) was the systems with species volume fractions of 0.15 for each one, and  $\lambda$  and  $\gamma$  varied. The regime map associated with this case is shown in Figure 3.7.

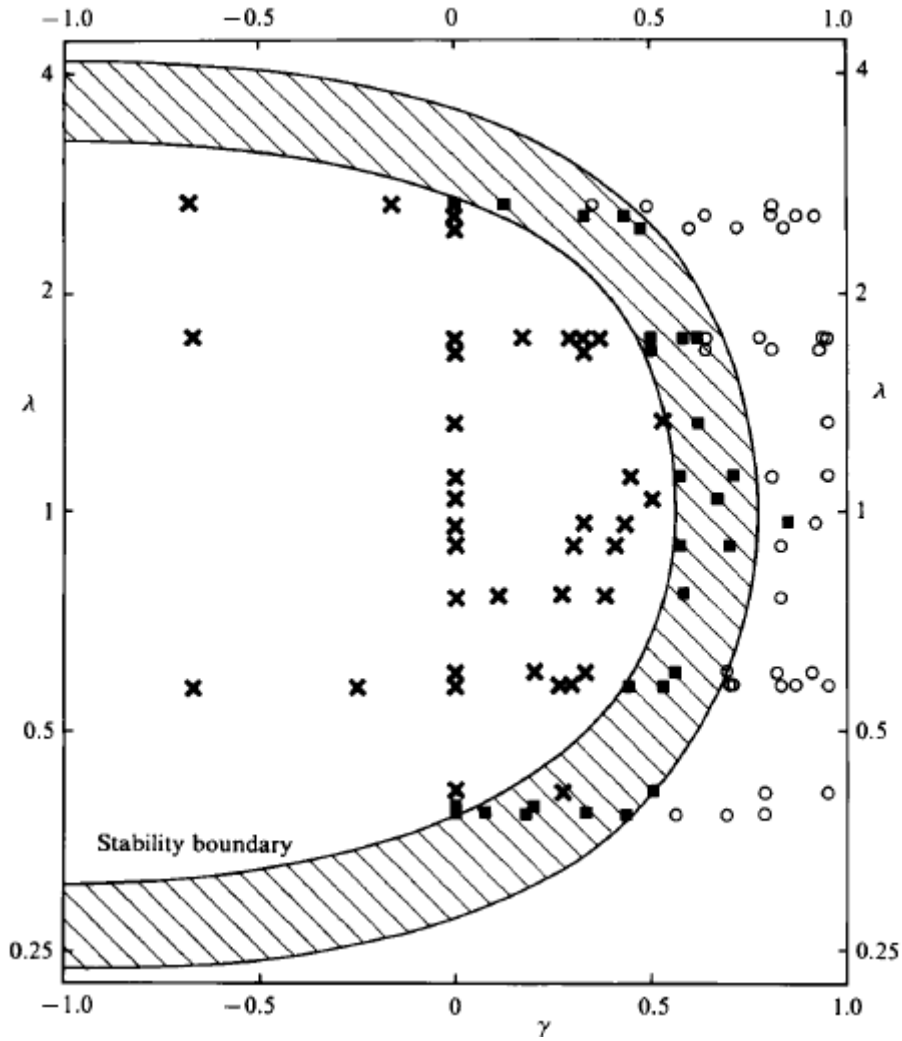


Figure 3.7: Regime map showing the (×) unstable, (■) marginally unstable and (○) stable systems when  $\phi_1 = \phi_2 = 0.15$  (Batchelor & Van Rensburg, 1986).

A theoretical parameter ( $I'$ ) was defined to indicate the stability in the suspensions.

$$I' = (\delta\phi_1 u_1 / \delta\phi_1 - \delta\phi_2 u_2 / \delta\phi_2)^2 + 4 \phi_1 \phi_2 (\delta u_1 / \delta\phi_2) (\delta u_2 / \delta\phi_1) \quad (3-1)$$

where  $u_1$  and  $u_2$  are the velocity of species which depends on  $\phi_1$ ,  $\phi_2$ ,  $\lambda$  and  $\gamma$ .

$I' = 0$  defines the critical condition. For  $I' < 0$ , the system was found to be unstable while for  $I' > 0$ , it was found to be stable. This parameter was found to approach a positive limit when either  $\phi_1$  or  $\phi_2$  approaches zero, which means that near the abscissa and ordinate in Figure 3.6 the system is stable and no streaming effect develops. For Case 1,  $\lambda = 1$  and  $\gamma = -1$ ,  $I'$  was calculated to be zero when  $\phi_1$  and  $\phi_2$  approach a specific values around 0.09. This point

clearly lies on the stability boundary in Figure 3.6. When  $\gamma > 0$ ,  $I'$  becomes zero for larger values of  $\phi_1$  and  $\phi_2$  compared to the case when  $\gamma < 0$ . In fact Figure 3.7 shows that the instability can also occur for some positive values of  $\gamma$ .

As a conclusion, the instability in a suspension was found to lead to the formation of streams and hence an increase in the species' settling velocity relative to the case where the other species was not present. This instability was shown to depend on four determining parameters,  $\phi_1$ ,  $\phi_2$ ,  $\lambda$  and  $\gamma$ . The interaction between these four parameters defines a parameter  $I'$  that determines the boundary between the unstable and stable conditions in suspensions. The theoretical prediction of critical conditions for instability using parameter  $I'$  was found to be consistent with the observations (Batchelor & Van Rensburg, 1986).

### **3.2.3 Similar phenomena to bulk streaming**

#### **3.2.3.1 Clustering and streaming in a gas-solid fluidized bed**

A phenomenon similar to bulk streaming motion in liquid-solid systems can also be seen in gas-solid fluidized beds, where it is referred to as cluster formation (Lim et al., 1995). Particles tend to gather together under specific hydrodynamic conditions, which gives completely different behaviour in terms of mass, heat and momentum transfer. Grace and Tuot (1979) related the formation of clusters to unstable dispersions of solid in the gas. Also in the bubbling regime of a fluidized bed, the bubble formation was reported to provide the mechanism for clustering phenomenon or instability (Cocco et al., 2010). There is not much information about the mechanism of this phenomenon in other fluidization regimes. The diameter of clusters was found to be related to their gravity and drag forces introduced to them (Horio et al., 1992). In fact when the solid particles move as a bulk in the suspension, their velocity increases due to a lower drag force compared to when they move as individual particles (Helland et al., 2007; Manyele et al., 2002). Figure 3.8 shows images of clusters formed in a solid-gas fluidized bed.

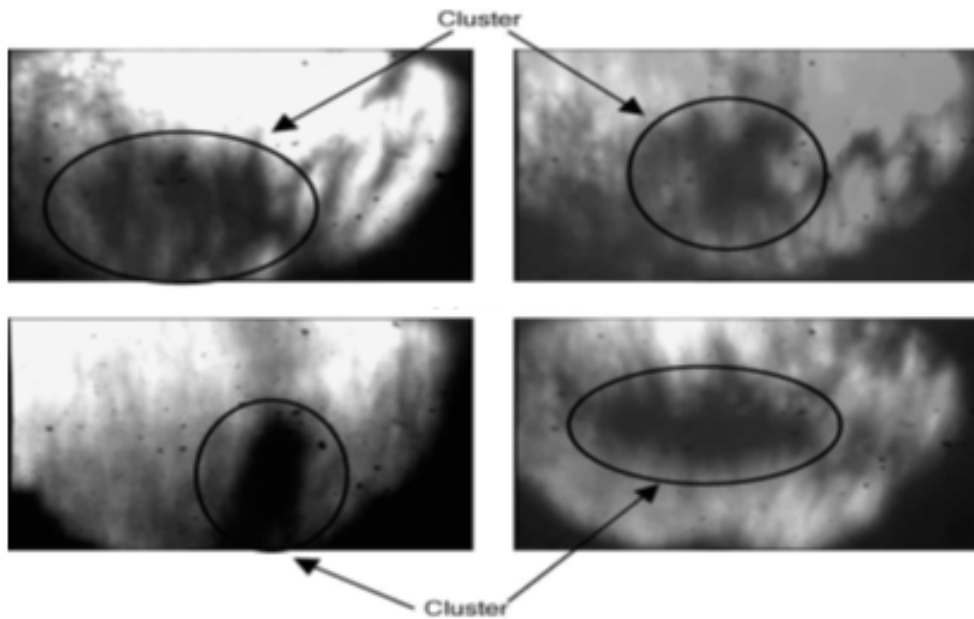


Figure 3.8: Formation of particles clusters in a gas-solid fluidized bed (Li et al., 1991).

### 3.2.3.2 Shear thinning behaviour of concentrated suspensions

Another phenomenon that bears similarities to bulk streaming is the shear thinning behaviour that occurs in concentrated suspensions. As shown in Figure 3.9, in concentrated suspensions which are in rest, or at low shear rates, the Brownian motion is dominant resulting in a random particles structure. In this random structure, the viscosity of the suspensions is independent of the shear rate. At high shear rates, the hydrodynamic interaction between the particles dominates the Brownian motion, and hence flow structures such as strings or sheets may develop. In these flow-structured suspensions, the viscosity is significantly lower than in the randomised-structured suspensions. Shear thinning behaviour occurs as a result of the transition between these two regimes, as the strings or sheets start to develop in the suspensions.

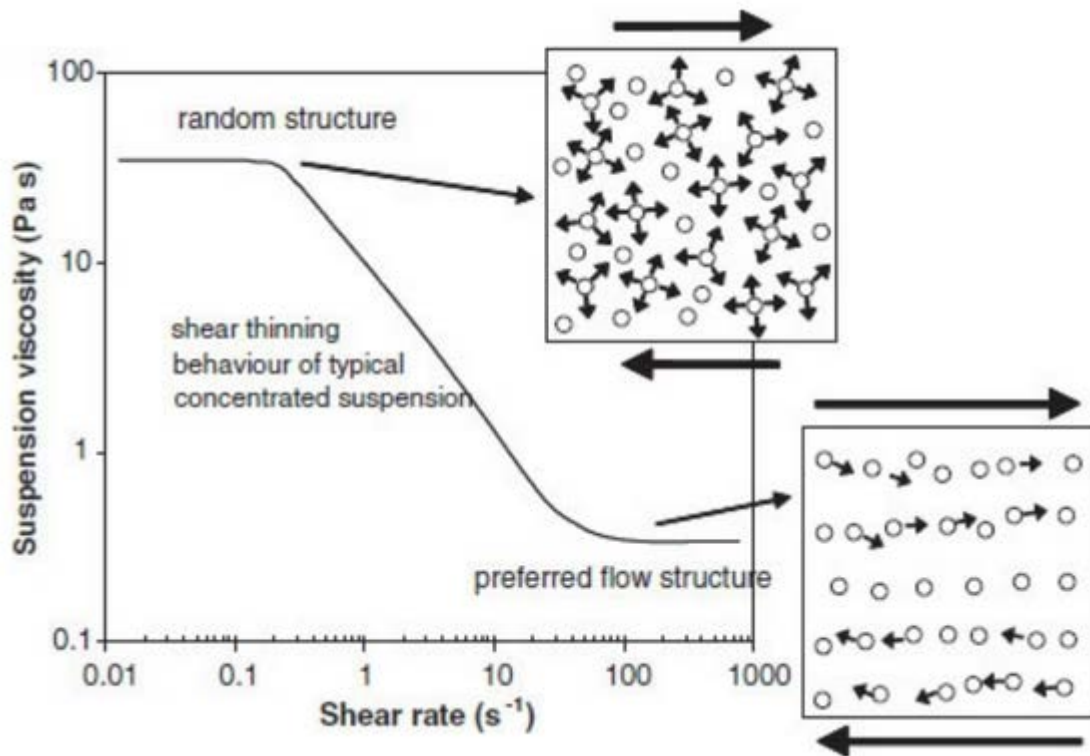


Figure 3.9: Shear thinning behaviour developed in a concentrated suspension at high shear rates (Rhodes, 2007).

### 3.3 Inclined settling

Inclined settling, first noted by Boycott (1920), provides an alternative method for increasing particle settling rates. Boycott observed that blood corpuscles settled much faster in an inclined tube rather than a vertical one. In one of his observations, after 20 hours, the clear proportion of the blood suspension was reported to be 4% in a vertical tube while 35% in the tube inclined about 45°. Since his observation, this effect is often referred to as the “Boycott effect”. At that time, this phenomenon was interpreted to depend on the vertical height of the suspension. Since Boycott’s observation, many investigations have been conducted to examine and analyse this method for increasing particle settling rates. It has practical application in the field of gravity settlers. Gravity settlers with inclined plates have a much higher effective area for sedimentation and hence increased capacity per unit footprint area occupied.

One explanation for the Boycott effect is that it is due to the ease of passage of the displaced water through the clear liquid zone beneath the downward facing wall of the inclined surface (Lundgren, 1927, 1928). In 1949, Kinoshita reported an enhancement in velocity up to about

100 times larger than that in a vertical container due to convection near the sedimentation boundaries, and assumed that this convection was the reason for the Boycott effect.

Many models have been proposed to predict the settling rates in inclined channels, but all have used some assumptions about the interface shape. Ponder (1925) and then Nakamura and Kuroda (1937) proposed the first models to predict inclined settling. Their model was for an inclined and rectangular tube, as shown in Figure 3.10 (a). In their models, the clear water emerging from the suspension was assumed to join the water layer ( $h$ ) above the horizontal interface. In other words, there was no layer of water underneath the upper wall of the vessel considered. At time  $t$ , the thickness of the clear water layer was  $h(t)$ , and after  $dt$ , the thickness of the clear water layer increases to  $h + dh$ . They proposed this thickness increases with time as:

$$h = (B + A \sin\Omega) [1 - \exp(-u (\sin\Omega) t/A)] \quad (3-2)$$

where  $\Omega$  is the inclination angle relative to the vertical,  $A$  is the width of the tube,  $B$  is the height of the suspension in the tube compared to its upper corner, and  $u$  is the settling velocity in a vertical tube.

The above equation estimates the upper limit for the sedimentation rate obtained in an inclined vessel. Later a lower and more accurate sedimentation rate was predicted by inserting an empirical coefficient into the above equation (Graham & Lama, 1963; Vohra & Ghosh, 1971). More recently, as shown in Figure 3.10 (b), the thin layer of clear water underneath the downward facing wall ( $h'$ ) was considered and combined with the clear water above the interface ( $h$ ), leading to a more complex model for predicting the sedimentation in inclined vessels (Zahavi & Rubin, 1975).

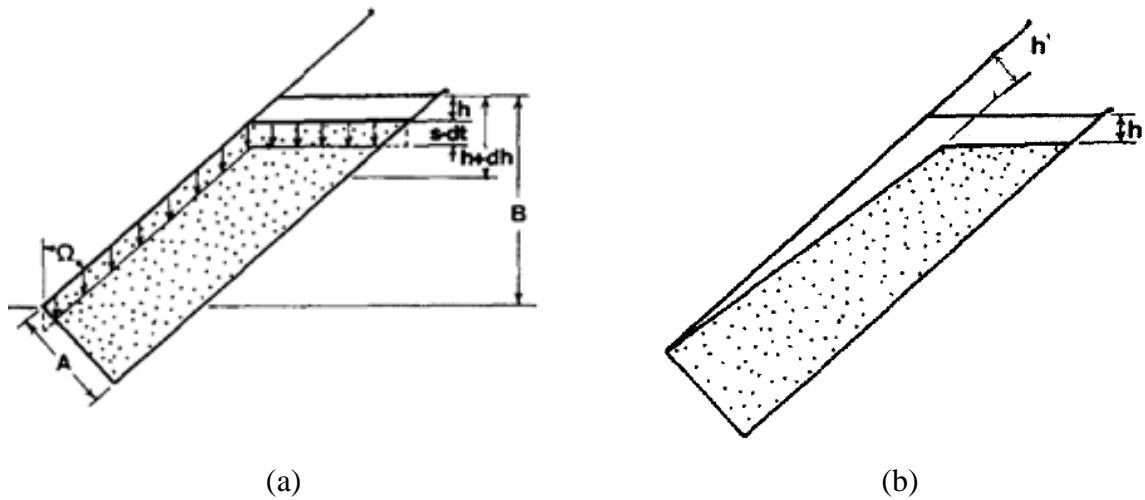


Figure 3.10: (a) Inclined settler related to the PNK theory (Hill et al., 1977), and (b) Inclined settling considering a more complex clear water-suspension interface (Zahavi & Rubin, 1975).

The settling of particles within inclined devices is best described using two dimensionless numbers: the Grashof number is the ratio of the (buoyant) gravity force to the viscous force, and the Reynolds number is the ratio of inertial force to the viscous force (Acrivos & Herbolzheimer, 1979; Davis et al., 1982). Ponder (1925) and Nakamura and Kuroda (1937) studied inclined sedimentation based on the geometrical and kinematic aspects and have suggested the velocity of the particles in an inclined container compared to that in a vertical one, known as the PNK theory, is:

$$U'/u = (1 + (B/A) \sin \Omega) \quad (3-3)$$

where  $U'$  is the settling velocity in an inclined container,  $u$  is the settling velocity in a vertical container,  $B$  is the vertical height of suspension,  $A$  is the space between the plates and  $\Omega$  is the angle of inclination with respect to the vertical. The validity of this approach has been examined in several studies. According to these investigations, this equation can be used to predict the settling velocity of particles in an inclined channel with the following characteristics (Acrivos & Herbolzheimer, 1979):

- Mono-disperse suspensions
- Uniform suspension concentration
- Low particles Reynolds number giving laminar flow

- Large ratio of sedimentation Grashof number to Reynolds number
- The interface between clear fluid and suspension remains stable

The Grashof number and Reynolds numbers are defined by:

$$Gr = l^3 g \rho_f (\rho_s - \rho_f) \phi_0 / \mu^2 \quad (3-4)$$

$$Re = \rho_f l u_t / \mu \quad (3-5)$$

where  $l$  is defined as the characteristic length of macroscale motions which Hill et al., (1977) reported to be equal to the vertical height of the suspension ( $B$ ),  $\phi_0$  is the initial volume fraction of solids in suspension, and  $\rho_f$  and  $\rho_s$  are the liquid and solid densities, respectively. The particle terminal settling velocity is shown by  $u_t$  and defined as equation 2-10. So the ratio of Grashof number to Reynolds number is calculated as:

$$A = l^2 g (\rho_s - \rho_f) \phi_0 / (\mu u_t) \quad (3-6)$$

In terms of the two dimensionless numbers which are usually used to explain the settling behaviour in a tilted container, a Grashof number equal to zero indicates non-convective flow. As the Grashof number increases the sedimentation time shortens. Further research on the settling rate of particles in a container with different shapes and orientation demonstrated that the settling velocity of particles in an inclined container may be several time faster than that in a vertical container due to the enhanced convection (Hill et al., 1977).

Most studies of inclined settling have been for mono-dispersed suspensions (Probstein et al., 1977; Probstein & Hicks, 1978; Herbolzheimer & Acrivos, 1981). Poly-dispersed suspensions, containing particles which are denser than the fluid, settling on an inclined surface have been studied by Davis et al., (1982) and Schaflinger (1985).

A theoretical investigation of such systems to show the sedimentation in inclined channels was conducted (Davis et al., 1982; Davis & Gecol, 1996). For simplicity, the hindered settling velocity of particles was assumed to be given by the settling velocity calculated by Stokes law multiplied by a parameter related to total solids fraction in the suspension. The

settling behaviour of  $N$  distinct particle types was firstly calculated and then extended to a continuous size and density distribution. Several regions of different concentration were formed in the tilted container. All species exist in the lowest region. The next region does not contain the particles with highest settling velocity (i.e.  $N - 1$  species are in this region,  $N - 2$  species in the next region and  $N - 3$  species in the next). In the highest region, only particles with the lowest settling velocity can be seen. In addition sediment appears on the upward facing surface, and water exists in the higher region and beneath the downward facing plate. Therefore, the concentration of each species in each region was measured so that the settling velocity of the particles could be calculated. The schematic representation of this method for  $N = 3$  is shown in Figure 3.11.

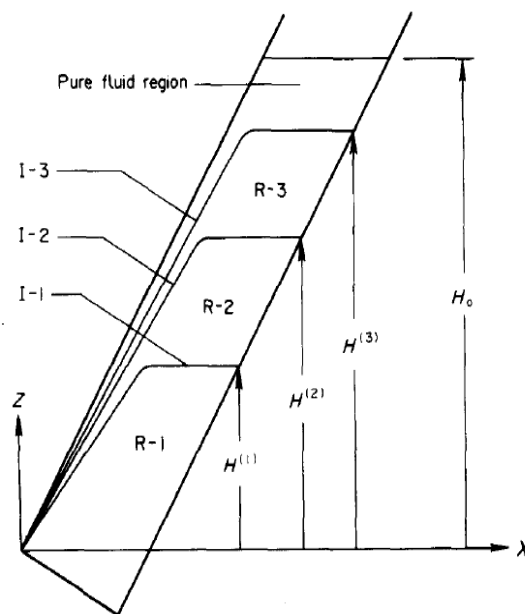


Figure 3.11: A simplified model for predicting the particles settling velocity in an inclined container (Davis et al., 1982).

More recently, studies have focused on the operational aspects and applications of inclined settling, examining the effects of operating conditions on their performance. It has been found that for a suspension containing light and heavy particles, the efficiency of the separator depends mostly on the feed rate, the ratio of the underflow rate to the feed rate, referred to as the split ratio, the solid content in the feed and degree of inclination. Because of hindered settling, increasing the feed solids content decreases the recovery. Also beyond an optimum feed rate, the recovery enhancement decreased with increasing feed rate. The degree of inclination also has a significant effect on the recovery and concentration of particles in the

underflow (Masliyah et al., 1989). When an inclined settler was used to classify particles, recycling the underflow stream was found to increase the separation efficiency. A recycle stream is advantageous where the fine particles have the chance to be recovered from a coarse stream. These experiments were conducted in a rectangular settler for a dilute suspension of polystyrene bead particles and clearly showed the benefits of the recycle stream (Zhang & Davis, 1990).

Increasing the effective area and decreasing the distance of settling were reported as two reasons for the enhancement of sedimentation rate in inclined containers (Davis & Gecol, 1996). Unlike many separation processes, at a constant feed rate, the efficiency of classification (defined here as the mass of fine particles in the fine fraction divided by that in the coarse fraction) was shown to increase by increasing the feed solids concentration. At a higher feed solids concentration, there is a higher hindered settling effect and hence a lower particle settling velocity is obtained. Therefore fine particles are less likely to enter the underflow, leading to an increase in the efficiency. Also by increasing the fraction of slower settling particles in the feed, more hindered settling occurs which results in a higher proportion of slow settling particles reporting to the overflow. In conclusion, if the aim is to separate slow settling particles from faster settling particles, the efficiency can be improved by increasing the solid content of the feed (Davis & Gecol, 1996). Figure 3.12 shows a diagram of their inclined settler used to classify a suspension of four different species.

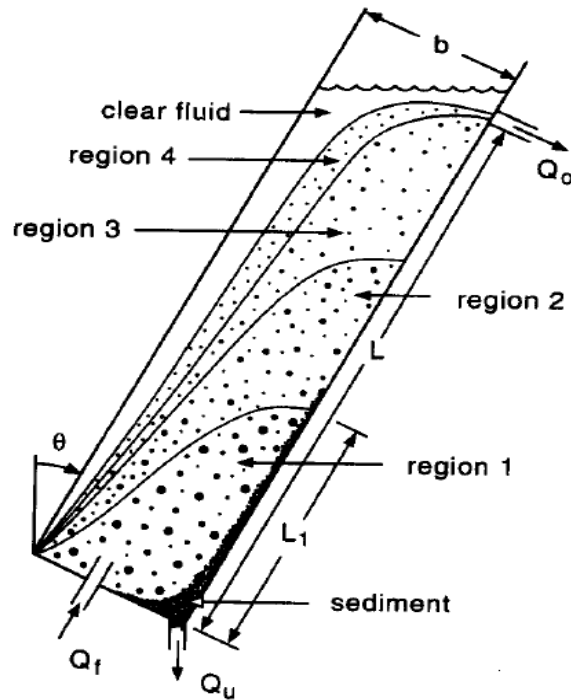


Figure 3.12: A continuous inclined settling of a suspension with four different species.  $Q_o$  was adjusted such that only the two smallest species could be carried to the overflow (Davis & Gecol, 1996).

Studies on inclined settlers led to the development of the lamella thickener, used in solid-liquid separation. Of course there remained a problem in scaling-up the system to ensure the delivery of a uniform feed to multiple inclined channels, essential for achieving a sharp overall separation. The REFLUX™ Classifier, which incorporates a fluidized bed system, and overflow weirs across each channel, addressed this problem.

### 3.4 REFLUX™ Classifier

In 2000, Nguyentranlam and Galvin investigated the development of an innovative method of particle separation based on density and size. They aimed to develop a classifier operating at higher throughput that provided a better separation compared with conventional fluidized beds. They examined the combination of the high segregation rate obtained in inclined channels with the separation achieved in conventional fluidized bed technology. Their preliminary results and their simple model showed the large potential of the system for classifying particles based on their density and size.

Galvin and Nguyentranlam (2002) extended their previous work by investigating the influence of parallel inclined channels on a fluidized bed as shown in Figure 3.13. The inclined channels were placed at different vertical positions. Interestingly, the inclined system prevented the solids from being elutriated into the overflow. Suspensions with different concentrations could be formed even at superficial velocities higher than the particle terminal settling velocity. Therefore this novel system is also capable of processing higher feed throughputs when compared to conventional fluidized beds. In this system, relatively dense particles settle down onto the channels and slide down the upward facing surface of the inclined plates and return to the bed. However, relatively light particles are not captured by the channels and are elutriated from the bed. A continuous feed to the lamella plates leads to mixing, ensuring that the entrained fine particles in the lower zone can be separated and returned to the channels. This self-recycling effect led to the term “REFLUX™” and hence the separator was named the REFLUX™ Classifier (RC™).

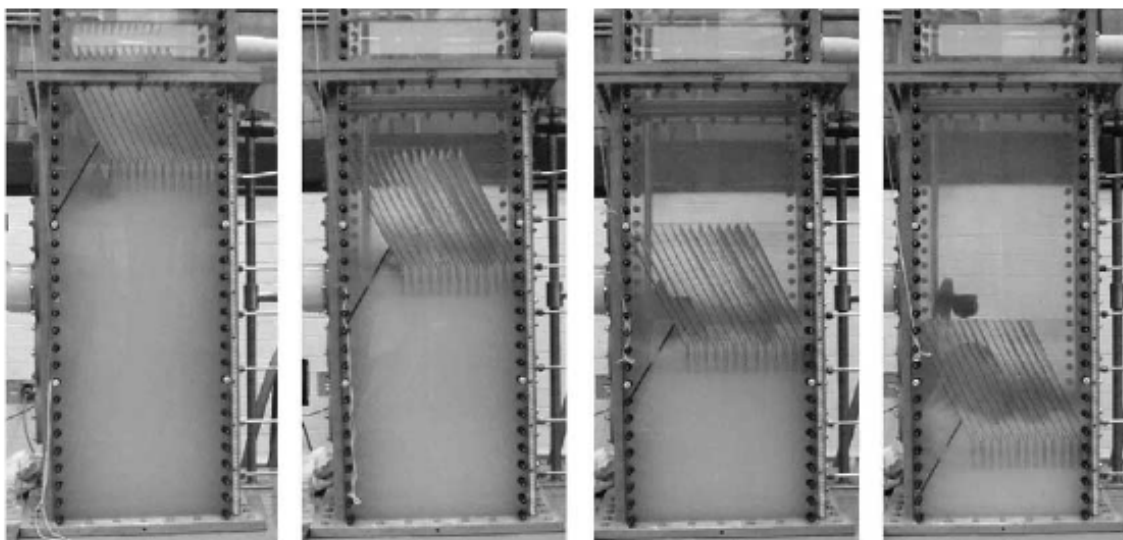


Figure 3.13: A fluidized bed with a system of inclined channels installed at its different vertical positions (Galvin & Nguyentranlam, 2002).

In order to find a relationship between the segregation through the inclined channels and the fluidization in the fluidized bed, a first-order model was developed for a simplified system as shown in Figure 3.14(a). They used a few assumptions such as having a uniform velocity profile through the channel, and perfect mixing between the solids that slide down on the upward facing plate and the suspension in the fluidized bed in order to simplify the analysis (Galvin & Nguyentranlam, 2002).

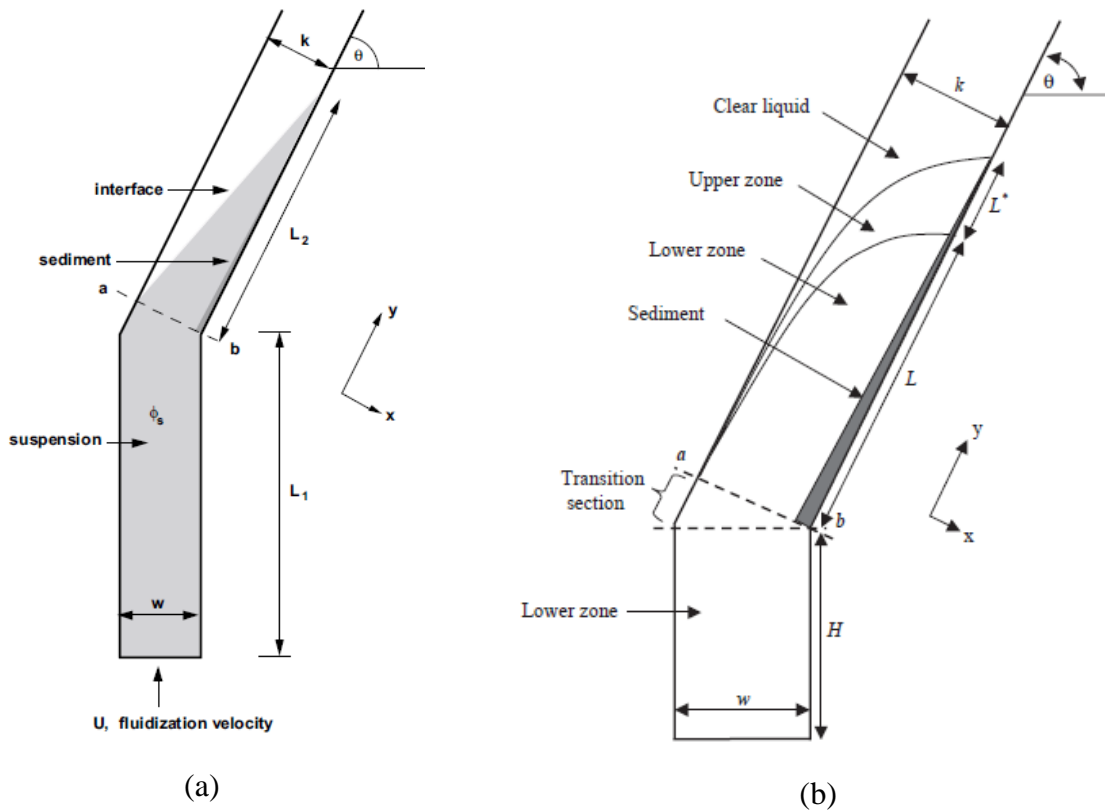


Figure 3.14: (a) A schematic of a simplified system containing an inclined channel and a fluidized bed (Galvin & Nguyentranlam, 2002), and (b) a more complex analysis of the system (Doroodchi et al., 2004).

The kinematic study on the bed expansion in a liquid fluidized bed connected to an inclined channel was theoretically and experimentally extended using mono- and bi-dispersed suspensions (Doroodchi et al., 2004). As shown in Figure 3.14(b), in their theoretical model, they assumed different zones of suspension formed through the channel, and considered the effects of the suspension length up through the inclined channel. In 2005, a fluidized bed coupled with inclined channels was used to for the first time to examine the classification of particles in a continuous steady-state process with both overflow and underflow removal. The aim was to achieve a sharp separation at a high feed solids concentration (Doroodchi et al., 2005). This system named the REFLUX™ Classifier provided a higher segregation rate due to the enhanced sedimentation area given by the inclined channels. A full scale version of this system was then successfully trialled for beneficiation of coal in the size range of 0.25-2.0 mm. The separation performance was found to be equivalent to that at the pilot scale in terms of  $d_{50}$  and  $E_p$  (Galvin et al., 2005).

### 3.4.1 The Laskovski et al. correlation

Laskovski et al. (2006) studied the semi-batch elutriation behaviour of particles from the RC<sup>TM</sup> and fitted their data to an empirical model that covered a wide range of experimental conditions (Eq. 3.7). This study was the first to provide a detailed assessment of the separation efficiency of a REFLUX<sup>TM</sup> Classifier with multiple inclined channels. A schematic diagram of the RC<sup>TM</sup> is shown in Figure 3.15.

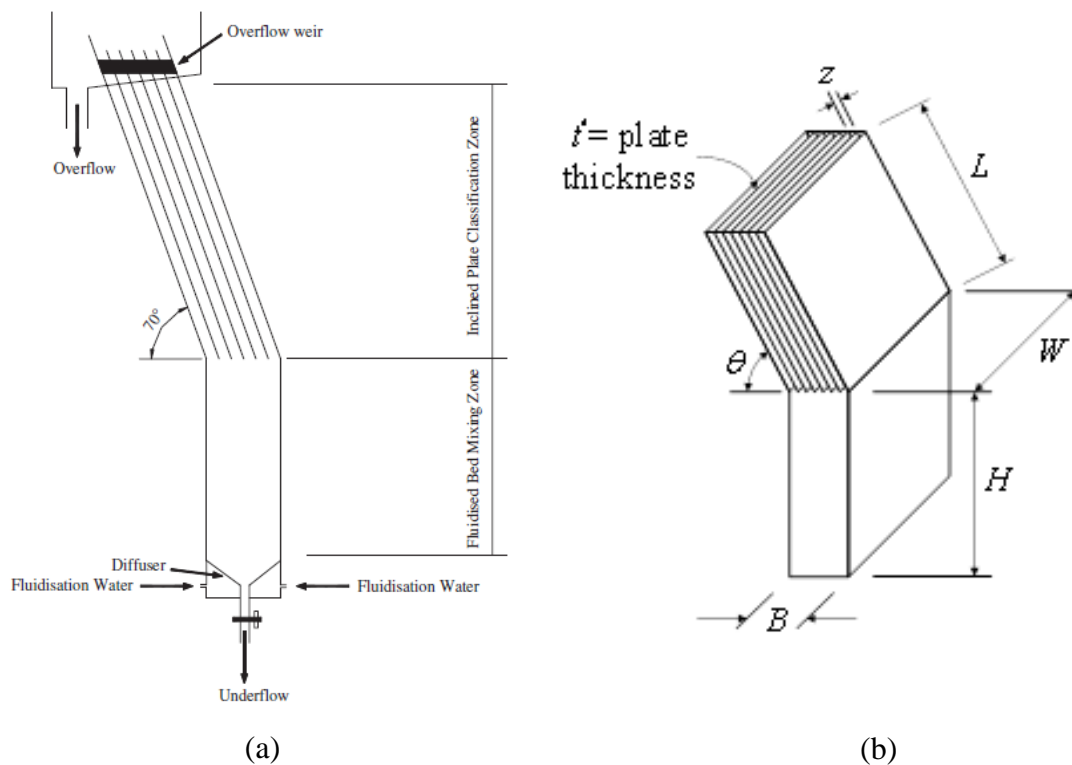


Figure 3.15: (a) A representation of the REFLUX<sup>TM</sup> Classifier as set up for semi-batch fractionation tests. In semi-batch tests, there is no underflow removal and no feed addition other than the initial batch of feed solids (Laskovski et al., 2006) & (b) A schematic diagram of the REFLUX<sup>TM</sup> Classifier showing its main dimensions (Li et al., 2014).

First an expression for describing the theoretical throughput advantage ( $F'$ ) was developed based on the segregation area of the inclined plates. Increasing the number of plates whilst keeping the total size of the unit constant, reduces the plate spacing  $z$  and thus increases the aspect ratio  $L/z$  and also the effective segregation area of the inclined channels. A kinematic approach was used to find the theoretical relationship between the throughput advantage and

aspect ratio  $L/z$ . This is an alternative expression to the PNK theory (Equation 3-3), given below as Equation 3-7.

$$F' = 1 + (L/z) \cos\theta \sin\theta \quad (3-7)$$

where  $\theta$  is the angle of inclination with respect to the horizontal.  $L$  and  $z$  are the length of the plates and the perpendicular distance between the plates, respectively. Equation 3-7 gives the increase in effective settling area compared to the area provided by a conventional fluidized bed with the same cross-section in the vertical section.

Equation 3-7 predicts that the throughput advantage should be able to be increased indefinitely by adding more plates to reduce the plate spacing  $z$ . However, not all particles that settle on the surface necessarily slide all the way back into the vertical section. As discussed later in Section 3.4.2, the high shear forces in narrow channels increase the tendency of particles to be resuspended (Acrivos & Herbolzheimer, 1979; Rampall & Leighton, 1994) and so there is a limit to the benefit of increasing the aspect ratio. Beyond this limit the particles tend to be hydraulically conveyed to the overflow, and hence the separation size decreases. Therefore the term “segregation efficiency” was introduced as a measure of how close the performance is to the theoretical throughput benefit predicted by the simple theory behind Equation 3-7.

The actual throughput advantage can be defined as the ratio of the superficial fluid velocity up through the fluidized bed and the terminal velocity of the largest particles reporting to the overflow. In a conventional fluidized bed, this ratio is equal to 1 (Callen et al., 2007). The segregation efficiency  $\eta$  is then defined as the ratio of the actual throughput advantage to the theoretical throughput advantage predicted by Equation 3-8 (Laskovski et al., 2006):

$$\text{Segregation efficiency } \eta = (U/u_t)/F' \quad (3-8)$$

$F'$  is the theoretical throughput advantage and  $U/u_t$  is the actual throughput advantage. The Buckingham-II dimensional analysis theorem was used to find a general expression for segregation efficiency. This efficiency is predicted to be a function of the particle Reynolds number, Froude number, the aspect ratio, and the  $d_{50}$ . However, when Laskovski et al. (2006)

fitted their experimental data, the influence of the Froude number was found to be insignificant. The general correlation they found for predicting the segregation efficiency is:

$$\eta = 1 / (1 + 0.133 Re_p^{1/3} \cos\theta (L/z)) \quad (3-9)$$

Hence using equations 3-7, 3-8 and 3-9, the actual throughput advantage is:

$$U/u_t = [1 + \cos\theta \sin\theta (L/z)] / [1 + 0.133 Re_p^{1/3} \cos\theta (L/z)] \quad (3-10)$$

In the limit as the aspect ratio approaches infinity, the actual throughput advantage approaches:

$$U/u_t = 7.5 Re_p^{-1/3} \quad (3-11)$$

Although the re-suspension of particles decreases the segregation efficiency, the performance of the separation based on the density becomes more effective. Using the force balance on a particle suspended in a fluid given by equation 2-7, and applying the correlations for  $C_D$  (Table 2.1) for Stokes' and Newton's regimes, and  $C_D = 18.5 / Re_p^{0.6}$  proposed by Vance and Moulton (1965) for the intermediate regime, the proportionality of terminal settling velocity as a function of particles size and density is given by equation 3-12. Then using equation 3-11, the proportionality of the superficial velocity required to achieve a separation as a function of particle density  $\rho_s$  and size  $d_p$  in the RC<sup>TM</sup> can predicted by Equation (3-13):

$$u_t \sim (\rho_s - \rho_f)^{1/(2-n)} d_p^{(1+n)/(2-n)} \quad (3-12)$$

$$U \sim (\rho_s - \rho_f)^{2/(6-3n)} d_p^{n/(2-n)} \quad (3-13)$$

where  $n$  depends on the particle Reynolds number ( $n = 1$  for Stokes' law regime, 0.6 for intermediate regime, 0 for Newton's regime). For a conventional fluidized bed, the superficial velocity is directly related to the terminal velocity  $U \sim u_t$ , and  $u_t$  and  $d_p$  are related by  $u_t \sim d_p^{(1+n)/(2-n)}$ . Hence, the dependence of superficial velocity on the particles size in the RC<sup>TM</sup> is less than that in a conventional fluidized bed. Table 3.2 summarises the dependency of superficial velocity on the particles size in a conventional fluidized bed and also the REFLUX<sup>TM</sup> Classifier for different regimes. This table shows that the separation efficiency

depends less on the particle size (Laskovski et al., 2006). It is clear that for  $Re_p > 508.4$ , the superficial velocity in the RC<sup>TM</sup> is independent of particle size, which is used as an advantageous phenomenon in processes in which the aim is a separation based on particle density.

Table 3.2: The dependency of the superficial velocity in fluidized beds and the REFLUX<sup>TM</sup> Classifier on particles size at different regimes (Laskovski et al., 2006).

Regime	Conventional fluidized bed	REFLUX <sup>TM</sup> Classifier
$Re_p < 1.9$ ( $n = 1$ )	$U \sim u_t \sim d_p^{2.0}$	$U \sim d_p^{1.0}$
$1.9 < Re_p < 508.4$ ( $n = 0.6$ )	$U \sim u_t \sim d_p^{1.1}$	$U \sim d_p^{0.43}$
$Re_p > 508.4$ ( $n = 0$ )	$U \sim u_t \sim d_p^{0.5}$	$U \sim d_p^{0.0}$

The potential of the REFLUX<sup>TM</sup> Classifier using an aspect ratio of about 200 for beneficiation of a minerals sand feed was studied by Zhou et al. (2006). At a throughput of 21 t/(m<sup>2</sup> h), a recovery of minerals about 97% was obtained. A very high product concentration of about 100% for the particle size between 90 and 180  $\mu\text{m}$  was also achieved. This work experimentally showed that in separating particles with a same size range but with different densities, a REFLUX<sup>TM</sup> Classifier with a high aspect ratio provided a more efficient separation. This finding was compatible with the Laskovski's findings that in a system with a high aspect ratio, re-suspension of low density particles facilitates separation based on density and decreases the influence of particles size.

### 3.4.2 Elutriation models for laminar high-shear flow in narrow channels

Galvin et al., (2009) developed a theoretical model of the elutriation behaviour of particles in the REFLUX<sup>TM</sup> Classifier when the channels are narrow enough to promote laminar flow. Assuming a laminar flow in a channel, the local velocity of the fluid introduced to the particle ( $u$ ) is measured by Equation (3-14) (Bird et al., 1976):

$$u = 6Ux(1 - x/z)/z \quad (3-14)$$

when  $U$  is the superficial velocity,  $x$  is the particle distance from the upward facing plate, and  $z$  is the channel spacing. At the critical condition for elutriation to occur, the local velocity would be equal to the terminal velocity of the particle. When the flow through the channels is laminar, near the wall ( $x \ll z$ ), the velocity gradient is approximately linear,

$$u = 6Ux/z \quad (3-15)$$

so particles resting on the inclined plates experience a local flow velocity  $u$  proportional to their diameter (Figure 3.16). It was assumed that a particle will elutriate when the tangential component of its settling velocity,  $u_t'$ , is less than the local velocity. This condition causes the power-law dependence of elutriation velocity on particle size to decrease by one. Hence the elutriation velocity should become more sensitive to particle density. In particular, for particles in the intermediate settling regime where the dependence of  $u_t$  on particle diameter is only  $\sim 1.1$  (Table 3.2), the dependence of elutriation velocity on size in a laminar flow field is predicted to drop to close to zero, making the separation almost entirely dependent only on particle density. These predictions were confirmed experimentally in semi-batch elutriations tests where it was found that narrow channels leads to a remarkable suppression of the influence of particle size on the separation density, as shown in Figure 3.17 (Galvin et al., 2009). Figure 3.17 also shows that the dependence of elutriation velocity on the particles size in a conventional elutriator is significantly large. So, a wide size range of particles of a given density are conveyed within a narrow range of hydraulic velocities. It should also be noted that the high shear rate through the inclined channels facilitates the flowability of the suspension and hence assists to prevent channel blockages. Also a more uniform flow is obtained through the narrow channels due to the larger pressure drop (Galvin et al., 2009). Later work confirmed that these benefits of narrow channels were also conferred in processing fine particles (Walton et al., 2010) and continuous steady-state separations (Galvin et al., 2010).

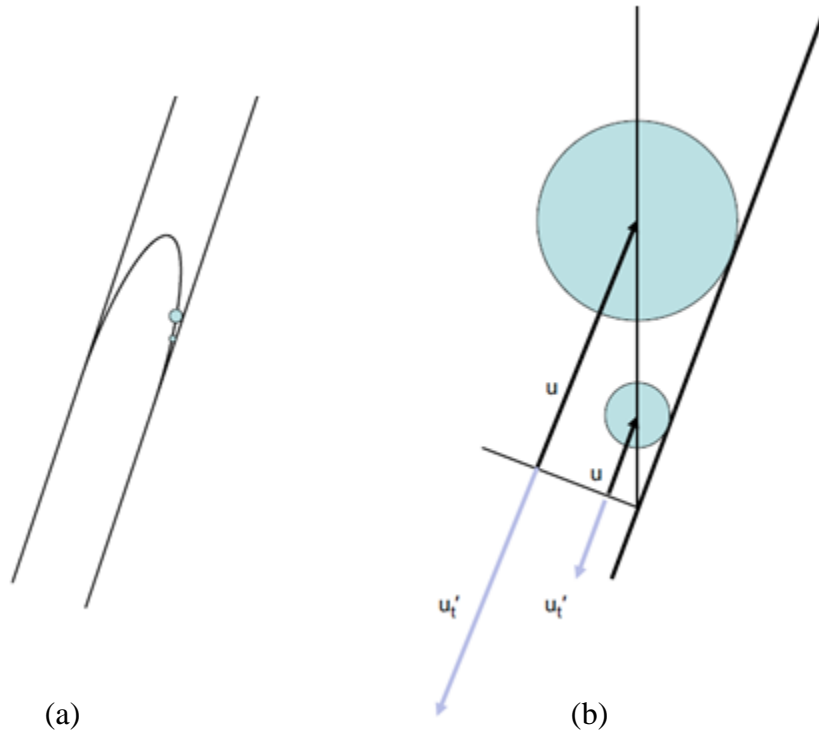


Figure 3.16: (a) The parabolic velocity profile for laminar flow in a narrow channel gives (b) a near linear velocity field close to the wall, such that the local conveying velocity  $u$  experienced by particles is approximately proportional to their size (Galvin et al., 2009).

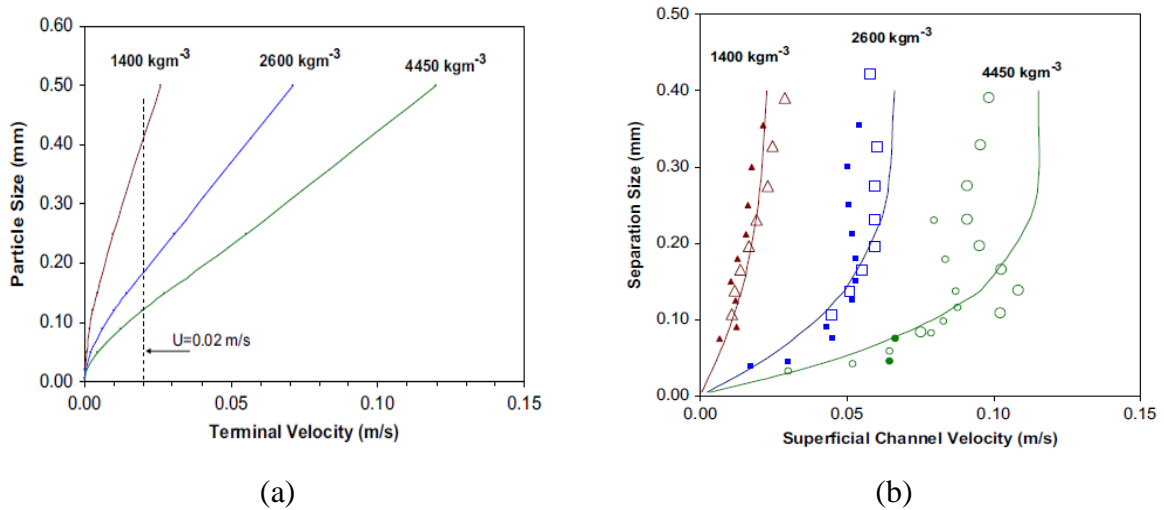


Figure 3.17: The dependency of elutriation velocity on the particles size for (a) a conventional elutriator and (b) a REFLUX™ Classifier with 1.77 mm spacing (Galvin et al., 2009).

Galvin and Liu (2011) developed a more accurate model of particle elutriation by including the effect of the shear-induced lift force. According to this model, not only does the local flow velocity need to exceed the tangential component of the particle's settling velocity, but there must also be a shear-induced lift force that is large enough to lift the particle off the surface.

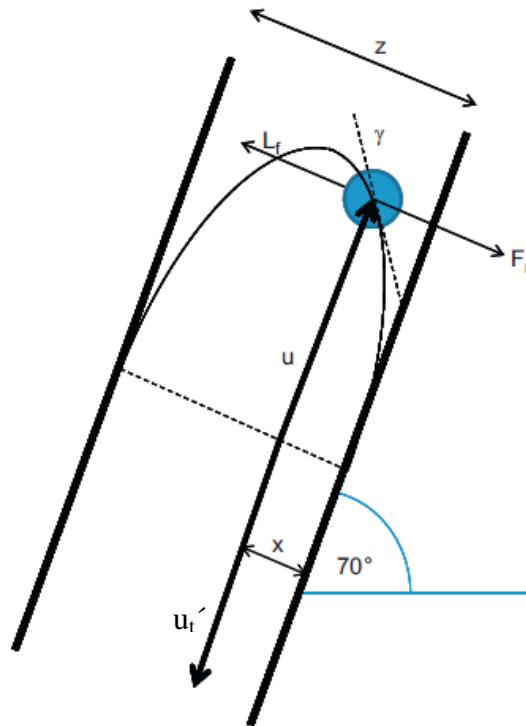


Figure 3.18: The equilibrium condition for a particle in a channel subjected to a laminar flow (Galvin & Liu, 2011).

As shown in Figure 3.18, the critical lift force ( $L_f$ ) should be also equal and opposite to the component of the particle's net weight force acting perpendicular to the plate ( $F_n$ ). They proposed an equation for the calculation of lift force as:

$$L_f = 0.0567 Re_p^{0.8} \rho \gamma^2 d_p^4 \quad (3-16)$$

where  $\gamma$  is the shear rate calculated by differentiating equation 3-14:

$$\gamma = 6U (1 - 2x/z)/z \quad (3-17)$$

Based on equations 3-16 & 3-17 narrowing the channels increases the shear rate, leading to an increase in the lift force introduced to the particle. Therefore the vertical component of the lift force ( $L_f$ ) would increase in this case, and hence the particle is more easily elutriated (Galvin & Liu, 2011).

### **3.5 Combined effects of Inclined Settling and Bulk Streaming Motion**

The batch settling behaviour of concentrated bi-dispersed suspensions of positively and negatively buoyant particles in an inclined settler was studied by Law et al. (1988). They measured the variation of bed height for each component versus time to indicate the velocity of each species, as shown in Figure 3.19. The heavy particles were dyed in order to be visually distinguished from the white light particles.

They carried out a comprehensive experimental and theoretical investigation on settling and rising velocity of suspensions at different concentrations of light and heavy particles in either vertical or inclined settlers. The Boycott effect was investigated by changing the inclination angle of the channels. They found that total solids concentration less than 16 vol.% hindered the settling and rising velocities of particles (Figure 3.19a). They were also the first to provide a photographical evidence of the bulk streaming motion phenomenon in systems with total solids concentrations greater than 35 vol.% (Figure 3.19b).

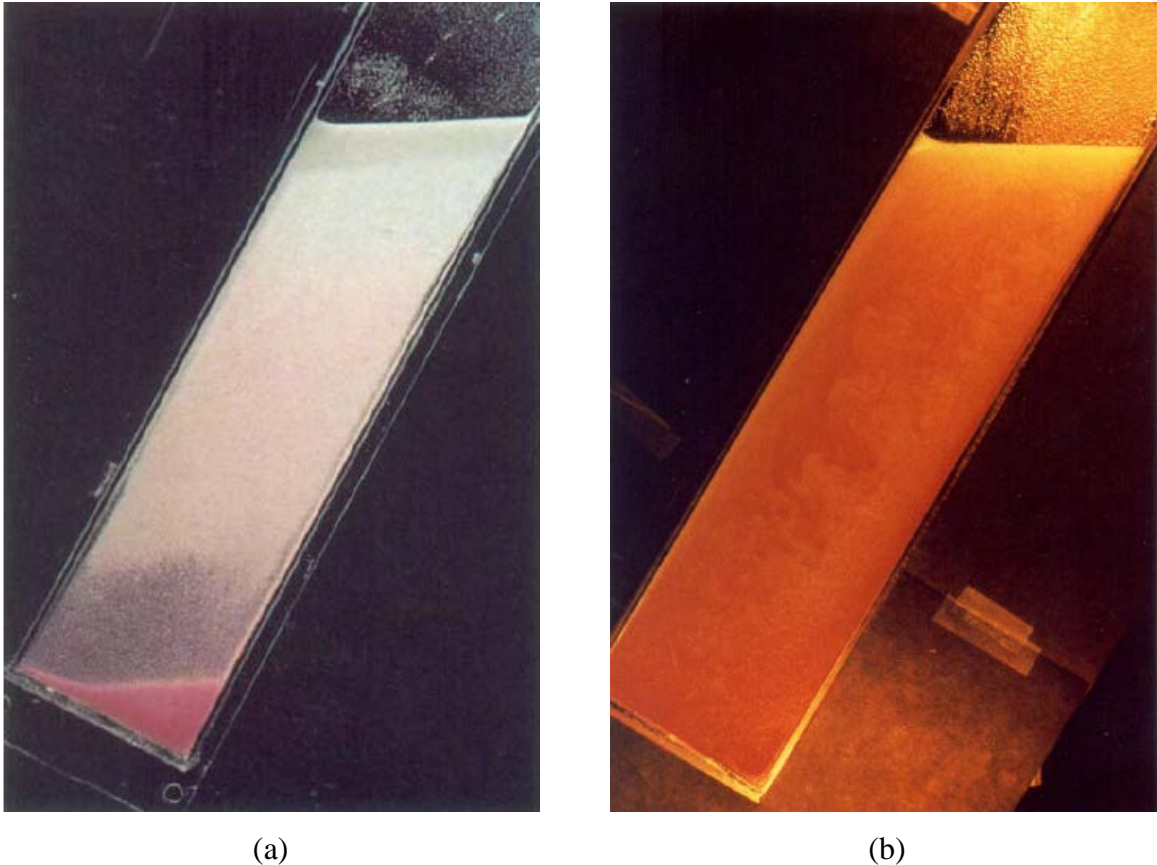


Figure 3.19: A system of light (white) and heavy particles (pink) in an inclined vessel at volume fractions of (a) 0.08 for each one, and (b) 0.20 and 0.15 for light and heavy ones, respectively (Law et al., 1988).

They adopted the PNK theory for the bi-dispersed systems, and found it worked well in predicting the experimental data when the total solids concentration were lower than 16 vol.%, while for higher concentrations, they assumed that an additional mechanism of the bulk streaming motion phenomenon should be considered.

MacTaggart et al., (1988) extended the initial work of Law et al. (1988), by evaluating the influences of both Boycott and streaming phenomenon on separation of particles in two systems. They investigated the effects of the vessel's dimensions, inclination angles and initial solids concentrations on the separation performance. The properties of the system used in their study are indicated in Table 3.3. Both phenomena were reported to affect the settling and rising velocity of the heavy and light particles, depending on the channel geometry, particle and fluid properties and the degree of inclination. A sample of their results is shown in Figure 3.20. This figure shows the velocity of light particles at different inclination angle compared to their terminal velocity ( $u_{lb}^0/u_{1m}^0$ ) at different concentrations of heavy particles. It

was found that by increasing the inclination angle from vertical, the light particle velocity increases and reaches a peak depending on the initial concentration of the species. At an inclination angle of 20° from the vertical, at the heavy particle concentrations of 10 vol.%, 15 vol.% and 20 vol.%,  $u_{lb}^{\theta}/u_{lm}^0$  of about 2 times, 4 times and 5 times were achieved. These enhancements reflect the combined effects of the inclined settling and the bulk streaming motion. It is noted again that the enhancement in particle velocity was reported to be different for various systems.

Table 3.3: Properties of the system and geometrical dimensions of the vessels used to examine the combined effects of Boycott and bulk streaming motion phenomenon (MacTaggart et al., 1988).

	Particle species		Suspending fluid
	Polystyrene (PS)	Polymethyl methacrylate (PMMA)	Aqueous NaCl
<b>System 1</b>			
$\rho$ (g/cm <sup>3</sup> )	1.05	1.186	1.120
$d_p$ (cm)	0.0241	0.0231	-
$\mu$ (g/(cm s))	-	-	0.0141
<b>System 2</b>			
$\rho$ (g/cm <sup>3</sup> )	1.050	2.835	1.23
$d_p$ (cm)	0.0438	0.0133	-
$\mu$ (g/(cm s))	-	-	0.1543
<b>Geometry</b>	Spacing (cm)	Width (cm)	Length (cm)
System 1	4	6	80
System 2	3	8	80

This work (MacTaggart et al., 1988) was the first to investigate the combination of bulk streaming motion phenomenon and the Boycott effect on the sedimentation of a bi-dispersed suspension. The works of Law et al. (1988) and MacTaggart et al. (1988) were both on batch systems. There are no published studies of how the Boycott and bulk streaming motion effects influence continuous processes. There are also no data or theories to specify the critical concentrations under different operating conditions required for the streaming phenomenon to develop in an inclined settler.

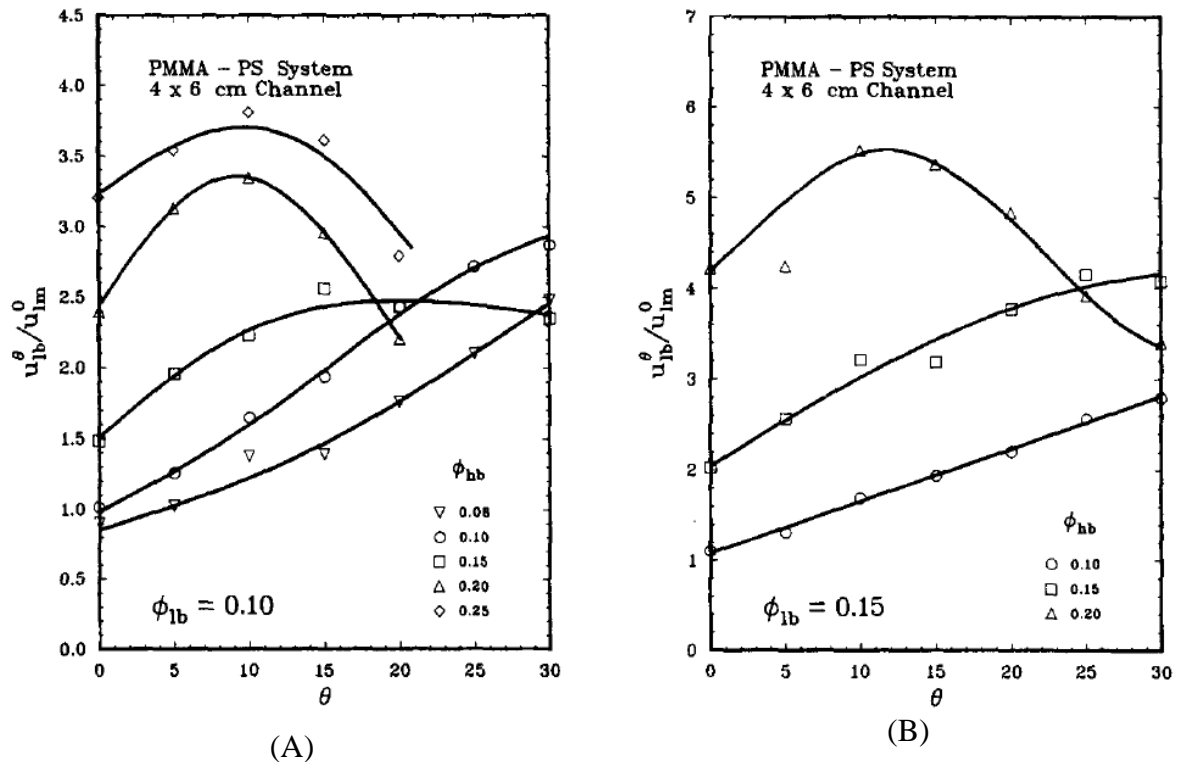


Figure 3.20: Dependency of the light particles' velocity relative to their terminal velocity ( $u_{lb}^{\theta}/u_{lm}^0$ ) on the angle of inclination  $\theta$  of the channel for different initial concentrations of heavy particles  $\phi_{hb}$  (MacTaggart et al., 1988).

Note that when bulk streaming occurs in an inclined channel, the concentrations of particles near the upward and downward facing plates are not the same as their initial concentrations. The study (MacTaggart et al., 1988) showed that the channel's dimensions played a strong role in determining whether bulk streaming motion occurred, which may reflect the effect of various concentrations near the walls for vessels with different dimensions.

### 3.6 The Potential for separating cenospheres from fly ash in an Inverted REFLUX™ Classifier

Figure 3.21(a) shows a schematic diagram of an Inverted REFLUX™ Classifier (IRC™). The inverted REFLUX™ Classifier can potentially provide some advantages over the standard REFLUX™ Classifier when it comes to the recovery of positively buoyant particles. Feed enters into the vertical section of the IRC™, where most of the cenospheres and some fine fly ash will rise towards the product exit, and most of the heavy fly ash particles and some fine entrained cenospheres are carried downwards to the inclined channels section. A

bed of low density particles can form in the upper part of the vertical section. Here wash water entering uniformly from the top of the IRC™ washes the unwanted entrained high-density material back into the underflow. The strong segregation rate in the inclined channels helps prevent the loss of any entrained fine cenospheres by returning them to the fluidized bed section of the IRC™ from where they can find their way back up to the low-density product. Therefore in this thesis, owing to the low density of the cenospheres relative to water, the performance of an inverted REFLUX™ Classifier was investigated.

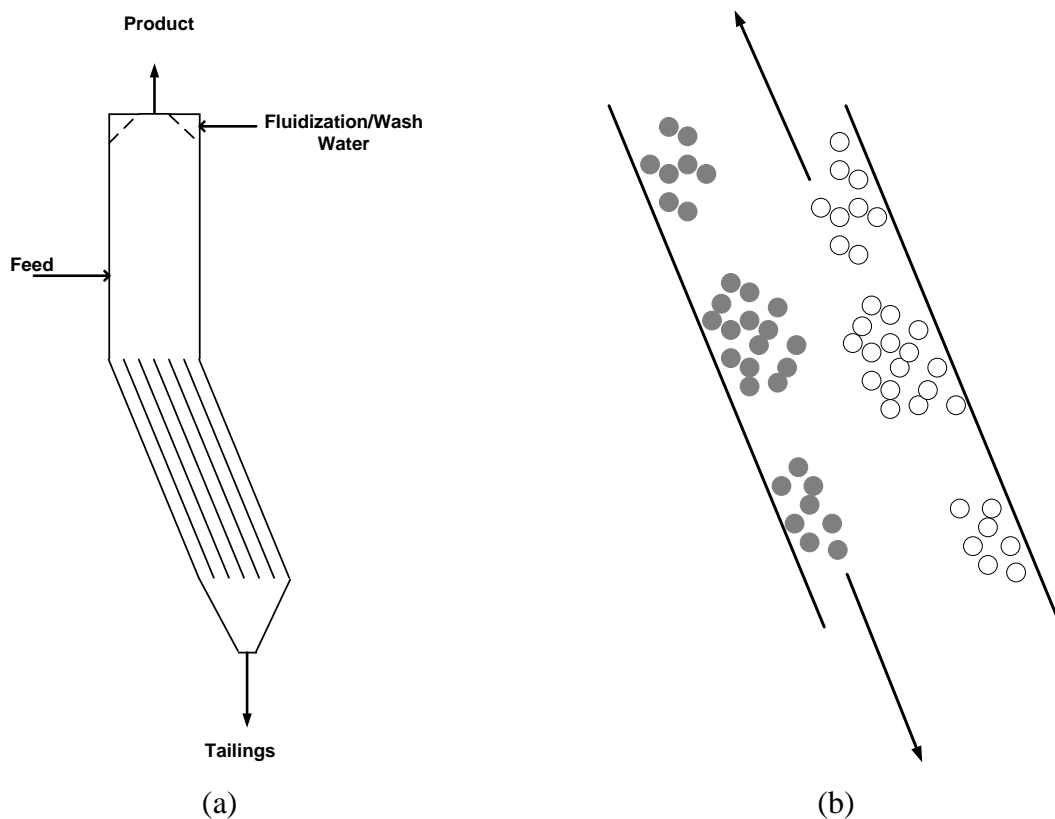


Figure 3.21: (a) A schematic diagram of an Inverted REFLUX™ Classifier and (b) bulk streaming motion phenomenon hypothesised to occur for ● negatively buoyant fly ash and ○ positively buoyant cenospheres.

The concentration of positively buoyant cenospheres in fly ash is of the order of about 1 wt.% or about 2 vol.%. So according to the literature, it seems this would not be sufficient to trigger the bulk streaming phenomenon. However in a continuous process, the reflux of captured buoyant particles back into the vertical section has the potential to increase the concentration of cenospheres inside the IRC™. In addition the very large density difference between fly ash and cenospheres can also increase the likelihood of streaming, despite the

low feed concentrations. A simple representation of the phenomenon hypothesised to occur for a mixture of fly ash and cenospheres is presented in Figure 3.21(b).

### **3.7 Summary**

In this chapter, two important effects that enhance the settling velocity of particles in suspensions were reviewed. First, in concentrated bi-disperse suspensions of particles of positive and negative buoyancy, there is a tendency for particles to move as a stream or viscous finger, referred to as bulk streaming motion. The origins of this phenomenon were explained by Batchelor and Van Rensburg (1986). This phenomenon was found to develop at specific species concentrations due to instabilities in the suspensions. However, whilst an empirical regime map was developed, there is a lack of any well-developed theory for making predictions about when this phenomenon will occur. This makes it hard to predict whether it will occur in a continuously operated inverted REFLUX™ Classifier, where conditions are quite different to previous studies of vertical batch settling.

The second important phenomenon reviewed is the enhanced settling that occurs in inclined channels, the Boycott effect. Developments on the inclined settling area were explained, introducing an innovative method of particle separation called the REFLUX™ Classifier. This method was shown to be very effective in separating particles based on their size and density. In particular, density-based selectivity is greatly enhanced when the channels are narrow enough for high shear laminar flow fields to develop. The development of theories that predict this effect was also outlined.

There has been a limited amount of work studying batch systems which shows that the bulk streaming and Boycott effects can both act together. However, there is no published research on the conditions under which these two phenomena can occur together in continuous processes. Finally the potential benefits of an Inverted REFLUX™ Classifier in separating positively and negatively buoyant particles were described. Whether these benefits do allow good separations to be achieved in an inverted REFLUX™ Classifier is the focus of the rest of this thesis.

## **Chapter 4**

# **Fly Ash and Cenosphere Characterization**

### Journal Article(s) Related to the Chapter and Authors' Contribution

**Kiani, A.,** Zhou, J. & Galvin, K.P. (2016). Detailed Characterization and Separation of Fly Ash Fed to the Inverted Reflux Classifier. *Fuel Processing Technology*, DOI: 10.1016/j.fuproc.2016.04.028

Author	Contribution
Ali Kiani	The lead author of the paper, collaborator in experimental design, experimental operator, analysis of data, and primary interpretation of results
James Zhou	Co-supervisor, experimental support
Kevin Galvin	Principal supervisor, collaborator in experimental design and results interpretation

## **4.1 Introduction**

This chapter briefly provides a detailed characterization of the fly ash and cenosphere particles. A typical fly ash feed sample was characterized in terms of surface morphology, elemental composition, density and size distribution, providing more detail of the fly ash feed properties and their possible effects on the separation performance.

## **4.2 Experimental**

### **4.2.1 Experimental procedure**

Fly ash feed samples were sourced from a power station in Australia.

#### **4.2.1.1 Cenosphere grade**

Standard sink-float funnels of 1 L volume were used in order to determine the portion of cenospheres (defined as particles of density less than water) in a fly ash sample. A sink-float separating funnel is shown in Figure 4.1a. This method of analysis was used with great care to prevent any significant errors in the results. The initial entrainment (rafting) of fine fly ash and black unburnt carbon particles into the floats portion is shown in Figure 4.1b. To minimize this, during the first few hours of settling the floats layer in the funnels was gently agitated several times using a stirring rod in order to facilitate the release of the entrained particles, but without being vigorous enough to cause major re-mixing. The sinks layer of fly ash and unburnt carbon particles and the floats layer of clean cenosphere product are shown in Figures 4.1c and 4.1d, respectively. The separated sinks and floats were placed in an oven to be dried, and the grade of cenospheres in the fly ash was calculated using the mass of dried samples. The grade of cenospheres in a raw fly ash feed sample (i.e. the fly ash before agitation in the mixing tank and use in any runs) was measured to be 1.41 wt.%.



(a)



(b)



(c)



(d)

Figure 4.1: (a) A sink-float funnel, (b) a top view photo of the sink-float funnel showing the entrained fly ash and unburnt carbon particles with the cenospheres, (c) the released fly ash and unburnt carbon particles, and (d) obtained clean cenospheres at the end of the sink-float test.

#### 4.2.1.2 Particle size

A subsample from sink and float portions was obtained for measuring the particle size distributions, using laser light scattering via the Mastersizer 3000. This equipment measures the volume-based size distributions of particles in a wet condition. A sieve shaker (Analysette 3) was also used to measure the mass-based size distributions of particles in a dry condition. It is noted that for particles of constant density over the size range, and for particles of strong sphericity, these two size distributions should be equivalent.

#### **4.2.1.3 Particle density**

The density of the particles was also measured using a gas pycnometer. The measured density of particles using this method can be completely different to that measured by water pycnometry when the particles are porous. The pycnometer measures the occupied volume of the particles and then calculates the density. The gas pycnometer measures the volume of the particles including the volume of the accessible pores while in water pycnometry, the water may not penetrate as far into the pores due to the viscosity and resistance that arises from capillary forces, and hence a larger volume of particles will be measured. Therefore the density measured by the water pycnometer is equal to or smaller than that measured by the gas pycnometer. The density of a fly ash sample was measured to be  $1895 \text{ kg/m}^3$  and about  $1500 \text{ kg/m}^3$  using the gas and water pycnometry methods, respectively. It should be noted that many of the fly ash particles contain fully enclosed air pockets, and hence their densities are below that of alumina-silicates. Further, for the purpose of this study the particles that have a density below that of water are deemed to be the cenospheres.

#### **4.2.1.4 Feed semi-batch fractionation**

As part of the feed analysis, a novel approach was adopted to quantify the density distribution of the feed. A REFLUX™ Classifier (RC™) with parallel inclined channels located above a liquid fluidized bed was used to fractionate the fly ash feed into different flow fractions with a narrow range of density. Note that this mode is very different to the IRC arrangement adopted in this study for recovering and concentrating the cenospheres on a continuous basis. The inclined section consisted of 23 stainless steel plates forming 24 channels with perpendicular spacing of 1.77 mm. Channels with close spacing are known to separate particles on the basis of their density, suppressing the effects of particle size (Galvin et al, 2009; Galvin & Liu, 2011). The vertical section located below the inclined section is 1 m long with a cross sectional area of  $100 \text{ mm} \times 60 \text{ mm}$ . The fluidization water was introduced from the base of the vertical section. The fractionation process is run under semi-batch conditions. Figure 4.2 shows a simple representation of the semi-batch REFLUX™ Classifier process.

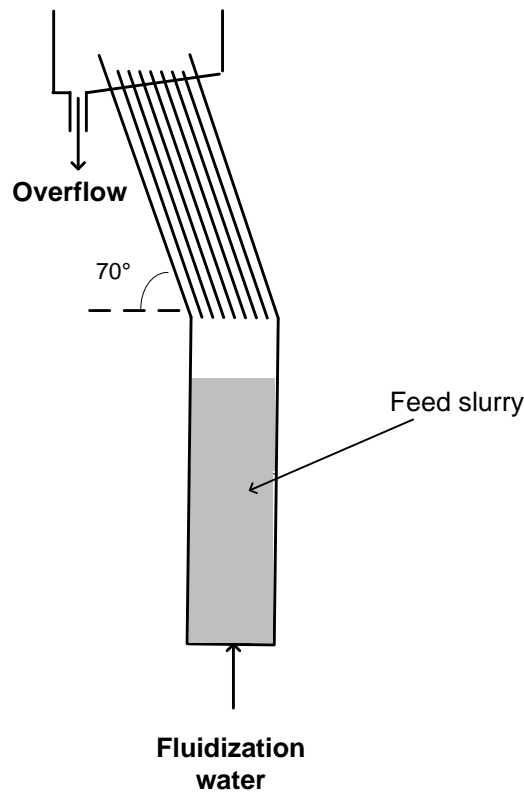


Figure 4.2: A simple representation of a semi-batch REFLUX™ Classifier process.

The REFLUX™ Classifier (RC™) was used in its traditional form under batch conditions to elutriate the fly ash feed into several overflow fractions. A sample of the feed was added to the RC™. Different fluidization water rates were used to generate the flow fractions in an increasing trend. At the lowest fluidization rate, cenospheres and very low density fly ash particles were carried up through the lower vertical section and then through the inclined channels, reporting to the overflow. This process was continued until there were negligible particles reporting to the overflow. By increasing the fluidization rate, a second flow fraction of higher density was produced. This approach was repeated several more times. On completion the remaining particles in the vessel were used to form the densest flow fraction. The sink-float test was then applied to Overflow 1 in order to separate cenospheres from the fine fly ash particles. These overflow samples were then fractionated based on their size using the sieve shaker (Analysette 3) for 30 minutes at an amplitude of 2. It is noted that in a more accurate analysis, prior to dry sieving, a wet size separation at 38  $\mu\text{m}$  was conducted on the overflows because the presence of slimes in the flows can lead to the formation of aggregates and hence generates errors in dry sieving. Each size fraction obtained from each flow fraction was placed in a gas pycnometer in order to measure the average density.

## 4.3 Results and Discussion

A data set characterizing a typical feed is presented in this section.

### 4.3.1 Morphology and compositions

A Scanning Electron Microscope (SEM) was used to examine the surface morphology of the particles in a fly ash sample. There were three main components observed. Figures 4.3a and 4.3b show the white spherical cenospheres which are hollow inside. It is the air trapped inside the hollow cenospheres that makes these particles positively buoyant in water. Some cenospheres were broken and hence heavier than water and therefore were lost to the underflow tailings of the IRC™. The shell thickness of the cenospheres was observed to be less than 10  $\mu\text{m}$ .

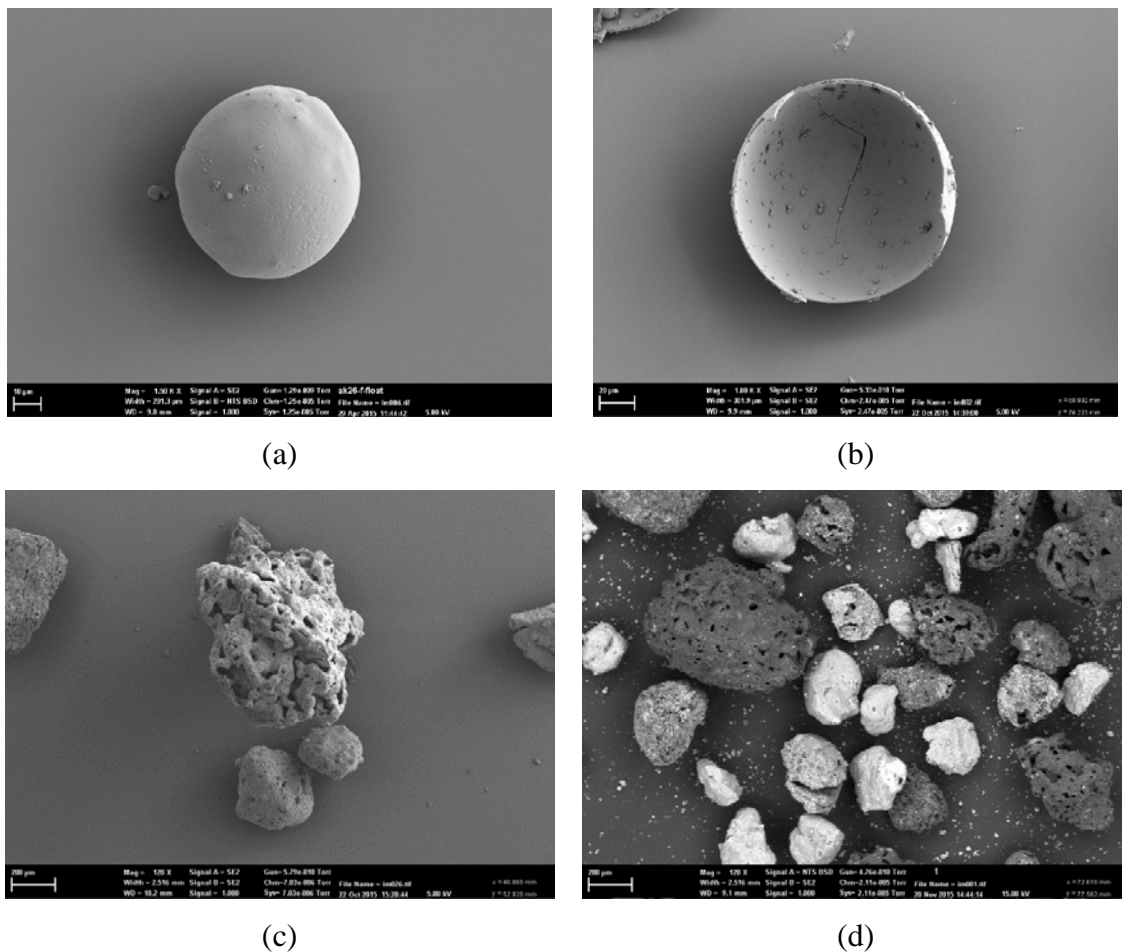


Figure 4.3: (a) A spherical cenosphere (Length Scale = 10  $\mu\text{m}$ ), (b) a broken cenosphere (Length Scale = 20  $\mu\text{m}$ ), (c) an unburnt carbon particle and (d) heavy particles in fly ash (silica, alumina, calcium and unburnt carbon). In (c) & (d), the length scales shown are 200  $\mu\text{m}$ .

Another component in the fly ash is unburnt carbon, black irregular particles, exhibiting porosity as shown in Figure 4.3c. In wet conditions, if there is insufficient time for the water to penetrate inside the pores, these particles can float. In these experiments the feed slurry was mixed for several hours, ensuring the particles were fully wetted. Thus the black particles initially present in the floats samples decreased with time. The last component observed in the fly ash is the white dense particles mainly consisting of silicon dioxide, aluminium oxide and calcium oxide. Figure 4.3d shows these particles and the black unburnt carbon in the fly ash.

Energy-Dispersive X-ray Spectroscopy (EDS) analysis was also carried out to show the chemical characterization of each component in the fly ash sample. Figure 4.4a shows that the black particles mostly consisted of carbon with small portions of other elements. Figures 4.4b and 4.4c show the elements in two different dense fly ash particles, illustrating that there is significant variation in the ratio of silica and alumina. In Figure 4.4d, the cenospheres are shown to also be mainly made of silica and alumina. It is because of this similar composition of the fly ash and cenospheres that flotation is ineffective for their separation.

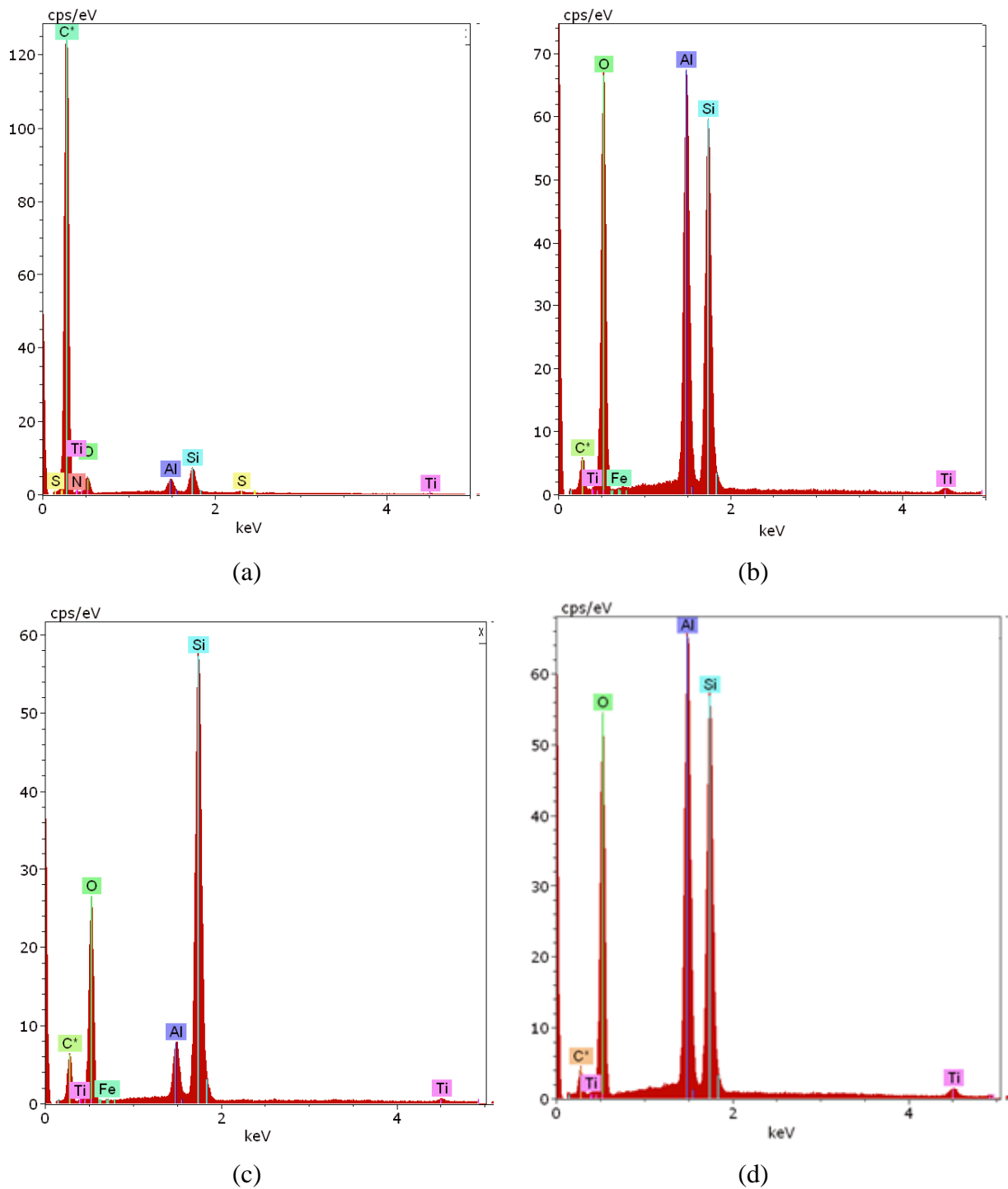


Figure 4.4: X-ray spectroscopy component analyses of (a) unburnt carbon particles, (b) dense fly ash particles, (c) silicate fly ash particles and (d) cenosphere particles.

#### 4.3.2 Feed fractionation using the semi-batch REFLUX™ Classifier

Table 4.1 lists the data for the double fractionation (by size and flow) of a fly ash feed sample. Using the semi-batch REFLUX™ Classifier process, the feed sample was divided

into 10 flow fractions (Overflow 1 to 10). Additionally Overflow 1 containing cenospheres and low density fly ash was divided into two fractions using the sink-float test. Each fraction was then sieved to 4 size intervals (-38  $\mu\text{m}$ , -90 +38  $\mu\text{m}$ , -180 +90  $\mu\text{m}$  and +180  $\mu\text{m}$ ). The densities of all 44 portions were then measured using the gas pycnometer. The sample densities were found to range from 770  $\text{kg/m}^3$  for cenospheres up to 2420  $\text{kg/m}^3$ . Table 4.1 presents the mass fractions and densities of all portions, providing a better description of the size and density of the fly ash feed. Table 4.2 uses an interpolation method (Iveson et al., 2015) to obtain the density and size distribution. It is noted that the mass of solids in some fractions was very small leading to slight errors in measuring their density. The presence of porous particles in the feed which as previously mentioned may show different hydrodynamic behaviour in wet and dry conditions can also produce slight inconsistencies in the fractionation data.

Table 4.1: Double fractionation data of a typical fly ash feed sample  
(Preliminary experiment).

Size ( $\mu\text{m}$ )	+180		-180 +90		-90 +38		-38	
	Mass Fraction (wt.%)	Density ( $\text{g/cm}^3$ )	Mass Fraction (wt.%)	Density ( $\text{g/cm}^3$ )	Mass Fraction (wt.%)	Density ( $\text{g/cm}^3$ )	Mass Fraction (wt.%)	Density ( $\text{g/cm}^3$ )
Overflow								
1-floats	0.07	0.85	0.87	0.78	0.40	0.77	0.00	-
1-sinks	0.05	1.39	0.26	1.13	0.13	1.09	0.01	1.56
2	0.02	1.53	0.09	1.14	0.15	1.04	1.48	2.21
3	0.00	-	0.02	1.08	0.07	1.06	2.37	2.15
4	0.02	1.31	0.36	1.36	1.34	1.63	6.53	2.10
5	0.01	1.56	0.44	1.79	1.56	1.87	5.52	2.16
6	0.17	1.72	0.90	1.44	2.15	1.65	3.25	2.07
7	0.32	1.90	1.06	1.60	2.23	1.75	2.37	2.07
8	0.79	1.95	2.57	1.73	4.23	1.86	1.80	2.03
9	1.46	2.42	12.07	2.14	15.69	2.08	1.85	2.24
10-remains	1.54	2.03	7.67	1.84	12.71	1.90	3.26	2.11

Table 4.2: Interpolation of data in Table 4.1 to obtain the density distribution  
(Preliminary experiment).

Density ( $\text{kg/m}^3$ )	700-1000	1000-1500	1500-2000	2000-2200	2200-2500
Size ( $\mu\text{m}$ )	Mass Fraction (wt.%)				
+180	0.07	0.08	1.68	1.06	1.57
-180+90	0.87	1.55	13.30	5.63	4.99
-90+38	0.40	0.84	25.26	8.65	5.56
-38	0.00	0.00	0.70	22.72	5.05
Total	1.34	2.47	40.94	38.06	17.17

Figure 4.5 shows the cumulative yield defined as the total amount of solids collected in the product at different density cut points. This figure shows that about 60 wt.% of the particles have a density higher than 2000 kg/m<sup>3</sup>. The fraction of particles less dense than 1000 kg/m<sup>3</sup> in the fly ash sample was as small as 1.3 wt.%, corresponding to the cenosphere grade in the fly ash sample measured earlier using the sink-float method.

The separation of cenospheres from this fly ash feed in the IRC<sup>TM</sup> is examined in Chapter 6. Note that the cenospheres grade here may be overestimated as the water was not given sufficient time to penetrate inside the pores of particles, and hence some broken cenospheres and porous particles floated due to the air trapped inside their pores (please see Figures I.16 & I.21). In contrast, in the main separation experiments in future chapters the feed was always well mixed for at least 4 hours before each experiment, thus giving time for the water to penetrate inside the particles' pores. Therefore the grade of cenospheres measured here is expected to be higher than that in the IRC<sup>TM</sup> runs.

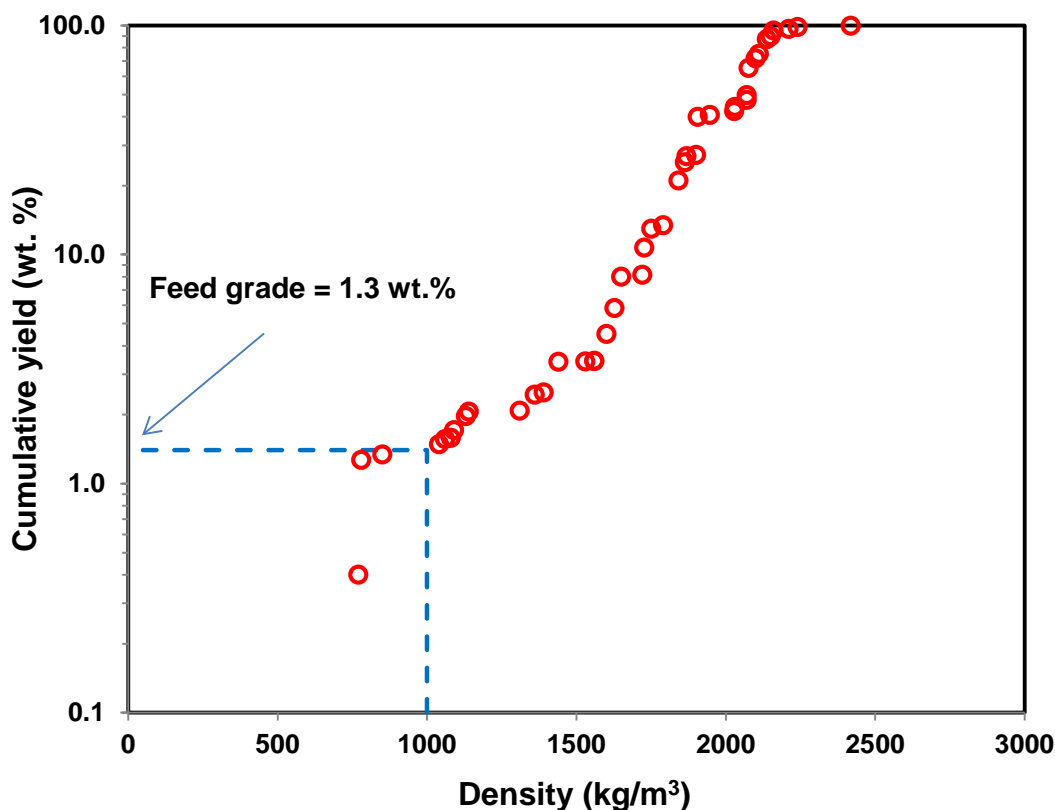


Figure 4.5: Cumulative yield at different density cut points (preliminary experiment).

A more accurate fractionation run was conducted to divide the feed into 13 overflows. The first overflow containing cenospheres and fine fly ash was divided into sinks and floats fractions. The slimes are more likely to be present in first overflow. Therefore the fraction 1-sinks and fractions 2-10 were wet split at 38  $\mu\text{m}$  first and then particles larger than 38  $\mu\text{m}$  were subjected to the dry sieving (-75, -150+75 and +150). Thus, the dry sieving was more accurate. The same procedure as the preliminary run was used to generate results. Tables 4.3 and 4.4, and Figure 4.6 present the fractionation results which are believed to be more accurate than the previous one. Again the mass of particles less dense than water corresponded to the cenospheres concentration in the fly ash measured in Section 4.2.1.1.

Table 4.3: Double fractionation data of a typical fly ash feed sample (main experiment).

Size ( $\mu\text{m}$ )	+150		-150+75		-75+38		-38	
	Mass Fraction (wt.%)	Density ( $\text{kg/m}^3$ )	Mass Fraction (wt.%)	Density ( $\text{kg/m}^3$ )	Mass Fraction (wt.%)	Density ( $\text{kg/m}^3$ )	Mass Fraction (wt.%)	Density ( $\text{kg/m}^3$ )
Overflow								
1-floats	0.15	810	0.89	780	0.38	780	0.02	830
1-sinks	0.07	1310	0.28	1050	0.18	1020	1.10	2180
2	0.01	1330	0.05	1070	0.08	1050	3.92	2230
3	0.01	1220	0.08	1070	0.12	1100	4.29	2150
4	0.01	1200	0.12	1110	0.18	1180	5.67	2130
5	0.35	1640	1.99	1500	3.20	1640	12.31	2070
6	0.71	1820	2.62	1700	3.15	1800	5.16	2090
7	0.49	1880	1.59	1750	1.34	1830	1.30	2110
8	0.81	1920	2.82	1820	2.76	1840	2.01	2100
9	0.80	1980	4.44	1870	3.65	1880	1.96	2120
10	0.49	2030	2.94	1930	3.48	1930	1.35	2170
11	0.65	2290	5.73	2110	5.45	2090	1.50	2310
12	0.39	2520	2.48	2470	2.91	2370	1.05	2580
13-remains	0.07	1860	0.09	1680	0.11	1950	0.23	2440

Table 4.4: Interpolation of data in Table 4.3 to obtain the density distribution (main experiment).

Density ( $\text{kg/m}^3$ )	700-1000	1000-1500	1500-2000	2000-2200	2200-2600
Size ( $\mu\text{m}$ )	Mass Fraction (wt.%)				
+150	0.15	0.20	2.99	0.76	0.92
-150+75	0.89	1.53	15.72	3.67	4.32
-75+38	0.38	1.64	17.56	3.43	3.99
-38	0.02	2.88	2.88	29.85	6.24
Total	1.43	6.25	39.14	37.71	15.47

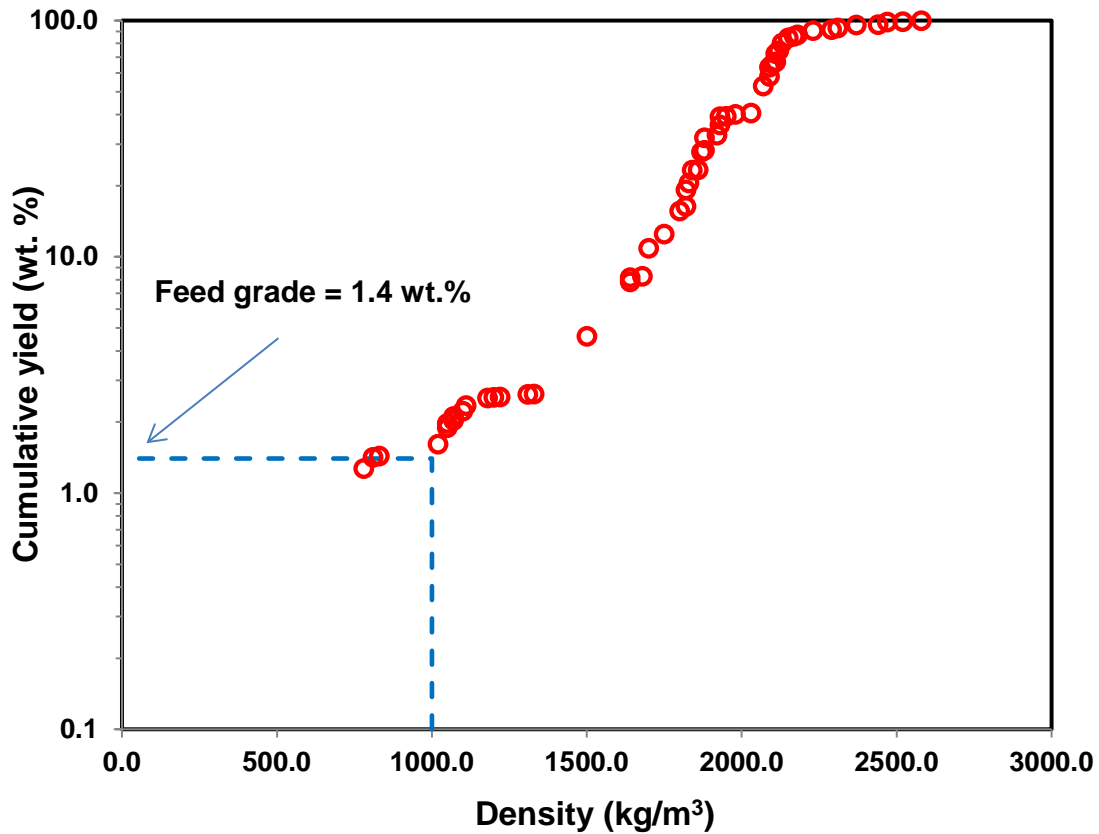


Figure 4.6: Cumulative yield at different density cut points (main experiment).

The difference between the results obtained from the preliminary and main fractionation is associated with the particles finer than 38  $\mu\text{m}$ , suggesting that the wet size separation produced more accurate fractionation results.

#### 4.3.3 Particle size and density

The volume-based size distribution measured by the laser scattering method (Malvern Mastersizer 3000) and the mass-based distribution generated from sieving (Analysette 3) should be identical if there is no size-dependence in the density distributions of the particles, and the particles are reasonably spherical. The cumulative size distributions of the cenospheres and fly ash based on the mass and volume measurements are shown in Figure 4.7. The close agreement between the mass-based and volume-based size distributions of the floats cenospheres can suggest that there is very little size-dependence in the variation of density of these particles. The mass-based distribution of the sinks fly ash particles is also similar to the volume-based distribution. It is noted that for each sample, the sieve shaker was stopped every 15 minutes to examine the quantity of material below 38 microns. Sieving was

continued until the mass variation was less than 2%. The required sieving time for the cenospheres and fly ash particles was found to be about 30 mins and 120 mins, respectively. It is also worth noting that comparing sizes measured by screening with those measured by light scattering is fraught with difficulty and assumptions. Hence no firm conclusions can be drawn other than that if there is any size-dependent variation in density, then it is not large.

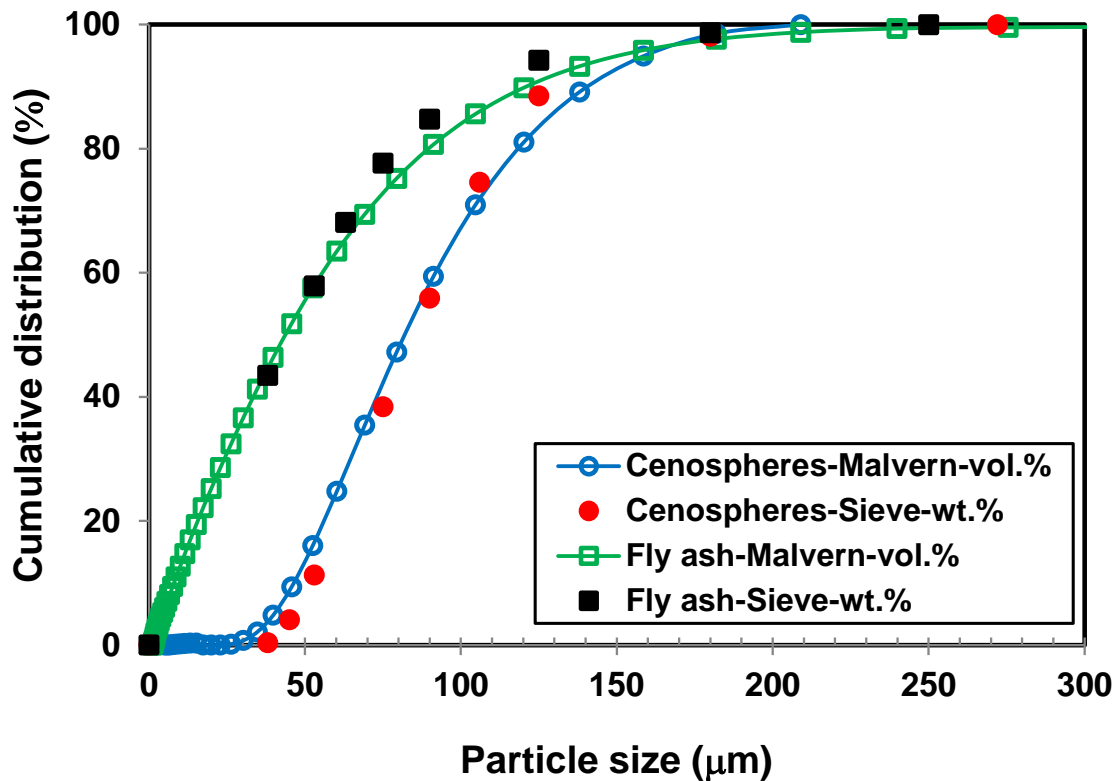


Figure 4.7: The mass-based and volume-based fractions of cenospheres and fly ash less than a given particle size.

The cenosphere particles were then divided into three different density intervals (+900, -900+800 and -800 in  $\text{kg/m}^3$ ) using water-acetone mixtures of different densities (Noda et al., 1982). Cenospheres less dense than  $900 \text{ kg/m}^3$  formed around 80 wt.% of the cenospheres. Figure 4.8 shows the size distributions of the cenospheres for these three density intervals are almost the same.

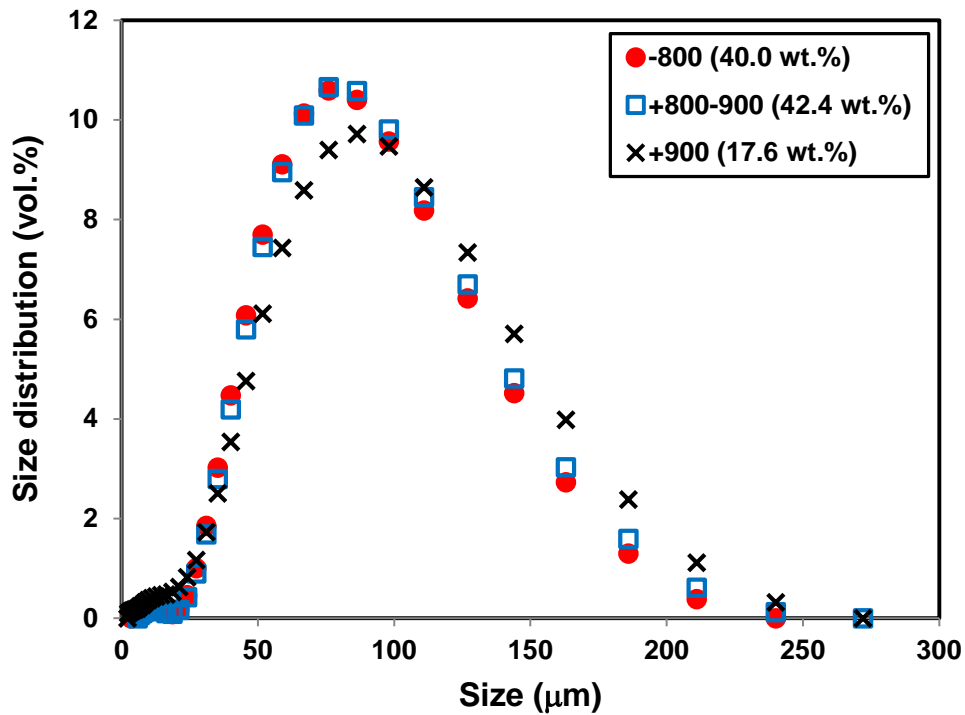


Figure 4.8: The volume-based size distributions of cenospheres particles at different density intervals in  $\text{kg/m}^3$ .

#### 4.4 Conclusions

A typical fly ash feed sample was characterized in several ways. SEM images revealed that cenospheres, unburnt carbon and dense particles (i.e. silicon dioxide, aluminum oxide and calcium oxide) were the three main components of the fly ash. The elemental composition of these three components was measured by the EDS method, showing the same chemical compositions for cenospheres and fly ash. Furthermore, a double fractionation test was conducted on a fly ash feed sample, providing more detail on the size and density of particles in the feed.

In the next Chapter, as a preliminary study, the separation of cenospheres from dense silica in the IRC<sup>TM</sup> is investigated first, and then the potential of the IRC<sup>TM</sup> for separating cenospheres from real fly ash feed is examined.

## **Chapter 5**

# **Preliminary Experiments on Upgrading Positively Buoyant Particles using an Inverted REFLUX™ Classifier**

### Journal Article(s) Related to the Chapter and Authors' Contribution

**Kiani, A.,** Zhou, J. & Galvin, K.P. (2015). Upgrading of Positively Buoyant Particles Using an Inverted Reflux Classifier. *Advance Powder Technology*, 26, 119-125.

Author	Contribution
Ali Kiani	The lead author of the paper, collaborator in experimental design, primary interpretation of results, experimental operator and primary analysis of data
James Zhou	Co-supervisor, experimental support
Kevin Galvin	Principal supervisor, collaborator in experimental design, results interpretation and data analysis, inventor and designer of system

## 5.1 Introduction

This chapter reports the results of preliminary experiments to study the potential of an Inverted REFLUX™ Classifier (IRC™) to upgrade and recover positively buoyant particles. This innovative enhanced gravity separation method combines a set of inclined channels mounted below a downwards fluidized bed. Initially a model feed is used, consisting of a mixture of commercial cenospheres and dense silica. Then this method is applied to the separation of cenospheres from real fly ash sourced from a coal-fired power station in Australia. The effects of different operating conditions such as fluidization water rate, feed rate and split ratio on the separation performance in the IRC™ are also examined. The analysis includes measuring the size partition curves.

## 5.2 Background

Gravity-based separation in water is the most obvious method for recovering cenospheres since the cenospheres are positively buoyant and the fly ash negatively buoyant. Considering the densities of cenospheres and fly ash as roughly  $800 \text{ kg/m}^3$  and  $2000 \text{ kg/m}^3$  respectively, equation 2-59 predicts that the free settling ratio will vary from around 5 down to 2.2 for Newton's through to Stokes' regimes respectively, indicating that there is potential for effective wet gravity separation (Wills, 1997). However, ultrafine fly ash will tend to split with the water, and hence tend to cause significant contamination of the rising cenospheres. Moreover, the rise velocity of the fine cenospheres is very low, meaning that long residence times are required for effective separation and also that many cenospheres are easily trapped beneath settling higher density solids.

As previously discussed in Chapter 3, the system of inclined channels used in the REFLUX™ Classifier increases the rate of segregation, leading to a throughput advantage over conventional fluidized beds (Laskovski et al., 2006). For a cenosphere  $50 \text{ }\mu\text{m}$  in diameter and  $800 \text{ kg/m}^3$  in density, the particle Reynolds number is 0.014 (Equation 2-13), and hence the theoretical maximum throughput advantage at large aspect ratios is  $U/u_t = 31$  (Equation 3-11). Thus the REFLUX™ Classifier has the potential to permit a feed rate some 31 times greater than a conventional fluidized bed, for the same separation. However, even with this large throughput advantage, in the standard REFLUX™ Classifier there will still be

a strong tendency for ultrafine, high density, silica to split to the overflow and contaminate the cenosphere product.

An Inverted REFLUX™ Classifier configuration can potentially reduce contamination of the overflow cenospheres by ultrafine silica through the washing action of the fluidization water entering through the top distributor, thus improving the cenosphere grade. This inverted fluidization will also have the tendency to entrain the low density cenospheres downwards; however, within the inclined channels, the cenospheres segregate strongly from the flow, returning to the upper fluidized bed zone and ultimately to the product overflow. Thus the Inverted REFLUX™ Classifier theoretically provides a powerful approach to both recover and to concentrate the positively buoyant cenospheres. The purpose of this chapter is to experimentally investigate the potential of this novel device, the Inverted REFLUX™ Classifier, in recovering and concentrating cenospheres, first from a model feed and then from real fly ash.

## **5.3 Experimental**

### **5.3.1 Experimental equipment**

Figure 5.1 shows an Inverted REFLUX™ Classifier (IRC™), a system of parallel inclined channels installed underneath a liquid fluidized bed. As shown in Figure 5.1, the Inverted REFLUX™ Classifier consists of a 1 m long vertical zone with a cross sectional area of 86 mm × 100 mm. A wash-water distributor with the same cross section as the vertical section of the IRC™ and a height of 110 mm is placed at the top. The chamber is narrowed down to a discharge port with a diameter of 20 mm. As shown in Figure 5.2, the fluidization water chamber includes 14 holes in each face (56 holes total), each with a diameter of 1 mm, to provide an even washing process. The inclined section, which is also  $L = 1$  m long, has an angle of  $\theta = 70^\circ$  with respect to the horizontal. It consists of 7 stainless-steel plates, each with a thickness of 0.7 mm, forming 8 channels of perpendicular spacing of  $z = 9.5$  mm.

The feed enters 300 mm above the junction between the vertical and inclined zones. It was crucial the product rate be controlled via a pump given this flow rate was relatively low, hence natural fluctuations would have potential sampling implications for the short term recoveries. It was also important to ensure the system was full at all times, and in fact under

positive pressure, otherwise there was a risk the level of material in the system could decrease below the outlet, resulting in no product. Naturally, there needs to be one degree of freedom in the system to allow for natural fluctuations. This was achieved by incorporating an upper vent connected to the tailings line. Thus the rates of the feed, overflow product and a portion of the underflow tailings (Tailings 1) were all controlled by specific peristaltic pumps. The flow rate of fluidization water from the mains was adjusted using a valve and measured using a rotameter. The vent tube from the tailings discharge was extended to a level above the device, resulting in a positive internal system pressure. If tailings were observed via the vent, then the system had to be full, with a hydrostatic head at the product discharge equal to the vent elevation above the unit. The required discharge rate of the tailings via the vent was arbitrary. The primary requirement was that a flow occurred via the vent. Nevertheless, it was desirable that significant tailings discharged via the main underflow line, thus allowing the coarser particles to discharge immediately. If the coarser particles were forced to discharge via the elevated vent, sediment could develop and cause a blockage in the elevated line. It is noted that sufficient upwards flow was required in the tailings line to the vent to prevent unrecovered cenospheres from blocking the line.

The Tailings 1 and Tailings 2 streams were combined, and then a sample of the combined stream was taken and analyzed in order to determine the composition of underflow tailings in the process. In general the rate of Tailings 1 was usually adjusted so that the excess Tailings 2 stream to the vent was roughly the same flow rate as the fluidization water.

Two pressure transducers were used in the vertical section of the IRC™ to measure the density of the suspension. The signal provides some indication of whether the system is operating at steady state, and the density value also indicates the likely grade of the product.

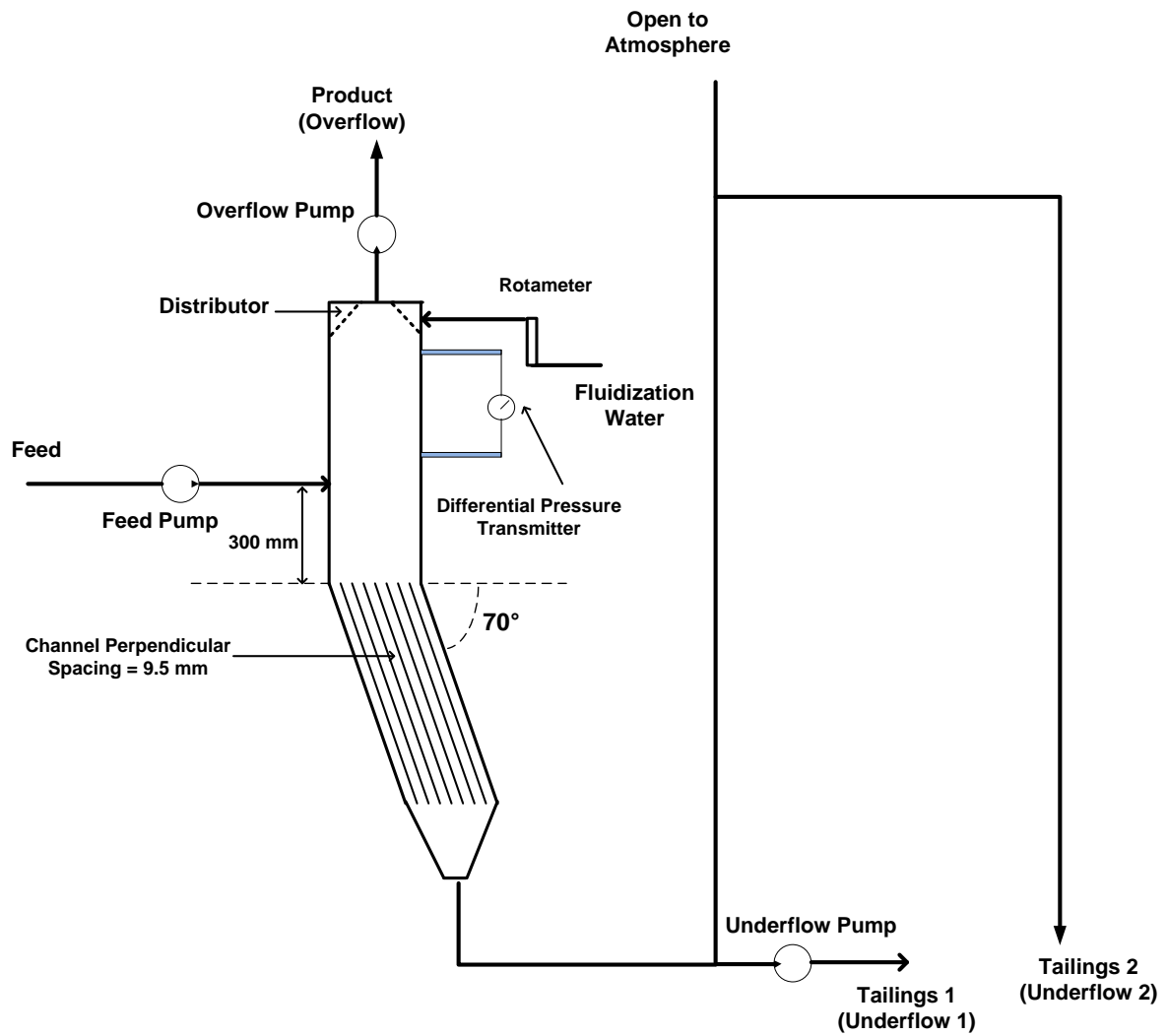


Figure 5.1: A schematic representation of the Inverted REFLUX™ Classifier used in this study.



Figure 5.2: The fluidization water distributor with 4 water inlets to the chamber and 14 holes in each face of the distributor.

### 5.3.2 Feed preparation

In the preliminary work a model feed, a mixture of silica flour (Sibelco, 400 G) and the 7040S grade of Q-Cell commercial cenospheres (Potters industries), was prepared in a mixing tank with a volume of 1200 L. About 35 wt.% of the supplied cenospheres were actually measured to be denser than water (Li et al., 2014). This composition reflects the fact that most commercial products are contaminated with unwanted dense particles, due to the fundamental difficulty of desliming these products to remove these very fine dense particles using existing technologies. It is emphasized that only the cenospheres lower in density than water are the focus of interest in this thesis. Thus it was crucial to establish this fact concerning the model feed, given the performance of the separation experiments is measured in terms of the recovery of the particles of density lower than water. Thus the concentration of the positively buoyant cenospheres in the model feed was adjusted to be 0.51 wt.%. The feed total solids content of the slurry was diluted significantly, and measured to be about 8.3 wt.%.

In the preparation of the model feed, two important issues were considered and carefully addressed. The first one was the low tendency of the very buoyant cenospheres to wet and mix in water, and the second one was the high tendency of the dense fine silica particles to settle and form very firm sediments at the bottom of the feed tank. To address the first issue, the cenosphere and silica particles were kept mixed for several hours before each experiment to ensure an appropriate homogenous feed in the tank. Regarding the latter issue, the bottom of the mixing tank was checked for any sediment before starting the experiments to verify that proper mixing was occurring in the tank.

In the second part of these preliminary studies, a real fly ash feed was used. The feed fly ash was sourced from an Australian coal-fired power plant. The grade of the cenospheres defined as the ratio of the cenosphere mass to the total solids mass in the feed was nominally 0.53 wt.% and typically 30 wt.% of the cenospheres were finer than 50  $\mu\text{m}$ . For this work, about 350 kg of dry solid fly ash was mixed with almost 650 kg of water in a mixing tank, forming around 850 L of slurry with a solids content of 30-35 % by mass. A single tank supplied enough uniform feed for 3 h of continuous operation, which was more than enough time to reach steady state.

### 5.3.3 Experimental procedure

The feed slurry was withdrawn via a vertical tube located near the inner wall of the tank, with its entrance elevated 100 mm off the base of the tank. This approach was essential given the strong tendency for the fly ash to sediment and pack tightly causing blockages when the flow or mixing ceased. The feed was pumped into the vertical section of the IRC™, about 300 mm above its junction with the inclined section.

As previously mentioned, two pressure transducers fitted to the vertical fluidized bed section of the Inverted REFLUX™ Classifier measured the average suspension density above the feed inlet, providing useful information for monitoring the state of the system. It is noted that solids sometimes entered the pressure transducer tubes, causing some inaccuracies in the pressure readings. However the relative fluctuations of these values could be still used to indicate whether the experiment was at steady state. Another indication of how close the system was to steady state was to monitor the solids fraction of the product. This was done by regularly collecting samples in a measuring cylinder and then comparing the heights of the sediment layers formed after a given time. No significant changes in the volume fractions gives some indication that steady state has been reached. The time required to reach steady state depended on the experimental operating parameters such as the feed cenosphere and total solids concentrations, and the product and feed rates. In general, 2 h was usually sufficient. After reaching steady state, timed samples of the overflow product, underflow tailings, and the feed were collected, dried, weighed and then analyzed.

During an experiment, the overflow and underflow streams were collected in separate buckets, which were later re-combined to use as feed in a subsequent experiment. To keep the feed particle size and grade constant for these later experiments, the following precautions were taken. First samples of the product and the tailings streams were always collected over the same time period. Secondly, dried samples were never returned to the feed tank, as a precaution in case aggregation had occurred during drying. Finally, before removing the excess water that had been added as fluidization during a previous experiment, the overflow and underflow buckets were left for a few days to settle until a clear intermediate layer of water was observed between floating cenospheres and sunken fly ash. The excess water was then carefully withdrawn from this layer using a small tube.

### 5.3.4 Samples analysis for grade and recovery

#### 5.3.4.1 Gas pycnometry method

The density of the dry samples was measured using gas pycnometry (Micromeritics AccuPyc 1330). This machine calculates the sample density  $\rho_{\text{solids}}$  by measuring the sample's occupied volume, divided by its dried weight. An accurate determination of the proportion of cenosphere floats and fly ash sinks material in each sample requires a sink-float separation (Section 5.3.4.2). These measurements are tedious and time-consuming, so in some of the early work, a quick approximate method was used to estimate the separation performance based only on the average density of each sample measured using gas pycnometry. This method was based on assumed densities of the dense fly ash component ( $\rho_s$ ) and the cenospheres ( $\rho_c$ ). The grade  $X_c$  and the recovery of cenospheres ( $R$ ) were estimated as:

$$X_c = (\rho_{\text{solids}} - \rho_s) / (\rho_c - \rho_s) \times \rho_c / \rho_{\text{solids}} \quad (5-1)$$

$$R = (X_c M_{\text{solid}})_{\text{product}} / (X_c M_{\text{solid}})_{\text{feed}} \quad (5-2)$$

where  $M_{\text{solid}}$  is the mass of solids in the relevant stream sample.

The reason this approach is only an approximation is because the density of each sinks and floats fraction varies between streams. For instance, the density of the fly ash (sinks fraction) that appears in the overflow is typically lower than the density of the fly ash that appears in the underflow, especially when the portion of the fly ash in the overflow is relatively small. A sensitivity analysis was therefore applied, by calculating the product grade and cenosphere recovery using a range of different assumed fly ash densities, to quantify this uncertainty.

The reason for using the above approximate method to calculate grades and recoveries was because of the much faster analysis time compared to carrying out tedious sink-float separations (Section 5.3.4.2). All that needed to be done was to dry each sample and measure its density using gas pycnometry, which could be done within 24 h of the experiment being completed. In contrast sink-float analysis took almost 5 days until accurate results were known.

#### **5.3.4.2 Sink-float separation method**

The more accurate sink-float approach was also used to measure the composition of each stream. In this method of analysis, the samples were left in 1 L separating funnels for 24 h (Figure 5.3). In the preliminary experiments involving the model feed, owing to the high tendency of silica particles to form hard sediments in the funnels, small batches of these sinks particles were regularly discharged from the base of the funnels. After 24 h, most of the heavy particles were separated from the floating light particles. Some fine cenospheres were entrained to the sinks fraction where they were seen floating to the surface, and so these were collected and returned to the float phase. After this step the sinks and floats fractions were dried and weighed. The floats fraction is usually referred to as the “cenosphere” fraction of the sample, and the sinks component as the “fly ash” fraction. As noted in Chapter 1, in practice, not all cenospheres are lower in density than water. Some hollow particles can still be higher in density than that of water. However, in this thesis, the cenospheres are defined as those particles that are lower in density than water. This definition is consistent with the sink-float method used to formally identify and hence quantify the grade of the cenospheres.

The sink-float procedure was repeated for the feed, product and tailings streams. From these measurements the grade in each stream was calculated, and then using the cenosphere masses in each stream, the recovery of cenospheres determined. This sink-float approach was very time consuming and hence was reserved for only a few runs in this preliminary phase of the research.

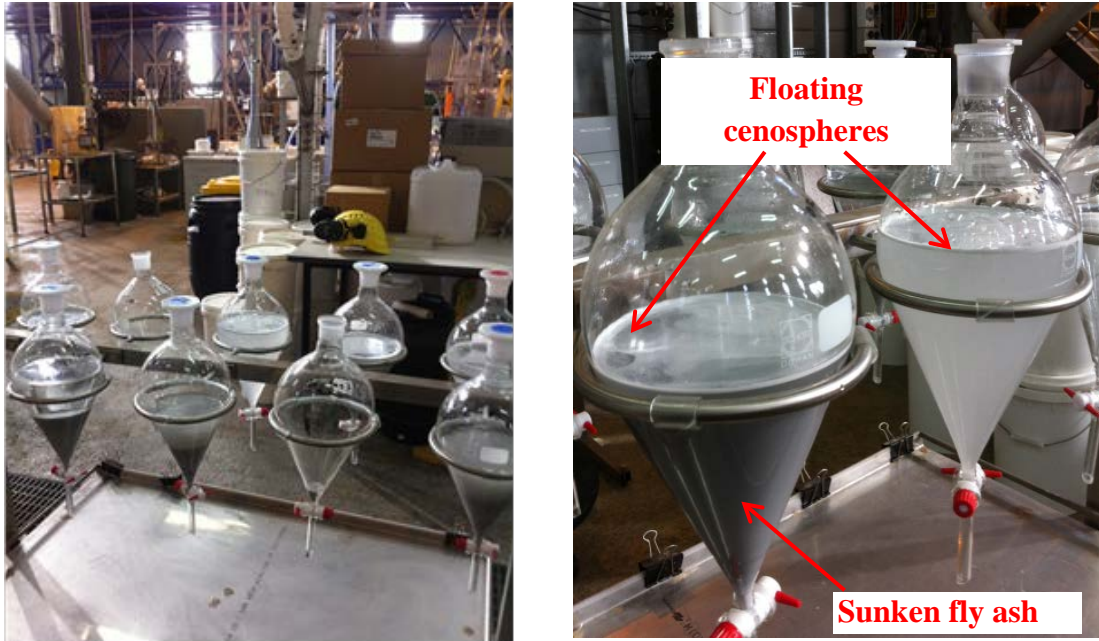


Figure 5.3: Separating funnels used for sink-float measurements of the grade of cenospheres in product, tailings and feed samples.

### 5.3.5 Mass balance reconciliation technique

Given that perfect steady state is more a goal than a reality, and given the inevitable errors that occur during sampling and analysis, there is always a discrepancy between the inlet and outlet masses in each density/size interval. In this study, a standard method of mass balance reconciliation was used in order to minimize these errors and hence quantify more accurately the recovery and the grade. A Simplex algorithm was used to achieve a least squares data adjustment according to material balance requirements and an objective function based around the data adjustment (Galvin et al., 1995). Previous work by Galvin et al. has demonstrated the potential for data improvement. The consistency of the raw data was then indicated by a comparing the outlet and inlet masses, and the required adjustment to the raw data. This procedure, shown in Appendix A, includes all raw and reconciled data.

### 5.3.6 Particle size measurement

In the set of runs analyzed by the sink-float test, small samples from all streams were taken and subjected to particle size measurement using laser light scattering (Malvern Mastersizer 2000). This machine measures the volume fraction of particles in each size interval. The volume frequency size distribution was then calculated by dividing the volume percentage

(vol.%) by the interval width ( $\Delta d$ ). Mass balance data reconciliation was also applied to the size distributions of the float fraction of each stream. By using these reconciled size distributions, the recovery of the cenospheres as a function of the particle size was calculated resulting in the size partition curve. This result provides a clear measure of the size separation performance of the process. A sample partition curve was shown in Figure 2.10.

## 5.4 Results and Discussion

When the mixture of cenospheres and fly ash enters into the IRC<sup>TM</sup>, most of the positively buoyant cenospheres naturally move upwards and exit via the product discharge line. The fluidization water washes away a significant amount of the dense fine particles that would otherwise be entrained with the exiting overflow product. However, the net downwards flow in the vertical section does carry some of the slow-rising fine cenospheres down into the inclined section. Here the enhanced segregation rate through the inclined channels, as previously mentioned, captures most of these particles and returns (refluxes) them back up into the fluidized bed section. Therefore the use of the inclined channels and the fluidization chamber potentially leads to an increase in the recovery and the product grade, respectively.

Results are presented first for the preliminary experiments conducted on the model cenosphere/silica feed. Then the results are presented from the initial experiments using a real fly ash feed. The effects of fluidization water rate, feed rate and the product rate on the separation performance in the IRC<sup>TM</sup> are investigated. The main reason for the low recovery in the process is explored by studying the size separation in the IRC<sup>TM</sup>. Also the evidence of density classification of cenospheres and fly ash is given. As previously noted, in this study, the product grade and cenosphere recovery were calculated based on mass-balance reconciled data. Therefore error bars are defined using a comparison between the results calculated from the balanced data and raw data.

### 5.4.1 Model feed

In the initial work, the Inverted REFLUX<sup>TM</sup> Classifier (IRC<sup>TM</sup>) was used to process a model feed consisting of a mixture of silica flour with an average density of about 2670 kg/m<sup>3</sup> and the 7040S grade Q-cell commercial cenospheres with an average density of about 470 kg/m<sup>3</sup>. The portion of the commercial “cenospheres” that floated in water was found to be about 68

wt.% with an average density of about  $382 \text{ kg/m}^3$ . The density of the sink fraction was measured to be  $1472 \text{ kg/m}^3$ . In this section, the floated particles (float fractions of commercial cenospheres) and sunken particles (silica flour and the sink fractions of commercial cenospheres) are simply named “cenospheres” and “silica” respectively. The size distributions of the cenospheres and silica in the feed of Run 1 are shown in Figure 5.4. All particles were finer than  $100 \mu\text{m}$ , with the silica having a large fraction less than  $10 \mu\text{m}$  in size, whereas there were almost no cenospheres less than  $10 \mu\text{m}$  in size.

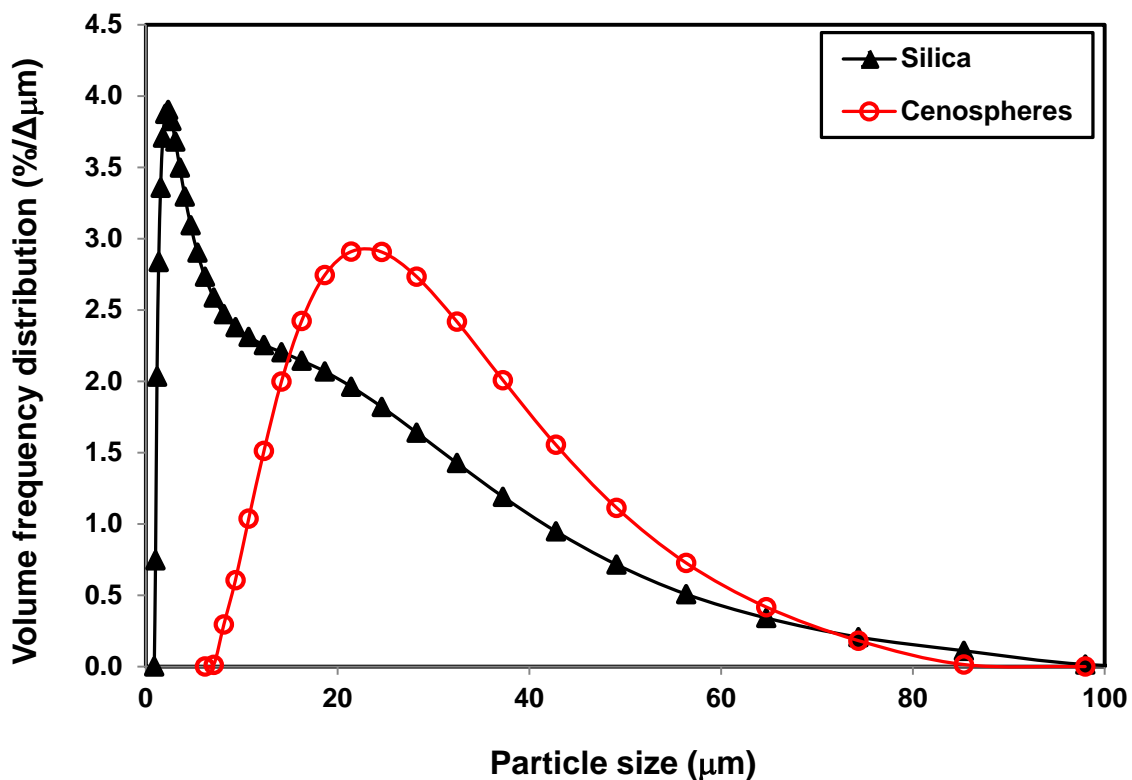


Figure 5.4: The volume frequency size distributions of the cenospheres and silica fractions in the model feed of Run 1 (raw data).

Table 5.1 shows the experimental data for different runs conducted on the model feed. The sink-float test was used to measure the product grade and cenosphere recovery. Feed slurry with about 8.3 wt.% solids and with a nominal cenosphere grade of 0.51 wt.% was prepared and fed into the device. In this set of experiments, the feed and wash water fluxes were kept constant at about  $7.0 \text{ m}^3/(\text{m}^2 \text{ h})$  and  $0.87 \text{ m}^3/(\text{m}^2 \text{ h})$ , respectively, with the overflow flux varied from 0.07 up to  $0.63 \text{ m}^3/(\text{m}^2 \text{ h})$ . So the underflow flux varied in a narrow range from 7.24 to  $7.8 \text{ m}^3/(\text{m}^2 \text{ h})$ . All flux values quoted here and in the following chapters are calculated

by dividing the volumetric flow rates by the horizontal cross-sectional area in the vertical section of the IRC™.

Note that the free rise velocity of cenospheres of size 75 µm and density 300 kg/m<sup>3</sup> is calculated to be about 7.23 m/h (Equation 2-13). This means that all cenospheres smaller or denser than the respective values given above can potentially be entrained by the downwards flux of feed in the vertical section of the IRC™.

Table 5.1: Experimental parameters and results obtained from the four runs using the model feed. Note that the mass of cenospheres in the tailings samples, all samples of Run 4 and the feed sample of Run 3 were too small for the gas pycnometry method to measure their density.

	Run 1	Run 2	Run 3	Run 4
Feed Cenospheres Density (kg/m <sup>3</sup> )	353	391	-	-
Feed Cenosphere Grade <sup>1</sup> (wt.%)	0.66*	0.58	0.56	0.27
Feed Solids Concentration (wt.%)	8.6	8.3	8.3	8.3
Feed Flux (m/h)	7.0	7.0	6.4	7.0
Wash Water Flux (m/h)	0.87	0.87	0.87	0.87
Overflow Product Flux (m/h)	0.37	0.17	0.07	0.63
Overflow Cenospheres Density (kg/m <sup>3</sup> )	257	271	261	-
Product Cenosphere Grade <sup>1</sup> (wt.%)	70.6	85.3	82.7	64.5
Tailings Cenosphere Grade <sup>1</sup> (wt.%)	0.35	0.23	0.28	0.19
Cenospheres Recovery <sup>2</sup> , $R_{Vc}$ (vol.%)	68.6	67.0	61.4	N.A.
Cenospheres Recovery <sup>1</sup> , $R_{Mc}$ (wt.%)	60.6	59.6	49.8	31.3
Equation 5-3: $R_{Vc} = (\rho_{cF}/\rho_{cP})R_{Mc}$	83.2	86.0	-	-
$d_{50}$ (µm)	21.5	29.0	26.0	-
$I$	0.19	0.21	0.21	-

<sup>1</sup> Calculated using cenospheres masses obtained from the sink-float method.

<sup>2</sup> Calculated from reconciled volume fraction size distributions using two-product formula.

\* The grade of cenospheres in the feed for Run 1 was measured using a sample taken at the beginning of the run, whereas other feed grades are based on feed samples collected at the same time as the steady state product and tailings flows.

#### 5.4.1.1 Separation at different product fluxes

In this set of experiments, the separation of positively buoyant cenospheres from silica particles was examined in the IRC™ at three different product fluxes of 0.37 m<sup>3</sup>/(m<sup>2</sup> h), 0.17 m<sup>3</sup>/(m<sup>2</sup> h) and 0.07 m<sup>3</sup>/(m<sup>2</sup> h) (i.e. Runs 1, 2 and 3). The resulting overflow product grade and recovery are shown in Figures 5.5. As expected, increasing the overflow product rate resulted in a decrease in grade and increase in recovery. The grade decreased from around 80

wt.% down to about 71 wt.%, but there was an increase in cenosphere recovery from 50 wt.% up to about 61 wt.%. The reduction in grade is presumably due to the increased entrainment of fine silica as the overflow flux increases.

It is noted that the grade and recovery values plotted in Figure 5.5 were calculated using the mass-balance reconciled experimental data. The error was found to be negligible for the grade values and hence is only showed for the recovery values. The error bars show the span of the three recovery values that can be calculated using the raw experimental data for the mass of solids in the feed, tailings and product (i.e. recovery =  $P/F$ ,  $(F - T)/F$  and  $P/(P + T)$ ). Sample calculations are shown in Appendix H.

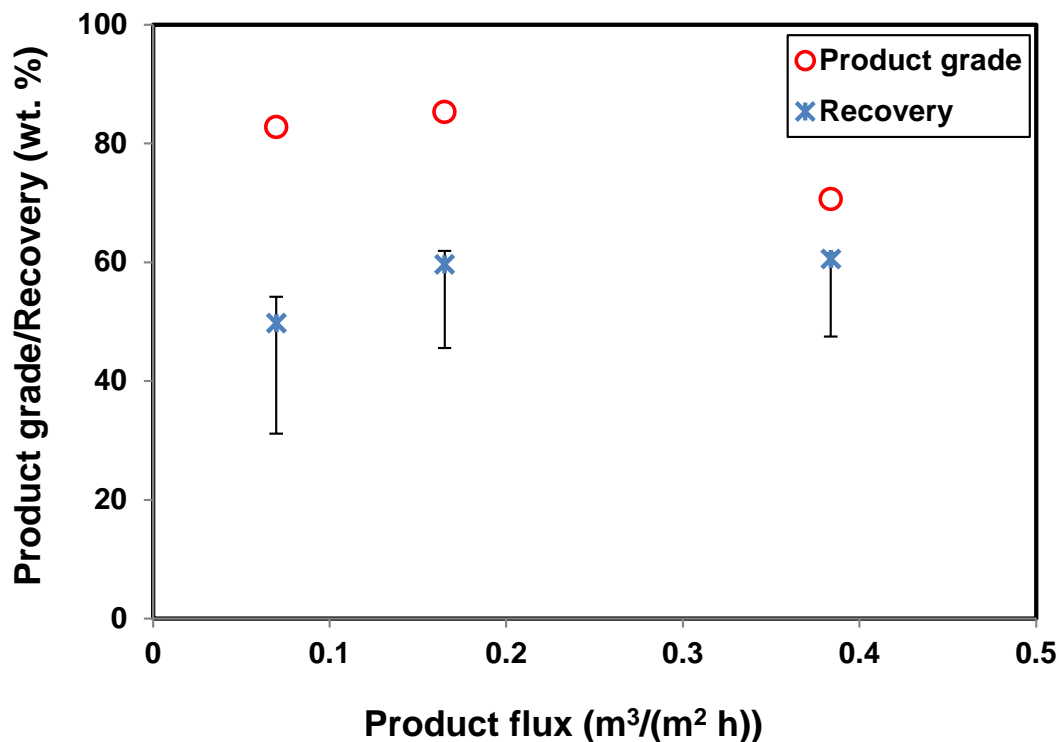


Figure 5.5: Product grade and cenosphere recoveries obtained at different overflow product fluxes for the model feed at constant feed and wash water fluxes of 7.0 m<sup>3</sup>/(m<sup>2</sup> h) and 0.87 m<sup>3</sup>/(m<sup>2</sup> h), respectively (based on balanced data). The error bars show the span of calculated recoveries based on the raw measurements of feed, product and tailings masses.

Figure 5.6 shows the size distributions of the cenosphere floats fractions in the product, tailings and feed for Run 2 with a product flux of 0.17 m<sup>3</sup>/(m<sup>2</sup> h). As clearly shown, the cenospheres in the tailings are much finer than that in the product. Most of the cenosphere losses were in the fine sizes, with around 50 vol.% of cenospheres in the tailings smaller than

20  $\mu\text{m}$ . As mentioned above, only the largest cenospheres with rise velocities greater than 7.23 m/h can segregate directly to the product stream (in the absence of hindered settling). The majority would initially be entrained downwards and be carried downwards into the inclined channels. It is only the high segregation rate in the channels that allows most of these particles to be captured and returned to the vertical section, from where dispersion eventually enables them to start to force their way out via the product stream. However, this mechanism is clearly not sufficient to capture the particles below 20  $\mu\text{m}$  in size. The free rise velocity of these cenospheres (for example those with a density of  $300 \text{ kg/m}^3$  and size of 10  $\mu\text{m}$ ) is only 0.13 m/h (Eqn. 2-13), and thus they would require a throughput advantage of  $7/0.13 = 54$  to be captured in the channels. Using Equation 3-11, the throughput advantage of the IRC<sup>TM</sup> for this size and density of cenospheres is calculated to be only 24, which is much less than the required 54. It is noted that for the next section involving real fly ash and cenospheres with a density closer to water, the separation of fine particles would be even more difficult.

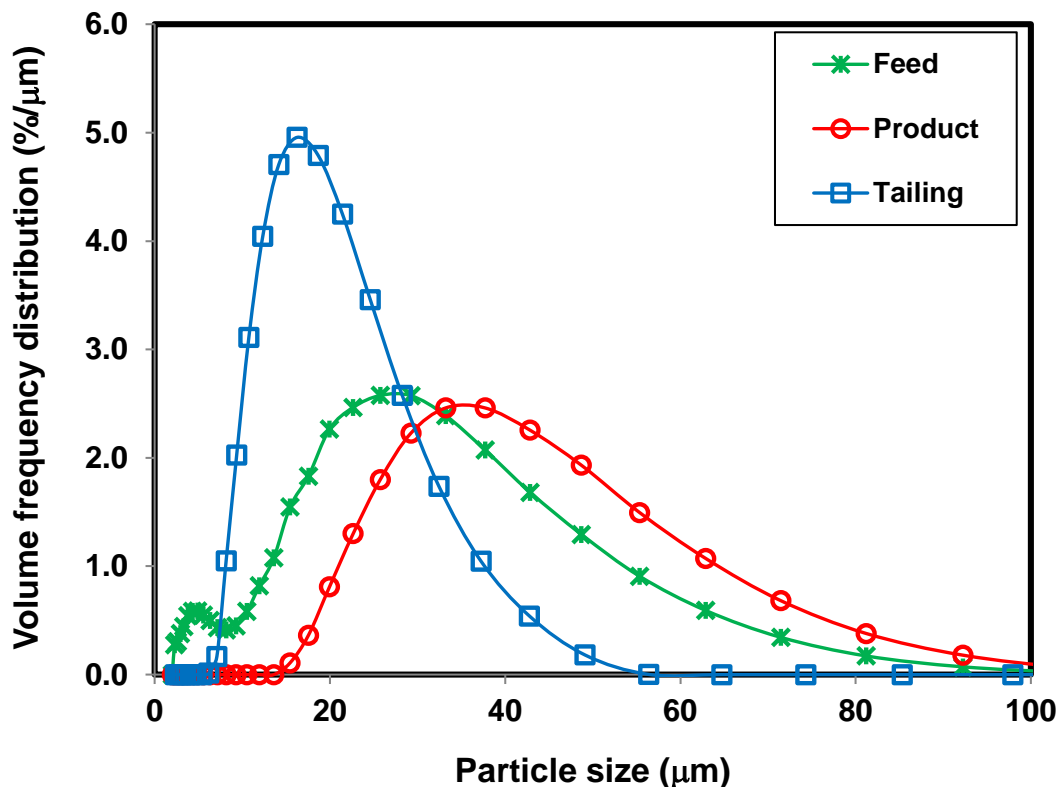


Figure 5.6: Floats volume frequency size distributions in the product, tailings and feed streams from Run 2 on the model feed at a product flux of  $0.17 \text{ m}^3/(\text{m}^2 \text{ h})$ . Raw data measured using Malvern 2000.

The cenosphere volume-based size distributions from each run were then material-balance reconciled and used to calculate the partition of cenospheres to the product stream as a function of their size. These partition curves are shown in Figure 5.7, and the calculated cut sizes and imperfections are given in Table 5.1. These show the volume-based recovery of different size fractions of cenospheres, which clearly show the poor performance below 20  $\mu\text{m}$  in size. The recoveries based only on cenospheres larger than 20  $\mu\text{m}$  in size, were about 78.0 vol.%, 76.4 vol.% and 69.0 vol.%, while the recoveries based on the entire size range were only around 69 vol.%, 67 vol.% and 61 vol.%, for Run 1, 2 and 3, respectively (decreasing overflow product flux).

Note that the volume-based recovery (partition number) was calculated using the particle volume-based size distributions, whereas the mass-based recovery reported in Figure 5.5 was calculated directly from the sample solids masses and calculated cenosphere grades. The density of cenospheres in the product is lower than in the feed (Table 5.1), as expected due to their higher rise velocities. This explains why the calculated volume-based recovery is usually larger than the estimated mass-based recovery (Table 5.1). Equation 5-3 shows how the volume-based recovery is theoretically related to the mass-based one:

$$R_{Vc} = (\rho_{cF}/\rho_{cP})R_{Mc} \quad (5-3)$$

where  $R_{Vc}$  and  $R_{Mc}$  are the volume-based and mass-based recoveries, respectively,  $\rho_{cF}$  and  $\rho_{cP}$  are the average density of cenospheres in the feed and the product. However, as shown in Table 5.1, this over predicts  $R_{Vc}$  compared to the value calculated from the Malvern size distribution data. This may reflect differences between the apparent volumes measured by light scattering compared with the skeletal volumes measured by gas pycnometry.

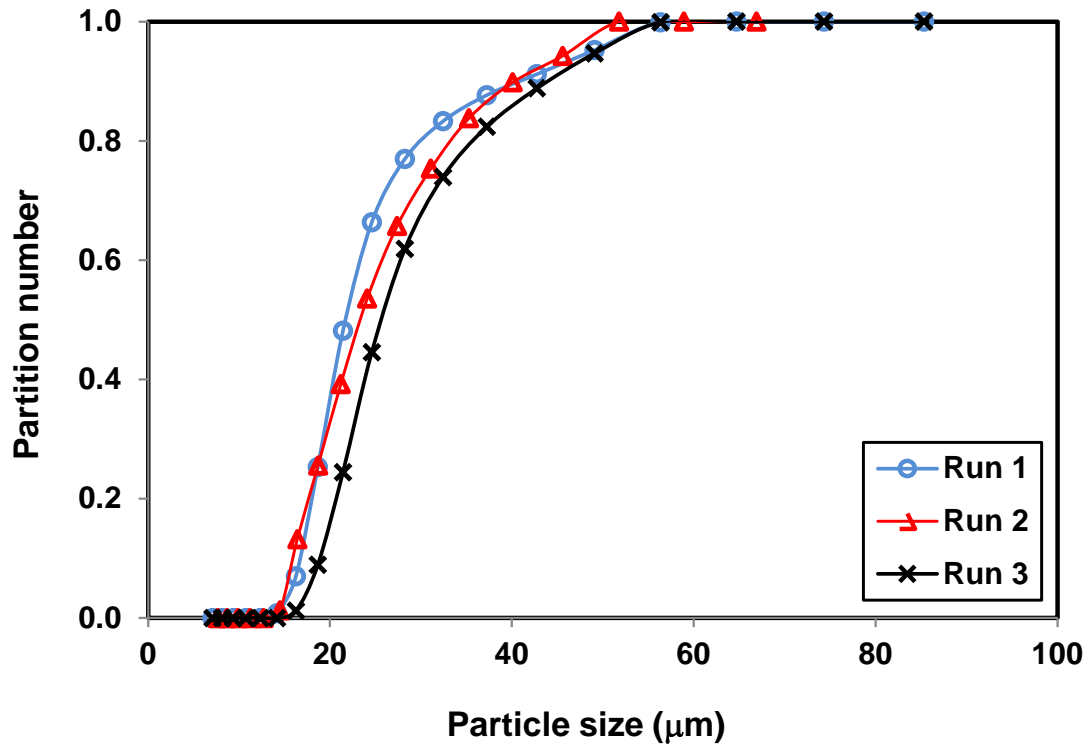


Figure 5.7: Partition of cenospheres to the product stream for experiments with the model feed at a volumetric flux of  $6.7 \text{ m}^3/(\text{m}^2 \text{ h})$  and slurry with 8.3% solids by mass. Curves based on material-balanced data.

A final experiment was performed using a model feed, but this time with a feed cenosphere grade of only 0.27 wt.%, which may be the case for some low grade raw fly ash feeds. In this experiment (Run 4), the feed and wash water fluxes, and the feed solids fraction, were set to the same levels used previously, but a higher product flux of about  $0.63 \text{ m}^3/(\text{m}^2 \text{ h})$  was used to increase the recovery of cenospheres. These conditions resulted in a product grade of 64.5 wt.%, but a recovery of only 31.3 wt.%. Hence although the inverted REFLUX™ Classifier has been shown to be effective at separating mixtures of positively and negatively buoyant particles, the recovery was much lower when processing feed with very low cenosphere grades. Assuming no difference in the feed particles size compared to the previous runs, this result suggests possible benefits from using feeds of higher grades, a hypothesis explored later in this thesis.

In the next section, the potential of this innovative method for separating cenospheres from real fly ash is studied.

### 5.4.2 Fly ash feed

This section concerns the separation of cenospheres from real fly ash feeds using the IRC™. The separation of cenospheres from fly ash was first studied at a very high feed solids concentration to maximize the solids processing rate. Then the role of the fluidization wash water on the process was examined by conducting an experiment with no fluidization water. Then in the main part of this section, the effects of different operating conditions on the separation process are investigated. The experimental results are reported firstly on the effects of fluidization wash water flux; then, two studies are reported showing the effects of increasing the feed volumetric flux. The first of these additional studies involved a volumetric product flux set at 20 % of the feed flux, while the second involved a volumetric product flux set at 40 % of the feed flux. Finally, the effects of the volumetric split ratio ( $P/F$ ), defined as the ratio of the product flux to the feed flux, on the separation performance is presented in detail. For this set of experiments, reported recoveries are based on both the entire size range and for a specified target size range (for example, greater than 50  $\mu\text{m}$ ), to show the losses of ultrafine cenospheres in the IRC™. Table 5.2 shows the experimental conditions for all experiments discussed in this section.

Table 5.2: Experimental parameters in different runs on real fly ash feed (based on raw data).

	Feed Cenosphere Grade (wt.%)	Feed Solids Concentration (wt.%)	Feed Flux (m/h)	Product Flux (m/h)	Wash Water Flux (m/h)	Volumetric Split Ratio (%)
Run 5	1.2	50.1	6.7	0.18	0.87	2.6
Run 6	0.93	49.3	6.6	0.36	0.87	5.5
Run 7	0.81	49.1	7.0	0.70	0.87	10.0
Run 8	0.73	51.1	7.0	0.68	0.00	9.8
Run 9	0.49	30.1	7.0	0.70	0.87	10.0
Run 10	0.60	31.3	7.0	1.4	0.87	20.0
Run 11	0.51	32.0	7.7	2.7	0.87	34.5
Run 12	0.71	32.0	6.4	2.8	0.35	43.6
Run 13	0.71	32.1	6.4	2.8	1.7	43.5
Run 14	0.78	32.1	6.3	2.7	2.8	42.2
Run 15	0.65	35.1	3.6	0.75	0.87	20.9
Run 16	0.50	34.8	13.9	2.8	0.87	20.3
Run 17	0.65	35.0	3.8	1.4	0.87	37.6
Run 18	0.61	35.4	9.8	2.1	0.87	21.4
Run 19	0.72	34.6	9.9	4.5	0.87	45.1
Run 20	0.72	35.3	12.6	5.3	0.87	42.2

#### **5.4.2.1 Separation at a high solids concentration**

In Runs 5-7, a very concentrated feed slurry with about 50 wt.% fly ash solids was used. The feed flux was about  $7.0 \text{ m}^3/(\text{m}^2 \text{ h})$  in all experiments. As shown in Figure 5.8, at three different product fluxes of about 0.18, 0.36 and  $0.70 \text{ m}^3/(\text{m}^2 \text{ h})$ , and fluidization water flux of about  $0.87 \text{ m}^3/(\text{m}^2 \text{ h})$ , product grades of around 77 wt.% were achieved. However, as shown in Figure 5.9 the recovery of the cenospheres was very low at around 30 wt.% in all three experiments, reflecting the dominant negative effects of the high feed suspension viscosity on the process.

#### **5.4.2.2 Zero-fluidization water effects**

Figure 5.8 and Figure 5.9 also present the cenosphere grade and recovery obtained in Run 8, which had similar conditions to Runs 5-7 except without any fluidization water. A very poor grade of about 1.8 wt.% was achieved showing the very important role of the fluidization water in washing the fine fly ash particles away from the product. The recovery of 15.2 wt.% was also very low, reflecting the dominant negative effect of high suspension viscosity. The lack of the effective mixing needed to separate cenospheres from fly ash in the device is also the other reason for the low cenosphere recovery in this experiment (Run 8). As a result, it was decided to use a lower feed solids concentration in subsequent experiments.

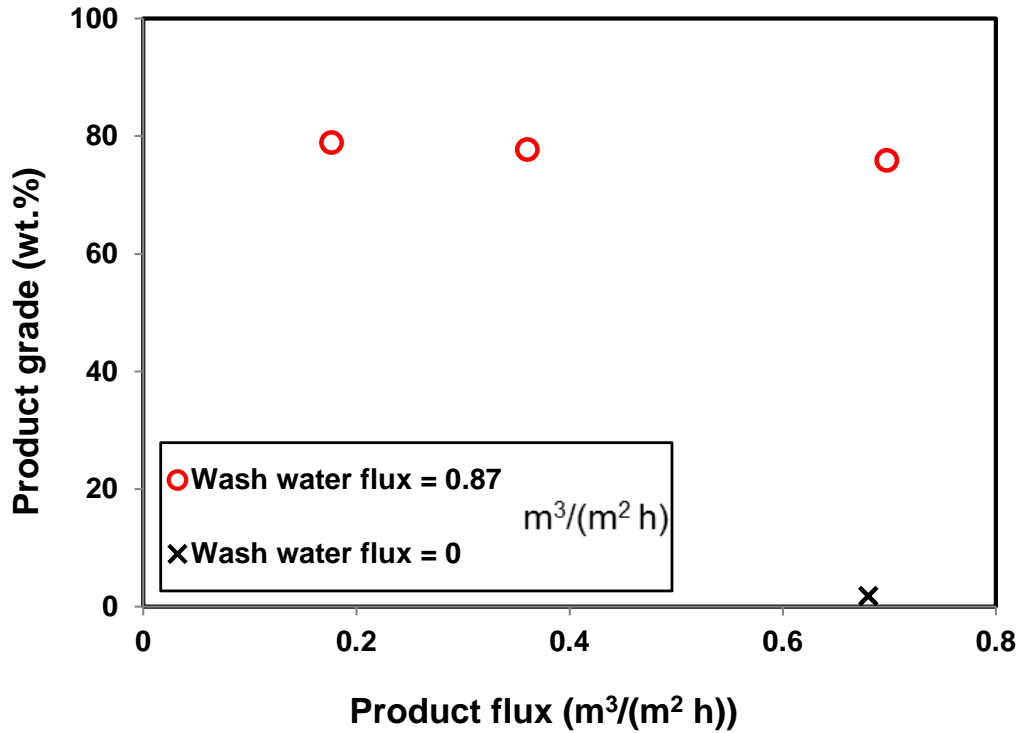


Figure 5.8: Product grade obtained at different product fluxes in the IRC™ at feed solids concentration of about 50 wt.% (Runs 5-8).

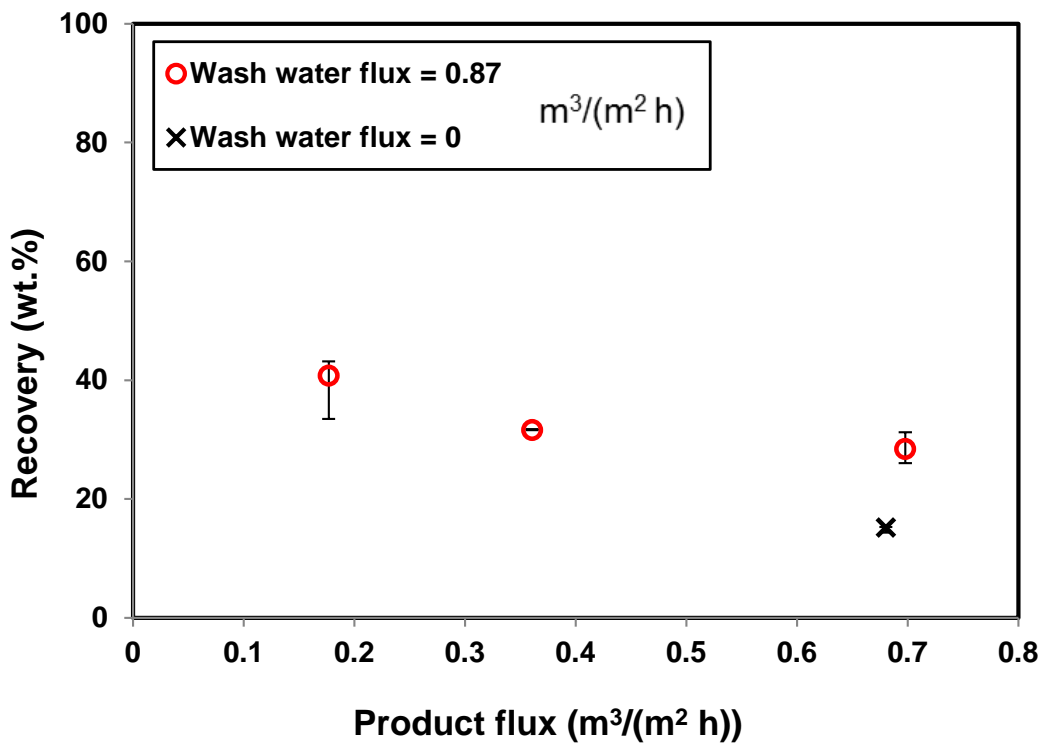


Figure 5.9: Cenosphere recovery for entire size range obtained at different product fluxes (Runs 5-8) in the IRC™ at feed solids concentration of about 50 wt.% based on reconciled data.

### 5.4.2.3 Effects of different operating conditions

A feed slurry containing around 0.53 wt.% cenospheres and 30 – 35 wt.% solids was prepared and used in Runs 9 – 20. The densities of the cenospheres floats and fly ash sinks fractions were measured to be about  $775 \text{ kg/m}^3$  and  $1873 \text{ kg/m}^3$  respectively, using gas pycnometry. The size distributions of cenospheres and fly ash sinks in the feed slurry are shown in Figure 5.10. The majority of the fly ash sinks particles is finer than  $100 \mu\text{m}$ , while the cenospheres are mostly between  $20 \mu\text{m}$  and  $200 \mu\text{m}$ . Note that there are small peaks in the cenosphere floats fraction less than about  $10 \mu\text{m}$ , most likely due to entrainment of very fine dense particles during the sink-float test.

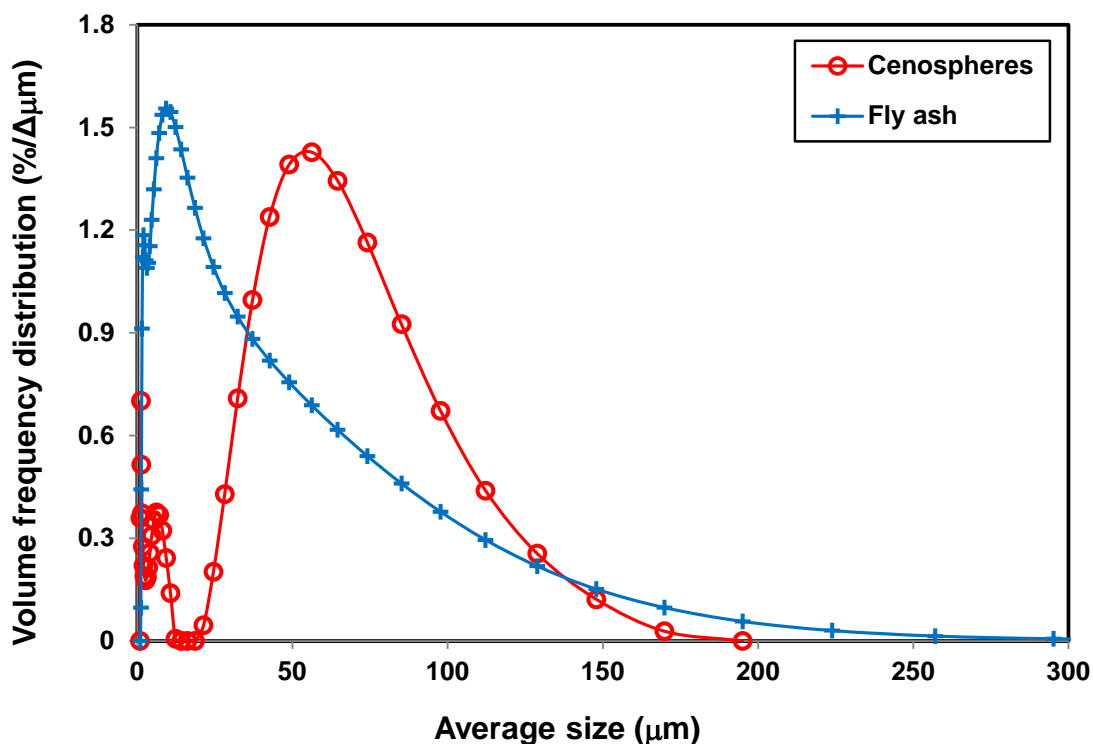


Figure 5.10: The volume frequency size distributions of the floats and sinks fractions in the fly ash feed slurry of Runs 9-20 as measured by a Malvern Mastersizer Model 2000 (raw data).

In this section (Runs 9-20) the first two sub-sections focus on the effects of fluidization water and feed fluxes on the separation process. In these parts, four sub-plots are presented in each of the Figures. These plots show (A) the product solids flux, (B) the product solids density, (C) the product grade of cenospheres, and (D) the recovery of the cenospheres. The product

solids flux and product solids density data were measured experimentally and curves fitted through the data using the error minimization technique (formulas shown on the related graphs). These curves were then used to calculate the cenosphere grade and recovery values as continuous curves. It is noted that the curves were used to present the trends of data more clearly and to provide further data points under different operating conditions.

Additional estimates of the cenosphere grades and recoveries were also calculated using Equations 5-1 and 5-2 directly from the raw gas pycnometry data, based on the assumption that the cenosphere density was  $\rho_c = 775 \text{ kg/m}^3$  and performing a sensitivity analysis by varying the assumed product's fly ash density ( $\rho_s = 1600$  to  $1830 \text{ kg/m}^3$ ). All raw data and sample calculations are presented in Appendix B and H.

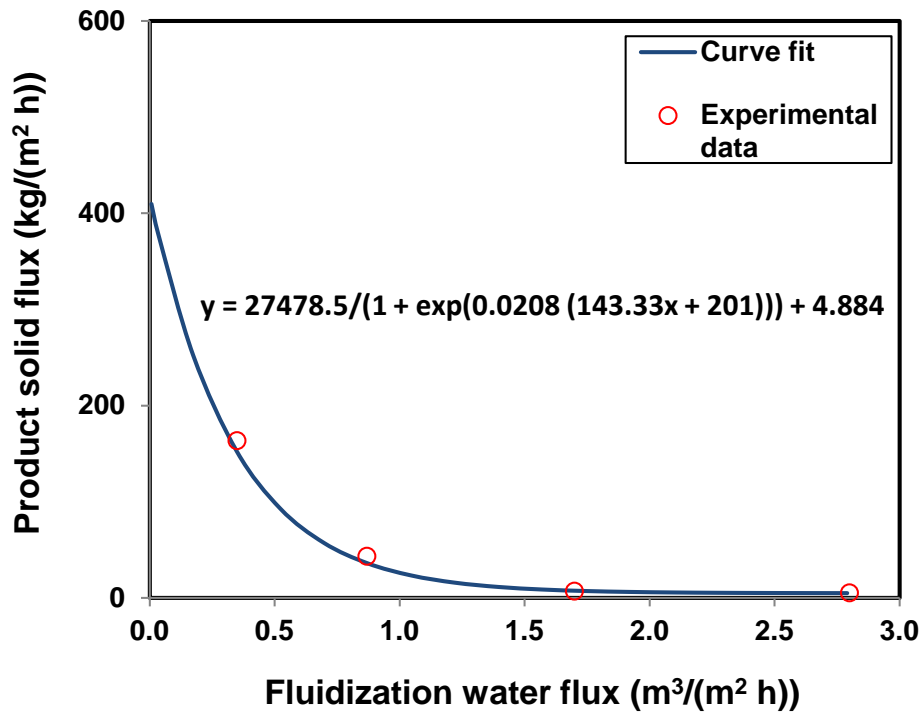
In the last part of this section, the effect of the split ratio ( $P/F$ ) on the separation process was examined using the accurate sink-float test, incorporating more detail on the particles size classification.

#### **5.4.2.3.1 Influence of fluidization rate**

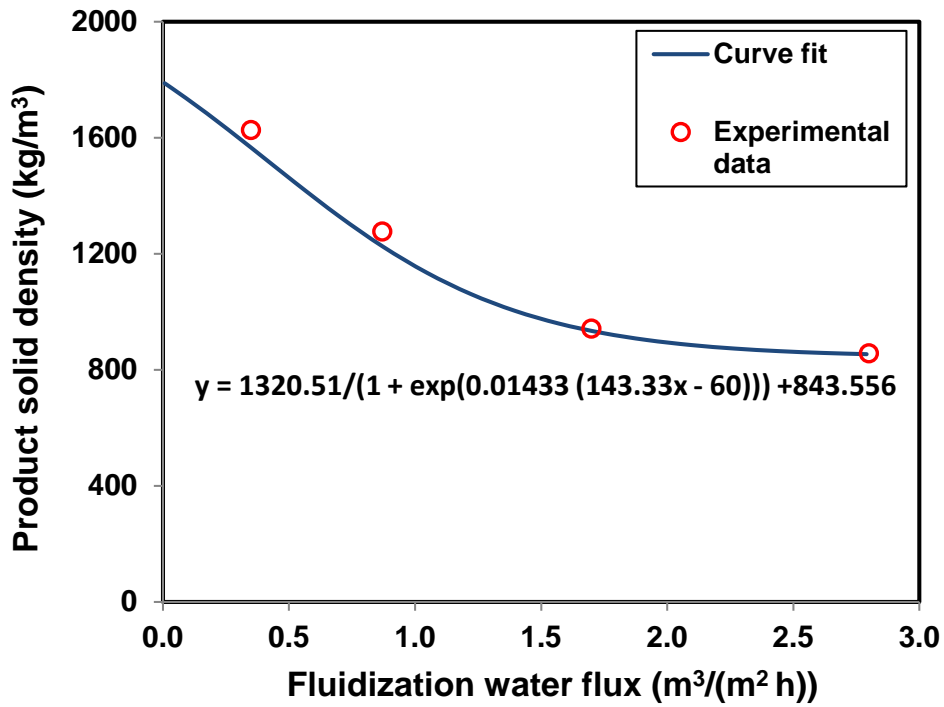
The fluidization rate, defined as the flux of water applied through the distributor for the purpose of washing the slimes from the final product, was found to have a significant effect on the separation of the cenospheres in the Inverted REFLUX™ Classifier. Figure 5.11 (A-D) shows the effects of the fluidization wash water flux on the system performance, with the feed total volumetric and solids mass fluxes fixed at about  $7.0 \text{ m}^3/(\text{m}^2 \text{ h})$  and  $2400 \text{ kg}/(\text{m}^2 \text{ h})$  respectively, and the overflow volumetric flux set at 40 % of the feed flux (Runs 11 – 14). From Figure 5.11A it is evident that the rate of product solids decreases exponentially as the wash water flux increases, reflecting the removal of unwanted ultrafine fly ash, and increasing losses of cenospheres. The average solids density of the product also decreases (Figure 5.11B), approaching the value of  $775 \text{ kg/m}^3$ , which is the nominal density of the clean cenospheres.

The smooth curves through data sets A and B were combined with the feed flux of the cenospheres, the clean cenosphere density of  $775 \text{ kg/m}^3$ , and the assumed density of the overflow fly ash, to calculate cenosphere grade and recovery curves using Equations 5.1 and 5.2 (Figure 5.11, subplots C and D respectively). It is evident that the cenosphere grade improved dramatically as the fluidization wash water flux increased. However, the recovery

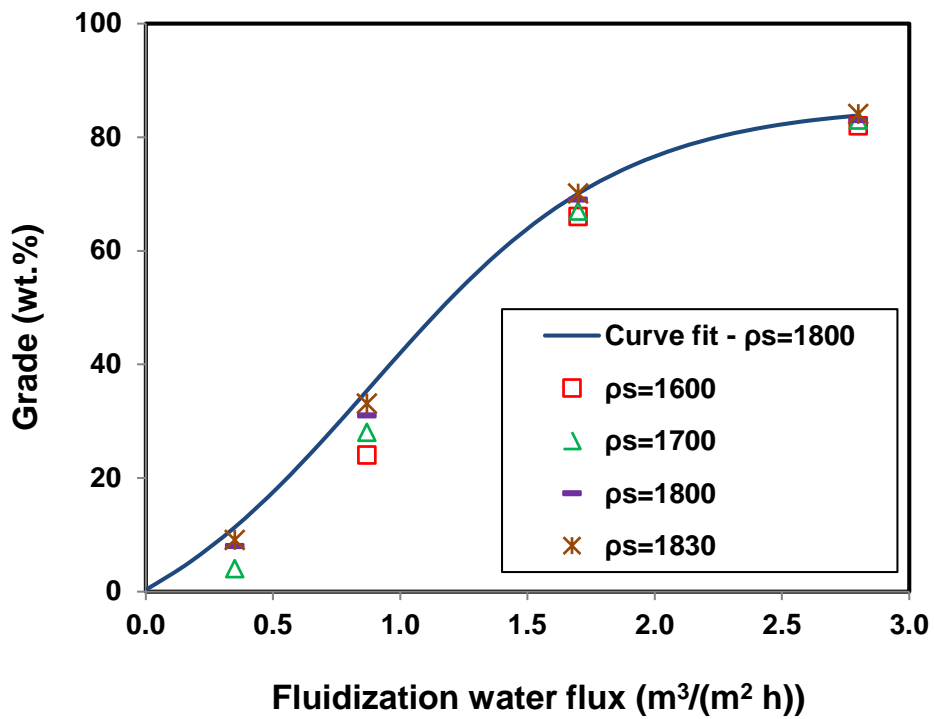
decreased significantly. The sensitivity of the results to the assumed fly ash density in the overflow product was assessed by recalculating the performance using different fly ash density values. This uncertainty of fly ash density had little effect on the grade. However, as the recovery is directly calculated from the cenosphere grade and the total mass of solids in the product, a slight error in the grade curve can generate a large error in the recovery curve. So the effect of the uncertainty in the fly ash density on recovery was significant.



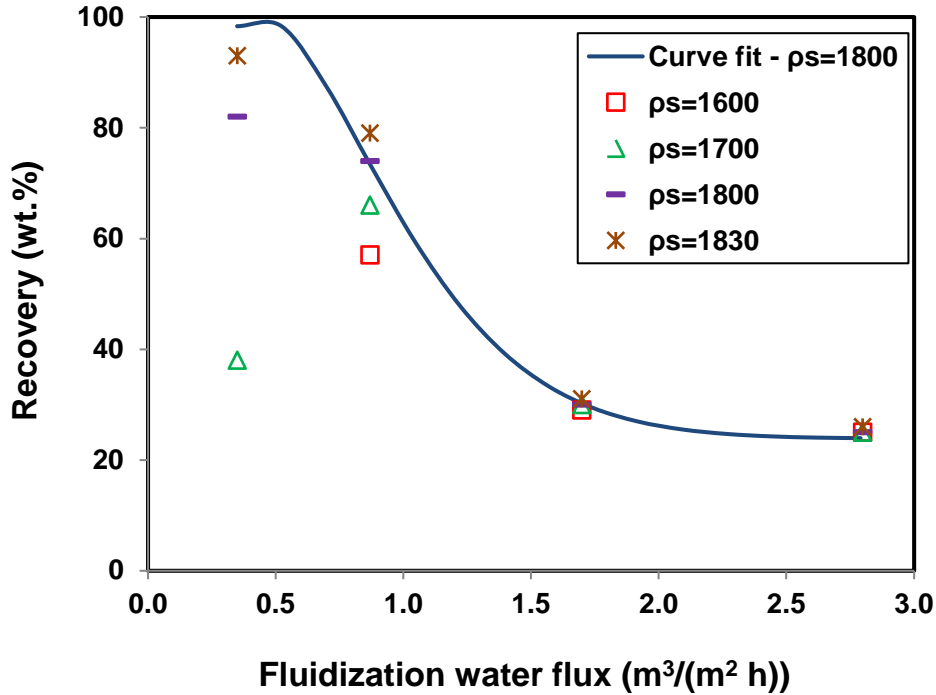
Graph A.



Graph B.



Graph C.



Graph D.

Figure 5.11: The influence of fluidization water on (A) product solid flux (B) product solid density (C) grade of cenospheres in product (D) recovery of cenospheres in product. Note that at the fluidization water flux of about  $0.35 \text{ m}^3/(\text{m}^2 \text{ h})$ , the measured average solids density was about  $1630 \text{ kg/m}^3$  (Graph B), so it makes no sense to calculate grades or recoveries based on an assumed fly ash density of  $1600 \text{ kg/m}^3$ .

#### 5.4.2.3.2 Influence of the feed rate

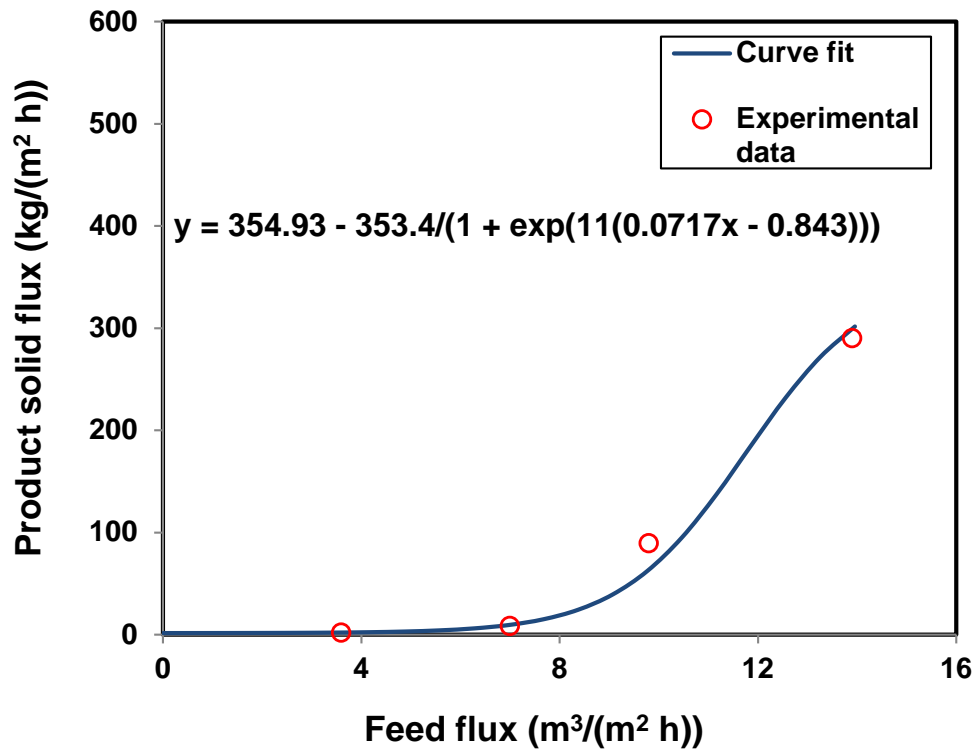
The separation performance in the Inverted REFLUX™ Classifier was also investigated using two different ratios of the product rate to the feed rate. Clearly, a doubling of the feed rate results in a doubling of the feed cenosphere rate and hence there is, in principle, a need to double the product rate to maintain recovery.

Case 1. Split ratio = 0.2

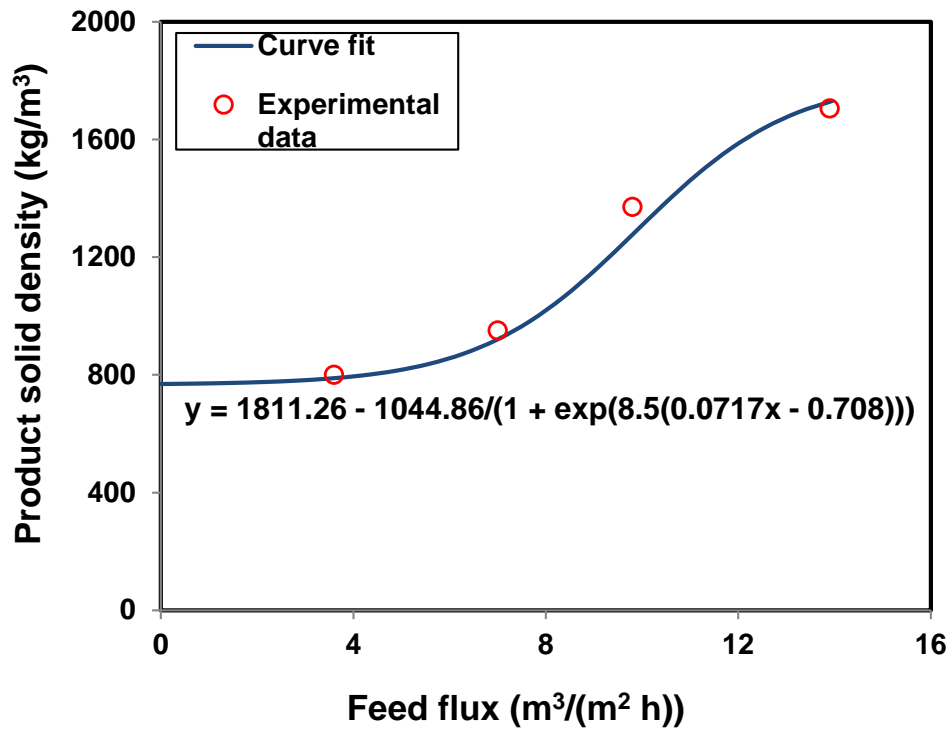
Figure 5.12 (A-D) shows the effects of changes in the volumetric feed flux, with fixed fluidization flux of  $0.87 \text{ m}^3/(\text{m}^2 \text{ h})$ , and a volumetric overflow flux set at 20 % of the volumetric feed flux (Runs 10, 15, 16 and 18). Once again, the first two graphs are based on precise experimental measurements, with smooth curves fitted. The other two graphs are again calculated from the first two graphs, with the usual assumptions applied to the

cenosphere and fly ash densities. It is evident that at low feed flux the product solids flux reporting to the overflow was negligible; however, the product flux suddenly increased once the feed flux increased above a critical level. This result is attributed to the effects of a fixed wash water fluidization flux, which generates a strong downwards net volumetric flux at low feed rates and so results in low product solids flux levels. The cenosphere grade is clearly very high at low feed fluxes due to the dominant effects of the wash water flux over the relatively low product flux. However, as expected, the grade declines with increasing feed flux.

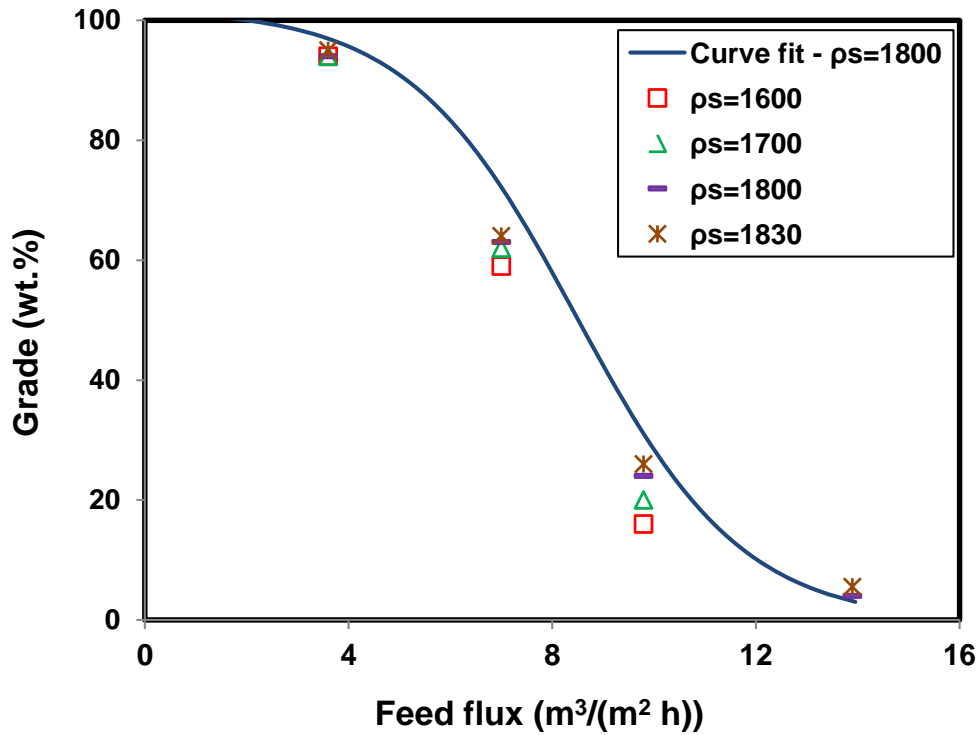
Two important factors, the fluidization water flux and the fluid velocity through the inclined channels, control the cenosphere recovery in the Inverted REFLUX™ Classifier. At a low feed rate and consequently a low product rate, the downwards fluidization water dilutes the upper zone. Under these conditions, the product rate is insufficient to recover all of the ceno-spheres, leading to a drop in the cenosphere recovery. By increasing the feed rate and the product rate, the role of the fluidization water in controlling the recovery decreases, allowing more ceno-spheres to be recovered. However, by further increasing the feed rate, the local fluid velocity through the inclined channels increases, resulting in more of the ceno-spheres being entrained to the underflow tailings stream. Therefore, interestingly, a strong optimum is apparent in the cenosphere recovery. This reflects the dominant effects of the fluidization wash water at low feed fluxes, and the limited residence time at high feed fluxes.



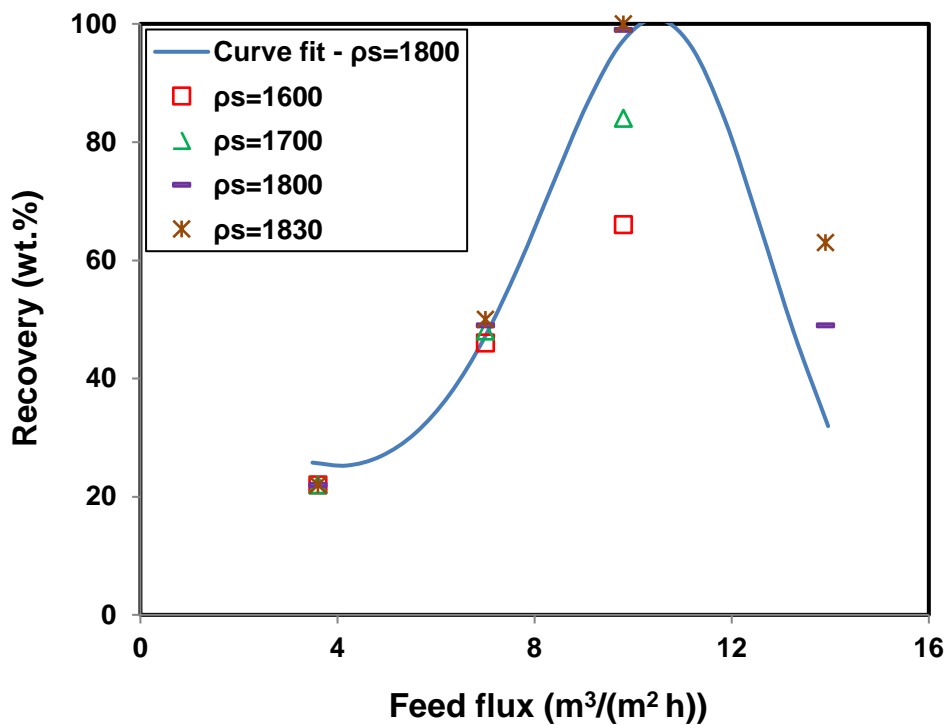
Graph A.



Graph B.



Graph C.

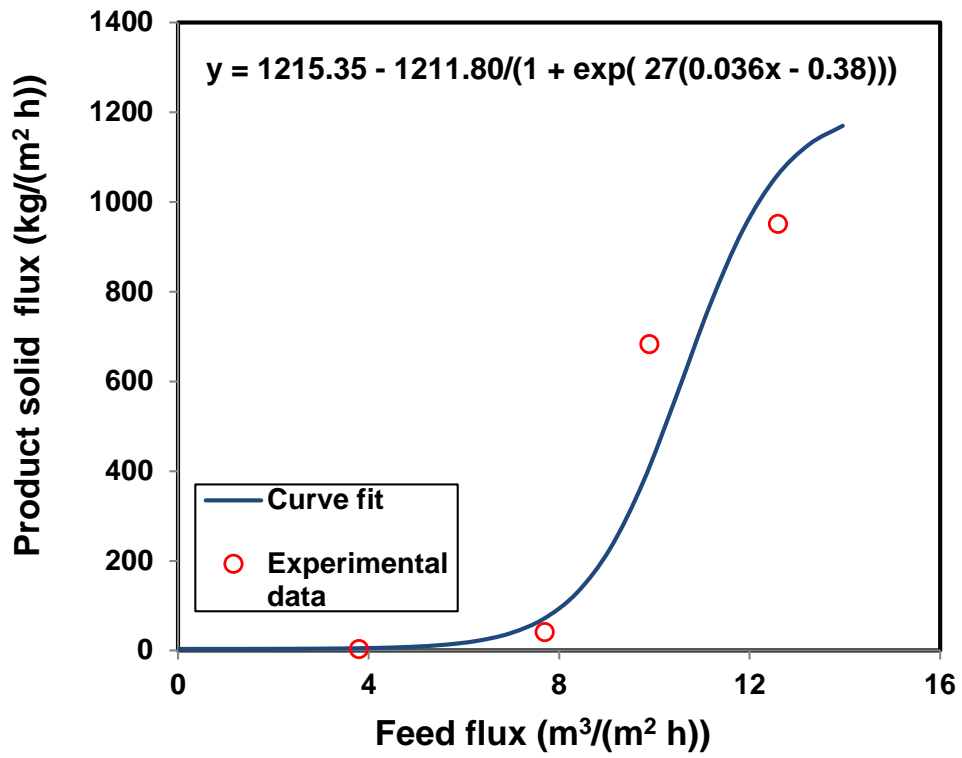


Graph D.

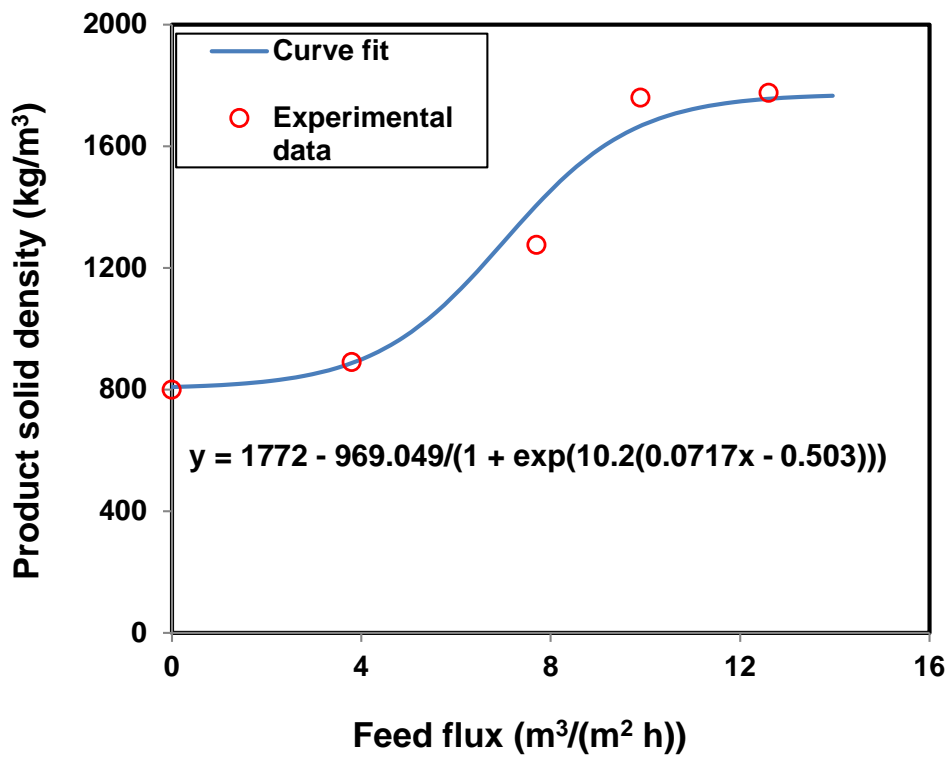
Figure 5.12: The investigation of feed flux variation (with ratio of product volumetric flux to feed volumetric flux set equal to 0.2) on (A) product solid flux (B) product solid density (C) grade of cenospheres in product (D) recovery of cenospheres in product.

## Case 2. Split ratio = 0.4

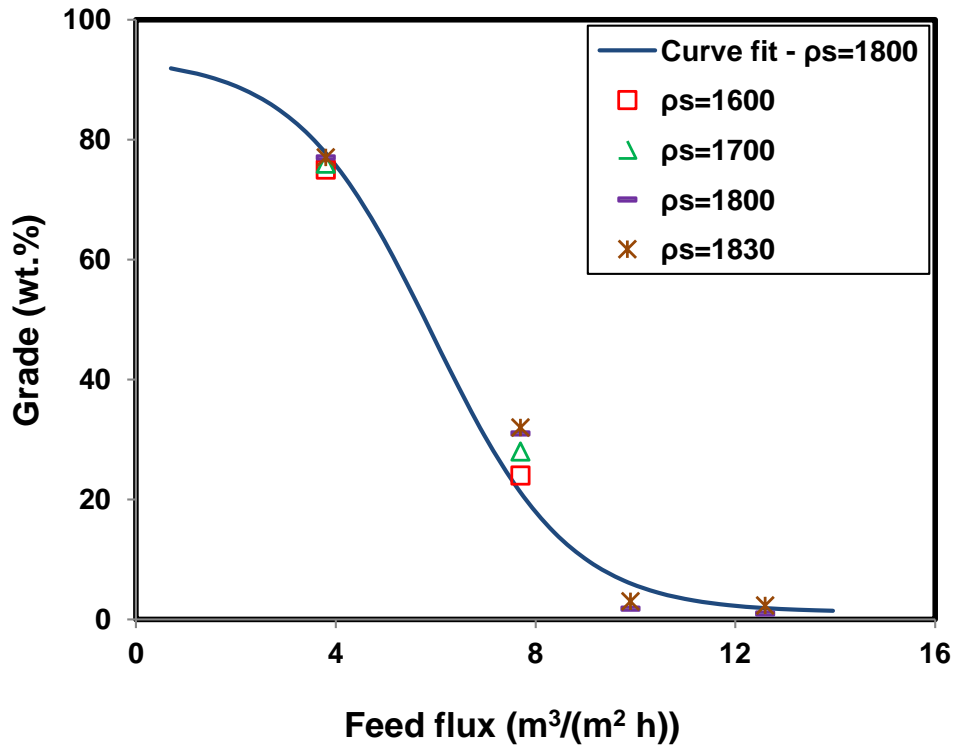
Figure 5.13 (A-D) shows the third series of results. This series is similar to that shown in Figure 5.12, except that the volumetric overflow flux of the product was set at 40% of the volumetric feed flux (Runs 11, 17, 19 & 20). Once again, at low volumetric feed flux values, the product solids flux was low due to the dominant effects of the fluidization wash water. As volumetric feed flux increased, the product solids flux increased rapidly to much higher levels than in the other experiments. Thus, in this case the grades were generally lower and the recoveries higher. These conditions make good sense in first stage processing where the goal should be to elevate the cenosphere grade to a satisfactory level, while insuring maximum recovery.



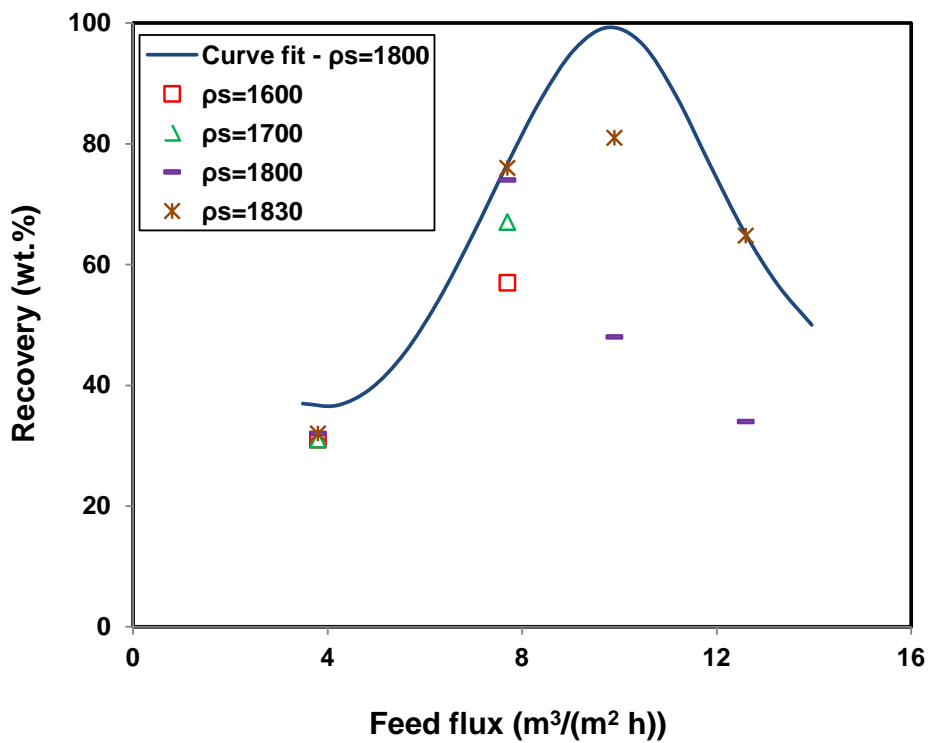
Graph A.



Graph B.



Graph C.



Graph D.

Figure 5.13: The investigation of feed flux variation (with ratio of product volumetric flux to feed volumetric flux set equal to 0.4) on (A) product solid flux (B) product solid density (C) grade of cenospheres in product (D) recovery of cenospheres in product.

### 5.4.2.3.3 Influence of the split ratio

The experiments in this part (Runs 9-11) were analyzed using the sink-float test in order to obtain a more accurate measurement of the system performance. The system was fed at a solids flux of about 2300 kg/(m<sup>2</sup> h), corresponding to a volumetric feed flux of 7.0 m<sup>3</sup>/(m<sup>2</sup> h). At a low split ratio ( $P/F$ ) (Run 9), a product grade of 76 wt.% was achieved, corresponding to an upgrade of 151. This is a remarkable result from a single separation stage. However, the recovery of the cenospheres was considered too low at 42 wt.%. By increasing the split ratio (Run 11), a significantly higher recovery of 64 wt.% was achieved, but at a much lower upgrade of 33. In another experiment with the same operating condition as in the last two cases, but at a moderate split ratio (Run 10), an upgrade of about 126 and a recovery of about 49 wt.% were achieved. The variation of grade and recovery of cenospheres with the split ratio is shown in Figure 5.14. When the product flux is increased, slow settling fly ash particles are entrained resulting in a decrease in the grade of cenospheres in the product. At the same time, slow floating cenosphere particles will convey with the product stream, increasing the recovery of the cenospheres.

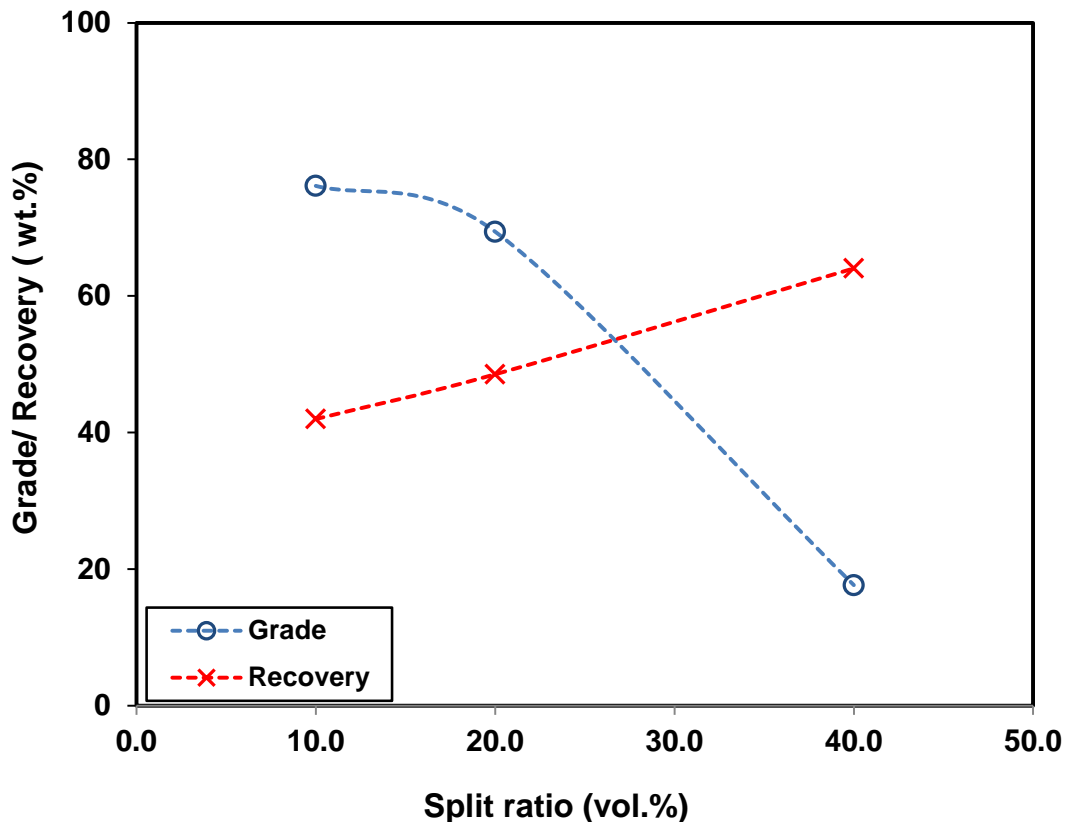


Figure 5.14: Grade and recovery of cenospheres at different split ratios (Runs 9-11).

#### 5.4.2.4 Variation in recovery with particle size

The recovery values presented in the last section were based on particles covering the full size range. If these recoveries were reported with respect to a target particle size range of, for example, greater than 50  $\mu\text{m}$ , the values would be significantly higher. To examine the drop in cenosphere recovery with particle size, the experiments in the previous section were analyzed in detail in terms of size classification.

In all cases most of the losses were found to be attributed to ultrafine (less than 50  $\mu\text{m}$ ) cenosphere particles, being entrained to the underflow. As shown in Figure 5.15, at the volumetric split ratios of about 10 %, 20 % and 35 %, the total volume-based recoveries were about 56 vol.%, 67 vol.% and 80 vol.% , however, the recoveries of particles larger than 50  $\mu\text{m}$  were 66 vol.%, 80 vol.% and 91 vol.%, respectively. These results confirm that the losses involved relatively fine particles.

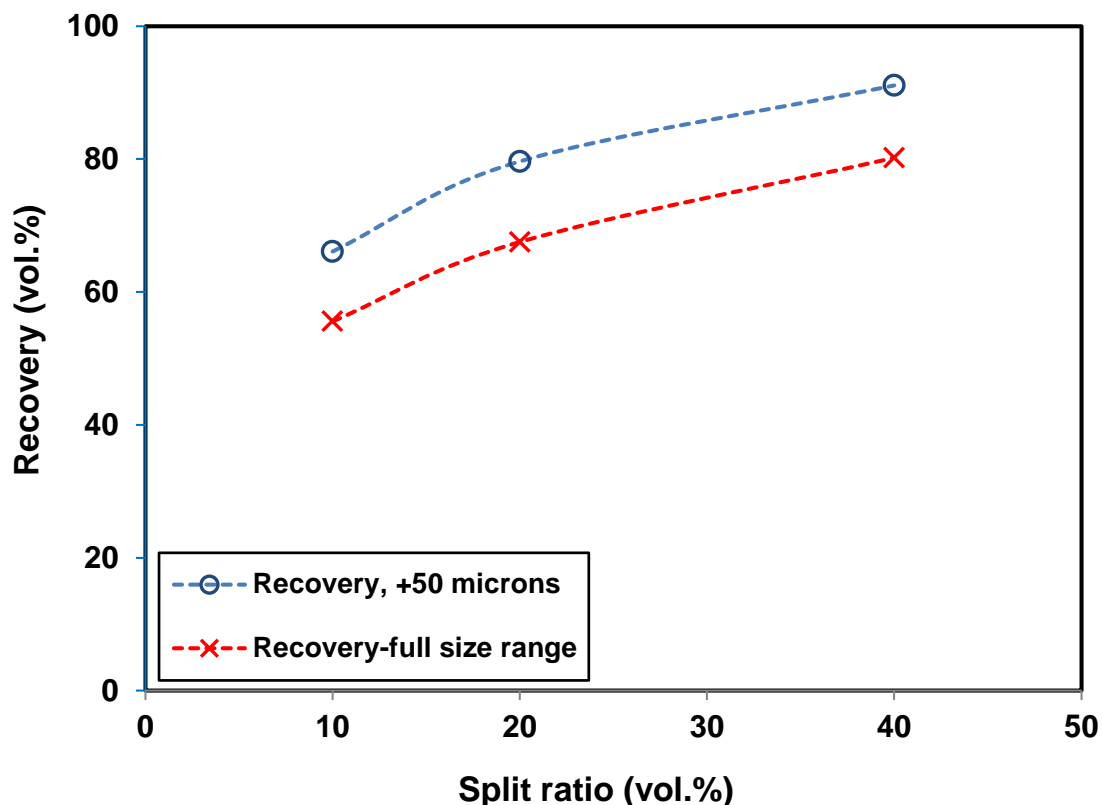


Figure 5.15: Volume-based recovery of cenospheres obtained at different split ratios for the full particles size range compared with recoveries based only on particles larger than 50  $\mu\text{m}$  (Runs 9-11).

Using the size distributions of cenospheres in the product, tailings and feed, a partition curve showing the recovery as a function of size was plotted for each experiment. As shown in Figure 5.16, increasing the product flux caused a decrease in the  $d_{50}$  as smaller cenospheres had a greater chance to exit in the product. Imperfection ( $I$ ), which indicates the sharpness of separation, was almost constant, probably reflecting the constant feed conditions in all these experiments. The  $d_{25}$ ,  $d_{50}$  and  $d_{75}$ , and  $I$  are presented in Table 5.3.

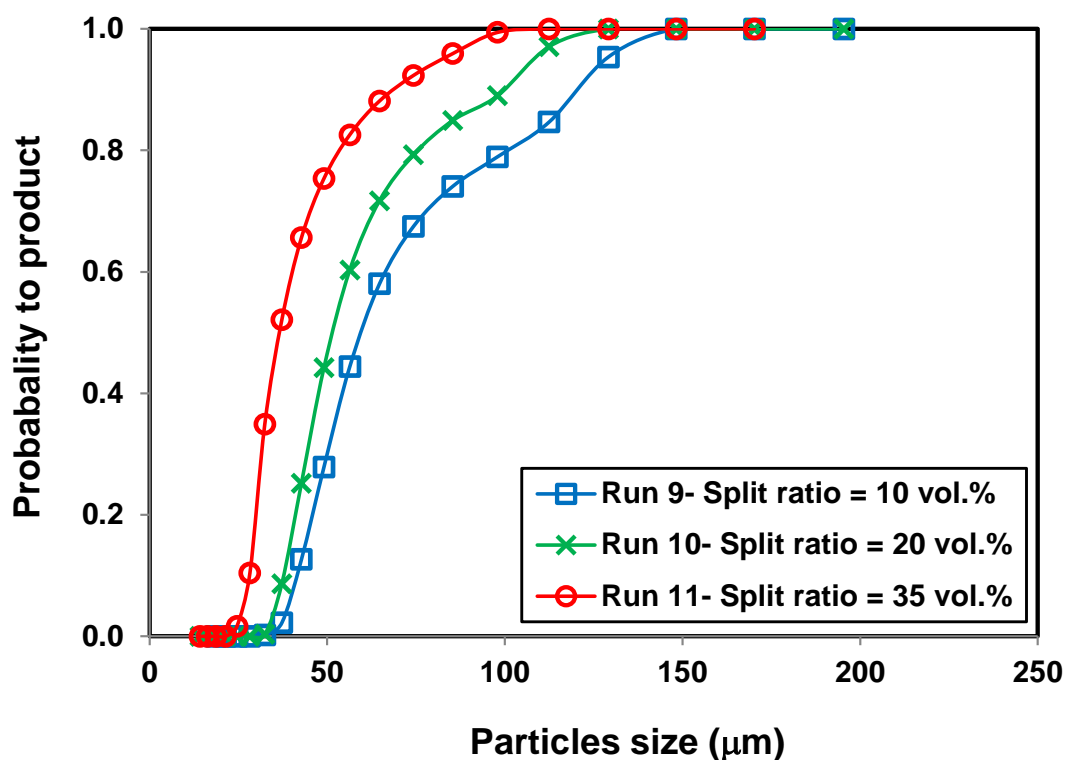


Figure 5.16: Partition curves at different split ratios (based on volume-balance reconciled data) (Runs 9-11).

Table 5.3:  $d_{25}$ ,  $d_{50}$ ,  $d_{75}$  and  $I$  for the runs at different product fluxes (Runs 9-11).

	Product flux ( $\text{m}^3/(\text{m}^2 \text{ h})$ )	Split ratio (vol.%)	$d_{25}$ ( $\mu\text{m}$ )	$d_{50}$ ( $\mu\text{m}$ )	$d_{75}$ ( $\mu\text{m}$ )	$I$
Run 9	0.7	10	48.0	59.0	88.0	0.34
Run 10	1.4	20	43.0	52.0	68.0	0.24
Run 11	2.5	35	30.5	36.5	49.0	0.25

#### 5.4.2.5 Combined effects of product rate and fluidization rate

The difference between the product flux,  $P$ , and wash-water flux,  $W$ , was found to be a key parameter, best represented by the difference,  $(P - W)$ , in controlling the product grades and cenosphere recoveries in the IRC<sup>TM</sup>. As shown in Figures 5.17 and 5.18, the grade of the cenospheres in the product decreased as  $(P - W)$  increased due to the entrainment of the dense fly ash particles, while the recovery of cenospheres in the product generally increased. The recovery data point at the highest  $(P - W)$  value in Figure 5.18 was for an experiment conducted using an excessive feed flux, resulting in a decrease in the cenosphere recovery due to the high velocity in the inclined channels. In fact the peak is at the same location as those in Figures 5-12(D) and 5-13(D). Clearly, the net upward flux,  $(P - W)$ , is an important factor in controlling the grade and recovery of the product, similar to the so-called “bias flux” (Mohanty & Honaker, 1999) used in froth flotation to describe the effect of wash water addition.

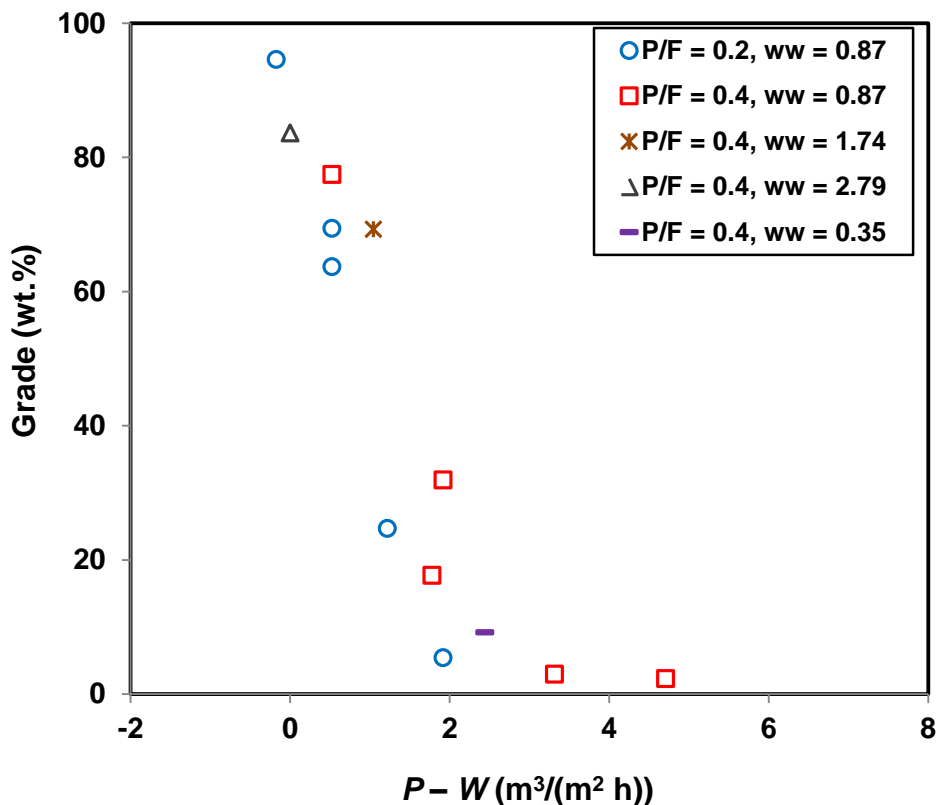


Figure 5.17: Product grade versus  $(P - W)$  parameter for the experiments at different operating conditions.

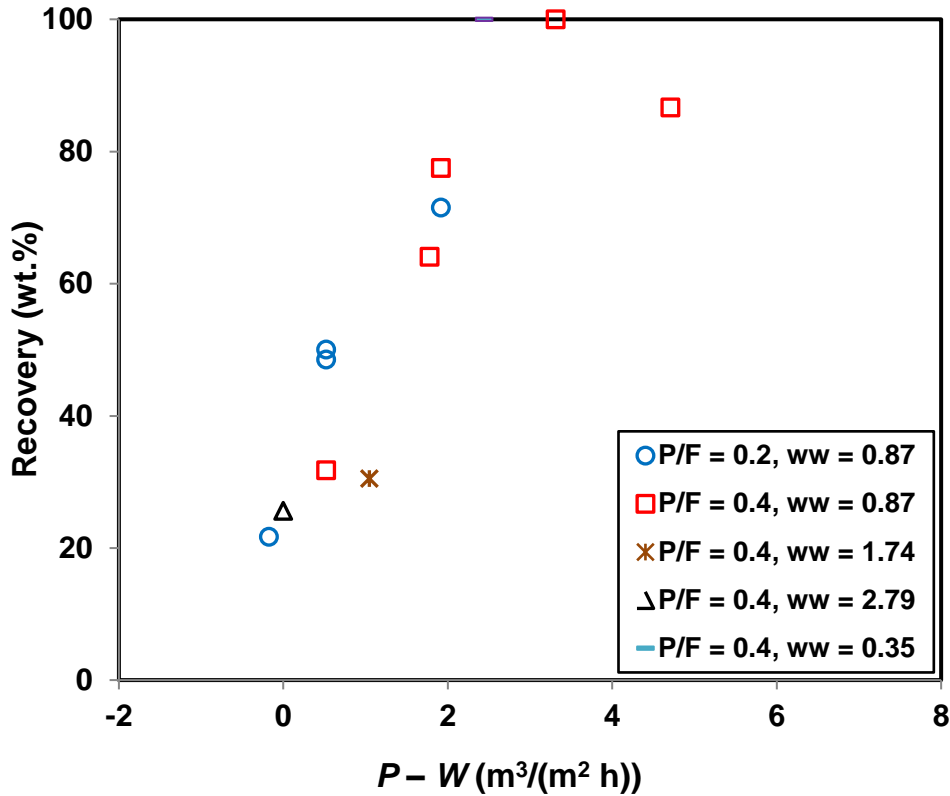


Figure 5.18: Recovery versus ( $P - W$ ) parameter for the experiments at different operating conditions.

#### 5.4.2.6 Density-based classification of cenospheres and fly ash in the IRC™

Table 5.4 shows the density of cenosphere particles in each stream of Runs 5, 6 and 7, reflecting the density classification of particles occurred in the IRC™. Lower density cenospheres provide a higher buoyancy driving force and hence are more likely to be recovered in the product. On the other hand, denser cenospheres can be entrained to the tailings stream. A density classification also occurred for fly ash particles, as lower density particles were more likely to entrain in the product while high density particles were more likely to exit in the tailings.

Table 5.4: Density of cenospheres and fly ash in feed, tailings and product of Runs 5, 6 & 7.

	Cenospheres density (kg/m <sup>3</sup> )			Fly ash density (kg/m <sup>3</sup> )		
	Feed	Product	Tailings	Feed	Product	Tailings
Run 5	837	733	859	1922	1320	1920
Run 6	825	713	974	1838	1510	1850
Run 7	789	732	941	1878	1719	1865

Table 5.5 shows the detailed density and size distributions of the cenospheres particles in the feed, product and tailings of Run 5. As predicted, in each size interval, the cenospheres density in the product is generally lower than the density values in the tailings and feed. Considering the density of cenospheres in the feed in different size intervals, it is evident that there is no significant difference between the cenospheres average density over the particle size ranges.

Table 5.5: Mass and density of cenospheres in feed, product and tailings for different size ranges (Run 5 based on reconciled data).

Size ( $\mu\text{m}$ )	Feed		Product		Tailings	
	Mass fraction (wt.%)	Density ( $\text{kg/m}^3$ )	Mass fraction (wt.%)	Density ( $\text{kg/m}^3$ )	Mass fraction (wt.%)	Density ( $\text{kg/m}^3$ )
-63	33.81	836	6.61	712	47.82	832
-106+63	47.27	828	51.14	700	45.27	880
+106	18.92	857	42.24	780	6.91	887

In fact, the rise and settling velocities of cenosphere and fly ash particles depend on both particle size and density. A more detailed analysis of the feed size and density distribution achieved using the novel, double fractionation technique, was provided in the previous chapter (Chapter 4).

## 5.5 Conclusions

The potential of the Inverted REFLUX™ Classifier system for separating positively buoyant cenospheres from dense materials was investigated via a series of preliminary experiments. The IRC™ consists of an inclined channel section, offering a very significant throughput advantage over conventional fluidized beds. A preliminary study involving the separation of commercial cenospheres from silica flour was carried out, showing the strong potential of the IRC™ to be used for separating cenospheres from real fly ash samples.

The effects of different operating parameters on the separation performance in the IRC™ were investigated in this chapter. Results showed that the fluidization wash water is an important factor in controlling the grade and recovery of the cenospheres, providing a means for washing the entrained ultrafine dense fly ash from the product stream. Excessive fluidization, however, led to significant product loss. The product grade decreased as the feed flux increased, while the product recovery exhibited a clear optimum with respect to the feed flux. In general, as the

product flux increased relative to the feed flux, the recovery increased, and the grade decreased. Furthermore, increasing the split ratio led to an increase in the cenosphere recovery and a decrease in the product grade. The Inverted REFLUX™ Classifier is based on gravity separation, and hence most of the loss in cenosphere recovery was shown to be related to the ultrafine cenosphere particles, less than 50 μm in diameter. The difference between the volumetric rate of product and fluidization wash water, was found to be a parameter that provided a useful measure of the performance of the Inverted REFLUX™ Classifier under different operating conditions. It was also evident that the particle classification based on density also occurred within the two floats and sinks fractions, which was another important reason for the loss in grade and recovery.

In the next chapter, a fly ash feed with a higher cenosphere concentration is used. With such high cenosphere concentrations, the separation of cenospheres from fly ash is hypothesized to be promoted by the combined effects of the inclined settling and the bulk streaming phenomena discussed in Chapter 3.

## **Chapter 6**

# **Enhanced Recovery and Concentration of Cenospheres from Fly Ash Particles in the Inverted REFLUX™ Classifier**

### Journal Article(s) Related to the Chapter and Authors' Contribution

**Kiani, A.,** Zhou, J. & Galvin, K.P. (2015). Enhanced Recovery and Concentration of Positively Buoyant Cenospheres from Negatively Buoyant Fly ash Particles using the Inverted Reflux Classifier. *Minerals Engineering*, 79, 1-9.

Author	Contribution
Ali Kiani	The lead author of the paper, collaborator in experimental design, primary interpretation of results, analysis of data, and experimental operator
James Zhou	Co-supervisor, experimental support
Kevin Galvin	Principal supervisor, collaborator in experimental design and results interpretation, inventor and designer of system

## 6.1 Introduction

This chapter examines the enhanced separation of valuable positively buoyant cenospheres from negatively buoyant fly ash particles using an Inverted REFLUX™ Classifier (IRC™). The effect of varying the feed suspension density on the recovery and concentration was studied. Feed pulp densities ranging from 10 wt.% to 46 wt.% were tested. Using a sufficiently high fly ash concentration, it is hypothesised that a powerful bulk streaming phenomenon develops (Batchelor & Van Rensburg, 1986) within the inclined channels, enhancing the segregation of the positively and negatively buoyant species. The separations are assessed in terms of the partitioning of the cenospheres between the overflow and underflow exit streams. The separation is then investigated using different feed flow rates, providing the basis needed for ensuring optimum performance in future pilot scale investigation of this novel technology.

## 6.2 Background

The previous chapter presented the results of preliminary trials which demonstrated the potential of an Inverted REFLUX™ Classifier (IRC™) to concentrate and recover positively buoyant cenospheres from fly ash. This chapter builds directly on the previous one, utilizing dense medium effects (i.e. the enhanced buoyancy driving force of light particles and/or the bulk streaming motion phenomenon) to promote an even more powerful overall separation.

In concentrated suspensions, equation 2-33 proposed by Richardson and Zaki (1954) is used to predict the hindered settling velocity. For a suspension involving mixtures of particles with varying densities, the behaviour is more complex and can be predicted based on the suspension average density using equation 2-36 proposed by Asif (1997). According to Asif's equation, for cenospheres with a density of about  $802 \text{ kg/m}^3$  in a fly ash suspension of density  $1214 \text{ kg/m}^3$  (38 wt.% pulp density, with the fly ash density  $1863 \text{ kg/m}^3$ ), the effective density difference driving force in the concentrated suspension is  $412 \text{ kg/m}^3$ , compared with  $198 \text{ kg/m}^3$  in a dilute suspension. These data, derived from the conditions of this study, give a dimensionless density ratio of 2.1:1. However, based on equation 2-31 proposed by Thomas (1965), the suspension viscosity, relative to the viscosity of the underlying liquid, increases by a similar factor, hence the pseudo fluid approach fails to predict any significant benefit.

Masliyah (1979) also developed equation 2-39 for the velocity of species in multi-component suspensions. Equations 2-33, 2-36 and 2-39 predict completely different species velocities in suspensions containing positively buoyant particles and dense particles. In such suspensions, as the heavy particles settle, the displaced water moves upward and hence enhances the rise velocity of the light particles. Moreover, for a suspension containing solids denser than water, increasing the suspension pulp density leads to an enhancement of the effective density of the suspension and hence increases the buoyancy driving force acting on the light particles. On the other hand, increased effective viscosity of the suspension hinders the rise velocity of the light particles.

Figure 6.1 shows an analysis performed on a fly ash suspension containing 1 wt.% cenospheres (i.e. same as the experimental case study in this chapter) with a density of  $802 \text{ kg/m}^3$  and a uniform size of  $81 \text{ }\mu\text{m}$ , mixed with 99 wt.% fly ash particles of density  $1880 \text{ kg/m}^3$  and uniform size of  $61 \text{ }\mu\text{m}$ . The ratio of the cenospheres predicted rise velocity in the suspensions relative to their terminal free rise velocity is plotted at different feed solids concentrations. The Masliyah model predicts a peak in the cenospheres rise velocity with increasing solids concentration. This reflects the dominant beneficial effect of the increased suspension density at lower feed solids concentrations and the dominant hindering effect of the rapidly increasing suspension viscosity at higher feed solids concentrations. According to Richardson-Zaki equation, the velocity of positively buoyant cenospheres decreases with increasing solids concentration. In contrast, the Asif model predicts a steady increase in the cenospheres' velocity with increasing solids concentration, which is clearly unrealistic. Predictions of these three models and their corresponding sample calculations are presented in Appendix F and H, respectively.

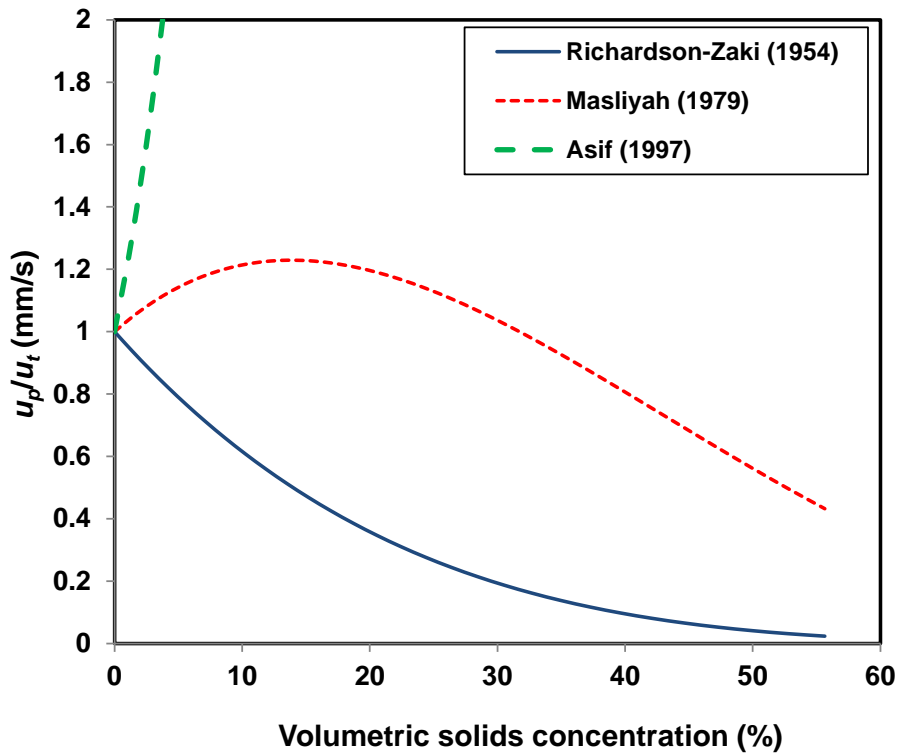


Figure 6.1: The rise velocity of cenospheres in fly ash slurry at different feed pulp densities predicted by three different models.

In suspensions containing both positively and negatively buoyant species, under the specific conditions that lead to instabilities in the suspension, the particles from each species gather together and form a chain of clusters which move as a bulk. Therefore the velocities of the species increase due to the significant convective effects of these clusters or streams. The regime maps based around dimensionless quantities to describe the circumstances that would lead to the instabilities in the suspension were shown in Figure 3.6 and 3.7. For the case study involving  $\lambda = 1$ ,  $\gamma = -1$  and variable values of  $\phi_1$  and  $\phi_2$ , based on Figure 3.6, the Batchelor & Van Rensburg (1986) model suggests that the cenosphere concentration within fly ash should be too low for instabilities to occur. However, in the vicinity of the downwards facing inclined surfaces much higher localised concentrations of the cenospheres should develop, hence the benefits arising from the associated instability of the suspension may still come into play. Indeed, as shown in Figure 6.2, there were visual signs of the formation of rising streams of concentrated cenospheres against the downward-facing surface of the channels.

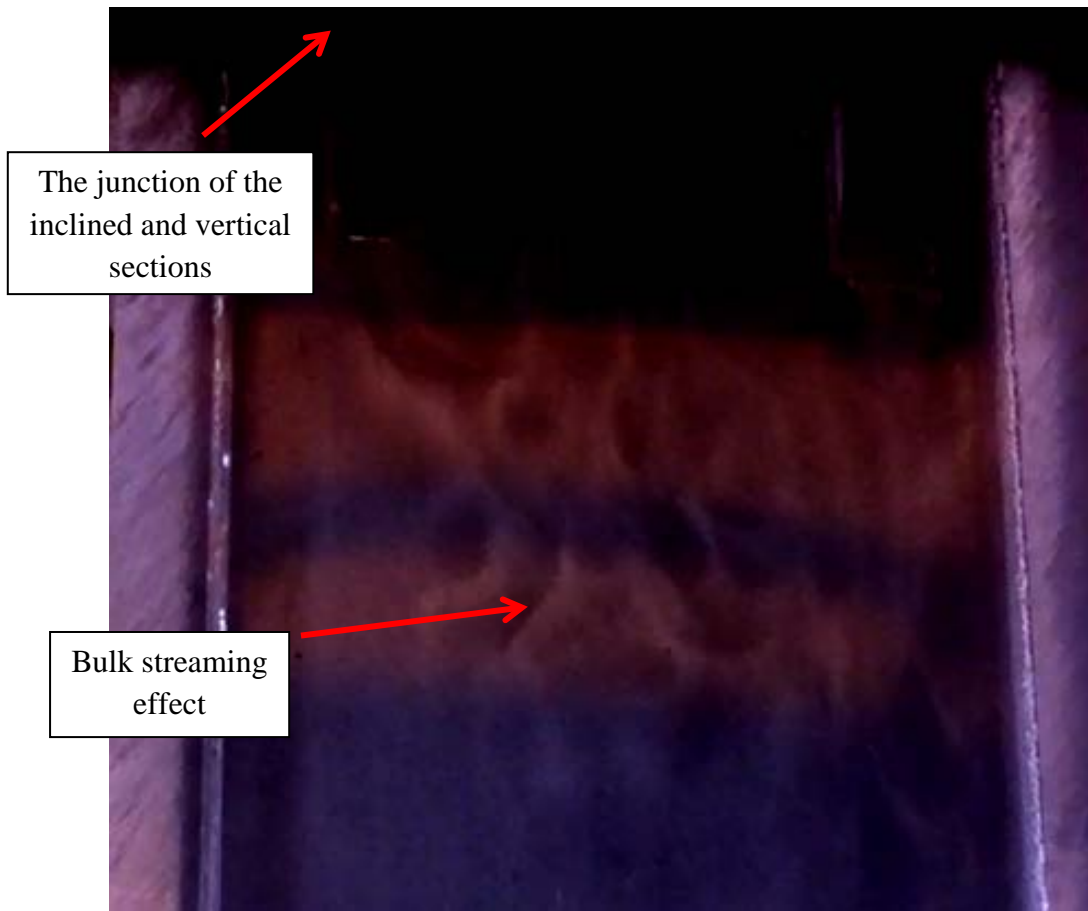


Figure 6.2: The visual sign of the streams forming against the downward facing surface of the Inclined channel.

It is therefore hypothesized that in the present study the beneficial streaming structure formation might be promoted by increasing the feed solids concentration of the fly ash. The dense medium also produces a higher effective buoyancy driving force, promoting the upward movement of the cenospheres, although the higher effective viscosity may counter this effect. The overall enhancement should be promoted further by the segregation that develops within the inclined channels, reflecting the combination of the two effects. In this study we investigate for the first time the segregation enhancement arising from the dense fly ash medium surrounding the cenospheres by examining the separation performance in the IRC<sup>TM</sup> as a function of the feed pulp density, at a fixed volumetric rate. Once optimised with respect to the feed pulp density, the operation is further explored as a function of the feed rate.

## 6.3 Experimental

### 6.3.1 Equipment

The Inverted REFLUX™ Classifier (IRC™) was applied to the separation of cenospheres from fly ash. As described in the previous chapter, the system of channels, inclined at an angle of 70° to the horizontal, consistent with the standard REFLUX™ Classifier, had a length of 1 m and a channel gap of  $z = 0.0095$  m. Fluidization water, regulated by a rotameter, washes fine gangue particles from the rising product. Two pressure sensors installed in the vertical fluidized bed section provide a measure of the suspension density of the system. A net positive pressure was maintained using a stand-pipe arrangement, with a vented exit point located 1 m above the system. The system was operated by discharging some portion of the underflow tailings upwards through this vented exit point. As discussed in chapter 5, this approach ensured the system remained full and prevented the pressure build-up in the device. A schematic representation of the experimental set-up is shown in Figure 5.1.

### 6.3.2 Methodology

The fly ash used in this study was sourced from an Australian coal fired power station. The grade of the cenospheres in the fly ash was in the order of 1 wt.%. Feed slurry of a given pulp density was prepared by mixing for several hours in the feed tank. The feed was extracted via a tube with its end point located 80 mm off the bottom of the feed tank. The feed was supplied to the IRC™ via a peristaltic pump, and entered the vertical section at an elevation 300 mm above the system of inclined channels.

When the fly ash entered the system there was a natural tendency for the positively buoyant cenospheres to rise upwards. However, a significant proportion would have been entrained downwards with the rest of the fly ash into the inclined channels. Moreover, the downwards fluidization wash water flow increased the tendency for the ultrafine fly ash to convey towards the entrance of the inclined channels. Meanwhile, the washed cenospheres were permitted to discharge via the central overflow exit point.

The suspension of fly ash and cenospheres experienced a strong degree of segregation within the inclined channels, with the denser particles migrating towards the upward facing surfaces

and the positively buoyant cenospheres migrating towards the downwards facing inclined surfaces. These cenosphere particles had a strong tendency to then return back towards the vertical section of the IRC™, located above the inclined channels. Once steady state was reached, equally timed samples were taken from the product and the tailings streams in order to preserve the grade of the remaining cenospheres in the feed for future experiments.

Note that the cenospheres grade in the fly ash feed was around 1 wt.% here which was less than that measured in Chapter 4. As previously discussed in Section 4.3.2, in the double fractionation tests (i.e. Chapter 4), some broken cenospheres and porous particles floated due to the trapped air inside their pores. However here the slurry of fly ash and water was kept mixed in a feed tank for several hours, hence water was given sufficient time to penetrate inside the particles pores and make them sink in the suspension. Therefore the lower grade of cenospheres was obtained (see Figures I.21 & 22 in Appendix I).

### **6.3.3 Measurements**

#### **6.3.3.1 Sink-float experiments**

In the experiments of this chapter, all of the samples were analysed using the sink-float method via separating funnels as shown in Figure 6-3(a). This standard method was applied to data analysis for a few cases in the previous chapters, however the separation technique used in the previous chapters was improved here to provide more accurate separation results. During the first few hours of the sink-float separation, the floats layer inside the funnel was gently agitated in order to release entrained ultrafine dense particles.

In addition to this procedure used in the chapters 4 and 5, the settled dense fly ash component was gradually discharged through the base of the funnel and into a bucket. Given some fine cenosphere particles were entrained by the fly ash to the sinks, a method was applied to recover these cenospheres. The material in the bucket was stirred very slowly allowing the settling of the heavy particles, leaving behind the entrained cenospheres as shown in Figure 6-3(b). These were then returned to the separating funnel. By repeating this method until no further cenospheres were recovered from the sink fraction (typically up to 5 times), it was possible to achieve good reconciliation in the cenosphere material balance. The

cenospheres and dense fly ash components were then dried and weighed, allowing the concentrations and recovery to be quantified.



(a)

(b)

Figure 6.3: (a) Sink and float analysis using a separating funnel, (b) entrained cenospheres recovered from the sinks fraction.

### 6.3.3.2 The particle size distribution

Laser light scattering (Malvern Mastersizer 2000) was used to measure the size distributions of the floats cenospheres and sinks fly ash fractions present in the feed, product, and tailings. Mass balance reconciliation, as described in Chapter 5, was used to make minor adjustments in the size distributions, and to in turn quantify the partition curves, and hence the nature of the size classification. Using the partition curves, the  $d_{25}$ ,  $d_{50}$  and  $d_{75}$ , and the sharpness of the particle size separation defined as the Imperfection,  $I = (d_{75} - d_{25})/(2d_{50})$  (Wills, 1997) was calculated and used to assess the size separation performance in the experiments. Figure 2.10 illustrates a typical partition curve, showing the key parameters.

### 6.3.3.3 Fly ash properties

The sink-float method of separation was applied to the feed prior to commencing the first experiment. Gas pycnometry was applied to each portion. The density of the cenospheres was found to be  $802 \text{ kg/m}^3$  and the density of the remaining fly ash  $1880 \text{ kg/m}^3$ , while the density of the overall fly ash, based on a separate sample of the feed, was  $1863 \text{ kg/m}^3$ . Note that at a feed pulp density of 38.1 wt.%, the volume fraction of the solids is 0.248, hence the calculated suspension density was  $0.248 \times 1863 + (1 - 0.248) \times 1000 = 1214.0 \text{ kg/m}^3$ .

The size distributions of the cenospheres and fly ash solids in the feed, obtained by laser light scattering (Malvern Mastersizer 2000), are shown in Figure 6.4. The fly ash covers a broad range of particles size from  $1 \mu\text{m}$  to about  $200 \mu\text{m}$ , while the cenospheres size range is from about  $20 \mu\text{m}$  to  $200 \mu\text{m}$ .

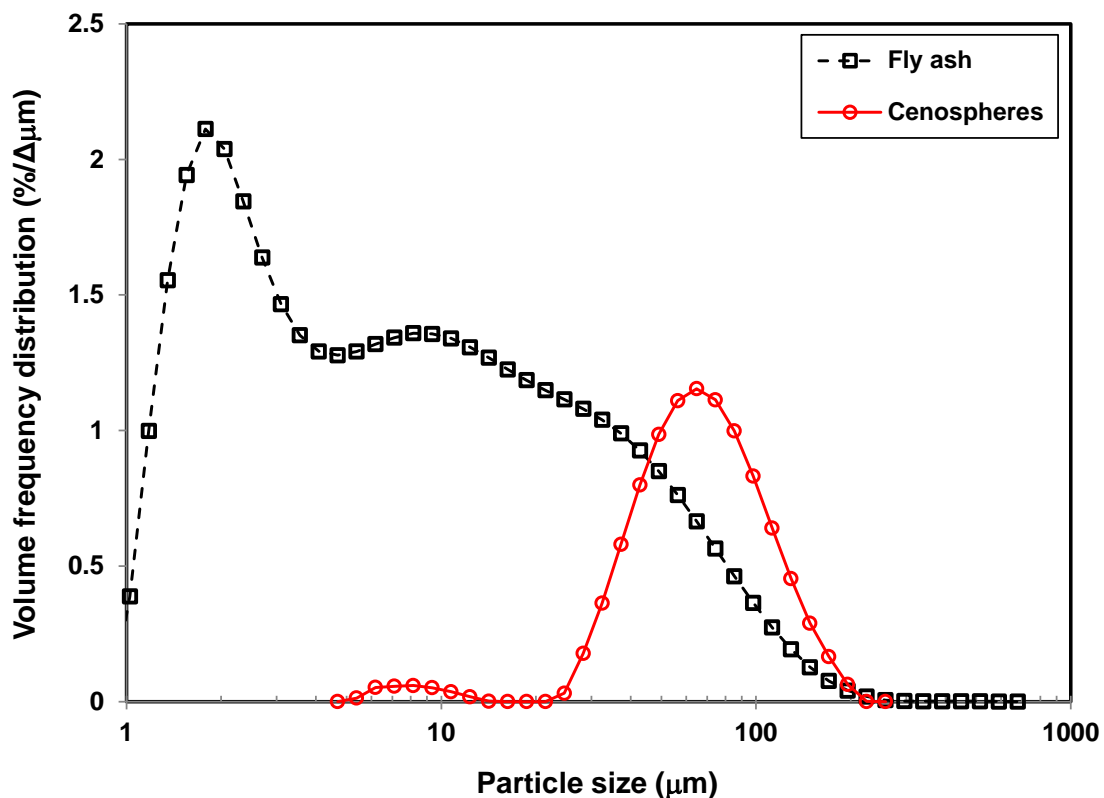


Figure 6.4: Volume frequency size distributions of floats cenospheres and sinks fly ash fractions in feed on a log scale (based on the unreconciled raw data).

## 6.4 Results and Discussion

The purpose of this study was to investigate the separation performance of the Inverted REFLUX™ Classifier (IRC™) on a fly ash feed sourced from a coal-fired power station. The primary goal was to establish the effect of the feed pulp density on the upgrade and the recovery of the cenospheres. The hypothesis was that there should be a strong enhancement in the performance when the concentrations of the positively and negatively buoyant particles reach a sufficient level to trigger the bulk streaming effect (Section 3.2.2). In most conventional density separation devices, at a fixed volumetric feed rate, the separation performance should decline as the solids concentration increases due to the increased level of hindered settling. But in mixtures of negatively and positively buoyant particles, if the conditions can yield the instability necessary for streaming structures to develop in the suspension, then there should be a range in which performance should improve with increasing solids concentration. The second objective was to explore the system performance at the optimum feed pulp density, varying the feed rate and overflow rate.

A total of 10 experiments were performed in this section of work. All experimental data points, including the operating conditions of each experiment, and also the mass balanced grade and recovery values are presented in Table 6.1. Note that the feed pulp densities in the first five runs covered a wide range of solids concentration from 10 up to 46 wt.%. Runs 6-10 were then performed to examine the separation performance at the optimum feed solids concentration under different operating conditions.

The inlet total mass of the slurry, solid fly ash, and cenospheres to the IRC™ compared to their outlet mass values are also presented in this table, demonstrating the consistency of the raw data. These data indicated a mere  $\pm 2\%$  discrepancy in most cases for the slurry and fly ash solids mass. However, owing to the small proportion of cenospheres in the separation process, and also difficulties in recovering all of the cenospheres in the sink and float technique, the discrepancy between the input and output for this component was higher at about  $\pm 10\%$ . This table also provides details on the extent of adjustment of the raw data required to achieve mass balance reconciliation (Refer to Appendix A for details).

Table 6.1: Details of the 10 experiments carried out using a raw fly ash feed. All data shown is mass-balance reconciled except for the total volumetric flow rate values which are based on the raw data.

	Run 1	Run 2	Run 3	Run 4	Run 5	Run 6	Run 7	Run 8	Run 9	Run 10
<b>Feed</b>										
Total volumetric rate (m <sup>3</sup> /(m <sup>2</sup> h))	6.45	7.67	7.67	7.33	6.80	11.16	11.16	9.77	3.84	5.23
Total mass rate (g/min)	934.5	1102.8	1172.0	1151.1	1089.9	1794.0	1719.8	1594.5	592.0	891.1
Fly ash mass rate (g/min)	93.1	209.5	356.4	434.3	500.5	678.6	670.4	654.4	235.9	355.2
Cenospheres mass rate (g/min)	1.08	2.63	3.41	4.76	4.75	6.11	5.83	6.73	1.94	3.03
Solids throughput (t/(m <sup>2</sup> h))	0.66	1.48	2.51	3.06	3.52	4.78	4.72	4.61	1.66	2.50
Pulp density (g solid/100 g slurry)	10.1	19.2	30.7	38.1	46.4	38.2	40.0	41.5	40.2	40.2
Cenospheres grade (%)	1.15	1.24	0.95	1.08	0.94	0.89	0.85	1.02	0.81	0.85
Split ratio to product (vol.%)	23.8	18.2	20.5	21.0	22.1	17.5	13.4	7.6	19.4	21.3
<b>Product (Overflow)</b>										
Total volumetric rate (m <sup>3</sup> /(m <sup>2</sup> h))	1.53	1.39	1.57	1.53	1.50	1.95	1.50	0.74	0.74	1.12
Total mass rate (g/min)	199.2	186.0	215.4	202.4	195.5	269.5	186.4	101.1	98.2	148.5
Fly ash mass rate (g/min)	0.3	0.6	1.2	2.5	1.0	18.6	1.0	0.3	0.2	0.5
Cenospheres mass rate (g/min)	0.67	1.68	2.89	4.28	2.86	4.87	3.75	2.45	1.47	2.35
Pulp density(g solid/100 g slurry)	0.5	1.2	1.9	3.3	2.0	8.7	2.6	2.7	1.7	1.9
Cenospheres grade (%)	68.5	73.3	70.3	63.5	74.5	20.8	78.9	89.7	85.7	81.8
<b>Tailings (Underflow)</b>										
Total volumetric rate (m <sup>3</sup> /(m <sup>2</sup> h))	6.28	6.98	7.15	6.98	6.28	9.77	11.16	10.05	3.91	5.16
Total mass rate (g/min)	861.0	1041.9	1081.7	1073.7	1019.4	1674.5	1683.3	1643.3	618.7	867.4
Fly ash mass rate (g/min)	92.8	208.9	355.2	431.9	499.5	660.1	669.4	654.2	235.9	354.6
Cenospheres mass rate (g/min)	0.42	0.95	0.52	0.48	1.89	1.24	2.07	4.28	0.47	0.68
Pulp density(g solid/100 g slurry)	10.8	20.1	32.9	40.3	49.2	39.5	39.9	40.1	38.2	41.0
Cenospheres grade (%)	0.45	0.45	0.15	0.11	0.38	0.19	0.31	0.65	0.20	0.19
<b>Fluidization water</b>										
Total volumetric rate (m <sup>3</sup> /(m <sup>2</sup> h))	0.87	0.87	0.87	0.87	0.87	1.05	1.05	1.05	0.87	0.87
<b>Process performance</b>										
Upgrade	59.5	59.1	74.1	58.6	79.3	23.3	91.5	88.2	105.4	96.6
Recovery (%)	61.7	64.0	84.7	89.9	60.2	79.7	64.4	36.4	75.9	77.5
<b>Consistency of raw data</b>										
In/out (total solids mass)	0.93	1.00	1.00	0.99	1.01	1.01	1.01	1.01	1.01	1.02
In/out (fly ash mass)	0.91	1.01	1.01	1.01	1.02	1.00	1.02	1.01	1.02	1.01
In/out (cenospheres mass)	0.97	0.99	0.94	0.89	1.01	0.96	0.97	1.09	1.12	0.91
Maximum adjustment (%)	5.17	0.74	3.59	6.36	5.73	2.22	1.93	5.72	7.08	5.29
Average absolute adjustment (%)	2.34	0.25	0.91	1.55	1.08	0.53	0.73	1.21	1.67	1.40

#### 6.4.1 The effects of the dense medium on the separation of positively buoyant cenospheres from fly ash in the IRC<sup>TM</sup>

In this section, the effect of the dense medium on the grade and the recovery of cenospheres in the IRC<sup>TM</sup> were investigated using different feed pulp densities (i.e. 10.1%, 19.2%, 30.7%, 38.1% and 46.4% by weight) (Runs 1-5). The feed cenosphere size distributions were measured to be almost the same in all experiments as shown in Figure 6.5.

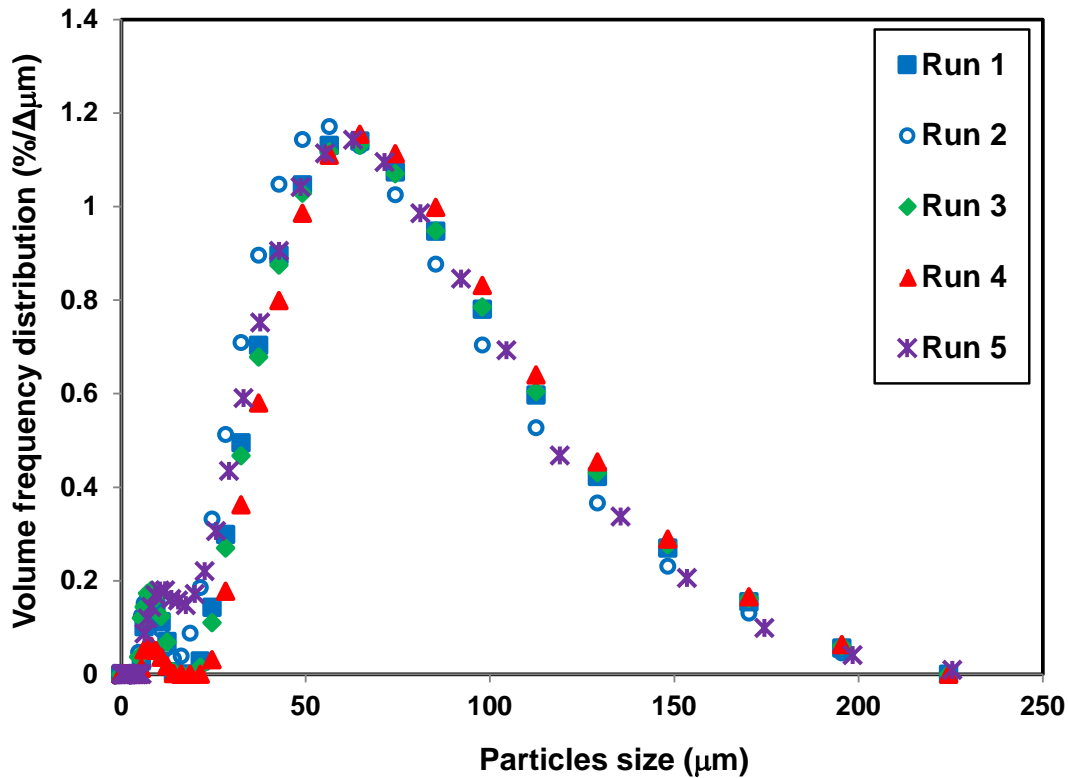


Figure 6.5: Feed cenosphere volume frequency size distributions in Runs 1-5 as measured by the Malvern Mastersizer 2000. It is noted that the small peaks at particle sizes smaller than 30  $\mu\text{m}$  are mainly due to the fine cenospheres and fly ash misplacement in the sink-float separation method.

In this set of experiments (Runs 1-5), The feed  $F$  and fluidization water  $W$  volumetric fluxes were kept constant in all experiments at an average of  $7.18 \text{ m}^3/(\text{m}^2 \text{ h})$  and  $0.87 \text{ m}^3/(\text{m}^2 \text{ h})$ , respectively. In all experiments, almost 20% of the volumetric feed flux went to the product. As the difference between the product  $P$  and the fluidization water volumetric fluxes were the same in all experiments conducted at different feed pulp densities, the product grade remained almost constant at about 70%. These results, shown in Figure 6.6, are consistent with the findings of the previous chapter which showed the difference between the product and the fluidization water fluxes (i.e.  $P - W$ ) as a significant factor in controlling the product grade. This factor,  $P - W$ , was about  $0.62 \text{ m}^3/(\text{m}^2 \text{ h})$  in the present study.

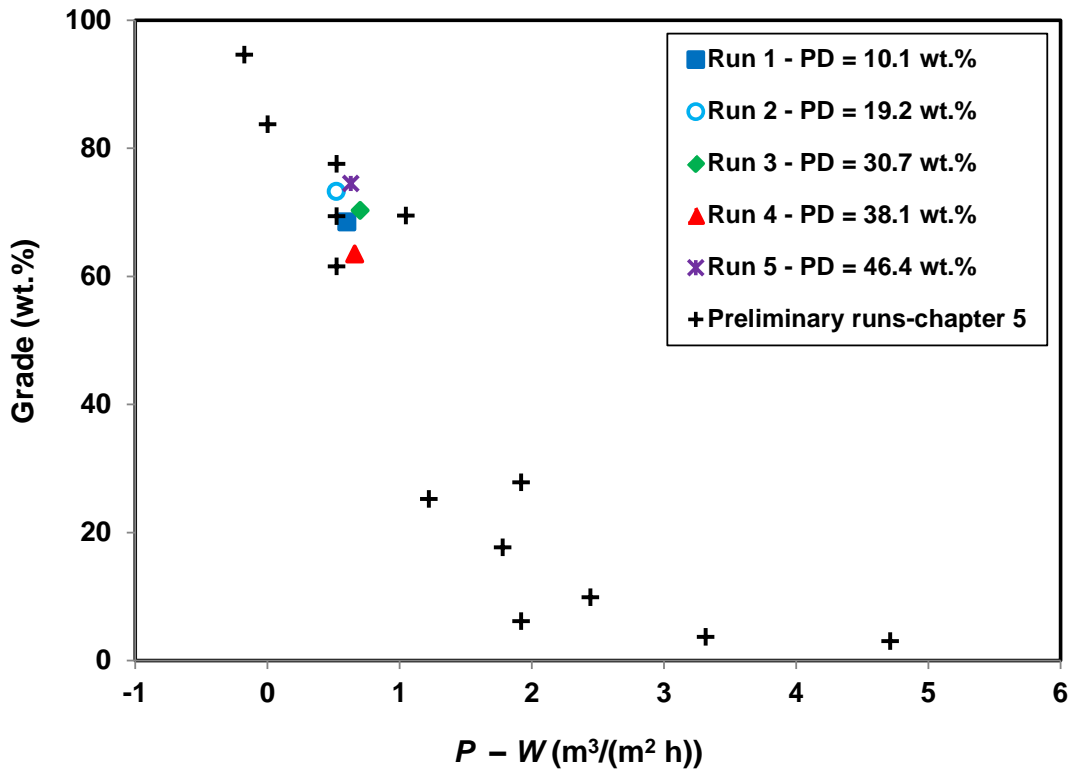


Figure 6.6: Dependence of product grade from Runs 1-5 (different feed pulp densities (PD)) on the difference between the product and fluidization volumetric fluxes, ( $P - W$ ).

Figure 6.7 shows the cenosphere recovery as a function of the feed pulp density. In Run 1, operating with a dilute feed (i.e. about 10.1 wt.% pulp density), 61.7 wt.% of the cenospheres was recovered. By increasing the solids content of the feed to about 38.1 wt.%, the recovery increased to 89.9 wt.% with a grade of 63 wt.%, an extraordinary result. In other words, the solids processing rate increased significantly, and in turn the separation performance increased significantly. However, when the feed pulp density increased to about 46.4 wt.% the recovery dropped to just over 60 wt.%, revealing a clear optimum in the separation conditions. According to Figure 6.7, the optimum feed pulp density for high cenosphere recovery was found to be about 38 wt.%. This optimum point reflects the dominant positive effects of the streaming phenomenon up to the pulp densities of about 38 wt.% and the dominant negative hindering effect of the suspension viscosity at higher pulp densities on cenospheres recovery. It is noted that the error bars show the difference between the results obtained from reconciled data and raw experimental data, calculated using the same procedure as used in Chapter 5 (refer to Appendix H for details).

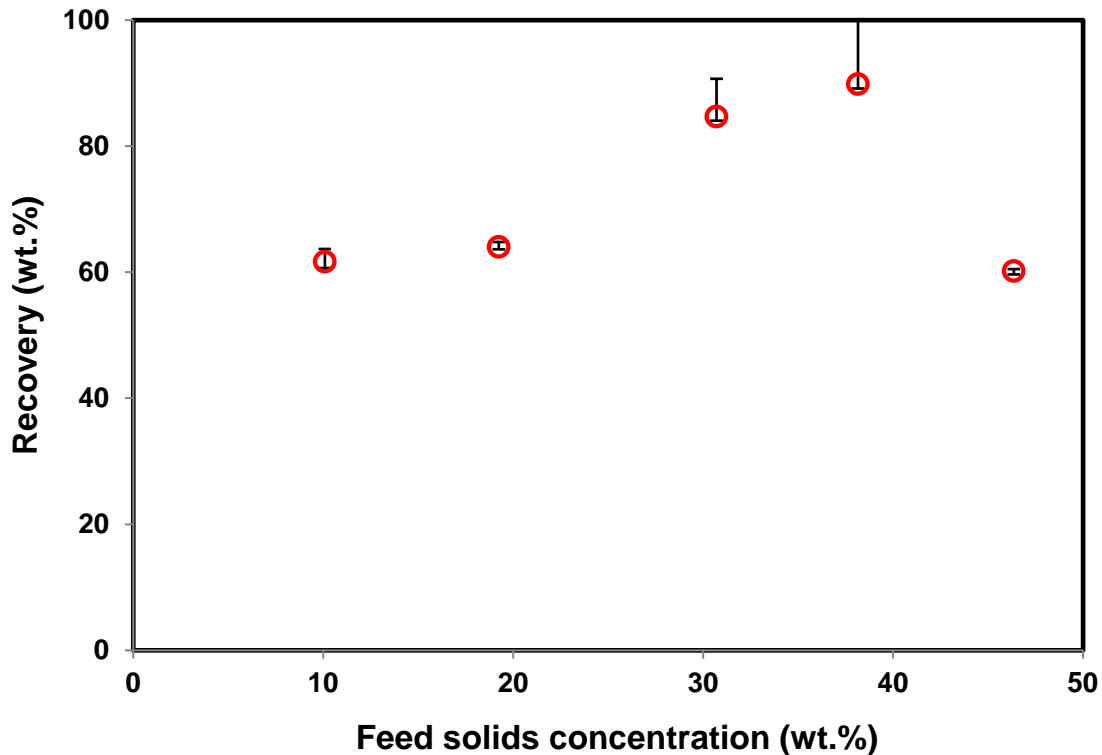


Figure 6.7: Recovery of cenospheres at different feed pulp densities from Runs 1-5 (based on reconciled data).

As previously discussed, the rise velocity of positively buoyant particles can be increased *en-masse* if the streaming structure develops. This condition is most likely within the inclined channels where the cenospheres segregate strongly forming higher concentrations. Commencing off a low base, the cenosphere concentration increases with increasing feed pulp density, possibly reaching the critical value required for instability and hence formation of clusters. This cluster structure then results in a significantly larger entity and higher buoyancy driving force, increasing the cenosphere recovery. However the effect of the suspension viscosity on hindering the segregation of the cenospheres becomes dominant with increasing feed pulp density beyond a critical value, and hence the cenospheres recovery decreases.

#### 6.4.2 Dense medium effects on the particles size classification in the IRC™

In this section, the effect of the dense medium on the size classification of the cenospheres in the IRC™ is examined. Figure 6.8 illustrates the cenosphere size distributions of the feed, the underflow tailings, and the overflow product based on Run 4 which was performed at about 38.1 wt.% feed pulp density. As expected, the cenospheres lost in the underflow tailings are

biased towards the finer size particles. This figure also shows that almost no cenospheres larger than 100  $\mu\text{m}$  were lost in the tailings.

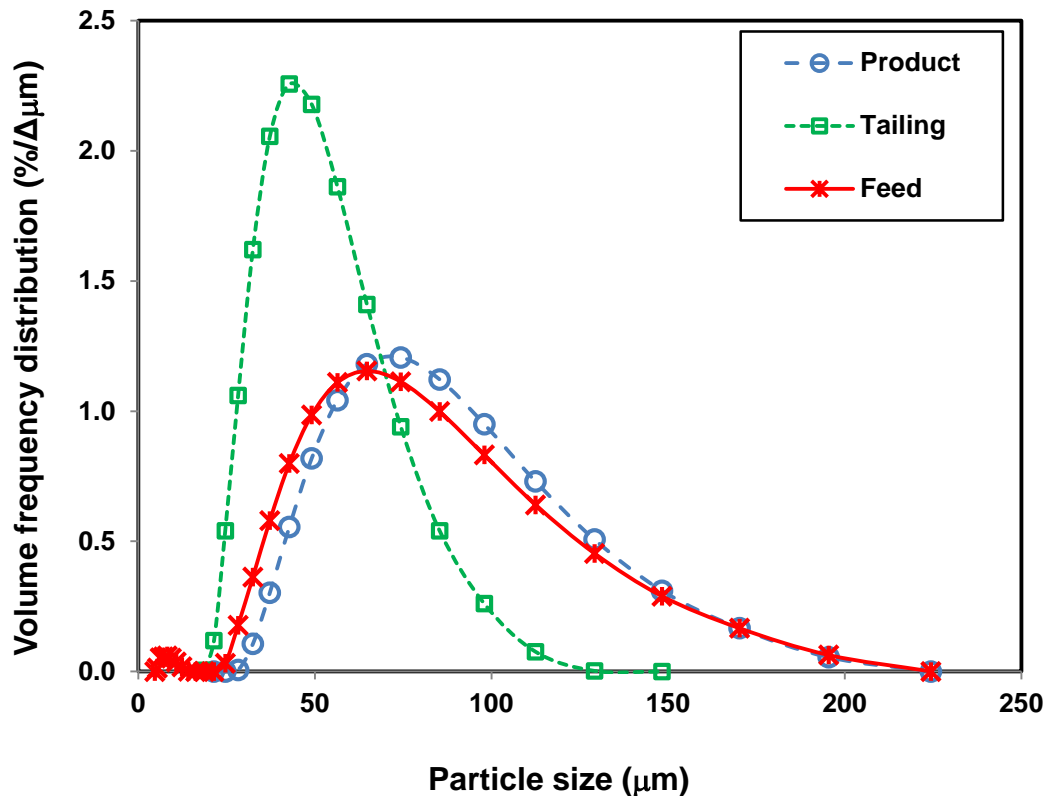


Figure 6.8: Cenosphere volume frequency size distributions in the feed, product and tailing for Run 4, conducted at 38.1 wt.% feed pulp density (unreconciled raw data).

The partition to product versus the size of the cenospheres was obtained using the material-balance reconciled data for the cenosphere size distributions in all three streams. Figure 6.9 shows the partition curves for different feed pulp densities. The partition curve at the optimum feed pulp density for maximizing cenosphere recovery (Run 4, 38.1 wt.%) is clearly the sharpest, while the poorest occurs at the highest feed pulp density of 46.4 wt.% solids. Table 6.2 shows the corresponding values of the  $d_{50}$  and Imperfections. The throughput advantage based on the system geometry and particle Reynolds number at the  $d_{50}$  size, calculated using Equation 3-10, is also shown. These values take into account the thickness of the plates, which limit the flow area by 7%. The actual throughput advantage derived from the experiments is also shown. The correlation of Laskovski et al. appears to be reasonably accurate at low pulp densities. However, it under-predicts the capacity advantage at high pulp densities by a factor of 2 to 3. Neglecting the expected errors, the discrepancies between the

theoretical and actual throughput advantages are largely attributed to a concentration induced enhancement arising from the positively buoyant cenospheres which concentrate near the downward facing inclined surfaces, within an environment of negatively buoyant fly ash particles. Table of data and all corresponding calculations are presented in Appendix E & H.

It is noted that the Laskovski correlation, equation 3-10, was derived for negatively buoyant particles in the standard RC<sup>TM</sup> configuration. In the inverted configuration (IRC<sup>TM</sup>), these particles are equivalent to the positively buoyant cenospheres. The fact that the buoyant cenospheres congregate against the downwards facing surface and rise rapidly back up into the vertical section is exactly analogous to negatively buoyant particle behaviour in the standard unit. So if there was a mixture of only buoyant cenospheres of varying density, then they would be expected to separate in the IRC<sup>TM</sup> in exactly the same way that negatively buoyant particles separate in a standard RC<sup>TM</sup>.

What is different when the IRC<sup>TM</sup> process is used to treat fly ash is the existence of both negatively and positively buoyant particles together. In the channels, as illustrated in Figure 3.21(b), as well as the accelerated settling of the buoyant cenospheres up against the downwards facing surfaces, there will also be an accelerated settling of the negatively buoyant particles onto the upwards facing surface, from where they will then flow more rapidly downwards towards the underflow exit. There is no analogy to this in the standard RC<sup>TM</sup>. Given that the bulk of solids are the dense ones, there is the potential here for this large sliding layer to create a quite different velocity gradient inside the channels, closer to linear across the entire channel rather than parabolic.

In the vertical section of the IRC<sup>TM</sup>, there is also the potential for streaming behaviour to develop. Normally this would not be expected at the low concentrations of buoyant particles present in the fly ash feed, but it may effectively be catalysed by the concentrated streams of buoyant cenospheres refluxing back up into the vertical section from the inclined channels (Figure 6.2). These concentrated streams also occur in the standard RC<sup>TM</sup>, forming a plume of dense solids that can penetrate a certain distance down into the vertical section. However, because all the particles have the same buoyancy direction, these plumes do not maintain their integrity and they appear to rapidly disperse back into the mixture. In the fly ash system, there is the potential that these refluxed streams of buoyant cenospheres will retain their integrity and thus benefit from the bulk streaming segregation enhancement. Unfortunately,

there was no visual confirmation of the existence of these streams in the vertical section. They would be difficult to clearly see, given the similar colour of the cenospheres and fly ash (most published experimental work on this effect has used contrasting colours for the negatively and positively buoyant particles).

Consider now an analysis at the optimum feed pulp density of 38.1 wt.% solids, with the  $d_{50}$  equal to 36.5  $\mu\text{m}$ . The state of the suspension within the inclines can be estimated using the tailings pulp density (40.3 wt.% solids) and the density of the solids in the tailings (1880  $\text{kg}/\text{m}^3$ ), corresponding to a volume fraction of 0.264. The density of the cenospheres within the inclined channels should be well represented by the feed value, 802  $\text{kg}/\text{m}^3$ . Thus the terminal velocity of the  $d_{50}$  particle is 0.52 m/h, with corresponding Reynolds number equal to 0.0052. The hindered settling velocity based on Equation 2-33 is 0.13 m/h using  $n = 4.5$ . Using the tailings flux of about 7  $\text{m}^3/(\text{m}^2 \text{ h})$  to denote the superficial velocity through the system of inclined channels, the actual throughput advantage is  $7/0.13 = 54$ , a remarkably large value. This result is significantly higher than the value predicted using Equation 3-10, which gives  $U/u_t = 18$ . The ratio,  $54/18 = 3$ , is defined as the *concentration induced enhancement* (Equation 6-1):

$$\text{Concentration induced enhancement} = \frac{\text{Actual throughput advantage}}{\text{Theoretical throughput advantage}} \quad (6-1)$$

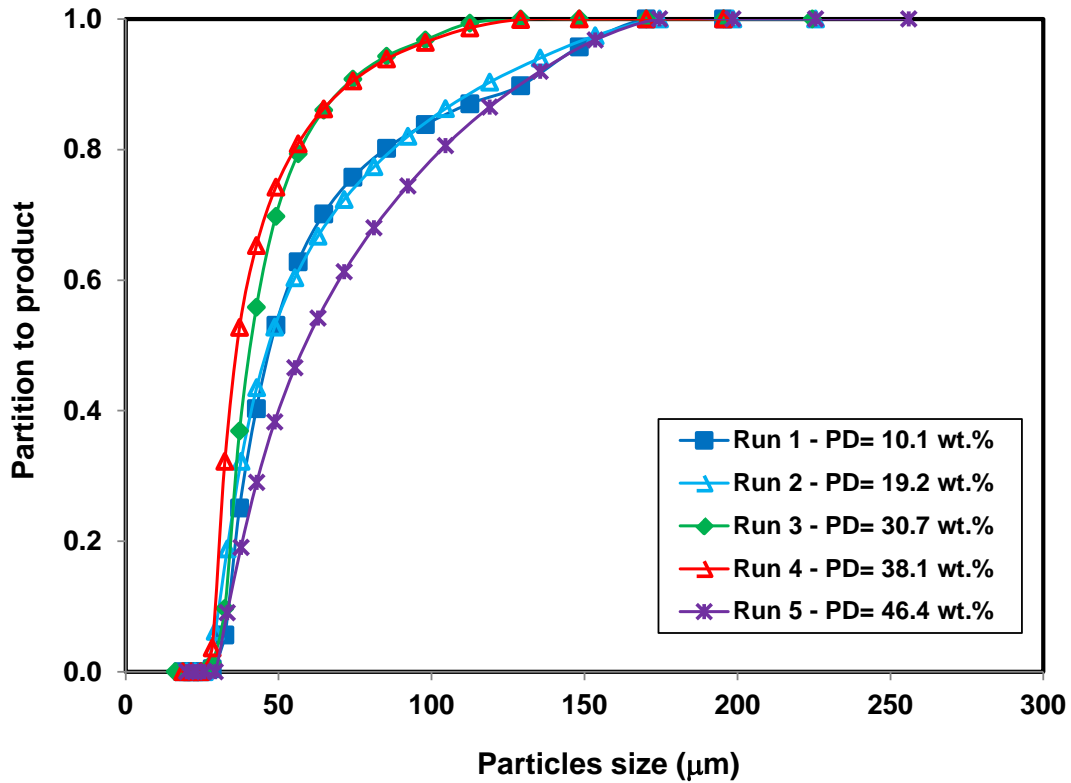


Figure 6.9: Partitioning to the product for different feed pulp densities (PD) (based on the mass-balance reconciled results).

Table 6.2:  $I$ ,  $d_{50}$  values, theoretical and actual throughput advantage for Runs 1-5 (based on the reconciled results).

Feed pulp density (%)	$I$ (Imperfection)	$d_{50}$ ( $\mu\text{m}$ )	Predicted throughput advantage, Eq. (3-10)	Actual throughput advantage	Concentration induced enhancement
10.1	0.38	47.5	16	10	0.6
19.2	0.43	46.5	16	15	0.9
30.7	0.21	41.0	17	31	1.8
38.1	0.21	36.5	18	54	3.0
46.4	0.46	58.5	14	31	2.2

Figure 6.10 shows the concentration induced enhancement as a function of the feed pulp density. The result expected for stable suspensions is given by the horizontal dashed line at 1.0. The result obtained at a feed pulp density of 19.2 wt.% solids involved an actual throughput advantage of 15, while the theoretical value predicted by Equation 3-10 is 16, giving a concentration induced enhancement of 0.93, close to 1.0. The errors here are considerable given the reliance on the Richardson and Zaki equation for describing the hindered settling of the cenospheres within the fly ash. It should be also noted that the Laskovski correlation 3-10 was fitted to batch elutriation data where hindered settling effects

would have been much lower than for continuous conditions. So it cannot be expected to necessarily work for a continuous process. The error bars shown are based on the results calculated using the  $d_{25}$  and  $d_{75}$  values from the partition curves of Figure 6.9. In fact the concentration induced throughput enhancement was recalculated based on the  $d_{25}$  and  $d_{75}$ , and hence the true error should be well within this range. Data and detailed calculations are shown in Appendix E & H. Hence we conclude the strong concentration induced enhancement is a real and significant effect. The error bars are amplified by the low hindered settling velocities that arise at the highest concentrations.

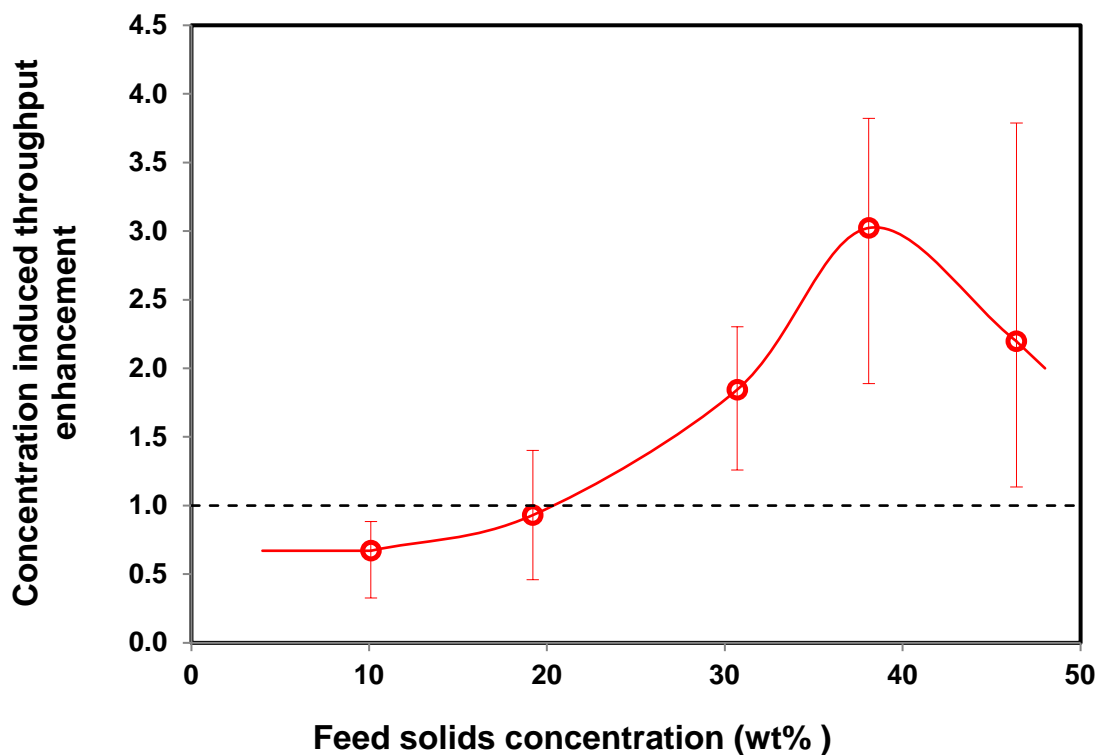


Figure 6.10: Concentration induced throughput advantage (Eq. 6.1) of the Inverted REFLUX™ Classifier. The curve is based on the  $d_{50}$  values while the error bars denote values ranging from the  $d_{25}$  to the  $d_{75}$  (see Appendix E & H). The dashed horizontal line denotes the base-line for the Inverted REFLUX™ Classifier.

#### 6.4.3 Varying product split at the optimum feed pulp density

This section discusses the results of Runs 6 to 8 where the feed pulp density was kept at the optimum value of around 40 wt.%, the feed volumetric flux was increased from the previous value of around  $7.2 \text{ m}^3/(\text{m}^2 \text{ h})$  used in Runs 1-5 up to around  $10.7 \text{ m}^3/(\text{m}^2 \text{ h})$  and the product volumetric flowrate was varied from 0.74 up to  $1.95 \text{ m}^3/(\text{m}^2 \text{ h})$ . This work was motivated by

the desire to maximize the solids throughput, while maintaining a high recovery. In this set of experiments, the feed solids mass flux was set at  $4.7 \text{ t}/(\text{m}^2 \text{ h})$ , higher than in Runs 1 to 5, while the fluidization water flux was kept constant at about  $1.05 \text{ m}^3/(\text{m}^2 \text{ h})$ .

Figure 6.11 shows the effects of varying the product flux on the product grade and recovery in Runs 6-8. As the product flux increases from  $0.74 \text{ m}^3/(\text{m}^2 \text{ h})$  to  $1.95 \text{ m}^3/(\text{m}^2 \text{ h})$ , the product grade decreased from 89.7 wt.% to about 20.8 wt.%. However the recovery increased from 36.4 wt.% to about 79.7 wt.%. This figure provides a good basis for choosing the best operating condition for a one-stage or a multi-stage process. A product rate given by 20% of the feed volumetric rate delivers a recovery higher than 80 wt.%, while the product grade is less than 20 wt.%, hence multi-stage processing becomes necessary at this higher throughput for achieving satisfactory grade.

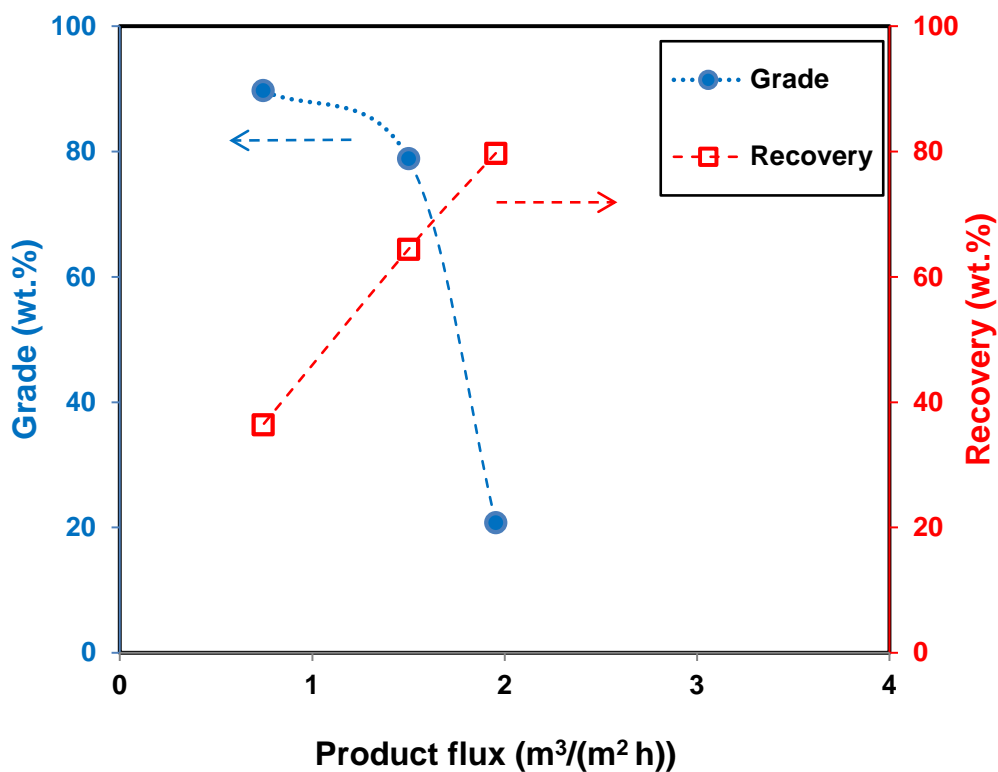


Figure 6.11: Grade and recovery of cenospheres as a function of product flux for Runs 6-8 at the optimum feed pulp density of 40 wt. % and a feed solids flux of  $4.7 \text{ t}/(\text{m}^2 \text{ h})$  (based on the reconciled data).

#### 6.4.4 Effect of the feed throughput at the optimum feed pulp density

This section compares the performance of the IRC™ in Runs 4, 6, 9 and 10 where different feed flow fluxes were used. These results are also compared to the results obtained in Chapter 5. The fluidization water flux was constant at about  $0.87 \text{ m}^3/(\text{m}^2 \text{ h})$  for Runs 4, 9 and 10 and a little higher at  $1.05 \text{ m}^3/(\text{m}^2 \text{ h})$  for Run 6. The ratio of the product volumetric flux to the feed volumetric flux was kept constant in all of the experiments, at about 20%. By decreasing the feed flux, the cenosphere grade in the product increased, due to the improved desliming achieved by the fluidization water, which although at a constant rate, had increasing significance relative to the reducing product rate. Again, the main parameter governing the product grade is the value of  $P - W$ , the difference between the product and the fluidization water flux. The strong dependence of product grade to this factor was previously shown in Figure 6.6 and more thoroughly in Chapter 5 (Section 5.4.2.5). Figure 6.12 compares the product grades achieved in this study with those in Chapter 5. The product rate relative to the feed rate, and fluidization water flux were almost the same in both studies. It is noted that the data of Chapter 5 was shown here based on the density of  $1800 \text{ kg/m}^3$  for fly ash solids in the product, while the error bars reflect the variation of the results obtained through the sensitivity analysis (please refer to Chapter 5 for details). The related sample calculations are shown in Appendix B.

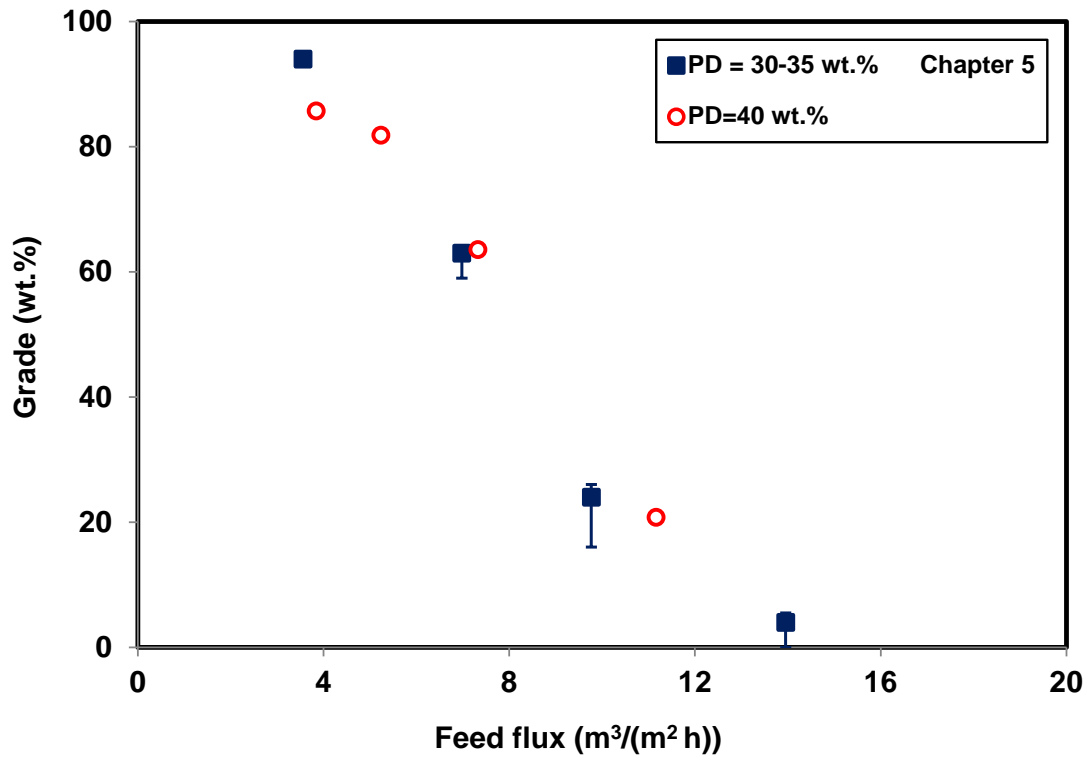


Figure 6.12: The effect of the feed flux on the product grade, at the optimum feed pulp density (PD) of about 40 wt.% (based on the mass balance reconciled results).

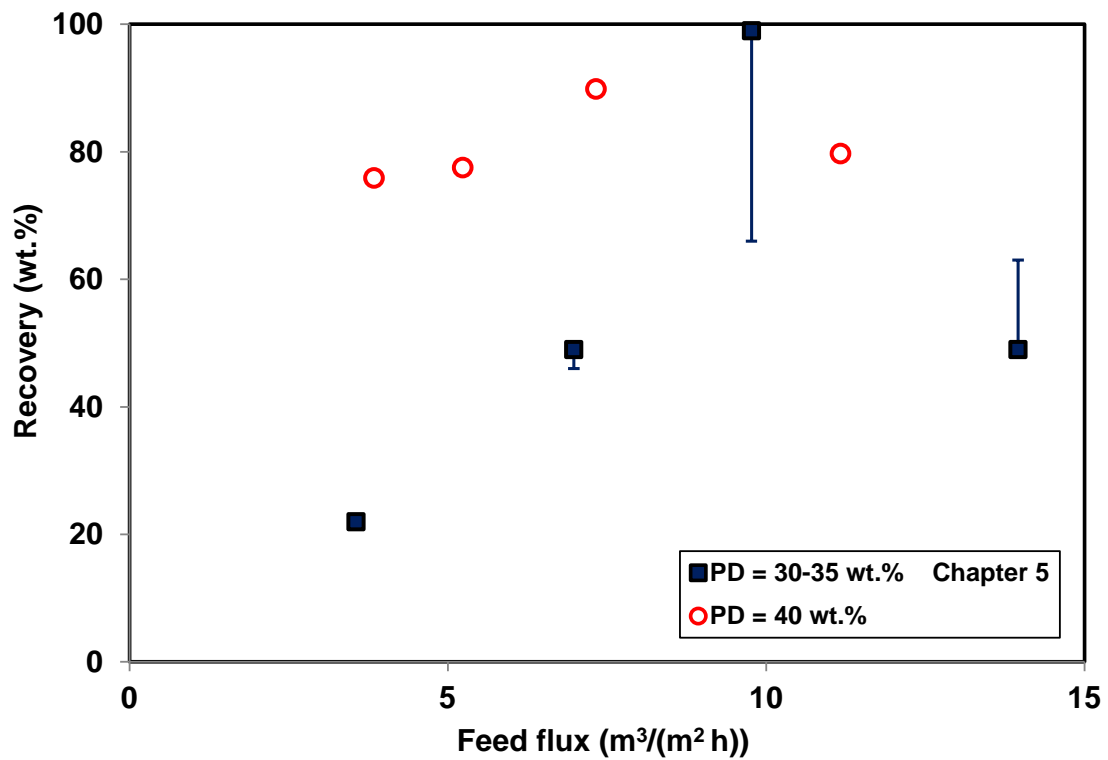


Figure 6.13: The effect of the feed flux on the cenosphere recovery, at the optimum feed pulp density of about 40 wt.% (based on the reconciled results).

As shown in Figure 6.13, increasing the feed flux, with the product to feed flux ratio fixed, led to a rise in the recovery of the cenospheres, but at much higher feed fluxes, the recovery decreased. This interesting trend was discussed in Chapter 5. The recoveries obtained at the optimum feed pulp density in this study are higher than those reported for the feed pulp density ranging from 30-35 wt.% in Chapter 5, where the feed grade of the cenospheres was much lower at 0.51 wt.%. Arguably the improvement here was also due to the higher grade of cenospheres in the feed.

#### **6.4.5 Grade-Recovery curve**

The grade-recovery curve provides useful insight into the performance of the IRC™ under different operating conditions. Figure 6.14 presents the grade-recovery curves at different feed throughputs. As shown, the curves of the runs conducted at about 40 wt.% feed pulp density with a grade of about 1% cenospheres are generally higher than the runs reported in Chapter 5 with a feed pulp density of 30 to 32 wt.% and only a 0.5 wt.% feed grade, even though those runs were at a lower feed volumetric flux. So a better separation performance is obtained at the optimum pulp density and the higher grade of cenospheres in the feed. As expected, a better separation is achieved at a lower feed throughput.

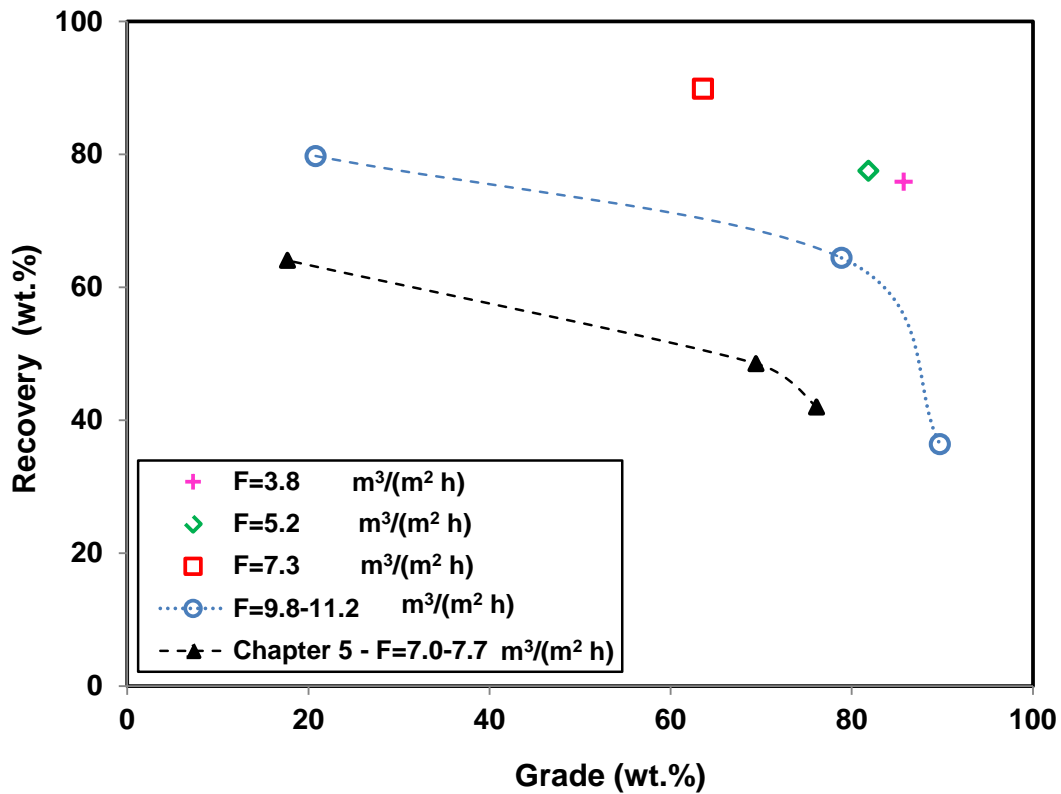


Figure 6.14: The grade-recovery curves for experiments conducted at different feed volumetric fluxes. The Chapter 5 results were based on pulp density of 30-32 wt.%, and feed grade 0.51 wt.%. All other data are based on Run 4 and Runs 6-10 involving a pulp density of 38.1 to 41.5 wt.% solids, and feed grade of 0.81 to 1.08 wt.%.

## 6.5 Conclusions

In this chapter the enhanced separation of positively buoyant cenospheres from negatively buoyant fly ash was studied using the Inverted REFLUX™ Classifier at different feed pulp densities. It was concluded that increasing the feed pulp density up to around 40 wt.% led to an enhancement in the separation performance due to a higher effective buoyancy driving force, and possibly the formation of hydrodynamic structures and bulk streaming of the cenospheres within the inclined channels. Specifically, the recovery of the cenospheres increased to an optimum recovery of 89.9 wt.% and upgrade of 58.6 when the feed pulp density increased to 38.1 wt.%, before declining at higher feed pulp densities. Analysis based on the correlation of Laskovski et al. (2006) predicted that the inclined channels should produce an underlying throughput advantage of 18. A further improvement factor of 3 was attributed to a combination of the dense medium effect and the bulk streaming phenomenon, resulting in an overall throughput advantage of 54 compared to a conventional fluidized bed.

The optimum performance was also evident in the partition curves used for describing the cenosphere size classification. At the optimum feed solids concentration, the effect of varying the feed and product flowrates was further explored in order to establish the best conditions for a future pilot scale study.

## **Chapter 7**

# **A Pilot Scale Study of Cenosphere Recovery and Concentration in the Inverted REFLUX™ Classifier**

### Journal Article(s) Related to the Chapter and Authors' Contribution

**Kiani, A.,** Zhou, J. & Galvin, K.P. (2015). A Pilot Scale Study of Cenosphere Recovery and Concentration using the Inverted Reflux Classifier, *Minerals Engineering*, 79, 17-23.

Author	Contribution
Ali Kiani	The lead author of the paper, collaborator in experimental design, primary interpretation of results, analysis of data, and experimental operator
James Zhou	Co-supervisor, experimental support and collaborator in experimental design
Kevin Galvin	Principal supervisor, collaborator in experimental design and results interpretation, inventor and designer of system

## **7.1 Introduction**

The previous chapter investigated the recovery and concentration of positively buoyant cenosphere particles in an Inverted REFLUX™ Classifier (IRC™) at laboratory scale with a cross-section  $0.100\text{ m} \times 0.086\text{ m}$ . A strong optimum was identified at a feed pulp density of 38 wt.% solids, with the solids mass flux throughput at  $3.1\text{ t}/(\text{m}^2\text{ h})$ , giving a recovery of 89.9 wt.%, and an upgrade of 58.6. The system throughput was found to be 54 times higher than estimated for a conventional fluidized bed, with a factor of 18 attributed to the inclined system geometry and factor of 3 attributed to the interaction between the positively and negatively buoyant species. While the previous laboratory scale study demonstrated remarkable separation performance, industrial application demands assessment at progressively larger scale.

However, there are no guarantees of success when the scale of operation is increased. There are compromises that are introduced when a system is scaled-up, for example, in reducing the number of fluidization nozzles located at the top of the system for fluidizing and hence washing the cenospheres. Therefore this chapter investigates the scale-up potential of the inverted REFLUX™ Classifier, utilizing a pilot scale device with cross-section  $0.3\text{ m} \times 0.3\text{ m}$ . The performance data are compared directly with those obtained at the smaller laboratory scale. Product grade and cenosphere recovery are examined at different feed split ratios (i.e. the ratio of product volumetric rate to the feed volumetric rate) and hence different solids yields. The performance is also examined as a function of the feed slurry flux. Success with this ten-fold scale-up will provide the necessary basis for proceeding with a full scale implementation of this technology.

## **7.2 Materials and Methods**

### **7.2.1 Pilot scale Inverted REFLUX™ Classifier**

The pilot-scale Inverted REFLUX™ Classifier (IRC™) had an inclined section 1.2 metres long which contained 38 channels formed by 37 parallel plates with a perpendicular spacing of 6 mm. A 2.7 m long vertical inverted fluidized bed with cross sectional area of about  $0.300\text{ m} \times 0.300\text{ m}$  was located above the inclined section. Two pressure sensors, placed about 0.200 m and 0.250 m respectively above the junction of the inclined channels and the vertical fluidized bed, were used to measure the suspension density in the vertical fluidized bed

section, providing an indication of whether the system was at steady state, and also information on the quality of the product. A lower suspension density reflected the higher proportion of low density cenospheres in the vertical section of the IRC™, and hence a higher product grade. A fluidization water distribution chamber was installed above the fluidized bed section, distributing the water used to suspend the bed of cenospheres, thus washing the entrained ultrafine fly ash particles from the cenosphere product.

In order to re-use the feed for later experiments it was necessary to remove a significant quantity of water from the tailings stream. This was done using a small lamellae thickener containing 24 channels with a perpendicular spacing of 2.6 mm. In some experiments a tube was used instead of the lamellae thickener. Water was drawn from the tailings stream at a rate sufficient to match the rate of water addition to the fluidized bed distributor, significantly less than the actual tailings rate. Some solids were still entrained to the drawn water and hence separated and returned to the feed for later experiments. This arrangement, which is shown in Figure 7.1, was also connected to a vented tube extended up to 1 m above the device, thus ensuring a positive pressure within the IRC™ during the experiments. A schematic and photo of the experimental set up are shown in Figure 7.1a and Figure 7.1b respectively.

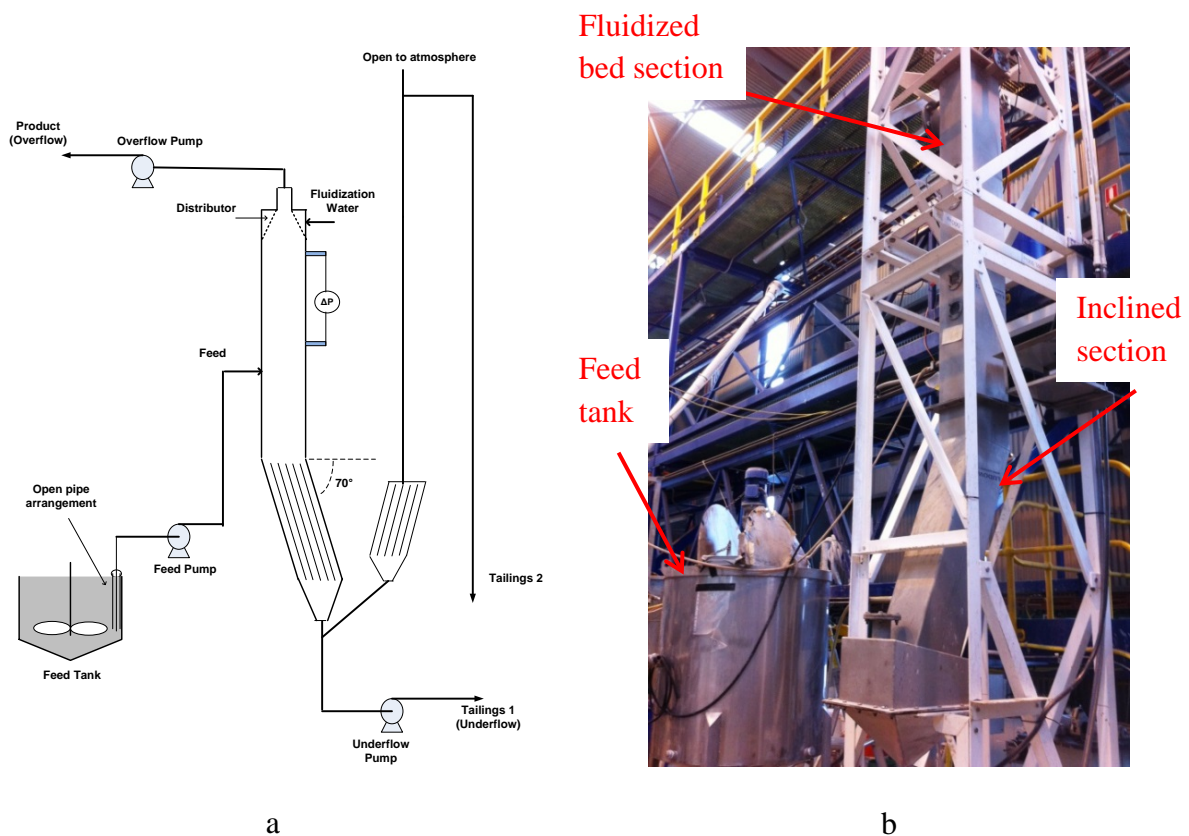


Figure 7.1: (a) A schematic representation and (b) A photo of the experimental set up.

## 7.2.2 Experimental procedure

A sample of about 1300 kg of actual fly ash solids from an Australian coal-fired power station was supplied in two 1 m<sup>3</sup> containers for use in this study. The sample was mixed with 1950 L of water to produce a feed of about 40 wt.% solids. This is the feed solids concentration that was found to be the optimum in the laboratory-scale unit (Chapter 6). After waiting until all the visible cenospheres and unburnt carbon were sunken and well mixed into the bulk (the presence of black particles in the floats layer in the feed slurry disappeared after about 4 hours), a pump was used to withdraw a small sample from 100 mm above the bottom of the feed tank in order to measure the feed cenosphere concentration. The concentration of cenospheres in the solid fly ash was measured to be approximately 0.9 wt.% using sink-float tests.

Two large mixing tanks with volumes of 1200 L and 1500 L were used to keep the feed slurry uniform during the experiments. Before each experiment, the contents of both tanks were kept the same by pumping the slurry between the tanks for several hours. A sample was taken from each tank on the day prior to a run to ensure the feed pulp density and the cenospheres grade were the same in both tanks. The samples were firstly poured into two volumetric flasks, allowing the cenosphere concentrations to be compared via the thickness of the cenosphere layer in each flask. Both samples were then placed in an oven, dried and weighed to assess the pulp density, allowing a final adjustment to be made prior to the run. The smaller tank with a volume of 1200 L was used as the main feed tank. The level of the feed in this tank was kept constant by transferring suspended feed from the larger tank to the feed tank at a rate equivalent to the feed rate.

Before each experiment, the pressure sensors were calibrated using both air and water. The water calibration was conducted when the device was filled with water. At the end of the calibration stage, the water was discharged and the feed was then pumped into the IRC<sup>TM</sup>. A peristaltic pump was used to withdraw the feed from the 1200 L tank at a location 100 mm above the bottom of the feed tank. This feed was delivered to the fluidized bed section of the IRC<sup>TM</sup> some 500 mm above its junction with the inclined section. When the feed was filling up the IRC<sup>TM</sup>, the underflow pump pulled out a small portion of the suspension to prevent blockage in the IRC<sup>TM</sup>. This also led to a degree of cenosphere separation and accumulation

forming a thick cenospheres layer at the top of the vertical section in the IRC™ over time. When the feed level in the IRC™ reached the upper sensor, the feed, tailings (tailings 1 and tailings 2), product and fluidization water were adjusted to the experimental required rates. By doing this, the thick layer of cenospheres formed in the vertical section of the IRC™ can help the system reach steady state more quickly. The other option was to stop the overflow product stream to assist the accumulation and concentration of cenospheres in the vertical section of the IRC™, however, this increased the risk of the overflow product line blocking.

The bulk of the feed including all but the most buoyant of the cenospheres is swept downwards towards the inclined channels. However, the enhanced segregation in the inclined channels captures the cenospheres and refluxes them back to the vertical fluidized bed section. The downwards fluidization, controlled by a peristaltic pump, suspended the cenospheres, washing the entrained fly ash particles in the downwards direction, increasing the product grade. Once steady state was reached, representative samples of the tailings and the product, followed by the feed, were taken. Like the procedure used in Chapter 6, the streams from adjacent lamellae (Tailings 1) and Tailings 2 were combined and then the representative tailings sample was taken. It is noted that timed samples of the same duration were collected from the tailings and the product in order to ensure the grade of the cenospheres remaining in the collected tailings and product was unchanged in the following runs. Also, the water removed by the adjacent lamellae chamber was stored in buckets allowing any entrained solids, at the surface and at the base, to be returned to the feed for the following run. Thus considerable effort was made to ensure there was no degradation in the nature of the feed during the program of work.

### **7.2.3 Data analysis**

Representative portions of the steady state samples were analysed using the sink-float method using a series of separating funnels, as shown in Figure 6.3 (A). This method of separation was thoroughly discussed in Sections 5.3.4.2 and 6.3.3.1. Some portions were also taken in order to measure the particle size distribution and the average particle density. Mass balance reconciliation (Galvin et al., 1995) was undertaken, adjusting the experimental data by minimizing an objective function (Refer to Appendix A).

### 7.2.3.1 Grade and recovery

Using water as the medium, the sink-float method, as described in the previous chapters, was applied to the separation of the cenospheres from the dense fly ash in each stream, allowing the determination of the cenosphere grade and recovery.

### 7.2.3.2 Particle size and density

The particle size distributions of the feed, product, and tailings were measured using a laser particle size analyser (Malvern Master Sizer 3000). Figure 7.2 illustrates the size distributions of the cenospheres and the dense fly ash in the feed. Mass balance reconciliation was used to examine the partitioning of the cenosphere particles between the product and tailings, to in turn produce the partition curve defining the separation. The degree of adjustment in the raw data performed by the mass balance reconciliation technique is presented in Appendix C.

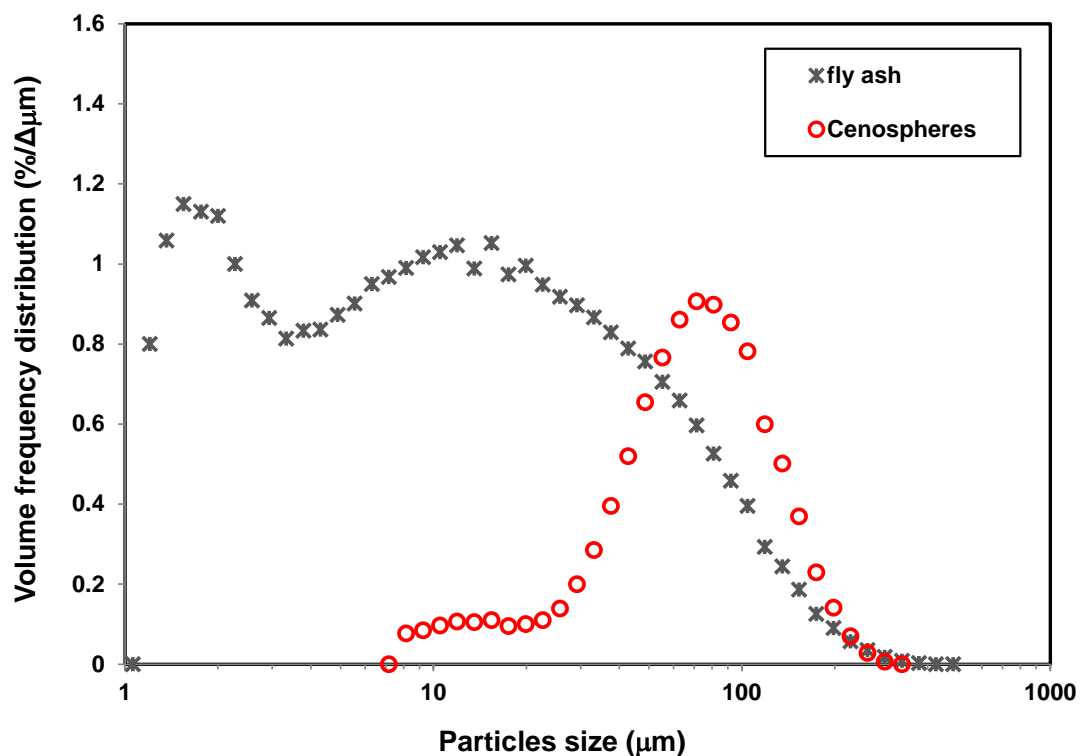


Figure 7.2: Cenospheres and fly ash volume frequency size distributions in the feed (based on the raw data).

A gas pycnometer was also used to measure the average density of the solids obtained under different operating conditions. The pycnometer used nitrogen gas to measure the occupied

volume of a known mass of solids. The average density of the feed solids was measured to be around 1870 kg/m<sup>3</sup>.

### 7.3 Results and Discussion

This section presents the results obtained using different feed split ratios and feed fluxes. In the first part, the feed split ratio, defined as the product volumetric rate divided by the feed volumetric rate ( $P/F$ ), was varied from 0.04 to 0.20, while the feed and fluidization water fluxes were kept constant at 8.3 m<sup>3</sup>/(m<sup>2</sup> h) and 0.83 m<sup>3</sup>/(m<sup>2</sup> h), respectively. These experiments are indicated as Runs 1, 2, 3 and 6 in Table 7.1. In Runs 1, 4 and 5, the effects of using different feed volumetric fluxes were examined at a constant split ratio. The feed pulp density was maintained at the optimum of about 40 wt.% in all runs.

The operating conditions and experimental results are reported in Table 7.1. The slurry mass rates ranged from about 475 kg/h to 1229 kg/h, and the corresponding solid fly ash rates ranged from 194 kg/h to 482 kg/h, thus the processing rates were significant. It is noted that due to the large volume of the samples taken from the pilot IRC<sup>TM</sup> it was difficult to measure their volume accurately. Hence mass-based measurements were used in this chapter in order to provide an accurate comparison between the pilot-scale and the laboratory-scale results. The consistency of the raw data was determined by comparing the inlet and outlet mass rates of the suspension, fly ash, and cenospheres. The discrepancy was the greatest for the cenospheres due to the relatively small quantities involved and the tendency for misplacement of some cenospheres in the sinks fractions. Table 7.1 also presents the maximum and average adjustment required in the mass balance reconciliation.

Table 7.1: Summary of experimental results, operating conditions, and parameters based on the reconciled data (note that the section labelled “Experimental conditions” is based on the raw data).

	Run 1	Run 2	Run 3	Run 4	Run 5	Run 6
<b>Feed</b>						
Total mass rate (kg/h)	936.4	947.2	933.5	1228.6	475.0	924.5
Fly ash mass rate (kg/h)	374.8	369.0	360.7	482.0	193.6	361.6
Cenospheres mass rate (kg/h)	3.6	3.1	3.2	4.5	1.7	3.2
Pulp density (kg solid/kg slurry) (wt.%)	40.4	39.3	39.0	39.6	41.1	39.5
Cenospheres grade (%)	0.96	0.83	0.88	0.93	0.88	0.88
<b>Product</b>						
Total mass rate (kg/h)	118.7	58.7	30.4	175.1	74.1	157.3
Fly ash mass rate (kg/h)	4.7	0.7	0.2	19.8	0.5	12.8
Cenospheres mass rate (kg/h)	2.7	1.9	1.4	3.0	1.2	2.6
Pulp density (kg solid/kg slurry) (%)	6.3	4.5	5.2	13.1	2.3	9.7
Cenospheres grade (wt.%)	36.7	72.0	88.2	13.3	72.9	16.7
<b>Tailings</b>						
Total mass rate (kg/h)	817.7	963.4	978.1	1128.5	475.9	842.1
Fly ash mass rate (kg/h)	370.0	368.2	360.6	462.1	193.2	348.8
Cenospheres mass rate (kg/h)	0.9	1.2	1.8	1.5	0.5	0.7
Pulp density (kg solid/kg slurry) (wt.%)	45.4	38.3	37.0	41.1	40.7	41.5
Cenospheres grade (wt.%)	0.24	0.32	0.50	0.32	0.25	0.19
<b>Experimental conditions</b>						
Fluidization water flux ( $\text{m}^3/(\text{m}^2 \text{h})$ )	0.83	0.83	0.83	0.83	0.83	0.83
Feed split ratio (vol.%)	16	8	4	16	16	20
Feed flux ( $\text{m}^3/(\text{m}^2 \text{h})$ )	8.3	8.3	8.3	11.3	5.3	8.3
<b>Process performance</b>						
Upgrade	38.2	86.7	100.4	14.3	83.3	18.9
Recovery (wt.%)	75.4	61.9	43.5	67.3	71.8	79.6
<b>Consistency of raw data</b>						
Inlet mass/outlet mass (total)	1.02	1.02	0.99	1.00	1.00	1.01
Inlet mass/outlet mass (fly ash)	0.98	0.98	0.96	0.98	0.96	1.00
Inlet mass/outlet mass (cenospheres)	1.00	1.15	1.08	0.87	1.04	1.03
Maximum adjustment by the reconciliation technique (%)	1.33	9.49	5.31	8.65	2.37	2.02
Average adjustment by the reconciliation technique (%)	0.45	2.25	1.54	2.13	0.92	0.55

### 7.3.1 Variation of the feed split ratio

One approach for operating the Inverted REFLUX™ Classifier (IRC™) is to establish the flow rates of the product and tailings according to a given flow split ratio. The solids yield, which is the percentage of the feed solids reporting to the product stream, correlates directly

with increases in the flow split ratio, and hence is an alternative way to represent the split condition, though its actual value must be determined experimentally.

Figure 7.3 shows the change in the suspension density in the vertical section of the IRC™ versus time at different feed split ratios during the initial start-up phase of an experiment before steady-state was reached. The suspension density value initially decreases, reflecting the accumulation of low density cenospheres in the vertical section, and the removal of the higher density fly ash particles in the underflow. The suspension density levelled off as the process approached steady state. At the lower split ratio, the rate of product removal was relatively low, hence the cenosphere concentration in the vertical section of the IRC™ increased, resulting in a lower suspension density. It is also noted that the fluidization water flux was significant compared to the lower product flux, hence the ultrafine dense fly ash was readily washed from the product. Therefore a higher product grade was achieved at a lower split ratio (Table 7.1). It is noted that feed flow started at  $t = 0$  with the IRC™ initially empty. The first density measurement at approximately  $t = 20$  min is when the liquid level in the unit first reached the upper pressure probe.

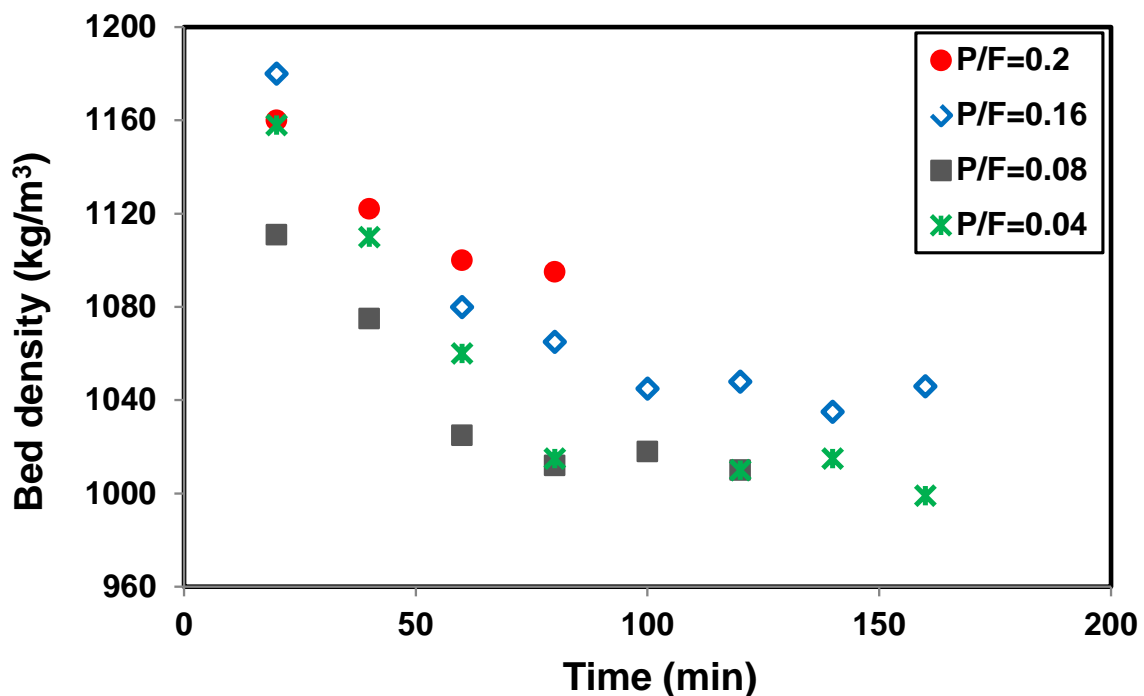


Figure 7.3: The suspension density formed in the vertical section of the IRC™ above the feed point versus time at different feed split ratios with the feed solids throughput and fluidization water flux kept constant at  $4.1 \text{ t}/(\text{m}^2 \text{ h})$  and  $0.83 \text{ m}^3/(\text{m}^2 \text{ h})$ , respectively.

Figures 7.4 and 7.5 show the variation in the average density and size of the cenospheres in the product with increasing product to feed volumetric split ratio. A high product overflow rate results in the direct recovery of cenospheres exhibiting a low rise velocity, and hence a finer and denser cenospheres product. Therefore the average density and size of cenospheres in the product approach the values for the feed as the feed split ratio increases. In other words, any drop in the cenosphere recovery at low feed split ratios is attributed mostly to the loss of fine and high density cenospheres being entrained to the tailings.

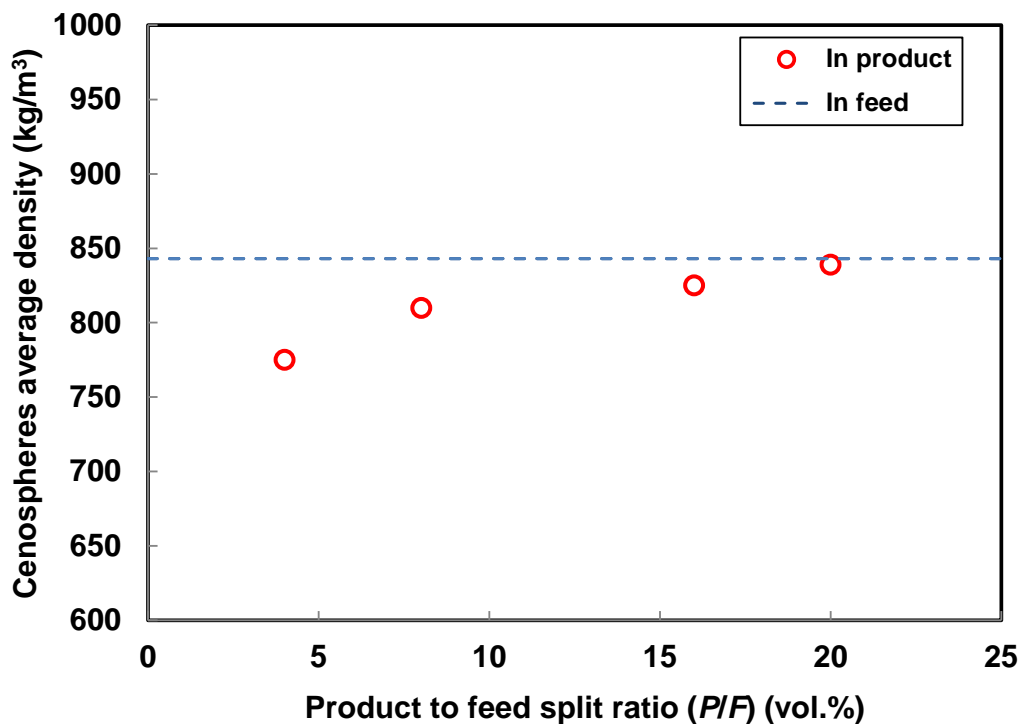


Figure 7.4: Variation of the average density of cenospheres in product at different feed split ratios (raw data) with the feed solids throughput and fluidization water fluxes kept constant at 4.1 t/(m<sup>2</sup> h) and 0.83 m<sup>3</sup>/(m<sup>2</sup> h), respectively.

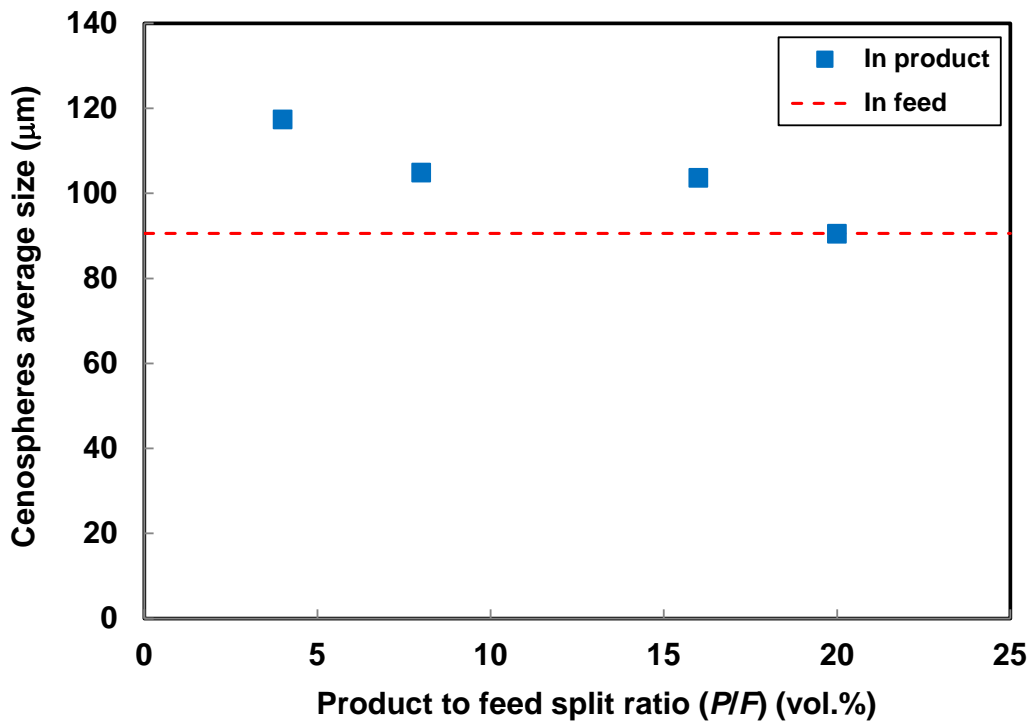


Figure 7.5: Variation of the average size of cenospheres in product at different feed split ratios (raw data) with the feed solids throughput and fluidization water flux kept constant at  $4.1 \text{ t}/(\text{m}^2 \text{ h})$  and  $0.83 \text{ m}^3/(\text{m}^2 \text{ h})$ , respectively.

Therefore an excessive product rate does ensure maximum recovery of cenospheres for the imposed feed rate as shown in Figure 7.6. By increasing the yield (defined as the ratio of solids mass in the product to solids mass in the feed) from 0.43 wt.% to 4.2 wt.%, the recovery of the cenospheres increased from 43.7 wt.% to about 79.1 wt.%. These pilot scale findings are consistent with the laboratory scale results in the previous chapter. It should be noted that these results are also dependent on the fluidization flux imposed (Section 5.4.2.5). It is also worth noting that in Figures 7.6 and 7.7, the data were compared with data from the laboratory-scale runs at approximately the same conditions, namely throughput and fluidization water flux of about  $4.7 \text{ t}/(\text{m}^2 \text{ h})$  and  $1.0 \text{ m}^3/(\text{m}^2 \text{ h})$  respectively. The feed pulp density was approximately 40 wt.% at both scales.

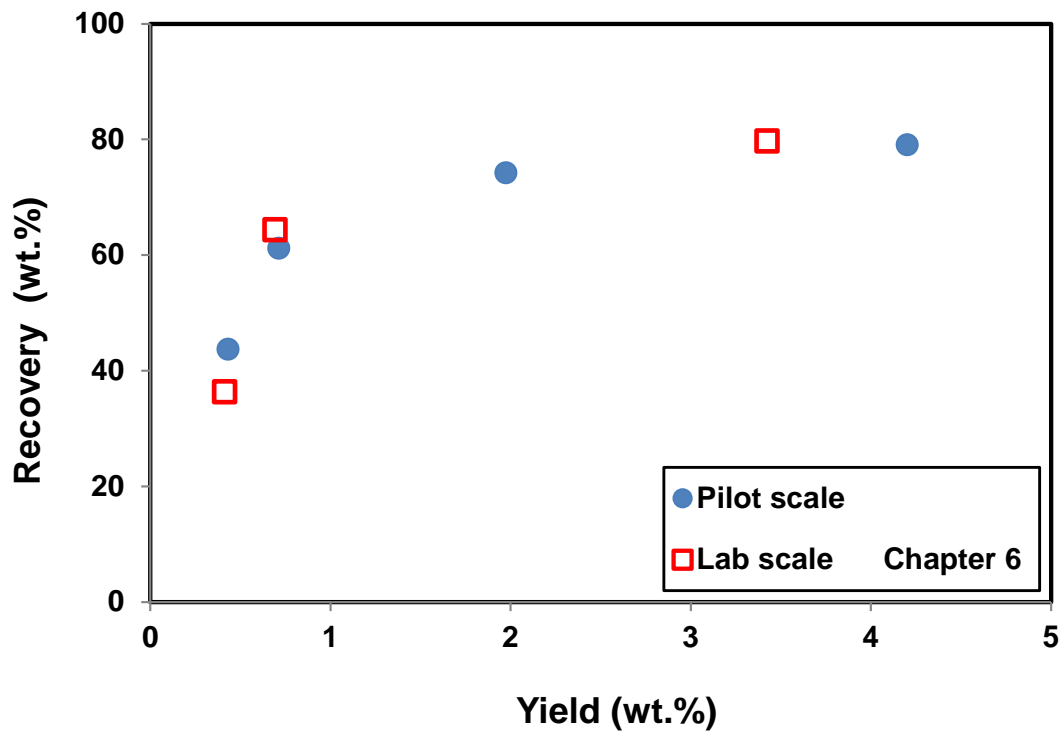


Figure 7.6: Recovery of cenospheres obtained at different yields from the pilot scale IRC<sup>TM</sup> (based on the reconciled data) with the feed solids throughput and fluidization water flux kept constant at 4.1 t/(m<sup>2</sup> h) and 0.83 m<sup>3</sup>/(m<sup>2</sup> h), respectively.

Conversely, an insufficient product overflow rate results in the growth of the fluidized bed of cenospheres at the top of the unit, which increases the likelihood of them being entrained in the downwards flow, and lost to the tailings, thereby reducing the yield of solids. At these low yields, the product grade is at a maximum for the imposed feed and fluidization rates, as shown in Figure 7.7. The product grade increased from about 17 wt.% to 88 wt.% when the split ratio decreased from 0.20 to 0.04, corresponding to a decrease in the solids yield from 4.2 wt.% to 0.43 wt.%. Figure 7.8 shows the density of suspension in the vertical section of the IRC<sup>TM</sup> at the steady state condition and the obtained product grades at different split ratios. It is evident that at higher split ratios, a higher proportion of the dense fly ash can be carried to the vertical section, and hence a higher suspension density and lower product grade were obtained.

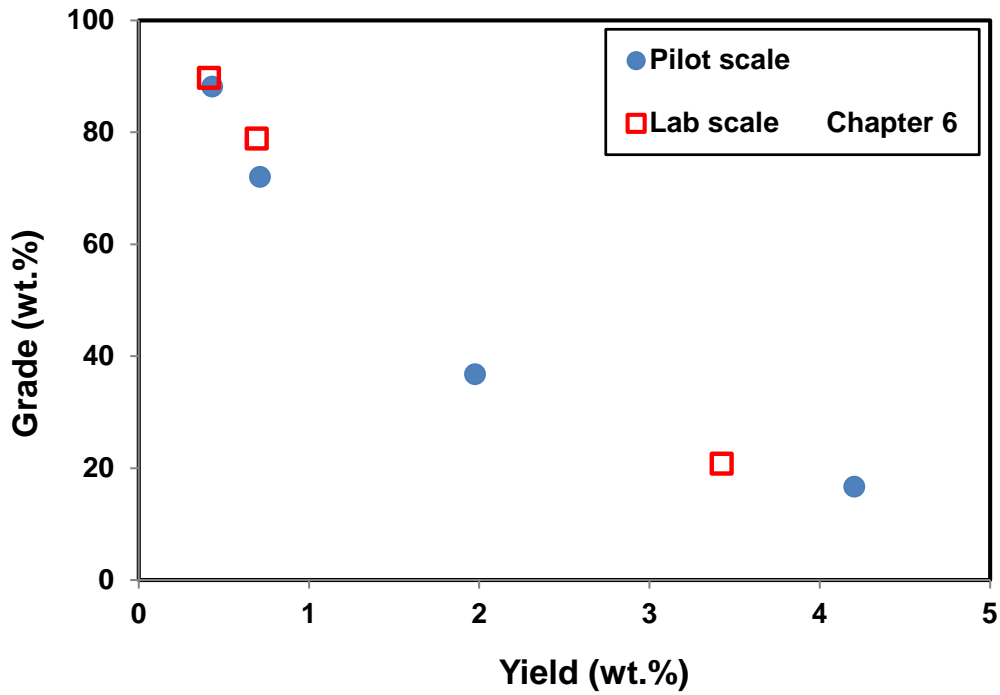


Figure 7.7: Product grades obtained at different yields from the pilot scale IRC<sup>TM</sup> (based on the reconciled data) with the feed solids throughput and fluidization water flux kept constant at 4.1 t/(m<sup>2</sup> h) and 0.83 m<sup>3</sup>/(m<sup>2</sup> h), respectively.

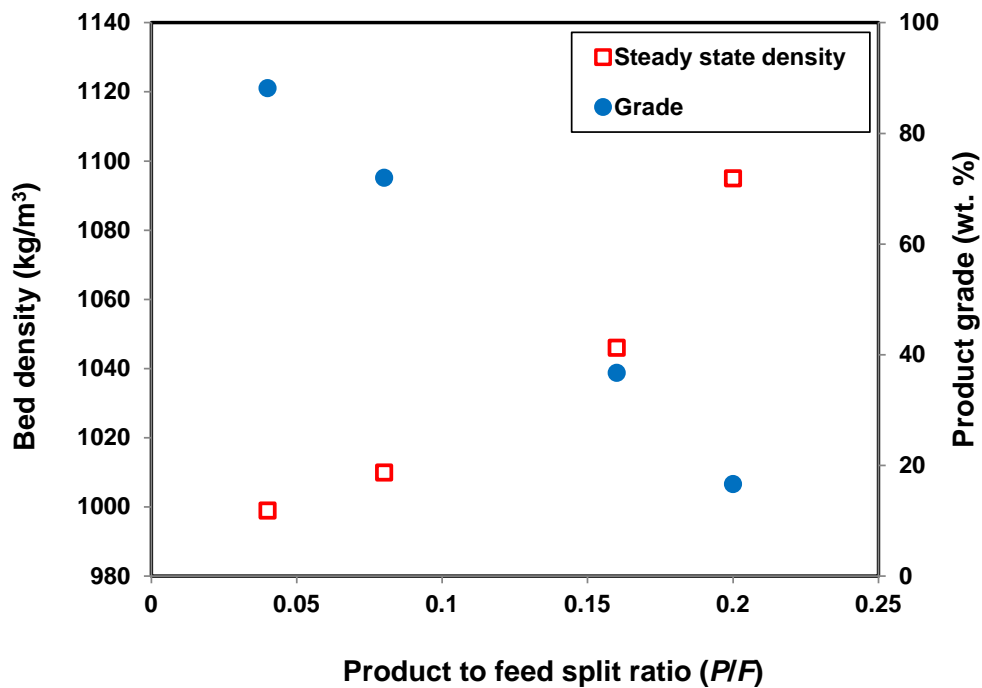


Figure 7.8: The bed density and product grade at different feed split ratios at the steady state condition.

The cenosphere grade is shown as a function of the cenosphere recovery in Figure 7.9. The results achieved from a single stage separation using the Inverted REFLUX™ Classifier are remarkable, with a recovery of 79 wt.% at a grade of 17 wt.%, hence an upgrade of 19. This condition delivers significant recovery and upgrade. Additional separation stages can be used to raise the grade to the required level. It is also evident that significant increases in grade can still be achieved in the first stage, initially with a modest cost of recovery. This grade – recovery curve applies to the feed volumetric and solids fluxes used here, with more favourable results achievable by reducing the feed throughput.

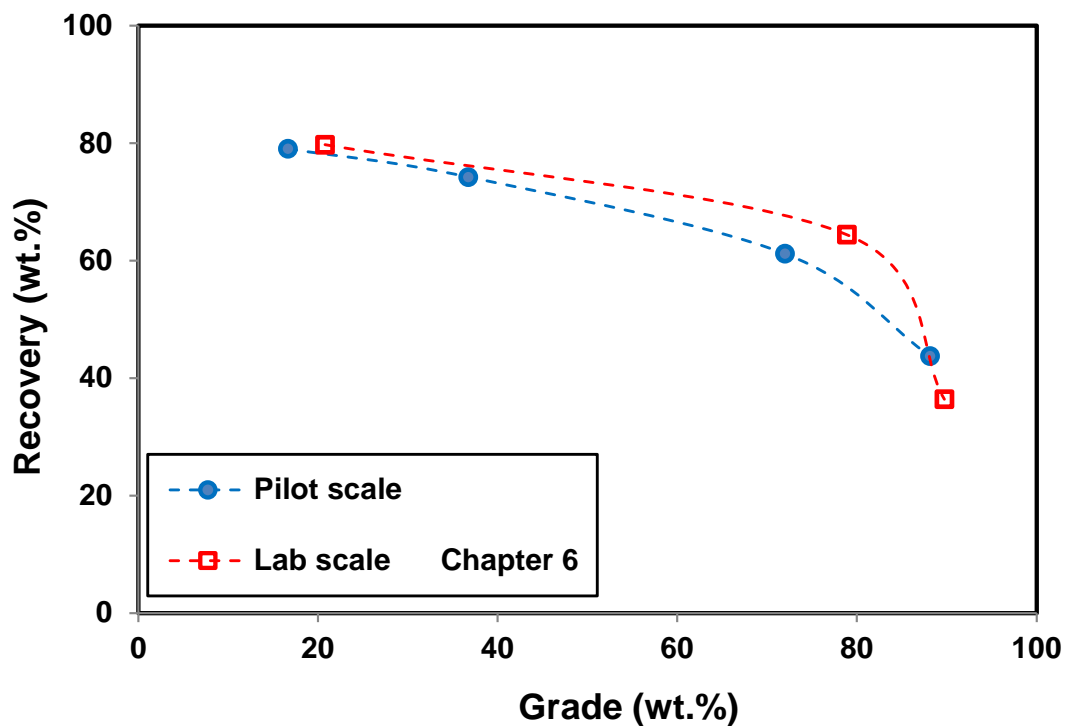


Figure 7.9: The grade-recovery curve achieved for the pilot scale IRC™ at a solid throughput of 4.1 t/(m<sup>2</sup> h) (based on the mass balanced data) with the fluidization water fluxes kept constant at 0.83 m<sup>3</sup>/(m<sup>2</sup> h). The feed solids throughput and fluidization water flux were about 4.7 t/(m<sup>2</sup> h) and 1.0 m<sup>3</sup>/(m<sup>2</sup> h) in the laboratory scale runs. The feed pulp density was around 40 wt.% at both scales.

### 7.3.2 Density and size classification of cenospheres and fly ash

Figure 7.10 shows that the size distributions of the dense fly ash particles in the feed, product, and tailings were very similar, while Figure 7.11 shows that a distinct size classification of the cenospheres was evident. The sink-float method was highly problematic for the particles

finer than 10  $\mu\text{m}$  due to their very low settling velocities, contributing to the discrepancies between the inputs and outputs shown in Table 7.1. These discrepancies mainly affect the size distributions of fly ash particles smaller than 10  $\mu\text{m}$  (Figure 7.10).

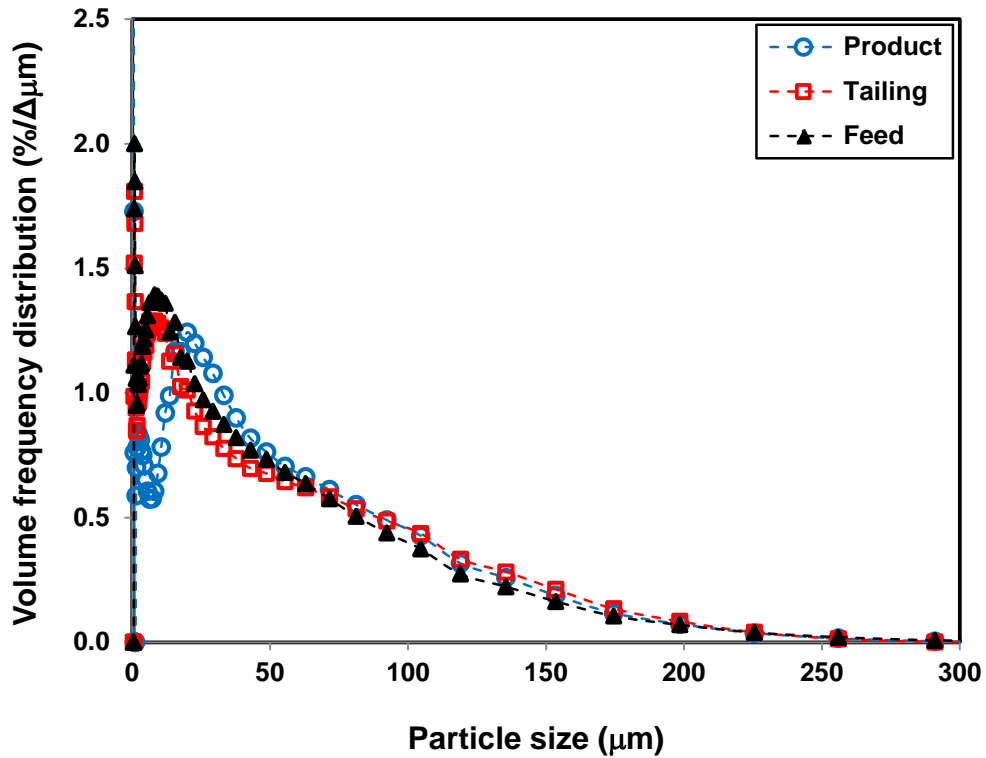


Figure 7.10: The volume frequency size distributions of sink fly ash particles in the product, tailings and feed for Run 3 (based on the raw data).

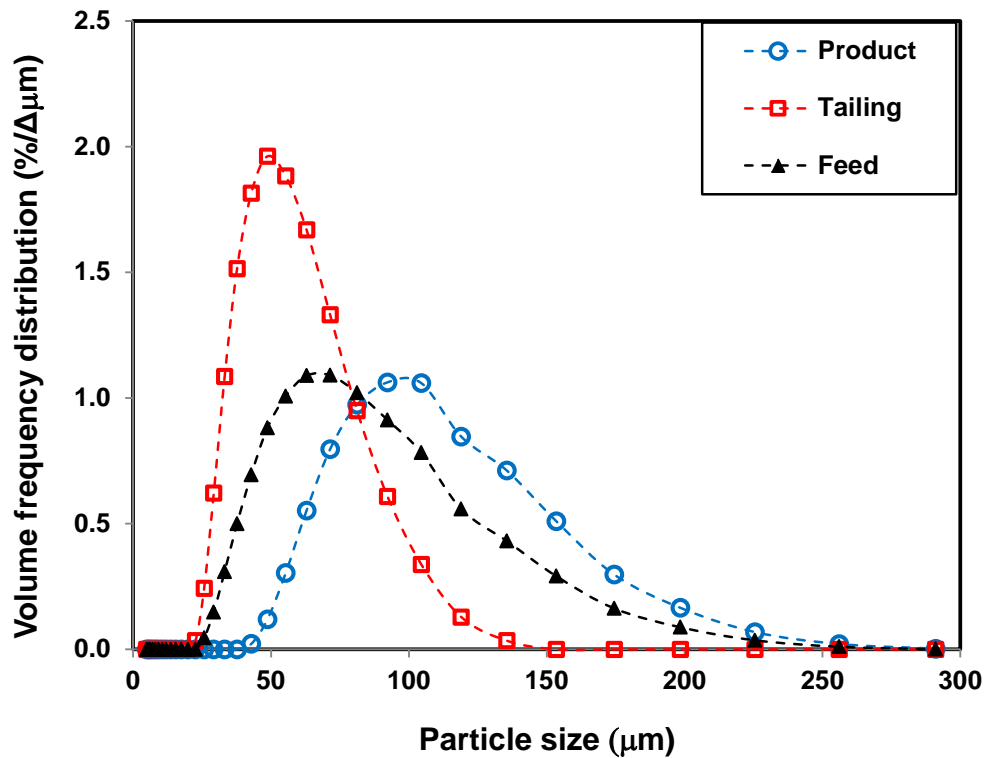


Figure 7.11: The volume frequency size distributions of float cenosphere particles in product, tailings and feed for Run 3 (based on the raw data).

The size distribution of the cenospheres in the tailings was relatively fine compared to the distribution in the product. Clearly the loss in cenosphere recovery can largely be explained by the fineness of the particles and hence their low rise velocities. Figure 7.12 provides the partition curves for Runs 1, 2, 3 and 6 denoting the probability of the cenosphere particles reporting to the product versus the particle size. For Run 3, it is evident that cenosphere particles with a diameter of 60 µm had a probability of 0.31 in reporting to the product while cenosphere particles with a diameter of 100 µm had a probability of more than 0.80 of reporting to the product. Based on this curve, all particles of diameter less than 40 µm were entrained to the tailings, and almost all cenospheres larger than 145 µm entered the product.

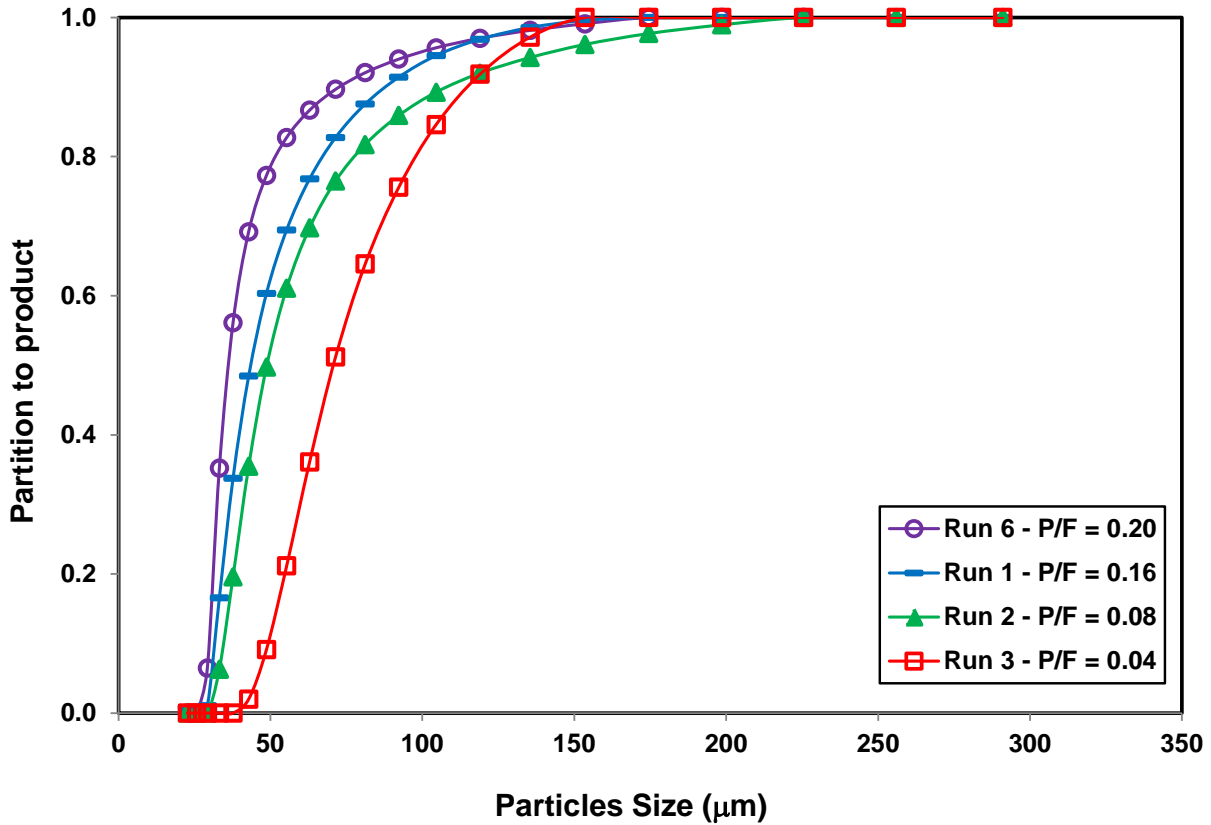


Figure 7.12: The partition curves for Run 1, 2, 3 and 6 (based on the reconciled data).

Using the partition curves shown in Figure 7.12, the values of  $d_{50}$  and  $I$  were obtained and are listed in Table 7.2. At a high feed split ratio, finer particles with lower rise velocities were recovered more easily to the product and hence the  $d_{50}$  is lower, while at a low feed split ratio, these particles will be entrained to the tailings. Imperfection ( $I$ ) defined as  $(d_{75} - d_{25})/2d_{50}$  shows the sharpness of separation, which is similar across all runs, showing the robust performance of the IRC™. Runs 3 and 6 were conducted at about 4% lower solids throughputs and hence their corresponding size separation is slightly sharper (i.e.  $I$  is lower).

Table 7.2:  $d_{50}$  and  $I$  obtained at different split ratios (Runs 1, 2, 3 and 6).

	Run 6 $P/F = 0.20$	Run 1 $P/F = 0.16$	Run 2 $P/F = 0.08$	Run 3 $P/F = 0.04$
$d_{50}$ (µm)	35	44	49	70
$I$	0.23	0.29	0.29	0.25

A particle's settling/rise velocity depends on its density and size. The average density of both the cenospheres and dense fly ash in the product, tailings and the feed for Run 3 are shown in Table 7.3. Clearly there is some classification based on the density, with the lower density

portion of the cenospheres reporting to the product, while the cenospheres with a density close to that of water reported to the tailings. Some density classification also occurred within the sinks fly ash particles. It is noted that there were difficulties in measuring the density of the cenospheres in the tailings and the density of the fly ash in the product because the sample mass was far too low for the pycnometer. Therefore the average density of the cenospheres in the tailings was calculated based on the measured densities of the cenospheres in the feed and the product. Similarly, the average density of the fly ash in the product was calculated using the measured densities of the overall solid product and the cenospheres in the product.

Table 7.3: Arithmetic average size and density of cenospheres and fly ash in product, tailings and feed for Run 3 (based on the raw Malvern & pycnometry data).

	Average size ( $\mu\text{m}$ )	Average density ( $\text{kg/m}^3$ )
<b>Cenospheres</b>		
Overflow product	117.4	775.4
Underflow tailings	62.1	*903.6
Feed	94.5	843.0
<b>Fly ash</b>		
Overflow product	68.1	*1230.0
Underflow tailings	68.5	1890.0
Feed	64.0	1887.0

\* Density of cenospheres in the tailings was calculated based on the measured densities of cenospheres in the feed and product, and the density of fly ash in the product was calculated based on the measured densities of the solids (i.e. fly ash and cenospheres) and cenospheres in product.

Table 7.3 also presents the average size, defined as the arithmetic mean of the volume equivalent size, of the cenospheres and fly ash particles in all streams, indicating clearly that the size classification occurred only for the cenosphere component, not for the dense fly ash which was on average 65  $\mu\text{m}$ . This is consistent with the finding of Figure 7.10 and 7.11. The cenospheres exhibited a narrower range of densities as previously shown in Tables 4.1, 4.3 and 5.4, hence classification was stronger on the basis of size. A detailed characterization of the fly ash and cenospheres was presented in Chapter 4, providing more information about the size and density distributions of particles.

### 7.3.3 Separation of cenospheres from fly ash at different feed throughputs

In this section, the effects of feed flux variation on the bed suspension density, and product grade and recovery of cenospheres are examined. In Runs 1, 4 and 5 shown in Table 7.1, the fluidization water flux was kept constant at  $0.83 \text{ m}^3/(\text{m}^2 \text{ h})$ . Different volumetric feed fluxes of 5.3, 8.3 and  $11.3 \text{ m}^3/(\text{m}^2 \text{ h})$  were used while the feed split ratio and feed pulp density were maintained at approximately 16 vol.% and 40 wt.%, respectively, in the experiments.

Figure 7.13 shows the bed (concentrated suspension) density as a function of time for three different feed volumetric fluxes (Runs 1, 4 & 5). As previously mentioned in Figure 7.3, the bed density initially jumps up to a peak value as the unit fills with suspension that is similar to the feed. Then the density gradually decreases as the concentration of the positively buoyant cenospheres increases, eventually approaching a constant value at steady state. The time taken to reach steady state appears to vary from about 1 h at high feed fluxes up to 2 h at the lowest feed flux, presumably due to the longer time needed to build up the inventory of low-density cenospheres in the vertical section. According to Figure 7.14, it is also evident that at a higher feed flux and hence a higher product flux, more dense fly ash particles were entrained upwards into the vertical section, leading to a higher suspension density and hence a lower grade product.

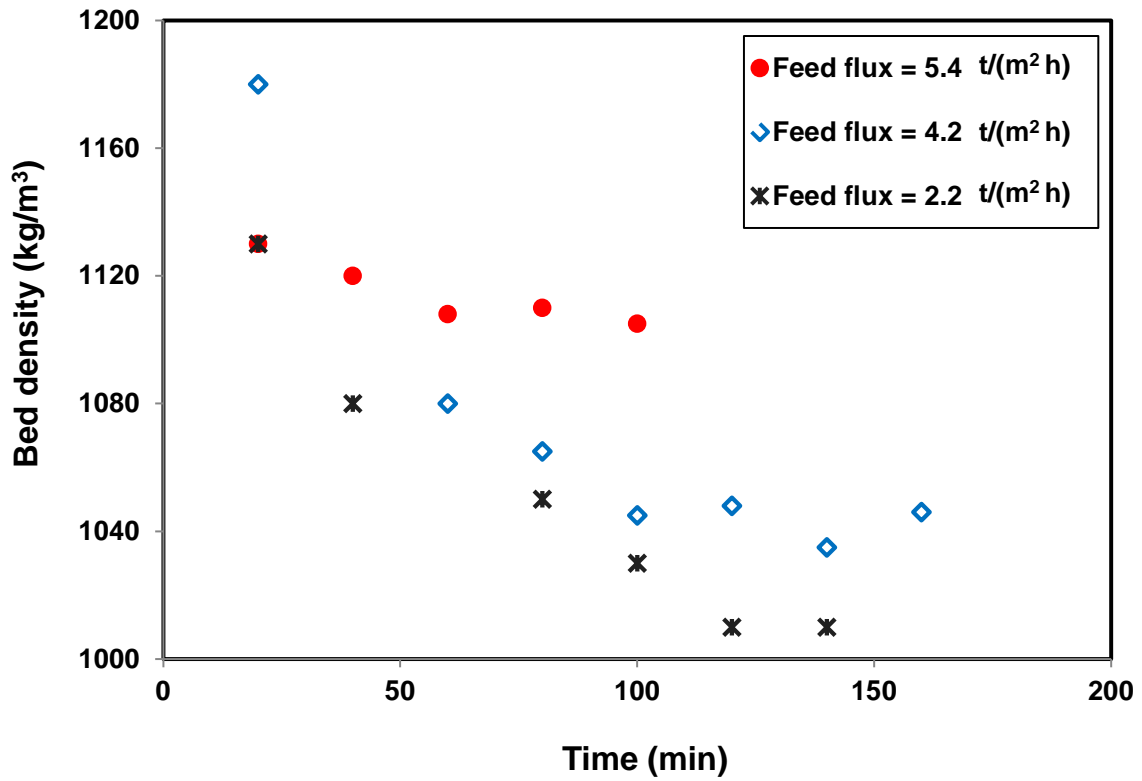


Figure 7.13: The bed density variation with time at different feed fluxes in the pilot scale IRC<sup>TM</sup>. Fluidization water flux, feed volumetric split ratio and feed pulp density were maintained approximately constant at 0.83 m<sup>3</sup>/(m<sup>2</sup> h), 16 vol.% and 40 wt.% respectively.

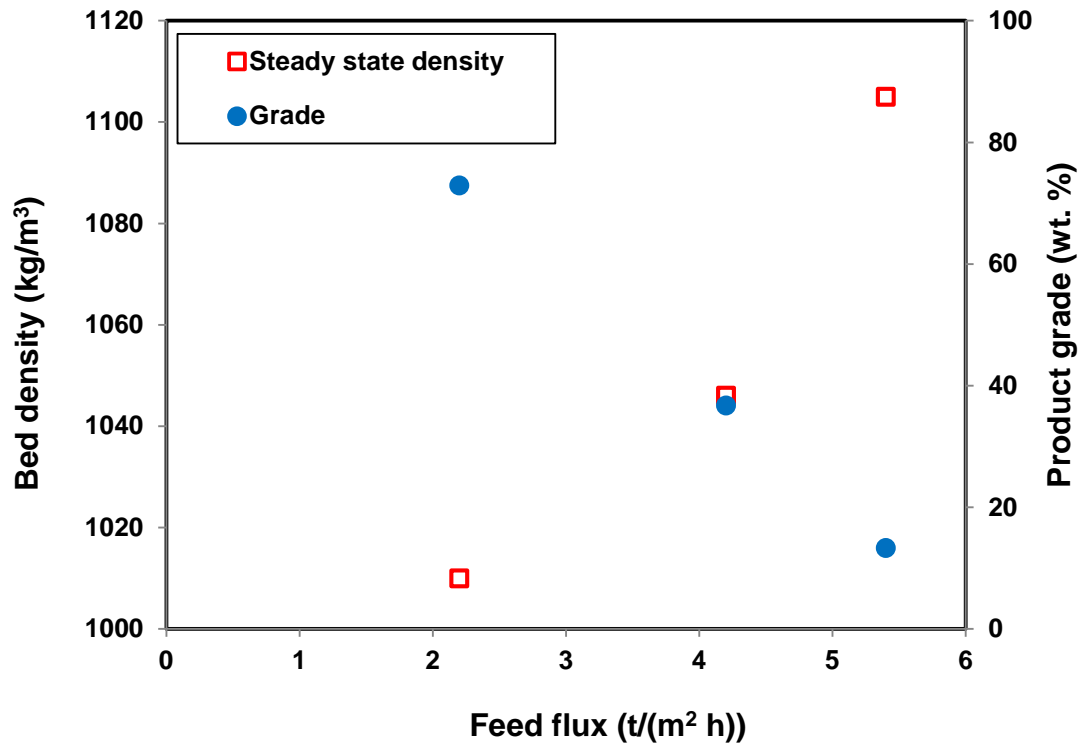


Figure 7.14: The bed density and product grade at different feed fluxes, at steady state.

Figure 7.15 shows the cenosphere grade in the product decreased from about 73 wt.% to approximately 13 wt.% as the feed mass flux increased from 5.3 t/(m<sup>2</sup> h) to about 13.7 t/(m<sup>2</sup> h). Further, it is evident the trend is consistent with the results obtained at the much smaller laboratory scale (Section 6.5.4). These results clearly demonstrate that the performance is consistent during scale-up by a factor of about 10 in the vessel cross-sectional area.

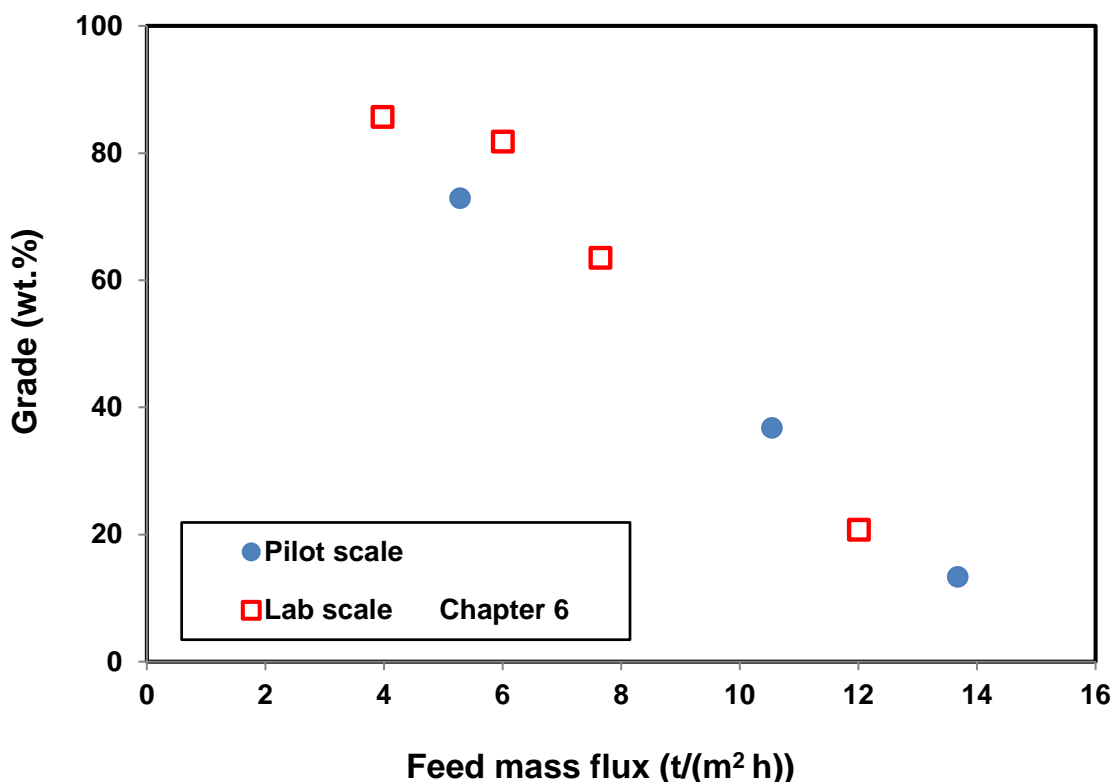


Figure 7.15: The variation of product grades at different feed slurry mass fluxes (based on the mass balanced data), comparing this chapter's pilot-scale results with the laboratory-scale results from Chapter 6. Fluidization water flux, feed volumetric split ratio and feed pulp density were maintained approximately constant at 0.83 m<sup>3</sup>/(m<sup>2</sup> h), 16 vol.% and 40 wt.% respectively in the pilot scales runs, while the feed volumetric split ratio was slightly higher at 20 vol.% in the lab scale runs.

As the feed flux increased the product flux increased due to the imposed constraint of a fixed split ratio. Figure 7.16 shows that the cenosphere recovery was nearly independent of the feed flux, however the previous laboratory scale work (Chapter 6) suggested the existence of an optimum. The optimum is quite subtle here, but was clearer in chapter 5. At a low feed flux, the product rate is low, hence the fluidization rate dominates, reducing the net transport of the

cenospheres to the overflow. At a higher feed flux, the volumetric rate to the tailings increases, entraining more cenospheres to the tailings, reducing the recovery.

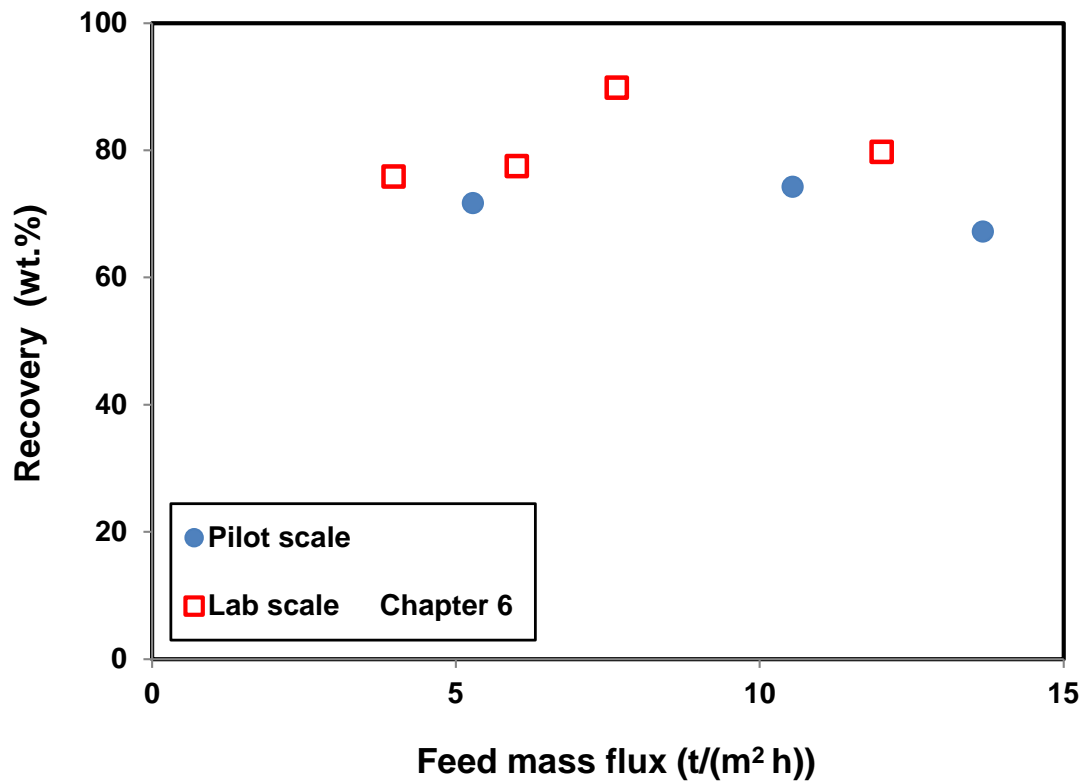


Figure 7.16: The recovery of cenospheres at different feed slurry mass fluxes (based on the reconciled data) comparing the present pilot-scale results with the laboratory-scale results from Chapter 6. Fluidization water flux, feed volumetric split ratio and feed pulp density were maintained approximately constant at  $0.83 \text{ m}^3/(\text{m}^2 \text{ h})$ , 16 vol.% and 40 wt.% respectively in the pilot scales runs, while the feed volumetric split ratio was slightly higher at 20 vol.% in the lab scale runs.

Before concluding it is worth noting the significance of the volumetric flux difference between the product and fluidization water,  $P - W$ . The fluidization water has two purposes, firstly to fluidize the cenospheres creating a bed of low density to promote gravity separation, and secondly to wash ultrafine dense fly ash particles from the fluidized bed. The fluidization flux should be set at the minimum rate necessary to fluidize. Insufficient fluidization will cause misplaced dense particles to become entrained within the overflow while excessive fluidization will prevent the formation of a distinct fluidized bed layer of cenospheres. Further, the fluidization flux also places a lower limit on the size of cenospheres that can report to the product.

At a low product flux, the net water flux in the vertical zone is downwards, favouring higher product grades at the expense of low recovery. However, as the product flux increases, the net water flux in the vertical zone drops to zero, and then becomes upwards. This condition leads to lower grades and higher recovery. Figure 7.17 shows the grade and recovery obtained from different runs (Runs 1-6) in the pilot scale IRC™ at different  $P - W$ . The last point in the recovery figure is related to Run 4 conducted at a high feed flux. This behaviour is similar to that presented in Figure 5.18, reflecting the detrimental effect at high feed rates of the resultant high suspension velocity through the inclined channels causing a drop in cenospheres recovery in the IRC™. This Figure is consistent with Figure 5.17 and 5.18 showing the effect of the parameter ( $P - W$ ) on the product grade and cenospheres recovery at a pilot scale IRC™.

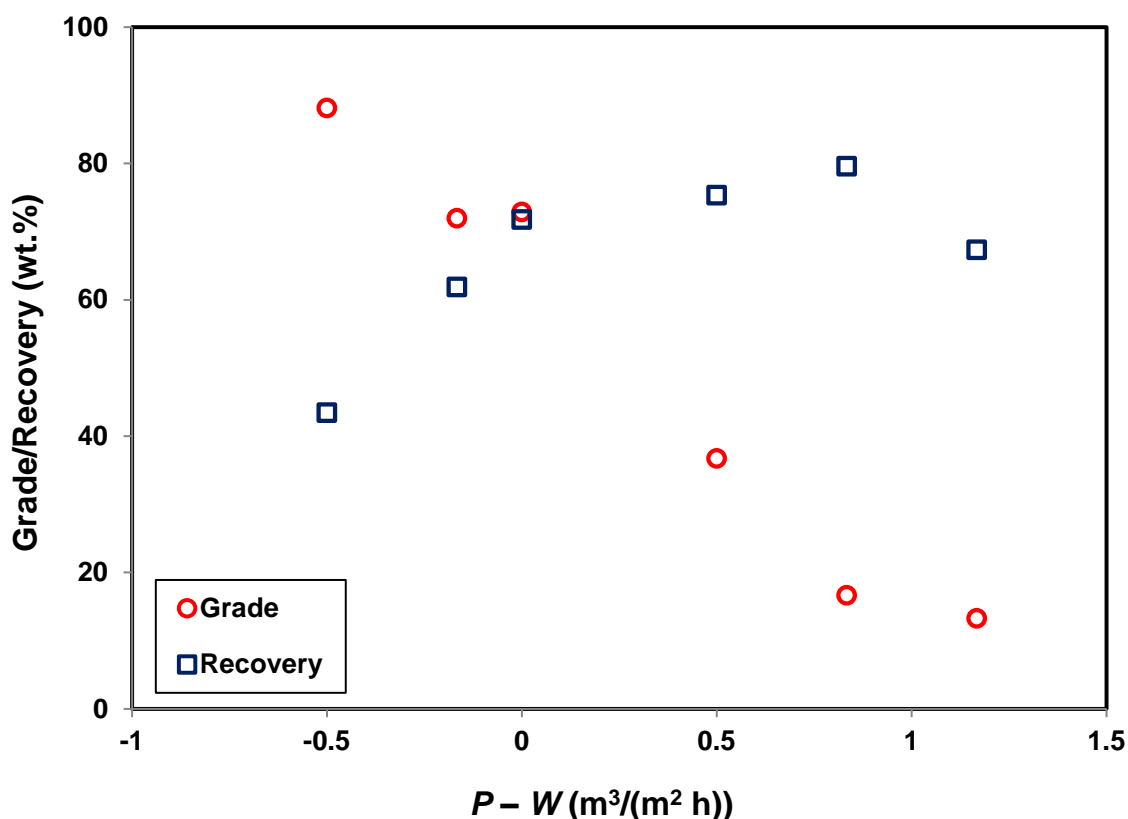


Figure 7.17: Product grade and cenospheres recovery obtained from different runs in the pilot scale IRC™ (Runs 1-6).

This study has demonstrated two things. Firstly, the results provide robust confirmation of the earlier laboratory scale work and supports the strong conclusions made in that work

concerning the considerable throughput advantage and separation performance of the Inverted REFLUX™ Classifier (IRC™). But, importantly, this chapter also shows the robust nature of the technology, in particular the potential to achieve scale-up of the findings. The work provides the necessary foundation required for proceeding with the implementation of a full-scale trial, especially in terms of the ideal conditions defined in terms of the solids feed flux, and target cenosphere grade and recovery. Clearly, the suspension density of the upper zone provides a rigorous measure of the probable product grade, and a simple method for insuring the presence of a fixed fluidized bed of cenospheres. The overflow discharge would be permitted in response to the suspension density decreasing below a specific set point value.

#### **7.4 Conclusions**

A pilot scale Inverted REFLUX™ Classifier was used to separate cenospheres from fly ash waste, in an attempt to validate the previous laboratory scale results. The results were quantitatively in good agreement and the effects of feed split ratio and feed flux on product grade and the cenosphere recovery followed similar trends. The cenosphere particle size distributions of the feed, product, and tailings were used to generate size partition curves. These showed that by increasing the feed split ratio to product, finer cenospheres were recovered and hence a smaller  $d_{50}$  was obtained. On the other hand, as the feed conditions including the feed flux and the feed solids concentration were almost similar in all runs, the sharpness of separation indicated by Imperfection ( $I$ ) was measured to be almost constant.

Analysis of the cenosphere densities in each stream showed that there was also some degree of separation based on density. Using pressure probes to measure the suspension density in the vertical section of the IRC™ was useful for assessing whether the system had reached steady state. Knowing the density of cenospheres, fly ash and water, this approach can also provide an estimation of the product quality (i.e. product grade). The consistency of these findings during scale up by a factor of 10 demonstrates that the Inverted REFLUX™ Classifier should be able to confidently be scaled-up even further to full-scale.

Based on the results obtained from a one-stage IRC™ in Chapters 5, 6 and 7, to extend the performance boundaries in terms of solids throughput, product grade and cenospheres recovery, it is suggested that a multi-stage IRC™ arrangement be used to achieve a

combination of high upgrade with simultaneous high recovery at large solids throughput. The performance of such a multi-stage arrangement is the focus of Chapter 8.

## **Chapter 8**

# **Multi-stage Concentration of Cenospheres in Fly Ash**

### Journal Article(s) Related to the Chapter and Authors' Contribution

**Kiani, A.,** Zhou, J. & Galvin, K.P. (2015). Multi-stage concentration of cenospheres in fly ash using the Inverted Reflux Classifier. *Coal Combustion and Gasification Products*, 7, 40-46.

Author	Contribution
Ali Kiani	The lead author of the paper, collaborator in experimental design, primary interpretation of results, analysis of data, and experimental operator
James Zhou	Co-supervisor, experimental support
Kevin Galvin	Principal supervisor, collaborator in experimental design and results interpretation, inventor and designer of system

## **8.1 Introduction**

Although wet processing methods offer the best prospect for achieving recovery and concentration of cenospheres, significant impediments remain for achieving satisfactory economics. This chapter is concerned with the recovery and concentration of cenospheres from different fly ash feeds using the Inverted REFLUX™ Classifier (IRC™), covering multi-stage processing. Chapters 6 and 7 demonstrated at laboratory and pilot scale respectively how the combined effects of inclined settling and bulk streaming enable a one-stage IRC™ to obtain either a high recovery or a high grade of cenospheres. This chapter studies use of a multi-stage series of IRC™s in an attempt to simultaneously obtain both high grade and high recovery. Cenospheres were recovered from fly ash feeds of varying initial cenosphere concentrations. This is the first time that the multi-stage application of IRC™s has ever been reported. In preliminary experiments, a fly ash feed with a very low cenosphere concentration was processed in a two-stage IRC™ process. Then in the main part of the study the same fly ash feed used in Chapter 7 with about 0.9 wt.% cenospheres concentration was processed in a three-stage IRC™ to achieve an almost pure cenosphere product. Thus this chapter provides further insight into the optimisation of cenosphere recovery from different fly ash feeds using multi-stage arrangements.

## **8.2 Experimental**

### **8.2.1 Materials**

In this chapter, the same laboratory and pilot scale Inverted REFLUX™ Classifiers (IRC™) already comprehensively described in previous chapters were applied to the multi-stage separation of cenospheres from fly ash. In the laboratory-scale unit, the inclined section consisted of 8 channels with perpendicular spacing of 9.5 mm, and the pilot-scale unit had 38 channels with a 6 mm perpendicular spacing.

### **8.2.2 Methods**

A multi-stage arrangement was used to upgrade the cenospheres in the fly ash. In the preliminary work, a series of two laboratory IRC™s was used to upgrade the cenospheres in a fly ash feed that was degraded to only 0.33 wt.% cenospheres. Then in the main part of the study the same fly ash feed used in Chapter 7 with around 0.9 wt.% cenospheres was

concentrated using a series of three IRC™s. The large pilot-scale IRC™ run in Chapter 7 (Run 6) was considered as the first of these three stages. The yield was adjusted to obtain a high recovery of partially upgraded cenospheres. In fact Run 6 in Chapter 7 was continued to generate a high quantity of partially upgraded product. This product was then used to feed the subsequent two stages which were both laboratory-scale IRC™s. The aim of the second stage was to deslime the product. The third stage was then used to further purify the product from the second stage. Samples of all streams in each stage were analysed. A simple representation of the three-stage process is shown in Figure 8.1. It is noted here that the product obtained from each stage was collected and kept mixed in a feed tank and then the mixture was fed to the later stages. Therefore the process here was different from a continuous multi-stage process in which the product of each stage is directly and continuously fed to the next stages.

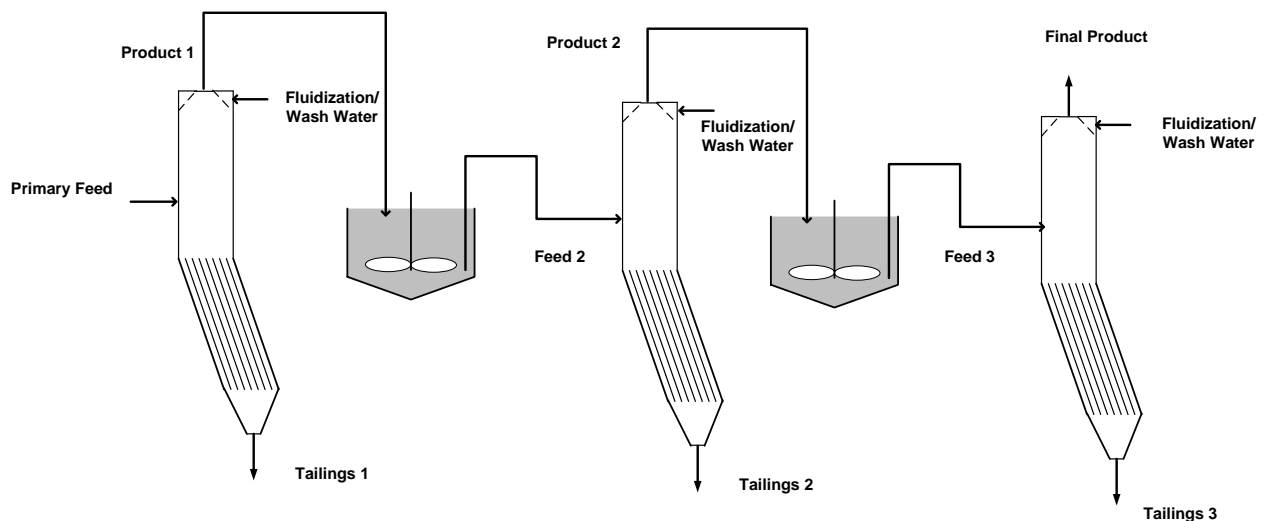


Figure 8.1: A schematic diagram of the three-stage IRC™ process.

### 8.2.3 Data analysis

Sink-float separation was used to measure the composition of the samples as per the procedures described in Chapters 5, 6 and 7. The masses of fly ash (sinks) and cenospheres (floats) were used to calculate the product grade and then the recovery of the cenospheres.

The laser scattering technique (Malvern Mastersizer 3000) was applied to measure the size distributions of the cenosphere and fly ash fractions in the preliminary and main runs. The errors in all experimental data were minimized using the mass balance reconciliation method. The cumulative size distributions of the cenospheres and fly ash in the feed used in the

preliminary study are shown in Figure 8.2. It is evident that 28 vol.% of the fly ash was finer than 20  $\mu\text{m}$ , making the upgrading process difficult. Furthermore, about 84 vol.% of the cenospheres were finer than 100  $\mu\text{m}$ , thus also difficult to recover. The arithmetic average particles size was calculated to be 72  $\mu\text{m}$  for the cenospheres and 59  $\mu\text{m}$  for the fly ash. It is noted that the size distributions of the sinks fractions in both fly ash feeds used in the multi-stage experiments in this chapter were almost identical, whereas the size distribution of floated cenospheres used in the preliminary study was slightly finer. The feed size distributions for both studies are shown in Appendix G.

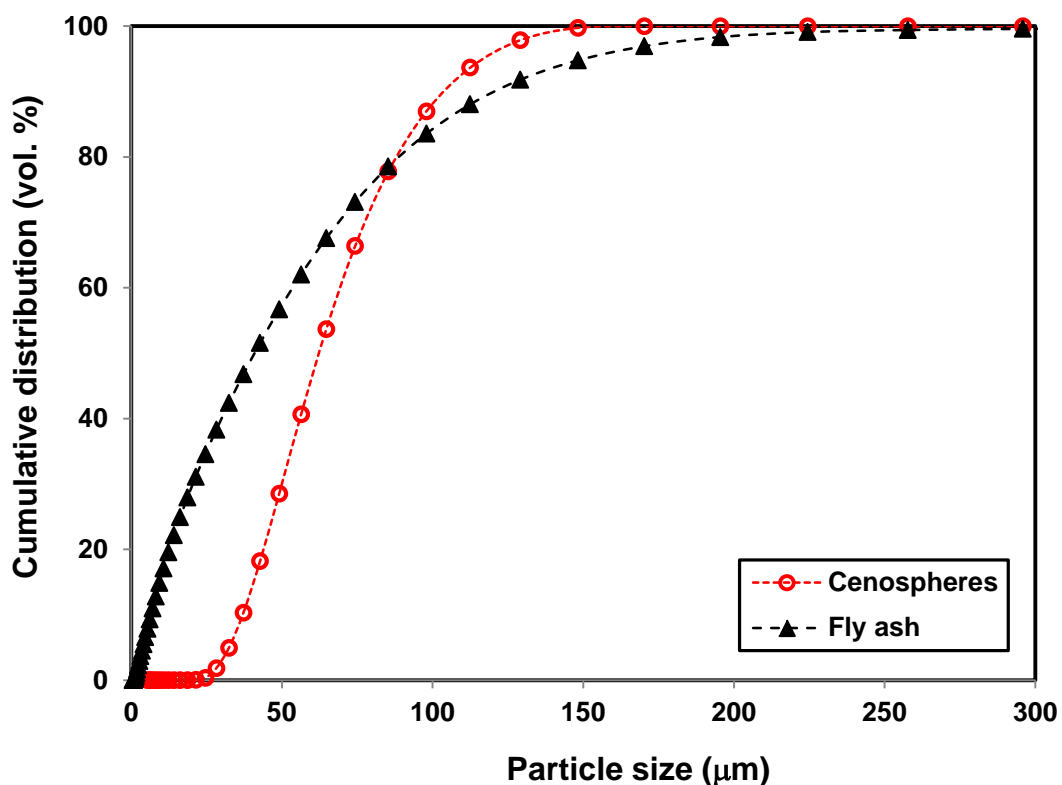


Figure 8.2: The cenosphere floats and fly ash sinks particle size distributions in the feed used for the preliminary two-stage trials.

The average density of the cenospheres and fly ash in the main three-stage feed were measured to be about 843  $\text{kg}/\text{m}^3$  and 1887  $\text{kg}/\text{m}^3$ , respectively, using the gas pycnometry method. However the feed cenosphere density in the preliminary two-stage work was measured to be slightly lower at about 807  $\text{kg}/\text{m}^3$ . Scanning Electron Microscopy (SEM) images of the feed fly ash and cenospheres fractions used in the preliminary and main experiments are shown in Figure 8.3.

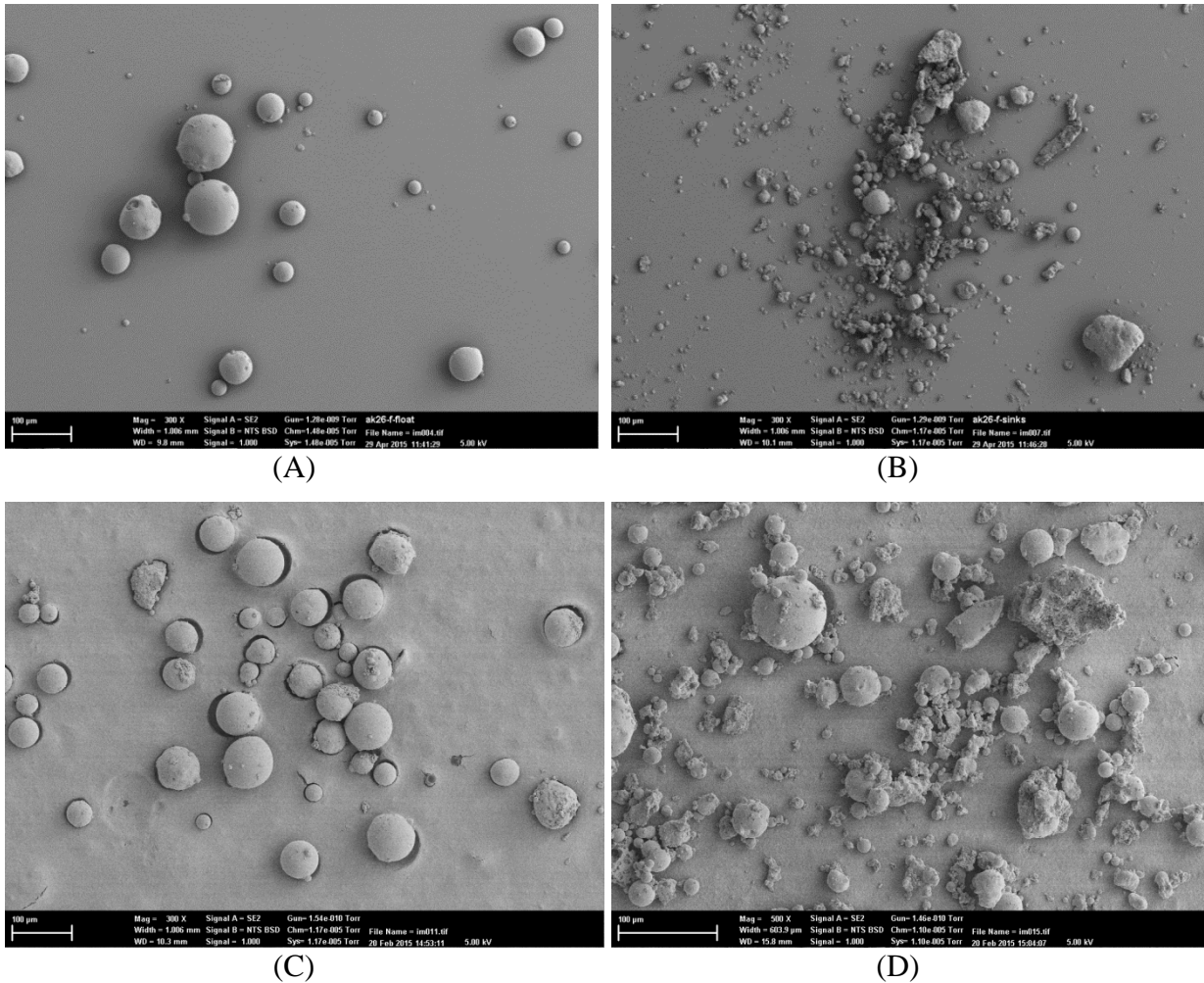


Figure 8.3: SEM images showing (A) the floats fraction and (B) the sinks fraction obtained from a sink-float separation of the preliminary fly ash feed containing 0.33 wt.% cenospheres, and (C) the floats fraction and (D) the sinks fraction obtained from a sink-float separation of the main fly ash feed containing about 0.9 wt.% cenospheres. The 100 µm length scale is shown in the bottom left hand corner of each image. Note the background material, on which the samples rest, is unrelated to the fly ash.

### 8.3 Results and Discussion

This work investigates use of multiple stages for the upgrading of cenospheres. In the preliminary experiments, a series of two IRC<sup>TM</sup>s was used to upgrade the cenospheres in the low grade fly ash containing 0.33 wt.% cenospheres. Then in the main experiments, a feed containing 0.9 wt.% cenospheres was upgraded in a series of three IRC<sup>TM</sup>s.

### 8.3.1 Upgrading cenospheres from a low-grade fly ash feed

A fly ash feed containing about 0.33 wt.% cenosphere concentration was processed in two stages of laboratory-scale IRC<sup>TM</sup>s. The first stage aimed to recover most of the cenospheres. The product obtained from this stage was then processed in a second stage to be upgraded. Approximately identical operating conditions were used in both stages. The volumetric split ratio was about 40 %, and the feed and fluidization water volumetric fluxes were about 7.3 and 0.87 m<sup>3</sup>/(m<sup>2</sup> h), respectively. Table 8.1 indicates the operating parameters and results obtained from this two-stage IRC<sup>TM</sup> process. As indicated in Table 8.1, the cenospheres were upgraded from 0.33 wt.% to about 3.8 wt.% in Stage 1. The recovery of this stage was around 82.5 wt.%. After processing the product of the first stage in the second stage, a final product grade of 21.3 wt.% and a recovery of 79.3 wt.% were achieved. Lower split ratios could be used in the process for obtaining a higher product grade, however the recovery would be lower in this case. As listed in Table 8.1, the overall product grade and recovery were calculated to be 21.3 wt.% and 65.4 wt.%, respectively. A higher product grade but a lower overall recovery could be achieved using another stage of the IRC<sup>TM</sup>. It was concluded that this two-stage IRC<sup>TM</sup> process was inefficient in separating cenospheres from the low grade fly ash.

It is worth noting that the whole process performance here was determined by combining the steady state results obtained from Stages 1 and 2, meaning that the overall product grade was actually the grade obtained from Stage 2, and the whole recovery was calculated by multiplying the recoveries obtained from Stages 1 and 2. In theory, in a continuous two-stage process, the product of the first stage is continuously fed to the second stage, and hence the feed grade of Stage 2 should be equal to the product grade of Stage 1. Here, however, the process is different, as the product of Stage 1 under both unsteady and steady state conditions (20-30 vol.% of the feed was consumed while reaching the steady state condition) was collected in a mixing tank, and then the mixture was fed to Stage 2. Therefore, the feed grade in Stage 2 was lower than the steady state product grade obtained from Stage 1. However, in a real continuous two-stage process in which the product of Stage 1 will be constantly fed to Stage 2, an even better performance than here will be obtained due to the higher feed cenosphere grade in Stage 2.

Table 8.1: Product grade and cenosphere recovery achieved at different stages of the process.

	Feed volumetric flux (m <sup>3</sup> /(m <sup>2</sup> h))	Split ratio (vol.%)	Feed pulp density (wt.%)	Feed grade (wt.%)	Product grade (wt.%)	Upgrade	Recovery (wt.%)
Run 1 (Stage 1)	7.3	38.0	32.8	0.33	3.8	11.4	82.5
Run 2 (Stage 2)	6.8	40.0	6.1	2.7	21.3	7.8	79.3
Whole process	-	-	-	0.33	21.3	64.6	65.4

### 8.3.2 Upgrading cenospheres from a high-grade fly ash feed

The optimum feed solids concentration for a fly ash with 1 wt.% cenospheres was established in Chapter 6. At the optimum, the pilot-scale IRC™ was used to process approximately 1 tonne of fly ash and generate a large quantity of product to feed to the next stages. Two additional laboratory-scale IRC™s in series were employed to purify the cenosphere product, while aiming for the maximum possible recovery. Error bars are used to show the discrepancy between the experimental data and the mass-balanced data. These error bars show the spread in the three different recovery values that can be calculated from the raw data by using three different routes: 1) the mass of cenospheres in product divided by the combined mass in product and tailings, 2) the mass in product divided by mass in feed, and 3) the mass in feed minus the mass in tailings divided by the mass in the feed. Appendix H presents sample calculations showing these calculations for defining these error bars. The same procedure could be applied for grade values. However, the errors were found to be negligible for the product grades, and hence the error bars are only shown for the recoveries. This error definition was previously discussed in Chapter 5.

In Chapter 6, the optimum feed solids concentration in the cenospheres separation process was found to be around 38 wt.%. At this optimum point, a product grade of 64 wt.% and a recovery of about 90 wt.% were achieved using a one-stage IRC™. Then in Chapter 7, results from a pilot-scale IRC™ were found to be in very close agreement with the laboratory-scale unit. Therefore, the pilot scale IRC™ at the optimum feed solids concentration was used as the first stage of a three-stage IRC™ process in order to obtain a high recovery and a satisfactory grade. All three stages' operating parameters and results are indicated in Table 8.2. Again, the performance of the whole process was assessed by combining the steady state results obtained from Stages 1-3 (Runs 3, 4 and 5). It is noted that Runs 6 and 7 in Table 8.2 were experiments to investigate the effect of changes in the operation of Stage 3 (Run 5) on the overall performance.

Table 8.2: The operating parameters (based on raw data) and the obtained results (based on mass-balanced data) for the three-stage separation in the IRC™.

	Feed volumetric flux (m <sup>3</sup> /(m <sup>2</sup> h))	Split ratio (vol.%)	Feed pulp density (wt.%)	Feed solids content (vol.%)	Feed grade (wt.%)	Product grade (wt.%)	Upgrade	Recovery (wt.%)
Run 3 (Stage 1)	8.3	20.1	39.5	25.8	0.88	16.7	18.9	79.6
Run 4 (Stage 2)	4.0	56.5	10.3	7.5	12.2	77.3	6.4	68.9
Run 5 (Stage 3)	2.1	18.3	1.8	1.7	80.9	96.9	1.2	91.8
Whole process	-	-	-	-	0.88	96.9	110.0	50.3
Run 6*	1.7	48.0	2.0	1.9	81.0	92.5	1.1	95.4
Run 7*	1.7	74.7	1.7	1.6	76.5	88.7	1.2	95.2

\* Two further runs to investigate the performance of Stage 3 at different operating conditions.

### 8.3.2.1 Product grades and cenosphere recovery

Three stages of IRC™ were applied to upgrade the cenospheres in the fly ash. The first stage IRC™, was operated at the optimum feed solids concentration of around 40 wt.% with the primary aim was to process a relatively high feed rate, while ensuring high recovery of the cenospheres. Here an upgrade of about 20 was deemed satisfactory. The focus of the latter stages was on the further upgrading of the cenospheres. Figure 8.4 shows the product grade obtained at different stages of the process.

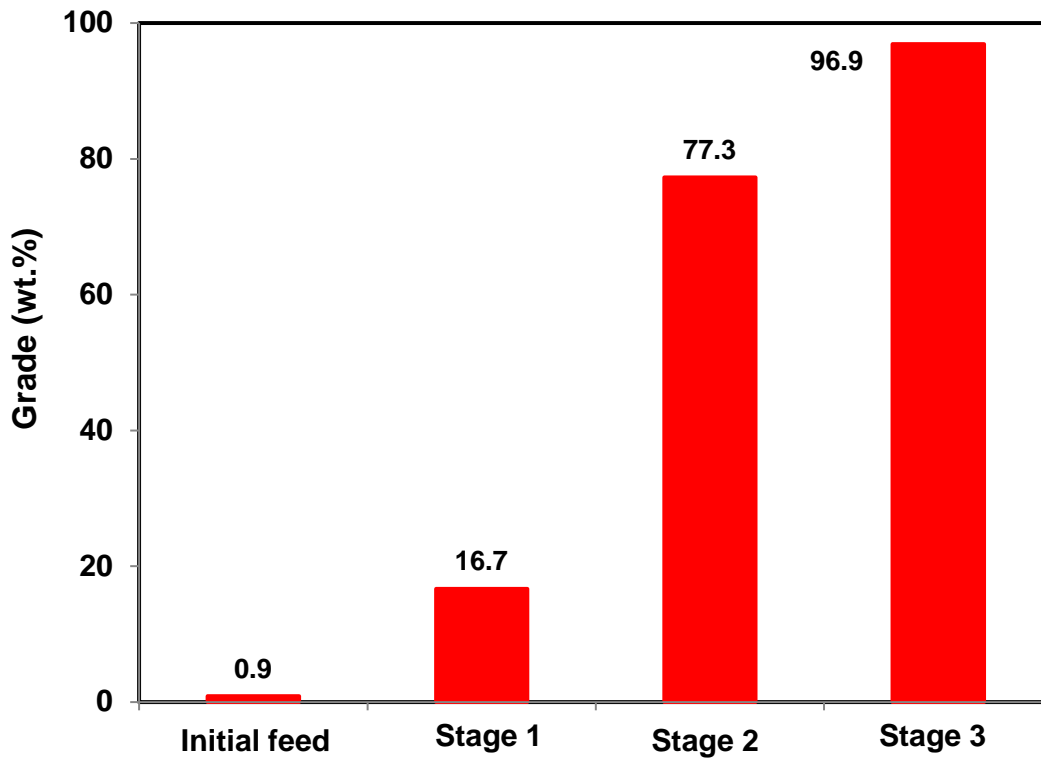


Figure 8.4: Product grade of cenospheres at different stages of the process.

The product grade of the first stage (Run 3) was relatively low at about 17 wt.% but the recovery was significant at about 80 wt.%, as analysed in detail in Chapter 7. This stage of the process was carried out at the optimum feed solids concentration of about 39 wt.% and the solids throughput of about 4.0 t/(m<sup>2</sup> h). The fluidization water was around 0.83 m<sup>3</sup>/(m<sup>2</sup> h), and the product rate was set at about 20 % of the feed volumetric rate (Table 8.2). In the second and third stages (Runs 4 and 5), however, lower feed fluxes and higher split ratios were used. In the second stage (Run 4), the product grade of cenospheres was raised to about 77 wt.%, however the recovery obtained from this stage was only about 69 wt.%. In the third stage (Run 5), the cenospheres grade was increased to about 97 wt.%, with a cenosphere recovery of around 92 wt.%.

The cenosphere recoveries obtained at different stages of the process are shown in Figure 8.5.

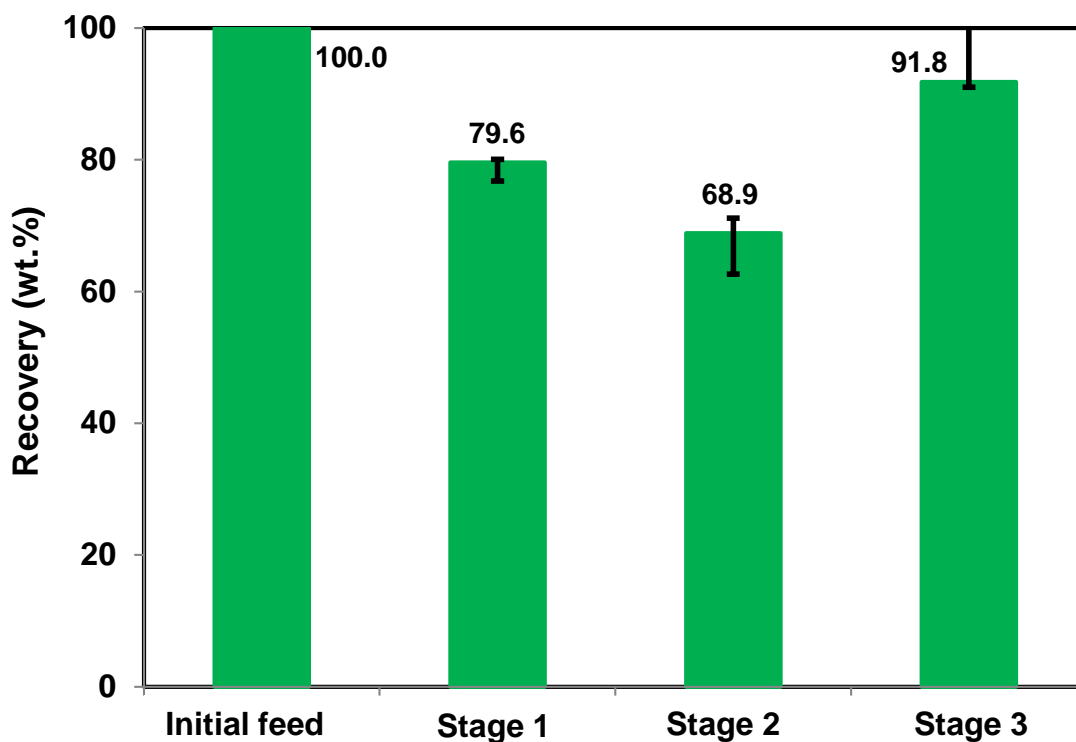


Figure 8.5: Cenospheres incremental recovery obtained at different stages of the process.

Figures 8.6 and 8.7 show the cumulative upgrade and recovery during the multi-stage processing, respectively. The combined upgrade and recovery of the cenospheres in the multi-stage IRC™ were about 110 and 50 wt.%, respectively. In fact, as the second stage of the process was conducted at a relatively low feed rate and a high split ratio (volumetric product to feed ratio), a higher recovery of cenospheres was expected. However the low solids concentration of the feed, about 10.3 wt.%, could be the reason for the relatively low recovery of this stage.

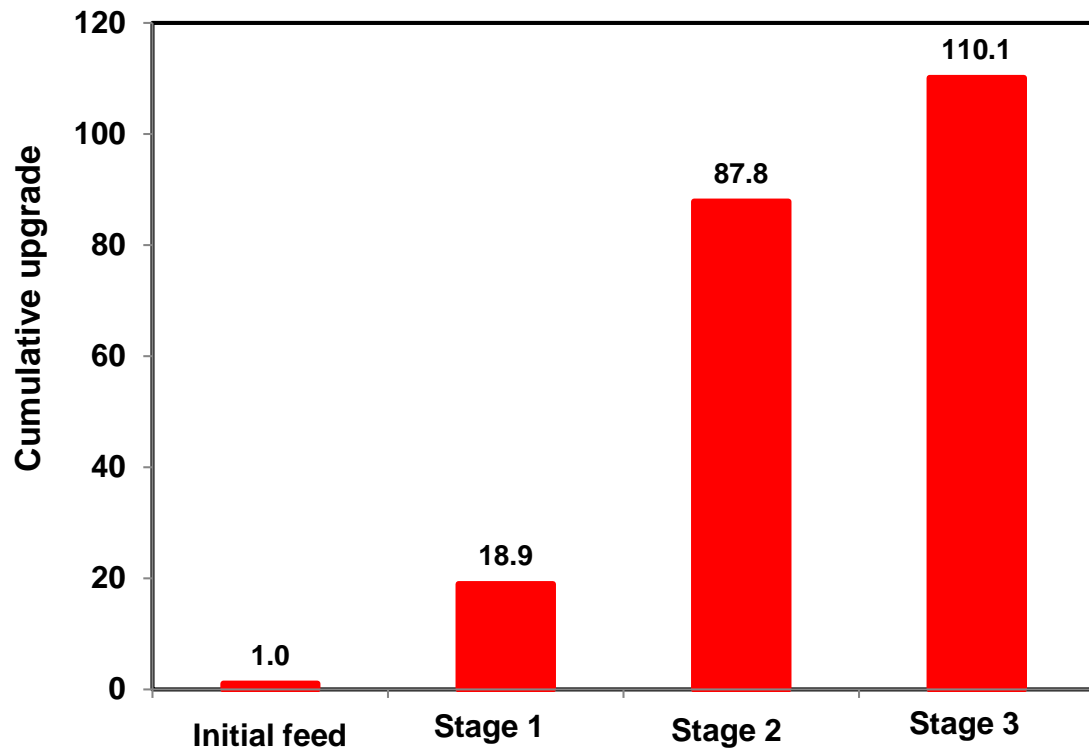


Figure 8.6: Cumulative upgrade after each stage of the process.

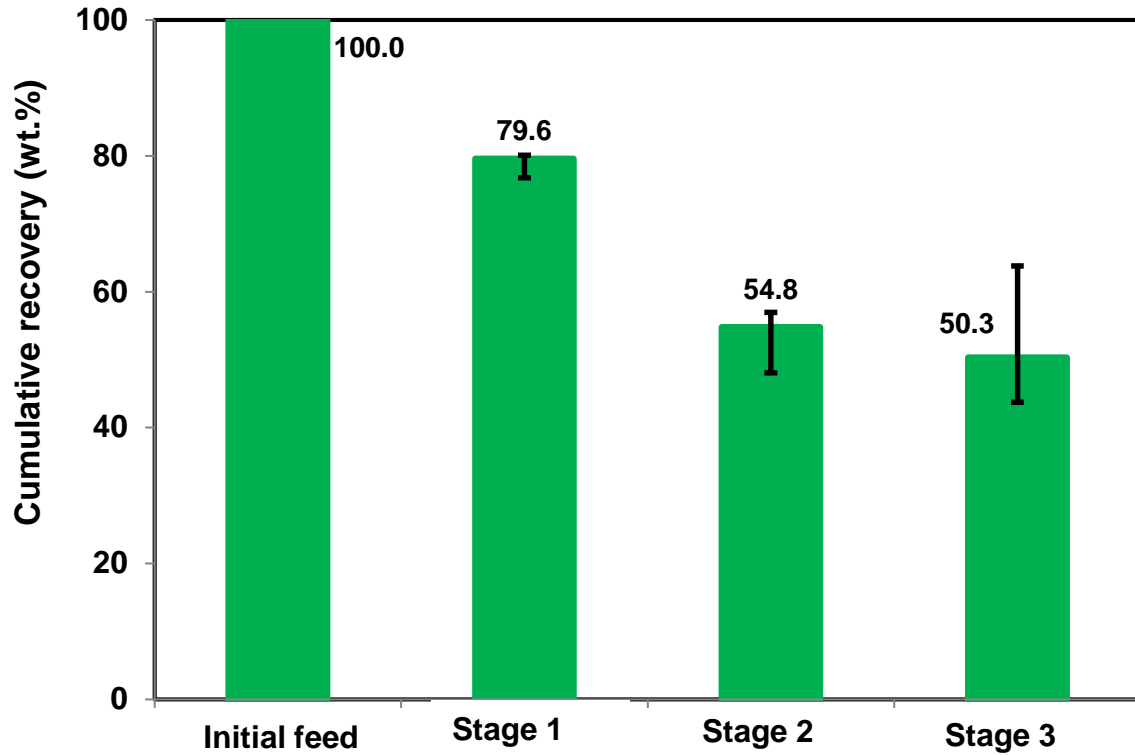


Figure 8.7: Cumulative cenosphere recovery after each stage of the process.

According to the literature (Fessas & Weiland, 1984) and the study in Chapter 6, in a mixture of positively and negatively buoyant particles, the presence of a high concentration of negatively buoyant particles can cause the streaming formation and hence promote the rise velocity of those particles. Based on the regime map proposed by Batchelor and Van Rensburg (1986) and discussed in Chapter 3, the system of positively buoyant cenospheres and negatively buoyant fly ash can be assumed to provide  $\lambda = 1$  and  $\gamma = -1$ . Here the feed cenosphere concentration in Stage 1 is as low as 0.51 vol.% which should be much lower than the critical concentration to develop streams. However the cenospheres segregate toward the downward facing wall of the inclined channels and are refluxed back into the vertical section. Hence their concentration can be significantly higher than their initial concentration in the feed. The other important parameter in the formation of the streams is the total solids concentration in the suspension. Based on the literature presented in Chapter 3, a volumetric solids concentration of at least 20% is required for the formation of streams. In Stage 1, the pulp density of the feed stream is about 25.8 vol.% (39.5 wt.%) which it is speculated was enough to trigger bulk streaming effects. However, in Stages 2 and 3 the feed concentration was much lower at about 7.5 vol.% and 1.7 vol.% respectively. So even with the build up in concentration caused by the reflux of buoyant cenospheres, it is speculated that the solids concentration in the vertical section may not have built up high enough to trigger the streaming effect. Unfortunately no samples were collected from the vertical section so the concentration there cannot be confirmed.

The recovery in Stage 3 was found to be significantly better than Stage 2 (Figure 8.5), even though the feed to Stage 2 was at a higher pulp density. This is consistent with the hypothesis that streaming phenomena did not occur in Stages 2 and 3 and so the higher pulp density was more of a hindrance than a benefit. The better performance of Stage 3 can then be explained by one or more of the following three effects. Firstly the more dilute conditions would have resulted in a lower degree of hindered settling in Stage 3 compared with Stage 2. Secondly, there was a lower feed volumetric flux in Stage 3, giving longer residence times for particles to segregate. Thirdly the majority of the slow rising cenospheres (i.e. fine and high density ones) would already have been removed in Stage 2 and so did not reduce the recovery in Stage 3. The size and density of particles are examined in detail in Section 8.3.3.2, providing more explanation about the performance of different stages.

Figure 8.8 shows the product grade and cenosphere recovery obtained from the third stage of the process at different product fluxes (Runs 5-7) while maintaining constant feed and fluidization water fluxes of about  $1.7 \text{ m}^3/(\text{m}^2 \text{ h})$  and  $0.87 \text{ m}^3/(\text{m}^2 \text{ h})$  respectively. As expected, the product grade decreased and the cenospheres recovery increased as the product flux increased from 0.38 (Run 5) through to  $1.30 \text{ m}^3/(\text{m}^2 \text{ h})$  (Run 7).

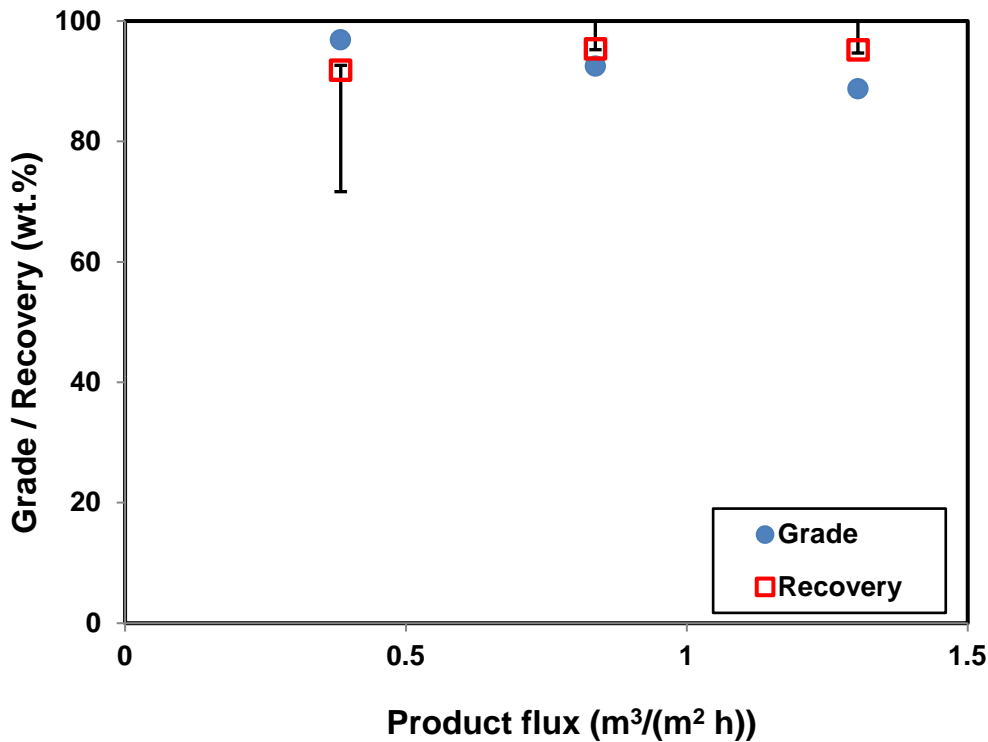


Figure 8.8: Product grade and cenospheres recovery obtained from the third stage of the process at different product fluxes.

Figure 8.9 shows the grade-recovery curves for each stage. It was appropriate to operate Stages 2 and 3 at relatively low feed volumetric fluxes given the significant upgrade following Stage 1. As the feed volumetric fluxes of Stages 2 and 3 were relatively low, their grade-recovery curves were higher than for Stage 1. It is noted here that the grade-recovery curve for Stage 1 was the one obtained for the pilot-scale IRC™ in Chapter 7. The operating point in which the recovery of 79.6 wt.% and grade of 16.7 wt.% were achieved was considered as the first stage of the three-stage separation process in this chapter.

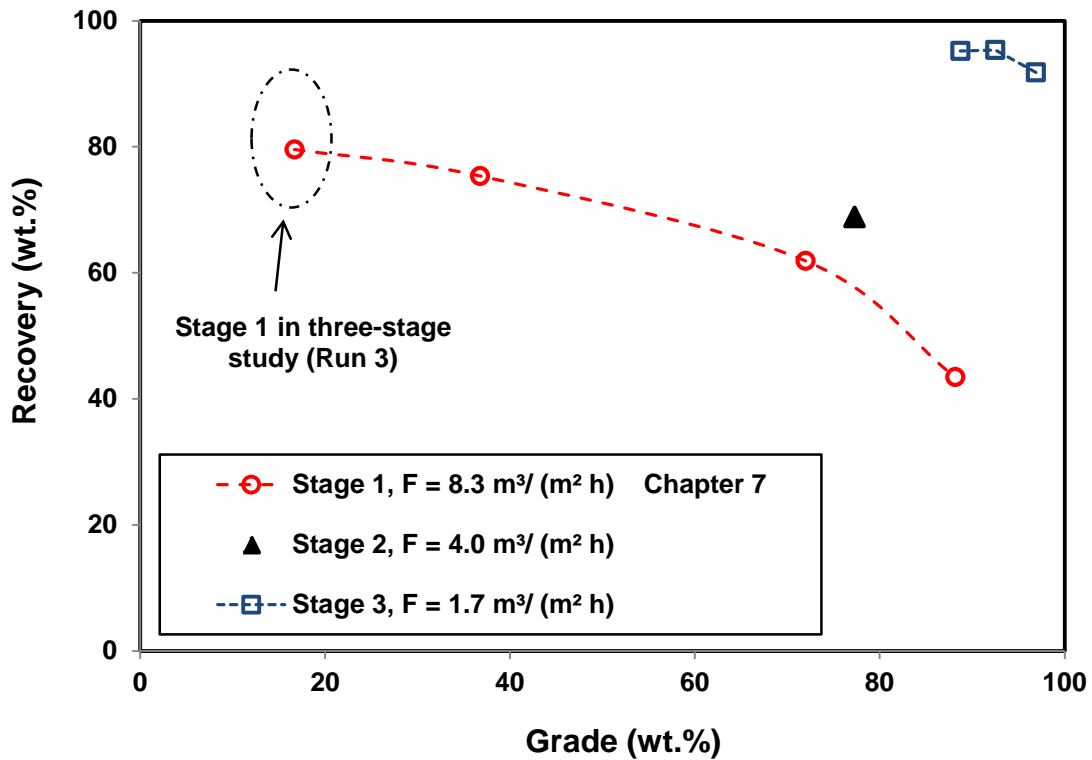


Figure 8.9: Grade-recovery curve for each stage of the process.

### 8.3.2.2 Size and density of cenospheres in the multi-stage IRC™ process

The size and density of the cenospheres in the product of each stage were measured to investigate the performance of the multi-stage IRC™ in more detail. Figure 8.10 presents the size distributions of the cenospheres in the products from all three stages (Run 3-5). The size distribution of the first and second stages had a significant difference, reflecting the loss of considerable proportions of fine cenospheres in Stage 2 (Run 4). However the size distribution of the cenospheres exhibited negligible change from Stage 2 (Run 4) to Stage 3 (Run 5).

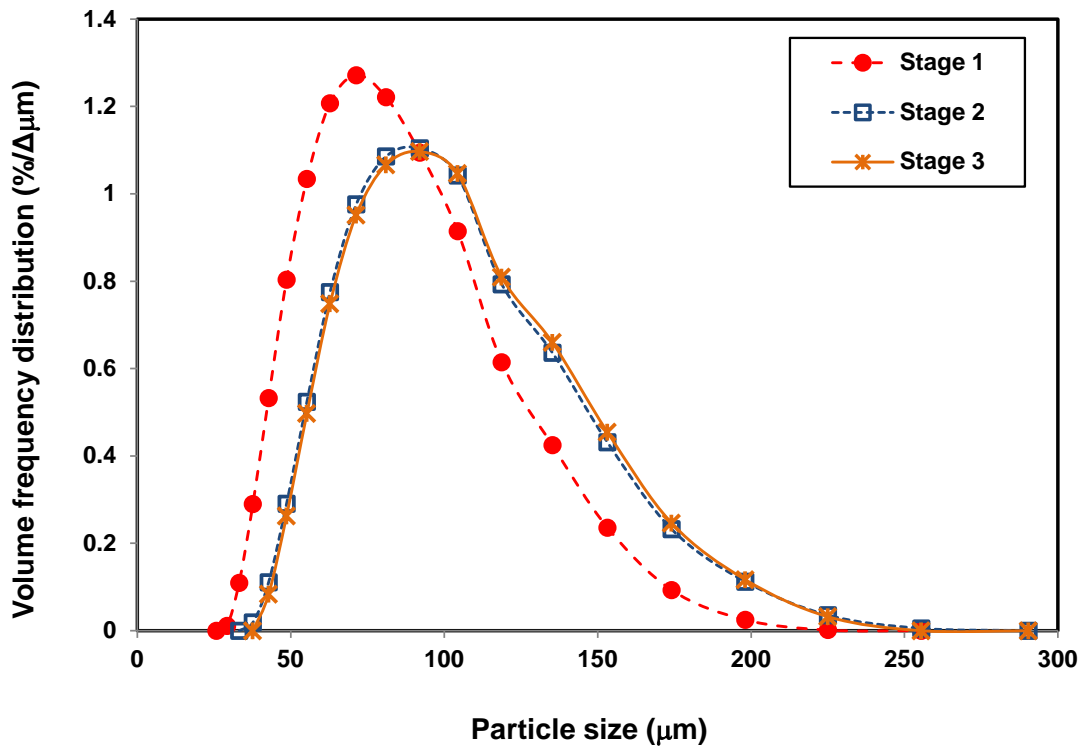


Figure 8.10: Size distributions of cenospheres in the product at different stages of the process.

Using the mass-balance reconciled particle size distributions of the feed, tailings and product, the size partition curves were calculated for each stage of the process. As shown in Figure 8.11, the second stage showed a poorer size separation compared to the first stage, due it is believed to the lack of bulk streaming phenomenon, reflecting the loss of fine and high density cenospheres in this stage. However, the third stage of the process which involved a very dilute feed containing less dense and larger cenospheres than the second stage provided a sharper separation. Table 8.3 presents the imperfection and  $d_{50}$  (Wills, 1996), indicating the efficiency of different stages of the process.

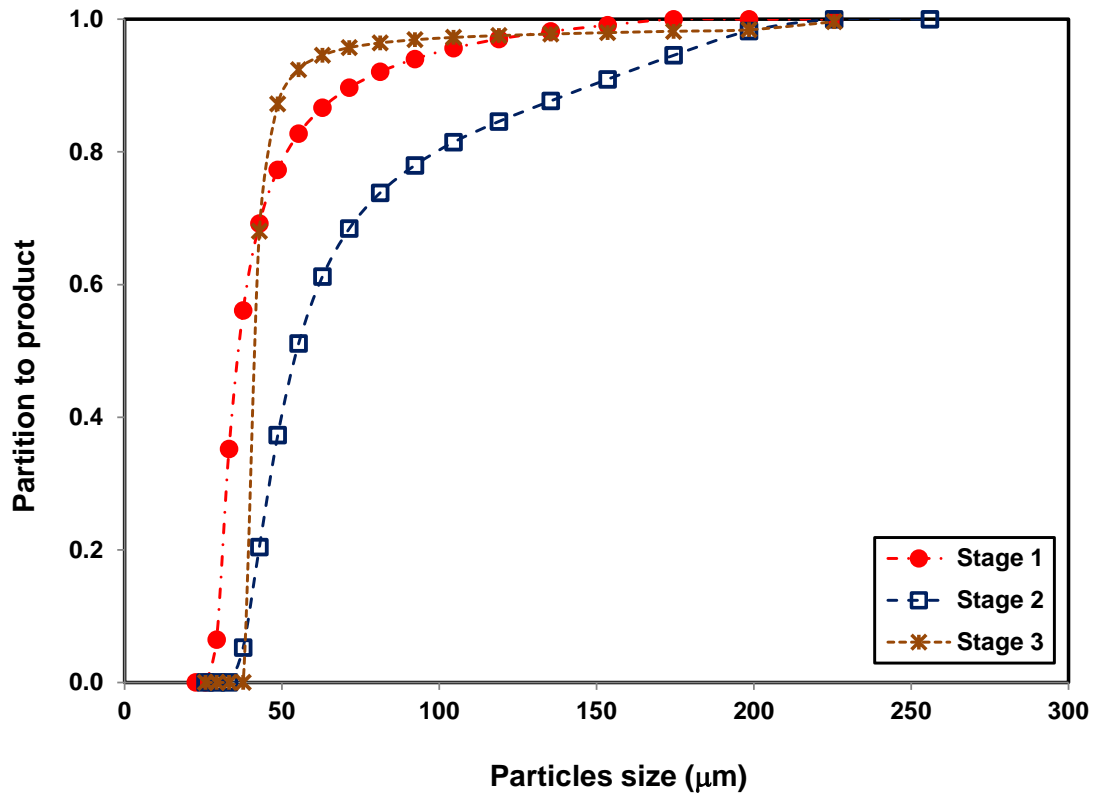


Figure 8.11: Partitioning to product obtained at different stages of the process.

Table 8.3:  $d_{50}$  and imperfection ( $I$ ) (Wills, 1996) showing the quality of separation in each stage.

	$d_{50}$	$I$
Stage 1 (Run 3)	36	0.21
Stage 2 (Run 4)	54	0.35
Stage 3 (Run 5)	40	0.06

Figure 8.12 shows the density of the total product solids and the cenospheres floats fraction in the product obtained from each stage compared to the average density of the cenospheres in the feed. The density of total solids in the product decreased from about 1413 kg/m<sup>3</sup> after Stage 1 down to about 778 kg/m<sup>3</sup> after Stage 3, showing the effective washing of the fine fly ash particles from the cenosphere product. The average density of the cenospheres in the product also slightly decreased from about 839 kg/m<sup>3</sup> after Stage 1 down to about 793 kg/m<sup>3</sup> after Stage 2 and then almost levelled off. These data reflect the already mentioned difficulties in the recovery of high density cenospheres in Stage 2. It is speculated that this difficulty was not apparent in Stage 1 due to the higher suspension density involved being enough to trigger bulk streaming.

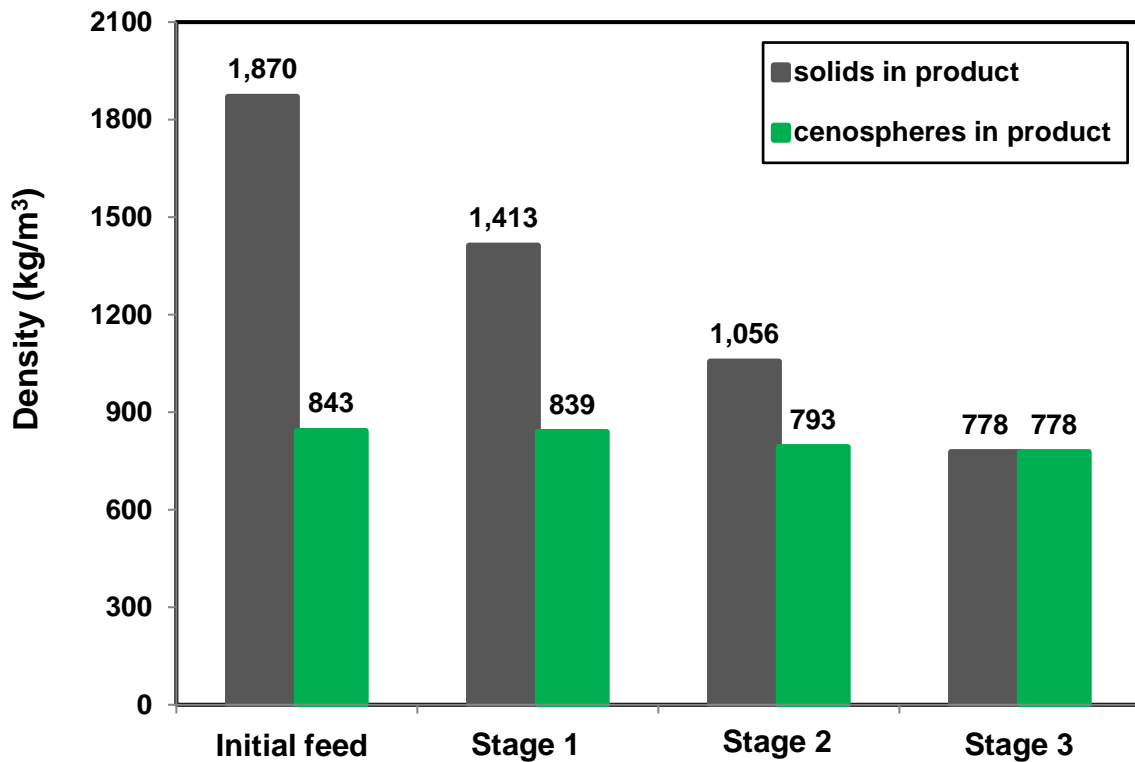


Figure 8.12: Average density of all product solids and only the cenospheres in the product at different stages of the process.

It was previously explained that the occurrence of bulk streaming motion depends on the concentrations of cenospheres and other solids in the suspension. In the second stage of the multi-stage IRC™, the feed total solids concentration was about 10 wt.%, which we speculate was insufficient to trigger streaming. If correct, then it means that in the second and third stages, the separation was only promoted by the Boycott effect while the first stage separation was promoted by both the Boycott and streaming effects. Hence Stage 2 may have suffered the deleterious effects of moderate solids loading, without the benefits of the streaming that occurs at higher solids loading.

Hence it is concluded that the use of a one-stage IRC™ at a lower throughput as shown in Section 6.5.4 may be a more appropriate option for achieving the target grade and recovery. For example, for the same feed, a recovery of about 90 wt.% and a product grade of 64 wt.% (Run 5 Chapter 6) were obtained at a lower solids throughput of about 3.1 t/(m<sup>2</sup> h) in the one-stage IRC™. Even at a higher throughput of about 4.7 t/(m<sup>2</sup> h) (Run 7 Chapter 6), a product grade of about 79 wt.% and a cenospheres recovery of about 64 wt.% were achieved using a

one-stage IRC™. Therefore the use of one-stage or multi-stage IRC™ processes mainly depends on the target product grade, recovery and throughput.

#### **8.4 Conclusions**

In this chapter, the ability of a multi-stage IRC™ process to achieve a high upgrade of the cenospheres was investigated. The results showed that a two-stage IRC™ arrangement was ineffective in processing a low grade fly ash containing only 0.33 wt.% cenospheres. However in the main part of the study involving a fly ash feed with around 0.9 wt.% cenospheres, a product grade of about 97 wt.% was achieved using a three-stage arrangement. However the recovery dropped to about 50 wt.% at the end of the three stages. The size and density analysis suggested that the second stage of the process was less effective in recovering the fine and dense cenospheres. The low total solids concentration of the feed in the latter stages and hence the lack of the bulk streaming effect were speculated to be the likely reason for the lower overall recovery. These results suggest that a one stage process, conducted at a reduced feed rate as shown in Section 6.3.3, may provide the best approach for achieving a high target grade and recovery.

However one-stage separation performance can still vary for different fly ash feeds depending on the cenosphere concentration and size. In the next chapter, the separation of cenospheres from a fly ash feed containing bigger cenospheres at a slightly higher concentration is examined and compared with the single-stage separation performance found in Chapter 5 and 6.

## **Chapter 9**

# **The Performance of the One-stage Inverted REFLUX™ Classifier Process in Separation of Cenospheres from Different Fly Ash Feeds**

### Journal Article(s) Related to the Chapter and Authors' Contribution

**Kiani, A.,** Zhou, J. & Galvin, K.P. (2016). Detailed Characterization and Separation of Fly Ash Fed to the Inverted Reflux Classifier. *Fuel Processing Technology*, DOI: 10.1016/j.fuproc.2016.04.028

Author	Contribution
Ali Kiani	The lead author of the paper, collaborator in experimental design, primary interpretation of results, analysis of data, and experimental operator
James Zhou	Co-supervisor, experimental support
Kevin Galvin	Principal supervisor, collaborator in experimental design and results interpretation, inventor and designer of system

## 9.1 Introduction

This chapter briefly provides a detailed analysis of the separation of valuable cenospheres from different fly ash feeds using the Inverted REFLUX™ Classifier (IRC™). Even though the one-stage IRC™ was found to be effective in recovering cenospheres in Chapters 5-7, the separation performance can vary depending on the cenosphere and fly ash properties. A fly ash containing larger cenospheres with a higher initial concentration of about 1.14 wt.%, simply named as Feed 3, was processed using a one-stage IRC™. The results obtained for this feed relatively late in the study are considered so significant that they should be presented as a separate chapter. Their significance is evident by comparing the results with those obtained in the previous chapters (Chapters 5 and 6). The fly ash feeds in Chapters 5 and 6 (named as Feed 1 and Feed 2) contained significantly less cenospheres, at concentrations of about 0.51 wt.% and 0.85 wt.%, respectively.

## 9.2 Experimental

A schematic representation of the Inverted REFLUX™ Classifier (IRC™) is shown in Figure 5.1. The laboratory-scale IRC™ was used to separate the cenospheres from different fly ash feeds. A detailed description of the IRC™ is given in Chapters 5 and 6.

Fly ash feed samples of different cenosphere concentrations ranging from 0.51 to 1.14 wt. % were sourced from a power station in Australia. The experimental procedure is exactly the same as discussed in Chapters 5 and 6. Standard sink-float funnels of 1 L volume were used in order to determine the grade of cenospheres in each sample and then calculate the cenosphere recovery. This standard test was comprehensively described in Chapters 5, 6 and 7. A subsample from each stream was obtained for measuring the particles size distributions, using Malvern Mastersizers 3000 or 2000. This equipment measures the volume-based size distributions of particles in a wet condition. The density of the particles was also measured using a gas pycnometer. The pycnometer measures the occupied volume of the particles and then calculates the density.

The cenosphere volume-based size distributions were reconciled using the material-balance method proposed by Galvin et al., (1995). The balanced data were then used to calculate the partition of cenospheres to the product stream as a function of size. It is noted again that the

volume-based recovery (partition number) is calculated using the volume-based size distributions, whereas the mass-based recovery (total recovery reported in wt.%) is calculated directly from the sample solids masses (i.e. the ratio of cenosphere mass in the product to that in the feed). The volume-based recovery is theoretically related to the mass-based recovery as  $R_{Vc} = (\rho_{cF}/\rho_{cP})R_{Mc}$  as presented in Equation 5-3.

### 9.3 Results and Discussion

The results achieved using the IRC™ is presented in this section for different feeds. Again, as the errors in product grade data were found to be negligible, the error bars were only reported for the recoveries. These error bars show the difference between the results obtained using the raw experimental data and those obtained using the mass-balanced data, as discussed in Chapter 5.

This section presents laboratory-scale results obtained from the processing of three different fly ash feeds. These are referred to as Feed 1, 2 and 3 and contained cenosphere concentrations of 0.55, 0.85, and 1.14 wt.% respectively, which were all sourced from a power station in Australia under different circumstances. In this chapter, the separation performance of Feed 3 is compared with Feeds 1 and 2 which have already been presented in Chapters 5 and 6 (Run 10 in Chapter 5 which is here referred to as “Run 1” & Run 7 in Chapter 6 which is here referred to as “Run 2”). The average density and size of the cenospheres and fly ash fractions in these three feeds are shown in Table 9.1. The cenosphere average density was roughly the same in all three feeds, whereas the average density of the fly ash in Feed 3 was slightly higher. Also the arithmetic volume average fly ash particle size in all three feeds was approximately the same while the average size of the cenospheres was larger in Feed 3. The size distribution of the cenosphere particles is also shown in Figure 9.1. It is noted that the arithmetic volume average size was calculated as  $\sum d_{arith-i} \times x_{ave-i}$ , where the  $d_{arith-i}$  is the arithmetic average size defined in Chapter 2 and  $x_{ave-i}$  is the volume fraction of particles, both for the interval  $i$ .

Table 9.1: Average size and density of the fly ash and the cenospheres at different feeds.

	Feed 1		Feed 2		Feed 3	
	Fly ash	Cenosphere	Fly ash	Cenosphere	Fly ash	Cenosphere
Average Size (µm)	59.5	73.4	63.1	75.3	56.9	131.9
Average Density (kg/m <sup>3</sup> )	1850	807	1876	802	2030	811

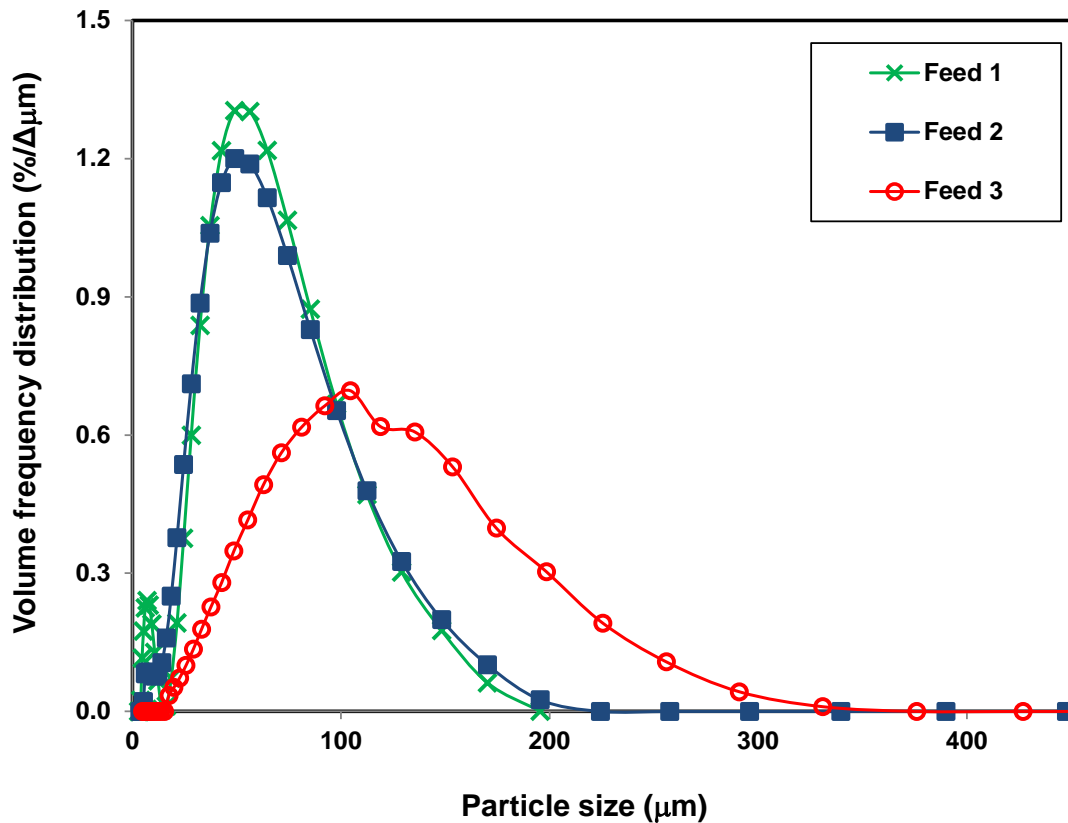


Figure 9.1: Volume size distributions of cenospheres in the different fly ash feeds.

For Feeds 2 and 3 (Runs 2 and 3), the laboratory-scale IRC™ was operated at almost identical operating conditions, while the feed volumetric flux for Feed 1 (Run 1) was lower. Stream samples were collected and analysed to measure cenosphere grade and size distributions. Recovery was calculated from the mass-balance reconciled data. Table 9.2 shows the experimental parameters and the results obtained from different runs, and also indicates the inconsistency in the raw experimental data reported as the ratio of inlet flows to outlet flows for the cenospheres, fly ash and total solids. Again, the error bars were only significant for the recoveries. The size partition curves defining the cenosphere separations in the IRC™ were also determined.

Table 9.2: The experimental parameters and the results obtained from the separation of cenospheres from different fly ash feeds in the IRC™.

	Run 1	Run 2	Run 3
Feed flux (m <sup>3</sup> /(m <sup>2</sup> h))	7.0	11.2	10.5
Feed solid concentration (wt.%)	31.3	40.0	38.9
Feed cenospheres concentration (wt.%)	0.55	0.85	1.14
Fluidization water Flux (m <sup>3</sup> /(m <sup>2</sup> h))	0.87	1.05	1.05
Split ratio (vol.%)	20.0	13.4	14.0
<i>P – W</i>	0.53	0.45	0.42
Product grade (wt.%)	69.4	78.9	79.7
Recovery (wt.%)	48.5	64.4	92.6
In/out (solids)	1.01	1.02	1.02
In/out (Fly ash)	1.01	1.02	1.02
In/out (Cenospheres)	1.13	0.97	1.08

For Feeds 2 and 3, the operating conditions were almost identical. The feed solids concentration was approximately 40 wt.%, and the feed and fluidization water fluxes were about  $10.8 \pm 0.3$  and  $1.0 \text{ m}^3/(\text{m}^2 \text{ h})$ , respectively. The split ratio defined as the ratio of the product volumetric flux to the feed volumetric flux was about 14 %. However for Feed 1, the feed and fluidization water volumetric fluxes were lower at  $7 \text{ m}^3/(\text{m}^2 \text{ h})$  and  $0.9 \text{ m}^3/(\text{m}^2 \text{ h})$ , respectively, and the volumetric split ratio was higher at 20 %.

As shown in Chapters 5, 6 and 7, the difference between the product and fluidization water fluxes (*P – W*) is an important factor in controlling the product grade. In this set of experiments, this factor was approximately the same in the runs conducted on Feed 2 and 3 (Runs 2 and 3), and slightly more for Feed 1 (Run 1). As a result, the product grades obtained for Feed 2 and 3 were almost the same at about 79 wt.% while it was lower at about 69 wt.% for Feed 1. Figure 9.2 presents the product grades obtained for the three fly ash feeds.

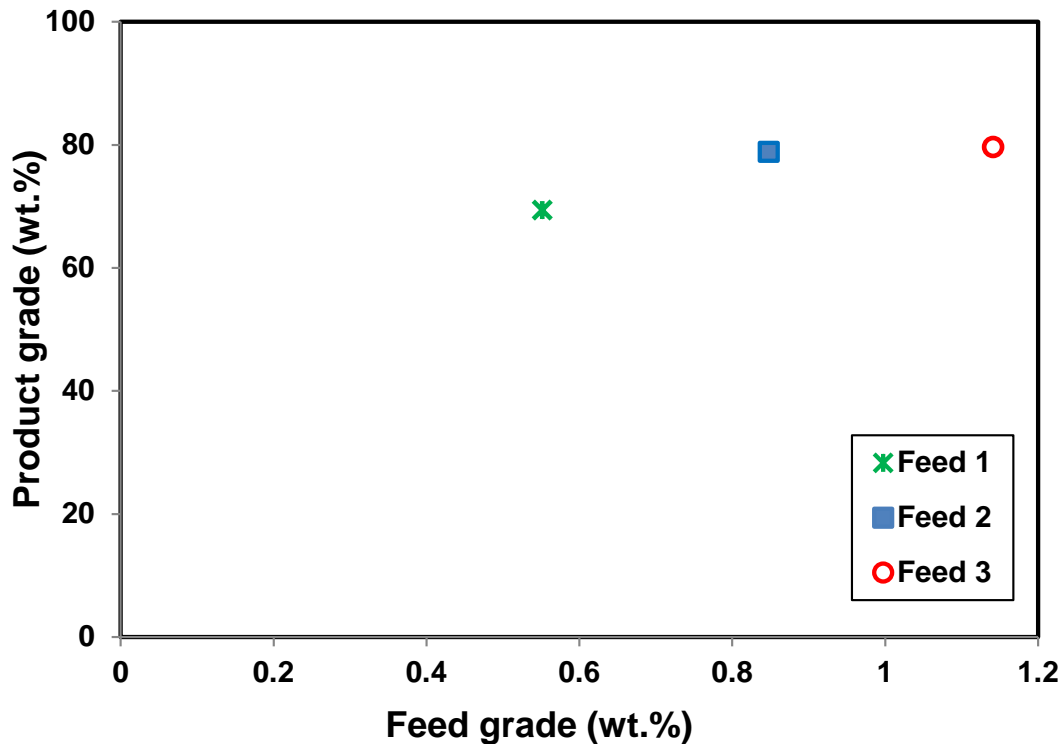


Figure 9.2: Product grades obtained from IRC™ in separating cenospheres from different fly ash feeds (Runs 1, 2 and 3).

Figure 9.3 shows the cenosphere recovery obtained for the three different fly ash feeds. For Feed 1, although the lower feed flux and a higher split ratio were more favourable for obtaining a higher recovery, the cenosphere grade and the solids concentration in the feed were very low at about 0.51 wt.% and 31 wt.%, respectively. It is suspected, therefore, that there was less bulk streaming motion in this case. This was comprehensively investigated and analysed in Chapter 6. As shown in Figure 9.3, the recoveries of cenospheres obtained for Feeds 2 and 3 were about 64 wt.% and 93 wt.%, respectively. This recovery for Feed 3 is remarkable, which suggests that the elevated cenosphere concentration of 1.14 wt.% led to enhanced bulk streaming, well beyond that observed for the other two runs. The result also suggests that a single-stage IRC™ can be utilized to recover cenospheres from fly ash, achieving high product grades and recoveries, at significant solids throughputs. As previously discussed in Chapter 6, according to Batchelor’s case study (Figure 3.6 in Chapter 3), bulk streaming is more likely to develop at higher species concentrations in a mixture of positively and negatively buoyant particles. The size of the cenospheres in Feed 3 was also larger, inducing a greater convective driving force and hence a larger cenosphere recovery.

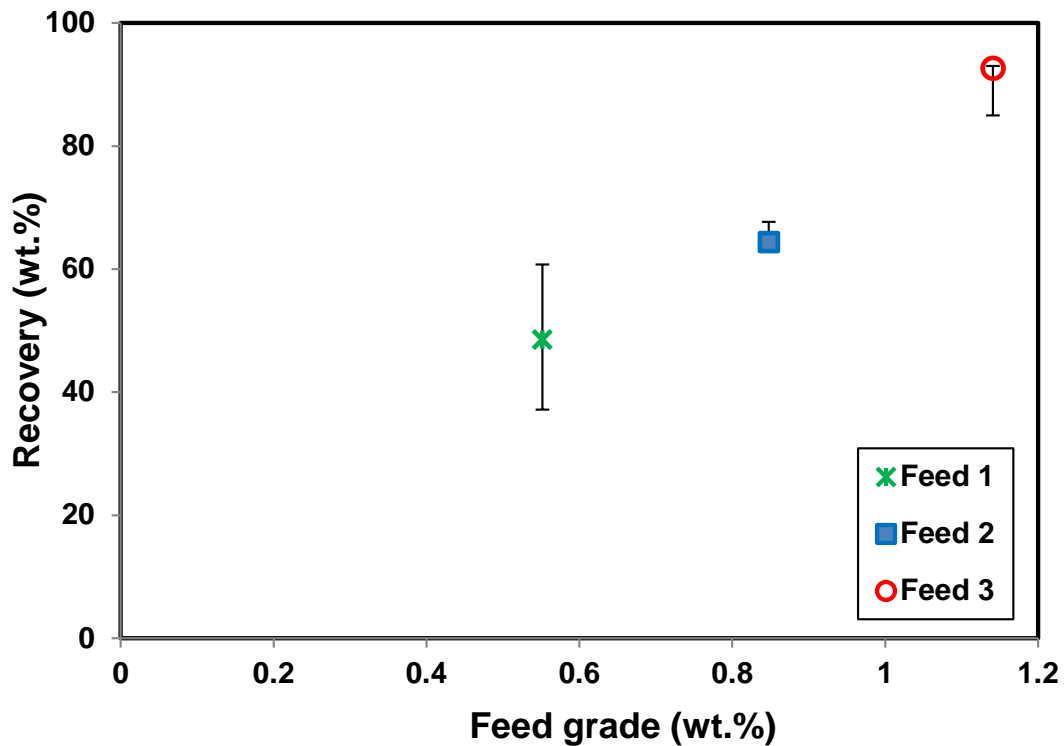


Figure 9.3: Cenosphere recovery obtained for different fly ash feeds processed in the IRC™.

In order to explore further the effects of these two factors (i.e. cenospheres concentration and cenospheres size) on the recovery of cenospheres from Feeds 2 and 3 (Runs 2 and 3), the partition curves between Runs 2 and 3 were compared. Figure 9.4 shows the size distribution of the cenospheres in the product, tailings and feed for Run 3. The size partition curves for Feed 2 and 3 (Runs 2 and 3) were determined from the reconciled volume particle size distributions and are plotted in Figure 9.5. The operating conditions used in the IRC™ for both Feeds 2 and 3 were the same and so, unsurprisingly the partition curves are similar. Therefore the higher recovery obtained for Feed 3 mostly reflects the fact that it contained a higher proportion of coarser cenospheres which were more easily recovered.

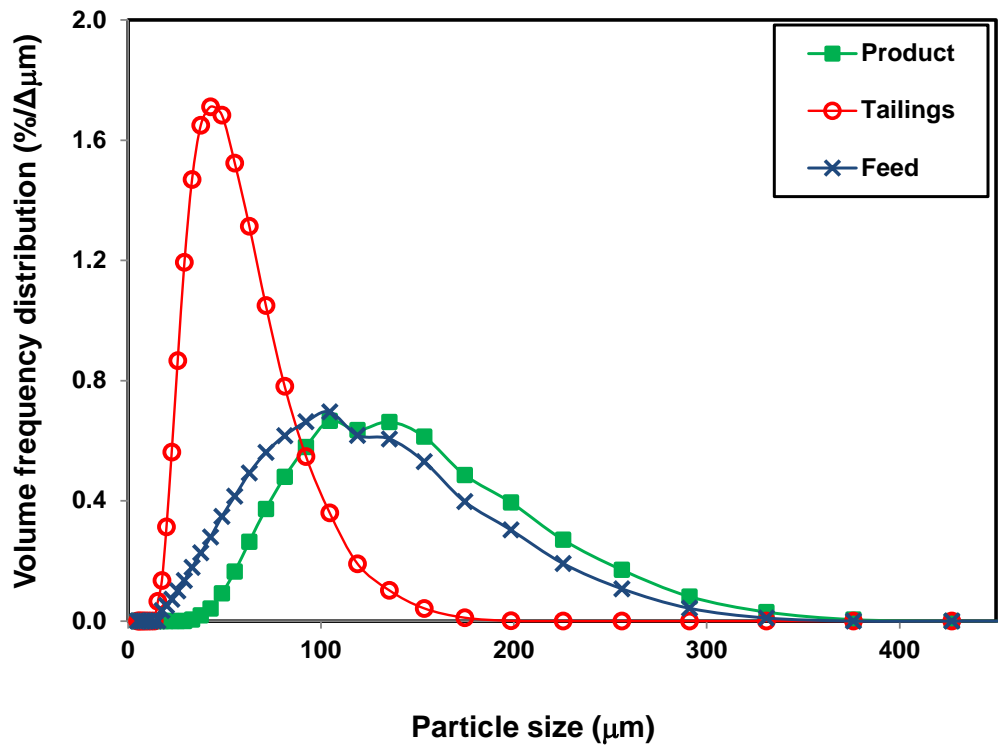


Figure 9.4: Volume-based frequency size distribution of cenospheres in product, tailings and feed for Run 3.

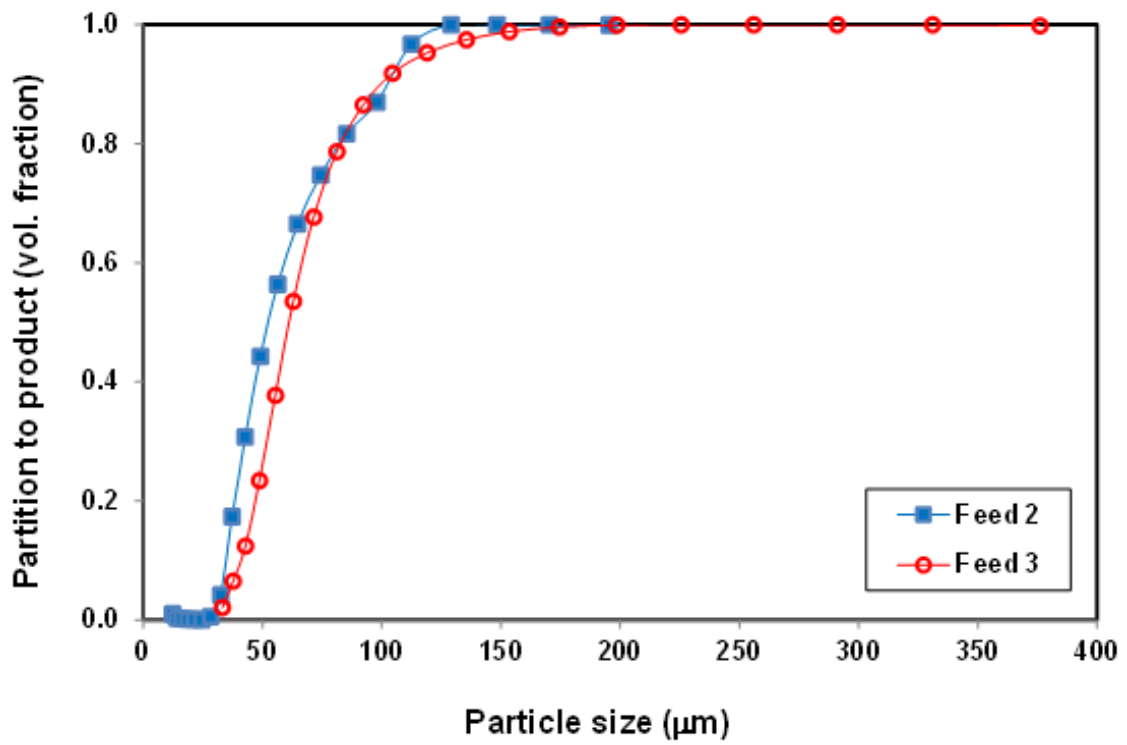


Figure 9.5: The size partition curves obtained for Feeds 2 and 3 (Runs 2 and 3).

## **9.4 Conclusions**

For the feed with 1.14 wt.% cenospheres, involving larger cenospheres, a remarkable recovery of about 92.6 wt.% was achieved at a grade of 79 wt %, with the solids throughput about 4.9 t/(m<sup>2</sup> h). The significance of this separation was established by comparing the findings with those from the feeds containing lower cenosphere grades. The size partition curve indicated that the higher recovery obtained for Feed 3 was associated with the presence of larger cenospheres. It is also suspected that much stronger bulk streaming was produced within the inclined channels as a result of these larger and more concentrated cenospheres.

# **Chapter 10**

## **Conclusions and Recommendations**

## 10.1 Conclusions

This study was concerned with investigating the separation performance of an Inverted REFLUX™ Classifier (IRC™) to recover and concentrate valuable, positively buoyant, cenospheres from negatively buoyant fly ash. This innovative system consisted of a set of parallel inclined channels located below a vertical liquid fluidized bed. The purpose of the inclined channels was to enhance the particles segregation rate, leading to a throughput advantage over a conventional fluidized bed (Laskovski et al., 2006). In other words, the inclined channels reduce the loss of cenospheres to the tailings, thus increasing their recovery at a given feed rate. A fluidization chamber was also installed above the IRC™, distributing water to wash the entrained high density ultrafine particles from the product, and therefore increase the product grade.

A typical fly ash feed was characterized in terms of surface structure, elemental composition, and size and density distribution. Using Scanning Electron Microscopy (SEM) and Energy Dispersive Spectroscopy (EDS) methods, the fly ash was found to mainly contain cenospheres, unburnt carbon, and dense particles (mainly aluminium oxide and silicon dioxide). The SEM images showed that some cenospheres were naturally broken and therefore denser than water. Some hollow spherical cenospheres can also be negatively buoyant if their shell thickness is sufficiently large. Thus, the term cenospheres was reserved in this study to particles of density lower than that of water. The EDS analysis showed that the surface property of the cenospheres and dense particles were almost the same confirming the need to focus on gravity separation rather than flotation.

The REFLUX™ Classifier (RC™) was also used to fractionate the fly ash feed into several flow fractions, providing a better understanding of the particles size and density distribution. This form of analysis has not been applied to fly ash previously. The fractionation data showed that 60 wt.% of particles had a density of more than 2000 kg/m<sup>3</sup>. However, the portion below a density of 1000 kg/m<sup>3</sup> was only about 1.4 wt.%, corresponding to the feed cenospheres concentration measured separately using the sink-float method. In some cases water may fail to penetrate immediately into partially broken cenospheres, hence the cenospheres concentration may vary with time. Ideally, in order to measure the true grade of cenospheres in the fly ash, the fly ash and water should be kept mixed for several hours.

The potential of the innovative approach, the Inverted REFLUX™ Classifier (IRC™), for separating positively buoyant particles was investigated initially via a series of so-called preliminary experiments. Here, the separation of commercial cenospheres from dense silica flour was examined in a laboratory-scale IRC™. The results obtained from the IRC™ were promising, showing a high product grade of about 85 wt.% under some operating conditions. Here the upgrade was about 148, reflecting the strong potential of the IRC™ for upgrading positively buoyant cenospheres.

The recovery and concentration of cenospheres in a low-grade fly ash feed were then examined in the IRC™ under different operating conditions. The cenospheres concentration of the first feed was about 0.51 wt.%. By increasing the fluidization water flux, more of the fine high-density fly ash was washed away from the cenosphere product leading to an increase in the product grade. Meanwhile, higher proportions of heavy cenospheres were also lost and hence the recovery decreased. By increasing the feed flux and hence the product flux, the entrainment of fine fly ash particles in the product increased and hence the grade decreased. The cenospheres recovery increased up to an optimum point and then decreased. At high feed fluxes and hence high product fluxes, the ratio of the product flux to the fluidization water flux became large resulting in a higher cenospheres recovery. However by further increasing the feed flux, the high velocity of the feed through the inclined channels led more entrainment of the fine cenospheres to the tailings and therefore a lower recovery. It was also found that the difference between the product and fluidization water fluxes ( $P - W$ ) is a critical factor in controlling the product grade in the IRC™. By increasing the feed split ratio and hence ( $P - W$ ), the product grade decreased and the cenospheres recovery increased.

The enhanced separation of cenospheres from fly ash in the IRC™ was investigated using different feed solids concentrations of about 10.1 wt.% up to 46.1 wt.%. The fly ash feed contained around 1.0 wt.% cenospheres. The operating conditions were similar in all experiments, and therefore, the critical factor ( $P - W$ ) was almost the same. As a result, similar product grades of about 70 wt.% were obtained in different runs. By increasing the feed solids concentration up to an optimum concentration, the cenospheres recovery increased significantly. This result was contrary to expectation given that performance would normally decline as the solids rate increased. The optimum feed solids concentration was found to be about 38.1 wt.%. By further increasing the feed solids concentration to 46.1 wt.%, the cenospheres recovery decreased, probably due to the high feed viscosity and its

hindrance effects. Using the partition curves obtained for different experiments, the sharpest separation was evident at the optimum feed solids concentration. At this optimum, a recovery of 90 wt.% and grade of 64 wt.% were achieved at a solids throughput of about 3.1 t/(m<sup>2</sup> h). Here, the actual and theoretical throughput advantage were calculated to be 54 and 18. An enhancement factor of  $54/18 = 3$  was attributed to the feed solids concentration. This is consistent with the literature (Batchelor and van Rensburg, 1986), stating that the velocity of positively buoyant particles can be induced in the presence of a specific concentration of negatively buoyant particles, referred to as bulk streaming. It was therefore concluded the separation of cenospheres in the IRC<sup>TM</sup> was enhanced at higher feed solids concentrations due to the development of bulk streaming. The separation performance at the optimum feed solids concentration was further studied in order to establish the best operating conditions for the pilot-scale experiments. In general, increasing the feed flux led to an increase in the recovery and a decrease in the product grade.

The separation of cenospheres from fly ash was then examined using a pilot scale IRC<sup>TM</sup>. Here the separation process was scaled up by a 10 fold factor to a pilot-scale IRC<sup>TM</sup> (cross sectional area: 300 mm × 300 mm). Around 1 tonne of fly ash was used to provide enough feed for the steady state runs in the pilot-scale IRC<sup>TM</sup>. The separation performance in the pilot scale IRC<sup>TM</sup> was examined at different feed split ratios and feed fluxes. Two parameters,  $I$  and  $d_{50}$ , were used to indicate the size separation performance in the pilot-scale runs at different feed split ratios. Since the feed conditions were the same in all runs, the sharpness of separation ( $I$ ) was similar. On the other hand, by increasing the feed split ratio, finer cenospheres were recovered and hence the  $d_{50}$  decreased. The results obtained from the pilot-scale runs were compared with those obtained from the laboratory-scale runs. The performance was found to be similar. Grade-recovery curves for both scales were also plotted, compared and found to be consistent. The size and density of the fly ash solids and cenospheres in the product, tailings and feed were also measured showing that the loss of fine and dense cenospheres was the main reason for the lower recovery in the pilot-scale IRC<sup>TM</sup>.

A multi-stage arrangement was also considered in order to optimise the separation of the cenospheres from fly ash in respect to solids throughput, product grade and recovery. The separation of cenospheres from low grade and high grade fly ash feeds was examined using two-stage and three-stage IRC<sup>TM</sup> processes, respectively. For the fly ash feed with only 0.33 wt.% cenospheres, the two-stage process was found to be inefficient. A three-stage IRC<sup>TM</sup>

process was applied to process a fly ash feed with about 0.9 wt.% cenospheres. After the third stage, a product grade of 97 wt.% (almost pure on a volume basis) was achieved, however the recovery was relatively low at about 50 wt.%. At Stage 2 of the process, a recovery of only about 69 wt.% was obtained. The reason for the low recovery of this stage was found to be the low feed solids concentration (about 10 wt.%) which based on the literature (Batchelor and van Rensburg, 1986) was much lower than the required threshold value for the bulk streaming to form. Having looked at Stage 2 more carefully, significant proportions of fine and dense cenospheres were lost in this stage. It is noted that Stage 3 was found to be very efficient due to the lower feed flux and solids concentration, and the absence of the fine and dense cenospheres remaining in this stage. Therefore, it was concluded that the one-stage process at a lower feed solids throughput is the preferred option for obtaining the required product grades and recovery.

Subsequent experiments demonstrated that the separation performance varied when different fly ash feeds were used. A fly ash feed containing larger cenospheres at a slightly higher concentration was therefore examined in the one-stage IRC<sup>TM</sup>, and the results were compared with those obtained from the previous two fly ash feeds (Chapters 5 & 6). The concentration of cenospheres in the fly ash feeds 1, 2 and 3 (new one) was about 0.51 wt.%, 0.85 wt.% and 1.1 wt.%, respectively. The arithmetic average size of the cenospheres in the new feed was 132  $\mu\text{m}$ , which was significantly larger than for the other two (73  $\mu\text{m}$ , 75  $\mu\text{m}$  for Feed 1 and 2, respectively). Again, the most important factor controlling the product grade was the difference between the product and fluidization fluxes ( $P - W$ ). The cenospheres recovery obtained for Feed 2 was higher than that for Feed 1 due to the further development of the bulk streaming at the elevated cenospheres concentration. However, a recovery of about 93 wt.% was achieved for Feed 3, reflecting the effects of the streaming phenomenon and the presence of the larger cenospheres. Here the product grade was about 80 wt.% at a throughput of about 4.9 t/(m<sup>2</sup> h). The partition curves plotted for Feed 2 and 3 indicated that the high recovery obtained for Feed 3 was mainly due to the presence of larger cenospheres.

## 10.2 Recommendations

The results of this study show a strong potential of the IRC™ in separating valuable cenospheres from fly ash waste. Based on these findings it is recommended:

1. The bulk streaming effect may further develop at higher feed cenosphere concentrations, and lead to an even more efficient separation process.
2. During the separation process in the IRC™, samples from the inclined channels and the fluidized bed section could be taken to reveal the local cenosphere concentration. These local concentrations could be compared with the required critical concentrations for the formation of bulk streaming reported in the literature.
3. The partitioning between the product and tailings is based on the particle size and density. Therefore in addition to the size partitioning studied in this thesis, the partitioning behaviour based on the particle density could be investigated to provide more detail about the separation process. This could be conducted through the sink-float test using liquids of different density or via an extension of the fractionation method used in this study.
4. The analysis used in this study to quantify the separation performance via the inclined channels could be extended to produce a two-component model of the IRC™. This model needs to effectively demonstrate the classification based on the size and density, and ideally consider the effect of the bulk streaming motion.
5. The final product from the IRC™ is generally very dilute, and hence the water needs to be removed in order to make the separation process more applicable and economical. An efficient method needs to be introduced for the filtration of positively buoyant cenospheres in the product. Some preliminary experiments using a pressurized filtration method provided promising results, showing a decrease in the product water content by around 70 wt.%.
6. The separation of other valuable components like unburnt carbon, magnetic particles, metals and scarce elements should be investigated.

7. Cenosphere is considered a valuable material due to its superior properties. A comprehensive study on economic aspects of the separation process in the IRC™ could be undertaken. If the process is found to be economical, the system could be studied at full scale.

8. The findings of this study including the determined optimum conditions, scaling up and the development of bulk streaming can be applied to any other separation processes involving a buoyant phase.

## Reference

- Acrivos, A. & Herbolzheimer, E. (1979). Enhanced Sedimentation in Settling Tanks with Inclined Walls, *Journal of Fluid Mechanics*, 92, 435.
- ADAA 2005, 'Total Ash Production and Beneficial Uses', <http://www.adaa.asn.au/statistics.htm>, last accessed, December 2005.
- Ahmaruzzaman, M. (2010). A review on the utilization of fly ash, *Progress in Energy and Combustion Science*, 36, 327–363.
- Arnold, H. D. (1911). Limitations imposed by slip and inertia terms upon Stokes's law for the motion of spheres through liquids, *Philosophical Magazine*, 22, 755–775.
- Asif, M. (1998). Segregation velocity model for fluidized suspension of binary mixture of particles, *Chemical Engineering and Processing*, 37, 279-286.
- Asif, M. (1997). Modeling of Multi-Solid Liquid Fluidized Bed, *Chemical Engineering & Technology*, 20, 485-490.
- Asif, M. & Petersen, J.N. (1993). Particle dispersion in a binary solid-liquid fluidized bed, *AIChE Journal*, 39, 9.
- Aziz, S., Soomro<sup>1</sup>, S. A., Tunio, A. H. & Nazir, I. (2010). Environmental & Health Hazards of Fly Ash & SO<sub>x</sub> from FBC Power Plant at Khanote, *Pakistan Journal of Analytical and Environmental Chemistry*, Vol. 11, No. 2, 56-62.
- Baeyens, J. & Geldart, D. (1974). An investigation into slugging fluidized beds, *Chemical Engineering Science*, 29, 255.
- Batchelor, G.K. (1988). A new theory of the stability of a uniform fluidized bed, *Journal of Fluid Mechanics*, 193, 75-110.

- Batchelor, G.K. & Van Rensburg, R.W. (1986). Structure formation in bidisperse sedimentation, *Journal of Fluid Mechanics*, 166, 379-407.
- Bird, R.B., Stewart, W.E. & Lightfoot, E.N. (1976). *Transport Phenomena*, John Wiley and Sons, 62.
- Blanco, F., Garcia, P. Mateos, P. & Ayala, J. (2000). Characteristic and properties of lightweight concrete manufactured with cenospheres, *Cement and Concrete Research*, 30 (11), 1715–1722.
- Boycott, A.E. (1920). Sedimentation of blood corpuscles, *Nature*, 104, 532.
- Burt, R.O. (1985). *Gravity Concentration Technology*, Amsterdam: Elsevier.
- Callen, A., Moghtaderi, B. & Galvin, K.P. (2007). Use of parallel inclined plates to control elutriation from a gas fluidized bed, *Chemical Engineering Science*, 62, 356 – 370.
- Carman, P.C. (1937). Fluid flow through granular beds, *Transactions, Institution of Chemical Engineers, London*, 15, 150-166.
- Chalivendra, V.B., Shukla, A., Bose, A. & Paramewaran, V. (2003). Processing and mechanical characterization of lightweight polyurethane composites, *Journal of Materials Science*, 38, 1631–1643.
- Clift, R., Seville, J.P.K., Moore, S.C. & Chavarie, C. (1987). Comments on buoyancy in fluidized beds, *Chemical Engineering Science*, 42(1), 191-194.
- Clift, R., Grace, J.R. & Weber, M.E. (1978). *Bubbles, Drops and Particles*, New York: Academic Press.
- Clift, R., & Gauvin, W.H. (1970). The motion of particles in turbulent gas streams, *Chemeca*, Butterworths, Australia, 1, 14-24.

- Cocco, R., Shaffer, F., Reddy Karry, S.B., Hays, R. & Knowlton, T. (2010). Particle clusters in fluidized beds, *The 13<sup>th</sup> international conference on fluidization-New paradigm in fluidization engineering, Art, 11*.
- Cole, J., Dunne, R. & Giblett, A. (2012). *Review of current enhanced gravity separation technologies and applications. In "Separation Technology for Minerals, coal and Earth Resources"*, Colorado: Englewood.
- Dallavalle, J. M. (1948). *Micromeritics: the Technology of Fine Particles*, 2nd Edition, Pitman Publishing Corp., New York.
- Darcy, H. (1856). *Les Fontaines Publiques de la ville de Dijon*, Dalmont, Paris.
- Davis, R.H. (1996). Hydrodynamic diffusion of suspended particles: a symposium, *Journal of Fluid Mechanics*, 310, 325-335.
- Davis, R.H. & Gecol, H. (1996). Classification of concentrated suspensions using inclined settlers, *International Journal of Multiphase Flow*, 22(3), 563-574.
- Davis, R.H. & Hassen, M.A. (1988). Spreading of the interface at the top of a slightly polydisperse sedimenting suspension, *Journal of Fluid Mechanics*, 196, 107-134.
- Davis, R.H., Herbolzhiemer, E. & Acrivos, A. (1982). The Sedimentation of Polydisperse Suspensions in Vessels Having Inclined Walls, *International Journal of Multiphase Flow*, 8(6), 571.
- Di Felice, R. (1995). Hydrodynamics of liquid fluidization, *Chemical Engineering Science*, 50, 1213-1245.
- Di Felice, R. & Gibilaro, L.G. (1988). On the inversion of binary-solid liquid fluidized beds, *Chemical Engineering Science*, 43(4), 979-981.
- Doroodchi, E., Zhou, J., Fletcher, D.F., & Galvin, K.P. (2005). Particle size classification in a fluidized bed containing parallel inclined plates, *Minerals Engineering*, 19, 161-172.

- Doroodchi, E., Fletcher, D.F. & Galvin, K.P. (2004). Influence of inclined plates on the expansion behaviour of particulate suspensions in a liquid fluidized bed, *Chemical Engineering Science*, 59, 3559-3567.
- Einstein, A. (1906). Eine neue Bestimmung der Moleküldimensionen, *Annalen der Physik*, 19 (2), 289.
- Epstein, N. & Leclair, B.P. (1985). Liquid fluidization of binary particle mixtures—II. Bed expansion, *Chemical Engineering Science*, 40, p. 1517.
- Ergun, S. (1952). Fluid Flow through Packed Columns, *Chemical Engineering Progress*, 48(2), 89-94.
- Faxen, H. (1923). Die bewegung einer starren kugel langs der achse eines mit zaher flussigkeit gefüllten rohres, *Ark Mat Astron Fys*, 17 (27), 1.
- Fessas, Y.P. & Weiland, R.H. (1984). The settling of suspensions promoted by rigid buoyant particles, *International Journal of Multiphase Flow*, 10, 485-507.
- Fessas, Y.P. & Weiland, R.H. (1982). Convective solids settling induced by a buoyant phase—A new method for the acceleration of thickening, *Resources and Conservation*, 9, 87-93.
- Fessas, Y.P. & Weiland R.H. (1981). Convective solids settling induced by a buoyant phase, *AIChE Journal*, 27(4), 588-592.
- Fenelonov, V.B., Mel'gunov, M.S. & Parmon, V.N. (2010). The Properties of Cenospheres and the Mechanism of Their Formation During High-Temperature Coal Combustion at Thermal Power Plants, *Boreskov Institute of Catalysis*, SB RAS.
- Francis, A.W. (1933). Wall effects in falling ball method for viscosity, *Physics*, 4, 403.
- Galvin, K.P. & Dickinson, J.E. (2013). Particle transport and separation in inclined channels subject to centrifugal forces, *Chemical Engineering Science*, 87, 294–305.

- Galvin, K.P. (2012). *Development of the Reflux Classifier, in, Challenges in Fine Coal Processing, Dewatering, and Disposal*, Edited by M. Klima, Published by SME, ISBN 978-0-87335-363-2. pp 159-185.
- Galvin, K.P. & Liu, H. (2011). Role of inertial lift in elutriating particles according to their density, *Chemical Engineering Science*, *66*, 3687-3691.
- Galvin, K.P., Walton, K. & Zhou, J. (2010). Application of closely spaced inclined channels in gravity separation of fine particles, *Minerals Engineering*, *23*, 326–338.
- Galvin, K.P., Walton, K. & Zhou, J. (2009). How to elutriate particles according to their density, *Chemical Engineering Science*, *64*, 2003 – 2010.
- Galvin, K.P., Swann, R., & Ramirez, W.F. (2006). Segregation and dispersion of a binary system of particles in a fluidized bed, *AIChE Journal*, *52*(10), 3401–3410.
- Galvin, K.P., Callen, A., Zhou, J. & Doroodchi, E. (2005). Performance of the REFLUX™ Classifier for gravity separation at full scale, *Minerals Engineering*, *18*, 19–24.
- Galvin, K.P. & Nguyentranlam, G. (2002). Influence of parallel inclined plates in a liquid fluidized bed system, *Chemical Engineering Science*, *57*, 1231-1234.
- Galvin, K.P., Belcher, B.D., Pratten, S.J., Callen, A.M., Lambert, M. & Nguyentranlam, G. (2002). Pilot scale Reflux Classifier for density and size separations, Grant Report, ACARP Project C10049, Department of Chemical Engineering, University of Newcastle, Australia.
- Galvin, K.P., Pratten, S. & Nguyen Tran Lam, G. (1999). A generalized empirical description for particle slip velocities in liquid fluidized beds, *Chemical engineering Science*, *54*, 1045-1052.

- Galvin, K.P., Compton, T. & Firth, B.A. (1995). Quantification of the Data Improvement Produced by Optimised Metallurgical Plant Mass Balances, *Minerals Engineering*, 8(7), 739-752.
- Geldart, D., Cullinan, J., Georghiades, S., Gilvray, D. & Pope, K. J. (1979). The effects of fines on entrainment from gas fluidized beds, *Transactions of the Institution of Chemical Engineers*, 57, 269.
- Gibilaro, L.G., Gallucci, K., Di Felice, R. & Pagliai, P. (2007). On the apparent viscosity of a fluidized bed, *Chemical Engineering Science*, 62, 294-300.
- Gibilaro, L.G., Di Felice, R., Waldram, S.P. & Foscolo, P.U. (1987). Authors' reply to comments by Cliff et al., *Chemical Engineering Science*, 42(1), 194-196.
- Gibilaro, L.G., Felice R. Di, Waldram, S.P. & Foscolo, P.U. (1986). A predictive model for the equilibrium composition and inversion of binary-solid liquid fluidized beds, *Chemical Engineering Science*, 41, p. 379.
- Grace, J.R. & Tuot, J. (1979). Theory for cluster formation in vertically conveyed suspensions of intermediate density, *Transactions of the Institution of Chemical Engineers*, 57, 49-54.
- Graf, W.H. (1984). *Hydraulics of sediment transport*, Colorado: Water Resource Publications, LLC.
- Graham, W. & Lama, R. (1963). Sedimentation in inclined vessels, *Canadian Journal of Chemical Engineering*, 41, 31-32.
- Gregory, J., (2005). *Particles in Water: Properties and Processes*. London: IWA.
- Haider, A. & Levenspiel, O. (1989). Drag coefficient and Terminal velocity of spherical and non-spherical particles, *Powder technology*, 58, 63–70.

- Happel, J. & Brenner, H. (1965). *Low Reynolds number hydrodynamics*, Englewood Cliffs, NJ: Prentice Hall.
- Heiskanen, K. (1993). *Particle Classification*, London; New York: Chapman & Hall.
- Helland, E., Bournot, H., Occelli, R. & Tadrist, L. (2007). Drag reduction and cluster formation in a circulating fluidized Bed, *Chemical Engineering Science*, 62, 148-158.
- Herbolzheimer, E. & Acrivos, A. (1981). Enhanced sedimentation in narrow tilted channels, *Journal of Fluid Mechanics*, 108, 485-499.
- Hill, W.D., Rothfus, R.R. & Kun, L. (1977). Boundary-enhanced sedimentation due to settling convection, *International Journal of Multiphase Flow*, 3(6), 561-583.
- Hoerner, S.F. (1958). *Fluid-Dynamic Drag*, Published by the Author, New York, USA.
- Honaker, R.Q. & Forrest, W.R. (2003). *Advances in gravity concentration*, Littleton : Society for Mining, Metallurgy & Exploration.
- Horio, M., Ishii, H. & Nishimuro, M. (1992). On the nature of turbulent and fast fluidized bed, *Powder Technology*, 70, 229-236.
- Huang, X., Hwang, J.Y. & Gillis, J.M. (2003). Processed Low NO<sub>x</sub> Fly Ash as a Filler in Plastics, *Journal of Minerals & Materials Characterization & Engineering*, Vol. 2, No.1, 11-31.
- Iveson, S.M., Hunter, D.M. & Galvin, K.P. (2015). A water-based method for measuring density-based partition curves of separators used in coal and mineral processing, *Minerals Engineering*, 79, 196-211.
- Jankowski, J., Ward, C.R., French, D. & Groves, S. (2006). Mobility of trace elements from selected Australian fly ashes and its potential impact on aquatic ecosystems, *Fuel*, 85, 243–256.

- Jean, R.H. & Fan, L.S. (1986). On the criteria of solid layer inversion in a liquid-solid fluidized bed containing a binary mixture of particles, *Chemical Engineering Science*, 41, p. 2811.
- Joshi, R.C. & Lothia, R.P. (1997). *Fly ash in concrete: production, properties and uses*. In: Advances in concrete technology, vol. 2. Gordon and Breach Science Publishers.
- Kennedy, S.C. & Bretton R.H. (1966). Axial dispersion of spheres fluidized with liquids, *AIChE Journal*, 12, 24.
- Khan, A.R. & Richardson, J.F. (1989). Fluid-particle interactions and flow characteristics of fluidized beds and settling suspensions of spherical particles, *Chemical Engineering Communications*, 78, 111.
- Kinosita, K. (1949). Sedimentation in tilted vessels, *Journal of Colloid and Interface Science*, 4, 525-536.
- Kozeny, J. (1927). Ueber kapillare Leitung des Wassers im Boden. *Sitzungsber Akad, Wiss., Wien*, 136(2a), 271-306.
- Kozeny, J. (1933). Theorie und Berechnung der Brunnen. *Wasserkraft und Wasserwirtschaft*, 28, 101- 105.
- Kruger, R.A. (1997). Fly ash beneficiation in South Africa: Creating new opportunities in the market-place, *Fuel*, 76 (8), 777–779.
- Kunii, D. & Levenspiel, O. (1991). *Fluidization Engineering*, 2<sup>nd</sup> Ed, Butterworth Heinemann.
- Lanchester, F.W. (1907). *Aerodynamics*, London.
- Laskovski, D., Duncan, P., Stevenson, P., Zhou, J. & Galvin, K.P. (2006). Segregation of hydraulically suspended particles in inclined channels, *Chemical Engineering Science*, 61, 7269–7278.

- Law, H.S., MacTaggart, R.S., Nandakumar, K. & Masliyah, J.H. (1988). Settling behaviour of heavy and buoyant particles from a suspension in an inclined channel, *Journal of Fluid Mechanics*, 187, 301-318.
- Li, J., Agarwal, A., Iveson, S.M., Kiani, A., Dickinson, J., Zhou, J. & Galvin, K.P. (2014). Recovery and concentration of buoyant cenospheres using an Inverted Reflux Classifier, *Fuel Processing Technology*, 123, 127-139.
- Li, H., Xia, Y., Tung, Y. & Kwauk, M. (1991). Micro-visualization of clusters in a fast fluidized bed, *Powder Technology*, 66, 231–235.
- Lilkov, V., Djabarov, N., Bechev, G. & Petrov, O. (1999). Properties and hydration products of lightweight and expansive cements Part II: Hydration products, *Cement and Concrete Research*, 29, 1641–1646.
- lim, K.S., Zhu, J.X. & Grace, J.R. (1995). Hydrodynamics of gas-solid fluidization, *International Journal of Multiphase Flow*, 21, 141.
- Lockett, M.J. & Al-Habbooby, H.M. (1973). Differential settling by size of two particle species in a liquid, *Transactions of the Institution of Chemical Engineers*, 51, 281-292.
- Lundgren, R. (1927). *Acta Medica Scandinavia*. 67, 63f.
- Lundgren, R. (1928). *Acta Med. Scandinavia*. 69, 405f.
- MacTaggart, R.S., Law, H.S., Masliyah, J.H. & Nandakumar, K. (1988). Gravity separation of concentrated bidisperse suspensions in inclined plate settlers, *International Journal of Multiphase Flow*, 14, 519-532.
- Manyele, S.V., Parssinen, J.H. & Zhu, J.X. (2002). Characterizing particle aggregates in high density and high flux CFB risers, *Chemical Engineering Journal*, 88, 151.

- Masliyah, J.H., Nasr-El-Din, H. & Nandakumar, K. (1989). Continuous separation of bidisperse suspensions in inclined channels, *International Journal of Multiphase Flow*, 15, 815-829.
- Masliyah, J. (1979). Hindered settling in a multi-species particle system, *Chemical Engineering Science*, 34, 1166-1168.
- McBride, S. P., Shukla, A. & Bose, A. (2002). Processing and characterization of lightweight concrete using cenospheres, *Journal of Materials Science*, 37, 4217– 4225.
- Miltzer, J., Kan, J.M., Hamdullahpur, F., Amyotte, P.R. & Al Taweel, A.M. (1989). Drag coefficient for axisymmetric flow around individual spheroidal particles, *Powder Technology*, 57, 193-195.
- Mohanty, M.K. & Honaker, R.Q. (1999). Performance Optimization of Jameson Flotation Technology for Fine Coal Cleaning, *Minerals Engineering*, 12(4), 367-381.
- Moritomi, H., Iwase, T. & Chiba, T. (1982). A comprehensive interpretation of solid layer inversion in liquid fluidized beds, *Chemical Engineering Science*, 37, 1751-1757.
- Munroe, H.S. (1888). *Transactions of the American Institute of Mining, Metallurgical and Petroleum Engineers*, 17, 637.
- Nakamura, H. & Kuroda, K. (1937). La Cause de l'accélération de la Vitesse de Sedimentation des Suspensions dans les Recipients Inclines, *Keijo J. Med.* 8, 256–296.
- Nguyentranlam, G. & Galvin, K.P. (2000). Development of an innovative classifier, Chemeca 2000, 28th Australian and New Zealand Chemical Engineers' Conference, Perth.
- Noda, K., Ohashi, M. & Ishida, K. (1982). Viscosities and Densities at 298.15 K for Mixtures of Methanol, Acetone, and Water, *Journal of Chemical Engineering Data*, 27, 326-328.

- Patel, B.K., Ramirez, W.F. & Galvin, K.P. (2008). A generalized segregation and dispersion model for liquid-fluidized beds, *Chemical Engineering Science*, 63(6), 1415- 1427.
- Ponder, E. (1925). On Sedimentation and Rouleaux Formation, *Quarterly Journal of Experimental Physiology*, 15, 235.
- Probstein, R.F. & Hicks, R. (1978). Lamella settlers: a new operating mode for high performance, *Ind. Water Eng.* 15, 6-8.
- Probstein, R.F., Yung, D. & Hick, R.E. (1977). A model for lamella settler, In Theory, Practice and Process Principles for Physical Separations; Proc. Engineering Conference Foundation Conf, Asilomar, Calif, 53-92.
- Raask, E. (1985). Mineral impurities in coal combustion-behaviour, problems, and remedial measures, *Hemisphere Publishing Corporation: Leatherhead*.
- Raask, E. (1968). Cenospheres in pulverized-fuel ash, *Journal of the Institute of Fuel*, 43, 339-344.
- Rampall, I. & Leighton, Jr. (1994). Influence of shear-induced migration on turbulent resuspension, *International Journal of Multiphase Flow*, 20 (3), 631–650.
- Reed, C.C. & Anderson, J.L. (1980). Hindered settling of a suspension at low Reynolds number, *AIChE Journal*, DOI: 10.1002/aic.690260515.
- Rhodes, M. (2007). *Introduction to Particle Technology*, 2<sup>nd</sup> Edition, Chichester: Wiley.
- Rhodes, M. (1998). *Introduction to Particle Technology*, Chichester: Wiley.
- Richardson, J.F. & Meikle, R.A. (1961). Sedimentation and fluidization: Part 4. *Transactions of the Institution of Chemical Engineers*, 39, 348.
- Richardson, J.F. & Zaki, W.N. (1954a). The sedimentation of a suspension of uniform spheres under conditions of viscous flow, *Chemical Engineering Science*, 3, 65-73.

- Richardson, J.F. & Zaki, W.N. (1954b). Sedimentation and Fluidization, *Transactions of the Institution of Chemical Engineers*, 32.
- Rushton, A., Ward, A.S. & Holdich, R.G. (1996). *Solid-Liquid Filtration and Separation Technology*. Weinheim, Germany: VCH.
- Sanders, G.J. (2007). *The principles of Coal Preparation*, 4th Ed. Australian Coal Preparation Society.
- Schaflinger, U. (1985). Influence of non-uniform particle size on settling beneath downward facing walls, *International Journal of Multiphase Flow*, 11, 783–796.
- Selberg, B.P. & Nicholls, J.A. (1968). *The American Institute of Aeronautics and Astronautics Journal*, 6, 401-408.
- Seville, J.P.K., Tuzun, U. & Clift, R. (1997). *Processing of Particulate Solids*, Chapman & Hall.
- Sivier, K.R. & Nicholls, J.A. (1969). *NASA Contract. Rep. CR-1392*.
- Stokes, G.G. (1851). On the effect of the internal friction of fluids on the motion of pendulums, *Transactions Cambridge Philosophical Society*, 9(8), 106.
- Thomas, D.G. (1965). Transport Characteristics of Suspension: VIII. A note on the viscosity of Newtonian suspensions of uniform spherical particles, *Journal of Colloid Science*, 20, 267-277.
- Tsiridis, V., Petala, M., Samaras, P., Kungolos, A. & Sakellariopoulos, G.P. (2012). Environmental hazard assessment of coal fly ashes using leaching and ecotoxicity tests, *Ecotoxicology and Environmental Safety*, 84, 212–220.

- Turton, R. & Levenspiel, O. (1986). A short note on the drag correlation for spheres, *Powder Technology*, 47(1), 83-86.
- Vance, W.H. & Moulton, R.W. (1965). A study of slip ratios for the flow of steam–water mixtures at high void fractions, *AIChE Journal*, 11 (6), 1114–1124.
- Vassilev, S. V. & Vassileva, C. G. (1996). Minerology of combustion wastes from coal-fired power stations, *Fuel Processing Technology*, 47 (3), 261–280.
- Vohra, D.K. & Ghosh, B. (1971). Studies of sedimentation in inclined tubes, *Ind. Chem. Engng*, 13, 32-40.
- Wadell, H. (1933). Sphericity and roundness of rock particles, *Journal of Geology*, 41(3), 310-331.
- Walton, K., Zhou, J. & Galvin, K.P. (2010). Processing of fine particles using closely spaced inclined channels, *Advanced Powder Technology*, 21, 386–391.
- Weiland, R.H., Fessas, Y.P. & Ramarao, B.V. (1984). On instabilities arising during sedimentation of two-component mixtures of solids, *Journal of Fluid Mechanics*, 142, 383-389.
- Weiland, R.H. & McPherson, R.R. (1979). Accelerated settling by addition of buoyant particles, *Industrial & Engineering Chemistry Fundamentals*, 18, 45-49.
- Wen, C.Y. & Yu, Y.H. (1966). Mechanics of Fluidization, *Chemical Engineering Progress*, Symposium, 62, 100 - 111.
- Whitmore, R.L. (1955). The sedimentation of suspensions of spheres, *British Journal of Applied Physics*, 6, 239-245.
- Williams, J.C. (1990). *Mixing and segregation in powders*, In *Principles of Powder Technology*, ed. M.J. Rhodes, John Wiley & Sons, Chichester.

- Williams, J.C. (1976). The Segregation of Particulate Material. A Review, *Powder Technology*, 15, 245-251.
- Wills, B.A. (1997). *Mineral Processing Technology*, 6th ed., Boston: Butterworth-Heinemann.
- Yang, W.C. (2003). *Bubbling fluidized bed in- Handbook of fluidization and fluid-particle system*, New York: Marcel Dekker, Ink.
- Zahavi, E. & Rubin, E. (1975). Settling of solid suspension under and between inclined surfaces, *Industrial & Engineering Chemistry Process Design and Development*, 14, 34-41.
- Zenz, F.A. & Weil, N.A. (1958). A theoretical-empirical approach to the mechanism of particle entrainment from fluidized beds, *AIChE Journal*, 4, 472.
- Zhang, X. & Davis, R.H. (1990). Particle classification using inclined settlers in series and with underflow recycle, *Industrial & Engineering Chemistry Research*, 29(9), 1894-1900.
- Zhou, J., Walton, K., Laskovski, D., Duncan, P. & Galvin, K.P. (2006). Enhanced separation of mineral sands using the REFLUX™ Classifier, *Minerals Engineering*, 19, 1573–1579.
- Zigrang, D.J. & Sylvester, N.D. (1981). An explicit equation for particle settling velocities in solid-liquid systems, *AIChE Journal*, 27(6), 1043-1044.
- Zimmels, Y. (1988). Simulation of Nonsteady Sedimentation of Polydisperse Particle mixtures, *Powder Technology*, 56, 227-250.
- Zimmels, Y. (1985). Theory of density separation of particulate systems, *Powder Technology*, 43, 127-139.

## **Appendix A: IRC™ raw experimental and reconciled data and results (grade and recovery by the sink-float method)**

In this set of experiments, the results were obtained using the sink-float method. The experimental data was reconciled using the error minimization method discussed in Chapters 5-9. In the following tables of data, the red numbers are values that were adjusted in order to minimize the sum of square standard error that is shown in blue. Constraints are the ratios of in/out which should be equal to 1 in a set of balanced data. Sample calculations are presented in Appendix H. Note that the first 4 runs in Chapter 5 were related to the preliminary stage of the work, studying the model feed (mixture of silica and commercial cenospheres).

As mentioned in previous chapters, the consistency of the raw data has been shown by comparing the measured inlet and outlet rates of each component (in/out ratios). These ratios are shown for each experiment. These values obviously equal 1 for the reconciled data. The sub-tables named “Relative error” show the percentage of adjustment made by the reconciliation technique to each set of raw experimental data.

## Chapter 5 - Run 1

### Experiment data

Stream	Total (g/min)	Silica (g/min)	Cenosphere (g/min)
Overflow	48.40	0.19	0.36
Underflow	1045.20	82.34	0.29
Feed	970.80	82.22	0.75
Wash water	125.00	-	-
in/out	1.00	1.00	1.16

### Balanced data

Stream	Total (g/min)	Silica (g/min)	Cenosphere (g/min)
Overflow	48.40	0.19	0.45
Underflow	1046.37	82.19	0.29
Feed	969.79	82.37	0.74
Wash water	124.98	-	-
in/out	1.0	1.0	1.0

### Square standard error

	Total	Silica	Cenosphere	Sum of errors
Overflow	0.0000	0.0000	0.0645	0.0645
Underflow	0.0000	0.0000	0.0000	0.0000
Feed	0.0000	0.0000	0.0003	0.0003
Wash water	0.0000	-	-	0.0000

Sum \* 100 = 6.4823

### Relative error (%)

	Total	Silica	Cenosphere
Overflow	0.01	0.00	25.40
Underflow	0.11	-0.19	0.64
Feed	-0.10	0.19	-1.67
Wash water	-0.01	-	-

### Results based on reconciled data

Stream	Pulp Density (wt.%)	Cenosphere Grade (wt.%)	Silica Grade (wt.%)	Cenosphere Recovery (wt.%)	Silica Recovery (wt.%)	Cenosphere Upgrade
Overflow	1.3	70.6	29.4	60.6	0.2	79.6
Underflow	7.9	0.4	99.6	39.4	99.8	-
Feed	8.6	0.9	99.1	-	-	-

## Chapter 5 - Run 2

### Experiment data

Stream	Total (g/min)	Silica (g/min)	Cenosphere (g/min)
Overflow	21.00	0.05	0.21
Underflow	1075.00	79.20	0.18
Feed	961.40	79.42	0.47
Wash water	125.00	-	-
in/out	0.99	1.00	1.20

### Balanced data

Stream	Total (g/min)	Silica (g/min)	Cenosphere (g/min)
Overflow	21.00	0.05	0.27
Underflow	1069.71	79.28	0.19
Feed	965.63	79.33	0.46
Wash water	125.07	-	-
in/out	1.00	1.00	1.00

### Square standard error

	Total	Silica	Cenosphere	Sum of errors
Overflow	0.0000	0.0000	0.0021	0.0021
Underflow	0.0000	0.0000	0.0003	0.0003
Feed	0.0000	0.0000	0.0003	0.0003
Wash water	0.0000	-	-	0.0000

Sum \* 100 = 0.2685

### Relative error (%)

	Total	Silica	Cenosphere
Overflow	-0.01	0.00	28.73
Underflow	-0.49	0.11	4.24
Feed	0.44	-0.11	-1.62
Wash water	0.06		

### Results based on balanced data

Stream	Pulp Density (wt.%)	Cenosphere Grade (wt.%)	Silica Grade (wt.%)	Cenosphere Recovery (wt.%)	Silica Recovery (wt.%)	Cenosphere Upgrade
Overflow	1.5	85.3	14.7	59.6	0.1	148.1
Underflow	7.4	0.2	99.8	40.4	99.9	-
Feed	8.3	0.6	99.4	-	-	-

## Chapter 5 - Run 3

### Experiment data

Stream	Total (g/min)	Silica (g/min)	Cenosphere (g/min)
Overflow	8.84	0.04	0.14
Underflow	1030.80	74.98	0.20
Feed	911.00	75.26	0.44
Wash water	125.00	-	-
in/out	1.00	1.00	1.30

### Balanced data

Stream	Total (g/min)	Silica (g/min)	Cenosphere (g/min)
Overflow	8.84	0.04	0.21
Underflow	1028.77	75.09	0.21
Feed	912.58	75.14	0.42
Wash water	125.03	-	-
in/out	1.00	1.00	1.00

### Square standard error

	Total	Silica	Cenosphere	Sum of errors
Overflow	0.0000	0.0000	0.0051	0.0051
Underflow	0.0000	0.0000	0.0009	0.0009
Feed	0.0000	0.0000	0.0009	0.0009
Wash water	0.0000	-	-	0.0000

Sum \* 100 = 0.6844

### Relative error (%)

	Total	Silica	Cenosphere
Overflow	0.00	0.00	55.22
Underflow	-0.20	0.16	6.46
Feed	0.17	-0.16	-2.96
Wash water	0.02	-	-

### Results based on balanced data

Stream	Pulp Density (wt.%)	Cenosphere Grade (wt.%)	Silica Grade (wt.%)	Cenosphere Recovery (wt.%)	Silica Recovery (wt.%)	Cenosphere Upgrade
Overflow	2.9	82.7	17.3	49.8	0.1	147.5
Underflow	7.3	0.3	99.7	50.2	99.9	-
Feed	8.3	0.6	99.4	-	-	-

## Chapter 5 - Run 4

### Experiment data

Stream	Total (g/min)	Silica (g/min)	Cenosphere (g/min)
Overflow	85.90	0.04	0.06
Underflow	1002.00	80.08	0.15
Feed	972.00	80.09	0.22
Wash water	125.00	-	-
in/out	1.01	1.00	1.08

### Balanced data

Stream	Total (g/min)	Silica (g/min)	Cenosphere (g/min)
Overflow	85.93	0.04	0.07
Underflow	1006.63	80.07	0.15
Feed	967.64	80.10	0.22
Wash water	124.93	-	-
in/out	1.00	1.00	1.00

### Square standard error

	Total	Silica	Cenosphere	Sum of errors
Overflow	0.0000	0.0000	0.0010	0.0010
Underflow	0.0000	0.0000	0.0004	0.0004
Feed	0.0000	0.0000	0.0009	0.0009
Wash water	0.0000	-	-	0.0000

Sum \* 100 = 0.2301

### Relative error (%)

	Total	Silica	Cenosphere
Overflow	0.04	0.00	12.73
Underflow	0.46	-0.02	1.93
Feed	-0.45	0.02	-2.95
Wash water	-0.06	-	-

### Results based on balanced data

Stream	Pulp Density (wt.%)	Cenosphere Grade (wt.%)	Silica Grade (wt.%)	Cenosphere Recovery (wt.%)	Silica Recovery (wt.%)	Cenosphere Upgrade
Overflow	0.1	64.5	35.5	31.3	0.0	237.6
Underflow	8.0	0.2	99.8	68.7	100.0	-
Feed	8.3	0.3	99.7	-	-	-

## Chapter 5 - Run 5

### Experiment data

Stream	Total (g/min)	Fly ash (g/min)	Cenosphere (g/min)
Overflow	23.33	0.71	2.23
Underflow	1199.00	560.90	3.79
Feed	1145.20	567.63	6.67
Wash water	125.00	-	-
in/out	1.04	1.01	1.11

### Balanced data

Stream	Total (g/min)	Fly ash (g/min)	Cenosphere (g/min)
Overflow	23.34	0.71	2.28
Underflow	1223.88	563.88	3.93
Feed	1122.50	564.58	6.22
Wash water	124.73	-	-
in/out	1.00	1.00	1.00

### Square standard error

	Total	Fly ash	Cenosphere	Sum of errors
Overflow	0.0000	0.0000	0.0005	0.0005
Underflow	0.0004	0.0000	0.0015	0.0019
Feed	0.0004	0.0000	0.0046	0.0050
Wash water	0.0000	-	-	0.0000

Sum \* 100 = 0.7

### Relative error (%)

	Total	Fly ash	Cenosphere
Overflow	0.04	0.00	2.26
Underflow	2.08	0.53	3.84
Feed	-1.98	-0.54	-6.76
Wash water	-0.22	-	-

### Results based on balanced data

Stream	Pulp Density (wt.%)	Cenosphere Grade (wt.%)	Fly ash Grade (wt.%)	Cenosphere Recovery (wt.%)	Fly ash Recovery (wt.%)	Cenosphere Upgrade
Overflow	14.4	78.9	21.1	40.8	0.1	69.4
Underflow	46.4	0.7	99.3	59.2	99.9	-
Feed	50.9	1.1	98.9	-	-	-

## Chapter 5 - Run 6

### Experiment data

Stream	Total (g/min)	Fly ash (g/min)	Cenosphere (g/min)
Overflow	49.23	0.46	1.60
Underflow	1163.60	536.14	3.46
Feed	1105.00	539.52	5.08
Wash water	125.00	-	-
in/out	1.01	1.01	1.00

### Balanced data

Stream	Total (g/min)	Fly ash (g/min)	Cenosphere (g/min)
Overflow	49.25	0.46	1.60
Underflow	1172.56	537.59	3.47
Feed	1096.92	538.05	5.07
Wash water	124.90	-	-
in/out	1.00	1.00	1.00

### Square standard error

	Total	Fly ash	Cenosphere	Sum of errors
Overflow	0.0000	0.0000	0.0000	0.0000
Underflow	0.0001	0.0000	0.0000	0.0001
Feed	0.0001	0.0000	0.0000	0.0001
Wash water	0.0000	-	-	0.0000

Sum \* 100 = 0.0130

### Relative error (%)

	Total	Fly ash	Cenosphere
Overflow	0.03	0.00	0.03
Underflow	0.77	0.27	0.07
Feed	-0.73	-0.27	-0.11
Wash water	-0.08	-	-

### Results based on balanced data

Stream	Pulp Density (wt.%)	Cenosphere Grade (wt.%)	Fly ash Grade (wt.%)	Cenosphere Recovery (wt.%)	Fly ash Recovery (wt.%)	Cenosphere Upgrade
Overflow	4.2	77.8	22.2	31.6	0.1	83.3
Underflow	46.1	0.6	99.4	68.4	99.9	-
Feed	49.5	0.9	99.1	-	-	-

## Chapter 5 - Run 7

### Experiment data

Stream	Total (g/min)	Fly ash (g/min)	Cenosphere (g/min)
Overflow	93.70	0.41	1.22
Underflow	1208.40	574.19	3.21
Feed	1177.00	573.33	4.67
Wash water	125.00	-	-
in/out	1.00	1.00	1.06

### Balanced data

Stream	Total (g/min)	Fly ash (g/min)	Cenosphere (g/min)
Overflow	93.70	0.41	1.30
Underflow	1208.35	573.55	3.26
Feed	1177.05	573.97	4.56
Wash water	125.00	-	-
in/out	1.00	1.00	1.00

### Square standard error

	Total	Fly ash	Cenosphere	Sum of errors
Overflow	0.0000	0.0000	0.0004	0.0004
Underflow	0.0000	0.0000	0.0003	0.0003
Feed	0.0000	0.0000	0.0006	0.0006
Wash water	0.0000	-	-	0.0000

Sum \* 100 = 0.1239

### Relative error (%)

	Total	Fly ash	Cenosphere
Overflow	0.00	0.00	6.76
Underflow	0.00	-0.11	1.62
Feed	0.00	0.11	-2.36
Wash water	0.00	-	-

### Results based on balanced data

Stream	Pulp Density (wt.%)	Cenosphere Grade (wt.%)	Fly ash Grade (wt.%)	Cenosphere Recovery (wt.%)	Fly ash Recovery (wt.%)	Cenosphere Upgrade
Overflow	1.8	75.9	24.1	28.5	0.1	96.3
Underflow	47.7	0.6	99.4	71.5	99.9	-
Feed	49.2	0.8	99.2	-	-	-

## Chapter 5 – Run 8

### Experiment data

Stream	Total (g/min)	Fly ash (g/min)	Cenosphere (g/min)
Overflow	109.45	34.92	0.65
Underflow	1022.40	543.67	3.65
Feed	1149.20	583.54	4.26
Wash water	0.00	-	-
in/out	1.02	1.01	0.99

### Balanced data

Stream	Total (g/min)	Fly ash (g/min)	Cenosphere (g/min)
Overflow	109.54	34.93	0.65
Underflow	1030.03	545.97	3.63
Feed	1139.56	580.89	4.28
Wash water	0.00	-	-
in/out	1.0	1.0	1.0

### Square standard error

	Total	Fly ash	Cenosphere	Sum of errors
Overflow	0.0000	0.0000	0.0000	0.0000
Underflow	0.0001	0.0000	0.0000	0.0001
Feed	0.0001	0.0000	0.0000	0.0001
Wash water	-	-	-	-

**Sum \* 100 = 0.0218**

### Relative error (%)

	Total	Fly ash	Cenosphere
Overflow	0.08	0.03	-0.08
Underflow	0.75	0.42	-0.47
Feed	-0.84	-0.45	0.55
Wash water	0.0	-	-

### Results based on balanced data

Stream	Pulp Density (wt.%)	Cenosphere Grade (wt.%)	Fly ash Grade (wt.%)	Cenosphere Recovery (wt.%)	Fly ash Recovery (wt.%)	Cenosphere Upgrade
Overflow	32.5	1.8	98.2	15.2	6.0	2.5
Underflow	53.4	0.7	99.3	84.8	94.0	-
Feed	51.4	0.7	99.3	-	-	-

## Chapter 5 - Run 9

### Experiment data

Stream	Total (g/min)	Fly ash (g/min)	Cenosphere (g/min)
Overflow	96.60	0.22	0.72
Underflow	1108.80	334.51	1.00
Feed	1091.00	327.30	1.61
Wash water	125.00		
in/out	1.01	0.98	0.94

### Balanced data

Stream	Total (g/min)	Fly ash (g/min)	Cenosphere (g/min)
Overflow	96.64	0.22	0.71
Underflow	1114.13	330.71	0.97
Feed	1085.84	330.93	1.68
Wash water	124.93	-	-
in/out	1.00	1.00	1.00

### Square standard error

	Total	Fly ash	Cenosphere	Sum of errors
Overflow	0.0000	0.0000	0.0003	0.0003
Underflow	0.0000	0.0001	0.0007	0.0008
Feed	0.0000	0.0001	0.0017	0.0018
Wash water	0.0000	-	-	0.0000

Sum \* 100 = 0.2990

### Relative error (%)

	Total	Fly ash	Cenosphere
Overflow	0.04	0.00	-1.84
Underflow	0.48	-1.13	-2.56
Feed	-0.47	1.11	4.12
Wash water	-0.05	-	-

### Results based on balanced data

Stream	Pulp Density (wt.%)	Cenosphere Grade (wt.%)	Fly ash Grade (wt.%)	Cenosphere Recovery (wt.%)	Fly ash Recovery (wt.%)	Cenosphere Upgrade
Overflow	1.0	76.1	23.9	42.0	0.1	150.8
Underflow	29.8	0.3	99.7	58.0	99.9	-
Feed	30.6	0.5	99.5	-	-	-

## Chapter 5 - Run 10

### Experiment data

Stream	Total (g/min)	Fly ash (g/min)	Cenosphere (g/min)
Overflow	190.32	0.39	0.85
Underflow	980.20	323.98	0.90
Feed	1054.00	328.30	1.97
Wash water	125.00	-	-
in/out	1.01	1.01	1.13

### Balanced data

Stream	Total (g/min)	Fly ash (g/min)	Cenosphere (g/min)
Overflow	190.46	0.39	0.88
Underflow	984.04	325.92	0.93
Feed	1049.56	326.31	1.81
Wash water	124.94	-	-
in/out	1.00	1.00	1.00

### Square standard error

	Total	Fly ash	Cenosphere	Sum of errors
Overflow	0.0000	0.0000	0.0013	0.0013
Underflow	0.0000	0.0000	0.0014	0.0015
Feed	0.0000	0.0000	0.0068	0.0068
Wash water	0.0000	-	-	0.0000

Sum \* 100 = 0.9541

### Relative error (%)

	Total	Fly ash	Cenosphere
Overflow	0.08	0.00	3.54
Underflow	0.39	0.60	3.75
Feed	-0.42	-0.61	-8.23
Wash water	-0.05	-	-

### Results based on balanced data

Stream	Pulp Density (wt.%)	Cenosphere Grade (wt.%)	Fly ash Grade (wt.%)	Cenosphere Recovery (wt.%)	Fly ash Recovery (wt.%)	Cenosphere Upgrade
Overflow	0.7	69.4	30.6	48.5	0.1	125.9
Underflow	33.2	0.3	99.7	51.5	99.9	-
Feed	31.3	0.6	99.4	-	-	-

## Chapter 5 - Run 11

### Experiment data

Stream	Total (g/min)	Fly ash (g/min)	Cenosphere (g/min)
Overflow	371.60	5.53	1.24
Underflow	844.20	339.89	0.68
Feed	1087.20	346.69	1.76
Wash water	125.00	-	-
in/out	1.00	1.00	0.92

### Balanced data

Stream	Total (g/min)	Fly ash (g/min)	Cenosphere (g/min)
Overflow	371.36	5.53	1.19
Underflow	842.95	340.51	0.67
Feed	1089.28	346.04	1.85
Wash water	125.03	-	-
in/out	1.00	1.00	1.00

### Square standard error

	Total	Fly ash	Cenosphere	Sum of errors
Overflow	0.0000	0.0000	0.0015	0.0015
Underflow	0.0000	0.0000	0.0005	0.0005
Feed	0.0000	0.0000	0.0030	0.0030
Wash water	0.0000	-	-	0.0000

Sum \* 100 = 0.4957

### Relative error (%)

	Total	Fly ash	Cenosphere
Overflow	-0.07	0.00	-3.85
Underflow	-0.15	0.18	-2.13
Feed	0.19	-0.19	5.48
Wash water	0.02	-	-

### Results based on balanced data

Stream	Pulp Density (wt.%)	Cenosphere Grade (wt.%)	Fly ash Grade (wt.%)	Cenosphere Recovery (wt.%)	Fly ash Recovery (wt.%)	Cenosphere Upgrade
Overflow	1.8	17.7	82.3	64.0	1.6	33.1
Underflow	40.5	0.2	99.8	36.0	98.4	-
Feed	31.9	0.5	99.5	-	-	-

## Chapter 6 - Run 1

### Experiment data

Stream	Total (g/min)	Fly ash (g/min)	Cenosphere (g/min)
Overflow	201.06	0.31	0.68
Underflow	897.20	97.82	0.42
Feed	898.25	88.89	1.06
Wash water	125.00	-	-
in/out	0.93	0.91	0.97

### Balanced data

Stream	Total (g/min)	Fly ash (g/min)	Cenosphere (g/min)
Overflow	199.25	0.31	0.67
Underflow	860.99	92.76	0.42
Feed	934.54	93.07	1.08
Wash water	125.70	-	-
in/out	1.00	1.00	1.00

### Square standard error

	Total	Fly ash	Cenosphere	Sum of errors
Overflow	0.0001	0.0000	0.0002	0.0002
Underflow	0.0016	0.0027	0.0001	0.0044
Feed	0.0016	0.0022	0.0004	0.0042
Wash water	0.0000	-	-	0.0000

Sum \*100 = 0.8853

### Relative error (%)

	Total	Fly ash	Cenosphere
Overflow	-0.90	-0.02	-1.25
Underflow	-4.04	-5.17	-0.77
Feed	4.04	4.70	1.96
Wash water	0.56	-	-

### Results based on balanced data

Stream	Pulp Density (wt.%)	Cenosphere Grade (wt.%)	Fly ash Grade (wt.%)	Cenosphere Recovery (wt.%)	Fly ash Recovery (wt.%)	Cenosphere Upgrade
Overflow	0.5	68.5	31.5	61.7	0.3	59.5
Underflow	10.8	0.4	99.6	38.3	99.7	-
Feed	10.1	1.2	98.8	-	-	-

## Chapter 6 - Run 2

### Experiment data

Stream	Total (g/min)	Fly ash (g/min)	Cenosphere (g/min)
Overflow	186.05	0.61	1.69
Underflow	1044.10	208.34	0.95
Feed	1100.40	210.14	2.61
Wash water	125.00	-	-
in/out	1.00	1.01	0.99

### Balanced data

Stream	Total (g/min)	Fly ash (g/min)	Cenosphere (g/min)
Overflow	185.98	0.61	1.68
Underflow	1041.90	208.93	0.95
Feed	1102.85	209.54	2.63
Wash water	125.03	-	-
in/out	1.00	1.00	1.00

### Square standard error

	Total	Fly ash	Cenosphere	Sum of errors
Overflow	0.0000	0.0000	0.0000	0.0000
Underflow	0.0000	0.0000	0.0000	0.0000
Feed	0.0000	0.0000	0.0001	0.0001
Wash water	0.0000	-	-	0.0000

**Sum \* 100 = 0.0109**

### Relative error (%)

	Total	Fly ash	Cenosphere
Overflow	-0.04	0.00	-0.48
Underflow	-0.21	0.28	-0.27
Feed	0.22	-0.28	0.74
Wash water	0.03	-	-

### Results based on balanced data

Stream	Pulp Density (wt.%)	Cenosphere Grade (wt.%)	Fly ash Grade (wt.%)	Cenosphere Recovery (wt.%)	Fly ash Recovery (wt.%)	Cenosphere Upgrade
Overflow	1.2	73.3	26.7	64.0	0.3	59.1
Underflow	20.1	0.5	99.5	36.0	99.7	-
Feed	19.2	1.2	98.8	-	-	-

## Chapter 6 - Run 3

### Experiment data

Stream	Total (g/min)	Fly ash (g/min)	Cenosphere (g/min)
Overflow	215.40	1.22	2.99
Underflow	1082.80	352.76	0.53
Feed	1170.70	358.95	3.30
Wash water	125.00		
in/out	1.00	1.01	0.94

### Balanced data

Stream	Total (g/min)	Fly ash (g/min)	Cenosphere (g/min)
Overflow	215.36	1.22	2.89
Underflow	1081.67	355.20	0.52
Feed	1172.01	356.42	3.42
Wash water	125.01	-	-
in/out	1.00	1.00	1.00

### Square standard error

	Total	Fly ash	Cenosphere	Sum of errors
Overflow	0.0000	0.0000	0.0011	0.0011
Underflow	0.0000	0.0000	0.0000	0.0001
Feed	0.0000	0.0000	0.0013	0.0013
Wash water	0.0000	-	-	0.0000

Sum \* 100 = 0.2487

### Relative error (%)

	Total	Fly ash	Cenosphere
Overflow	-0.02	0.00	-3.26
Underflow	-0.10	0.69	-0.57
Feed	0.11	-0.71	3.59
Wash water	0.01	-	-

### Results based on balanced data

Stream	Pulp Density (wt.%)	Cenosphere Grade (wt.%)	Fly ash Grade (wt.%)	Cenosphere Recovery (wt.%)	Fly ash Recovery (wt.%)	Cenosphere Upgrade
Overflow	1.9	70.3	29.7	84.7	0.3	74.1
Underflow	32.9	0.1	99.9	15.3	99.7	-
Feed	30.7	0.9	99.1	-	-	-

## Chapter 6 - Run 4

### Experiment data

Stream	Total (g/min)	Fly ash (g/min)	Cenosphere (g/min)
Overflow	202.55	2.45	4.57
Underflow	1077.10	428.77	0.49
Feed	1147.20	437.56	4.48
Wash water	125.00		
in/out	0.99	1.01	0.89

### Balanced data

Stream	Total (g/min)	Fly ash (g/min)	Cenosphere (g/min)
Overflow	202.43	2.45	4.28
Underflow	1073.69	431.87	0.48
Feed	1151.07	434.33	4.76
Wash water	125.05	-	-
in/out	1.00	1.00	1.00

### Square standard error

	Total	Fly ash	Cenosphere	Sum of errors
Overflow	0.0000	0.0000	0.0040	0.0040
Underflow	0.0000	0.0001	0.0000	0.0001
Feed	0.0000	0.0001	0.0039	0.0040
Wash water	0.0000	-	-	0.0000

Sum \* 100 = 0.8105

### Relative error (%)

	Total	Fly ash	Cenosphere
Overflow	-0.06	0.00	-6.36
Underflow	-0.32	0.72	-0.68
Feed	0.34	-0.74	6.24
Wash water	0.04	-	-

### Results based on balanced data

Stream	Pulp Density (wt.%)	Cenosphere Grade (wt.%)	Fly ash Grade (wt.%)	Cenosphere Recovery (wt.%)	Fly ash Recovery (wt.%)	Cenosphere Upgrade
Overflow	3.3	63.5	36.5	89.9	0.6	58.6
Underflow	40.3	0.1	99.9	10.1	99.4	-
Feed	38.1	1.1	98.9	-	-	-

## Chapter 6 - Run 5

### Experiment data

Stream	Total (g/min)	Fly ash (g/min)	Cenosphere (g/min)
Overflow	195.35	0.98	2.85
Underflow	1016.20	472.42	1.89
Feed	1093.70	485.46	4.78
Wash water	125.00		
in/out	1.01	1.03	1.01

### Balanced data

Stream	Total (g/min)	Fly ash (g/min)	Cenosphere (g/min)
Overflow	195.47	0.98	2.86
Underflow	1019.43	499.51	1.89
Feed	1089.95	500.49	4.75
Wash water	124.95	-	-
in/out	1.00	1.00	1.00

### Square standard error

	Total	Fly ash	Cenosphere	Sum of errors
Overflow	0.0000	0.0000	0.0000	0.0000
Underflow	0.0000	0.0033	0.0000	0.0033
Feed	0.0000	0.0010	0.0000	0.0010
Wash water	0.0000	-	-	0.0000

Sum \* 100 = 0.4319

### Relative error (%)

	Total	Fly ash	Cenosphere
Overflow	0.06	0.00	0.35
Underflow	0.32	5.73	0.23
Feed	-0.34	3.09	-0.58
Wash water	-0.04	-	-

### Results based on balanced data

Stream	Pulp Density (wt.%)	Cenosphere Grade (wt.%)	Fly ash Grade (wt.%)	Cenosphere Recovery (wt.%)	Fly ash Recovery (wt.%)	Cenosphere Upgrade
Overflow	2.0	74.5	25.5	60.2	0.2	79.3
Underflow	49.2	0.4	99.6	39.8	99.8	-
Feed	46.4	0.9	99.1	-	-	-

## Chapter 6 - Run 6

### Experiment data

Stream	Total (g/min)	Fly ash (g/min)	Cenosphere (g/min)
Overflow	269.40	18.57	4.96
Underflow	1668.73	660.00	1.24
Feed	1800.70	678.68	5.98
Wash water	150.00	-	-
in/out	1.01	1.00	0.96

### Balanced data

Stream	Total (g/min)	Fly ash (g/min)	Cenosphere (g/min)
Overflow	269.55	18.57	4.87
Underflow	1674.45	660.06	1.24
Feed	1794.04	678.63	6.11
Wash water	149.95	-	-
in/out	1.00	1.00	1.00

### Square standard error

	Total	Fly ash	Cenosphere	Sum of errors
Overflow	0.0000	0.0000	0.0003	0.0003
Underflow	0.0000	0.0000	0.0000	0.0000
Feed	0.0000	0.0000	0.0005	0.0005
Wash water	0.0000	-	-	0.0000

Sum \* 100 = 0.0881

### Relative error (%)

	Total	Fly ash	Cenosphere
Overflow	0.06	0.00	-1.84
Underflow	0.34	0.01	-0.46
Feed	-0.37	-0.01	2.22
Wash water	-0.03	-	-

### Results based on balanced data

Stream	Pulp Density (wt.%)	Cenosphere Grade (wt.%)	Fly ash Grade (wt.%)	Cenosphere Recovery (wt.%)	Fly ash Recovery (wt.%)	Cenosphere Upgrade
Overflow	8.7	20.8	79.2	79.7	2.7	23.3
Underflow	39.5	0.2	99.8	20.3	97.3	-
Feed	38.2	0.9	99.1	-	-	-

## Chapter 6 - Run 7

### Experiment data

Stream	Total (g/min)	Fly ash (g/min)	Cenosphere (g/min)
Overflow	186.25	1.01	3.80
Underflow	1670.00	675.15	2.09
Feed	1734.20	686.98	5.72
Wash water	150.00	-	-
in/out	1.02	1.02	0.97

### Balanced data

Stream	Total (g/min)	Fly ash (g/min)	Cenosphere (g/min)
Overflow	186.42	1.01	3.75
Underflow	1683.32	680.47	2.07
Feed	1719.84	681.47	5.83
Wash water	149.89	-	-
in/out	1.00	1.00	1.00

### Square standard error

	Total	Fly ash	Cenosphere	Sum of errors
Overflow	0.0000	0.0000	0.0002	0.0002
Underflow	0.0001	0.0001	0.0000	0.0002
Feed	0.0001	0.0001	0.0004	0.0005
Wash water	0.0000	-	-	0.0000

Sum \* 100 = 0.0848

### Relative error (%)

	Total	Fly ash	Cenosphere
Overflow	0.09	0.00	-1.29
Underflow	0.80	0.79	-0.71
Feed	-0.83	-0.80	1.93
Wash water	-0.07	-	-

### Results based on balanced data

Stream	Pulp Density (wt.%)	Cenosphere Grade (wt.%)	Fly ash Grade (wt.%)	Cenosphere Recovery (wt.%)	Fly ash Recovery (wt.%)	Cenosphere Upgrade
Overflow	2.6	78.9	21.1	64.4	0.1	93.0
Underflow	40.5	0.3	99.7	35.6	99.9	-
Feed	40.0	0.8	99.2	-	-	-

## Chapter 6 - Run 8

### Experiment data

Stream	Total (g/min)	Fly ash (g/min)	Cenosphere (g/min)
Overflow	101.10	0.28	2.40
Underflow	1637.84	652.69	4.14
Feed	1599.70	655.93	7.14
Wash water	150.00	-	-
in/out	1.01	1.00	1.09

### Balanced data

Stream	Total (g/min)	Fly ash (g/min)	Cenosphere (g/min)
Overflow	101.12	0.28	2.45
Underflow	1643.31	654.16	4.28
Feed	1594.48	654.44	6.73
Wash water	149.95	-	-
in/out	1.00	1.00	1.00

### Square standard error (%)

	Total	Fly ash	Cenosphere	Sum of errors
Overflow	0.0000	0.0000	0.0004	0.0004
Underflow	0.0000	0.0000	0.0011	0.0011
Feed	0.0000	0.0000	0.0033	0.0033
Wash water	0.0000	-	-	0.0000

Sum \* 100 = 0.4776

### Relative error (%)

	Total	Fly ash	Cenosphere
Overflow	0.02	0.00	1.93
Underflow	0.33	0.23	3.32
Feed	-0.33	-0.23	-5.72
Wash water	-0.03	-	-

### Results based on balanced data

Stream	Pulp Density (wt.%)	Cenosphere Grade (wt.%)	Fly ash Grade (wt.%)	Cenosphere Recovery (wt.%)	Fly ash Recovery (wt.%)	Cenosphere Upgrade
Overflow	2.7	89.7	10.3	36.4	0.0	88.2
Underflow	40.1	0.6	99.4	63.6	100.0	-
Feed	41.5	1.0	99.0	-	-	-

## Chapter 6 - Run 9

### Experiment data

Stream	Total (g/min)	Fly ash (g/min)	Cenosphere (g/min)
Overflow	98.07	0.24	1.40
Underflow	614.60	233.87	0.46
Feed	595.90	238.17	2.08
Wash water	125.00	-	-
in/out	1.01	1.02	1.12

### Balanced data

Stream	Total (g/min)	Fly ash (g/min)	Cenosphere (g/min)
Overflow	98.17	0.24	1.47
Underflow	618.70	235.86	0.47
Feed	592.04	236.11	1.94
Wash water	124.83	-	-
in/out	1.00	1.00	1.00

### Square standard error

	Total	Fly ash	Cenosphere	Sum of errors
Overflow	0.0000	0.0000	0.0023	0.0023
Underflow	0.0000	0.0001	0.0002	0.0004
Feed	0.0000	0.0001	0.0050	0.0051
Wash water	0.0000	-	-	0.0000

Sum \* 100 = 0.7760

### Relative error (%)

	Total	Fly ash	Cenosphere
Overflow	0.11	0.00	4.76
Underflow	0.67	0.85	1.56
Feed	-0.65	-0.87	-7.08
Wash water	-0.14	-	-

### Results based on balanced data

Stream	Pulp Density (wt.%)	Cenosphere Grade (wt.%)	Fly ash Grade (wt.%)	Cenosphere Recovery (wt.%)	Fly ash Recovery (wt.%)	Cenosphere Upgrade
Overflow	1.7	85.7	14.3	75.9	0.1	105.4
Underflow	38.2	0.2	99.8	24.1	99.9	-
Feed	40.2	0.8	99.2	-	-	-

## Chapter 6 - Run 10

### Experiment data

Stream	Total (g/min)	Fly ash (g/min)	Cenosphere (g/min)
Overflow	148.30	0.52	2.46
Underflow	858.90	353.57	0.69
Feed	900.40	356.28	2.88
Wash water	125.00	-	-
in/out	1.02	1.01	0.91

### Balanced data

Stream	Total (g/min)	Fly ash (g/min)	Cenosphere (g/min)
Overflow	148.55	0.52	2.35
Underflow	867.36	354.65	0.68
Feed	891.10	355.18	3.03
Wash water	124.82	-	-
in/out	1.00	1.00	1.00

### Square standard error

	Total	Fly ash	Cenosphere	Sum of errors
Overflow	0.0000	0.0000	0.0020	0.0020
Underflow	0.0001	0.0000	0.0002	0.0003
Feed	0.0001	0.0000	0.0028	0.0029
Wash water	0.0000	-	-	0.0000

Sum \* 100 = 0.5224

### Relative error (%)

	Total	Fly ash	Cenosphere
Overflow	0.17	0.00	-4.52
Underflow	0.99	0.31	-1.27
Feed	-1.03	-0.31	5.29
Wash water	-0.14	-	-

### Results based on balanced data

Stream	Pulp Density (wt.%)	Cenosphere Grade (wt.%)	Fly ash Grade (wt.%)	Cenosphere Recovery (wt.%)	Fly ash Recovery (wt.%)	Cenosphere Upgrade
Overflow	1.9	81.8	18.2	77.5	0.1	96.6
Underflow	41.0	0.2	99.8	22.5	99.9	-
Feed	40.2	0.8	99.2	-	-	-

## Chapter 7 - Run 1

### Experiment data

Stream	Total (g/min)	Fly ash (g/min)	Cenosphere (g/min)
Overflow	1974.50	78.81	45.79
Underflow	13475.60	6224.11	14.96
Feed	15816.60	6190.17	60.71
Wash water	1250.00	-	-
in/out	1.02	0.98	1.00

### Balanced data

Stream	Total (g/min)	Fly ash (g/min)	Cenosphere (g/min)
Overflow	1977.78	78.81	45.77
Underflow	13628.35	6167.43	14.96
Feed	15606.13	6246.23	60.73
Wash water	1250.00	-	-
in/out	1.00	1.00	1.00

### Square standard error

	Total	Fly ash	Cenosphere	Sum of errors
Overflow	0.0000	0.0000	0.0000	0.0000
Underflow	0.0001	0.0001	0.0000	0.0002
Feed	0.0002	0.0001	0.0000	0.0003
Wash water	0.0000	-	-	0.0000

Sum \* 100 = 0.0474

### Relative error (%)

	Total	Fly ash	Cenosphere
Overflow	0.17	-0.01	-0.03
Underflow	1.13	-0.91	-0.01
Feed	-1.33	0.91	0.04
Wash water	0.00	-	-

### Results based on balanced data

Stream	Pulp Density (wt.%)	Cenosphere Grade (wt.%)	Fly ash Grade (wt.%)	Cenosphere Recovery (wt.%)	Fly ash Recovery (wt.%)	Cenosphere Upgrade
Overflow	6.3	36.7	63.3	75.4	1.3	38.2
Underflow	45.4	0.2	99.8	24.6	98.7	-
Feed	40.4	1.0	99.0	-	-	-

## Chapter 7 - Run 2

### Experiment data

Stream	Total (g/min)	Fly ash (g/min)	Cenosphere (g/min)
Overflow	978.50	12.40	30.31
Underflow	15884.60	6213.08	19.00
Feed	15961.80	6077.21	56.84
Wash water	1250.00	-	-
in/out	1.02	0.98	1.15

### Balanced data

Stream	Total (g/min)	Fly ash (g/min)	Cenosphere (g/min)
Overflow	979.15	12.40	31.85
Underflow	16057.23	6137.31	19.60
Feed	15787.46	6149.71	51.45
Wash water	1248.93	-	-
in/out	1.00	1.00	1.00

### Square standard error

	Total	Fly ash	Cenosphere	Sum of errors
Overflow	0.0000	0.0000	0.0026	0.0026
Underflow	0.0001	0.0001	0.0010	0.0013
Feed	0.0001	0.0001	0.0090	0.0093
Wash water	0.0000	-	-	0.0000

Sum \* 100 = 1.3106

### Relative error (%)

	Total	Fly ash	Cenosphere
Overflow	0.07	0.00	5.06
Underflow	1.09	-1.22	3.17
Feed	-1.09	1.19	-9.49
Wash water	-0.09	-	-

### Results based on balanced data

Stream	Pulp Density (wt.%)	Cenosphere Grade (wt.%)	Fly ash Grade (wt.%)	Cenosphere Recovery (wt.%)	Fly ash Recovery (wt.%)	Cenosphere Upgrade
Overflow	4.5	72.0	28.0	61.9	0.2	86.8
Underflow	38.3	0.3	99.7	38.1	99.8	-
Feed	39.3	0.8	99.2	-	-	-

## Chapter 7 - Run 3

### Experiment data

Stream	Total (g/min)	Fly ash (g/min)	Cenosphere (g/min)
Overflow	507.50	3.11	22.65
Underflow	16402.60	6132.68	29.28
Feed	15468.80	5898.15	56.21
Wash water	1250.00	-	-
in/out	0.99	0.96	1.08

### Balanced data

Stream	Total (g/min)	Fly ash (g/min)	Cenosphere (g/min)
Overflow	507.40	3.11	23.14
Underflow	16301.71	6009.23	30.09
Feed	15558.53	6012.34	53.23
Wash water	1250.58	-	-
in/out	1.00	1.00	1.00

### Square standard error

	Total	Fly ash	Cenosphere	Sum of errors
Overflow	0.0000	0.0000	0.0005	0.0005
Underflow	0.0000	0.0004	0.0008	0.0012
Feed	0.0000	0.0004	0.0028	0.0032
Wash water	0.0000	-	-	0.0000

Sum \* 100 = 0.4897

### Relative error (%)

	Total	Fly ash	Cenosphere
Overflow	-0.02	0.00	2.14
Underflow	-0.62	-2.01	2.77
Feed	0.58	1.94	-5.31
Wash water	0.05	-	-

### Results based on balanced data

Stream	Pulp Density (wt.%)	Cenosphere Grade (wt.%)	Fly ash Grade (wt.%)	Cenosphere Recovery (wt.%)	Fly ash Recovery (wt.%)	Cenosphere Upgrade
Overflow	5.2	88.1	11.9	43.5	0.1	100.5
Underflow	37.0	0.5	99.5	56.5	99.9	-
Feed	39.0	0.9	99.1	-	-	-

## Chapter 7 - Run 4

### Experiment data

Stream	Total (g/min)	Fly ash (g/min)	Cenosphere (g/min)
Overflow	2917.20	330.98	54.46
Underflow	18776.00	7787.66	25.43
Feed	20515.00	7943.92	69.39
Wash water	1250.00	-	-
in/out	1.00	0.98	0.87

### Balanced data

Stream	Total (g/min)	Fly ash (g/min)	Cenosphere (g/min)
Overflow	2917.98	330.82	50.77
Underflow	18808.30	7702.10	24.62
Feed	20476.42	8032.93	75.39
Wash water	1249.86	-	-
in/out	1.00	1.00	1.00

### Square standard error

	Total	Fly ash	Cenosphere	Sum of errors
Overflow	0.0000	0.0000	0.0046	0.0046
Underflow	0.0000	0.0001	0.0010	0.0011
Feed	0.0000	0.0001	0.0075	0.0076
Wash water	0.0000	-	-	0.0000

Sum \* 100 = 1.3341

### Relative error (%)

	Total	Fly ash	Cenosphere
Overflow	0.03	-0.05	-6.79
Underflow	0.17	-1.10	-3.17
Feed	-0.19	1.12	8.65
Wash water	-0.01	-	-

### Results based on balanced data

Stream	Pulp Density (wt.%)	Cenosphere Grade (wt.%)	Fly ash Grade (wt.%)	Cenosphere Recovery (wt.%)	Fly ash Recovery (wt.%)	Cenosphere Upgrade
Overflow	13.1	13.3	86.7	67.3	4.1	14.3
Underflow	41.1	0.3	99.7	32.7	95.9	-
Feed	39.6	0.9	99.1	-	-	-

## Chapter 7 - Run 5

### Experiment data

Stream	Total (g/min)	Fly ash (g/min)	Cenosphere (g/min)
Overflow	1235.20	7.60	20.13
Underflow	7924.80	3291.80	8.00
Feed	7924.20	3160.69	29.20
Wash water	1250.00	-	-
in/out	1.00	0.96	1.04

### Balanced data

Stream	Total (g/min)	Fly ash (g/min)	Cenosphere (g/min)
Overflow	1235.37	7.60	20.46
Underflow	7931.73	3219.62	8.05
Feed	7917.27	3227.23	28.51
Wash water	1249.83	-	-
in/out	1.00	1.00	1.00

### Square standard error

	Total	Fly ash	Cenosphere	Sum of errors
Overflow	0.0000	0.0000	0.0003	0.0003
Underflow	0.0000	0.0005	0.0000	0.0005
Feed	0.0000	0.0004	0.0006	0.0010
Wash water	0.0000	-	-	0.0000

Sum \* 100 = 0.1796

### Relative error (%)

	Total	Fly ash	Cenosphere
Overflow	0.01	-0.01	1.63
Underflow	0.09	-2.19	0.65
Feed	-0.09	2.11	-2.37
Wash water	-0.01	-	-

### Results based on balanced data

Stream	Pulp Density (wt.%)	Cenosphere Grade (wt.%)	Fly ash Grade (wt.%)	Cenosphere Recovery (wt.%)	Fly ash Recovery (wt.%)	Cenosphere Upgrade
Overflow	2.3	72.9	27.1	71.8	0.2	83.3
Underflow	40.7	0.2	99.8	28.2	99.8	-
Feed	41.1	0.9	99.1	-	-	-

## Chapter 7 - Run 6

### Experiment data

Stream	Total (g/min)	Fly ash (g/min)	Cenosphere (g/min)
Overflow	2620.00	212.96	41.94
Underflow	13963.40	5820.98	10.89
Feed	15496.80	6017.97	54.63
Wash water	1250.00	-	-
in/out	1.01	1.00	1.03

### Balanced data

Stream	Total (g/min)	Fly ash (g/min)	Cenosphere (g/min)
Overflow	2622.53	212.95	42.60
Underflow	14035.21	5813.26	10.93
Feed	15408.32	6026.21	53.53
Wash water	1249.42	-	-
in/out	1.00	1.00	1.00

### Square standard error

	Total	Fly ash	Cenosphere	Sum of errors
Overflow	0.0000	0.0000	0.0002	0.0002
Underflow	0.0000	0.0000	0.0000	0.0000
Feed	0.0000	0.0000	0.0004	0.0004
Wash water	0.0000	-	-	0.0000

Sum \* 100 = 0.0731

### Relative error (%)

	Total	Fly ash	Cenosphere
Overflow	0.10	0.00	1.55
Underflow	0.51	-0.13	0.40
Feed	-0.57	0.14	-2.02
Wash water	-0.05	-	-

### Results based on balanced data

Stream	Pulp Density (wt.%)	Cenosphere Grade (wt.%)	Fly ash Grade (wt.%)	Cenosphere Recovery (wt.%)	Fly ash Recovery (wt.%)	Cenosphere Upgrade
Overflow	9.7	16.7	83.3	79.6	3.5	18.9
Underflow	41.5	0.2	99.8	20.4	96.5	-
Feed	39.5	0.9	99.1	-	-	-

## Chapter 8 - Run 1

### Experiment data

Stream	Total (g/min)	Fly ash (g/min)	Cenosphere (g/min)
Overflow	388.80	24.60	0.93
Underflow	816.20	327.40	0.20
Feed	1080.60	354.80	1.22
Wash water	125.00	-	-
in/out	1.00	1.01	1.08

### Balanced data

Stream	Total (g/min)	Fly ash (g/min)	Cenosphere (g/min)
Overflow	388.85	24.61	0.96
Underflow	816.40	328.68	0.20
Feed	1080.25	353.29	1.17
Wash water	125.00	-	-
in/out	1.00	1.00	1.00

### Square standard error

	Total	Fly ash	Cenosphere	Sum of errors
Overflow	0.0000	0.0000	0.0013	0.0013
Underflow	0.0000	0.0000	0.0001	0.0001
Feed	0.0000	0.0000	0.0022	0.0023
Wash water	0.0000	-	-	0.0000

Sum \* 100 = 0.3634

### Relative error (%)

	Total	Fly ash	Cenosphere
Overflow	0.01	0.03	3.60
Underflow	0.02	0.39	0.78
Feed	-0.03	-0.43	-4.74
Wash water	0.00	-	-

### Results based on balanced data

Stream	Pulp Density (wt.%)	Cenosphere Grade (wt.%)	Fly ash Grade (wt.%)	Cenosphere Recovery (wt.%)	Fly ash Recovery (wt.%)	Cenosphere Upgrade
Overflow	6.6	3.8	96.2	82.5	7.0	11.4
Underflow	40.3	0.1	99.9	17.5	93.0	-
Feed	32.8	0.3	99.7	-	-	-

## Chapter 8 - Run 2

### Experiment data

Stream	Total (g/min)	Fly ash (g/min)	Cenosphere (g/min)
Overflow	366.20	4.87	1.25
Underflow	769.00	54.57	0.34
Feed	989.80	59.47	1.80
Wash water	125.00	-	-
in/out	0.98	1.00	1.13

### Balanced data

Stream	Total (g/min)	Fly ash (g/min)	Cenosphere (g/min)
Overflow	364.61	4.87	1.32
Underflow	761.99	54.59	0.34
Feed	1001.41	59.46	1.66
Wash water	125.19	-	-
in/out	1.00	1.00	1.00

### Square standard error

	Total	Fly ash	Cenosphere	Sum of errors
Overflow	0.0000	0.0000	0.0029	0.0029
Underflow	0.0001	0.0000	0.0002	0.0003
Feed	0.0001	0.0000	0.0059	0.0060
Wash water	0.0000	-	-	0.0000

Sum \* 100 = 0.9218

### Relative error (%)

	Total	Fly ash	Cenosphere
Overflow	-0.43	0.00	5.34
Underflow	-0.91	0.02	1.45
Feed	1.17	-0.03	-7.69
Wash water	0.15	-	-

### Results based on balanced data

Stream	Pulp Density (wt.%)	Cenosphere Grade (wt.%)	Fly ash Grade (wt.%)	Cenosphere Recovery (wt.%)	Fly ash Recovery (wt.%)	Cenosphere Upgrade
Overflow	1.7	21.3	78.7	79.3	8.2	7.8
Underflow	7.2	0.6	99.4	20.7	91.8	-
Feed	6.1	2.7	97.3	-	-	-

## Chapter 8 – Run 3 (is the same as Chapter 7 – Run 6)

### Chapter 8 - Run 4

#### Experiment data

Stream	Total (g/min)	Fly ash (g/min)	Cenosphere (g/min)
Overflow	331.60	1.45	4.78
Underflow	370.00	49.86	2.20
Feed	576.40	52.56	7.63
Wash water	125.00	-	-
in/out	1.00	1.02	1.09

#### Balanced data

Stream	Total (g/min)	Fly ash (g/min)	Cenosphere (g/min)
Overflow	331.56	1.45	4.95
Underflow	369.95	50.45	2.24
Feed	576.51	51.90	7.19
Wash water	125.01	-	-
in/out	1.00	1.00	1.00

#### Square standard error

	Total	Fly ash	Cenosphere	Sum of errors
Overflow	0.0000	0.0000	0.0013	0.0013
Underflow	0.0000	0.0001	0.0003	0.0004
Feed	0.0000	0.0002	0.0033	0.0035
Wash water	0.0000	-	-	0.0000

Sum \* 100 = 0.5191

#### Relative error (%)

	Total	Fly ash	Cenosphere
Overflow	-0.01	0.03	3.61
Underflow	-0.01	1.18	1.66
Feed	0.02	-1.24	-5.76
Wash water	0.00	-	-

#### Results based on balanced data

Stream	Pulp Density (wt.%)	Cenosphere Grade (wt.%)	Fly ash Grade (wt.%)	Cenosphere Recovery (wt.%)	Fly ash Recovery (wt.%)	Cenosphere Upgrade
Overflow	1.9	77.3	22.7	68.9	2.8	6.4
Underflow	14.2	4.2	95.8	31.1	97.2	-
Feed	10.2	12.2	87.8	-	-	-

## Chapter 8 - Run 5

### Experiment data

Stream	Total (g/min)	Fly ash (g/min)	Cenosphere (g/min)
Overflow	49.30	0.11	3.71
Underflow	309.05	0.70	0.30
Feed	253.40	0.93	3.32
Wash water	105.00	-	-
in/out	1.00	1.15	0.83

### Balanced data

Stream	Total (g/min)	Fly ash (g/min)	Cenosphere (g/min)
Overflow	49.30	0.11	3.33
Underflow	309.08	0.75	0.30
Feed	253.38	0.86	3.62
Wash water	105.00	-	-
in/out	1.00	1.00	1.00

### Square standard error

	Total	Fly ash	Cenosphere	Sum of errors
Overflow	0.0000	0.0001	0.0108	0.0109
Underflow	0.0000	0.0038	0.0001	0.0038
Feed	0.0000	0.0065	0.0086	0.0152
Wash water	0.0000	-	-	0.0000

Sum \* 100 = 2.9866

### Relative error (%)

	Total	Fly ash	Cenosphere
Overflow	0.00	0.92	-10.39
Underflow	0.01	6.13	-0.84
Feed	-0.01	-8.09	9.28
Wash water	0.00	-	-

### Results based on balanced data

Stream	Pulp Density (wt.%)	Cenosphere Grade (wt.%)	Fly ash Grade (wt.%)	Cenosphere Recovery (wt.%)	Fly ash Recovery (wt.%)	Cenosphere Upgrade
Overflow	7.0	96.9	3.1	91.8	12.5	1.2
Underflow	0.3	28.4	71.6	8.2	87.5	-
Feed	1.8	80.9	19.1	-	-	-

## Chapter 8 - Run 6

### Experiment data

Stream	Total (g/min)	Fly ash (g/min)	Cenosphere (g/min)
Overflow	110.67	0.29	3.68
Underflow	241.80	0.57	0.18
Feed	243.80	1.16	4.10
Wash water	105.00	-	-
in/out	0.99	1.35	1.06

### Balanced data

Stream	Total (g/min)	Fly ash (g/min)	Cenosphere (g/min)
Overflow	110.35	0.31	3.78
Underflow	240.28	0.62	0.18
Feed	245.34	0.93	3.97
Wash water	105.29	-	-
in/out	1.00	1.00	1.00

### Square standard error

	Total	Fly ash	Cenosphere	Sum of errors
Overflow	0.0000	0.0025	0.0008	0.0034
Underflow	0.0000	0.0096	0.0000	0.0096
Feed	0.0000	0.0404	0.0011	0.0415
Wash water	0.0000	-	-	0.0000

Sum \* 100 = 5.4565

### Relative error (%)

	Total	Fly ash	Cenosphere
Overflow	-0.29	5.05	2.91
Underflow	-0.63	9.80	0.15
Feed	0.63	-20.10	-3.25
Wash water	0.27	-	-

### Results based on balanced data

Stream	Pulp Density (wt.%)	Cenosphere Grade (wt.%)	Fly ash Grade (wt.%)	Cenosphere Recovery (wt.%)	Fly ash Recovery (wt.%)	Cenosphere Upgrade
Overflow	3.7	92.5	7.5	95.4	33.0	1.1
Underflow	0.3	22.8	77.2	4.6	67.0	-
Feed	2.0	81.0	19.0	-	-	-

## Chapter 8 - Run 7

### Experiment data

Stream	Total (g/min)	Fly ash (g/min)	Cenosphere (g/min)
Overflow	191.33	0.39	2.88
Underflow	169.80	0.60	0.16
Feed	243.70	1.05	3.71
Wash water	105.00	-	-
in/out	0.97	1.05	1.22

### Balanced data

Stream	Total (g/min)	Fly ash (g/min)	Cenosphere (g/min)
Overflow	187.98	0.40	3.13
Underflow	167.16	0.61	0.16
Feed	249.14	1.01	3.29
Wash water	106.01	-	-
in/out	1.00	1.00	1.00

### Square standard error

	Total	Fly ash	Cenosphere	Sum of errors
Overflow	0.0003	0.0002	0.0076	0.0081
Underflow	0.0002	0.0004	0.0000	0.0007
Feed	0.0005	0.0012	0.0127	0.0143
Wash water	0.0001	-	-	0.0001

Sum \* 100 = 2.3204

### Relative error (%)

	Total	Fly ash	Cenosphere
Overflow	-1.75	1.29	8.75
Underflow	-1.55	1.97	0.47
Feed	2.23	-3.43	-11.26
Wash water	0.96	-	-

### Results based on balanced data

Stream	Pulp Density (wt.%)	Cenosphere Grade (wt.%)	Fly ash Grade (wt.%)	Cenosphere Recovery (wt.%)	Fly ash Recovery (wt.%)	Cenosphere Upgrade
Overflow	1.9	88.7	11.3	95.2	39.4	1.2
Underflow	0.5	20.4	79.6	4.8	60.6	-
Feed	1.7	76.5	23.5	-	-	-

**Chapter 9 - Run 1 (is the same as Chapter 5 - Run 10)**

**Chapter 9 - Run 2 (is the same as Chapter 6 – Run 7)**

**Chapter 9 - Run 3**

**Experiment data**

Stream	Total (g/min)	Fly ash (g/min)	Cenosphere (g/min)
Overflow	187.25	1.88	7.09
Underflow	1732.40	678.86	0.58
Feed	1808.60	694.32	8.29
Wash water	150.00	-	-
in/out	1.02	1.02	1.08

**Balanced data**

Stream	Total (g/min)	Fly ash (g/min)	Cenosphere (g/min)
Overflow	187.47	1.88	7.35
Underflow	1750.87	685.50	0.58
Feed	1788.47	687.37	7.93
Wash water	149.86	-	-
in/out	1.00	1.00	1.00

**Square standard error**

	Total	Fly ash	Cenosphere	Sum of errors
Overflow	0.0000	0.0000	0.0013	0.0014
Underflow	0.0001	0.0001	0.0000	0.0002
Feed	0.0001	0.0001	0.0018	0.0021
Wash water	0.0000	-	-	0.0000

**Sum \* 100 = 0.3639**

**Relative error (%)**

	Total	Fly ash	Cenosphere
Overflow	0.12	0.00	3.67
Underflow	1.07	0.98	0.30
Feed	-1.11	-1.00	-4.30
Wash water	-0.09	-	-

**Results based on balanced data**

Stream	Pulp Density (wt.%)	Cenosphere Grade (wt.%)	Fly ash Grade (wt.%)	Cenosphere Recovery (wt.%)	Fly ash Recovery (wt.%)	Cenosphere Upgrade
Overflow	4.9	79.7	20.3	92.6	0.3	69.8
Underflow	39.2	0.1	99.9	7.4	99.7	-
Feed	38.9	1.1	98.9	-	-	-

## Appendix B: IRC™ raw experimental data and results (grade and recovery by pycnometry)

In this set of runs, samples taken from all the streams were placed in an oven to be dried. Then the density of the dried solids was measured using the gas pycnometer. From the density of solids and the known densities of pure dense fly ash and cenospheres, the percentage of each component (i.e. cenospheres and fly ash) was calculated. The density of fly ash in the product varied depending on the experimental conditions, and hence a sensitivity analysis was applied. The complete procedure of this method was explained in Chapter 5. The sample calculations from this set of runs are presented in Appendix H.

### Chapter 5 - Run 10 -pycnometry

#### Raw experimental data

	Feed	Product	Fluidization water
Volumetric rate (m <sup>3</sup> /(m <sup>2</sup> h))	7.0	1.4	0.87
Solids weight (g)	328.1	1.3	-
Total solids average density (kg/m <sup>3</sup> )	1860.0	980.0	-
Cenospheres average density (kg/m <sup>3</sup> )	775.0	775.0	-
Dense fly ash average density (kg/m <sup>3</sup> )	1873.0	Varied	-

#### Sensitivity analysis results

Product fly ash density (kg/m <sup>3</sup> )	Product grade (wt.%)	Recovery (wt.%)
1600	59.4	46.4
1700	61.6	48.1
1800	63.3	49.4
1830	63.7	49.8

## Chapter 5 - Run 11 - pycnometry

### Raw experimental data

	Feed	Product	Fluidization water
Volumetric rate (m <sup>3</sup> /(m <sup>2</sup> h))	7.7	2.7	0.87
Solids weight (g)	368.3	16.3	
Total solids average density (kg/m <sup>3</sup> )	1853.0	1276.0	
Cenospheres average density (kg/m <sup>3</sup> )	775.0	775.0	
Dense fly ash average density (kg/m <sup>3</sup> )	1873.0	Varied	

### Sensitivity analysis results

Product fly ash density (kg/m <sup>3</sup> )	Product grade (wt.%)	Recovery (wt.%)
1600	23.8	57.0
1700	27.8	66.5
1800	31.1	74.2
1830	31.9	76.2

---

## Chapter 5 - Run 12 - pycnometry

### Raw experimental data

	Feed	Product	Fluidization water
Volumetric rate (m <sup>3</sup> /(m <sup>2</sup> h))	7.0	2.8	0.35
Solids weight (g)	487.4	23.4	
Total solids average density (kg/m <sup>3</sup> )	1854.3	1626.4	
Cenospheres average density (kg/m <sup>3</sup> )	775.0	775.0	
Dense fly ash average density (kg/m <sup>3</sup> )	1873.0	Varied	

### Sensitivity analysis results

Product fly ash density (kg/m <sup>3</sup> )	Product grade (wt.%)	Recovery (wt.%)
1600	-	-
1700	3.8	38.3
1800	8.1	81.6
1830	9.2	93.0

## Chapter 5 - Run 13 - pycnometry

### Raw experimental data

	Feed	Product	Fluidization water
Volumetric rate (m <sup>3</sup> /(m <sup>2</sup> h))	7.0	2.8	1.7
Solids weight (g)	479.7	1.0	
Total solids average density (kg/m <sup>3</sup> )	1845.0	941.9	
Cenospheres average density (kg/m <sup>3</sup> )	775.0	775.0	
Dense fly ash average density (kg/m <sup>3</sup> )	1873.0	Varied	

### Sensitivity analysis results

Product fly ash density (kg/m <sup>3</sup> )	Product grade (wt.%)	Recovery (wt.%)
1600	65.6	28.8
1700	67.4	29.6
1800	68.9	30.3
1830	69.3	30.4

## Chapter 5 - Run 14 - pycnometry

### Raw experimental data

	Feed	Product	Fluidization water
Volumetric rate (m <sup>3</sup> /(m <sup>2</sup> h))	7.0	2.8	2.8
Solids weight (g)	471.0	1.5	
Total solids average density (kg/m <sup>3</sup> )	1852.5	856.0	
Cenospheres average density (kg/m <sup>3</sup> )	775.0	775.0	
Dense fly ash average density (kg/m <sup>3</sup> )	1873.0	Varied	

### Sensitivity analysis results

Product fly ash density (kg/m <sup>3</sup> )	Product grade (wt.%)	Recovery (wt.%)
1600	81.7	25.0
1700	82.6	25.3
1800	83.4	25.6
1830	83.6	25.6

## Chapter 5 - Run 15 - pycnometry

### Raw experimental data

	Feed	Product	Fluidization water
Volumetric rate (m <sup>3</sup> /(m <sup>2</sup> h))	3.6	0.7	0.87
Solids weight (g)	187.8	0.8	
Total solids average density (kg/m <sup>3</sup> )	1856.0	800.0	
Cenospheres average density (kg/m <sup>3</sup> )	775.0	775.0	
Dense fly ash average density (kg/m <sup>3</sup> )	1873.0	Varied	

### Sensitivity analysis results

Product fly ash density (kg/m <sup>3</sup> )	Product grade (wt.%)	Recovery (wt.%)
1600	93.9	21.5
1700	94.3	21.6
1800	94.5	21.6
1830	94.6	21.7

## Chapter 5 - Run 16 - pycnometry

### Raw experimental data

	Feed	Product	Fluidization water
Volumetric rate (m <sup>3</sup> /(m <sup>2</sup> h))	13.9	2.8	0.87
Solids weight (g)	373.4	43.5	
Total solids average density (kg/m <sup>3</sup> )	1859.8	1704.4	
Cenospheres average density (kg/m <sup>3</sup> )	775.0	775.0	
Dense fly ash average density (kg/m <sup>3</sup> )	1873.0	Varied	

### Sensitivity analysis results

Product fly ash density (kg/m <sup>3</sup> )	Product grade (wt.%)	Recovery (wt.%)
1600	-	-
1700	-	-
1800	4.2	49.2
1830	5.4	62.9

## Chapter 5 - Run 17 - pycnometry

### Raw experimental data

	Feed	Product	Fluidization water
Volumetric rate (m <sup>3</sup> /(m <sup>2</sup> h))	3.8	1.4	0.87
Solids weight (g)	199.7	1.4	
Total solids average density (kg/m <sup>3</sup> )	1856.0	891.0	
Cenospheres average density (kg/m <sup>3</sup> )	775.0	775.0	
Dense fly ash average density (kg/m <sup>3</sup> )	1873.0	Varied	

### Sensitivity analysis results

Product fly ash density (kg/m <sup>3</sup> )	Product grade (wt.%)	Recovery (wt.%)
1600	74.8	30.6
1700	76.1	31.1
1800	77.1	31.6
1830	77.4	31.7

---

## Chapter 5 - Run 18 - pycnometry

### Raw experimental data

	Feed	Product	Fluidization water
Volumetric rate (m <sup>3</sup> /(m <sup>2</sup> h))	9.8	2.1	0.87
Solids weight (g)	263.9	6.7	
Total solids average density (kg/m <sup>3</sup> )	1857.0	1370.0	
Cenospheres average density (kg/m <sup>3</sup> )	775.0	775.0	
Dense fly ash average density (kg/m <sup>3</sup> )	1873.0	Varied	

### Sensitivity analysis results

Product fly ash density (kg/m <sup>3</sup> )	Product grade (wt.%)	Recovery (wt.%)
1600	15.8	65.9
1700	20.2	84.3
1800	23.7	99.2
1830	24.7	100.0

## Chapter 5 - Run 19 - pycnometry

### Raw experimental data

	Feed	Product	Fluidization water
Volumetric rate (m <sup>3</sup> /(m <sup>2</sup> h))	9.9	4.5	0.87
Solids weight (g)	258.4	51.2	
Total solids average density (kg/m <sup>3</sup> )	1854.0	1759.0	
Cenospheres average density (kg/m <sup>3</sup> )	775.0	775.0	
Dense fly ash average density (kg/m <sup>3</sup> )	1873.0	Varied	

### Sensitivity analysis results

Product fly ash density (kg/m <sup>3</sup> )	Product grade (wt.%)	Recovery (wt.%)
1600	-	-
1700	-	-
1800	1.8	48.3
1830	3.0	81.2

---

## Chapter 5 - Run 20 - pycnometry

### Raw experimental data

	Feed	Product	Fluidization water
Volumetric rate (m <sup>3</sup> /(m <sup>2</sup> h))	12.6	5.3	0.87
Solids weight (g)	346.4	71.3	
Total solids average density (kg/m <sup>3</sup> )	1854.0	1775.0	
Cenospheres average density (kg/m <sup>3</sup> )	775.0	775.0	
Dense fly ash average density (kg/m <sup>3</sup> )	1873.0	Varied	

### Sensitivity analysis results

Product fly ash density (kg/m <sup>3</sup> )	Product grade (wt.%)	Recovery (wt.%)
1600	-	-
1700	-	-
1800	1.1	30.3
1830	2.3	64.8

## **Appendix C: Size distribution data and partition numbers**

In this section, the size distribution raw data used in different chapters is presented. They are mainly the size data of the cenosphere (floats) component, however a few sets of fly ash size data are also shown. This section also shows the results of applying the “mass” balance reconciliation technique to the size data and the yield to product value (strictly speaking it is actually a “volume” balance that is used, not a mass balance). Again, the numbers in the red cells are adjusted in order to minimize the sum of square standard error (blue cell). The SSE column shows the sum of square standard errors for product, tailings and feed in that size interval. Using this error minimization method, balanced data was obtained and then used to calculate partition numbers. Sample calculations from this set of data are shown in Appendix H.

Chapter 5 – Run 1 (Raw and mass balanced cenospheres size distribution)

Size (µm)		Raw data size distribution (vol.%)			Raw data - volume frequency (%/Δµm)			Balanced data size distribution (vol.%)				
Size Interval	Average size	Product	Tailings	Feed	Product	Tailings	Feed	Product	Tailings	Feed	Partition number	SSE
5.75	5.38	0.00	0.00	0.00	0.00	0.00	0.00	0.00	0.00	0.00		
6.61	6.18	0.00	0.02	0.00	0.00	0.03	0.00	0.00	0.02	0.01	0.00	
7.59	7.10	0.00	0.47	0.01	0.00	0.48	0.01	0.00	0.04	0.01	0.00	0.00
8.71	8.15	0.00	1.46	0.33	0.00	1.30	0.29	0.00	1.16	0.38	0.00	0.83
10.00	9.35	0.00	2.95	0.78	0.00	2.29	0.61	0.00	2.60	0.85	0.00	0.06
11.48	10.74	0.00	4.90	1.54	0.00	3.31	1.04	0.00	4.77	1.55	0.00	0.02
13.18	12.33	0.00	7.09	2.57	0.00	4.17	1.51	0.00	7.36	2.40	0.00	0.00
15.14	14.16	0.04	9.28	3.90	0.02	4.75	2.00	0.04	10.09	3.31	0.01	0.01
17.38	16.26	0.42	11.06	5.43	0.19	4.93	2.42	0.42	12.23	4.27	0.07	0.03
19.95	18.67	1.91	12.15	7.06	0.74	4.72	2.74	2.01	13.08	5.62	0.24	0.06
22.91	21.43	4.81	12.29	8.60	1.63	4.16	2.91	5.23	12.47	7.59	0.46	0.05
26.30	24.61	9.11	11.43	9.86	2.68	3.37	2.91	9.71	10.90	10.10	0.65	0.02
30.20	28.25	13.70	9.75	10.65	3.52	2.50	2.73	13.68	9.03	12.16	0.76	0.01
34.67	32.44	17.00	7.55	10.82	3.80	1.69	2.42	15.91	7.01	13.01	0.82	0.03
39.81	37.24	17.57	5.23	10.32	3.42	1.02	2.01	16.11	4.96	12.47	0.87	0.05
45.71	42.76	15.13	3.13	9.17	2.57	0.53	1.56	14.39	3.04	10.69	0.91	0.05
52.48	49.09	10.74	1.23	7.54	1.59	0.18	1.11	11.20	1.23	7.95	0.95	0.03
60.26	56.37	6.12	0.02	5.64	0.79	0.00	0.73	7.12	0.02	4.80	1.00	0.00
69.18	64.72	2.64	0.00	3.72	0.30	0.00	0.42	3.22	0.00	2.17	1.00	0.05
79.43	74.31	0.77	0.00	1.87	0.08	0.00	0.18	0.92	0.00	0.62	1.00	0.22
91.20	85.32	0.04	0.00	0.17	0.00	0.00	0.01	0.05	0.00	0.03	1.00	0.48
104.71	97.96	0.00	0.00	0.00	0.00	0.00	0.00	0.00	0.00	0.00		0.66
<b>Sum</b>		<b>100</b>	<b>100</b>	<b>100</b>				<b>100</b>	<b>100</b>	<b>100</b>		<b>2.66</b>
<b>Yield to Product</b>		<b>0.674</b>										

<b>Relative errors (%)</b>											
<b>average size</b>	Product	Tailings	Feed	<b>average size</b>	Product	Tailings	Feed	<b>average size</b>	Product	Tailings	Feed
<b>2.35</b>	0.00	0.00	0.00	<b>10.74</b>	0.00	-2.80	1.18	<b>49.09</b>	4.29	-0.69	5.42
<b>2.70</b>	0.00	0.00	0.00	<b>12.33</b>	0.00	3.81	-6.76	<b>56.37</b>	16.28	0.01	-14.86
<b>3.10</b>	0.00	0.00	0.00	<b>14.16</b>	0.13	8.72	-15.16	<b>64.72</b>	22.21	0.00	-41.66
<b>3.56</b>	0.00	0.00	0.00	<b>16.26</b>	1.47	10.58	-21.37	<b>74.31</b>	19.30	0.00	-66.71
<b>4.08</b>	0.00	0.00	0.00	<b>18.67</b>	5.42	7.65	-20.49	<b>85.32</b>	14.19	0.00	-79.73
<b>4.69</b>	0.00	0.00	0.00	<b>21.43</b>	8.72	1.49	-11.76	<b>97.96</b>	0.00	0.00	0.00
<b>5.38</b>	0.00	0.00	0.00	<b>24.61</b>	6.58	-4.62	2.37				
<b>6.18</b>	0.00	-0.01	0.00	<b>28.25</b>	-0.18	-7.41	14.19				
<b>7.10</b>	0.00	-90.82	7.77	<b>32.44</b>	-6.39	-7.06	20.23				
<b>8.15</b>	0.00	-20.84	14.09	<b>37.24</b>	-8.34	-5.15	20.88				
<b>9.35</b>	0.00	-11.68	8.73	<b>42.76</b>	-4.95	-2.85	16.49				

Chapter 5 - Run 2 (Raw and mass balanced cenospheres size distribution)

Size ( $\mu\text{m}$ )		Raw data size distribution (vol.%)			Raw data - volume frequency ( $\%/\Delta\mu\text{m}$ )			Balanced data size distribution (vol.%)				
Size Interval	Average size	Product	Tailings	Feed	Product	Tailings	Feed	Product	Tailings	Feed	Partition number	SSE
5.21	5.57	0.00	0.01	0.39	0.00	0.01	0.55	0.58	0.01	0.39		0.00
5.92	6.32	0.00	0.16	0.40	0.00	0.17	0.50	0.00	0.11	0.04	0.00	0.84
6.72	7.18	0.00	1.18	0.40	0.00	1.05	0.43	0.00	0.60	0.20	0.00	0.29
7.64	8.16	0.00	2.61	0.43	0.00	2.03	0.41	0.00	1.38	0.46	0.00	0.01
8.68	9.27	0.00	4.61	0.53	0.00	3.11	0.45	0.00	1.91	0.63	0.00	0.17
9.86	10.53	0.00	6.88	0.78	0.00	4.04	0.58	0.00	2.83	0.93	0.00	0.23
11.20	11.95	0.00	9.19	1.23	0.00	4.71	0.82	0.00	4.41	1.46	0.00	0.17
12.70	13.60	0.00	11.11	1.94	0.00	4.96	1.08	0.00	6.55	2.16	0.00	0.05
14.50	15.45	0.21	12.33	2.94	0.11	4.79	1.55	0.06	9.18	3.07	0.01	0.01
16.40	17.55	0.84	12.56	4.21	0.36	4.25	1.83	0.84	11.22	4.27	0.13	0.00
18.70	19.95	2.03	11.74	5.66	0.81	3.46	2.26	2.07	12.21	5.42	0.26	0.00
21.20	22.65	3.77	10.04	7.15	1.30	2.58	2.47	3.94	12.35	6.72	0.39	0.01
24.10	25.75	5.94	7.77	8.50	1.80	1.74	2.58	6.34	11.14	7.92	0.54	0.01
27.40	29.25	8.25	5.37	9.52	2.23	1.05	2.57	8.88	9.38	9.04	0.66	0.01
31.10	33.20	10.33	3.19	10.04	2.46	0.54	2.39	11.08	7.36	9.85	0.75	0.01
35.30	37.70	11.81	1.23	9.95	2.46	0.18	2.07	12.55	4.92	10.03	0.84	0.00
40.10	42.85	12.40	0.01	9.25	2.25	0.00	1.68	12.87	2.96	9.60	0.90	0.00
45.60	48.70	11.98	0.00	8.02	1.93	0.00	1.29	12.03	1.49	8.54	0.94	0.00
51.80	55.35	10.61	0.00	6.44	1.49	0.00	0.91	10.36	0.00	6.94	1.00	0.01
58.90	62.90	8.57	0.00	4.73	1.07	0.00	0.59	7.84	0.00	5.25	1.00	0.02
66.90	71.45	6.21	0.00	3.13	0.68	0.00	0.34	5.31	0.00	3.56	1.00	0.04
76.00	81.20	3.95	0.00	1.79	0.38	0.00	0.17	3.10	0.00	2.08	1.00	0.07
86.40	92.25	2.10	0.00	0.84	0.18	0.00	0.07	1.48	0.00	0.99	1.00	0.12
98.10	104.55	0.84	0.00	0.27	0.06	0.00	0.02	0.49	0.00	0.33	1.00	0.22
111.00	119.00	0.19	0.00	0.00	0.01	0.00	0.00	0.19	0.00	0.12	1.00	0.00
<b>Sum</b>		<b>100</b>	<b>100</b>	<b>100</b>				<b>100</b>	<b>100</b>	<b>100</b>		<b>2.28</b>
<b>Yield to Product</b>		<b>0.67</b>										

Relative errors (%)											
average size	Product	Tailings	Feed	average size	Product	Tailings	Feed	average size	Product	Tailings	Feed
<b>5.57</b>	0.00	-0.01	0.34	<b>17.55</b>	0.30	-4.94	1.37	<b>55.35</b>	-2.37	0.00	7.73
<b>6.32</b>	0.00	7.49	-91.12	<b>19.95</b>	2.20	-0.76	-4.27	<b>62.90</b>	-8.43	0.00	11.05
<b>7.18</b>	0.00	20.58	-50.21	<b>22.65</b>	4.34	-0.38	-6.08	<b>71.45</b>	-14.48	0.00	13.63
<b>8.16</b>	0.00	-7.74	6.31	<b>25.75</b>	6.63	-0.53	-6.79	<b>81.20</b>	-21.41	0.00	16.06
<b>9.27</b>	0.00	-36.38	18.96	<b>29.25</b>	7.70	-1.31	-5.00	<b>92.25</b>	-29.29	0.00	18.24
<b>10.53</b>	0.00	-43.43	19.78	<b>33.20</b>	7.28	-1.88	-1.85	<b>104.55</b>	-41.98	0.00	20.45
<b>11.95</b>	0.00	-36.96	18.51	<b>37.70</b>	6.25	-1.69	0.77	<b>119.00</b>	0.11	0.00	0.00
<b>13.60</b>	0.00	-18.15	11.49	<b>42.85</b>	3.82	-1.34	3.77				
<b>15.45</b>	-71.87	-8.17	4.50	<b>48.70</b>	0.42	-0.88	6.54				

Chapter 5- Run 3 (Raw and mass balanced cenospheres size distribution)

Size (µm)		Raw data size distribution (vol.%)			Raw data - volume frequency (%/Δµm)			Balanced data size distribution (vol.%)				
Size Interval	Average size	Product	Tailings	Feed	Product	Tailings	Feed	Product	Tailings	Feed	Partition number	SSE
5.75	5.38	0.00	0.00	0.11	0.00	0.00	0.15	0.00	0.00	0.00		
6.61	6.18	0.00	0.00	0.06	0.00	0.00	0.07	0.00	0.00	0.00		
7.59	7.10	0.00	0.01	0.08	0.00	0.01	0.08	0.00	0.01	0.01	0.00	0.87
8.71	8.15	0.00	0.45	0.22	0.00	0.40	0.20	0.00	0.50	0.19	0.00	0.03
10.00	9.35	0.00	1.46	0.55	0.00	1.13	0.43	0.00	1.44	0.56	0.00	0.00
11.48	10.74	0.00	3.19	1.14	0.00	2.15	0.77	0.00	3.05	1.18	0.00	0.00
13.18	12.33	0.00	5.52	2.00	0.00	3.24	1.17	0.00	5.33	2.06	0.00	0.00
15.14	14.16	0.00	8.26	3.17	0.00	4.23	1.63	0.00	8.22	3.17	0.00	0.00
17.38	16.26	0.09	10.87	4.60	0.04	4.85	2.05	0.09	11.24	4.39	0.01	0.00
19.95	18.67	0.82	12.86	6.20	0.32	5.00	2.41	0.83	13.53	5.74	0.09	0.01
22.91	21.43	2.81	13.71	7.81	0.95	4.64	2.64	2.90	14.23	7.27	0.24	0.01
26.30	24.61	6.40	13.18	9.26	1.88	3.88	2.73	6.65	13.15	9.16	0.45	0.00
30.20	28.25	11.04	11.39	10.31	2.83	2.92	2.64	11.18	10.94	11.09	0.62	0.01
34.67	32.44	15.40	8.74	10.79	3.44	1.95	2.41	14.83	8.30	12.31	0.74	0.02
39.81	37.24	17.72	5.85	10.59	3.45	1.14	2.06	16.52	5.62	12.31	0.82	0.03
45.71	42.76	16.97	3.28	9.69	2.88	0.56	1.64	16.01	3.21	11.07	0.89	0.02
52.48	49.09	13.48	1.22	8.21	1.99	0.18	1.21	13.55	1.21	8.79	0.95	0.00
60.26	56.37	8.77	0.01	6.37	1.13	0.00	0.82	9.69	0.01	5.95	1.00	0.02
69.18	64.72	4.49	0.00	4.38	0.50	0.00	0.49	5.33	0.00	3.27	1.00	0.10
79.43	74.31	1.75	0.00	2.63	0.17	0.00	0.26	2.12	0.00	1.30	1.00	0.30
91.20	85.32	0.25	0.00	0.28	0.02	0.00	0.02	0.30	0.00	0.18	1.00	0.16
104.71	97.96	0.01	0.00	0.00	0.00	0.00	0.00	0.00	0.00	0.00		
<b>Sum</b>		100.0	100.0	98.5				<b>100</b>	<b>100</b>	<b>100</b>		<b>1.59</b>
<b>Yield to Product</b>		<b>0.614</b>										

Relative errors (%)							
average size	Product	Tailings	Feed	average size	Product	Tailings	Feed
<b>5.38</b>	0.00	0.00	0.00	<b>24.61</b>	4.04	-0.26	-1.03
<b>6.18</b>	0.00	0.00	0.00	<b>28.25</b>	1.24	-3.95	7.56
<b>7.10</b>	0.00	6.03	-93.13	<b>32.44</b>	-3.69	-4.97	14.11
<b>8.15</b>	0.00	10.05	-12.71	<b>37.24</b>	-6.77	-3.85	16.30
<b>9.35</b>	0.00	-1.31	1.19	<b>42.76</b>	-5.67	-2.06	14.17
<b>10.74</b>	0.00	-4.29	3.77	<b>49.09</b>	0.54	-0.48	6.99
<b>12.33</b>	0.00	-3.48	2.94	<b>56.37</b>	10.49	0.00	-6.59
<b>14.16</b>	0.00	-0.47	-0.05	<b>64.72</b>	18.52	0.00	-25.42
<b>16.26</b>	0.10	3.37	-4.45	<b>74.31</b>	21.55	0.00	-50.44
<b>18.67</b>	1.08	5.20	-7.52	<b>85.32</b>	19.23	0.00	-35.03
<b>21.43</b>	3.10	3.81	-6.90	<b>97.96</b>	0.00	0.00	0.00

**Chapter 5 - Run 9 (Raw and mass balanced cenospheres size distribution)**

Size ( $\mu\text{m}$ )		Raw data size distribution (vol.%)			Raw data - volume frequency ( $\%/\Delta\mu\text{m}$ )			Balanced data size distribution (vol.%)				
Size Interval	Average size	Product	Tailings	Feed	Product	Tailings	Feed	Product	Tailings	Feed	Partition number	SSE
17.38	16.26	0.00	0.00	0.00	0.00	0.00	0.00	0.00	0.00	0.00		0.00
19.95	18.67	0.00	0.25	0.00	0.00	0.10	0.00	0.00	0.25	0.11	0.00	0.00
22.91	21.43	0.00	1.37	0.14	0.00	0.46	0.05	0.00	0.36	0.16	0.00	0.57
26.30	24.61	0.00	2.93	0.69	0.00	0.86	0.20	0.00	1.85	0.82	0.00	0.18
30.20	28.25	0.00	5.00	1.67	0.00	1.28	0.43	0.00	4.22	1.87	0.00	0.04
34.67	32.44	0.01	7.33	3.17	0.00	1.64	0.71	0.01	7.26	3.23	0.00	0.00
39.81	37.24	0.19	9.59	5.12	0.04	1.87	1.00	0.19	10.35	4.70	0.02	0.01
45.71	42.76	1.43	11.42	7.31	0.24	1.94	1.24	1.46	12.58	6.40	0.13	0.03
52.48	49.09	3.98	12.47	9.43	0.59	1.84	1.39	4.18	13.53	8.33	0.28	0.02
60.26	56.37	7.83	12.53	11.10	1.01	1.61	1.43	8.36	13.10	10.47	0.44	0.01
69.18	64.72	12.17	11.58	12.00	1.36	1.30	1.34	12.85	11.63	12.31	0.58	0.00
79.43	74.31	15.58	9.80	11.93	1.52	0.96	1.16	15.90	9.58	13.09	0.67	0.01
91.20	85.32	16.87	7.48	10.89	1.43	0.64	0.93	16.52	7.24	12.39	0.74	0.02
104.71	97.96	15.55	5.09	9.08	1.15	0.38	0.67	14.78	4.93	10.41	0.79	0.02
120.23	112.47	12.15	2.67	6.82	0.78	0.17	0.44	11.60	2.63	7.61	0.85	0.02
138.04	129.13	7.98	0.49	4.55	0.45	0.03	0.26	8.08	0.49	4.71	0.95	0.00
158.49	148.26	4.26	0.00	2.49	0.21	0.00	0.12	4.42	0.00	2.45	1.00	0.00
181.97	170.23	1.74	0.00	0.67	0.07	0.00	0.03	1.38	0.00	0.77	1.00	0.06
208.93	195.45	0.27	0.00	0.00	0.01	0.00	0.00	0.28	0.00	0.15	1.00	0.00
239.88	224.41	0.00	0.00	0.00	0.00	0.00	0.00	0.00	0.00	0.00		0.00
<b>Sum</b>		100.01	100.00	97.04				<b>100</b>	<b>100</b>	<b>100</b>		<b>1.00</b>
<b>Yield to Product</b>		<b>0.56</b>										

Relative errors (%)											
average size	Product	Tailings	Feed	average size	Product	Tailings	Feed	average size	Product	Tailings	Feed
<b>16.26</b>	0.00	0.00	0.00	<b>56.37</b>	6.79	4.52	-5.70	<b>195.45</b>	0.16	0.00	0.00
<b>18.67</b>	0.00	0.03	N/A	<b>64.72</b>	5.64	0.44	2.56	<b>224.41</b>	0.00	0.00	0.00
<b>21.43</b>	0.00	-73.90	16.58	<b>74.31</b>	2.02	-2.24	9.71				
<b>24.61</b>	0.00	-36.94	19.67	<b>85.32</b>	-2.11	-3.23	13.85				
<b>28.25</b>	0.00	-15.63	12.24	<b>97.96</b>	-4.89	-2.97	14.65				
<b>32.44</b>	0.00	-0.93	1.85	<b>112.47</b>	-4.54	-1.69	11.72				
<b>37.24</b>	0.27	7.97	-8.05	<b>129.13</b>	1.25	-0.10	3.48				
<b>42.76</b>	2.18	10.16	-12.46	<b>148.26</b>	3.74	0.00	-1.33				
<b>49.09</b>	5.04	8.48	-11.62	<b>170.23</b>	-20.52	0.00	14.90				

Chapter 5 - Run 10 (Raw and mass balanced cenospheres size distribution)

Size (µm)		Raw data size distribution (vol.%)			Raw data - volume frequency (%/Δµm)			Balanced data size distribution (vol.%)				
Size Interval	Average size	Product	Tailings	Feed	Product	Tailings	Feed	Product	Tailings	Feed	Partition number	SSE
15.14	14.16	0.00	0.05	0.01	0.00	0.02	0.00	0.00	0.03	0.01	0.00	0.12
17.38	16.26	0.00	0.39	0.03	0.00	0.17	0.01	0.00	0.10	0.03	0.00	0.59
19.95	18.67	0.00	1.32	0.19	0.00	0.51	0.07	0.00	0.69	0.22	0.00	0.27
22.91	21.43	0.00	2.66	0.57	0.00	0.90	0.19	0.00	2.01	0.65	0.00	0.08
26.30	24.61	0.00	4.52	1.28	0.00	1.33	0.38	0.00	4.15	1.35	0.00	0.01
30.20	28.25	0.00	6.66	2.34	0.00	1.71	0.60	0.00	6.82	2.22	0.00	0.00
34.67	32.44	0.02	8.85	3.75	0.00	1.98	0.84	0.02	9.67	3.15	0.00	0.03
39.81	37.24	0.53	10.74	5.41	0.10	2.09	1.05	0.54	11.87	4.22	0.09	0.06
45.71	42.76	1.98	11.99	7.18	0.34	2.03	1.22	2.10	12.93	5.62	0.25	0.06
52.48	49.09	4.43	12.36	8.83	0.65	1.83	1.30	4.86	12.74	7.42	0.44	0.04
60.26	56.37	7.64	11.76	10.13	0.98	1.51	1.30	8.47	11.58	9.48	0.60	0.02
69.18	64.72	11.02	10.27	10.87	1.23	1.15	1.22	11.96	9.81	11.26	0.72	0.01
79.43	74.31	13.70	8.20	10.93	1.34	0.80	1.07	14.28	7.75	12.16	0.79	0.02
91.20	85.32	14.97	5.79	10.28	1.27	0.49	0.87	14.93	5.52	11.87	0.85	0.03
104.71	97.96	14.44	3.70	9.01	1.07	0.27	0.67	13.88	3.57	10.54	0.89	0.03
120.23	112.47	12.27	0.75	7.30	0.79	0.05	0.47	11.91	0.75	8.28	0.97	0.02
138.04	129.13	9.13	0.00	5.39	0.51	0.00	0.30	8.84	0.00	5.97	1.00	0.01
158.49	148.26	5.80	0.00	3.59	0.28	0.00	0.18	5.69	0.00	3.84	1.00	0.01
181.97	170.23	3.11	0.00	1.46	0.13	0.00	0.06	2.50	0.00	1.69	1.00	0.06
208.93	195.45	0.98	0.00	0.01	0.04	0.00	0.00	0.02	0.00	0.01	1.00	0.97
<b>Sum</b>		100.00	100.00	98.55				<b>100</b>	<b>100</b>	<b>100</b>		<b>2.42</b>
<b>Yield to Product</b>		<b>0.67</b>										

Relative errors (%)											
average size	Product	Tailings	Feed	average size	Product	Tailings	Feed	average size	Product	Tailings	Feed
<b>14.16</b>	0.00	-29.29	17.59	<b>49.09</b>	9.82	3.12	-15.93	<b>170.23</b>	-19.48	0.00	15.72
<b>16.26</b>	0.00	-74.95	16.13	<b>56.37</b>	10.89	-1.52	-6.38	<b>195.45</b>	-98.37	0.00	1.60
<b>18.67</b>	0.00	-47.49	20.49	<b>64.72</b>	8.56	-4.53	3.59				
<b>21.43</b>	0.00	-24.28	15.35	<b>74.31</b>	4.19	-5.48	11.24				
<b>24.61</b>	0.00	-8.10	5.73	<b>85.32</b>	-0.27	-4.77	15.51				
<b>28.25</b>	0.00	2.50	-5.11	<b>97.96</b>	-3.84	-3.49	16.90				
<b>32.44</b>	0.06	9.25	-15.92	<b>112.47</b>	-2.94	-0.70	13.42				
<b>37.24</b>	1.99	10.58	-22.01	<b>129.13</b>	-3.15	0.00	10.73				
<b>42.76</b>	6.03	7.82	-21.80	<b>148.26</b>	-1.80	0.00	6.97				

Chapter 5 - Run 11 (Raw and mass balanced cenospheres size distribution)

Size ( $\mu\text{m}$ )		Raw data size distribution (vol.%)			Raw data - volume frequency ( $\%/\Delta\mu\text{m}$ )			Balanced data size distribution (vol.%)				
Size Interval	Average size	Product	Tailings	Feed	Product	Tailings	Feed	Product	Tailings	Feed	Partition number	SSE
15.14	14.16	0.00	0.24	0.00	0.00	0.12	0.00	0.00	0.24	0.05	0.00	0.00
17.38	16.26	0.00	1.09	0.07	0.00	0.49	0.00	0.00	0.39	0.08	0.00	0.45
19.95	18.67	0.00	2.56	0.35	0.00	1.00	0.05	0.00	2.01	0.40	0.00	0.07
22.91	21.43	0.00	4.66	0.90	0.00	1.58	0.20	0.00	4.58	0.91	0.00	0.00
26.30	24.61	0.03	7.21	1.79	0.01	2.13	0.43	0.03	7.80	1.57	0.02	0.02
30.20	28.25	0.31	9.82	3.02	0.08	2.52	0.71	0.31	10.87	2.41	0.10	0.05
34.67	32.44	1.60	12.00	4.54	0.36	2.68	1.00	1.67	12.62	3.84	0.35	0.03
39.81	37.24	3.41	13.26	6.23	0.66	2.58	1.24	3.62	13.44	5.57	0.52	0.02
45.71	42.76	5.88	13.29	7.92	1.00	2.25	1.39	6.18	13.08	7.55	0.66	0.01
52.48	49.09	8.59	12.05	9.38	1.27	1.78	1.43	8.85	11.70	9.42	0.75	0.00
60.26	56.37	11.07	9.83	10.40	1.42	1.26	1.34	11.16	9.53	10.83	0.83	0.00
69.18	64.72	12.83	7.09	10.82	1.44	0.79	1.16	12.68	6.92	11.53	0.88	0.01
79.43	74.31	13.46	4.48	10.57	1.31	0.44	0.93	13.11	4.40	11.39	0.92	0.01
91.20	85.32	12.82	2.16	9.67	1.09	0.18	0.67	12.44	2.14	10.40	0.96	0.01
104.71	97.96	11.07	0.26	8.26	0.82	0.02	0.44	10.85	0.26	8.75	0.99	0.00
120.23	112.47	8.57	0.00	6.50	0.55	0.00	0.26	8.47	0.00	6.79	1.00	0.00
138.04	129.13	5.88	0.00	4.66	0.33	0.00	0.12	5.91	0.00	4.74	1.00	0.00
158.49	148.26	3.42	0.00	2.96	0.17	0.00	0.03	3.57	0.00	2.86	1.00	0.00
181.97	170.23	1.07	0.00	1.02	0.05	0.00	0.00	1.15	0.00	0.93	1.00	0.02
208.93	195.45	0.00	0.00	0.00	0.00	0.00	0.00	0.00	0.00	0.00		
<b>Sum</b>		<b>100.00</b>	<b>100.00</b>	<b>99.07</b>				<b>100</b>	<b>100</b>	<b>100</b>		<b>0.68</b>
Yield to Product		<b>0.80</b>										

Relative errors (%)											
average size	Product	Tailings	Feed	average size	Product	Tailings	Feed	average size	Product	Tailings	Feed
<b>16.26</b>	0.00	-0.05	N/A	<b>56.37</b>	3.05	-2.91	0.43	<b>195.45</b>	8.14	0.00	-9.20
<b>18.67</b>	0.00	-64.09	19.23	<b>64.72</b>	0.75	-3.08	4.20	<b>224.41</b>	0.00	0.00	0.00
<b>21.43</b>	0.00	-21.43	14.32	<b>74.31</b>	-1.21	-2.51	6.56				
<b>24.61</b>	0.00	-1.71	0.60	<b>85.32</b>	-2.56	-1.69	7.68				
<b>28.25</b>	0.19	8.10	-12.26	<b>97.96</b>	-2.94	-0.84	7.50				
<b>32.44</b>	1.77	10.78	-20.26	<b>112.47</b>	-2.02	-0.10	5.92				
<b>37.24</b>	4.94	5.24	-15.33	<b>129.13</b>	-1.25	0.00	4.36				
<b>42.76</b>	6.03	1.42	-10.69	<b>148.26</b>	0.64	0.00	1.65				
<b>49.09</b>	5.09	-1.53	-4.68	<b>170.23</b>	4.36	0.00	-3.26				

**Chapter 6 - Run 1 (Raw and mass balanced cenospheres size distribution)**

Size (µm)		Raw data size distribution (vol.%)			Raw data - volume frequency (%/Δµm)			Balanced data size distribution (vol.%)				
Size Interval	Average size	Product	Tailings	Feed	Product	Tailings	Feed	Product	Tailings	Feed	Partition number	SSE
15.14	14.16	0.00	0.00	0.00	0.00	0.00	0.00	0.00	0.00	0.00	0.00	
17.38	16.26	0.00	0.00	0.00	0.00	0.00	0.00	0.00	0.00	0.00	0.00	
19.95	18.67	0.00	0.24	0.00	0.00	0.00	0.00	0.00	0.15	0.04	0.00	0.00
22.91	21.43	0.00	1.17	0.09	0.00	0.40	0.03	0.00	0.37	0.10	0.00	0.50
26.30	24.61	0.00	2.39	0.49	0.00	0.71	0.14	0.00	2.01	0.55	0.00	0.04
30.20	28.25	0.01	4.08	1.18	0.00	1.05	0.30	0.01	4.17	1.15	0.00	0.00
34.67	32.44	0.15	6.04	2.23	0.03	1.35	0.50	0.15	6.63	1.92	0.06	0.03
39.81	37.24	1.06	8.04	3.64	0.21	1.57	0.71	1.09	8.64	3.15	0.25	0.02
45.71	42.76	2.50	9.81	5.34	0.42	1.67	0.90	2.62	10.29	4.71	0.40	0.02
52.48	49.09	4.60	11.06	7.15	0.68	1.64	1.06	4.81	11.31	6.59	0.53	0.01
60.26	56.37	7.10	11.59	8.87	0.91	1.49	1.14	7.37	11.62	8.53	0.63	0.00
69.18	64.72	9.66	11.30	10.27	1.08	1.27	1.15	9.88	11.19	10.24	0.70	0.00
79.43	74.31	11.79	10.27	11.11	1.15	1.00	1.08	11.87	10.10	11.38	0.76	0.00
91.20	85.32	13.06	8.65	11.25	1.11	0.74	0.96	12.96	8.50	11.74	0.80	0.00
104.71	97.96	13.17	6.74	10.65	0.98	0.50	0.79	12.93	6.63	11.21	0.84	0.00
120.23	112.47	12.09	4.73	9.35	0.78	0.31	0.60	11.80	4.67	9.85	0.87	0.00
138.04	129.13	10.06	2.99	7.60	0.56	0.17	0.43	9.83	2.97	7.95	0.90	0.00
158.49	148.26	7.46	0.89	5.57	0.36	0.04	0.27	7.46	0.89	5.66	0.96	0.00
181.97	170.23	4.86	0.00	3.68	0.21	0.00	0.16	4.99	0.00	3.62	1.00	0.00
208.93	195.45	2.44	0.00	1.53	0.09	0.00	0.06	2.25	0.00	1.64	1.00	0.01
239.88	224.41	0.00	0.00	0.00	0.00	0.00	0.00	0.00	0.00	0.00	0.00	0.00
<b>Sum</b>		<b>100.00</b>	<b>100.00</b>	<b>100.00</b>				<b>100</b>	<b>100</b>	<b>100</b>		<b>0.65</b>
<b>Yield to Product</b>		<b>0.73</b>										

Relative errors (%)											
average size	Product	Tailings	Feed	average size	Product	Tailings	Feed	average size	Product	Tailings	Feed
<b>14.16</b>	0.00	-29.29	17.59	<b>49.09</b>	4.67	2.25	-7.84	<b>170.23</b>	2.57	0.00	-1.58
<b>16.26</b>	0.00	0.00	0.00	<b>56.37</b>	3.78	0.25	-3.85	<b>195.45</b>	-7.54	0.00	6.98
<b>18.67</b>	0.00	-35.27	N/A	<b>64.72</b>	2.31	-1.01	-0.29				
<b>21.43</b>	0.00	-68.05	18.34	<b>74.31</b>	0.67	-1.62	2.46				
<b>24.61</b>	0.00	-15.85	11.76	<b>85.32</b>	-0.80	-1.75	4.32				
<b>28.25</b>	0.01	2.14	-2.68	<b>97.96</b>	-1.87	-1.57	5.27				
<b>32.44</b>	0.71	9.78	-14.03	<b>112.47</b>	-2.39	-1.20	5.34				
<b>37.24</b>	3.07	7.36	-13.50	<b>129.13</b>	-2.30	-0.79	4.67				
<b>42.76</b>	4.51	4.90	-11.63	<b>148.26</b>	0.00	-0.16	1.67				

Chapter 6- Run 2 (Raw and mass balanced cenospheres size distribution)

Size (µm)		Raw data size distribution (vol.%)			Raw data - volume frequency (%/Δµm)			Balanced data size distribution (vol.%)				
Size Interval	Average size	Product	Tailings	Feed	Product	Tailings	Feed	Product	Tailings	Feed	Partition number	SSE
16.40	17.55	0.00	0.00	0.00	0.00	0.00	0.00	0.00	0.00	0.00	0.00	0.00
18.70	19.95	0.00	0.43	0.12	0.00	0.19	0.05	0.00	0.41	0.13	0.00	0.00
21.20	22.65	0.00	1.30	0.41	0.00	0.52	0.16	0.00	1.32	0.40	0.00	0.00
24.10	25.75	0.00	2.70	0.94	0.00	0.93	0.32	0.00	2.86	0.88	0.00	0.01
27.40	29.25	0.14	4.53	1.74	0.04	1.37	0.53	0.14	4.82	1.57	0.06	0.01
31.10	33.20	0.69	6.60	2.84	0.19	1.78	0.77	0.70	6.86	2.59	0.19	0.01
35.30	37.70	1.79	8.61	4.20	0.43	2.05	1.00	1.83	8.74	3.95	0.32	0.00
40.10	42.85	3.44	10.28	5.73	0.72	2.14	1.19	3.49	10.26	5.56	0.44	0.00
45.60	48.70	5.52	11.33	7.29	1.00	2.06	1.33	5.52	11.18	7.25	0.53	0.00
51.80	55.35	7.77	11.62	8.70	1.25	1.87	1.40	7.68	11.43	8.83	0.60	0.00
58.90	62.90	9.86	11.09	9.80	1.39	1.56	1.38	9.68	10.93	10.06	0.67	0.00
66.90	71.45	11.45	9.83	10.41	1.43	1.23	1.30	11.21	9.71	10.75	0.72	0.00
76.00	81.20	12.27	8.05	10.44	1.35	0.88	1.15	11.99	7.96	10.76	0.77	0.00
86.40	92.25	12.14	6.02	9.85	1.17	0.58	0.95	12.00	5.96	10.16	0.82	0.00
98.10	104.55	11.06	4.02	8.69	0.95	0.34	0.74	11.04	3.99	8.88	0.86	0.00
111.00	119.00	9.21	2.29	7.11	0.71	0.18	0.55	9.32	2.27	7.16	0.90	0.00
127.00	135.50	6.88	1.02	5.30	0.43	0.06	0.33	7.07	1.02	5.22	0.94	0.00
144.00	153.50	4.46	0.28	3.50	0.26	0.02	0.21	4.67	0.28	3.33	0.97	0.00
163.00	174.50	2.35	0.00	1.94	0.12	0.00	0.10	2.54	0.00	1.76	1.00	0.01
186.00	198.50	0.85	0.00	0.81	0.04	0.00	0.04	0.96	0.00	0.67	1.00	0.05
211.00	225.50	0.12	0.00	0.18	0.00	0.00	0.01	0.14	0.00	0.10	1.00	0.24
<b>Sum</b>		<b>100.00</b>	<b>100.00</b>	<b>100.00</b>				<b>100</b>	<b>100</b>	<b>100</b>		<b>0.36</b>
Yield to Product		<b>0.69</b>										

<b>Relative errors (%)</b>											
<b>average size</b>	Product	Tailings	Feed	<b>average size</b>	Product	Tailings	Feed	<b>average size</b>	Product	Tailings	Feed
<b>17.55</b>	0.00	0.00	0.00	<b>55.35</b>	-1.19	-1.65	1.44	<b>174.50</b>	7.89	0.00	-9.30
<b>19.95</b>	0.00	-5.00	4.18	<b>62.90</b>	-1.84	-1.43	2.68	<b>198.50</b>	13.05	0.00	-17.67
<b>22.65</b>	0.00	1.43	-1.58	<b>71.45</b>	-2.12	-1.22	3.26	<b>225.50</b>	20.50	0.00	-44.25
<b>25.75</b>	0.00	6.07	-6.77	<b>81.20</b>	-2.25	-1.11	3.07				
<b>29.25</b>	0.46	6.42	-9.61	<b>92.25</b>	-1.11	-0.92	3.11				
<b>33.20</b>	1.66	3.89	-8.98	<b>104.55</b>	-0.15	-0.75	2.24				
<b>37.70</b>	2.41	1.47	-6.05	<b>119.00</b>	1.23	-0.97	0.76				
<b>42.85</b>	1.46	-0.20	-2.94	<b>135.50</b>	2.79	-0.06	-1.52				
<b>48.70</b>	0.00	-1.29	-0.50	<b>153.50</b>	4.77	-0.04	-4.90				

**Chapter 6 - Run 3 (Raw and mass balanced cenospheres size distribution)**

Size (µm)		Raw data size distribution (vol.%)			Raw data - volume frequency (%/Δµm)			Balanced data size distribution (vol.%)				
Size Interval	Average size	Product	Tailings	Feed	Product	Tailings	Feed	Product	Tailings	Feed	Partition number	SSE
15.14	14.16	0.00	0.00	0.01	0.00	0.00	0.01	0.00	0.00	0.00	0.00	0.00
17.38	16.26	0.00	0.10	0.00	0.00	0.04	0.00	0.00	0.10	0.01	0.00	0.00
19.95	18.67	0.00	0.78	0.00	0.00	0.30	0.00	0.00	0.78	0.11	0.00	0.00
22.91	21.43	0.00	2.17	0.04	0.00	0.73	0.02	0.00	0.35	0.05	0.00	0.72
26.30	24.61	0.00	4.27	0.38	0.00	1.26	0.11	0.00	3.08	0.44	0.00	0.11
30.20	28.25	0.02	6.87	1.05	0.00	1.76	0.27	0.02	7.06	1.02	0.01	0.00
34.67	32.44	0.19	9.60	2.09	0.04	2.15	0.47	0.19	10.76	1.70	0.10	0.05
39.81	37.24	1.19	11.92	3.48	0.23	2.32	0.68	1.25	12.86	2.91	0.37	0.04
45.71	42.76	2.75	13.31	5.16	0.47	2.26	0.87	2.93	13.91	4.50	0.56	0.02
52.48	49.09	4.96	13.44	6.96	0.73	1.98	1.03	5.26	13.67	6.46	0.70	0.01
60.26	56.37	7.54	12.28	8.69	0.97	1.58	1.12	7.86	12.29	8.49	0.79	0.00
69.18	64.72	10.12	10.10	10.10	1.13	1.13	1.13	10.31	10.05	10.27	0.86	0.00
79.43	74.31	12.17	7.43	10.97	1.19	0.72	1.07	12.14	7.38	11.46	0.91	0.00
91.20	85.32	13.27	4.74	11.16	1.13	0.40	0.95	13.04	4.72	11.85	0.94	0.00
104.71	97.96	13.15	2.56	10.61	0.97	0.19	0.79	12.79	2.55	11.33	0.97	0.01
120.23	112.47	11.82	0.45	9.38	0.76	0.03	0.60	11.53	0.45	9.95	0.99	0.00
138.04	129.13	9.61	0.00	7.68	0.54	0.00	0.43	9.41	0.00	8.07	1.00	0.00
158.49	148.26	6.90	0.00	5.67	0.34	0.00	0.28	6.83	0.00	5.86	1.00	0.00
181.97	170.23	4.36	0.00	3.81	0.19	0.00	0.16	4.43	0.00	3.80	1.00	0.00
208.93	195.45	1.86	0.00	1.65	0.07	0.00	0.06	1.89	0.00	1.62	1.00	0.00
239.88	224.41	0.11	0.00	0.00	0.00	0.00	0.00	0.11	0.00	0.09	1.00	0.00
<b>Sum</b>		<b>100.00</b>	<b>100.00</b>	<b>98.88</b>				<b>100</b>	<b>100</b>	<b>100</b>		<b>0.97</b>
<b>Yield to Product</b>		<b>0.86</b>										

Relative errors (%)											
average size	Product	Tailings	Feed	average size	Product	Tailings	Feed	average size	Product	Tailings	Feed
<b>14.16</b>	0.00	0.00	0.00	<b>49.09</b>	6.07	1.70	-7.29	<b>170.23</b>	1.74	0.00	-0.23
<b>16.26</b>	0.00	0.00	N/A	<b>56.37</b>	4.22	0.15	-2.20	<b>195.45</b>	2.04	0.00	-1.40
<b>18.67</b>	0.00	-0.02	N/A	<b>64.72</b>	1.89	-0.52	1.75	<b>224.41</b>	0.04	0.00	N/A
<b>21.43</b>	N/A	-83.74	12.14	<b>74.31</b>	-0.23	-0.65	4.51				
<b>24.61</b>	N/A	-27.82	17.08	<b>85.32</b>	-1.78	-0.51	6.19				
<b>28.25</b>	0.03	2.75	-3.11	<b>97.96</b>	-2.72	-0.30	6.81				
<b>32.44</b>	1.46	12.08	-18.60	<b>112.47</b>	-2.45	-0.05	6.10				
<b>37.24</b>	5.19	7.92	-16.46	<b>129.13</b>	-2.05	0.00	5.09				
<b>42.76</b>	6.78	4.49	-12.82	<b>148.26</b>	-0.95	0.00	3.27				

**Chapter 6 - Run 4 (Raw and mass balanced cenospheres size distribution)**

Size (µm)		Raw data size distribution (vol.%)			Raw data - volume frequency (%/Δµm)			Balanced data size distribution (vol.%)				
Size Interval	Average size	Product	Tailings	Feed	Product	Tailings	Feed	Product	Tailings	Feed	Partition number	SSE
15.14	14.16	0.00	0.00	0.00	0.00	0.00	0.00	0.00	0.00	0.00	0.00	0.00
17.38	16.26	0.00	0.00	0.00	0.00	0.00	0.00	0.00	0.00	0.00	0.00	0.00
19.95	18.67	0.00	0.01	0.00	0.00	0.00	0.00	0.00	0.01	0.00	0.00	0.15
22.91	21.43	0.00	0.35	0.00	0.00	0.12	0.00	0.00	0.35	0.04	0.00	0.00
26.30	24.61	0.00	1.83	0.11	0.00	0.54	0.03	0.00	1.07	0.13	0.00	0.21
30.20	28.25	0.02	4.13	0.69	0.01	1.06	0.18	0.02	4.63	0.57	0.04	0.05
34.67	32.44	0.47	7.25	1.62	0.11	1.62	0.36	0.49	7.83	1.37	0.32	0.03
39.81	37.24	1.56	10.56	2.98	0.30	2.06	0.58	1.62	10.87	2.72	0.53	0.01
45.71	42.76	3.27	13.31	4.71	0.56	2.26	0.80	3.36	13.34	4.54	0.65	0.00
52.48	49.09	5.55	14.75	6.67	0.82	2.18	0.99	5.59	14.61	6.66	0.74	0.00
60.26	56.37	8.10	14.48	8.63	1.04	1.86	1.11	8.05	14.28	8.79	0.81	0.00
69.18	64.72	10.54	12.59	10.31	1.18	1.41	1.15	10.38	12.42	10.62	0.86	0.00
79.43	74.31	12.37	9.64	11.41	1.21	0.94	1.11	12.12	9.54	11.82	0.90	0.00
91.20	85.32	13.20	6.36	11.75	1.12	0.54	1.00	12.95	6.32	12.16	0.94	0.00
104.71	97.96	12.83	3.52	11.24	0.95	0.26	0.83	12.65	3.51	11.56	0.96	0.00
120.23	112.47	11.32	1.18	9.93	0.73	0.08	0.64	11.29	1.18	10.09	0.99	0.00
138.04	129.13	9.03	0.04	8.08	0.51	0.00	0.45	9.14	0.04	8.06	1.00	0.00
158.49	148.26	6.34	0.00	5.92	0.31	0.00	0.29	6.54	0.00	5.77	1.00	0.00
181.97	170.23	3.90	0.00	3.90	0.17	0.00	0.17	4.14	0.00	3.65	1.00	0.01
208.93	195.45	1.48	0.00	1.71	0.05	0.00	0.06	1.65	0.00	1.46	1.00	0.03
239.88	224.41	0.00	0.00	0.01	0.00	0.00	0.00	0.00	0.00	0.00		
<b>Sum</b>		<b>100.00</b>	<b>100.00</b>	<b>99.68</b>				<b>100</b>	<b>100</b>	<b>100</b>		<b>0.51</b>
Yield to Product		<b>0.88</b>										

Relative errors (%)											
average size	Product	Tailings	Feed	average size	Product	Tailings	Feed	average size	Product	Tailings	Feed
<b>16.26</b>	0.00	0.00	0.00	<b>56.37</b>	-0.63	-1.37	1.88	<b>195.45</b>	11.41	0.00	-14.68
<b>18.67</b>	0.00	-38.93	-18.44	<b>64.72</b>	-1.55	-1.31	3.06	<b>224.41</b>	0.00	0.00	-91.24
<b>21.43</b>	0.00	-0.02	N/A	<b>74.31</b>	-1.98	-1.02	3.55				
<b>24.61</b>	0.00	-41.61	20.16	<b>85.32</b>	-1.94	-0.66	3.48				
<b>28.25</b>	0.53	12.14	-17.55	<b>97.96</b>	-1.45	-0.35	2.90				
<b>32.44</b>	4.15	7.93	-15.88	<b>112.47</b>	-0.30	-0.10	1.58				
<b>37.24</b>	4.20	2.95	-8.74	<b>129.13</b>	1.27	0.00	-0.24				
<b>42.76</b>	2.55	0.28	-3.56	<b>148.26</b>	3.14	0.00	-2.56				
<b>49.09</b>	0.77	-0.97	-0.19	<b>170.23</b>	6.20	0.00	-6.54				

**Chapter 6- Run 5 (Raw and mass balanced cenospheres size distribution)**

Size (µm)		Raw data size distribution (vol.%)			Raw data - volume frequency (%/Δµm)			Balanced data size distribution (vol.%)				
Size Interval	Average size	Product	Tailings	Feed	Product	Tailings	Feed	Product	Tailings	Feed	Partition number	SSE
16.40	17.55	0.00	0.75	0.34	0.00	0.33	0.15	0.00	0.75	0.34	0.00	0.00
18.70	19.95	0.00	1.19	0.43	0.00	0.48	0.17	0.00	1.16	0.45	0.00	0.00
21.20	22.65	0.00	1.90	0.64	0.00	0.66	0.22	0.00	1.78	0.68	0.00	0.01
24.10	25.75	0.00	2.90	1.01	0.00	0.88	0.31	0.00	2.77	1.07	0.00	0.01
27.40	29.25	0.00	4.20	1.61	0.00	1.14	0.44	0.00	4.25	1.64	0.00	0.00
31.10	33.20	0.37	5.71	2.48	0.09	1.36	0.59	0.37	5.91	2.51	0.09	0.00
35.30	37.70	1.13	7.30	3.61	0.24	1.52	0.75	1.13	7.65	3.64	0.19	0.00
40.10	42.85	2.38	8.77	4.98	0.43	1.59	0.91	2.38	9.28	5.04	0.29	0.00
45.60	48.70	4.10	9.90	6.46	0.66	1.60	1.04	4.10	10.54	6.58	0.38	0.00
51.80	55.35	6.14	10.50	7.91	0.86	1.48	1.11	6.14	11.22	8.10	0.47	0.01
58.90	62.90	8.26	10.42	9.14	1.03	1.30	1.14	8.27	11.13	9.37	0.54	0.01
66.90	71.45	10.14	9.62	9.97	1.11	1.06	1.10	10.18	10.24	10.20	0.61	0.00
76.00	81.20	11.50	8.21	10.25	1.11	0.79	0.99	11.58	8.67	10.46	0.68	0.00
86.40	92.25	12.06	6.38	9.90	1.03	0.55	0.85	12.18	6.67	10.05	0.74	0.00
98.10	104.55	11.72	4.41	8.94	0.91	0.34	0.69	11.86	4.55	9.04	0.81	0.00
111.00	119.00	10.50	2.59	7.49	0.66	0.16	0.47	10.63	2.64	7.55	0.87	0.00
127.00	135.50	8.59	1.19	5.73	0.51	0.07	0.34	8.65	1.20	5.78	0.92	0.00
144.00	153.50	6.30	0.33	3.91	0.33	0.02	0.21	6.26	0.33	3.98	0.97	0.00
163.00	174.50	3.99	0.00	2.28	0.17	0.00	0.10	3.85	0.00	2.37	1.00	0.00
186.00	198.50	2.04	0.00	1.03	0.08	0.00	0.04	1.83	0.00	1.12	1.00	0.02
211.00	225.50	0.71	0.00	0.28	0.02	0.00	0.01	0.53	0.00	0.33	1.00	0.09
240.00	256.00	0.06	0.00	0.00	0.00	0.00	0.00	0.06	0.00	0.04	1.00	0.00
<b>Sum</b>		<b>99.99</b>	<b>96.27</b>	<b>98.39</b>				<b>100</b>	<b>100</b>	<b>100</b>		<b>0.17</b>
Yield to Product		<b>0.69</b>										

Relative errors (%)											
average size	Product	Tailings	Feed	average size	Product	Tailings	Feed	average size	Product	Tailings	Feed
<b>17.55</b>	0.00	0.00	0.00	<b>55.35</b>	-0.02	6.83	2.36	<b>174.50</b>	-3.42	0.00	3.85
<b>19.95</b>	0.00	-2.92	3.59	<b>62.90</b>	0.08	6.86	2.54	<b>198.50</b>	-10.50	0.00	8.92
<b>22.65</b>	0.00	-6.54	6.98	<b>71.45</b>	0.37	6.49	2.34	<b>225.50</b>	-25.33	0.00	16.34
<b>25.75</b>	0.00	-4.33	5.91	<b>81.20</b>	0.67	5.66	2.03	<b>256.00</b>	0.01	0.00	N/A
<b>29.25</b>	0.00	1.31	1.89	<b>92.25</b>	1.00	4.49	1.57				
<b>33.20</b>	-0.03	3.47	1.01	<b>104.55</b>	1.20	3.16	1.14				
<b>37.70</b>	0.02	4.83	0.97	<b>119.00</b>	1.23	1.88	0.78				
<b>42.85</b>	0.06	5.86	1.26	<b>135.50</b>	0.74	0.84	0.87				
<b>48.70</b>	0.00	6.46	1.90	<b>153.50</b>	-0.56	0.20	1.71				

**Chapter 7 - Run 1 (Raw and mass balanced cenospheres size distribution)**

Size (µm)		Raw data size distribution (vol.%)			Raw data - volume frequency (%/Δµm)			Balanced data size distribution (vol.%)				
Size Interval	Average size	Product	Tailings	Feed	Product	Tailings	Feed	Product	Tailings	Feed	Partition number	SSE
16.40	17.55	0.08	0.00	0.04	0.03	0.00	0.02	0.06	0.00	0.05	1.00	
18.70	19.95	0.00	0.00	0.00	0.00	0.00	0.00	0.09	0.00	0.07	1.00	
21.20	22.65	0.00	0.29	0.00	0.00	0.10	0.00	0.00	0.03	0.00	0.01	0.79
24.10	25.75	0.00	1.22	0.12	0.00	0.37	0.04	0.00	0.93	0.14	0.00	0.08
27.40	29.25	0.00	2.94	0.44	0.00	0.79	0.12	0.01	2.93	0.44	0.01	0.00
31.10	33.20	0.19	5.32	1.07	0.05	1.27	0.25	0.19	5.57	0.99	0.17	0.01
35.30	37.70	0.72	8.04	2.03	0.15	1.68	0.42	0.74	8.33	1.87	0.34	0.01
40.10	42.85	1.73	10.58	3.32	0.31	1.92	0.60	1.77	10.77	3.11	0.48	0.01
45.60	48.70	3.20	12.43	4.88	0.52	2.00	0.79	3.30	12.42	4.66	0.60	0.00
51.80	55.35	5.08	13.20	6.57	0.72	1.86	0.93	5.21	13.10	6.38	0.69	0.00
58.90	62.90	7.15	12.75	8.20	0.89	1.59	1.03	7.28	12.60	8.07	0.77	0.00
66.90	71.45	9.13	11.19	9.57	1.00	1.23	1.05	9.25	11.05	9.52	0.83	0.00
76.00	81.20	10.71	8.89	10.46	1.03	0.85	1.01	10.80	8.79	10.50	0.88	0.00
86.40	92.25	11.65	6.30	10.75	1.00	0.54	0.92	11.62	6.24	10.82	0.91	0.00
98.10	104.55	11.75	3.90	10.37	0.91	0.30	0.80	11.71	3.88	10.54	0.95	0.00
111.00	119.00	10.96	2.01	9.35	0.69	0.13	0.58	10.86	2.00	9.55	0.97	0.00
127.00	135.50	9.42	0.78	7.82	0.55	0.05	0.46	9.28	0.78	8.01	0.99	0.00
144.00	153.50	7.35	0.17	5.98	0.39	0.01	0.31	7.19	0.17	6.15	1.00	0.00
163.00	174.50	5.09	0.00	4.09	0.22	0.00	0.18	4.95	0.00	4.22	1.00	0.00
186.00	198.50	2.99	0.00	2.39	0.12	0.00	0.10	2.90	0.00	2.47	1.00	0.00
211.00	225.50	1.36	0.00	1.09	0.05	0.00	0.04	1.32	0.00	1.12	1.00	0.00
240.00	256.00	0.37	0.00	0.30	0.01	0.00	0.01	0.36	0.00	0.31	1.00	0.00
272.00	291.00	0.00	0.00	0.00	0.00	0.00	0.00	0.04	0.00	0.03	1.00	
<b>Sum</b>		<b>98.93</b>	<b>100.01</b>	<b>98.84</b>				<b>100</b>	<b>100</b>	<b>100</b>		<b>0.91</b>
Yield to Product		<b>0.85</b>										

Relative errors (%)											
average size	Product	Tailings	Feed	average size	Product	Tailings	Feed	average size	Product	Tailings	Feed
<b>17.55</b>	0.00	0.00	0.00	<b>55.35</b>	2.46	-0.74	-2.90	<b>174.50</b>	-2.71	N/A	3.08
<b>19.95</b>	0.00	0.00	0.00	<b>62.90</b>	1.89	-1.19	-1.54	<b>198.50</b>	-3.13	N/A	3.24
<b>22.65</b>	N/A	-88.99	N/A	<b>71.45</b>	1.39	-1.27	-0.52	<b>225.50</b>	-2.86	N/A	2.84
<b>25.75</b>	N/A	-23.59	15.47	<b>81.20</b>	0.81	-1.13	0.39	<b>256.00</b>	-2.69	N/A	2.59
<b>29.25</b>	N/A	-0.36	0.04	<b>92.25</b>	-0.20	-0.88	0.69				
<b>33.20</b>	1.15	4.71	-7.26	<b>104.55</b>	-0.34	-0.57	1.67				
<b>37.70</b>	2.55	3.62	-7.91	<b>119.00</b>	-0.92	-0.32	2.10				
<b>42.85</b>	2.34	1.78	-6.47	<b>135.50</b>	-1.51	-0.09	2.46				
<b>48.70</b>	3.03	-0.05	-4.59	<b>153.50</b>	-2.14	-0.02	2.82				

**Chapter 7 - Run 2 (Raw and mass balanced cenospheres size distribution)**

Size (µm)		Raw data size distribution (vol.%)			Raw data - volume frequency (%/Δµm)			Balanced data size distribution (vol.%)				
Size Interval	Average size	Product	Tailings	Feed	Product	Tailings	Feed	Product	Tailings	Feed	Partition number	SSE
16.40	17.55	0.00	0.00	0.00	0.00	0.00	0.00	0.00	0.00	0.00		
18.70	19.95	0.00	0.00	0.00	0.00	0.00	0.00	0.00	0.00	0.00		
21.20	22.65	0.00	0.12	0.00	0.00	0.04	0.00	0.00	0.12	0.02	0.00	0.00
24.10	25.75	0.00	0.71	0.00	0.00	0.22	0.00	0.00	0.71	0.14	0.00	0.00
27.40	29.25	0.00	1.97	0.23	0.00	0.53	0.06	0.00	1.36	0.27	0.00	0.13
31.10	33.20	0.06	3.84	0.75	0.01	0.91	0.18	0.06	3.66	0.78	0.06	0.00
35.30	37.70	0.38	6.10	1.65	0.08	1.27	0.34	0.38	6.30	1.56	0.20	0.00
40.10	42.85	1.17	8.43	2.95	0.21	1.53	0.54	1.20	8.77	2.71	0.35	0.01
45.60	48.70	2.54	10.41	4.61	0.41	1.68	0.74	2.64	10.69	4.25	0.50	0.01
51.80	55.35	4.46	11.71	6.49	0.63	1.65	0.91	4.65	11.87	6.09	0.61	0.01
58.90	62.90	6.73	12.11	8.38	0.84	1.51	1.05	6.99	12.14	8.02	0.70	0.00
66.90	71.45	9.05	11.55	10.04	0.99	1.27	1.10	9.35	11.51	9.78	0.77	0.00
76.00	81.20	11.02	10.19	11.20	1.06	0.98	1.08	11.31	10.13	11.07	0.82	0.00
86.40	92.25	12.27	8.28	11.67	1.05	0.71	1.00	12.51	8.23	11.65	0.86	0.00
98.10	104.55	12.54	6.16	11.32	0.97	0.48	0.88	12.71	6.13	11.40	0.89	0.00
111.00	119.00	11.78	4.14	10.16	0.74	0.26	0.64	11.84	4.12	10.30	0.92	0.00
127.00	135.50	10.09	2.46	8.32	0.59	0.14	0.49	10.02	2.45	8.51	0.94	0.00
144.00	153.50	7.80	1.23	6.08	0.41	0.06	0.32	7.59	1.23	6.32	0.96	0.00
163.00	174.50	5.32	0.47	3.79	0.23	0.02	0.16	4.95	0.47	4.05	0.98	0.01
186.00	198.50	3.06	0.11	1.84	0.12	0.00	0.07	2.56	0.11	2.07	0.99	0.04
211.00	225.50	1.36	0.00	0.53	0.05	0.00	0.02	0.80	0.00	0.64	1.00	0.21
240.00	256.00	0.37	0.00	0.00	0.01	0.00	0.00	0.37	0.00	0.30	1.00	0.00
272.00	291.00	0.00	0.00	0.00	0.00	0.00	0.00	0.08	0.00	0.06		
<b>Sum</b>		<b>100.00</b>	<b>99.99</b>	<b>100.01</b>				<b>100</b>	<b>100</b>	<b>100</b>		<b>0.43</b>
Yield to Product		<b>0.80</b>										

Relative errors (%)											
average size	Product	Tailings	Feed	average size	Product	Tailings	Feed	average size	Product	Tailings	Feed
<b>17.55</b>	0.00	0.00	0.00	<b>55.35</b>	3.64	1.28	-6.63	<b>174.50</b>	-7.40	-0.21	6.58
<b>19.95</b>	0.00	0.00	0.00	<b>62.90</b>	3.10	0.25	-4.82	<b>198.50</b>	-16.61	-0.16	12.45
<b>22.65</b>	N/A	-0.01	N/A	<b>71.45</b>	2.37	-0.33	-3.28	<b>225.50</b>	-41.66	N/A	20.22
<b>25.75</b>	N/A	-0.07	N/A	<b>81.20</b>	1.55	-0.60	-1.98	<b>256.00</b>	0.00	N/A	N/A
<b>29.25</b>	N/A	-30.74	17.94	<b>92.25</b>	0.87	-0.63	-1.03				
<b>33.20</b>	-0.26	-4.35	3.92	<b>104.55</b>	0.22	-0.55	-0.26				
<b>37.70</b>	0.99	3.40	-5.40	<b>119.00</b>	-0.46	-0.43	0.50				
<b>42.85</b>	2.66	3.95	-8.36	<b>135.50</b>	-1.49	-0.32	1.53				
<b>48.70</b>	3.60	2.68	-8.14	<b>153.50</b>	-3.39	-0.25	3.30				

Chapter 7- Run 3 (Raw and mass balanced cenospheres size distribution)

Size (µm)		Raw data size distribution (vol.%)			Raw data - volume frequency (%/Δµm)			Balanced data size distribution (vol.%)				
Size Interval	Average size	Product	Tailings	Feed	Product	Tailings	Feed	Product	Tailings	Feed	Partition number	SSE
16.40	17.55	0.00	0.00	0.00	0.00	0.00	0.00	0.00	0.00	0.00		
18.70	19.95	0.00	0.00	0.00	0.00	0.00	0.00	0.00	0.00	0.00		
21.20	22.65	0.00	0.10	0.00	0.00	0.03	0.00	0.00	0.10	0.04	0.00	0.00
24.10	25.75	0.00	0.80	0.15	0.00	0.24	0.05	0.00	0.49	0.18	0.00	0.19
27.40	29.25	0.00	2.30	0.55	0.00	0.62	0.15	0.00	1.73	0.64	0.00	0.09
31.10	33.20	0.00	4.56	1.30	0.00	1.09	0.31	0.00	3.91	1.44	0.00	0.03
35.30	37.70	0.00	7.27	2.40	0.00	1.51	0.50	0.00	6.83	2.52	0.00	0.01
40.10	42.85	0.12	9.98	3.82	0.02	1.81	0.69	0.12	10.03	3.78	0.02	0.00
45.60	48.70	0.74	12.16	5.46	0.12	1.96	0.88	0.75	12.67	5.15	0.09	0.01
51.80	55.35	2.16	13.37	7.15	0.30	1.88	1.01	2.21	14.04	6.58	0.21	0.01
58.90	62.90	4.42	13.35	8.71	0.55	1.67	1.09	4.59	13.87	8.02	0.36	0.01
66.90	71.45	7.25	12.11	9.92	0.80	1.33	1.09	7.60	12.36	9.36	0.51	0.01
76.00	81.20	10.12	9.88	10.62	0.97	0.95	1.02	10.59	9.93	10.35	0.65	0.00
86.40	92.25	12.43	7.12	10.68	1.06	0.61	0.91	12.86	7.09	10.73	0.76	0.00
98.10	104.55	13.66	4.35	10.10	1.06	0.34	0.78	13.92	4.32	10.37	0.85	0.00
111.00	119.00	13.54	2.06	8.93	0.85	0.13	0.56	13.56	2.05	9.31	0.92	0.00
127.00	135.50	12.10	0.59	7.33	0.71	0.03	0.43	11.89	0.59	7.71	0.97	0.00
144.00	153.50	9.68	0.00	5.53	0.51	0.00	0.29	9.31	0.00	5.87	1.00	0.01
163.00	174.50	6.84	0.00	3.75	0.30	0.00	0.16	6.39	0.00	4.03	1.00	0.01
186.00	198.50	4.13	0.00	2.20	0.17	0.00	0.09	3.78	0.00	2.38	1.00	0.01
211.00	225.50	2.00	0.00	1.05	0.07	0.00	0.04	1.81	0.00	1.14	1.00	0.02
240.00	256.00	0.69	0.00	0.34	0.02	0.00	0.01	0.60	0.00	0.38	1.00	0.03
272.00	291.00	0.11	0.00	0.02	0.00	0.00	0.00	0.04	0.00	0.02	1.00	0.47
<b>Sum</b>		<b>99.99</b>	<b>100.00</b>	<b>100.01</b>				100	100	100		<b>0.90</b>
Yield to Product		<b>0.63</b>										

Relative errors (%)											
average size	Product	Tailings	Feed	average size	Product	Tailings	Feed	average size	Product	Tailings	Feed
<b>17.55</b>	0.00	0.00	0.00	<b>55.35</b>	2.20	4.99	-8.02	<b>174.50</b>	-6.54	N/A	7.50
<b>19.95</b>	0.00	0.00	0.00	<b>62.90</b>	3.88	3.92	-7.92	<b>198.50</b>	-8.54	N/A	8.28
<b>22.65</b>	N/A	0.00	N/A	<b>71.45</b>	4.83	2.05	-5.67	<b>225.50</b>	-9.64	N/A	8.54
<b>25.75</b>	N/A	-39.16	19.86	<b>81.20</b>	4.66	0.46	-2.59	<b>256.00</b>	-13.49	N/A	10.72
<b>29.25</b>	N/A	-24.88	16.04	<b>92.25</b>	3.47	-0.42	0.47				
<b>33.20</b>	N/A	-14.36	10.96	<b>104.55</b>	1.88	-0.63	2.70				
<b>37.70</b>	N/A	-6.04	5.13	<b>119.00</b>	0.14	-0.44	4.23				
<b>42.85</b>	0.05	0.53	-1.00	<b>135.50</b>	-1.76	-0.18	5.24				
<b>48.70</b>	0.71	4.19	-5.69	<b>153.50</b>	-3.84	N/A	6.15				

Chapter 7- Run 3 (Raw fly ash size distribution)

Size (µm)		Raw data size distribution (vol.%)			Raw data - volume frequency (%/Δµm)			Size (µm)		Raw data size distribution (vol.%)			Raw data - volume frequency (%/Δµm)		
Size Interval	Average size	Product	Tailings	Feed	Product	Tailings	Feed	Size Interval	Average size	Product	Tailings	Feed	Product	Tailings	Feed
<b>0.405</b>	<b>0.43</b>	0.15	0	0	2.727	0.000	0.000	<b>16.4</b>	<b>17.55</b>	2.68	2.36	2.63	1.165	1.026	1.143
<b>0.460</b>	<b>0.49</b>	0.19	0	0	3.016	0.000	0.000	<b>18.7</b>	<b>19.95</b>	3.11	2.53	2.82	1.244	1.012	1.128
<b>0.523</b>	<b>0.56</b>	0.19	0	0	2.676	0.000	0.000	<b>21.2</b>	<b>22.65</b>	3.48	2.69	3.01	1.200	0.928	1.038
<b>0.594</b>	<b>0.63</b>	0.14	0.08	0.09	1.728	0.988	1.111	<b>24.1</b>	<b>25.75</b>	3.77	2.86	3.21	1.142	0.867	0.973
<b>0.675</b>	<b>0.72</b>	0.07	0.14	0.16	0.761	1.522	1.739	<b>27.4</b>	<b>29.25</b>	3.99	3.05	3.43	1.078	0.824	0.927
<b>0.767</b>	<b>0.82</b>	0	0.19	0.21	0.000	1.810	2.000	<b>31.1</b>	<b>33.20</b>	4.16	3.27	3.67	0.990	0.779	0.874
<b>0.872</b>	<b>0.93</b>	0	0.2	0.22	0.000	1.681	1.849	<b>35.3</b>	<b>37.70</b>	4.32	3.54	3.94	0.900	0.737	0.821
<b>0.991</b>	<b>1.06</b>	0	0.19	0.21	0.000	1.367	1.511	<b>40.1</b>	<b>42.85</b>	4.5	3.84	4.24	0.818	0.698	0.771
<b>1.130</b>	<b>1.21</b>	0	0.17	0.19	0.000	1.133	1.267	<b>45.6</b>	<b>48.70</b>	4.73	4.2	4.55	0.763	0.677	0.734
<b>1.280</b>	<b>1.37</b>	0.1	0.16	0.18	0.588	0.941	1.059	<b>51.8</b>	<b>55.35</b>	5.01	4.58	4.84	0.706	0.645	0.682
<b>1.450</b>	<b>1.55</b>	0.14	0.17	0.19	0.700	0.850	0.950	<b>58.9</b>	<b>62.90</b>	5.31	4.96	5.09	0.664	0.620	0.636
<b>1.650</b>	<b>1.77</b>	0.18	0.2	0.22	0.783	0.870	0.957	<b>66.9</b>	<b>71.45</b>	5.57	5.31	5.24	0.612	0.584	0.576
<b>1.880</b>	<b>2.01</b>	0.21	0.24	0.26	0.840	0.960	1.040	<b>76</b>	<b>81.20</b>	5.74	5.57	5.26	0.552	0.536	0.506
<b>2.130</b>	<b>2.28</b>	0.24	0.28	0.3	0.828	0.966	1.034	<b>86.4</b>	<b>92.25</b>	5.74	5.7	5.13	0.491	0.487	0.438
<b>2.420</b>	<b>2.59</b>	0.27	0.33	0.35	0.818	1.000	1.061	<b>98.1</b>	<b>104.55</b>	5.52	5.63	4.83	0.428	0.436	0.374
<b>2.750</b>	<b>2.94</b>	0.3	0.38	0.41	0.811	1.027	1.108	<b>111</b>	<b>119.00</b>	5.07	5.34	4.38	0.317	0.334	0.274
<b>3.120</b>	<b>3.34</b>	0.33	0.45	0.48	0.767	1.047	1.116	<b>127</b>	<b>135.50</b>	4.4	4.8	3.79	0.259	0.282	0.223
<b>3.550</b>	<b>3.79</b>	0.36	0.54	0.57	0.750	1.125	1.188	<b>144</b>	<b>153.50</b>	3.58	4.04	3.12	0.188	0.213	0.164
<b>4.030</b>	<b>4.31</b>	0.39	0.64	0.67	0.709	1.164	1.218	<b>163</b>	<b>174.50</b>	2.69	3.1	2.42	0.117	0.135	0.105
<b>4.580</b>	<b>4.90</b>	0.41	0.75	0.79	0.651	1.190	1.254	<b>186</b>	<b>198.50</b>	1.83	2.1	1.75	0.073	0.084	0.070
<b>5.210</b>	<b>5.57</b>	0.43	0.88	0.93	0.606	1.239	1.310	<b>211</b>	<b>225.50</b>	1.08	1.17	1.14	0.037	0.040	0.039
<b>5.920</b>	<b>6.32</b>	0.46	1.03	1.09	0.575	1.288	1.363	<b>240</b>	<b>256.00</b>	0.51	0.46	0.66	0.016	0.014	0.021
<b>6.720</b>	<b>7.18</b>	0.53	1.18	1.26	0.576	1.283	1.370	<b>272</b>	<b>291.00</b>	0.16	0.07	0.31	0.004	0.002	0.008
<b>7.640</b>	<b>8.16</b>	0.63	1.34	1.45	0.606	1.288	1.394	<b>310</b>	<b>331.00</b>	0	0	0.1	0.000	0.000	0.002
<b>8.680</b>	<b>9.27</b>	0.8	1.51	1.64	0.678	1.280	1.390								
<b>9.860</b>	<b>10.53</b>	1.05	1.69	1.84	0.784	1.261	1.373								
<b>11.200</b>	<b>11.95</b>	1.38	1.86	2.04	0.920	1.240	1.360								
<b>12.700</b>	<b>13.60</b>	1.78	2.03	2.24	0.989	1.128	1.244								
<b>14.500</b>	<b>15.45</b>	2.22	2.2	2.44	1.168	1.158	1.284								

Chapter 7- Run 6 (Raw and mass balanced cenospheres size distribution) (is the same as Chapter 8 – Run 3)

Size (µm)		Raw data size distribution (vol.%)			Raw data - volume frequency (%/Δµm)			Balanced data size distribution (vol.%)				
Size Interval	Average size	Product	Tailings	Feed	Product	Tailings	Feed	Product	Tailings	Feed	Partition number	SSE
16.40	17.55	0.00	0.00	0.00	0.00	0.00	0.00	0.00	0.76	0.09		
18.70	19.95	0.00	0.21	0.00	0.00	0.08	0.00	0.00	0.00	0.00		1.00
21.20	22.65	0.00	0.91	0.00	0.00	0.31	0.00	0.00	0.91	0.10	0.00	0.00
24.10	25.75	0.00	2.21	0.15	0.00	0.67	0.05	0.00	1.57	0.18	0.00	0.11
27.40	29.25	0.04	4.08	0.63	0.01	1.10	0.17	0.04	4.46	0.55	0.06	0.02
31.10	33.20	0.46	6.29	1.49	0.11	1.50	0.35	0.48	6.83	1.22	0.35	0.04
35.30	37.70	1.39	8.53	2.74	0.29	1.78	0.57	1.49	8.92	2.35	0.56	0.03
40.10	42.85	2.93	10.44	4.33	0.53	1.90	0.79	3.11	10.61	3.98	0.69	0.01
45.60	48.70	4.98	11.69	6.09	0.80	1.89	0.98	5.18	11.68	5.93	0.77	0.00
51.80	55.35	7.34	12.06	7.83	1.03	1.70	1.10	7.47	11.93	7.98	0.83	0.00
58.90	62.90	9.66	11.50	9.34	1.21	1.44	1.17	9.62	11.34	9.82	0.87	0.00
66.90	71.45	11.57	10.13	10.38	1.27	1.11	1.14	11.31	9.98	11.16	0.90	0.01
76.00	81.20	12.70	8.20	10.84	1.22	0.79	1.04	12.26	8.10	11.78	0.92	0.01
86.40	92.25	12.80	6.06	10.62	1.09	0.52	0.91	12.29	6.00	11.57	0.94	0.01
98.10	104.55	11.80	4.00	9.76	0.91	0.31	0.76	11.40	3.97	10.54	0.96	0.01
111.00	119.00	9.83	2.29	8.38	0.61	0.14	0.52	9.69	2.28	8.84	0.97	0.00
127.00	135.50	7.22	1.07	6.67	0.42	0.06	0.39	0.00	0.76	0.09	0.98	0.00
144.00	153.50	4.48	0.34	4.86	0.24	0.02	0.26	0.00	0.00	0.00	0.99	0.02
163.00	174.50	2.14	0.00	3.17	0.09	0.00	0.14	0.00	0.91	0.10	1.00	0.12
186.00	198.50	0.62	0.00	1.77	0.02	0.00	0.07	0.00	1.57	0.18	1.00	0.43
211.00	225.50	0.04	0.00	0.77	0.00	0.00	0.03	0.04	4.46	0.55	1.00	0.91
240.00	256.00	0.00	0.00	0.21	0.00	0.00	0.01	0.48	6.83	1.22		
272.00	291.00	0.00	0.00	0.00	0.00	0.00	0.00	1.49	8.92	2.35		
<b>Sum</b>		<b>99.99</b>	<b>100.00</b>	<b>100.01</b>				100	100	100		<b>2.74</b>
Yield to Product		<b>0.89</b>										

Relative errors (%)											
average size	Product	Tailings	Feed	average size	Product	Tailings	Feed	average size	Product	Tailings	Feed
<b>17.55</b>	0.00	0.00	0.00	<b>55.35</b>	1.71	-1.05	1.87	<b>174.50</b>	18.41	N/A	-29.22
<b>19.95</b>	0.00	0.00	0.00	<b>62.90</b>	-0.43	-1.40	5.15	<b>198.50</b>	19.77	N/A	-62.79
<b>22.65</b>	0.00	-0.07	N/A	<b>71.45</b>	-2.25	-1.44	7.44	<b>225.50</b>	4.38	N/A	-95.22
<b>25.75</b>	0.00	-28.86	17.42	<b>81.20</b>	-3.49	-1.25	8.68	256.00	N/A	N/A	-100.00
<b>29.25</b>	0.66	9.23	-12.59	<b>92.25</b>	-3.95	-0.95	8.98	291.00	N/A	N/A	N/A
<b>33.20</b>	5.26	8.57	-18.36	<b>104.55</b>	-3.42	-0.63	8.04				
<b>37.70</b>	7.05	4.61	-14.28	<b>119.00</b>	-1.39	-0.32	5.52				
<b>42.85</b>	6.14	1.62	-8.10	<b>135.50</b>	2.81	-0.07	0.37				
<b>48.70</b>	4.08	-0.12	-2.61	<b>153.50</b>	9.81	0.06	-9.56				

**Chapter 8 - Run 1 (Raw cenospheres size distribution)**

Size (μm)		Raw data size distribution (vol.%)			Raw data - volume frequency (%/Δμm)			Cumulative distribution (Vol.%)
Size Interval	Average size	Product	Tailings	Feed	Product	Tailings	Feed	Feed
10.00	9.33	0.00	0.00	0.00	0.00	0.00	0.00	0.00
11.48	10.72	0.00	0.00	0.00	0.00	0.00	0.00	0.00
13.18	12.30	0.00	0.00	0.00	0.00	0.00	0.00	0.00
15.14	14.13	0.00	0.00	0.00	0.00	0.00	0.00	0.00
17.38	16.22	0.00	0.54	0.00	0.00	0.24	0.00	0.00
19.95	18.62	0.00	2.20	0.00	0.00	0.85	0.00	0.00
22.91	21.38	0.00	4.16	0.04	0.00	1.41	0.01	0.04
26.30	24.55	0.22	6.64	0.32	0.06	1.96	0.10	0.36
30.20	28.18	1.30	9.13	1.48	0.33	2.34	0.38	1.84
34.67	32.36	2.92	11.30	3.12	0.65	2.52	0.70	4.96
39.81	37.15	5.18	12.69	5.36	1.01	2.47	1.04	10.32
45.71	42.66	7.77	13.04	7.89	1.32	2.21	1.34	18.21
52.48	48.98	10.28	12.26	10.30	1.52	1.81	1.52	28.50
60.26	56.23	12.21	10.51	12.13	1.57	1.35	1.56	40.63
69.18	64.57	13.17	8.13	13.01	1.48	0.91	1.46	53.64
79.43	74.13	12.93	5.46	12.74	1.26	0.53	1.24	66.39
91.20	85.11	11.55	3.39	11.38	0.98	0.29	0.97	77.76
104.71	97.72	9.35	0.54	9.22	0.69	0.04	0.68	86.99
120.23	112.20	6.74	0.00	6.66	0.43	0.00	0.43	93.65
138.04	128.82	4.25	0.00	4.21	0.24	0.00	0.24	97.86
158.49	147.91	1.89	0.00	1.90	0.09	0.00	0.09	99.76
181.97	169.82	0.22	0.00	0.24	0.01	0.00	0.01	100.00
208.93	194.98	0.00	0.00	0.00	0.00	0.00	0.00	100.00

**Chapter 8 – Run 3 (Raw and mass balanced cenospheres size distribution) (is the same as Chapter 7- Run 6)**

**Chapter 8 - Run 4 (Raw and mass balanced cenospheres size distribution)**

Size (µm)		Raw data size distribution (vol.%)			Raw data - volume frequency (%/Δµm)			Balanced data size distribution (vol.%)				
Size Interval	Average size	Product	Tailings	Feed	Product	Tailings	Feed	Product	Tailings	Feed	Partition number	SSE
16.40	17.55	0.00	0.00	0.00	0.00	0.00	0.00	0.00	0.76	0.20		
18.70	19.95	0.00	0.00	0.00	0.00	0.00	0.00	0.00	1.06	0.28		
21.20	22.65	0.00	0.00	0.00	0.00	0.00	0.00	0.00	1.62	0.43		
24.10	25.75	0.00	0.32	0.00	0.00	0.10	0.00	0.00	0.32	0.08	0.00	0.00
27.40	29.25	0.00	1.09	0.15	0.00	0.29	0.04	0.00	0.68	0.18	0.00	0.18
31.10	33.20	0.00	2.39	0.59	0.00	0.57	0.14	0.00	2.30	0.61	0.00	0.00
35.30	37.70	0.09	4.16	1.45	0.02	0.87	0.30	0.09	4.53	1.27	0.05	0.02
40.10	42.85	0.61	6.21	2.73	0.11	1.13	0.50	0.63	6.79	2.26	0.20	0.04
45.60	48.70	1.80	8.30	4.40	0.29	1.34	0.71	1.89	8.82	3.73	0.37	0.03
51.80	55.35	3.72	10.12	6.30	0.52	1.43	0.89	3.92	10.41	5.64	0.51	0.01
58.90	62.90	6.20	11.38	8.20	0.77	1.42	1.03	6.48	11.39	7.78	0.61	0.00
66.90	71.45	8.88	11.87	9.86	0.98	1.30	1.08	9.12	11.67	9.80	0.68	0.00
76.00	81.20	11.29	11.50	11.01	1.09	1.11	1.06	11.38	11.20	11.33	0.74	0.00
86.40	92.25	12.92	10.33	11.46	1.10	0.88	0.98	12.79	10.03	12.06	0.78	0.00
98.10	104.55	13.44	8.52	11.12	1.04	0.66	0.86	13.13	8.29	11.85	0.81	0.01
111.00	119.00	12.69	6.36	10.03	0.79	0.40	0.63	12.32	6.22	10.70	0.85	0.01
127.00	135.50	10.82	4.16	8.35	0.64	0.24	0.49	10.53	4.10	8.83	0.88	0.00
144.00	153.50	8.19	2.25	6.32	0.43	0.12	0.33	8.09	2.23	6.54	0.91	0.00
163.00	174.50	5.34	0.87	4.25	0.23	0.04	0.18	5.44	0.87	4.23	0.95	0.00
186.00	198.50	2.81	0.15	2.43	0.11	0.01	0.10	3.01	0.15	2.25	0.98	0.01
211.00	225.50	1.03	0.00	1.07	0.04	0.00	0.04	1.17	0.00	0.86	1.00	0.06
240.00	256.00	0.17	0.00	0.28	0.01	0.00	0.01	0.00	0.00	0.00	1.00	1.97
272.00	291.00	0.00	0.00	0.00	0.00			0.00	0.00	0.00		
<b>Sum</b>		<b>100</b>	<b>99.98</b>	<b>100</b>				<b>100</b>	<b>100</b>	<b>100</b>		<b>0.39</b>
Yield to Product		<b>0.73</b>										

Relative errors (%)											
average size	Product	Tailings	Feed	average size	Product	Tailings	Feed	average size	Product	Tailings	Feed
<b>17.55</b>	0.00	N/A	N/A	<b>55.35</b>	5.50	2.83	-10.45	<b>174.50</b>	1.86	-0.11	-0.51
<b>19.95</b>	0.00	N/A	N/A	<b>62.90</b>	4.47	0.07	-5.14	<b>198.50</b>	7.02	0.10	-7.39
<b>22.65</b>	0.00	N/A	N/A	<b>71.45</b>	2.73	-1.71	-0.64	<b>225.50</b>	13.97	N/A	-19.36
<b>25.75</b>	0.00	-0.051	N/A	<b>81.20</b>	0.76	-2.64	2.89	<b>256.00</b>	-98.82	N/A	-99.47
<b>29.25</b>	0.00	-37.88	19.58	<b>92.25</b>	-0.98	-2.90	5.25				
<b>33.20</b>	0.00	-3.83	3.21	<b>104.55</b>	-2.31	-2.69	6.54				
<b>37.70</b>	0.60	8.93	-12.62	<b>119.00</b>	-2.93	-2.14	6.71				
<b>42.85</b>	2.98	9.36	-17.18	<b>135.50</b>	-2.65	-1.42	5.74				
<b>48.70</b>	5.06	6.31	-15.28	<b>153.50</b>	-1.19	-0.69	3.49				

**Chapter 8 - Run 5 (Raw and mass balanced cenospheres size distribution)**

Size (µm)		Raw data size distribution (vol.%)			Raw data - volume frequency (%/Δµm)			Balanced data size distribution (vol.%)				
Size Interval	Average size	Product	Tailings	Feed	Product	Tailings	Feed	Product	Tailings	Feed	Partition number	SSE
16.40	17.55	0.00	0.00	0.00	0.00	0.00	0.00	0.00	0.00	0.00		
18.70	19.95	0.00	0.00	0.00	0.00	0.00	0.00	0.00	0.00	0.00		
21.20	22.65	0.00	0.00	0.00	0.00	0.00	0.00	0.00	0.00	0.00		
24.10	25.75	0.00	0.00	0.00	0.00	0.00	0.00	0.00	0.00	0.00		
27.40	29.25	0.00	0.09	0.00	0.00	0.02	0.00	0.00	0.09	0.00	0.00	0.00
31.10	33.20	0.00	0.50	0.00	0.00	0.12	0.00	0.00	0.50	0.02	0.00	0.00
35.30	37.70	0.00	1.40	0.04	0.00	0.29	0.01	0.00	1.31	0.04	0.00	0.01
40.10	42.85	0.19	2.81	0.41	0.03	0.51	0.07	0.21	2.97	0.30	0.68	0.09
45.60	48.70	1.00	4.68	1.37	0.16	0.75	0.22	1.09	4.74	1.20	0.87	0.02
51.80	55.35	2.71	6.81	3.00	0.38	0.96	0.42	2.78	6.82	2.91	0.92	0.00
58.90	62.90	5.30	8.93	5.23	0.66	1.12	0.65	5.21	8.91	5.33	0.95	0.00
66.90	71.45	8.43	10.73	7.75	0.93	1.18	0.85	8.02	10.70	8.11	0.96	0.00
76.00	81.20	11.48	11.90	10.18	1.10	1.14	0.98	10.74	11.86	10.78	0.96	0.01
86.40	92.25	13.75	12.22	12.05	1.18	1.04	1.03	12.81	12.18	12.79	0.97	0.01
98.10	104.55	14.66	11.60	12.99	1.14	0.90	1.01	13.78	11.57	13.71	0.97	0.01
111.00	119.00	13.94	10.10	12.80	0.87	0.63	0.80	13.39	10.08	13.28	0.98	0.00
127.00	135.50	11.74	7.95	11.50	0.69	0.47	0.68	11.68	7.94	11.56	0.98	0.00
144.00	153.50	8.56	5.49	9.32	0.45	0.29	0.49	8.95	5.49	8.84	0.98	0.00
163.00	174.50	5.18	3.16	6.68	0.23	0.14	0.29	5.76	3.17	5.68	0.98	0.04
186.00	198.50	2.37	1.34	4.08	0.09	0.05	0.16	2.80	1.34	2.76	0.98	0.14
211.00	225.50	0.64	0.30	1.96	0.02	0.01	0.07	2.75	0.31	2.68	1.00	11.05
240.00	256.00	0.02	0.00	0.61	0.00	0.00	0.02	0.02	0.00	0.02	1.00	0.94
272.00	291.00	0.00	0.00	0.04	0.00	0.00	0.00	0.00	0.00	0.00		
<b>Sum</b>		<b>99.97</b>	<b>100.01</b>	<b>100.01</b>				<b>100</b>	<b>100</b>	<b>100</b>		<b>12.32</b>
Yield to Product		<b>0.97</b>										

<b>Relative errors (%)</b>											
<b>average size</b>	Product	Tailings	Feed	<b>average size</b>	Product	Tailings	Feed	<b>average size</b>	Product	Tailings	Feed
<b>17.55</b>	0.00	0.00	0.00	<b>55.35</b>	2.61	0.17	-2.94	<b>174.50</b>	11.25	0.22	-14.99
<b>19.95</b>	0.00	0.00	0.00	<b>62.90</b>	-1.79	-0.18	1.82	<b>198.50</b>	18.25	0.35	-32.47
<b>22.65</b>	0.00	0.00	0.00	<b>71.45</b>	-4.86	-0.30	4.61	<b>225.50</b>	330.38	1.99	36.48
<b>25.75</b>	0.00	0.00	0.00	<b>81.20</b>	-6.43	-0.32	5.88	<b>256.00</b>	0.00	0.00	-96.83
<b>29.25</b>	0.00	0.01	0.00	<b>92.25</b>	-6.81	-0.30	6.17				
<b>33.20</b>	0.00	-0.04	0.00	<b>104.55</b>	-6.02	-0.25	5.51				
<b>37.70</b>	0.00	-6.73	5.92	<b>119.00</b>	-3.95	-0.17	3.76				
<b>42.85</b>	11.80	5.86	-26.33	<b>135.50</b>	-0.50	-0.07	0.52				
<b>48.70</b>	8.54	1.32	-12.11	<b>153.50</b>	4.59	0.06	-5.15				

Chapter 9 – Run 1 (Raw and mass balanced cenospheres size distribution) (is the same as Chapter 5 – Run 10)

Chapter 9 - Run 2 (Raw and mass balanced cenospheres size distribution) (is the same as Chapter 6 – Run 7)

Size (µm)		Raw data size distribution (vol.%)			Raw data - volume frequency (%/Δµm)			Balanced data size distribution (vol.%)				
Size Interval	Average size	Product	Tailings	Feed	Product	Tailings	Feed	Product	Tailings	Feed	Partition number	SSE
11.48	10.74	0.00	0.00	0.11	0.00	0.00	0.08	0.00	0.00	0.00		
13.18	12.33	0.00	0.14	0.14	0.00	0.08	0.08	0.00	0.16	0.06	0.01	0.34
15.14	14.16	0.00	0.55	0.21	0.00	0.28	0.11	0.00	0.55	0.21	0.00	0.00
17.38	16.26	0.00	1.28	0.36	0.00	0.57	0.16	0.00	1.07	0.40	0.00	0.04
19.95	18.67	0.00	2.41	0.64	0.00	0.94	0.25	0.00	1.96	0.73	0.00	0.05
22.91	21.43	0.00	3.90	1.11	0.00	1.32	0.38	0.00	3.33	1.24	0.00	0.03
26.30	24.61	0.00	5.69	1.82	0.00	1.68	0.54	0.00	5.24	1.95	0.00	0.01
30.20	28.25	0.03	7.58	2.77	0.01	1.95	0.71	0.03	7.50	2.81	0.01	0.00
34.67	32.44	0.25	9.34	3.96	0.06	2.09	0.89	0.25	9.75	3.79	0.04	0.00
39.81	37.24	1.37	10.70	5.33	0.27	2.08	1.04	1.39	11.17	5.03	0.17	0.01
45.71	42.76	3.05	11.43	6.77	0.52	1.94	1.15	3.13	11.88	6.39	0.31	0.01
52.48	49.09	5.37	11.37	8.13	0.79	1.68	1.20	5.50	11.66	7.80	0.44	0.00
60.26	56.37	8.02	10.54	9.24	1.03	1.36	1.19	8.17	10.67	9.10	0.56	0.00
69.18	64.72	10.57	9.03	9.95	1.18	1.01	1.11	10.67	9.05	10.06	0.67	0.00
79.43	74.31	12.50	7.13	10.14	1.22	0.70	0.99	12.46	7.10	10.46	0.75	0.00
91.20	85.32	13.40	5.03	9.75	1.14	0.43	0.83	13.22	5.00	10.16	0.82	0.00
104.71	97.96	13.04	3.23	8.82	0.96	0.24	0.65	12.77	3.22	9.21	0.87	0.00
120.23	112.47	11.49	0.66	7.44	0.74	0.04	0.48	11.59	0.66	7.52	0.97	0.00
138.04	129.13	9.14	0.00	5.80	0.51	0.00	0.33	9.26	0.00	5.81	1.00	0.00
158.49	148.26	6.40	0.00	4.07	0.31	0.00	0.20	6.48	0.00	4.07	1.00	0.00
181.97	170.23	3.91	0.00	2.37	0.17	0.00	0.10	3.85	0.00	2.42	1.00	0.00
208.93	195.45	1.46	0.00	0.68	0.05	0.00	0.03	1.22	0.00	0.77	1.00	0.04
239.88	224.41	0.00	0.00	0.00	0.00	0.00	0.00	0.00	0.00	0.00		
<b>Sum</b>		<b>100.01</b>	<b>100.01</b>	<b>100.00</b>				<b>100</b>	<b>100</b>	<b>100</b>		<b>0.55</b>
Yield to Product		<b>0.63</b>										

Relative errors (%)											
average size	Product	Tailings	Feed	average size	Product	Tailings	Feed	average size	Product	Tailings	Feed
<b>12.33</b>	0.26	20.39	-54.88	<b>42.76</b>	2.62	4.01	-5.64	<b>129.13</b>	1.32	0.00	0.22
<b>14.16</b>	0.00	0.42	-0.35	<b>49.09</b>	2.42	2.55	-4.07	<b>148.26</b>	1.26	0.00	-0.16
<b>16.26</b>	-0.02	-15.79	12.03	<b>56.37</b>	1.88	1.28	-1.48	<b>170.23</b>	-1.36	0.00	2.03
<b>21.43</b>	-0.01	-14.56	11.42	<b>64.72</b>	0.87	0.21	1.13	<b>195.45</b>	-16.77	-0.01	12.68
<b>24.61</b>	0.00	-8.01	7.21	<b>74.31</b>	-0.33	-0.38	3.18				
<b>28.25</b>	0.00	-0.99	1.43	<b>85.32</b>	-1.28	-0.54	4.17				
<b>32.44</b>	0.25	4.39	-4.44	<b>97.96</b>	-2.03	-0.45	4.43				
<b>37.24</b>	1.11	4.39	-5.67	<b>112.47</b>	0.87	-0.01	1.14				

Chapter 9 – Run 3 (Raw and mass balanced cenospheres size distribution)

Size (µm)		Raw data size distribution (vol.%)			Raw data - volume frequency (%/Δµm)			Balanced data size distribution (vol.%)				
Size Interval	Average size	Product	Tailings	Feed	Product	Tailings	Feed	Product	Tailings	Feed	Partition number	SSE
14.5	15.450	0.00	0.12	0.00	0.00	0.07	0.00	0.24	0.12	0.23		
16.40	17.55	0.00	0.31	0.08	0.00	0.13	0.03	0.00	0.37	0.05	0.00	0.14
18.70	19.95	0.00	0.78	0.13	0.00	0.31	0.05	0.00	0.83	0.12	0.00	0.01
21.20	22.65	0.00	1.63	0.21	0.00	0.56	0.07	0.00	1.51	0.22	0.00	0.01
24.10	25.75	0.00	2.86	0.33	0.00	0.87	0.10	0.00	2.47	0.37	0.00	0.03
27.40	29.25	0.00	4.42	0.50	0.00	1.19	0.14	0.00	3.77	0.56	0.00	0.04
31.10	33.20	0.02	6.17	0.75	0.00	1.47	0.18	0.02	5.46	0.83	0.02	0.02
35.30	37.70	0.09	7.92	1.09	0.02	1.65	0.23	0.09	7.38	1.17	0.07	0.01
40.10	42.85	0.23	9.41	1.54	0.04	1.71	0.28	0.23	9.34	1.58	0.12	0.00
45.60	48.70	0.57	10.44	2.16	0.09	1.68	0.35	0.58	10.83	2.10	0.23	0.00
51.80	55.35	1.17	10.82	2.95	0.17	1.52	0.42	1.21	11.45	2.73	0.38	0.01
58.90	62.90	2.11	10.51	3.94	0.26	1.31	0.49	2.23	11.11	3.55	0.54	0.02
66.90	71.45	3.40	9.56	5.11	0.37	1.05	0.56	3.65	9.99	4.59	0.68	0.02
76.00	81.20	4.99	8.12	6.42	0.48	0.78	0.62	5.40	8.37	5.84	0.79	0.02
86.40	92.25	6.78	6.41	7.76	0.58	0.55	0.66	7.34	6.53	7.22	0.87	0.01
98.10	104.55	8.59	4.65	8.98	0.67	0.36	0.70	9.25	4.70	8.57	0.92	0.01
111.00	119.00	10.17	3.05	9.89	0.64	0.19	0.62	10.83	3.06	9.68	0.95	0.00
127.00	135.50	11.27	1.73	10.31	0.66	0.10	0.61	11.83	1.74	10.33	0.98	0.00
144.00	153.50	11.66	0.81	10.09	0.61	0.04	0.53	12.00	0.81	10.34	0.99	0.00
163.00	174.50	11.19	0.26	9.15	0.49	0.01	0.40	11.21	0.26	9.58	1.00	0.00
186.00	198.50	9.87	0.02	7.58	0.39	0.00	0.30	9.53	0.02	8.12	1.00	0.01
211.00	225.50	7.84	0.00	5.56	0.27	0.00	0.19	7.18	0.00	6.11	1.00	0.02
240.00	256.00	5.45	0.00	3.44	0.17	0.00	0.11	4.59	0.00	3.91	1.00	0.04
272.00	291.00	3.11	0.00	1.62	0.08	0.00	0.04	2.24	0.00	1.91	1.00	0.11
310.00	331.00	1.26	0.00	0.43	0.03	0.00	0.01	0.61	0.00	0.52	1.00	0.31
352.00	376.00	0.23	0.00	0.00	0.00	0.00	0.00	0.03	0.00	0.02		
400.00	427.00	0.00	0.00	0.00	0.00	0.00	0.00	0.00	0.00	0.00		
<b>Sum</b>		<b>99.97</b>	<b>100.01</b>	<b>100.01</b>				<b>100</b>	<b>100</b>	<b>100</b>		<b>0.83</b>
Yield to Product		<b>0.85</b>										

Relative errors (%)											
average size	Product	Tailings	Feed	average size	Product	Tailings	Feed	average size	Product	Tailings	Feed
<b>17.55</b>	0.00	18.42	-31.99	<b>55.35</b>	2.99	5.63	-7.68	<b>174.50</b>	-0.48	0.02	4.06
<b>19.95</b>	0.00	5.25	-5.77	<b>62.90</b>	5.34	5.52	-10.12	<b>198.50</b>	-3.92	0.00	6.55
<b>22.65</b>	0.00	-7.44	6.66	<b>71.45</b>	7.08	4.29	-10.46	<b>225.50</b>	-8.81	0.00	9.56
<b>25.75</b>	0.00	-13.68	10.97	<b>81.20</b>	7.84	2.93	-9.31	<b>256.00</b>	-16.05	0.00	13.25
<b>29.25</b>	0.00	-14.75	11.75	<b>92.25</b>	7.75	1.83	-7.32	<b>291.000</b>	-27.89	0.00	17.73
<b>33.20</b>	-0.22	-11.59	10.23	<b>104.55</b>	7.02	1.07	-5.01	<b>331.000</b>	-51.66	0.00	20.84
<b>37.70</b>	-0.49	-6.84	7.41	<b>119.00</b>	5.88	0.57	-2.71	<b>376.000</b>	0.13	0.00	0.00
<b>42.85</b>	-0.24	-0.94	2.56	<b>135.50</b>	4.25	0.28	-0.46				
<b>48.70</b>	0.87	3.65	-2.99	<b>153.50</b>	2.19	0.10	1.75				

## Appendix D: Double fractionation data obtained from the RC™

In Chapter 4 the REFLUX™ Classifier was applied to fractionate fly ash feed to different size and density intervals. In a preliminary run, the feed was divided to 11 overflows in total, and each one was sieved to 4 different size intervals. No de-sliming was performed in this preliminary run. The mass and density of these 44 samples are shown in Tables D.1 to D.3. Then a main run was also conducted similar to the preliminary run, but in this run, all the overflow samples were wet screened at 38 microns to separate slimes, before more detailed dry sieving. For this main run there were 56 samples, which are shown in Tables D.4 to D.6.

**Table D.1: Mass of dried solids obtained from the preliminary fractionation run**

Mass of dried solids (g)												
Size (µm)		flow 1 floats	flow1 sinks	flow 2	flow 3	flow 4	flow 5	flow 6	flow 7	flow 8	flow 9	flow 10
	38	0.001	0.011	1.477	2.370	6.539	5.525	3.256	2.374	1.802	1.853	3.268
38	90	0.400	0.127	0.148	0.076	1.337	1.562	2.159	2.234	4.239	15.707	12.727
90	180	0.869	0.262	0.090	0.023	0.364	0.439	0.900	1.058	2.576	12.089	7.677
180		0.070	0.055	0.018	0.001	0.020	0.011	0.171	0.316	0.795	1.467	1.538

**Table D.2: Density of dried solids obtained from the preliminary fractionation run**

Density of dried solids (kg/m <sup>3</sup> )												
Size (µm)		flow 1 floats	flow1 sinks	flow 2	flow 3	flow 4	flow 5	flow 6	flow 7	flow 8	flow 9	flow 10
	38	-	1560	2210	2150	2100	2160	2070	2070	2030	2240	2110
38	90	770	1090	1040	1060	1630	1870	1650	1750	1860	2080	1910
90	180	780	1130	1140	1080	1360	1790	1440	1600	1730	2140	1840
180		850	1390	1530	-	1310	1560	1720	1900	1950	2420	2030

**Table D.3: Mass fraction and cumulative yield versus solids density**

<b>Density (kg/m<sup>3</sup>)</b>	<b>Mass fraction (wt.%)</b>	<b>Cumulative yield (wt.%)</b>	<b>Density (kg/m<sup>3</sup>)</b>	<b>Mass fraction (wt.%)</b>	<b>Cumulative yield</b>
<b>770.0</b>	0.40	0.40	<b>1841.5</b>	7.68	21.09
<b>780.0</b>	0.87	1.27	<b>1862.8</b>	4.24	25.33
<b>850.0</b>	0.07	1.34	<b>1862.8</b>	4.24	25.33
<b>1040.0</b>	0.15	1.49	<b>1868.6</b>	1.56	26.90
<b>1060.0</b>	0.08	1.56	<b>1900.0</b>	0.32	27.21
<b>1080.0</b>	0.02	1.59	<b>1905.6</b>	12.73	39.94
<b>1090.1</b>	0.13	1.71	<b>1946.8</b>	0.79	40.73
<b>1130.0</b>	0.26	1.98	<b>2027.3</b>	1.54	42.27
<b>1140.0</b>	0.09	2.07	<b>2030.0</b>	1.80	44.07
<b>1310.0</b>	0.02	2.08	<b>2070.0</b>	3.26	47.33
<b>1360.0</b>	0.36	2.45	<b>2070.0</b>	2.37	49.70
<b>1390.0</b>	0.06	2.50	<b>2076.4</b>	15.71	65.41
<b>1440.0</b>	0.90	3.40	<b>2100.0</b>	6.54	71.95
<b>1530.0</b>	0.02	3.42	<b>2110.0</b>	3.27	75.22
<b>1560.0</b>	0.01	3.43	<b>2136.7</b>	12.09	87.31
<b>1560.0</b>	0.01	3.44	<b>2150.0</b>	2.37	89.68
<b>1600.0</b>	1.06	4.50	<b>2160.0</b>	5.53	95.20
<b>1627.6</b>	1.34	5.84	<b>2210.0</b>	1.48	96.68
<b>1650.0</b>	2.16	8.00	<b>2240.0</b>	1.85	98.53
<b>1720.0</b>	0.17	8.17	<b>2417.7</b>	1.47	100.00
<b>1726.9</b>	2.58	10.75			
<b>1750.0</b>	2.23	12.98			
<b>1790.0</b>	0.44	13.42			

**Table D.4: Mass of dried solids obtained from the main fractionation run**

		Mass of dried solids (g)														
Size (µm)		flow 1 floats	flow1 sinks	flow 2	flow 3	flow 4	flow 5	flow 6	flow 7	flow 8	flow 9	flow 10	flow 11	flow 12	flow 13	
<b>38</b>	<b>38</b>	0.018	1.099	3.923	4.287	5.671	12.309	5.161	1.300	2.010	1.961	1.349	1.495	1.047	0.231	
	<b>75</b>	0.382	0.177	0.084	0.116	0.177	3.204	3.155	1.340	2.765	3.652	3.483	5.449	2.907	0.106	
	<b>75</b>	<b>150</b>	0.887	0.280	0.053	0.079	0.124	1.988	2.623	1.593	2.822	4.437	2.938	5.729	2.481	0.093
	<b>150</b>		0.146	0.071	0.009	0.007	0.014	0.351	0.714	0.488	0.808	0.803	0.488	0.652	0.395	0.067

**Table D.5: Density of dried solids obtained from the main fractionation run**

		Density of dried solids (kg/m <sup>3</sup> )														
Size (µm)		flow 1 floats	flow1 sinks	flow 2	flow 3	flow 4	flow 5	flow 6	flow 7	flow 8	flow 9	flow 10	flow 11	flow 12	flow 13	
<b>38</b>	<b>38</b>	830	2180	2230	2150	2130	2070	2090	2110	2100	2120	2170	2310	2580	2440	
	<b>75</b>	780	1020	1050	1100	1180	1640	1800	1830	1840	1880	1930	2090	2370	1950	
	<b>75</b>	<b>150</b>	780	1050	1070	1070	1110	1500	1700	1750	1820	1870	1930	2110	2470	1680
	<b>150</b>		810	1310	1330	1220	1200	1640	1820	1880	1920	1980	2030	2290	2520	1860

**Table D.6: Mass fraction and cumulative yield versus solids density in the main fractionation run**

<b>Density (kg/m<sup>3</sup>)</b>	<b>Mass fraction (wt.%)</b>	<b>Cumulative yield (wt.%)</b>	<b>Density (kg/m<sup>3</sup>)</b>	<b>Mass fraction (wt.%)</b>	<b>Cumulative yield (wt.%)</b>	<b>Density (kg/m<sup>3</sup>)</b>	<b>Mass fraction (wt.%)</b>	<b>Cumulative yield (wt.%)</b>
<b>780.0</b>	0.38	0.38	<b>1830.0</b>	1.34	20.51	<b>2310.0</b>	1.50	92.94
<b>780.0</b>	0.89	1.27	<b>1840.0</b>	2.76	23.27	<b>2370.0</b>	2.91	95.85
<b>810.0</b>	0.15	1.42	<b>1860.0</b>	0.07	23.34	<b>2440.0</b>	0.23	96.08
<b>830.0</b>	0.02	1.43	<b>1870.0</b>	4.44	27.78	<b>2470.0</b>	2.48	98.56
<b>1020.0</b>	0.18	1.61	<b>1880.0</b>	0.49	28.27	<b>2520.0</b>	0.39	98.95
<b>1050.0</b>	0.28	1.89	<b>1880.0</b>	3.65	31.92	<b>2580.0</b>	1.05	100.00
<b>1050.0</b>	0.08	1.97	<b>1920.0</b>	0.81	32.73			
<b>1070.0</b>	0.05	2.03	<b>1930.0</b>	3.48	36.21			
<b>1070.0</b>	0.08	2.11	<b>1930.0</b>	2.94	39.15			
<b>1100.0</b>	0.12	2.22	<b>1950.0</b>	0.11	39.25			
<b>1110.0</b>	0.12	2.35	<b>1980.0</b>	0.80	40.06			
<b>1180.0</b>	0.18	2.53	<b>2030.0</b>	0.49	40.54			
<b>1200.0</b>	0.01	2.54	<b>2070.0</b>	12.31	52.85			
<b>1220.0</b>	0.01	2.55	<b>2090.0</b>	5.16	58.01			
<b>1310.0</b>	0.07	2.62	<b>2090.0</b>	5.45	63.46			
<b>1330.0</b>	0.01	2.63	<b>2100.0</b>	2.01	65.47			
<b>1500.0</b>	1.99	4.61	<b>2110.0</b>	1.30	66.77			
<b>1640.0</b>	3.20	7.82	<b>2110.0</b>	5.73	72.50			
<b>1640.0</b>	0.35	8.17	<b>2120.0</b>	1.96	74.46			
<b>1680.0</b>	0.09	8.26	<b>2130.0</b>	5.67	80.14			
<b>1700.0</b>	2.62	10.88	<b>2150.0</b>	4.29	84.42			
<b>1750.0</b>	1.59	12.48	<b>2170.0</b>	1.35	85.77			
<b>1800.0</b>	3.15	15.63	<b>2180.0</b>	1.10	86.87			
<b>1820.0</b>	0.71	16.35	<b>2230.0</b>	3.92	90.79			
<b>1820.0</b>	2.82	19.17	<b>2290.0</b>	0.65	91.44			

## Appendix E: The concentration induced enhancement obtained in Chapter 6, Runs 1-5 at different pulp densities

In Chapter 6, the recovery of cenospheres at different feed solids concentrations was examined. The theoretical throughput advantage based on the geometry of the IRC™ was calculated and compared with the actual throughput advantage obtained in each run. The error bar was defined as the difference between the enhancement factor for  $d_{50}$  and those for  $d_{25}$  and  $d_{75}$ . Tables E.1 to E.3 show the results of these calculations. Sample calculations are shown in Appendix H (sub-section H.15).

Table E.1: The concentration induced enhancement for  $d_{50}$

Pulp density (wt.%)	$d_{50}$ ( $\mu\text{m}$ )	Terminal rise velocity ( $u_t$ ) (m/h)	Hindered rise velocity ( $u_h$ ) (m/h)	Actual throughput advantage ( $U/u_h$ )	Theoretical throughput advantage	Concentration induced enhancement
10.1	48.0	0.89	0.67	10.47	15.61	0.67
19.2	46.5	0.84	0.48	14.68	15.78	0.93
30.7	41.0	0.65	0.23	30.99	16.8	1.84
38.1	36.5	0.52	0.13	53.63	17.74	3.02
46.4	58.5	1.33	0.20	30.67	13.96	2.20

Table E.2: The concentration induced enhancement for  $d_{25}$

Pulp density (wt.%)	$d_{25}$ ( $\mu\text{m}$ )	Terminal rise velocity ( $u_t$ ) (m/h)	Hindered rise velocity ( $u_h$ ) (m/h)	Actual throughput advantage ( $U/u_h$ )	Theoretical throughput advantage	Concentration induced enhancement	Positive deviation
10.1	37.2	0.54	0.40	15.53	17.59	0.88	0.22
19.2	35.5	0.49	0.28	25.18	17.96	1.40	0.47
30.7	35.5	0.49	0.17	41.34	17.96	2.30	0.46
38.1	31.5	0.39	0.10	72.31	18.92	3.82	0.80
46.4	40.5	0.64	0.10	64.00	16.9	3.79	1.59

Table E.3: The concentration induced enhancement for  $d_{75}$

Pulp density (wt.%)	$d_{75}$ ( $\mu\text{m}$ )	Terminal rise velocity ( $u_t$ ) (m/h)	Hindered rise velocity ( $u_h$ ) (m/h)	Actual throughput advantage ( $U/u_h$ )	Theoretical throughput advantage	Concentration induced enhancement	Negative deviation
10.10	73.5	2.10	1.58	3.98	12.21	0.33	0.34
19.20	76.0	2.24	1.27	5.49	11.97	0.46	0.47
30.70	53.0	1.09	0.38	18.55	14.74	1.26	0.59
38.10	50.0	0.97	0.24	28.70	15.20	1.89	1.13
46.40	94.0	3.43	0.53	11.88	10.46	1.14	1.06

## Appendix F: Three different models in predicting cenosphere hindered rise velocity in suspensions at different solids concentrations

This appendix presents the results of cenosphere hindered rise velocity calculations at different solids concentrations determined using three different models (Eqs. 2-33, 2-36 and 2-39). These results were presented in Chapter 6. The sample calculations are presented in Section H.14.

Pulp density (wt.%)	Suspension density (kg/m <sup>3</sup> )	Solids fraction (vol.%)	$\alpha_1$	$\alpha_f$	$\alpha_2$	$u_t$ Stokes (mm/s)	$u_p$ Masliyah (mm/s)	$u_p$ R-Z (mm/s)	$u_p$ Asif (m/s)
0.000	1000.000	0.000	0.000	1.000	0.000	0.847	0.847	0.085	0.815
0.025	1011.628	0.014	0.000	0.986	0.013	0.863	0.886	0.080	1.060
0.050	1023.531	0.028	0.001	0.972	0.027	0.877	0.921	0.074	1.367
0.075	1035.720	0.042	0.001	0.958	0.041	0.887	0.952	0.070	1.749
0.100	1048.204	0.056	0.001	0.944	0.055	0.892	0.978	0.065	2.222
0.125	1060.994	0.071	0.002	0.929	0.070	0.894	1.000	0.060	2.805
0.150	1074.102	0.087	0.002	0.913	0.085	0.893	1.017	0.056	3.520
0.175	1087.539	0.102	0.002	0.898	0.100	0.887	1.029	0.052	4.394
0.200	1101.319	0.118	0.003	0.882	0.116	0.879	1.037	0.047	5.457
0.225	1115.455	0.135	0.003	0.865	0.132	0.867	1.041	0.043	6.748
0.250	1129.960	0.152	0.004	0.848	0.148	0.852	1.039	0.040	8.309
0.275	1144.849	0.169	0.004	0.831	0.165	0.834	1.033	0.036	10.191
0.300	1160.138	0.187	0.004	0.813	0.183	0.814	1.023	0.033	12.456
0.325	1175.842	0.206	0.005	0.794	0.201	0.791	1.008	0.029	15.175
0.350	1191.980	0.225	0.005	0.775	0.219	0.765	0.988	0.026	18.431
0.375	1208.569	0.244	0.006	0.756	0.238	0.735	0.964	0.023	22.324
0.400	1225.629	0.264	0.006	0.736	0.258	0.703	0.936	0.021	26.970
0.425	1243.180	0.284	0.007	0.716	0.278	0.667	0.904	0.018	32.507
0.450	1261.243	0.305	0.007	0.695	0.298	0.626	0.868	0.016	39.097
0.475	1279.841	0.327	0.008	0.673	0.320	0.581	0.828	0.014	46.930
0.500	1298.998	0.350	0.008	0.650	0.342	0.530	0.785	0.012	56.232
0.525	1318.740	0.373	0.009	0.627	0.364	0.475	0.739	0.010	67.267
0.550	1339.094	0.397	0.009	0.603	0.387	0.414	0.690	0.008	80.349
0.575	1360.090	0.421	0.010	0.579	0.411	0.351	0.639	0.007	95.849
0.600	1381.756	0.446	0.010	0.554	0.436	0.287	0.586	0.006	114.204
0.625	1404.128	0.473	0.011	0.527	0.462	0.226	0.531	0.004	135.931
0.650	1427.239	0.500	0.012	0.500	0.488	0.171	0.476	0.004	161.644
0.675	1451.126	0.528	0.012	0.472	0.515	0.124	0.421	0.003	192.072
0.700	1475.830	0.556	0.013	0.444	0.544	0.086	0.366	0.002	228.077

## Appendix G: Cumulative size distribution of cenospheres and fly ash in the preliminary and main feeds used in multi-stage study in Chapter 8.

In Chapter 8, two fly ash feeds with different cenosphere concentrations were examined using the multi-stage process. The following figure shows that there was no significant difference between the feeds' size distributions.

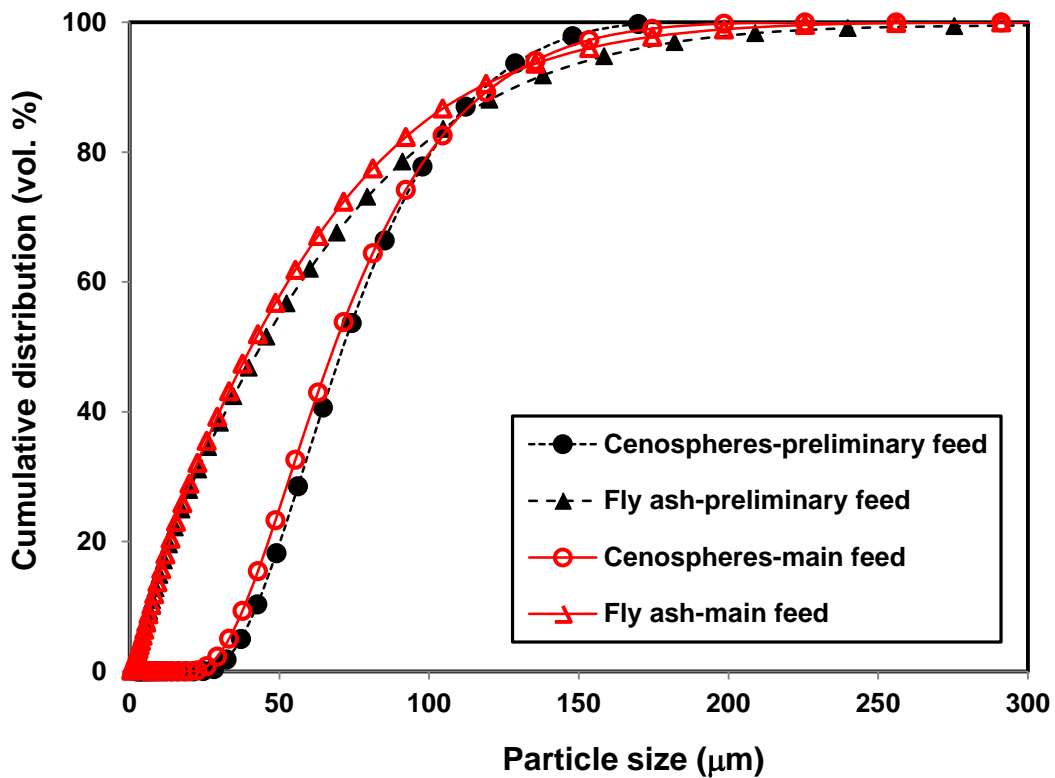


Figure G.1: The size distributions of cenospheres and fly ash in the preliminary and main feeds used in Chapter 8.

## Appendix H: Sample calculations

### H.1 Free settling ratio

In Section 5.2, the free settling ratio was calculated to vary from 5 down to 2.2 as conditions varied from the Newtonian regime to the Stokes regime.

Based on Eq. 2-59:

$$d_{p2}/d_{p1} = [(\rho_{p1} - \rho_f) / (\rho_{p2} - \rho_f)]^n \quad (2-59)$$

when  $\rho_{p1} = 2000 \text{ kg/m}^3$ ,  $\rho_{p2} = 800 \text{ kg/m}^3$  and  $\rho_f = 1000 \text{ kg/m}^3$ ,

for Stokes regime  $n = 0.5$ ,  $d_{p2}/d_{p1} = [(2000 - 1000) / (800 - 1000)]^{0.5} = 2.2$ ,

and for Newtonian regime  $n = 1$ ,  $d_{p2}/d_{p1} = [(2000 - 1000) / (800 - 1000)]^1 = 5$

### H.2 Throughput advantage

For a cenosphere of  $800 \text{ kg/m}^3$  density and  $50 \text{ }\mu\text{m}$  size, the throughput advantage of the REFLUX™ Classifier over the conventional fluidized bed was calculated to be 31.

Based on Eqs. 3-11 & 2-13:

$$U/u_t = 7.5 Re_p^{-1/3} \quad (3-11)$$

$$Re_p = [(14.51 + 1.83(g(\rho_p - \rho_f) \rho_f)^{0.5} d_p^{1.5}/\mu)^{0.5} - 3.81]^2 \quad (2-13)$$

So  $Re_p = [(14.51 + 1.83(9.806(800 - 1000) 1000)^{0.5} (50 \times 10^{-6})^{1.5}/0.001)^{0.5} - 3.81]^2 = 0.014$ ,  
and hence:

$$U/u_t = 7.5 (0.014)^{-1/3} = 31$$

### H.3 Volumetric flux

The volumetric flux was calculated by dividing the volumetric flow rate to the horizontal cross section area of the IRC™. For example, in Chapter 5.4.1, the feed rate was 1.0 L/min equal to:

$$\text{Flux} = \text{flow rate} / \text{horizontal cross section} = (1.0 \times 60 / 1000) / (86 \times 10^{-4}) = 7.0 \text{ m}^3 / (\text{m}^2 \text{ h})$$

#### H.4 Rise velocity of a typical cenosphere

In Section 5.4.1, the rise velocity of a cenosphere 75  $\mu\text{m}$  size and the density of 300  $\text{kg/m}^3$  was calculated as:

Based on Eq. 2-13:

$Re_p = [(14.51 + 1.83(9.806(300 - 1000) 1000)^{0.5} (75 \times 10^{-6})^{1.5}/0.001)^{0.5} - 3.81]^2 = 0.16$ , and hence,

$$u_t = Re_p \times \mu / (\rho_f \times d_p) = 0.16 \times 0.001 / (1000 \times 75 \times 10^{-6}) = 7.23 \text{ m/h}$$

#### H.5 Grade and Recovery (wt.%) using the sink-float test

In each experiment, samples were taken from each stream and poured in sink-float funnels. The separated cenospheres and dense particles were dried and hence their mass was used for calculation of grade and recovery. For example in Run 1 in Chapter 5 (refer to Appendix A):

$$\text{Product grade} = (\text{cenospheres mass in product}) / (\text{mass of total solids in product}) \times 100 = 0.45 / (0.45 + 0.18) \times 100 = 71$$

$$\text{Upgrade} = (\text{cenospheres grade in product}) / (\text{cenospheres grade in feed}) = 71/0.9 = 80$$

$$\text{Recovery} = (\text{cenospheres mass in product}) / (\text{cenospheres mass in feed}) \times 100 = 0.45/0.74 \times 100 = 61$$

$$\text{Pulp density}_{\text{product}} = (\text{solids mass} / \text{total mass})_{\text{product}} = (0.45 + 0.18)/48.4 \times 100 = 1.3$$

The similar procedure was used to calculate grades in different streams and the recovery of other components. It is noted that the grade and recovery values were calculated based on the reconciled data.

#### H.6 Mass balance reconciliation on raw experimental data

The inlet mass of cenospheres, dense silica or fly ash and slurry is not always balanced with the masses of outlet flows. Therefore these masses were adjusted using the Solver function in Excel in order to make a balance between the inlet and outlet (i.e. in/out = 1) and minimize the errors between the raw data and the adjusted data. For example in Chapter 5, Run 1:

The experimental mass of cenosphere in product and underflow was 0.36 and 0.29, respectively, while the mass in the feed was 0.75. Therefore  $\text{out/in} = 0.75/(0.36 + 0.29) = 1.16$ . So the values were changed in order to obtain  $\text{out/in} = 1$  and minimize the error. The adjusted values for cenospheres in product, underflow and feed were 0.45, 0.29 and 0.74. At the same time, the similar procedure was done on all the mass of all components.

For cenospheres in product:

$$\text{Square Standard Error (SSE)} = (\text{adjusted data} - \text{experiment data})^2 / (\text{experiment data})^2 = (0.45 - 0.36)^2 / (0.36)^2 = 0.06$$

$$\text{Relative error} = (\text{adjusted data} - \text{experiment data}) / (\text{experiment data}) = (0.45 - 0.36) / (0.45) \times 100 = 25$$

### H.7 Error bars on recovery data

The error bars show the span of the three recovery values that can be calculated using the raw experimental data for the mass of cenospheres in the feed, tailings and product (i.e.  $\text{recovery} = P/F$ ,  $(F - T)/F$  and  $P/(P + T)$ ), and their difference with that calculated using the balance data.

For example in Chapter 5, Run 1,  $C_p$ ,  $C_f$  and  $C_t$  are assumed to be the mass of cenospheres in product, feed and tailings, respectively. So,

$$\text{Recovery (1)} = C_p / C_f \times 100 = 0.36/0.75 \times 100 = 48$$

$$\text{Recovery (2)} = (C_f - C_t) / C_f \times 100 = (0.75 - 0.29)/0.75 \times 100 = 61$$

$$\text{Recovery (3)} = C_p / (C_p + C_t) \times 100 = 0.45/(0.45 + 0.29) \times 100 = 61$$

$$\text{Recovery using balance data} = 61$$

Therefore the positive difference is  $61 - 61 = 0$ , and negative difference =  $48 - 61 = 13$ .

## H.8 Size distribution and partition curve

In this thesis, the size distributions of the particles were measured and then reconciled using the error minimization method. The raw size data and the balance data are shown in Appendix B. Sample calculations for Chapter 1, Run 1, and the size interval 22.91 – 26.30  $\mu\text{m}$  is shown below:

$$\text{Arithmetic average size} = (22.91 + 26.30)/2 = 24.61 \mu\text{m}.$$

$$\begin{aligned} (\text{Volume frequency})_{\text{product}} &= (\text{Volume distribution})_{\text{product}} / \text{interval width} = 9.11/(26.30-22.91) \\ &= 2.68 \text{ \%/}\Delta\mu\text{m} \end{aligned}$$

## H.9 Mass balance reconciliation technique on size data

All size data were adjusted in order to make the inlet and outlet balanced, and also to minimize the errors between the adjusted values and experimental data. The volume distribution of cenospheres in each size interval in product, tailings and feed can be related as below:

$$\text{Volume fraction in product} = x_p$$

$$\text{Volume fraction in tailings} = x_T$$

$$\text{Volume fraction in feed} = x_F$$

$$\text{yield to product} = Y$$

$$x_p \times Y + x_T \times (1 - Y) = x_F$$

$$\text{So } 9.71 \times 0.674 + (10.90 \times (1 - 0.674)) = 10.10 \text{ which is } x_F.$$

In this formula, the yield to product value also needs to be known. Therefore, Solver in Excel adjusts the yield as well as the size values. Here, the constraints are the in/out ratios which should all equal 1, and also the sum of size fractions for each stream which should add to 100 %.

$$\text{Constraints: in/out values} = 1$$

$$\text{Sum (volume fractions in all size intervals for each stream)} = 100$$

For example in Chapter 1, Run 1, volume fractions in all size intervals as well as the yield (shown in red in Appendix C) were adjusted by Solver. Using the balanced data, partition number for each size interval was calculated:

$$\text{Partition number} = Y \times x_P / x_F = 0.674 \times 9.71/10.90 = 0.65$$

SSE and relative errors were also defined as described above.

The yield or total recovery in volume basis can be calculated directly using the size balanced data as:

$$Y = (x_F - x_T)/(x_P - x_T) = (10.1 - 10.9)/(9.7 - 10.9) = 0.67$$

To calculate the recovery for particles larger than 20  $\mu\text{m}$ ,

$$x_F \text{ for } 20^+ = \sum x_{Fi}^{+20} = 87.2$$

$$x_P \text{ for } 20^+ = \sum x_{Pi}^{+20} = 99.5$$

$$x_T \text{ for } 20^+ = \sum x_{Ti}^{+20} = 61.7$$

The volume based recovery is actually the partition number, so based on the equation above,

$$\text{Recovery}^{+20 \mu\text{m}} = Y \times x_P / x_F = (87.2 - 61.7)/(99.5 - 61.7) \times 99.5/87.2 = 0.77$$

Volume based recovery can be also calculated using Equation 5-3:

$$R_{Vc} = (\rho_{cF}/\rho_{cP})R_{Mc} \tag{5-3}$$

So for Run 1 in Chapter 1,

$$R_{Vc} = (353/257) \times 60.6 = 83.2 \text{ vol.}\%$$

### H.10 Imperfection (*I*)

In Chapter 5, Run 1,

Using Figure 5.7,  $d_{25} = 19 \mu\text{m}$ ,  $d_{50} = 21 \mu\text{m}$  and  $d_{75} = 27 \mu\text{m}$ , so

$$I = (d_{75} - d_{25})/(2 d_{50}) = (27 - 19)/(2 \times 21) = 0.19$$

### H.11 Volumetric split ratio

The ratio of product volumetric rate to the feed volumetric rate, for example in Chapter 1, Run 7, product and feed fluxes are 0.7 and 7, respectively. So the split ratio is:

$$\text{Split ratio} = 0.7/7 \times 100 = 10 \%$$

### H.12 Grade and recovery using pycnometry method

In section 5.4.2.3, the grade and recovery values were calculated using the density of cenospheres, dense fly ash and total solids. Equations 5-1 & 5-2 were used to calculate the grade and recovery of cenospheres. For instance, in Chapter 5, Run 10:

$$X_c = (\rho_{\text{solids}} - \rho_s) / (\rho_c - \rho_s) \times \rho_c / \rho_{\text{solids}} \quad (5-1)$$

$$R = (X_c M_{\text{solid}})_{\text{product}} / (X_c M_{\text{solid}})_{\text{feed}} \quad (5-2)$$

Assuming  $\rho_s = 1600 \text{ kg/m}^3$ ,

$$X_{c\text{-product}} = (\rho_{\text{solids}} - \rho_s) / (\rho_c - \rho_s) = (980 - 1600) / (775 - 1600) \times 775 / 980 = 0.59$$

$$X_{c\text{-Feed}} = (\rho_{\text{solids}} - \rho_s) / (\rho_c - \rho_s) = (1860 - 1873) / (775 - 1860) \times 775 / 1860 = 0.0049$$

$$R = (0.594 \times 1.26) / (0.0049 \times 328.1) = 0.46$$

For sensitivity analysis, the above calculations were repeated assuming different densities for the dense fly ash in product.

### H.13 Curve fit on the solid mass and density data (pycnometry data)

In Chapter 5, in order to generate more data point, curves were fitted to the solids mass data and solids density data. In fact the constants A, B, C and D in following equation were adjusted using Solver routine in EXCEL in order to minimize the sum of square errors (i.e. the difference between the experimental and fitted data).

$$y = A / (1 + \exp(B \times x - C)) + D$$

For example, in Figure 5.11(A),  $A = 27478.50$ ,  $B = 2.98$ ,  $C = 4.18$  and  $D = 4.88$  were fixed by Solver and the sum of square error was obtained about 0.036. This curve fitting procedure was performed for the solids density as well.

#### H.14 Prediction of hindered rise velocity of cenospheres by three different models

In Section 2.3.3, an analysis was done to show the complexity in multi-component suspensions. In a mixture of light particle and heavy particles with the density of  $800 \text{ kg/m}^3$  and  $2000 \text{ kg/m}^3$ , respectively, and average size of  $100 \text{ }\mu\text{m}$ , for the case of 2 vol.% light particles and 25 vol.% heavy ones, the hindered rise velocity of light particles was calculated using three models:

Based on Equation 2.13, the rise velocity of light particles is calculated to be  $1.04 \text{ m/s}$ . Now using Richardson-Zaki equation:

$$u_p = u_r \epsilon^n = u_r (1 - \phi)^n \quad (2-33)$$

$$u_p = 1.04 \times 0.73^{4.6} = 0.24 \text{ m/s}$$

Based on equation 2-36:

$$u_r = u_t [(\rho_p - \rho_{susp}) / (\rho_p - \rho_f)]^{n-1} \quad (2-36)$$

$$\rho_{susp} = \sum (\phi_{pi} \rho_{pi}) + \phi_f \rho_f = 0.02 \times 800 + 0.25 \times 2000 + 0.73 \times 1000 = 1246 \text{ kg/m}^3$$

$$u_p = 1.04 [(800 - 1246) / (800 - 1000)]^{4.6} = 41.6 \text{ m/s}$$

and based on equation 2-39:

$$u_{pi} = g \phi_f^{2.7} / 18 \mu [d_i^2 (1 - \phi_{pi}) (\rho_{pi} - \rho_{susp}) - d_j^2 \phi_{pj} (\rho_{pj} - \rho_{susp})] \quad (2-39)$$

$$u_{pi} = 9.806 \times 0.73^{2.7} / (18 \times 0.001) [0.0001^2 (1 - 0.02) (800 - 1246) - 0.0001^2 \times 0.25 (2000 - 1246)] = 1.46 \text{ m/s}$$

Here the solids concentration was about 0.27. In Chapter 6, Figure 6.1 shows the predictions by these three models for a range of suspension solids concentrations. In fact, in that chapter, the same calculations as above were carried out for the suspensions with different feed solids concentrations.

## H.15 Concentration induced enhancement

Sample calculations are shown for Chapter 6, Run 4. Reading  $d_{50} = 36.5 \mu\text{m}$  from Figure 6.9, and using Equation 3.10, the theoretical throughput advantage was calculated.

$$U/u_t = [1 + \cos\theta \sin\theta (L/z)]/[1 + 0.133 Re_p^{1/3} \cos\theta (L/z)] \quad (3-10)$$

$$Re_p = ((14.51 + (9.8 \times (1000 - 802) \times 1000))^{0.5} \times 1.83 \times (0.0365/1000)^{1.5} / 0.001)^{0.5} - 3.81)^2 \\ = 0.052$$

$$U/u_t = [1 + \cos(70 \pi/180) \sin(70 \pi/180) (1/0.095)]/[1 + 0.133 \times 0.052^{1/3} \cos(70 \pi/180) \\ (1/0.095)] = 18.9$$

Considering area fraction of 0.95, actual throughput advantage ( $U/u_t$ ) is obtained 17.8.

From the experimental conditions, feed velocity was 6.98 m/h. the rise velocity of the cenosphere was also calculated to be 0.13 m/h using Equation 2-13. Therefore the actual throughput advantage is  $6.98/0.13 = 54$ . The concentration induced enhancement is  $54/18 = 3$ .

For other experiments (different pulp densities), the same procedure as explained above was used to calculate the concentration induced enhancement.

## H.16 Error bars on the concentration induced enhancement results

To show the possible error in the results, the enhancement factor was also calculated for  $d_{25}$  and  $d_{75}$ . Therefore the difference between the factors calculated for  $d_{50}$  and those calculated for  $d_{25}$  and  $d_{75}$  was defined as the error bars. For example for Run 4 in Chapter 6, the enhancement factor was calculated to be 1.9 and 3.8 for  $d_{25} = 31.5 \mu\text{m}$  and  $d_{75} = 50 \mu\text{m}$ . Therefore the difference between these factors and that calculated for  $d_{50}$  was defined as positive and negative errors.

$$\text{Positive deviation} = 3.8 - 3.0 = 0.8$$

$$\text{Negative deviation} = 3.0 - 1.9 = 1.1$$

The same procedure was used for the other results in Figure 6.10.

### **H.17 Whole process performance in multi-stage study**

The product grade in whole process is the last stage product grade, and the whole recovery is calculated by multiplying the recovery values obtained at all stages. For example, in Chapter 8, in the three-stage process,

Product grade = product grade in stage 3 = 96.9 wt.%

Whole recovery =  $0.8 \times 0.69 \times 0.92 = 0.50$  or 50 wt.%

## Appendix I: Photos of the experiments and laboratory and pilot scale Inverted REFLUX™ Classifier

In this appendix, the photos taken from the laboratory and pilot scale devices are presented. Figure I.16 shows the porous black particles floated in a water-fly ash mixture. As mentioned in Chapters 4 and 6, if the feed is not mixed for sufficient time to allow water to penetrate all the pores, then the air trapped inside the particle pores leads to the floating of porous particles. Figures I.18 and I.19 show cloudy areas through the inclined channels, which were believed to be the streams. The two following sections show the photos from the laboratory and pilot scale IRC™ runs.

### I.1 Laboratory scale photos



Figure I.1: The laboratory scale IRC™.



Figure I.2: Feed tank used in the lab scale runs.



Figure I.3: The vertical section of the IRC™.



Figure I.4: The inclined section of the IRC™.



Figure I.5: The pressure transducer tubes.



Figure I.6: Overflow pump used in the lab IRC™.



Figure I.7: Product exit and the tube connected to the atmosphere in the lab IRC™.



Figure I.8: Fluidization chamber in the IRC™.



Figure I.9: Inlets to the fluidization chamber.



Figure I.10: Pressure transducer, feed inlet and fluidization chamber.

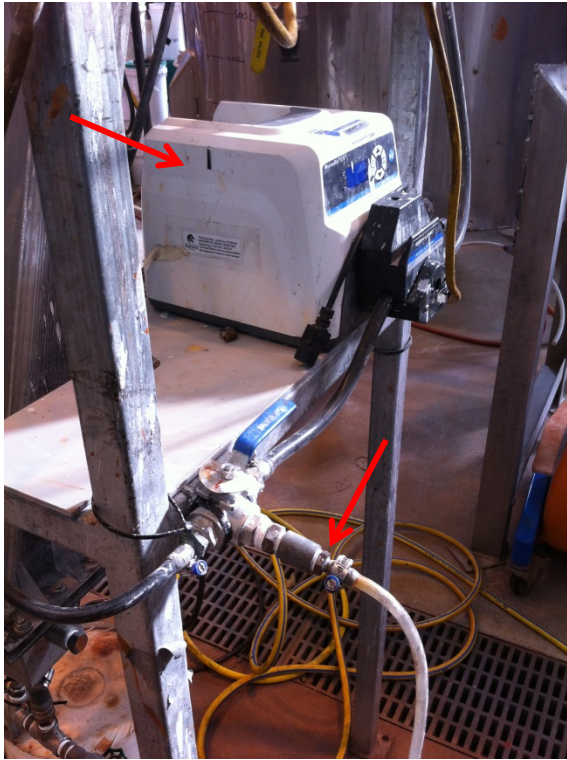


Figure I.11: Feed pump and feed sampling tube.



Figure I.12: The tube extended to 1 m above the IRC™ to make the system pressure balanced.

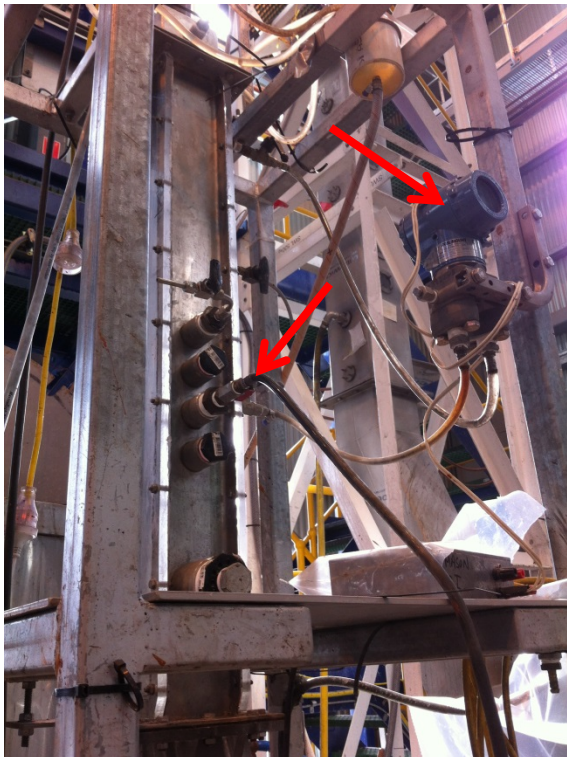


Figure I.13: Feed inlet and pressure transducer.



Figure I.14: The location of pressure transducer tubes.



Figure I.15: The junction of inclined and vertical sections.



Figure I.16: Black porous particles floated in a fresh fly ash-water mixture.



Figure I.17: No sign of the white streams through the inclined channel near the underflow exit.

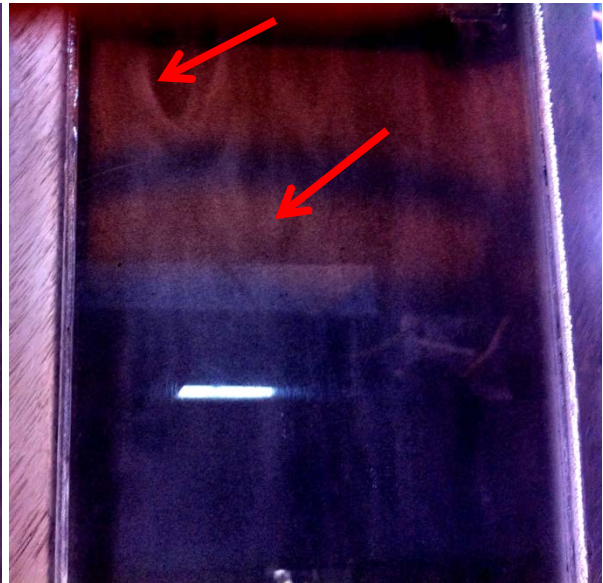


Figure I.18: The white streams developed within the inclined channel near the vertical sections.



Figure I.19: The white streams developed within the inclined channel near the vertical section.

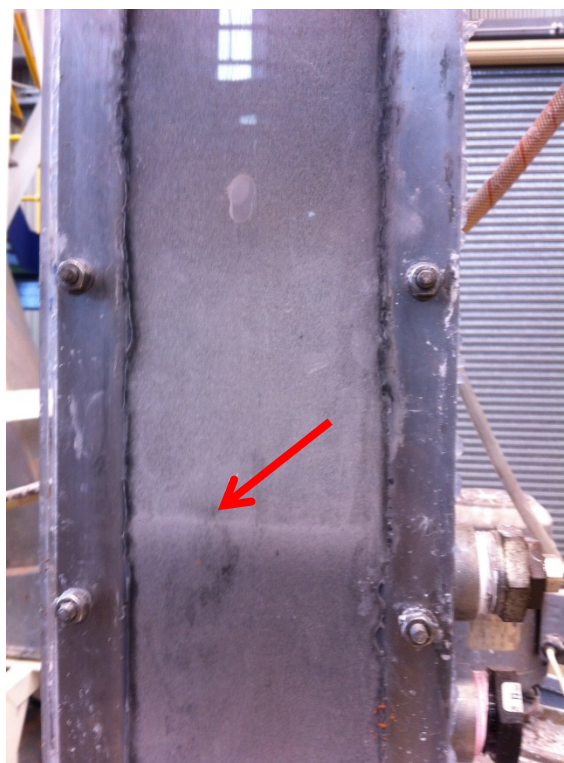


Figure I.20: Interface between light and heavy particles in the vertical section of the IRC™.

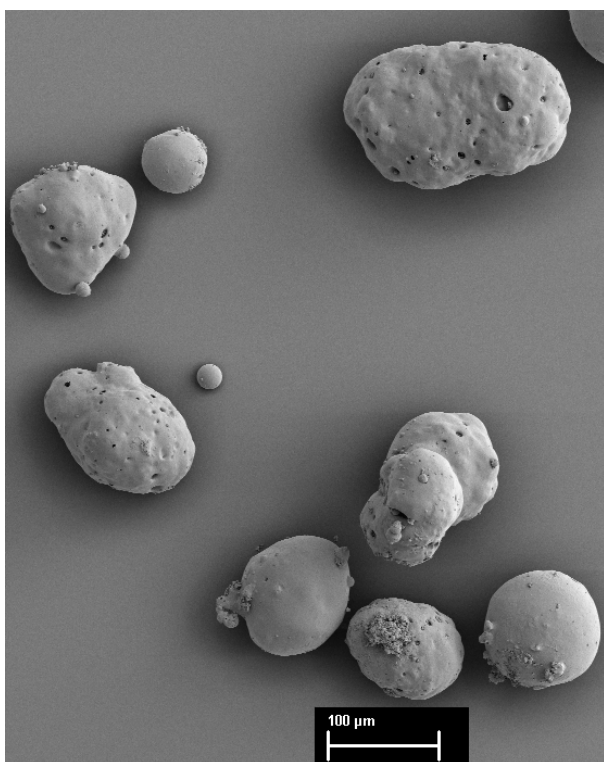


Figure I.21: The porous particles recovered with cenospheres in the double fractionation run.

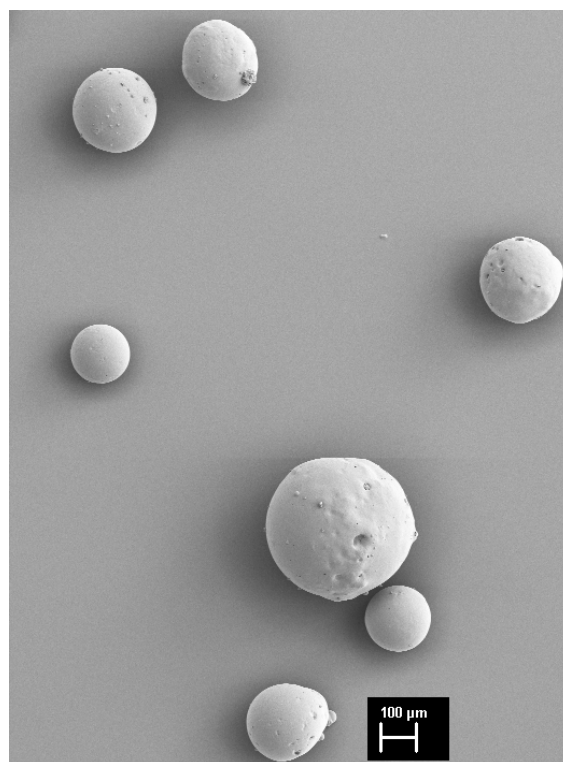


Figure I.22: The spherical cenosphere particles in the feed used in the IRC™ runs.

## I.2 Pilot scale photos



Figure I.23: The pilot scale IRC™.



Figure I.24: The feed tank and feed pump used in the pilot scale runs.



Figure I.25: The inclined channels used at the side of the pilot scale IRC™ to remove solids from underflow.



Figure I.26: The underflow exit and the underflow pump in the pilot scale runs.



Figure I.27: Upper pressure sensor and fluidization chamber in the pilot scale IRC™.



Figure I.28: The two feed tanks used in the pilot scale runs.



Figure I.29: Fly ash and cenospheres volume fraction comparison between two tanks used in the pilot runs.



Figure I.30: Product cenospheres obtained from the multi-stage IRC™ process.



Figure I.31: Final cenospheres powder product obtained from the multi-stage IRC™ process.